

Solar-Terrestrial Predictions Proceedings

Volume 3: Solar Activity Predictions

Richard F. Donnelly, Editor

Space Environment Laboratory
Boulder, Colorado



U.S. DEPARTMENT OF COMMERCE

National Oceanic and Atmospheric Administration

Environmental Research Laboratories

SOLAR-TERRESTRIAL PREDICTIONS PROCEEDINGS

VOLUME III

SOLAR ACTIVITY PREDICTIONS

Edited by

Richard F. Donnelly
Space Environment Laboratory
Boulder, Colorado 80303, U.S.A.

March 1980

The International Solar-Terrestrial Predictions Proceedings and Workshop Program was hosted by the NOAA Space Environment Laboratory. The workshop was held April 23-27, 1979, at the College Inn in Boulder, Colorado.

Science co-sponsors of the program:

AGU: American Geophysical Union
AMS: American Meteorological Society
COSPAR: Committee on Space Research
IAGA: International Association of Geomagnetism and Aeronomy
IAU: International Astronomical Union
IUWDS: International URSIGRAM and World Days Service
SCOSTEP: Scientific Committee on Solar-Terrestrial Physics
URSI: Union Radio Scientifique Internationale; Commissions E and G

Science and financial co-sponsors of the program:

Air Force Geophysics Laboratory
Air Force Office of Scientific Research
Department of Energy
National Aeronautics and Space Administration
National Science Foundation
NOAA Environmental Research Laboratories



UNITED STATES
DEPARTMENT OF COMMERCE
Philip M. Klutznick, Secretary

NATIONAL OCEANIC AND
ATMOSPHERIC ADMINISTRATION
Richard A. Frank, Administrator

Environmental Research
Laboratories
Wilmot N. Hess, Director

NOTICE

The papers in this volume express the opinions and suggestions of the authors. They are presented here in the spirit of encouraging further study, testing and development of solar-terrestrial predictions. The presentation of the papers in this volume does not constitute endorsement or approval by the Environmental Research Laboratories or by the cosponsors of the International Solar-Terrestrial Predictions Proceedings and Workshop Program.

The Environmental Research Laboratories do not approve, recommend, or endorse any proprietary product or proprietary material mentioned in this publication. No reference shall be made to the Environmental Research Laboratories or to this publication furnished by the Environmental Research Laboratories in any advertising or sales promotion which would indicate or imply that the Environmental Research Laboratories approve, recommend, or endorse any proprietary product or proprietary material mentioned herein, or which has as its purpose an intent to cause directly or indirectly the advertised product to be used or purchased because of this Environmental Research Laboratories publication.

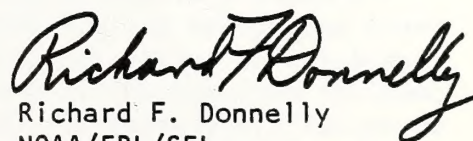
PREFACE

The International Solar-Terrestrial Prediction Proceedings and Workshop Program (ISTP/P-W Program) included the following: (1) an open call for contributed papers on solar-terrestrial predictions; (2) invited review papers about (a) the prediction, warning and monitoring services of groups that regularly issue solar-terrestrial predictions; (b) the current and future needs for predictions by groups that use solar-terrestrial predictions, and (c) current knowledge of selected topics in solar-terrestrial physics and applications; (3) working groups on fourteen areas of interest for solar-terrestrial predictions; (4) a preprint exchange from October, 1978 through March, 1979; (5) a workshop of representatives of the working groups; and (6) the Solar-Terrestrial Predictions Proceedings. These proceedings consist of four volumes:

Volume I.	Prediction Group Reports (GPO No. 003-023-00041-9)
Volume II.	Working Group Reports and Reviews (003-017-00471-6)
Volume III.	Solar Activity Predictions
Volume IV.	Prediction of Terrestrial Effects of Solar Activity

Volume I reviews the current practice in solar-terrestrial predictions. Volume II presents the recommendations and reports developed by the working groups at the workshop. Topical reviews and papers on the current and future needs for predictions are also included. Volumes III and IV present individual suggestions for particular prediction schemes.

The goals of the program were as follows: (1) to determine and document the current state-of-the-art of solar-terrestrial predictions, the applications of these predictions, and the future needs for solar-terrestrial predictions, (2) to encourage research, development and evaluation of solar-terrestrial predictions, and (3) to provide indepth interaction of prediction users, forecasters and scientists involved in the research and development of prediction techniques. To achieve the first goal, we invited forecast groups and user groups to review their activities. The working groups concentrated on deriving recommendations for future needs pertinent to solar-terrestrial predictions. The early call for contributed papers was made to achieve the second goal, i.e. authors had more than a year to orient their work towards a paper on predictions. The workshop was aimed at the third goal. The criteria used for selecting working-group representatives to attend the workshop included the goal of having at least one forecaster per group. The working groups on solar-activity, magnetospheric physics, ionospheric physics, etc., were aimed at attracting scientists. On the other hand, the working groups on communications, geomagnetic applications, and space-craft and man-in-space applications were intended to attract prediction users as well as applications scientists.


Richard F. Donnelly

NOAA/ERL/SEL

Boulder, Colorado 80303 USA

February 11, 1980

OVERVIEW

Volume III includes contributed papers about predicting solar activity. An open call for papers was made in 1977 and 1978 by mailing announcements and by publishing notices in technical journals and professional society bulletins. These notices called for papers on solar-terrestrial predictions, including solar activity predictions. The goal of the open call for contributed papers was to encourage research, development and evaluation of solar-terrestrial prediction techniques.

Contributed papers were reviewed and distributed as preprints to the members of the appropriate working groups. In most cases, the working groups discussed the contributed papers through correspondence before the workshop. The instructions for contributed papers asked that authors describe: (1) how the predictions are made, (2) what is predicted, (3) applications of the predictions, (4) the empirical or theoretical basis for the prediction technique, if not already published elsewhere, (5) an example of using the technique to make a prediction, and (6) if possible, a summary of evaluations of the prediction technique. Authors were requested to provide print-ready manuscripts, but in some cases revisions were made by the proceedings editorial staff.

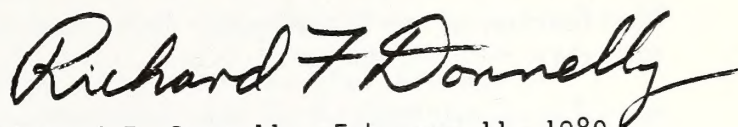
Chapter A includes the contributions on long-term solar-activity predictions. Most of these papers involve statistical techniques. Fougere uses the recently popular maximum entropy technique. Vasilyev et al. use a statistical model of solar periodicity consisting of an oscillating process with a regular component plus a strong noise component. They hope that studies of non-radial solar pulsations (p. A-19) will lead to future improvements in long term predictions. The current solar cycle is now far enough along to show that some predictions of the current solar cycle differ significantly from recent observations. Most papers in this volume were written in the summer or fall of 1978, and some discuss predictions made at an earlier date. The majority of the papers in Chapter A involve long-term predictions of sunspot numbers because there is a longer period of quantitative data on sunspots than for any other measure of solar activity. Some authors who are concerned with particular terrestrial applications, predict other quantities. Suda emphasizes long-term predictions of geomagnetic activity as well as sunspot number for sun-weather applications.

Chapter B presents predictions of the interplanetary magnetic field. Some of the papers suggest ways of using observations of the interplanetary magnetic field structure to predict terrestrial disturbances. Others describe how to use ground-based observations to infer the interplanetary magnetic field structure.

Chapter C discusses solar flare and active region predictions. Most of these papers use optical data with high spatial resolution to determine the complexity of active regions, especially the magnetic field structure. Others consider preflare conditions at microwave or X-ray wavelengths. Although no universal flare precursor has yet been identified, preflare features have been identified for special cases. Perhaps improved flare predictions will require using a large variety of precursors or preflare conditions, each for a particular special case.

Chapter D contains papers about using the optical, microwave or x-ray data to make short-term predictions of the particle radiation at Earth. Microwave emission has had the most success at predicting energetic particles. Optical data are still the main source of information on the location of the flare on the sun, which is essential data for the prediction of the particular particle fluxes that reach Earth. In the future, soft x-ray measurements with moderate spatial resolution may play a larger role in monitoring the location of solar flares. Also, hard x-ray measurements may in the future be used instead of microwave measurements to estimate energetic particle fluxes. However, enough x-ray data exist now to test whether x-rays have any advantage over microwave data in predicting energetic particle fluxes from solar flares.

The many prediction schemes presented throughout this volume will now need to be examined and tested by prediction groups to determine whether they provide an improvement over current practice. If a prediction technique requires data that are not normally available at a prediction center, the improvement in predictions would have to be large enough to justify the expense and work required to obtain the new data in real time at the prediction center.



Richard F. Donnelly, February 11, 1980
ISTP/P-W Program Chairman

ACKNOWLEDGEMENTS

The editor wishes to thank the financial sponsors listed on the title page. I thank Rush Services and Lindsay Murdock of NOAA for their help in revising some of the papers in Volume III. I also thank Millie Bolme, Kristi Brubaker, Ken Davies, Vi Hill, Huu Hoang, Judy Jasan, Linda Kishimoto, David Klock, Andy Smith and Marianne Wiarda for their help in completing Volume III. Without their support, this volume would not have been published.

SOLAR-TERRESTRIAL PREDICTIONS PROCEEDINGS

VOLUME III SOLAR ACTIVITY PREDICTIONS

TABLE OF CONTENTS

Preface.....	iii
Overview.....	iv
Acknowledgements.....	v
A. LONG-TERM SOLAR ACTIVITY PREDICTIONS	
Sunspots: Power Spectra and a Forecast — P. F. Fougere.....	A - 1
A Statistical Model of Solar Periodicity and Its Prediction — O. B. Vasilyev and K. A. Kandaurova.....	A - 10
Application of an Eigenvector Technique to Prediction of Sunspot Activity — H. E. Hunter.....	A - 22
Solar Activity Prediction for Cycle 21 — C. A. Wood.....	A - 37
Babcock Dynamo Theory and the Maunder Minimum — K. H. Schatten.....	A - 41
On the Prediction of Solar Activity Taking Into Account Its Extraneous Conditionality — G. I. Vassilyeva, A. A. Schpitalnaya, and N. S. Petrova.....	A - 45
Forecasting of Solar and Geomagnetic Activity Based on the Relation Between Geomagnetic Disturbance and High-Latitude Magnetic Field of the Sun — Y. I. Feldstein, M. A. Livshits, and T. E. Valtchuk.....	A - 58
Modification of Methods of Forecasting Monthly and Quarterly Wolf Numbers — Yu. I. Vitinsky and B. M. Rubashev.....	A - 71
Prediction of the Radio Emission Indices of the Sun in the Frequency Range $1000 \leq F \leq 3750$ MHz — J. N. Xanthakis and C. Poulakos.....	A - 77
An Attempt at Prediction of Solar-Activity Indices Which Are Closely Related to Climate — T. Suda.....	A - 96
Sunspot Turning-Points and Aurorae Since A. D. 1510 — D. J. Schove.....	A - 111
A Level of Geomagnetic Disturbance and a Distribution of Superlarge- Scale Magnetic Fields on the Sun — M. I. Pudovkin, D. I. Ponyavin, and A. D. Chertkov.....	A - 121

B. INTERPLANETARY MEDIUM PREDICTIONS

- Inference of Sector Polarity of the Interplanetary Magnetic Field From the Cosmic Ray North-South Asymmetry — S. Mori, S. Yasue, Y. Munakata, and K. Nagashima.....B - 1
- Cosmic Ray Anisotropy and the Gross Structure of the Interplanetary Magnetic Field — H. S. Ahluwalia.....B - 13
- On the Diagnosis of the IMF Parameters by the Vertical Ionosonde Data From Vostok Station, Antarctica — A. S. Besprozvannaya, A. V. Shirochkov, and T. I. Shchuka.....B - 23
- Prediction of Active Processes in the Solar Space — N. N. Kontor and G. P. Lyubimov.....B - 29
- Solar-Terrestrial Predictions Using IPS Technique — T. Watanabe.....B - 38
- Space Plasma Monitoring: Two New Capabilities for the Coming Decade — D. P. Cauffman.....B - 48
- The Structure and Geoefficiency of High Velocity Solar Wind Streams — M. I. Pudovkin, S. A. Zaitzeva, A. D. Chertkov, and E. M. Fomina.....B - 56
- The Possibility of Forecasting Magnetic Activity from Observations of Interplanetary Space and Sun — N.I. Dvinskikh, B.G. Dolgoarshinnyh, V.V. Mihnevitch, Yu. V. Pisanko, N.M. Rudneva, and P.M. Svidsky.....B - 66

C. ACTIVE REGION AND FLARE PREDICTIONS

- Prediction of Some Great Flares Based on the Magnetic Field Configuration and Evolution of Sunspot Groups — K. Tanaka.....C - 1
- Short-Term Prediction of the Potential of an Active Region to Produce Recurrent Proton Flares — S. M. P. McKenna Lawlor.....C - 12
- Forecasting of Solar Flares Based on Magnetic Field Configurations — K. L. Harvey and S. F. Martin.....C - 30
- Photospheric Velocity Fields as Indicators of Flare Activity — K. Harvey and J. Harvey.....C - 41
- Short-Term Flare Predictions and Their Stationarity During the 11-Year Cycle — M. Jakimiec and J. Wasiucioneck.....C - 54
- The Application of Multivariate Discriminant Analysis to Solar Flare Forecasting — J. W. Hirman, D. F. Neidig, P. H. Seagraves, W. E. Flowers, and P. H. Wiborg.....C - 64

Logistic Regression for Solar Flare Probability Forecasting — D. F. Vecchia, G. A. Caldwell, P. V. Tryon and R. H. Jones.....	C - 76
Forecasting Parameters of Energy Build-Up in the Chromospheric Active Region — V. V. Kasinsky.....	C - 94
Prediction of Sunspot Group Flare Activity 1-10 Days in Advance — V. B. Gumanitsky, V. I. Efimenko, V. M. Efimenko and V. V. Telnyuk-Adamchuk..	C - 103
New Aspects of Solar Activity Found With High Time Resolution and High Sensitivity Observations at CM- and MM-Wavelengths — P. Kaufmann, F. M. Strauss, J. C. Raffaelli and R. Opher.....	C - 115
Solar Flare Prediction Using Radio Wavelength Interferometers — K. R. Lang.....	C - 131
Soft X-Ray Emission From the Non-Flaring Sun as a Precursor to Flare Activity — D. M. Horan, R. W. Kreplin and K. P. Dere.....	C - 144
Relations Between Solar X-Ray Bursts, Sudden Enhancements of Atmospherics and Regions of Solar Activity — B. Leroy.....	C - 152
Prediction of Solar X-Ray Fluxes Based on Sunspot Structure — J. M. Mosher.....	C - 159
Frequency of Class M and X Flares by Sunspot Class (1969-1976) — K. J. N. Kildahl.....	C - 166
A Prediction Method for the Soft X-Ray Flux of Solar Flares — D. L. Teuber, E. J. Reichmann, R. M. Wilson and J. B. Smith, Jr.....	C - 173
The Study of Evolution of Extreme Ultraviolet Sources Over Sunspots as Given by OSO-4 Data and Some Implications for Predicting Sunspot Evolution and Flare Activity — E. V. Ivanov.....	C - 189
A Computation Scheme Toward Objective Prediction of Solar Flares — T. Yeh and Y. Nakagawa.....	C - 204
Probable Short-Term Prediction of Solar Activity I. Prediction of the Evolution of Active Regions — E. I. Mogilevsky.....	C - 209
Probabilistic Short-Term Prediction of Solar Activity II. Prediction of Flares in Flare-Active Regions — E. I. Mogilevsky.....	C - 222
Forecasting Flare Activity by Pattern Recognition Technique — V. A. Burov, J. W. Hirman and W. E. Flowers.....	C - 235

D. DIAGNOSIS OF SOLAR FLARE ELECTROMAGNETIC RADIATION AND SHORT-TERM
PREDICTIONS OF PARTICLE RADIATION

Application of Integrated Radio Burst Fluxes to the Prediction of Solar Energetic Proton Flux Increases — W. R. Barron and P. Bakshi.....	D - 1
Prediction of Solar Flare Proton Spectrum From Radio Burst Characteristics — P. Bakshi and W.R. Barron.....	D - 7
Quantitative Forecasts of Solar Protons Based on Solar Flare Radio Data — S. T. Akinyan, I. M. Chertok, and V. V. Fomichev.....	D - 14
Determination of PCA Value from the Characteristics of Solar Radio Bursts — S. T. Akinyan, I. M. Chertok, E. M. Zhulina.....	D - 27
Prediction of Solar Proton Events Using Hard X-Ray Emission — S. R. Kane and R. P. Lin.....	D - 34
Diagnostics of Solar Flares and Forecast of Their Geoeffectiveness — S. G. Frolov.....	D - 36
On Some Peculiarities of the Generation of Solar Flare Electromagnetic and Corpuscular Radiation — M.N. Belovsky and Yu, P. Ocheikov.....	D - 46
Prediction of Solar Flare Corpuscular Intensity on the Basis of Radio Burst Observations — A. P. Molchanov and I. E. Pogodin	D - 56
E. ERRATA.....	E - 1
F. WORKSHOP ATTENDEES.....	F - 1

A. LONG-TERM SOLAR ACTIVITY PREDICTIONS

SUNSPOTS: POWER SPECTRA AND A FORECAST

Paul F. Fougere
Air Force Geophysics Laboratory
Hanscom AFB, MA 01731, U.S.A.

High resolution power spectra of the Zürich sunspot numbers for the period 1849 to 1978 are obtained using the maximum entropy technique of Burg. The monthly means are first smoothed using a digital, least-squares, band-pass filter with 193 weights, and then decimated to obtain a more manageable series. An overall power spectrum, which displays multiple structure and harmonic series is then obtained.

In order to explain the complications in the spectrum, a dynamic spectrum is displayed. This is obtained by finding the spectra of data samples 66 years long, repeatedly slipped by 2 years for a total of 78 spectra. The spectra are then much simpler and vary smoothly with epoch. The nominal 11-year line varies in period from about 10 to $12\frac{1}{2}$ years.

In the process of obtaining a power spectrum a prediction error filter is derived. This linear filter may then be used to make predictions as follows: using sets of data containing 5 solar cycles of unsmoothed monthly values beginning with cycles 9 through 15, predictions of the next 12 months of the time series are made and compared to the observed values. RMS errors vary between 5 and 33 and lead to an expectation that the error of prediction for cycle 21 will be about 20. The entire cycle 21 is then predicted using 50, 100, 150 prediction error coefficients. The maximum of cycle 21 is predicted to be 130 ± 20 at 1980.1 ± 0.2 .

Introduction

The subject of this paper is the time series of Zürich sunspot numbers, R_z . The basic data set consists of monthly mean values of R_z beginning in 1749 and running without gaps to October 1978, the latest available value. See Chernosky and Hagan (1958) for the earlier data. There is some smoothing built into the way in which sunspot counts are obtained, because each daily count uses the entire visible hemisphere, which is rotating with a period of 27 days, or a rate of $13\frac{1}{3}$ degrees per day. Thus the daily count is really a $13\frac{1}{3}$ -day running mean of those spots and groups which could be observed on a $13\frac{1}{3}$ degree lune centered at central meridian. Despite the low-pass filter, one of the striking features of the series of monthly means of R_z is the large amplitude, high frequency noise which rides

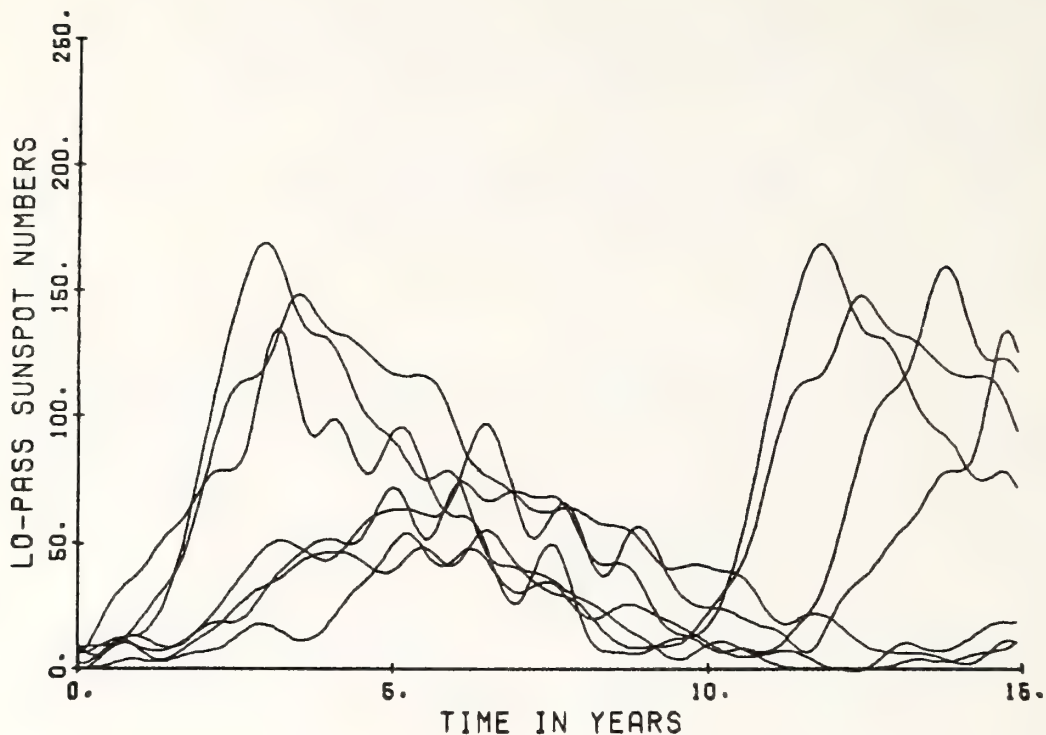


FIGURE 1. SOLAR CYCLES 1-7. DIGITAL LOW-PASS FILTER WITH 13 WEIGHTS HAS BEEN USED. EACH CYCLE BEGINS AT TIME OF SMOOTHED MINIMUM.

on top of the other striking feature, the 11-year period. Accordingly, it has become customary, for example in the monthly Solar Geophysical Data bulletin, to further smooth the monthly averages by using a running mean of 13 monthly values with the 2 extreme months weighted at $\frac{1}{2}$.

So dominant is the appearance of the 11-year cycle that the individual cycles have been assigned numbers beginning with cycle 1 in 1755 to cycle 21, the current cycle, which started in mid-1976. Since the time of minimum can be located with reasonable accuracy, the cycles begin and end at a minimum. Figure 1 shows the first 7 cycles with the time origin set at the time of minimum. These data have been smoothed using a 13-point digital least-squares, low-pass filter following the method of Behannon and Ness (1966). This simple filter has a more nearly accurate low-pass response than that of the 13-point running mean.

Despite the use of the filter, the extreme variability of the data is evident. All of the cycles are bumpy; cycle length, from minimum to minimum, varies between 9 and 15 years; time from minimum to maximum varies from about $2\frac{1}{2}$ to 6 years, and the size of the maximum varies by a factor of 4. These early 7 cycles have been criticized in the classical paper on sunspot prediction by McNish and Lincoln (1949). According to that paper the early data are considerably less reliable and even belong to a different statistical population from the modern data beginning in 1834.

Cycles 8 through 20, the modern data, are shown in Figure 2. For these data, the length of the cycle varies less, between 10 and $12\frac{1}{2}$ years. The

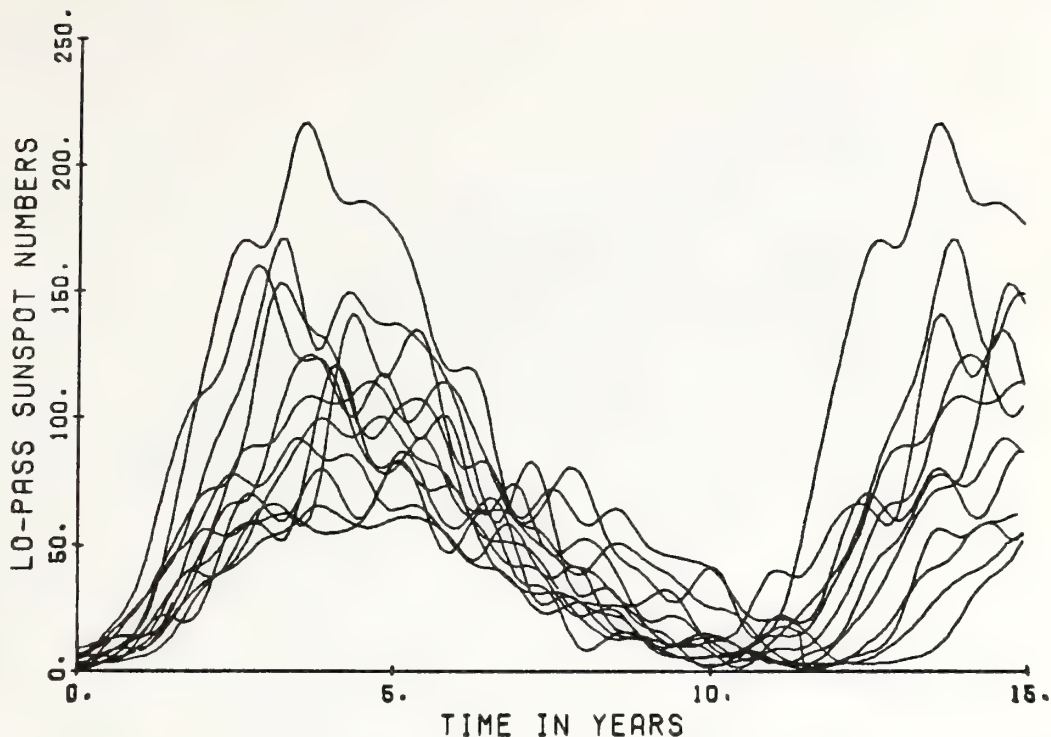


FIGURE 2. SOLAR CYCLES 8-20. DIGITAL LOW-PASS FILTER WITH 13 WEIGHTS HAS BEEN USED. EACH CYCLE BEGINS AT TIME OF SMOOTHED MINIMUM.

time to maximum is now about $2\frac{1}{2}$ to $4\frac{1}{2}$ years, but the height of the maximum still varies by a factor of 4: from about 50 to more than 200.

The extreme variability of these data is further illustrated in Figure 3, showing a 3-dimensional representation of all 20 cycles. Cycle 19, the largest ever, which began in 1954, is so large that it completely hides cycle 20.

Power Spectra

Now we would like to determine the power spectrum of this time series using the maximum entropy method (Burg, 1975) which works admirably on rather short time series. The original 2758 monthly means constitute a rather long series. We can easily remedy this by decimation but only after smoothing to prevent aliasing. Accordingly, a low-pass filter with a cutoff period of $2\frac{1}{2}$ years was designed. At the same time, a high-pass filter was used to remove the mean and very long time trends. The response of the resulting band-pass filter is shown in Figure 4. The digital least-squares filter used 193 weights to achieve this response. Notice the filter beginning to cut off at about $2\frac{1}{2}$ years, as designed, so that the response at 2 years and shorter times (high frequencies) is close to zero. Thus we can sample the output safely once a year and introduce no aliasing because all frequencies higher than the new Nyquist frequency of 0.5 cycles per year have been removed.

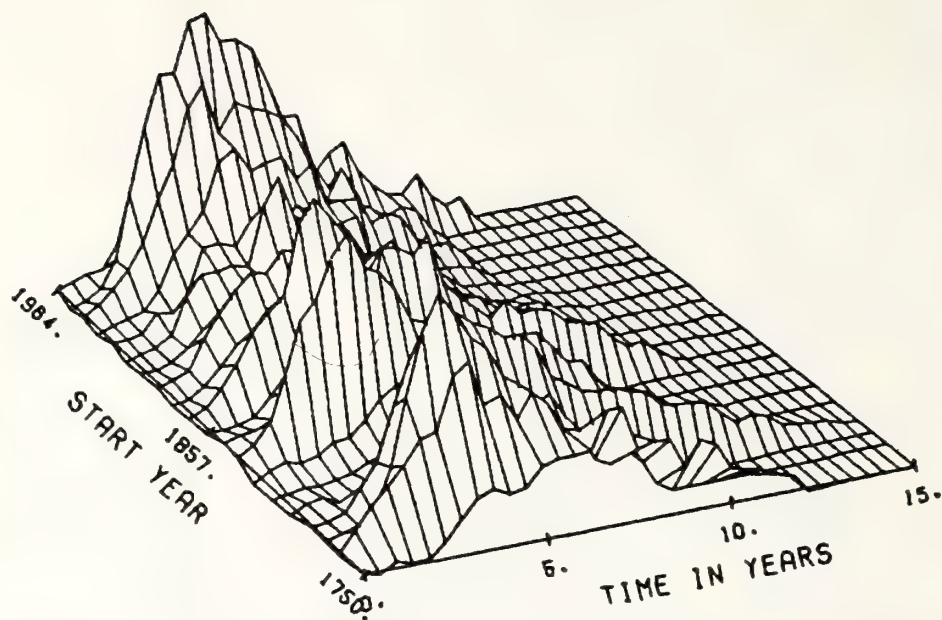


FIGURE 3. PERSPECTIVE PLOT OF CYCLES 1-20.

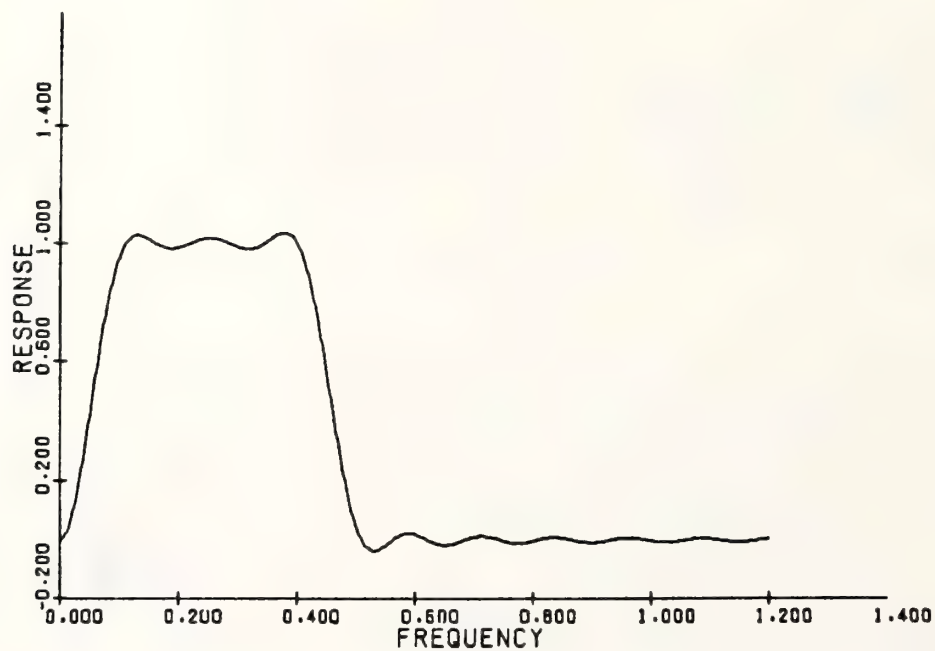


FIGURE 4. RESPONSE OF DIGITAL LEAST-SQUARES, BAND-PASS FILTER. 193 WEIGHTS ARE USED. FREQUENCY IS IN UNITS OF CYCLES PER YEAR.

The results are shown in Figure 5. The original unsmoothed, monthly means are given in the bottom panel with values ranging from 0 to 250 and the dates ranging from the year 1750 to the year 2000. The band-pass filtered output is shown in the top panel, and the differences between the original and band-pass data, the residuals, are given in the middle panel. Thus the original data set in the bottom panel is the sum of the top 2 panels, month by month. The top panel shows a smooth, zero-mean time series which is still not stationary because the amplitudes are quite variable. The residual series, in the central panel, contains essentially all of the high-frequency noise plus the slowly-varying mean or DC level. It is now quite safe to decimate the band-pass filtered series by 12 to obtain 211 yearly values.

The maximum entropy method of Burg (1975) was applied to these 211 numbers and the number of prediction error filter weights, analogous to the number of lags in a Blackman-Tukey spectrum, was varied from 4 to 130. The 3-dimensional representation of these spectra is shown in Figure 6. The nominal 11-year line, which carries most of the power, splits into two very stable lines with periods of about 11.0 and 10.0 years. There is also clear evidence of power peaking at about 12 years and again at about $8\frac{1}{2}$ years. The second harmonic of the 11-year doublet is also a doublet at about 5.5 and 4.8 years. The richness of structure in the spectrum is simply another manifestation of the extreme variability of the time series.

The complicated spectrum also can be explained by taking small overlapping segments of data, performing spectral analysis on each and watching the spectrum change with time. Such a dynamical spectrum is shown in Figure 7. Each spectrum is based on a segment of data 66 years long.

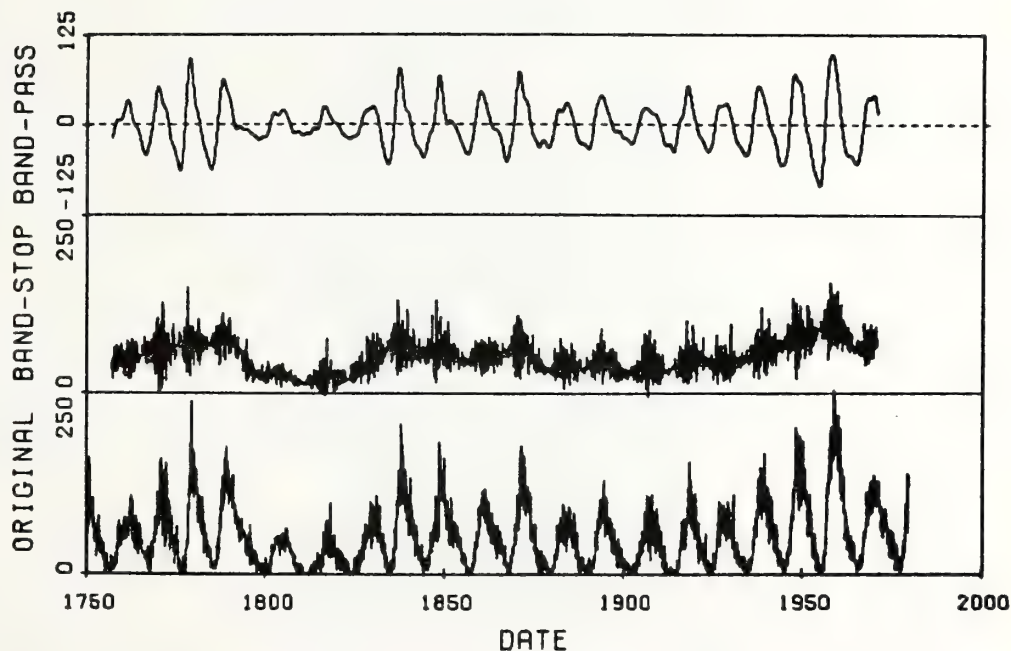


FIGURE 5. SUNSPOT NUMBERS VERSUS DATA FROM 1750 TO PRESENT (OCT. 1978).
 TOP PANEL: BAND-PASS FILTERED DATA (193 WEIGHTS).
 MIDDLE PANEL: ORIGINAL MINUS BAND-PASS.
 BOTTOM PANEL: ORIGINAL, UNSMOOTHED MONTHLY MEANS.

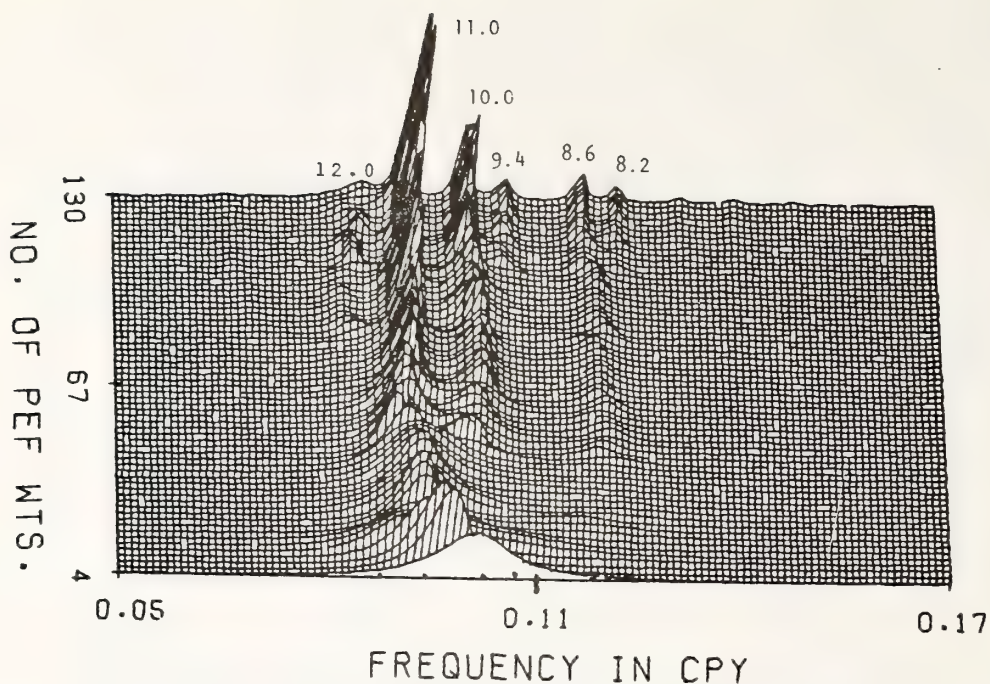


FIGURE 6. PERSPECTIVE PLOT OF MAXIMUM ENTROPY SPECTRA OF BAND-PASS FILTERED DATA SAMPLED ONCE PER YEAR. THE NUMBER OF PREDICTION ERROR FILTER (PEF) WEIGHTS RANGES BETWEEN 4 AND 130 IN STEPS OF 2. PERIODS IN YEARS ARE GIVEN AT APPROPRIATE PEAKS.

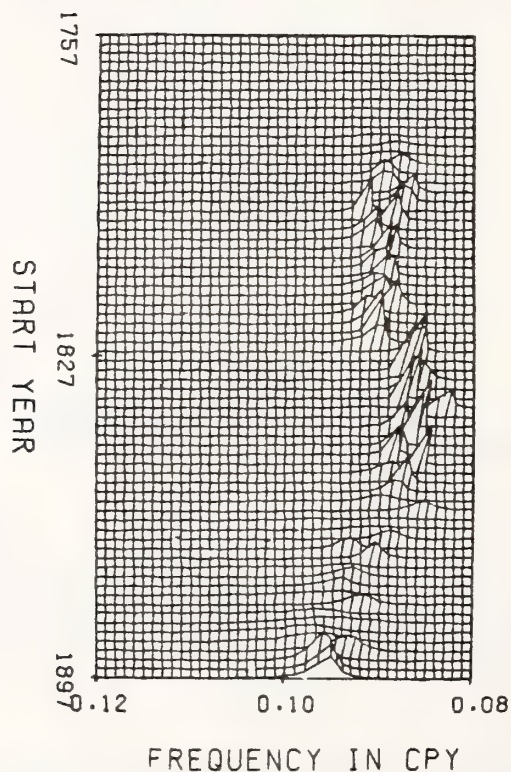


FIGURE 7. DYNAMIC MAXIMUM ENTROPY SPECTRUM OF 66 YEARS (APPROXIMATELY 6 CYCLES) OF BAND-PASS FILTERED DATA SAMPLED ONCE PER YEAR. THE START YEAR ADVANCES BY 2 YEARS FOR EACH SPECTRUM SHOWN.

The segments are overlapped by 64 points, so that the start year moves by 2 years for each new segment. We are now concentrating on a narrow band of periods between 8 and $12\frac{1}{2}$ years. The peaks in the earliest data are too small to be seen in these linear power spectral density plots. The nominal 11-year line shows an instantaneous period varying between 10 and $12\frac{1}{2}$ years while the power spectral density varies by over two orders of magnitude.

Predictions

At the heart of the maximum entropy method is the determination of a prediction error filter. This is a linear filter whose scalar product with a segment of data yields the error in a one-step-ahead prediction. We find the filter essentially by minimizing the sum of squares of such prediction errors over the set of observations. Once we have such a filter we can use it to make predictions off both ends of the series as far as we wish to go simply by applying the filter and moving over the data and the newly acquired predictions.

The predictions of the sunspot numbers were tested as follows. Beginning in 1843, 5 cycles of original unsmoothed monthly values, containing 708 monthly values, constitute a data set for which spectra are obtained for a number of prediction-error filter-weights ranging from 50 to 300 in steps of 50. For each filter, predictions were made for the following 12 months and the RMS prediction error was determined. This is possible because predictions and observed values which had not been used to obtain the predictions are available. The entire procedure was repeated seven times, using 5 cycles of monthly data beginning with cycles 9, 10, 11 through cycle 15, and making predictions into cycles 14 through 20 respectively.

The mean square prediction errors, all quite reasonable numbers from a low of 5 to a high of 33, are shown in Figure 8. Here are plotted the cycle numbers from 14 through 21 and the RMS prediction errors for 12 predictions ranging from 0 through 40. Curiously, the RMS error seems to alternate in magnitude, being low for even cycles, and appreciably higher for odd-numbered cycles. Accordingly a guess is made that the RMS prediction error for the real predictions for cycle 21 will be around 20 for predictions up to 12 months ahead.

Predictions were made using 50 to 300 weights for the entire cycle 21 and plotted. The most consistent behavior for the entire cycle comes from sets with 100, 150, and 200 weights and these are shown in Figure 9. Smoothing these results, the predictions of the maximum and its date become:

$$\text{MAX } (R_z) = 130 \pm 20$$

$$\text{DATE} = 1980.1 \pm 0.2$$

The entire cycle seems quite reasonable with a minimum around 1986.2.

Of the 12 predictions tested for each of the cycles 14 thru 21, the prediction errors were essentially oscillatory. This reflects the noise in the data set rather than any monotonic degradation in the prediction as the prediction time increases. The number 12 was chosen because of the prior

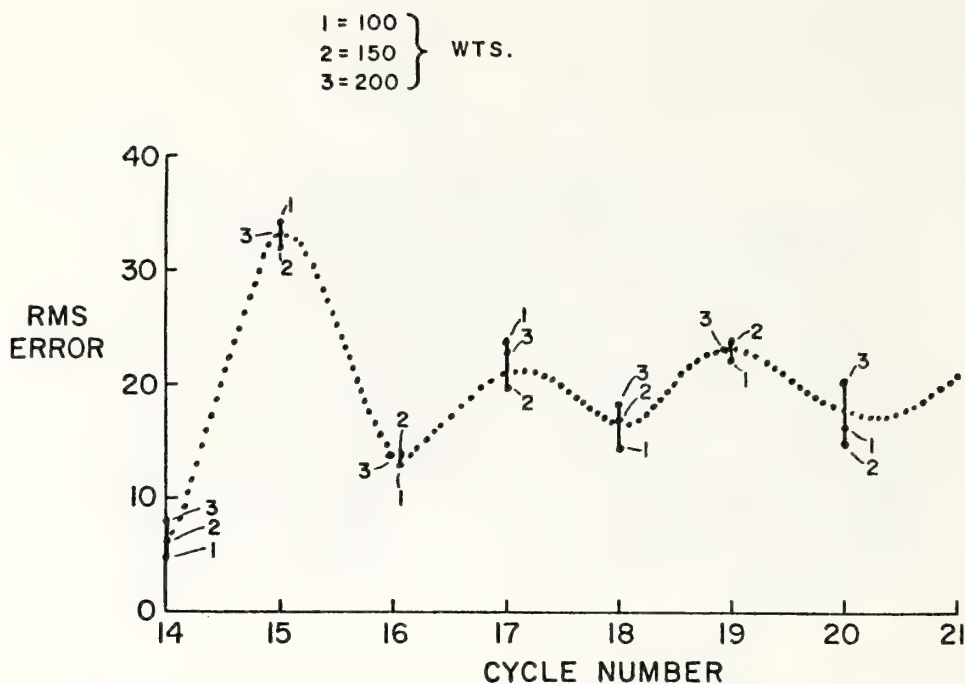


FIGURE 8. RMS ERRORS, FOR PREDICTION OF MONTHLY MEANS 1,2,3,.....,12 MONTHS AHEAD FOR 100, 150 AND 200 WEIGHTS. FIVE SOLAR CYCLES OF ORIGINAL UNSMOOTHED MONTHLY MEAN ARE USED AS INPUT TO THE MAXIMUM ENTROPY POWER SPECTRAL ANALYSIS PROGRAM. NUMBER OF OBSERVATIONS WAS 708, 708, 684, 684, 660, 648 AND 624 RESPECTIVELY.

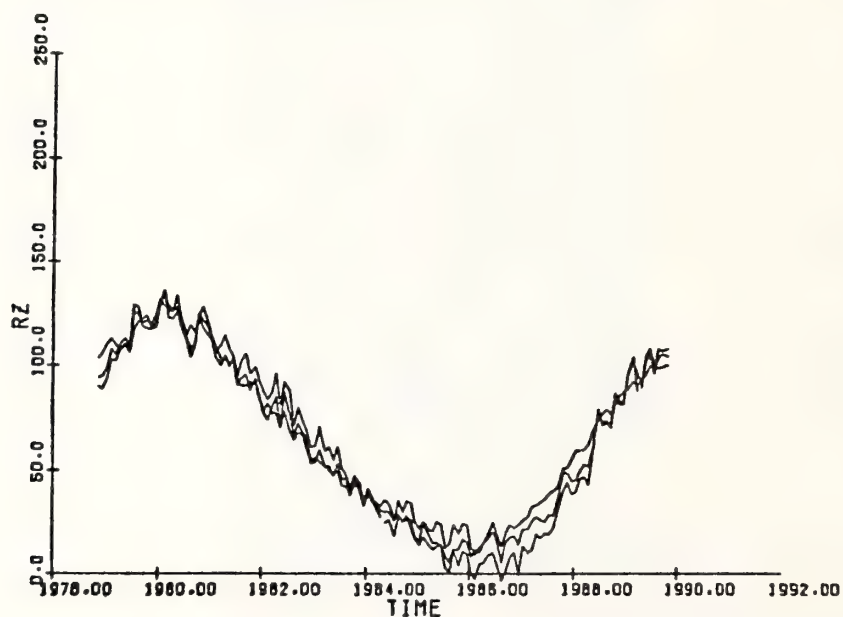


FIGURE 9. PREDICTION OF UNSMOOTHED SUNSPOT NUMBERS MADE USING THREE DIFFERENT SETS OF PREDICTION ERROR FILTERS WITH 100, 150 AND 200 WEIGHTS. DATA USED ARE 670 ORIGINAL UNSMOOTHED MONTHLY MEANS STARTING IN JANUARY, 1923.

expectation that the maximum of cycle 21 was about 12 months away from the date of the latest available observed monthly mean sunspot number (Oct 1978). Thus the expected error should be quite close to 20 even for predictions 14 to 16 months ahead.

In summary, the sunspot data have been displayed and their extreme variability discussed. The data have been filtered with a digital band-pass filter and the resulting series has been decimated. Maximum entropy power spectra vary in a stable manner as the number of weights is varied. A dynamic spectrum showed that the nominal 11-year line varies in period between 10 and $12\frac{1}{2}$ years. A prediction technique has been tested using seven separate data sets each five cycles long. For predictions of monthly means 1,2,3,.....12 months ahead, the RMS prediction error varied between 5 and 35 and lead to the expectation that the RMS prediction error should be about ± 20 for the prediction of the maximum of cycle 21. A forecast for the entire cycle has been given, with the maximum expected to be 130 ± 20 at 1980.1 ± 0.2 .

The programs used here, the filter design program, the three-dimensional plotting program, and the maximum entropy spectral analysis program, are all available on request to seriously interested scientists. Also available is a small card deck containing all of the sunspot monthly means.

References

- Behannon, K.W. and N.F. Ness, (1966), The Design of Numerical Filters for Geomagnetic Data Analyses, NASA TN D-3341.
- Burg, J.P., (1975), Maximum Entropy Spectral Analysis, Ph.D. Thesis, Stanford University.
- Chernosky, E.J. and M.P. Hagan, (1958), The Zürich Sunspot Number and Its Variations for 1700-1957, J. Geophys. Res., 63, (4).
- McNish, A.G. and J.V. Lincoln, (1949), Prediction of Sunspot Numbers, Trans, AGU, 30, 673-685.

A STATISTICAL MODEL OF SOLAR PERIODICITY AND ITS PREDICTION

Vasilyev O.B., Kandaurova K.A.
Main Astronomical Observatory
Leningrad, 196140, USSR

The statistical model of Solar periodicity consists of an oscillating process with a regular part and a noise component that are based on a frequency-statistical analysis of sunspot number series. This mathematical model has been used for developing a method of statistical prediction of solar activity characteristics with a variable length of forecast.

1. A STATISTICAL MODEL OF SOLAR PERIODICITY

Beginning with the middle of 1975, the forecasting of monthly quarter-annual and annual mean values of Wolf sunspot numbers has been performed at the Main Astronomical Observatory of the USSR Academy of Sciences by a principally new method. It is based on frequency-time and statistical analysis of the Zurich series of Wolf sunspot numbers for 1749-1975 and the Greenwich series of the mean areas of solar spots for 1874-1968 (Vasilyev O.B. and Kandaurova K.A., 1968; Kandaurova K.A., 1976).

According to these investigations, the process of spot formation is a multiperiodic one, which is non-stationary in its frequency spectrum and consequently in its correlation moment, and it contains a powerful noise component. In our case, frequency spectra are built from calculations of estimates of the autocorrelation function (ACF) using several "temporal windows." To calculate the fine structure of the spectrum we use a frequency-coordinate elimination (successive or simultaneous) of periodic components with repeated combined calculations of the amplitudes of the oscillation components by means of the least squares method (Vasilyev O.B., 1973).

All the calculations of frequency spectra of solar activity were accompanied by detailed statistical analysis of both the initial series and of the remainder after the subtraction of harmonics. Such an analysis makes it possible to obtain the statistical structure of the series (homogeneity, the kind of distribution, etc.). It also forms one of the possible ways for correctly determining the regular component.

The results of calculating frequency and statistical characteristics of the Zurich series of Wolf numbers and of the series of remainders formed

after successive subtraction of 12 harmonics are presented in the upper part of Table 1.

Table 1

Statistical characteristics of the Zurich series of
Wolf sunspot numbers and their remainders with
subsequently eliminated harmonics.

P		M(w)	D(w)	C _i (W)	$\frac{D_{i-1}}{D_i}$	A(w)	E(w)	λ(w)	κ ²
No.	(years)								
Ordinary series									
		47.40	1460			1.04	0.81	2.20	56.3
1	11.01	47.21	1071	26	1.44	1.32	2.58	1.38	46.5
2	9.91	47.38	880	13	1.10	1.00	1.74	0.82	25.4
3	92.40	47.36	708	12	1.12	0.93	1.78	0.91	24.0
4	10.57	47.30	595	8	1.09	1.05	1.96	0.81	27.3
5	55.35	47.17	504	6	1.08	0.94	1.56	0.99	23.8
6	11.84	47.21	429	5	1.08	0.86	1.32	0.88	22.5
7	8.46	47.11	384	3	1.06	0.81	0.85	0.81	18.2
8	46.01	47.10	350	2	1.06	0.62	0.51	0.46	7.8
9	12.98	47.09	316	2	1.06	0.55	0.87	0.67	12.5
10	9.38	47.10	284	2	1.05	0.40	0.72	0.74	10.6
11	8.12	47.11	261	1.5	1.05	0.28	0.26	0.41	4.6
12	10.18	47.04	239	1.5	1.04	0.21	0.22	0.36	8.9
Sign-alternating series									
		0	3777			-0.21	0.10	0.53	3.6
1	21.97	-0.94	1339	64	2.80	0.20	3.18	1.26	29.8
2	17.86	0.74	1018	8	1.14	0.18	1.95	0.62	9.8
3	20.32	-1.31	711	8	1.20	0.31	2.35	1.07	11.0
4	24.53	-1.30	592	3	1.09	0.07	1.90	0.50	6.3
5	15.95	-1.12	515	2	1.07	-0.05	1.60	0.80	7.4
6	36.25	-0.94	470	1	1.06	-0.08	1.60	0.59	6.2
7	12.54	-0.91	422	1	1.05	-0.05	1.29	0.57	8.5

The regular component of the process is determined by harmonics 5-10, which are significantly non-random, according to different statistical estimates: the variation of residual dispersion D, the changes in the asymmetry A and excess E, and the magnitudes of the Pearson criterion κ^2 and the Kolmogorov criterion λ . The power of the regular component constitutes about 80% of the total power in the process. The frequency spectrum (Fig. 1) contains three distinct groups of harmonics: a centennial (170-190) years) with 20% of the power, a decennial (8-12 years) with 60% of the power, and a short-term (less than 6 years) with 2% of the power.

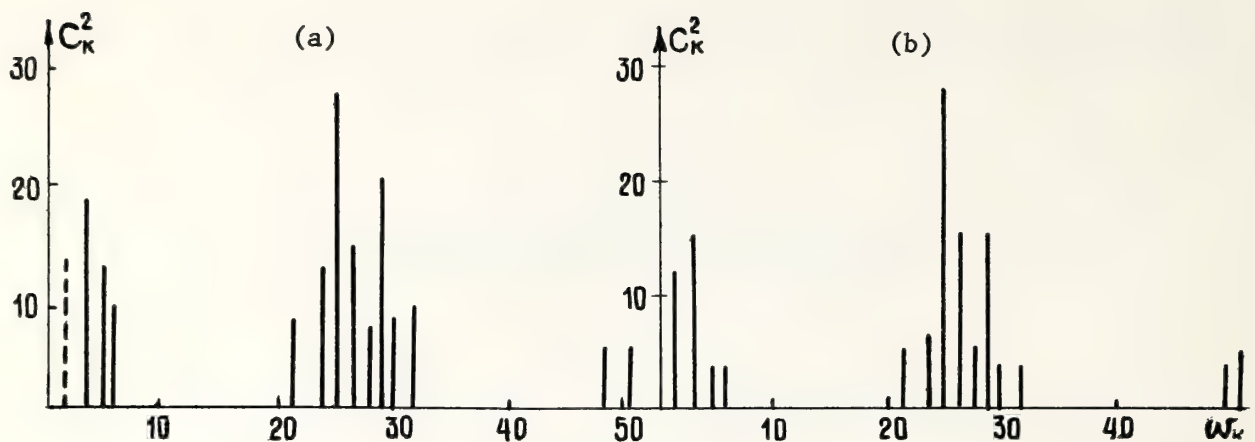


Figure 1. Frequency spectra for a) the Zurich series of the Wolf sunspot numbers (1749-1976); b) the modelled series of the kind ω^*

It is possible to determine the temporal variations of the basic characteristics of the harmonics (amplitude, phase, period) from the calculation of frequency-time spectra (the dynamic spectral picture (Fig. 2)).

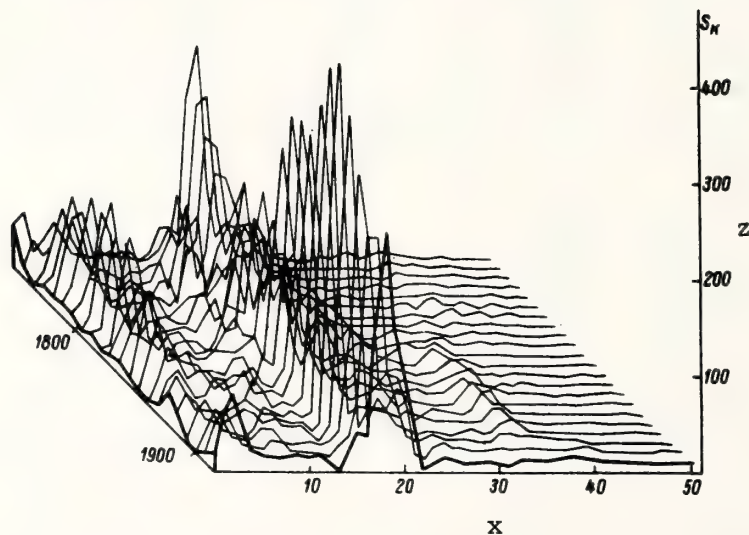


Figure 2. Frequency-time spectra of the Zurich series of Wolf numbers from a 96-year sliding window along the x axis. The dimensionless frequency $\omega_1 = 2T/P$, where P is the period in years, is plotted along the x axis; the time in years is plotted along the y axis; and the spectral estimate of C_1 to the nearest thousandth as obtained from ACF is plotted along the z axis.

Analyses of these spectra make it possible to draw the following conclusions. Decennial periods are characteristic of high temporal stability; their amplitudes are, however, unstable, the amplitude of the 11-year period varying in counter-phase with those of their periods. The mean value of the series and amplitude of the 11-year period are subject to oscillations with the centennial period (Vasilyev O.B., 1970).

Both series of spot indices, after the exclusion of the regular multi-periodic part with components whose periods exceed 6 years, contain a noise component whose power is approximately half the total power of the remainder series. The frequency-time spectra of the Wolf sunspot number series after subtraction of the long-period component ($p > 6$ years) reveal that short-time periods actually exist. Because their power is comparable to that of the noise, they appear and disappear periodically in the frequency spectra of the series, but always appear at the same frequencies. Their duration is, as a rule, only one to three 11-year cycles. The total power of the short-period components changes synchronously with the centennial variation of solar activity (Kandaurova K.A., 1971a).

A detailed statistical analysis of the random component of the Zurich series of Wolf sunspot numbers with the regular part excluded was performed in Kandaurova (1971b). Analysis of two intervals (1870-1904; 1916-1952) has shown that the remainder of the series obeys the normal distribution law. On the whole the process appeared to be non-stationary, but in the time interval of 2-5 years with a sufficient degree of significance it can be considered locally stationary in the "narrow sense." The series of remainders with the regular part excluded can be considered as a combination of correlated and non-correlated components:

$$D(t) = D(t)_{\text{uncor}} + D(t)_{\text{cor}}$$

where $D(t)$, $D(t)_{\text{uncor}}$, and $D(t)_{\text{cor}}$ are the dispersions of the remainder series and its non-correlated and correlated components. The dispersion of the non-correlated component will be dependent not only on the properties of the processes under examination, but also on the interval between adjacent observations. Its value can be assessed from formula below (Vasilyev O.B. and Sakharov V.I., 1971).

$$D_{\text{uncor}} = \lim_{i \rightarrow \infty} \sum_k \delta_k^{(i)} / (n-i) S_i, \quad (1)$$

where the $\delta_k^{(i)}$ equals the i th difference of the series examined, n equals the total number of values in the series, k equals the order of the difference, and S_i equals the sum of the squares of the binomial coefficients.

A standard deviation of the correlated component in the remainder series constitutes ± 10 units, i.e. 64% of the total power of the process. The standard deviation of the non-correlated component is ± 9 units. The high value of $D(t)_{\text{cor}}$ reveals that it is not only possible, but also necessary to extrapolate the random component of the series of monthly mean Wolf numbers. The change in the standard deviation of the remainder series and in that of its non-correlated component occurs synchronously with the variations of the Wolf numbers.

A similar statistical and frequency investigation has been performed with a sign-alternating series because the existence of the 22-year cycle is physically grounded both in the Hale law and in the variations of the solar constant and Sun's radius.

The results of the analysis presented in Table 1(b) have been defined as non-random to a 95% level of confidence for harmonics 3-5 with periods 22, 20, 18, etc., years; the power of the regular component contributes 80% of the power of which 67% can be attributed to the 22-year period and 8% to the remaining two. The noise component of the sign-alternating series is a non-stationary process with a normal distribution.

The average curve for the 11-year cycle, when subdivided into even and odd cycles and graphed as a histogram of the distribution of the duration of these two cycles, has shown that they differ significantly from each other. We assume that the even and odd cycles are two phases of the same physical process whose average duration is 22 years. The W^* series has been modelled as the sum of two summands taken over the modulus. The first summand is the sum of three harmonics with overtones (22.1; 17.9 and 20.2 years); the second one is a series of random numbers whose standard deviation is 6 units. The expression below gives the form of the W^* series.

$$W^* = \left| \sum C_i \sin(\omega_i t + \varphi_i) + \xi \right| \quad (2)$$

Figure 1 shows the calculated frequency spectra of the Wolf numbers and the W^* series. Table 2 contains the values of the periods and amplitudes calculated by the method of frequency-coordinate elimination. P_v equals the probability that the calculated harmonic is non-random. Note the fair

Table 2
Frequency spectra characteristics of the Wolf
sunspot numbers and the W^* series

The Wolf sunspot numbers					W* series			
P (years)	ω_i (see Fig. 2)	Ci (w)		P _v	P (years)	ω_i (see Fig. 2)	Ci (w)	P _v
T	R	E	N	D	198	1.4	12	0.999
92.4	2.96	18		0.999	90.6	3.0	15	0.999
55.4	4.95	13		0.999	58	4.7	-	0.891
46.0	5.96	8		0.999	44	6.3	3	0.900
12.9	21.1	8		0.994	12.6	21.7	3	0.940
11.8	23.1	12		0.999	11.3	24.1	5	0.999
11.01	24.7	27		0.999	11.0	24.8	28.6	0.999
10.6	25.9	15		0.999	10.5	26.0	15.6	0.999
10.2	26.9	7		0.981	10.0	27.0	5.0	0.981
9.9	27.6	19		0.999	9.9	27.6	15.0	0.999
9.4	29.2	8		0.994	9.4	29.0	4.0	0.975
8.5	32.4	9		0.997	8.8	30.8	3.0	0.891
5.4	50.1	5		0.950	5.2	52.4	3.0	0.984
5.6	38.0	5		0.972	5.7	47.7	5.0	0.982

agreement between the frequency characteristics of both series.

The frequency-statistical investigation performed made it possible to build a model of solar periodicity in the form of an oscillating process with a powerful noise component. The regular part is a periodic process that consists of a set of harmonics (5-10) of the centennial, decennial and short-time periods. The random component includes the correlated one with a correlation interval of 4-15 months. A good representation of the observed Wolf number curve can be obtained by using the 22-year period and 2 periods close to it in frequency and by subsequently calculating the modulus of the sum of the oscillations.

2. A STATISTICAL METHOD FOR FORECASTING

The mathematical model of the spot formation process serves as a basis for statistical forecasting. Its general scheme involves the performance of three kinds of extrapolation.

1. for long periods ($P > 7$ years)--by reconstructing the interval spot formation process from its frequency spectrum, which in turn is calculated from the annual mean values of the Wolf numbers for the whole period of observation (extrapolated monthly mean values of this index were determined by calculations with a step of $1/12$ year);
2. for short periods ($P < 6$ years)--by reconstructing the observed spot formation process from its frequency spectrum, which is calculated from the previously eliminated monthly mean values of the Wolf numbers for the previous 30 years of observation;
3. and for the random component--by making use of Kolmogorov's method of calculating their values for one or more months in advance.

The revelation of hidden periodicities in the real sunspot formation process and the determination of the parameters of the harmonics make it possible to approximate the variation of the regular part of the given process for a finite time interval by a certain multiharmonic function. In reconstructing the interval of the spot formation process from its frequency spectrum, the most difficult part is to distinguish between the spectral lines of the regular and random components. It is only the maximum use of physically real and steady harmonics that will give a minimum error in the extrapolation; in determining these harmonics, the best results can be obtained by using successive refinements of the regression equation for the prediction interval. The statistical significance of the decrease in residual dispersion was estimated according to Fischer's criterion; the significance of the correlation coefficient was also calculated.

The accuracy of extrapolating the regular component of the series increases at the division between the spectral lines of the high- and low-frequency components because the time period for constructing the regression equations is different for periods differing in value by an order of magnitude.

Verification of the extrapolation of long periods for 11-year cycles No. 9, 10, 11, 14, 17 and 19 has shown that the existing 270-year series does not exceed the optimal length or sample size for calculating the spectrum. The errors in verification of the forecast for annual and monthly mean values of the Wolf numbers constitute ± 15 units and ± 23 units, respectively. The error in the prediction of the epoch of maximum or minimum of the 11-year cycle is of the order of 6 months. In the forecast of the 20th cycle the error was 17; the error in the epoch of the minimum was 0.1 year. The verification of extrapolation of short periods was performed for cycles No. 9, 11, 14 and 18.

The optimal length the observations should span is 30 years, where the periods are stable in frequency and amplitude. Accounting for short periods improves forecasting of the process, on the whole, and reduces the error of prediction of monthly mean Wolf numbers to ± 18 .

Since the total power of short periods is correlated with the centennial variation of solar activity, it is evident that their inclusion is most efficient in the epochs of maximum of the centennial cycle.

The necessity for extrapolating the correlated part of the random component follows from the high value of its standard deviation. Kolmogorov's method (Kolmogorov N.I., 1941), which was developed for stationary sequences, is a linear smoothing technique and predicts according to the least squares method. The accuracy of the approximation can be estimated from the quantity that the least squares method minimizes--the difference between the predicted value and the true value.

$$D_m = M \left[(y_{i+m} - L)^2 \right], \quad (3)$$

where L is a linear combination of random values $y_{i-1}, y_{i-2}, y_{i-3}, \dots, y_{i-n}$ that belong to some process $Y(t)$. The polynomial L has the following form:

$$L = a_1^m y_{i-1} + a_2^m y_{i-2} + \dots + a_n^m y_{i-n},$$

where y_{i+m} is the value predicted.

The discrete random process $Y(t)$ must satisfy the requirements of stationarity, i.e. it must be time-independent.

$$M_x(t) = \text{const} = M_x, D_x(t) = \text{const} = D_x \text{ and } B(\tau) = B(-\tau),$$

where M_x equals the annual mean value of the Wolf number, D_x equals the dispersion of the annual mean values of the Wolf No., and $B(\tau)$ equals the correlation function.

Because the random component of the series is locally stationary for 2-5 years, the coefficients of the linear polynomial L are found by the method of least squares from the previous 60 months of observed Wolf sunspot numbers. The optimum number of predictors is determined from the ACF analysis. The character of the ACF of the sliding samples of the remainder series studied appeared to be such that the optimal number of predictors in

different years had values of 4 to 9. A verification of the extrapolation gave the same value for the optimal number of predictors--the location of the first significant ACF minimum in most cases corresponding to the value of the optimal number of predictors.

The minimum error value of the statistical forecasting method was determined by the standard deviation of the non-correlated component of the process. A comparison of the variation of the values of W with $D^*(t)$ forecast dispersion and with $D(t)_{\text{uncor}}$ revealed their synchronous change. The correlation coefficients were 0.80 for R_W, D_{uncor} and 0.62 for R_W, D^* forecast. The variation of the relative forecast error δ , which depends on the value of the monthly mean sunspot numbers, has the form

$$\delta = \frac{D_{\text{for}}^*}{W} = 0.056 + \frac{4.2}{W}.$$

In the table below δ has been evaluated for several representative values of W .

Monthly Mean Wolf No.	W	10	25	50	100	150	200
Relative fore- cast error	δ	48%	22%	14%	10%	9%	8%

In our case the forecast error does not exceed the non-correlated component standard deviation. Verification of forecast has been carried out for the periods 1916-1952 and 1970-1974.

Routine forecasting of monthly and quarter-annual mean values of the Wolf numbers has been going on since July 1975. The distribution of errors of the verification forecast and the operational one obey a normal distribution law. The error of forecasting constitutes ± 10 units. This indicates that the prediction scheme of this solar activity indices is an optimal one.

A comparison of the method described here for statistical forecasting with those existing today, as well as an analysis of justification of the methods performed according to meteorological criteria are given in (Vitinsky Yu.I. and Kandaurova K.A., 1975). From the viewpoint of sign and value, the forecast made by means of the statistical method with separate extrapolations of the regular and random components is a good one and may be considered optimal for the time being.

The final program of extrapolation of Wolf numbers has been accomplished with an appropriate algorithm on the "Minsk-22" and "ES-1020" electronic computers at the Main Astronomical Observatory of the USSR Academy of Sciences.

The prediction for long-time periods is made 11 years in advance--once each year, after the new annual mean value of the sunspot number has been obtained. The extrapolation of short-time periods is performed monthly after obtaining the next monthly mean value of the index under consideration. Forecasts of the random component are also made each month (toward the end

of the month) by using a preliminary value of the monthly mean Wolf number for the current month--a value based on approximately 25 days of observations. This extrapolation is performed 1, 2 or more months in advance.

Thus, on the 25th day of every month forecasts of the following values of the Wolf number (W) are made:

- 1) monthly mean values of W for the next 3 months;
- 2) quarter-annual values of W for the current and the next quarter of the year;
- 3) values of the regular component of the W series for the next 12 months;
- 4) annual mean values of W for the current year and the next;
- 5) and annual mean values for 11 years in advance.

Figure 3 shows the forecast of monthly mean Wolf numbers. The extrapolation error constitutes ± 10 units.

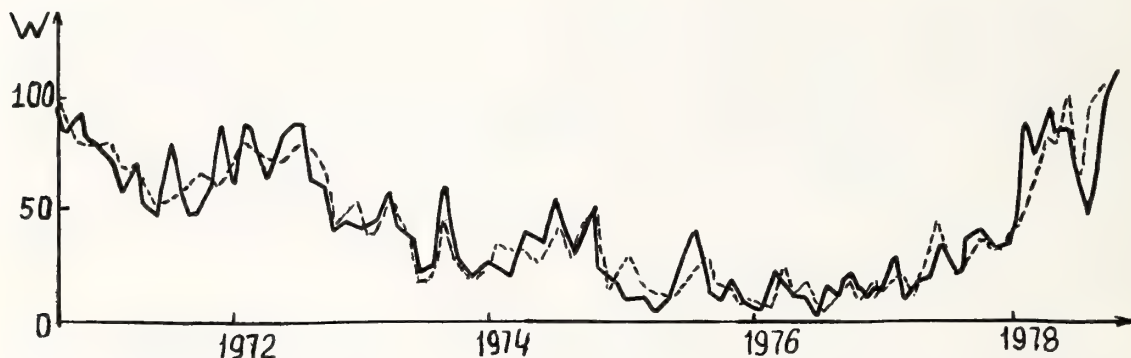


Figure 3. Forecast of monthly mean Wolf numbers. The solid line denotes the observed values; the dotted one, the predicted values.

Table 3 presents the expected values of the annual mean Wolf numbers (W) for the next 12 years, as calculated in 1978.

Table 3

Year	W	Year	W	Year	W
1979	86	1983	41	1987	10
1980	97	1984	16	1988	17
1981	87	1985	9	1989	35
1982	68	1986	5	1990	49

When the forecast of the 21st cycle of solar activity generated in 1975 (Vasilyev O.B. et al., 1975) according to the method described above was compared with other forecasts, it gave the maximum value within 70-110 units of the Wolf numbers and the maximum epoch in mid-1980.

3. INTERPRETATION OF STATISTICAL MODEL AS SURFACE LAYER PULSATIONS

Improvement of forecast accuracy should be sought in further development of theoretical knowledge of solar activity and in construction of a physical model of the activity. In this connection, of great importance is an attempt to relate some peculiar features of the Sun's activity to its possible non-radial pulsations. The results of a physical interpretation of the statistical model of solar activity from the point of view of the pulsation hypothesis are presented in Vasilyev O.B. and Kandaurova K.A. (1976).

Comparing variations in the rate of change of the Sun's radius with the Wolf numbers, comparing variations in the Sun's radius with the solar constant (Fig. 4), and investigating their phase relationships--all make it possible to obtain an integral description of variations of different solar parameters with the basic 22-year period.

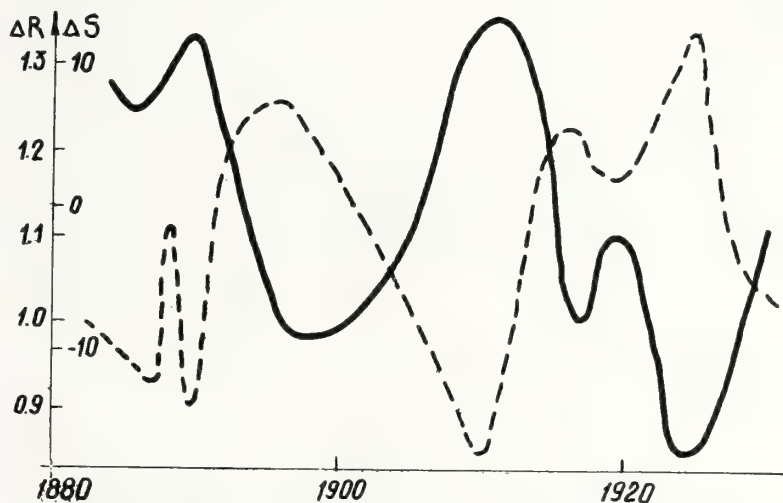


Figure 4. Relative change of the solar constant S (1873-1930) plotted as a dashed line and the Sun's radius (1876-1930) plotted as a solid line.

The non-adiabatic character of the excitation of oscillations follows from an analysis of the time profile of changes in solar radius. For energy

assessment of the oscillations, a Δp - Δv diagram (Fig. 5) has been built.

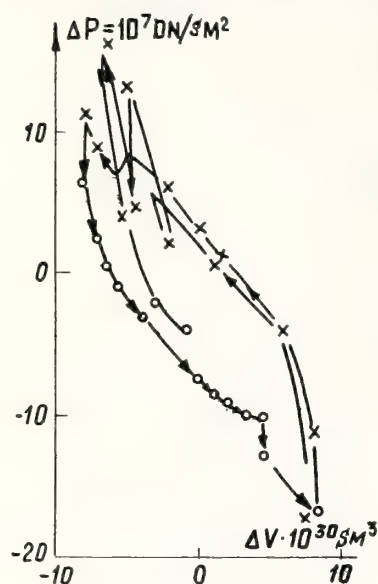


Figure 5. Diagram Δp - Δv (1873-1930).

x - points corresponding to odd-number cycles;

o - points corresponding to even-number cycles.

Calculation of the area inside the loop formed by the average PV curve gives the amount of energy dissipated during a single 22-year cycle as $E = 10^{38}$ ergs. This energy value is in fair agreement with the quantity of magnetic energy dissipated by spots during a 22-year cycle ($2 \cdot 10^{37}$ ergs). Comparison of the value E with the kinetic energy of the moving layers makes it possible to assume that the energy loss in every 22-year cycle may be accounted for by the expenditure of energy required for the excitation of convection in sub-photospheric layers, which in turn, determines the process of spot formation. Estimation of the pulsation period, under the assumption that the Sun's subphotospheric layers perform thermal relaxation oscillations in the regime of soft excitation, gives a value that coincides with the duration of the 22-year cycle.

REFERENCES

- Kandaurova, K. A. (1971a): A study of short-period variations in the series of Solar activity. Solnechnye Dannye. No. 5.
- Kandaurova, K. A. (1971b): The statistic analysis and forecast of the Zurich series of Wolf's Numbers with the regular part extracted. Solnechnye Dannye No. 11.
- Kandaurova, K. A. (1976): A statistical model of Solar cycles. Solnechnye Dannye. No. 5.
- Kolmogorov, N. I. (1941): Interpolation and extrapolation of stationary time series. Izvestiya of USSR Acad. Sci. Ser. Mathem. 5.3.

- Vasilyev, O. V. (1970): Frequency-time spectrum of the Zurich series of Wolf's numbers (1701-1964). Solnechnye Dannye. No. 1.
- Vasilyev, O. B. (1973): Analysis of hidden periodicities of complex processes. Izvestia of Main Astronomical Observ. of USSR Acad. Sci. No. 191.
- Vasilyev, O. B., and K. A. Kandaurova (1968): Preliminary results of the investigations of the frequency Wolf's numbers 1749-1967. Solnechnye Dannye. No. 12.
- Vasilyev, O. B., and K. A. Kandaurova (1970): Statistical long range forecast of the Zurich series of Wolf's numbers. Solnechnye Dannye. No. 2.
- Vasilyev, O. B., and K. A. Kandaurova (1976): On possible relationships between variations of Solar activity, Solar radius and Solar constant. Solnechnye Dannye. No. 10.
- Vasilyev, O. B., and V. I. Sakharov (1971): On the selection of the optimum smoothing parameter of experimental data. Sov. Astron. J. 50.3.
- Vasilyev, O. B., Yu.I. Vitinsky, and K. A. Kandaurova (1975): Forecast for Solar cycle 21. Solnechnye Dannye. No. 10.
- Vitinsky, Yu.I., and K. A. Kandaurova (1975): To the problem on estimating the validity of forecasts of the mean monthly and quarterly Wolf's numbers. Solnechnye Dannye. No. 3.

APPLICATION OF AN EIGENVECTOR TECHNIQUE TO PREDICTION OF SUNSPOT ACTIVITY

Herbert E. Hunter
ADAPT Service Corporation
P. O. Box 58
Reading, Massachusetts 01867

An eigenvector analysis procedure is used to analyze and develop algorithms for predicting sunspot numbers. The sunspot number from the preceding two solar cycles and magnetic index data from the preceding cycle are used to make the predictions. Predictions are presented for Cycles 21 and 22. The 3-month mean of the monthly sunspot number for Cycle 21 is predicted to rapidly reach a peak of approximately 120 in 1979 after which it will drop rapidly to less than 80. The two sigma accuracy on these predictions is approximately 20 sunspot numbers in the region of the peak and 10 sunspot numbers early and late in the cycle.

It is shown that the eigenvector technique used has three useful functions. These functions are: 1) to provide a way to reduce the dimensionality of the problem to allow application of classical regression techniques to a very large number of variables, 2) to provide additional insight into the nature of the sunspot cycles especially with respect to the validity of the earlier sunspot data and 3) to provide a way of representing the sunspot cycles by a limited number of numbers which may be predicted and then used to reconstruct the cycle.

The eigenvector analysis suggested that the gross features of the early cycles (i.e. cycles 1 through 11) are valid but that some of the finer structure has changed since the early cycles and some of the fine structure for the early cycles does not appear to have been obtained with sufficient accuracy.

1. Introduction

The eigenvector analysis procedures for this study have been developed by the ADAPT Service Corporation over the past ten years. These are empirical procedures which incorporate an economical and efficient derivation of the eigenvector representation for large quantities of data. This allows one to utilize the eigenvector expansion to provide an efficient representation prior to applying regression or pattern recognition techniques. This approach is described briefly in several text

books such as Andrews 1972. One of the better descriptions of the efficiencies possible with this technique can be found in Watanabe (1965).

The ADAPT service Corporation has applied its eigenvector analysis programs to many different problems. Some examples of these applications are included in Hunter 1972, Shenk 1973, Hunter 1976, Hunter et al 1977. For applications to problems such as the prediction of solar activity, the procedures may be summarized as follows:

Step 1 - Develop the eigenvector expansion for the parameters used to make the predictions.

Step 2 - Determine the coefficients of the eigenvector expansion found in Step 1 for the particular cases to be used to derive the predictive algorithm.

Step 3 - Develop a regression line relating the quantity to be predicted to the coefficients found in Step 2.

Step 4 - Transform the regression line derived in Step 3 back to the original space to create the algorithm

by using the inverse of the eigenvector transformation derived in Step 1. (Because of orthogonality the inverse is equal to the transpose).

The ADAPT eigenvector analysis techniques were first applied to the problem of predicting sunspots in 1972 (Hunter, 1972). The 1972 studies were motivated by a need for NASA to predict the satellite life times of the HEAO satellite which at that time was expected to be orbited near the beginning of sunspot Cycle 21. Thus, the major effort of the 1972 study was to develop an extrapolation technique to extrapolate solar activity to the end of Cycle 20 based on the portion of Cycle 20 which already had occurred. Initial studies of prediction methods which will be reported in this paper were started at that time but since Cycle 20 was approximately two-thirds complete the extrapolation techniques were emphasized.

The present paper gives results of a study to develop techniques for predicting future sunspot cycles based on the preceding two sunspot cycles plus the AA magnetic index during the preceding cycle. In addition, studies were performed to understand the validity of the earlier data on sunspot numbers. This has been discussed extensively in the literature (McNish, 1949), (Eddy, 1977) and (Sargent, 1978). Eddy presents convincing evidence that sunspot activity essentially stopped during the second half of the 17th century. The existence of such anomalies must be considered when evaluating the expected confidence in any estimate of future solar activity based on an empirical approach. Another concern has been whether the data obtained in the late 18th century and early 19th century is of

the same quality as the more recent data. Both McNish and Sargent have presented arguments that this earlier data is suspect. In this paper, we shall study this question in considerable detail and suggest that the validity of the earlier data has a more complex answer than a simple yes or no.

2. Eigenvector Representation of the Sunspot Cycles

Figure 1A contains two curves: the lower branch plots the variation explained by each eigenvector and the upper branch gives the cumulative sum of the explained variation. This figure shows that the first eigenvector explains approximately 68% of the variation in the entire set of 21 sunspot cycles. The second eigenvector explains approximately 15% so that the first two eigenvectors taken together explain 83% (upper curve at eigenvector-2) of the variation in the sunspot cycles. The remaining eigenvectors explain considerably less of the variation.

The remainder of the plots presented in Figure 1 are all plots of eigenvectors. Eigenvectors have the same abscissa as the data from which they are derived. Thus, the abscissa is the month after the start of the sunspot cycle. They may be visualized as the vector which when used to form a dot product with a sunspot cycle produce the coefficient of the corresponding term in the generalized Fourier series expansion of the sunspot cycle in terms of these eigenvectors. Thus, the ordinant of the eigenfunction is the relative amount of the variation explained by that eigenfunction which can be attributed to each of the months after the start of the cycle. It also shows the monthly contribution of that term to the reconstructed sunspot cycle.

Figures 1B and 1C show the first two eigenvectors associated with the sunspot cycles. Referring to Figure 1A we see that the first eigenvector shown in Figure 1B explains 68% of the variation associated with the sunspot cycles and the second eigenvector shown in Figure 1C explains 15% of the variation associated with the sunspot cycles. Figure 1B has negative values for the first 90 months of the sunspot cycle. Thus, all of the first 90 months variation associated with this eigenvector act in the same direction and this eigenvector can only explain variations in the total magnitude of the sunspot cycle over the first 90 month. We may conclude that at least 68% of the variation of the sunspot cycles is associated with the gross change in magnitude of the sunspot cycles. Figure 1C shows that the first half of the second eigenvector is negative while the second half is positive. Thus, the contribution of

FIGURE 1A - EXPLAINED VARIATION AS A FUNCTION OF
NUMBER OF TERMS RETAINED IN EIGENVECTOR EXPANSION

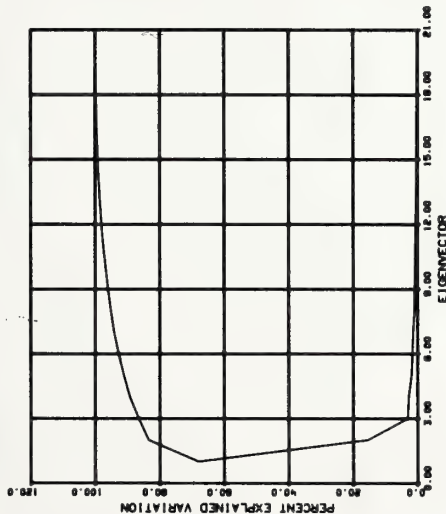


FIGURE 1B - FIRST EIGENVECTOR FOR REPRESENTING
SUNSPOT CYCLES DERIVED USING ALL CYCLES SINCE 1750

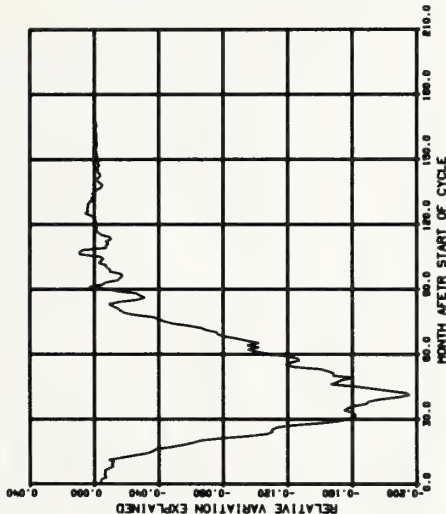


FIGURE 1C - SECOND EIGENVECTOR FOR REPRESENTING
SUNSPOT CYCLES DERIVED USING ALL CYCLES SINCE 1750

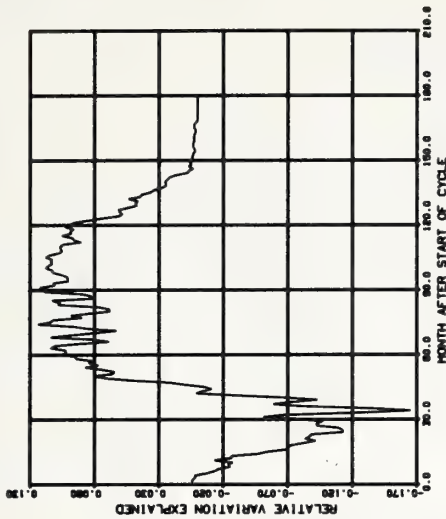


FIGURE 1D - FIRST EIGENVECTOR DERIVED
USING ONLY SUNSPOT CYCLES OCCURRING BEFORE 1870

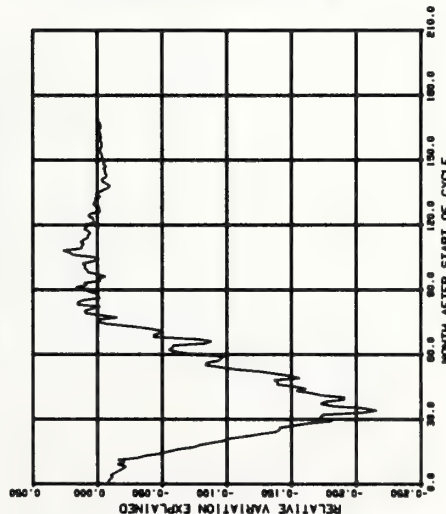


FIGURE 1E - FIRST EIGENVECTOR DERIVED
USING ONLY SUNSPOT CYCLES OCCURRING AFTER 1870

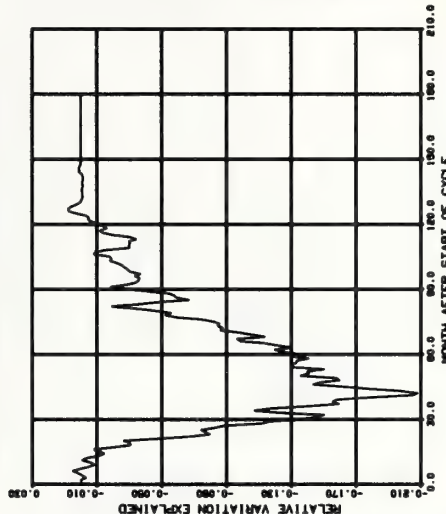
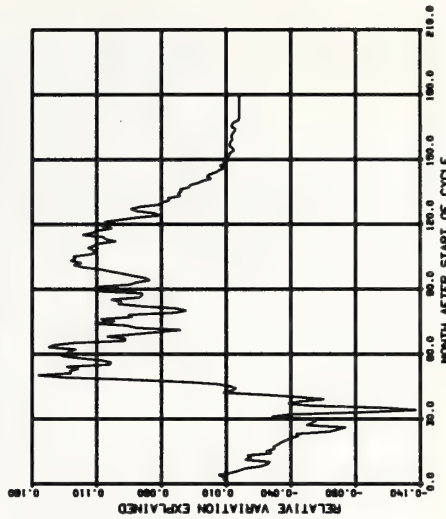


FIGURE 1F - SECOND EIGENVECTOR DERIVED
USING ONLY SUNSPOT CYCLES OCCURRING BEFORE 1870



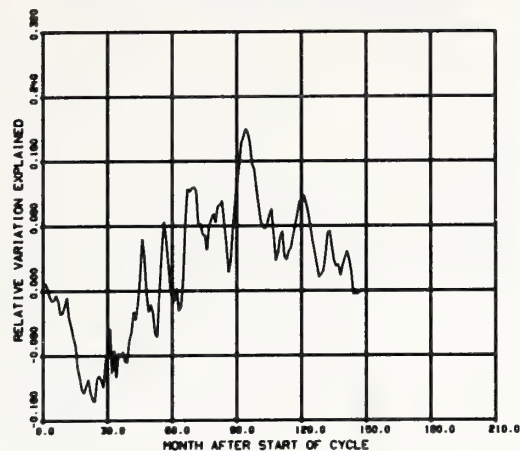
this term to the construction of the sunspot cycle will cause a peak of the sunspot cycle to move towards the later portions of the cycle if this eigenfunction has a positive coefficient and towards the beginning of the cycle if it has a negative coefficient. Also, if the sunspot cycle has an early high peak because of the contribution of this term it must also decrease more rapidly than the average sunspot cycle after the 45th month. Reference to Figure 1A shows that approximately 15% of the variation explains whether the sunspot cycle has an early or late peak. The third eigenvector determines more detail structure of the peak which is also related to the decay of the cycle. The remainder of the eigenvectors determine the fine structure of the sunspot cycles and account for about 14% of the variation.

An analysis was made of the eigenvectors to try to understand the validity of the earlier data. Figures 1D and 1E present the first eigenvector derived from only the sunspot cycles prior to 1870 and only the cycles after 1870, respectively. The split at 1870 has been selected because this is approximately the time from which the AA index data is available. Figures 1D and 1E should also be compared with 1B which was derived using all of the available cycles. McNish suggests that the data before 1830 is suspect and Sargent makes the point that he believes that his estimates are better than earlier estimates both because of the use of the magnetic data and because he only uses the data subsequent to 1870.

Examination of Figure 1D and 1B shows that if one had developed the eigenvector expansion over 100 years ago, the first eigenvector which explains 68% of the variation would have been very much like the one that has been derived using all of the presently available data. Figure 1E shows that there is little change in this eigenvector even if only the modern cycles are used. This implies that the variation explained by the first eigenvector has not changed significantly since the mid 18th century.

Figure 1F shows the second eigenvector as derived in 1870 would be quite similar to the one that we derived today, but Figure 1G shows the modern sunspot cycles used by themselves lead to an eigenvector which is quite different. Examination of the higher order eigenvector shows that, in general, there is considerable difference between the modern and the prior to 1870 eigenvectors. This suggests that the early data was sufficiently accurate to define the gross structure of the sunspot cycles. However, the differences in the higher order eigenvectors suggests that either the earlier data was not sufficiently accurate to define the fine structure or there has been a

FIGURE 1G - SECOND EIGENVECTOR DERIVED
USING ONLY SUNSPOT CYCLES OCCURRING AFTER 1870



change in the fine structure associated with the solar activity between these two periods of time.

The transformation to the eigenvector space maximizes the amount of explained variation in each coordinate of this new orthogonal system. The coordinates have been ordered such that the greatest variation is explained in the first direction the next greatest in the second, etc. Thus, the projection of the data onto the first two coordinates (i.e. eigenvectors) is an efficient way to examine large quantities of data in two dimensions. This has been done and is reported in (Hunter, 1978) where it is shown that this projection leads to three natural groupings of the sunspot cycles which have been labeled x, y and z. Examination of the distribution of these groups with time is interesting. Prior to 1870, Group Z is the most common groups but since 1870, there has been only one Group Z sunspot cycle which is Cycle 20. This suggests that there has been a change in the average character of the sunspot cycles over this time period. These groups are defined primarily by the second coefficient, thus, these are the same changes which caused the differences observed between the 1870 and modern second eigenvectors. This change was with respect to whether the peak is early or late. Since a Group Z cycle has occurred in the second set, one is suspicious that at least with respect to the second eigenvector these changes are real and not due to inaccuracies in the early recording of the data. It also appears that "throw backs" are possible. There is insufficient evidence in similar plots of the higher order eigenvectors to reach any conclusion as to the reason for these

differences, however, one would expect that both small changes in solar behavior and inaccuracies in taking the data would have a much greater effect on eigenvectors which only explain two to three percent of the variation than eigenvectors which explain large percentages of the variation.

It must also be noted that if radical changes in the character of the sunspot cycle occur such as those that apparently occurred in the Maunder minimum (Eddy, 1977), the character of the eigenvectors can be expected to change considerably. It would be very interesting to determine if the dominant eigenvectors for the sunspot cycles occurring before the Maunder minimum are similar to those occurring after the minimum. However, it is extremely unlikely that sufficient data will ever be recovered for these earlier cycles to allow one to accomplish this with any degree of confidence.

3. Algorithms for Estimating the Coefficients of the Sunspot Eigenvectors

The sunspot cycle can be constructed as a generalized Fourier series of the eigenvectors if we know the value of the coefficient to be associated with the eigenvector for a given cycle. The ADAPT procedures described in Section 1.0 were used to estimate each of these coefficients. That is a regression was used to relate each of the coefficients of the sunspot cycles to be estimated to the coefficients of the eigenvector representation of sunspot numbers of the preceding two sunspot cycles and the preceding AA index.

The steps required to predict the next sunspot cycle may be summarized as: 1) derive the eigenvector expansion of the individual sunspot cycles using all of the available data, 2) expand the cycles in terms of these eigenvectors, 3) derive algorithms (as described in Section 1.0) to predict the coefficients of each term in these expansions and 4) use the predicted coefficients to reconstruct the next sunspot history.

Table 1 presents the performance that was achieved for the algorithms used to calculate the first six coefficients of the eigenvector representation of the sunspot cycles. The performance shown is based on the "one-out" test procedure or (Lochenbruch, 1968)'s "U" method. It was not possible to derive successful prediction algorithms for coefficients 7 through 15. The first column of Table 1 lists the term in the eigenvector expansion. The second column gives the variation explained by this term and is the same as the values plotted in the lower curve in Figure 1A.

The algorithms whose performance is given in Table 1 were

TABLE 1 - PREDICTION PERFORMANCE FOR EACH PREDICTOR SET

RECONST. COEF. EST. VAR(%)	EXP'D VAR(%)	DATES USED SYMBOL	CORRELATION COEFFICIENT									END-REFERENCE AA-MAG
			SUNSPOT ONLY DERIVED FROM 1755-1976 EVALUATED USING DATA FROM			MODERN SUNSPOT			AA-MAG			
			1755-1976 (SS)	1755-1870 (SS)	1870-1976 (SS)	1870-1976 (MSS)	1870-1976 (AA)	1870-1976 (C)	1870-1976 (EAA)			
			2	3	4	5	6	7	8	9		
		COL NUMBER	2	3	4	5	6	7	8	9		
		1	68%	.80	.88	.72	.46	.92	.25	.81		
		2	15%	.62	.89	I*	.86	.63	I*	0.97		
		3	3%	.76	.91	.49	.61	I*	.33	.63		
		4	3%	.85	.92	.64	.49	.26	.93	.68		
		5	2%	.53	I*	.80	I*	I*	.68	0.79		
		6	2%	.58	.46	.69	I*	.81	.58	I*		
TOTAL			93%									

*I - denotes an imaginary correlation coefficient, i.e. the mean coefficients to be estimated is a better estimate than the regression.

derived using five different combinations of the sunspot and AA index data as predictors which we shall designate as "SS" for sunspot only, "MSS" for modern sunspot, "AA" for magnetic index, "C" for combined and EAA for End-Referenced magnetic index. The SS and MSS data sets used only the sunspot number information from the two preceding cycles and the performance using these data sets to estimate sunspot numbers is shown in Columns 3 through 6. Column 3 gives performance using the data from 1755 to 1976. This algorithm performance was also evaluated using only the data before 1870 and then using only the data after 1870, the performances obtained are given in Columns 4 and 5, respectively. The prediction performance labeled "MSS" used only data after 1870 both to derive the algorithms and evaluate the algorithms performance and thus is called the modern sunspot predictor. Its performance is given in Column 6. The AA magnetic predictor used only AA index data. The AA magnetic performance is given in Column 7. The predictions made by Sargent (78), which are based on using only the last three years of the AA-magnetic index, were modeled by referencing the AA data to the end of the cycle and only using the last 3 years of data. The results obtained are given in Column 9 of Table 1. Note, that the combined predictor and the AA magnetic index predictors are only available for those cycles occurring after 1870.

Table 1 shows that the first eigenvector could be best estimated using the AA magnetic index which gave a correlation coefficient of 0.92. Examination of Table 1 shows that the first coefficient is next best estimated using the sunspot only data. However, this estimate is best for the early data and is not nearly as good for the modern data.

Examination of Table 1 for the second coefficient shows that the best estimate is made using the End-Referenced AA-magnetic data. However, the sunspot data is also a good predictor by itself. For the early cycles, this estimate should be based on all of the sunspot cycles. However, this estimate is useless for estimating the second coefficient for the sunspot cycles occurring after 1870. However, if only the sunspot data since 1870 is used an algorithm can be derived which is good for estimating the second coefficient for the modern sunspot cycles. (See Column 6). Note, that this is further confirmation that the character of the second eigenvector has changed much more than the first eigenvector between the early and modern cycles. The better performance of the sunspot only algorithms on the modern data for coefficients 5 and 6 combined with the poor performance of the modern sunspot estimates suggest the information required to characterize these eigenvectors hasn't changed significantly but was not measured

with sufficient accuracy prior to 1870.

The conclusion for the third coefficient is very similar to that for the second coefficient. For the fourth coefficient, we find a similar conclusion with respect to estimating the early sunspot cycles but the use of the combined data set yields the best estimate for the modern cycles. We do not know how well that predictor would do for the early cycles since the AA index is not available over a time period required to evaluate this.

In order to arrive at a prediction for a future sunspot cycle, we must decide which of these combinations of sunspots and magnetic data should be used to estimate each of the coefficients. For most of the coefficients such as the first, second, fourth, and sixth, this decision is relatively easy because one of the predictors far out performs the others. The details of the selection procedures used for the more difficult cases are presented in (Hunter, 1978) and (Hunter, 1979).

It is also important to consider the capability to estimate future sunspot cycles if the magnetic data is not available, because we have not at present developed a technique to forecast the magnetic data for the next cycle. Thus, the approach that is used in this paper to obtain estimates for Cycle 21 and 22 consists of using the magnetic and sunspot data just discussed to estimate Cycle 21 and then combine the estimate of sunspot Cycle 21 with the available actual sunspot numbers for Cycles 21 and 20 to make a sunspot only estimate of Cycle 22.

The inverse of the eigenvector transformation may be used to transform the expected errors in the coefficient to an expected error in sunspot number. This has been done for the expected two sigma errors using the sunspot only and the magnetic plus sunspot predictors. This analysis indicates a two sigma accuracy for these predictions of approximately 20 sunspot numbers in the region of the peak and 10 sunspot numbers early and late in the cycle. These values are increased by about 50% if the magnetic data is not used.

A more detailed understanding of these errors can be obtained by reviewing the comparison of the predicted and actual cycles. These predictions were all derived with the sunspot cycle being predicted removed from the data set, i.e. using the one-out test procedure (Lochenbruch, 1968). Figure 2 presents selected samples of these cycles and Hunter (1979) gives the complete set for the predictions using both sunspot and magnetic data and Hunter (1978) gives the complete set when the predictions are based only on sunspot data.

FIGURE 2A - COMPARISON OF ADAPT PREDICTION WITH
ACTUAL CYCLE NO 12 - START OF CYCLE (MONTH-1) = (NOV 1876)

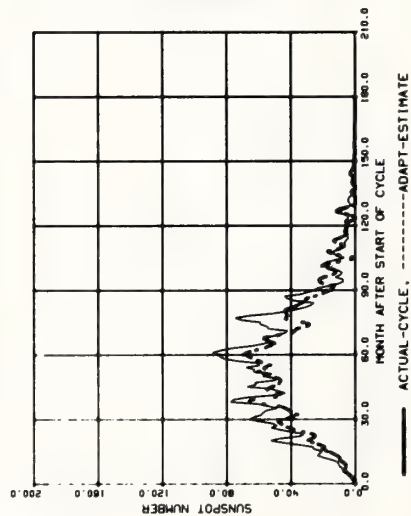


FIGURE 2B - COMPARISON OF ADAPT PREDICTION WITH
ACTUAL CYCLE NO 14 - START OF CYCLE (MONTH-1) = (JAN 1902)

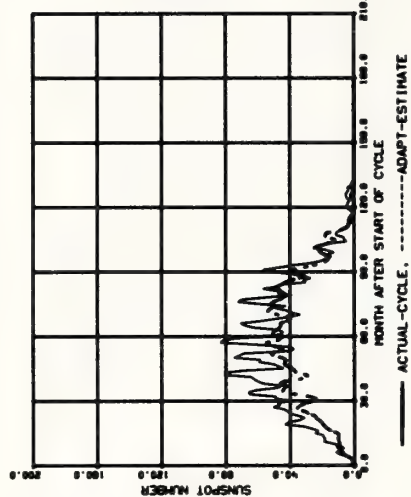


FIGURE 2C - COMPARISON OF ADAPT PREDICTION WITH
ACTUAL CYCLE NO 16 - START OF CYCLE (MONTH-1) = (JULY 1903)

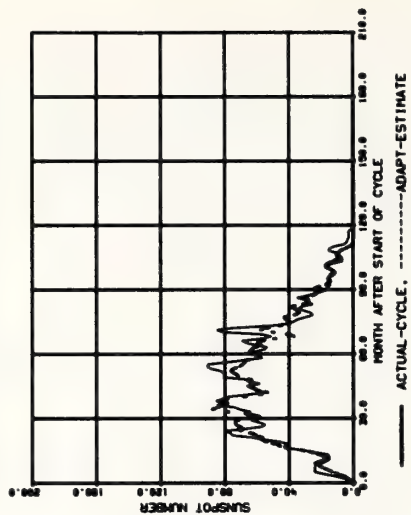


FIGURE 2D - COMPARISON OF ADAPT PREDICTION WITH
ACTUAL CYCLE NO 18 - START OF CYCLE (MONTH-1) = (FEB 1904)

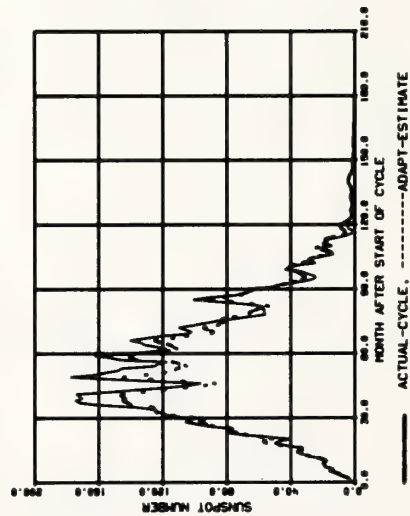


FIGURE 2E - COMPARISON OF ADAPT PREDICTION WITH
ACTUAL CYCLE NO 19 - START OF CYCLE (MONTH-1) = (APRIL 1904)

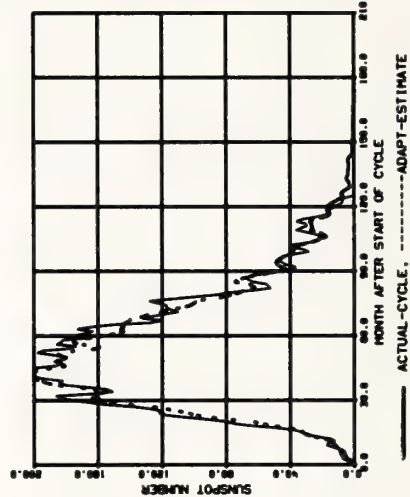
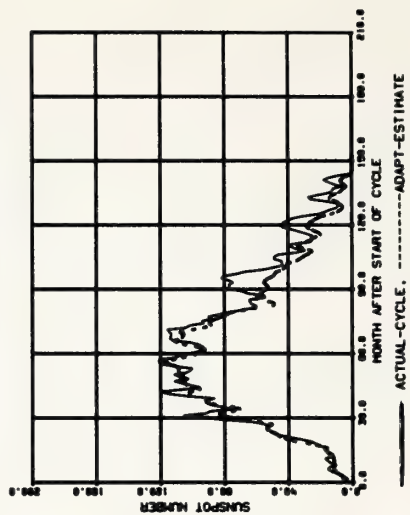


FIGURE 2F - COMPARISON OF ADAPT PREDICTION WITH
ACTUAL CYCLE NO 20 - START OF CYCLE (MONTH-1) = (OCT 1904)



4. Prediction for Cycles 21 and 22

The procedures developed and discussed in the preceding section were used to estimate the sunspot numbers for Cycles 21 and 22. These estimates have been plotted in Figure 3. These predictions were delivered to NASA in January of 1979.

Figure 4 presents a comparison of the ADAPT estimates of Cycle 21 using both the sunspot and magnetic data with the prediction given in Sargent (1978). Note, that Sargent's predictions are for the 13 month running mean assigned to the mid point and the ADAPT predictions are for a 3 month running average assigned to the end point. This figure also shows the actual sunspot Cycle 21 through April of 1979. This figure shows that the ADAPT forecast for Cycle 21 are significantly below those of Sargent, especially for the last three quarters of 1979 and the first quarter of 1980. It is also interesting to note that up to this point the ADAPT estimates are doing a reasonable job of predicting the occurrence of the small scale structure.

The first studies in which the eigenvector analysis was applied to a combination of sunspot and magnetic data (Hunter 1978) led to the conclusion that the magnetic data should be used in a significantly different manner than suggested by Sargent (78). Analysis of the reasons for these differences suggested that the information which is available from the magnetic index can be modified by either: 1) normalization or 2) whether the data vector is fixed relative to the beginning of the sunspot cycle or the end of the sunspot cycle. In Hunter (79) it is shown that the results presented by Sargent, (78) used different information from the magnetic index than Hunter (78) because Hunter used normalized as opposed to unnormalized data, and Hunter's data was fixed relative to the beginning of the sunspot cycle as opposed to the end of the sunspot cycle. After these differences are removed, the eigenvector approach yields a mechanism for estimating the coefficient of the first eigenvector which is in excellent agreement with the mechanism proposed by Sargent. Since the first eigenvector explains 68% of the variation and is primarily associated with the magnitude (see Section 2.0) of the sunspot cycle and Sargent only proposes his approach for estimating the peak sunspot number agreement in mechanism should only be expected for estimating the coefficient of the first eigenvector.

5. Conclusions

FIGURE 3 - RECOMMENDED ESTIMATE OF 3 MONTH
RUNNING AVERAGE SUNSPOT NUMBER FOR CYCLES 21 + 22

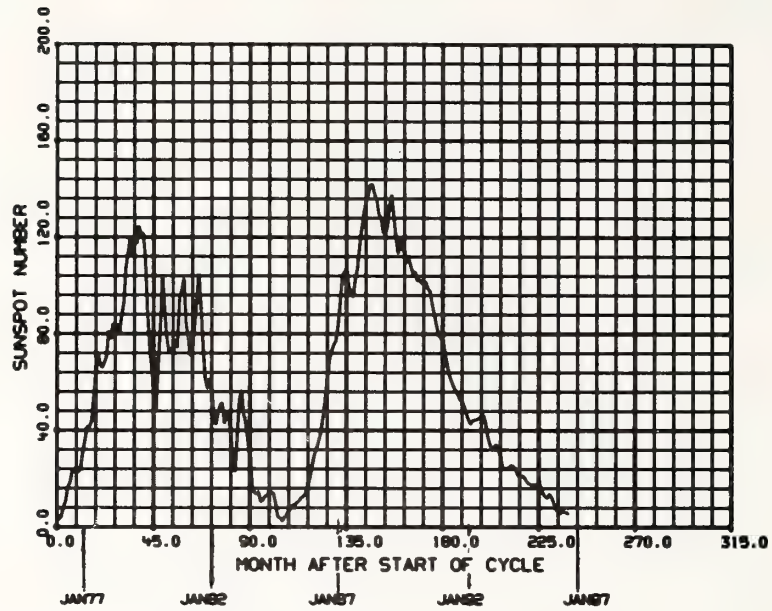
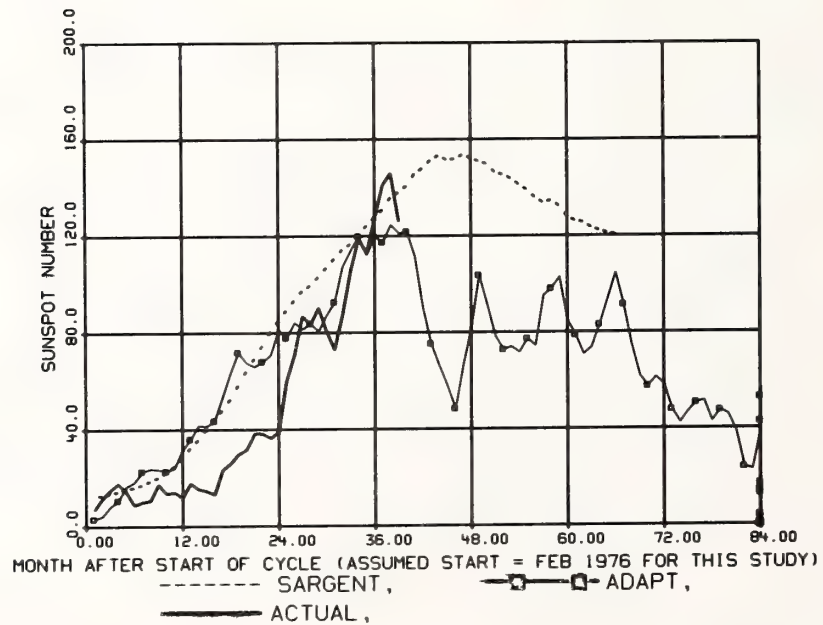


FIGURE 4 - COMPARISON OF ADAPT AND
SARGENT ESTIMATES OF SUNSPOT CYCLE 21



The studies and analyses which are reported in this report have led to new monthly predictions for the three month running average sunspot number expected to occur during Cycles 21 and 22 over the period from 1976 through 1998. The expected maximum errors in the reconstruction of Cycle 21 is approximately 20 sunspot numbers occurring near the region approximately $3\frac{1}{2}$ years after the beginning of the cycle. Significantly smaller errors will occur at the early and late portions of the cycle. These accuracies are based on the assumption that no gross changes such as the Maunder minimum occur over the time of the predictions. If the sunspot numbers for the preceding two cycles are used by themselves to make the predictions as was done for Cycle 22, the maximum error increases to approximately 30 sunspot numbers. Studies have also led to the following specific conclusions:

- 1) Both the sunspot activity over the preceding two cycles and the AA magnetic index during the preceding cycle appear to have predictive value for forecasting future sunspot activity. A comparison of the predictions made using the combination of the magnetic plus sunspot data with the sunspot data only has shown that whenever there is a significant difference, the magnetic plus sunspot has proved the better of the two.

- 2) The dominant variation in sunspot cycles as defined by the first eigenvector has remained essentially constant over the past two centuries. But the variation as defined by the second through fourth eigenvectors although apparently measured with sufficient accuracy to allow its prediction during the early sunspot cycles has changed in character during the modern period. However, we have also seen that throwbacks to the early sunspot cycle characteristics do occur. Finally, some of the information such as that characterized by the fifth and sixth eigenvectors was probably not measured with sufficient accuracy in the early cycles.

- 3) The new predictions for Cycle 21 show it to be quite similar to the mean cycle having an early peak of approximately 120 occurring $3\frac{1}{2}$ years after the start of the cycle or early 1979 followed by a local minimum 6 month to a year later of about 60 after which it will rapidly rise to a value of 100. The prediction for Cycle 22 shows that it should have a slightly greater magnitude than Cycle 21.

This work was supported by NASA Marshall Space Flight Center under Contract NAS8-32851. The author wants to thank Drs. C.A. Lundquist, R.E. Smith, and W.W. Vaughan of NASA/MSFC's Space Science Laboratory for suggesting this application and their interest and support during the course of the work. Thanks are also due to Mrs. Patricia Gaudet of the ADAPT Service Corporation for carrying out much of the computation required for this study.

References

- Andrews, H.C. 1972, "Introduction to Mathematical Techniques in Pattern Recognition", John Wiley & Sons, Inc.
- Eddy, John A., "The Case of the Missing Sunspots", *Scientific American* 236:15, May 1977, pp 80-92.
- Hunter and Amato, "Application of AVCO Data Analysis and Prediction Techniques (ADAPT) to Prediction of Sunspot Activity", AVSD-0287-72-CR, August 1972.
- Hunter, "Effect of Mechanical Cooling Devices on Ambient Salt Concentration", EPA Report No. EPA-600/3-76-034, April 1976
- Hunter, Rodgers and Shenk, "Objective Parameter Estimation and Forecasting Using NIMBUS-5 ESMR Measurements", Proceedings of 11th Technical Conference on Hurricanes and Tropical Meteorology" pp 496-501, American Meteorological Society, Boston, December 1977.
- Hunter, "Final Report - Updating of ADAPT Predictions of Sunspot Activity", ADAPT Service Corporation Report, July 78.
- Hunter, "Final Report - Comparison of ADAPT and Sargent Predictions of Sunspot Activity", ADAPT Service Corporation Report, January 1979.
- Jose, P.D., "Suns Motion and Sunspots", *Astron J.*, 70 1965, pp 193-200.
- Lochenbruch and Mickey, "Estimation of Error Rates in Discriminant Analysis", *Technometrics*, Vol 10, No. 1, Feb. 68.
- McNish and Lincoln, "Prediction of Sunspot Numbers", *Transaction American Geophysical Union*, Vol 30, No. 5, Oct. 49.
- Sargent, H.H., "A Prediction for the Next Solar Cycle", Presented at IEEE Vehicular Technology Conference, Mar 78.
- Shenk, William E.; Hunter, Herbert E.; Menkello, Frederick V.; Holub, Robert; Salomonson, Vincent B.; "The Estimation of Extratropical Cyclone Parameters from Satellite Radiation Measurements", *Journal of Applied Meteorology*, April 1973
- Watanabe, S., "Karhunen-Loeve Expansion and Factor Analysis Theoretical Remarks and Predictions", Transaction of the 4th Prague Conference on Information Theory, Statistical Decision Functions, and Random Processes; 1965 pg635-660

SOLAR ACTIVITY PREDICTION FOR CYCLE 21

Charles A. Wood
NHB Stop 119*
Smithsonian Institution
Washington, DC 20560 USA

* Now at Geophysics Branch, Goddard Space Flight Center, Greenbelt, Maryland, 20771, U.S.A.

Improved accuracy in prediction of sunspot numbers is needed to utilize proposed solar-terrestrial relationships. A simple correlation between sunspot number at solar minimum (R_{\min}) and the following maximum (R_{\max}) predicts that solar cycle 21 will have a maximum of about 145 ± 24 . Like many other statistical correlations of solar behavior this relation, while generally valid, has broken down (in 1957). Such deviations from normal solar activity weaken the confidence of predictions, but also focus attention on times of anomalous solar behavior. It is noteworthy that R_{\min} , which must be physically related to R_{\max} , is comprised equally of high latitude sunspots of the new solar cycle and near-equatorial sunspots of the old cycle.

1. Introduction

Possible relations between terrestrial weather and solar activity have long been a topic of intense scientific discussion. Typically, statistical correlations are presented linking rainfall, temperature, pressure, etc. with sunspot numbers. Other solar-activity indices are less frequently used because they are not available for periods longer than 10 (e.g. solar sector structure) to 60 (solar magnetic fields) years. Thus, sunspot numbers, with all the uncertainties in our knowledge of them (e.g. Eddy, 1976; Mayaud, 1977), must remain the principle index of solar activity for any investigation of long-term solar-terrestrial relations.

Despite more than 200 years of nearly continuous sunspot observations, and the detection of periodicities of roughly 11, 90, and 200 years in solar activity (Cohen and Lintz, 1974), accurate prediction of future sunspot numbers is still uncertain. Within the last year different statistical patterns of solar activity have been used to make predictions of the sunspot number (R) at the next solar maximum (cycle 21) ranging from $R_{\max} = 58$ (Sakurai, 1977) to $R_{\max} = 195$ (Ramaswamy, 1977). This spread of values illustrates that we can not confidently predict if the coming solar maximum will be one of the weakest in the last 200 years or the highest ever observed. Additionally, since the only reasonably reliable method of predicting the date of solar maximum depends upon estimation of R_{\max} , there is considerable uncertainty if maximum will occur in 1979 or 2 or 3 years later. Because of the possibility that the timing and severity of some droughts (Wood and Lovett,

1974) and other significant weather changes (King, 1973) may be influenced by cyclic solar variations, prediction accuracy must be refined. Toward this end a simple correlation between sunspot numbers at solar minimum and solar maximum is documented. This work was originally done in 1975, and although it is similar to the independent analysis by Brown (1976), a short description is presented to (1) predict R_{\max} for cycle 21, and (2) illustrate how apparently reliable statistical solar-activity relations can unaccountably break down.

2. R_{\min} as a Predictor of R_{\max}

Solar cycles with high maxima tend to follow high minima, and low maxima tend to follow low minima. This is well illustrated in Figure 1, where each point represents the yearly mean values of the sunspot numbers at minimum and the following maximum from AD 1711 to 1968; data from Waldmeier, 1961. The least squares fit to 23 R_{\min}/R_{\max} pairs yields:

$$R_{\max} = 6.11(R_{\min}) + 61.9 \quad \text{S.E.E.} = 24.2 \quad (1)$$

only the exceptionally strong maximum of 1957 ($R_{\max} = 190$) fails to conform to the general relation (and is not included in the analysis above). Neglecting this anomalous point - and Schöve's (1955) estimates of the strength of R_{\max} for the last 2600 years suggest that only the solar maximum of AD 1372 was possibly as strong - the correlation coefficient, r , equals 0.68, which is significant at the 0.02% level. If the 1957 maximum is included, $r = 0.53$ for a significance level of 0.4%. Although scatter reduces the predictive accuracy of this relation the value of 13.4 for R_{\min} in 1976 (Waldmeier, 1978) suggests that for solar cycle 21, R_{\max} will be between 120 and 170, with a most probable value of 145. Using this value and Waldmeier's (1935) relation between rise time and R_{\max} , solar maximum should occur in late 1979.

The correlation between R_{\min} and R_{\max} indicates that the series of sunspot observations from 1711 AD onwards is generally reliable. This conclusion contrasts with Danjon's (1920) belief that sunspot numbers prior to 1823 are inaccurate.

Although R_{\min} is a predictor of the following R_{\max} , there is no significant correlation between (1) R_{\max} and the following R_{\min} , (2) successive values of R_{\min} , and (3) successive values of R_{\max} .

3. The Breakdown of Statistical Relations

Predictions of future sunspot numbers are notoriously inaccurate, even though all forecasts are based upon observed patterns of solar activity that have been maintained throughout previous cycles. These statistical relations are valuable, albeit imperfect, descriptions of the general behavior of the sun. The breakdown of such a relation (e.g. Equation 1 predicts $R_{\max} = 90$ for 1957) weakens confidence in predictions of solar activity, but provides an opportunity to investigate unsuspected (and thankfully infrequent) irregularities in solar activity. The most spectacular example was the breakdown

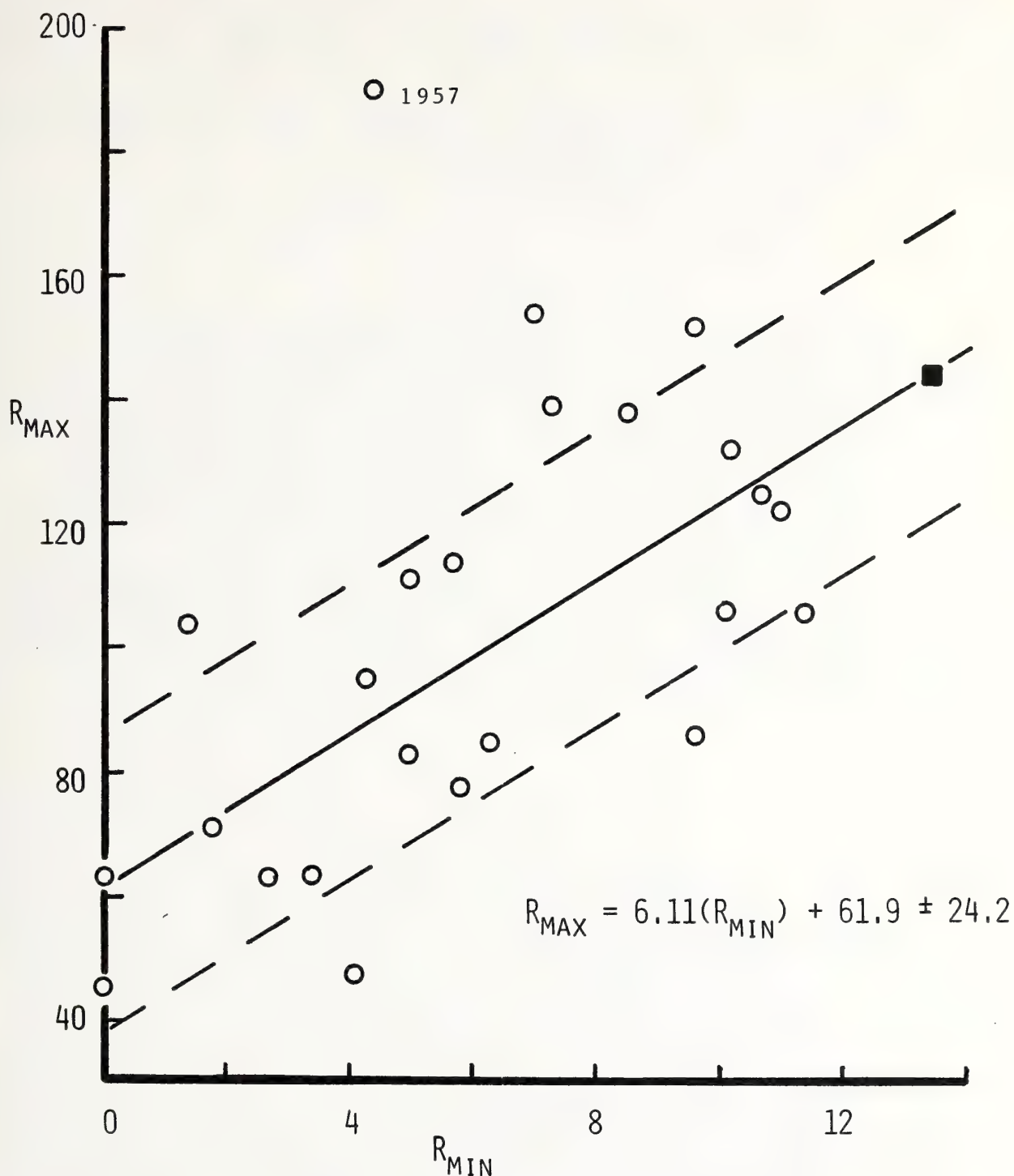


Fig. 1: Observed relation between yearly mean sunspot numbers at solar minimum (R_{min}) and the following maximum (R_{max}). The relation breaks down for cycle 19 (1957 maximum) which is not included in the least squares fit. The black square marks the predicted R_{max} for cycle 21 based on $R_{\text{min}} = 13.4$ (Waldmeier, 1978), but any value between 120 and 170 will be within one sigma (dashed lines) of the prediction.

of the 11-year sunspot cycle itself during the Maunder Minimum (AD 1645 to 1715) and during earlier times (Eddy, 1976). It is thus suggested that investigation of some of the less spectacular solar-activity anomalies can also lead to a better understanding of solar dynamics. The 1957 anomaly is worthy of investigation because (1) it was the largest sunspot maximum ever recorded, (2) the rise time/ R_{\max} relationship failed (King-Hele, 1966), and (3) the R_{\min}/R_{\max} relation (Fig. 1) failed.

4. R_{\min}

A final consideration prompted by Figure 1 concerns the interaction of sunspots at high and low solar latitudes. It is well known that the first sunspots at the beginning of a solar cycle appear at latitudes of 35° - 40° , and later sunspots occur at progressively lower latitudes. High-latitude sunspots, initiating a new solar cycle, appear before the last near-equatorial sunspots of the previous cycle vanish, so that R_{\min} is dependent upon both old and new sunspots. Examination of the latitude distributions of sunspot groups in the solar minimum years of 1923, 1933, 1944, 1954, and 1964 shows that 49% of the sunspots occurring in the 12-month periods centered on the months of minimum had latitudes of 10° or less, and thus belonged to the old solar cycle. The remaining 51% of the sunspots occurred in the latitude zone 11° - 45° and represent waxing activity of the new cycle. Thus, sunspots in different latitude zones and with opposite magnetic polarities (which change every solar cycle) equally contribute to R_{\min} which in turn influences the following R_{\max} .

5. References

- Brown, G.M. (1976). Mon. Not. R. Astr. Soc., 174:185.
 Cohen, T.J., and P.R. Lintz (1974). Nature, 250:398.
 Danjon, A. (1920). Compt. Rend., 171:1207.
 Eddy, J.A. (1976). Science, 192:1189.
 King, J.W. (1973). Nature, 245:443.
 King-Hele, D.G. (1966). Nature, 209:285.
 Mayaud, P.N. (1977). J. Geophys. Res., 82:1271.
 Ramaswamy, G. (1977). Nature, 265:713.
 Sakurai, K. (1977). Nature, 269:401.
 Schove, D.J. (1955). J. Geophys. Res., 60:127.
 Waldmeier, M. (1935). Astron. Mitt. Zurich, 14: No. 133.
 Waldmeier, M. (1961). The Sunspot Activity in the Years 1610-1960, (Schulthess, Zurich).
 Waldmeier, M. (1978). Vierteljahrsschrift Naturforsch. Gesell. Zurich, 123: 135.
 Wood, C.A., and R.R. Lovett (1974). Nature, 251:594.

BABCOCK DYNAMO THEORY AND THE MAUNDER MINIMUM

Kenneth H. Schatten
Astronomy Department *
Boston University
Boston, Massachusetts 02215

* Now at NASA Goddard Space Flight Center

Babcock dynamo theory is related to the Maunder Minimum and Gleissberg cycles using polar field variability. Schatten et al. (1978) utilized the sun's polar field observed in 1976 and the sun's polar field variability aspect of conventional Babcock dynamo theory as a first order parameter to predict solar activity during solar cycle 21. A comparison suggests that solar activity agrees closely with the prediction - the prediction of a larger than normal cycle was correct! Detailed yearly average behavior also appears to be remarkably precise. Although not realized previously, Babcock's solar dynamo theory may be able to explain the unusual behavior of spot motions during the Maunder Minimum. The increased differential rotation of the photosphere observed may be related to a reduced solar dynamo drag associated with a polar field (and sunspot) decrease during the Maunder and other such minima.

1. INTRODUCTION

The conventional dynamo theory of Babcock (1961), furthered by the work of Leighton (1969), and others, described by Parker (1977) utilizes a mechanical method of transforming energy from the sun's differential rotation to the magnetic field. Simply expressed - the sun's poloidal field is transformed by differential rotation into a toroidal field; this toroidal field gives rise to subsequent spots and solar activity. Following this, latitudinal wandering ("random walk") reverses the sense of the sun's polar field.

McIntosh (1979) describes the work of Shove, Brown, Sargent, and others to predict the current level of solar activity from principally the behavior of geomagnetic indices (aa, AE, H component), during the declining phase of the previous cycle. These methods appear to work and possibly relate to the work of Schatten et al. (1978) via a tie-in between long-lived interplanetary recurrent streams in the latter half of the solar cycle with the strength of the sun's polar field.

The method of Schatten et al. (1978) was to use the magnitude of the sun's polar field at sunspot minimum (1976) to predict the average yearly value at solar maximum. The relation to Babcock theory is evident. The

toroidal flux (and sunspots) generated by differential rotation is proportional to the poloidal flux. Thus Figure 1 shows the prediction using the 1976 polar magnetic field data. A rather good agreement appears to exist. The length of the cycle was not predicted, thus the curve after solar maximum is just an "average" decline which may or may not occur. Conventional dynamo theory, if assumed correct, has other implications for the Maunder Minimum.

2. RELATION OF POLAR FIELD VARIABILITY TO THE MAUNDER MINIMUM

Recently Herr (1978) and Eddy et al. (1977) have uncovered from historical records the solar rotation during the time of the Maunder Minimum (see Eddy, 1978). The solar rotation during this past epoch, in the 17th century, was found by measurements and calculations of the sunspot drawings of Harriot, Scheiner, and Hevelius. These findings show an increased differential rotation of the lower sunspot latitudes with the inception of the Maunder Minimum. At first this is somewhat puzzling, as dynamo theory might suggest that a more rapid rotation of the lower latitudes would imply a greater field-winding capability and thus an increase in sunspot activity following this behavior. Dynamo theory may reconcile the situation.

A clue to the resolution of the above dilemma may be provided by considering other solar parameters which are varying at the same time as the solar rotation during this past epoch and play a more important or overriding role in determining the level of solar activity. Recently Sargent (1977) and Feynman and Crooker (1978), have related the level of solar activity to geomagnetic indices (aa). They find considerable changes in the solar wind over the past century. Schatten et al., as we have seen, have related the level of solar activity during the sunspot maximum with the preceding solar minimum polar field strength. The Maunder Minimum may then be a likely consequence of the type of variability reported by Feynman and Crooker (1978) carried to an extreme. As the sun's polar field reverses sign by regeneration each solar activity cycle, the possibility is open for a near cancellation of polar field strength due to the inherent variability and randomness present in the migratory dynamo process. That is, Gleissberg or Eddy type of Maunder Minimum periods (100 years) may be intervals when polar fields are gradually deteriorating or regenerating. For example, Sheeley (1976) has examined north and south polar faculae from 1906-1975 showing polar field variability throughout this time. By no means does the polar field return to the same value at the end of each cycle. This polar field variability is often, in recent times, a factor of 2, whereas even the Maunder Minimum rotation variations are of the order of ten percent (Herr, 1978; Eddy et al. 1977). Thus, this author feels polar field variability is the prime control governing long term solar activity variations.

Accordingly, if a near complete cancellation of polar field develops, little toroidal flux would be wound in subsequent cycles. Although dynamo action would still occur, it could do so at a greatly reduced level (see Link, 1978). The 80 to 100 year variability (Gleissberg cycle) in solar activity reported by many authors (seen also in Feynman and Crooker's work), compares with the time scale for the sun's polar field to recover from a weakening (Sheeley, 1976). It is also consistent with the length of the

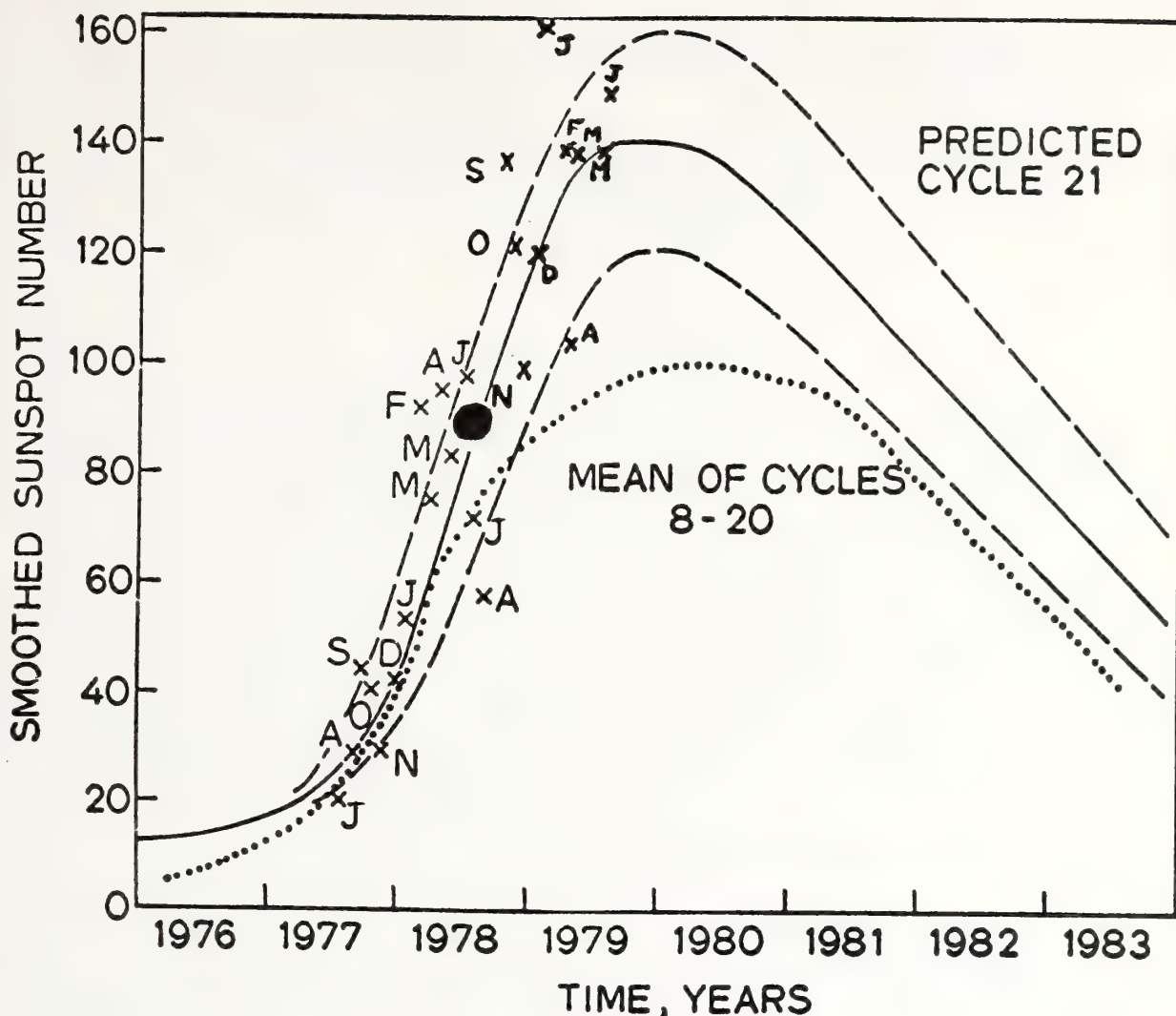


Figure 1. Predicted smoothed sunspot number based upon dynamo theory utilizing data from 1976 (solid curve). Estimated yearly average uncertainties (dashed curves) are smaller than in many other predictions and show that a larger than average cycle (dotted curve) is definitely predicted. Crosses show individual monthly sunspot numbers, labelled with the first letter of the month. The large dot shows the yearly average sunspot number, with which the solid curve was designed to be compared, for 1978. Recent 1979 data have been added and again agree remarkably well.

Maunder Minimum. Similar decreases in solar activity seem to relate to temporary coolings in the earth's climate (see Siscoe, 1978) and thus may be important to humanity.

A reduction in dynamo action during a Maunder type minimum, would have a concomitant effect on the sun's surface rotation. A reduction in this drag would allow the driving mechanism for the sun's differential rotation

to reach a new equilibrium state with a faster surface equatorial rotation rate (see Howard (1978) for a review of solar rotation and driving mechanisms of the differential rotation). Thus the careful sunspot observations by scientists hundreds of years ago, uncovered by diligent searches through ancient records, and subsequently interpreted for their scientific content with our modern-day understanding and computer capability, allow new light to be shed on the behavior of solar rotation and dynamo theory.

3. ACKNOWLEDGEMENT

The author thanks J. Feynman, J. Eddy, and M. Mendillo for useful comments.

REFERENCES

- Babcock, H.W. (1961): Astrophys. J., 133, 572.
- Eddy, J.A. (1976): Science, 192, 1189.
- Eddy, J.A., P.A. Gilman, and D.E. Trotter (1977): Science, 198, 824.
- Feynman, J. and N.U. Crooker (1978): Nature, 275, 626.
- Herr, R.B. (1978): Science, 202, 1079.
- Howard, R.H. (1978): Rev. of Geophys. and Space Phys., 16, 721.
- Leighton, R.B. (1969): Astrophys.J., 156, 1.
- Link, F. (1978): Solar Phys., 59, 175.
- McIntosh, P. (1979): Report of Long Term Forecast of Solar Activity, NOAA's International Solar Activity Predictions Proceedings Conference, to appear.
- Parker, E.N. (1977): Am. Rev. of Astron. and Astrophys., 15, 45.
- Sargent, H.H. (1977): Proc. Amer. Geophys. Union, San Francisco.
- Schatten, K.H., P.H. Scherrer, L. Svalgaard, and J.M. Wilcox (1978): Geophys. Res. Lett., 5, 411.
- Sheeley Jr., N.R. (1976): J. Geophys. Res., 81, 3462.
- Siscoe, G.L. (1978): Nature, 276, 348.

ON THE PREDICTION OF SOLAR ACTIVITY TAKING INTO ACCOUNT ITS EXTRANEEOUS CONDITIONALITY

G. I. Vassilyeva, A. A. Schpitalnaya, and N. S. Petrova
Pulkovo Observatory
Leningrad, USSR

The techniques of phase analysis are used to describe the state of the interplanetary medium in conventional units of a relative level of solar activity. The structure of the interplanetary medium revealed by this method is suspected to be an ecliptic projection of the solar magnetosphere, determined by orientation and motion of the solar system in the galaxy. This structure is used for the prediction of sunspot activity.

Consideration of solar flare and earthquake zeniths over the celestial sphere and the investigation of cosmic factors for their origin indicate galactic influence on solar and geo-activity. Flares and earthquakes seem to belong to the same class of phenomena and a common method for predicting them is possible.

1. INTRODUCTION

The idea of solar activity as a phenomenon of the solar system as a whole in response to the galaxy opens new ways for predicting different events of solar activity. In rejecting heliocentrism from the understanding of the solar activity, the treatment of the solar data is as follows:

1. The phase analysis of the continuous sets of relative sunspot numbers (W) and sunspot areas (Sp); and
2. Analysis of the distributions of the number of solar flares over the celestial sphere.

2. THE PHASE ANALYSIS

For the phase analysis of the W and Sp sets, the W and Sp values are distributed over the specific ecliptic longitude intervals of the planets in accordance with the length of time each planet remains in each longitude interval.

Investigation of the seasonal solar activity variations is a special case of the phase analysis application. This method searches the components of the solar activity variations associated with each planet as a function of their ecliptic longitude (λ).

The normalized distributions of the monthly relative solar numbers, W , for the period of 1749 to 1973 over 15-degree ecliptic longitude intervals

for 19 revolutions of Jupiter about the Sun are shown in Table 1 (Vassilyeva et al., 1975a).

The variable helioefficiency of Jupiter, $\phi_4(\lambda)$, in its orbit is revealed as a useful signal against the noise background by the summing of data over columns in Table 1, for odd and even revolutions separately (Figure 1).

Positions of Jupiter corresponding to two solar activity extrema near $\lambda = 135$ and $\lambda = 315$ coincide with the ecliptic projection of the galactic magnetic field direction ($b'' = 0$; $l'' = 70$). This magnetic field direction ($b'' = 0$; $l'' = 80$) has been discussed by Schatten and Wilcox (1969) in connection with the cosmic ray diurnal anisotropy.

Phase analysis brings the positions of the planets in their orbits (λ) into correspondence with their relative level of variable helioefficiency, $\phi_i(\lambda)$, and describes the state of the interplanetary medium in conventional units at their heliocentric distances.

1.1 Sector Structure of the Interplanetary Medium beyond the Jupiter Orbit

The interplanetary sector structure of the outer part of the solar system has been revealed with the phase analysis using the telescopic solar activity set of W and Schöve's set of W back to 649 B.C. (Figure 2).

Table 1. The normalized distributions of the monthly relative solar numbers, W, for the period of 1749 to 1973 over 15-degree ecliptic longitude intervals for 19 revolutions of Jupiter about the Sun.

0-15	15-30	30-45	45-60	60-75	75-90	90-105	105-120	120-135	135-150	150-165	165-180	180-195	195-210	210-225	225-240	240-255	255-270	270-285	285-300	300-315	315-330	330-345	345-0	
1.01	1.96	1.04	1.24	0.93	1.19	0.98	0.86	0.46	0.32	0.28	0.12	0.33	0.20	0.39	0.32	1.08	1.04	1.03	1.36	1.38	1.14	1.57	1.78	I
1.27	0.94	1.24	0.84	0.88	0.86	0.49	0.43	0.35	0.30	0.11	0.56	0.76	1.04	1.37	1.63	2.33	1.49	1.40	1.59	1.66	1.0	0.97	0.66	II
0.54	0.95	0.95	0.14	0.40	0.23	0.28	0.18	1.74	2.51	3.09	2.42	2.15	1.72	1.39	1.49	0.96	0.74	0.57	0.52	0.26	0.17	0.18	0.22	III
0.47	0.69	1.26	1.61	1.81	2.15	1.91	1.79	1.70	1.69	1.27	1.08	0.95	0.94	0.85	0.79	0.58	0.62	0.55	0.42	0.27	0.32	0.21	0.10	IV
0.28	0.20	0.12	0.22	0.45	0.14	0.42	0.82	1.28	1.63	1.93	1.96	1.64	2.09	1.79	2.42	1.73	1.48	1.13	0.78	0.54	0.11	0.46	0.40	V
0.21	0	0	0	0	0.16	0.14	0.25	0.42	0.80	0.76	0.76	1.59	2.15	2.97	2.10	2.61	1.60	1.93	1.34	1.20	1.30	0.98	0.71	VI
0.26	0.19	0.19	0.10	0	0	0.27	0.23	0.35	0.35	0.62	1.12	1.49	1.60	1.94	1.84	2.06	2.07	2.30	2.07	1.63	1.32	1.29	0.49	VII
0.75	0.14	0.17	0.11	0.40	0.74	1.59	2.14	2.61	2.68	2.14	2.09	1.59	1.58	1.34	1.10	0.71	0.72	0.47	0.42	0.78	0.19	0.35	0.30	VIII
0.39	0.75	0.72	1.11	1.17	1.12	2.27	2.09	2.37	1.94	1.50	1.19	1.22	1.14	1.16	0.23	0.84	0.75	0.45	0.58	0.31	0.13	0.06	0.06	IX
0.13	0.30	0.66	0.86	1.41	1.67	2.15	1.85	2.20	1.91	1.62	1.30	1.36	1.07	0.79	1.10	0.90	0.73	0.52	0.43	0.16	0.08	0.24	0.52	X
0.81	1.08	1.63	1.86	2.86	2.43	2.38	1.77	1.91	1.91	1.21	1.02	0.82	0.50	0.26	0.25	0.18	0.30	0.16	0.09	0.05	0.03	0.16	0.35	XI
1.07	1.06	1.57	1.45	1.77	1.56	1.56	1.94	2.10	1.35	1.83	0.94	0.94	0.29	0.43	0.26	0.14	0.17	0.23	0.09	0.24	0.34	1.17	1.49	XII
1.86	2.60	2.11	2.40	2.13	2.09	1.35	1.60	1.24	1.10	0.77	0.68	0.67	0.72	0.33	0.28	0.28	0.11	0.01	0.06	0.09	0.23	0.51	0.90	XIII
1.07	1.36	1.72	1.78	1.77	1.94	1.80	1.60	1.36	1.79	1.35	1.05	0.93	0.53	0.23	0.10	0.10	0.12	0	0	0.21	0.36	1.05	1.74	XIV
1.11	1.17	1.22	2.09	2.15	1.88	1.44	1.56	1.03	0.69	0.69	0.57	0.50	0.15	0.13	0.15	0.14	0.49	0.46	1.05	1.38	1.29	1.11	1.27	XV
1.20	1.56	1.19	1.08	1.24	0.76	0.51	0.48	0.29	0.26	0.16	0.14	0.05	0.17	0.25	0.59	1.21	1.73	2.03	2.23	1.79	2.10	1.71	1.78	XVI
1.06	0.93	0.85	0.54	0.76	0.84	0.25	0.34	0.16	0.09	0.16	0.33	0.55	1.61	1.52	2.12	1.87	2.10	1.85	1.77	1.74	1.36	0.83	1.08	XVII
0.78	0.39	0.42	0.24	0.23	0.49	0.03	0.15	0.37	1.10	1.70	2.05	2.44	2.78	2.23	2.16	1.54	1.44	1.30	0.72	0.61	0.55	0.41	0.28	XVIII
0.57	0.94	0.59	0.48	0.24	0.30	0.70	1.11	1.46	1.72	1.75	1.81	1.81	1.76	1.77	1.08	0.98	1.23	1.35	0.77	0.61	0.50	0.90		XIX

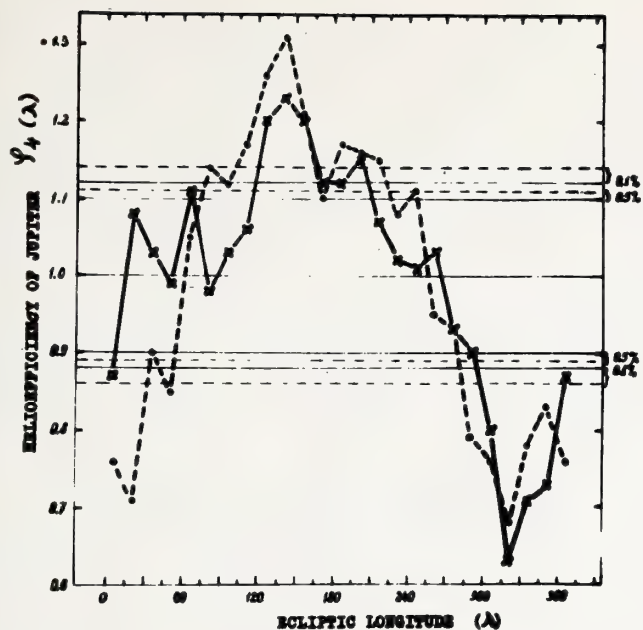


Figure 1. The variable helioefficiency of Jupiter based on the monthly relative solar number for the period of 1749 to 1973. Confidence intervals for the 0.5% and 0.1% significance levels according to Student's t criterion are shown.

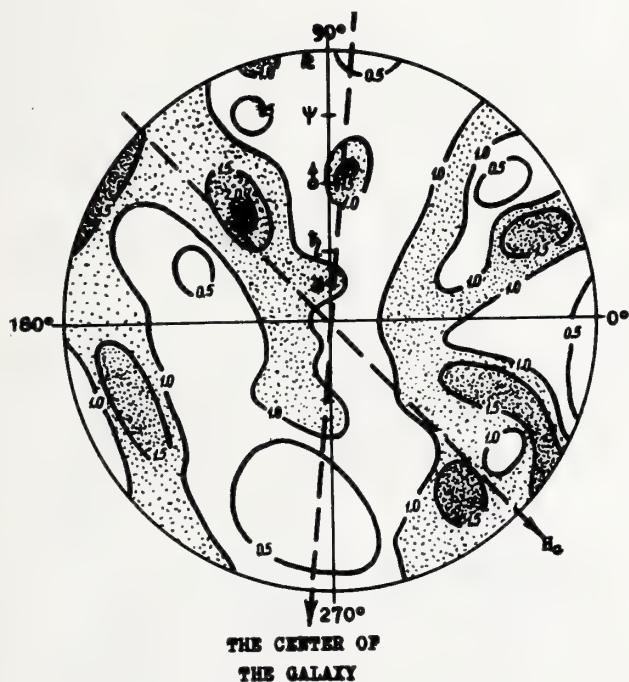


Figure 2. Map of lines of equal solar activity level in the conventional units of the solar activity beyond Jupiter's orbit obtained with phase analysis. Ecliptic longitudes are marked.

The shaded (active) regions in space are characterized by an increase of the solar activity level $[\phi_i(\lambda) > 1]$, when planets fall within these regions, regardless of what their mutual disposition is. The passive regions are characterized by a decrease of the solar activity level $[\phi_i(\lambda) < 1]$.

The detection of this structure is possible because the helioefficiency of some planets, $\phi_i(\lambda)$, changes in phase. On the other hand, the existence of this structure and orientation of the sector axes seem to prove an ex-

traneous action of the galaxy on solar activity (Vassilyeva et al., 1975d).

The axis of passive sectors is a line of nodes of the galactic equator and the ecliptic.

The axis of active sectors coincides with the ecliptic projection of the galactic magnetic field direction ($b'' = 0$; $l'' = 70$) and the direction of the solar motion relative to the stars of 14^m0-15^m0 ($d = 302.5$; $\delta = 32.5$). This anisotropic picture of the interplanetary medium seems to be evidence of ecliptic projection of the solar magnetosphere, because the most active sector is aligned toward the antiapex of the solar motion in the direction of the galactic magnetic field. Assuming the interconnection of the solar and galactic magnetic field force lines, the solar magnetosphere has to deviate from the ecliptic plane far beyond the solar system, as much as $\pm 50^\circ$ with the ecliptic projection along the axis $\lambda = 135 \div 315$.

Thus, side by side with the well-known sector structure of IMF observed at 1AU, which corotates with the Sun and is associated with the large-scale background solar magnetic field, the existence of another magnetic field sector structure beyond the Jupiter orbit is proposed. This sector structure is revealed by means of the phase solar activity analysis. It does not corotate with the Sun and is associated with both the magnetic field of sunspots and the orientation and the motion of the solar system in the galaxy.

2.2 Structure of the Interplanetary Medium Inside Mars' Orbit

The longitude distribution of the monthly and daily Wand Sp sets over orbits of Mercury, Venus, the Earth and Mars have been found to vary over the solar cycle (Vassilyeva et al., 1974a and 1974b).

In Figure 3 normalized monthly W distributions over the Earth's orbit averaged through the last 13 solar cycles, the variable helioefficiency of the Earth $\phi_{\oplus}(\lambda)$ at the solar minimum and maximum, are shown.

The $\phi_{\oplus}(\lambda)$ dependence on the phase of the 11-year solar cycle is a source of many discrepancies in the results of investigators (see references in Vassilyeva et al., 1974a). The variable helioefficiency of Mercury, Venus, the Earth and Mars over the solar cycle indicates the active role of the interplanetary medium in the formation of solar activity and implies the existence of feed-backs between solar activity and the planetary action on the Sun.

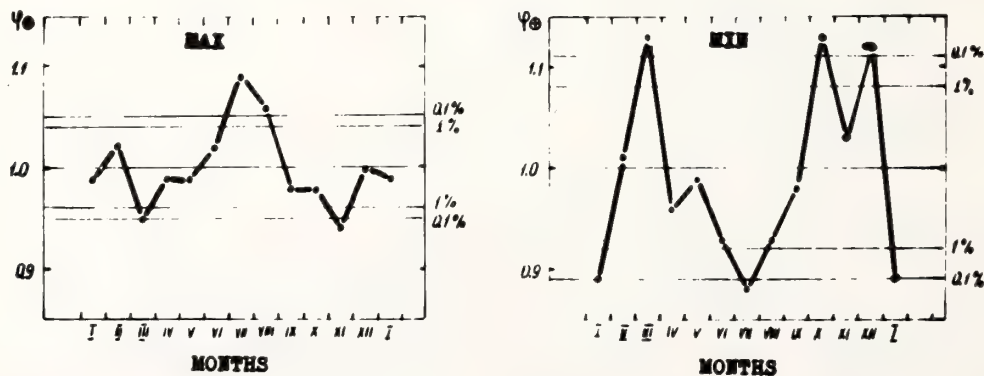


Figure 3. The seasonal variations averaged over the last 13 solar cycles at the solar maximum and the solar minimum. Confidence intervals for the 1% and 0.1% significance levels according to Student's t criterion are shown.

2.3 The Prediction of the Sunspot Area (Sp) 4-6 Months in Advance

The 4-6 month prediction of the sunspot area, Sp , is based on the daily Sp sets of the two last years and the daily positions of the four planets nearest to the Sun (Vassilyeva et al., 1975c). From the beginning, the table of 36×4 values of $\phi_i(\lambda)$ is created as a result of the daily Sp distributions over 10-degree ecliptic longitude intervals of Mercury, Venus, the Earth, and Mars.

This table is supplemented with 36 values of $\phi(\lambda_c)$ as a result of the daily Sp value distributions over the 10-degree Carrington longitude intervals of the central meridian. This table of 36×5 values describes the state of the interplanetary medium inside Mars' orbit and solar surface in the conventional units of the solar activity of the last two years.

In Figure 4, the variable helioefficiency of the four planets for the period of 1/IV-1974 to 1/IV-1976 is shown as a map of equal solar activity.

The shaded regions in space are characterized by an increase of solar activity [$\phi_i(\lambda) \geq 1$], when planets fall within these regions irrespective of their mutual disposition.

Predicted values of Sp for the following 4-6 months are calculated as $\overline{Sp} \prod \phi_i(\lambda)$, the values $\phi_i(\lambda)$ being taken from the table discussed above. The ecliptical longitude of the planets and Carrington's longitudes for the following dates are used as arguments. Influence of other planets may be taken into account with the help of a slowly varying supplementary coefficient. The observed sunspot areas (solid line) in comparison with those forecast by means of the phase analysis (dashed line) are shown in Figure 5a.

The observed relative solar numbers (solid line) in comparison with those forecast by Mayot's method in advance of 3 months are shown in Figure 5b.

This method empirically accounts for the phase changes of planetary helioefficiency $\phi_i(\lambda)$ over the solar cycle and assumes that the solar magnetosphere has an active role in the origin of the sunspot activity.

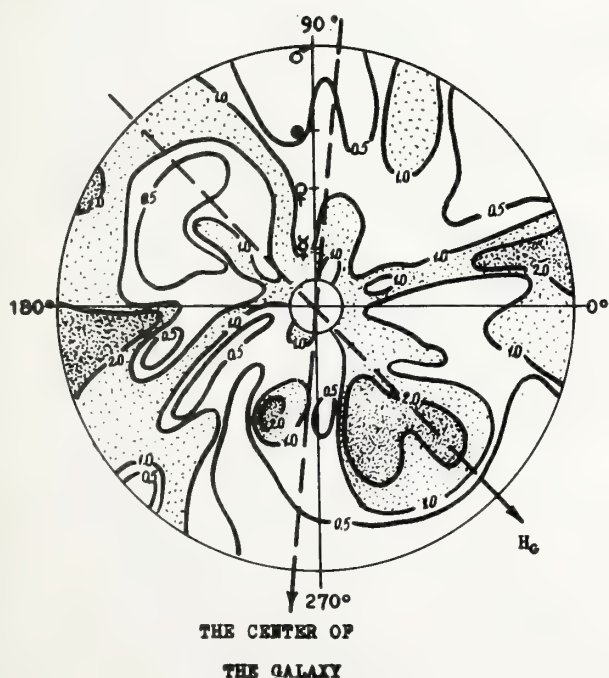


Figure 4. Map of the lines of equal solar activity level in conventional units of the solar activity inside Mars' orbit obtained from the phase analysis. Ecliptic longitudes are marked (1.IV.1974-1.IV.1976).

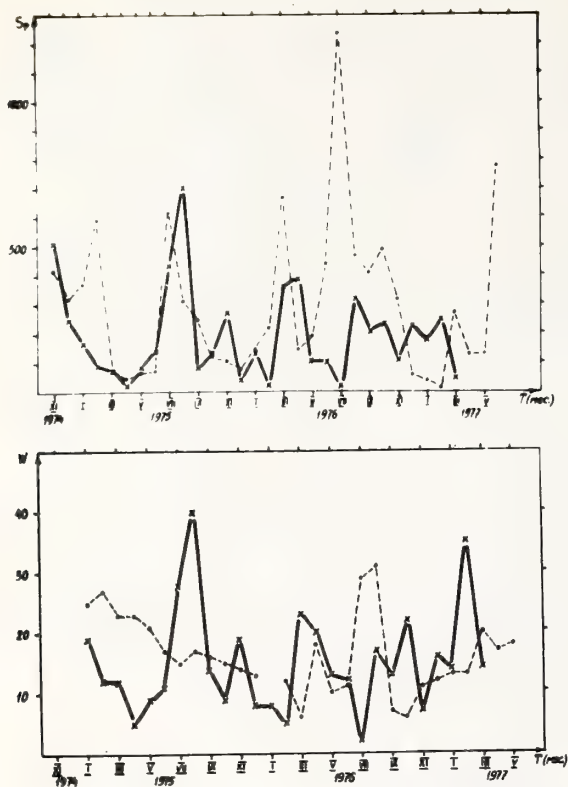


Figure 5. The observed (solid line) and forecast (dashed line) $Sp(a)$ and $W(b)$ in advance of 0-6 months (a) and in advance of 3 months (b).

The formation and the structure of the solar magnetosphere seem to be determined by the orientation and the motion of the solar system in the galaxy.

3. ANALYSIS OF THE COMMON COSMIC CONDITIONS OF THE SOLAR FLARES AND EARTHQUAKES

It is possible to look for the extraneous factors of the solar flares in quite another way. Positions of flare zeniths over the celestial sphere may be determined because of the sudden start and short duration of these events. If the external sources of flares are absent, the flare number distribution over the specific longitude intervals in a system of coordinates that is not connected with the solar rotation about the axis, have to be uniform or have random deviations from the uniform distribution. Moreover, in this system of coordinates it is possible to look for some universal regularities that are characteristic of a given region of the galaxy and are able to be manifested in the solar activity as well as in the geoactivity (Vassilyeva et al., 1978; Schpitalnaya et al., 1975).

The method of treating solar flares has been applied to earthquakes because of the sudden start and short duration of both phenomena; evidence of common morphological and dynamical features of their evolution; the existence of the experimental prerequisites for the consideration of the extraneous factors of the solar activity in general (Jose, 1965; Romanchuk, 1965, 1967; Trellis, 1967; Andis, 1977; Khlystov, 1978) and of the solar flares and

earthquakes in particular (Blizard, 1969; Prokudina, 1973; Bagby, 1973; Kropotkin and Liustkh, 1974; Kozelov, 1975; Schpitalnaya et al., 1975).

There is an idea that the flares and earthquakes can be identified with the response of whatever force field is both out of the Sun and out of the Earth and inherent to our region of the galaxy. To prove this idea, 5600 flares (1B-3B) and 2600 earthquakes, divided into four groups in magnitude M and depth of their focus h (I: $h < 70$, $M \geq 6$; II: $145 > h \geq 70$; III: $375 > h \geq 145$; IV: $h \geq 375$) have been investigated in the same system of coordinates that is not connected with the axes of the solar and Earth rotation (ecliptic heliocentric and ecliptic geocentric, respectively). The flare and earthquake sets are analyzed for the whole 11-year solar cycle to exclude the effects of the phase of the solar activity cycle (1962-1973).

The objectives of this investigation are: to study the spatial and temporal correlation between flares and earthquakes; to clarify the correlation between the positions of the zeniths of flares and earthquakes with the position of the planets in the same system of coordinates; and to study the character of the seasonal variations.

To increase statistical accuracy and ensure the spatial distributions of flares, this set has been supplemented with 7400 observations for 1961-1974 and 18,000 observations for 1954-1963.

3.1 Spatial Anisotropy of Flares and Earthquakes

The results of investigating the distributions of the zenith of flares and earthquakes over the celestial sphere in the ecliptic heliocentric and ecliptic geocentric system of coordinates, respectively, are as follows:

1. There is a spatial anisotropy of the distribution of the number of flares for the period of 1961-1974 and of 1954-1963, associated with the line of nodes of the galactic equator and the ecliptic longitude, the maximum of the flare distribution being directed to the center of the galaxy (Figure 6), and the maximum of the earthquake distribution being oppositely directed (Figure 7). The χ^2 criterion shows that the hypothesis of the uniform distribution has to be rejected with a probability as high as 0.999.

2. The longitudinal distributions of the total numbers of flares and the spatial modulation of the background $L\alpha$ -intensity (Fehlau et al., 1971; Bertaux and Blamont, 1971; Thomas and Krassa, 1971; Fahr, 1971) have a correlation coefficient of ~ 0.8 .

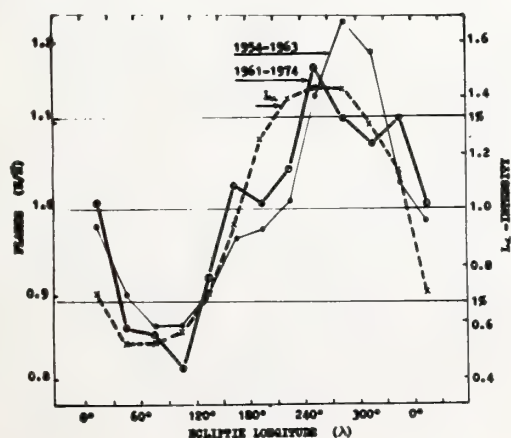


Figure 6. Normalized distributions of the number of flares over 30-degree ecliptic longitude intervals for the period 1961-1974 and for the period 1954-1963 (solid lines). Spatial modulation of the background $L\alpha$ -intensity is shown by the dashed line (Fehlau et al., 1971). Confidence intervals for the 1% level of significance according to Student's t criterion are shown for the period 1961-1974.

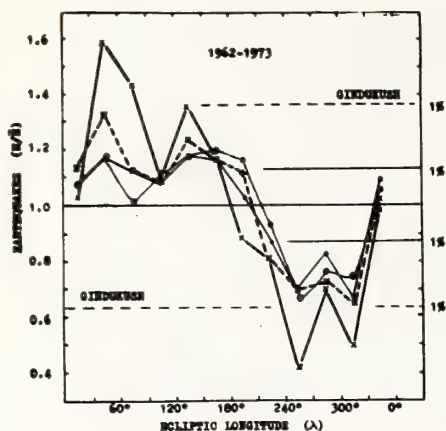


Figure 7. Normalized distributions of the number of earthquakes over 30-degree ecliptic longitude intervals for the period 1962-1973 for the different groups of earthquakes: (x—x), Gundukush (N = 535); (x---x), earthquakes with $h < 70$, $M \geq 6$; (o—o), all earthquakes (N = 2670). Confidence intervals for the 1% level of significance according to Student's t criterion are shown for the Gundukush distribution and for the distribution with N = 2670.

3. The spatial distribution of 2-3B flares (N = 522) and earthquakes with a depth of seismic focus of ≥ 375 km have a correlation coefficient of ~ 0.8 (Figure 8). Of particular interest is the evidence of high spatial correlation between these two sets in the absence of the temporal correlation.

3.2 Spatial Correlation of Flares and Earthquakes with Planets

The role of planets in the origin of flares and earthquakes has been discussed because they seem to be frequently on the meridians of flares and earthquake epicenters (Blizard, 1969; Prokudina, 1973; Bagby, 1973; Kozelov, 1975).

To clarify this role, the positions of the planets have been fixed at the time when 2-3B flares and earthquakes occurred, and the distributions of all planet positions summarized over the specific ecliptic longitude intervals have been analyzed.

The 2-3B flare zenith distributions of 522 flares for the two periods 1962-1967 and 1967-1972 are compared with the summarized planetary distributions of 522 $\times 9$ positions for the same periods in Figure 9.

The spatial anisotropy of 2-3B flares is found to be emphasized by the non-uniform distributions at the time of flares. This means that planets are really clustered on the flare meridian in general.

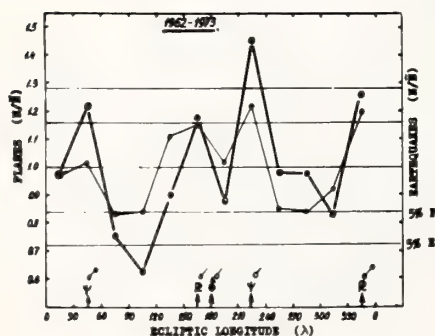


Figure 8. Normalized 2-3B flares (open circles) and earthquakes of $h \geq 375$ km (black circles) number distributions over ecliptic longitudes (heliocentric for flares, geocentric for earthquakes). Confidence intervals for a 5% significance level according to Student's t criterion are shown for flares and earthquakes. Positions of Neptune, Uranus, and Pluto are marked (1962-1973).

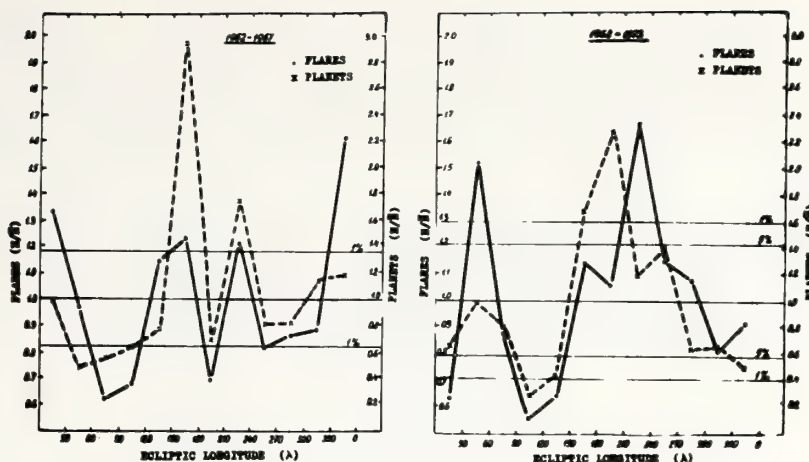


Figure 9. Normalized distributions of the 2-B flares ($N = 522$) (solid lines) and the planetary positions ($N' = 522 \times 9$) at the time of the flares (dashed lines) over ecliptic heliocentric longitudes (1962-1975).

In Figure 10 the normalized distribution of the number of earthquakes ($N = 288$) with a depth of seismic focus, $h \geq 375$ km, in comparison with the normalized summarized distribution of the positions of the Sun, the Moon, Mercury, Venus, and Mars ($N = 288 \times 5$) at the time of earthquakes over ecliptic geocentric longitudes is shown.

This result indicates the active role of planetary dispositions in the formation of the earthquakes and flares as well as the related origin of these two phenomena.

3.3 Temporal Correlation between Solar Flare and Earthquake Sets

Correlations between earthquakes and flares lead to different conclusions about the sign of this correlation and even that about its existence (see references in Vassilyeva et al., 1978). All of these conclusions may be compatible if the earthquake separates into groups over the depth of the seismic focus and the frequency of the solar and seismic activity variations is taken into account.

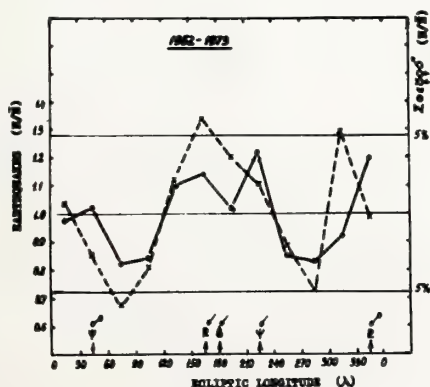


Figure 10. Normalized distributions of earthquakes ($h \geq 375$; $N = 288$) (solid line) and normalized distribution of the positions of the Sun, the Moon, Mercury, Venus, and Mars ($N' = 288 \times 5$) over ecliptic geocentric longitudes (1962-1973).

In the one case, the correlation coefficient (R) is a function of the temporal interval in which the data of two sets analyzed for the period 1962-1973 are averaged (Figure 11). In the other case, the behavior of the correlation coefficient is quite different for the two groups of earthquakes ($h < 70$ or $h \geq 70$).

The value of R is close to zero for the daily sets of all groups of earthquakes. The value of R is positive for the monthly and yearly sets of earthquakes with $h < 70$, but R is negative for the monthly and yearly sets of earthquakes with $h \geq 70$ km. As a result, it seems very doubtful that flares may be responsible for triggering earthquakes.

3.4 The Seasonal Variations of Flares and Earthquakes

Seasonal variations of flares and earthquakes have been discussed by many authors (e.g., Svestka, 1968; Kropotkin and Liustikh, 1974). Analysis of the seasonal variations for the simultaneous sets of flares and earthquakes for 1962-1973 shows their similar character (Figure 12).

A common cause for the similarity of the seasonal variations of flares as well as earthquakes may be the change of the Sun-Earth vector orientation in space during the year. Flare and seismic activity is a minimum when this vector is along the line of nodes of the galactic equator and the ecliptic. Flare and seismic activity is a maximum when this vector is close to the ecliptic projection of the galactic magnetic field direction.

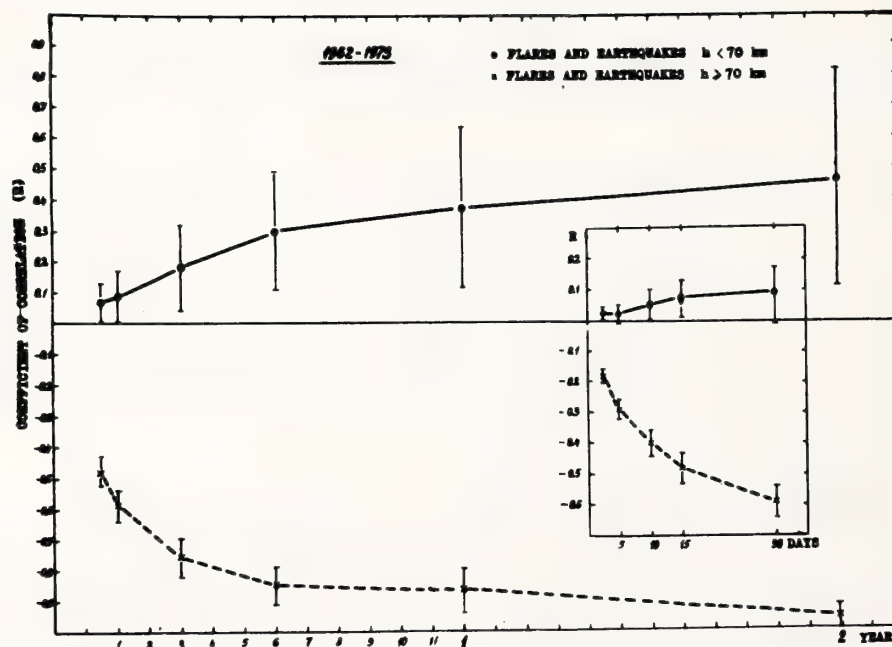


Figure 11. Coefficient of correlation between earthquake and flare sets for the period 1962-1973. Earthquakes are separated into two groups, taking into account the depth of the earthquakes [$h < 70$ km (solid line) and $h \geq 70$ km (dashed line)]. Time along the x-axis is a temporal interval of data averaging.

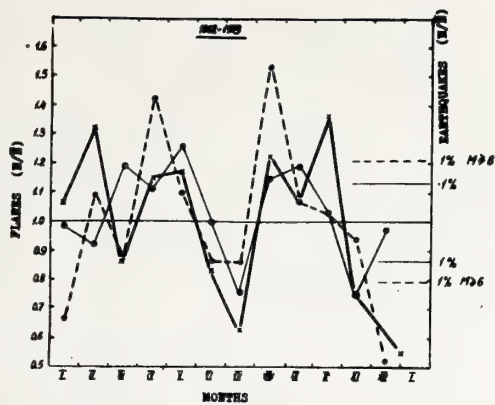


Figure 12. Normalized seasonal variations averaged over the solar cycle of simultaneous sets of flares and earthquakes (1962-1973). Seasonal variations of the earthquakes with $h < 70$, $M \geq 6$ (dashed line) are similar to those of 2-3B flares (solid line) and weak flares (open circles).

4. CONCLUSION

1. As a result of the new methods of treating solar activity data, there is evidence that solar activity is a complex phenomenon of the solar system as a whole. Variable helioefficiency of planets depends on many conditions including the mutual disposition of planets, their positions in orbits, the non-uniform structure of the solar magnetosphere and the phase of the 11-year solar cycle.

2. In many aspects the presence of galactic action to solar activity is revealed. It seems that the problem of planetary influence on the solar activity should be transformed into the problem of galactic influence on the solar activity by means of planets.

3. Some common cosmic conditions of the flare and earthquake origin as well as dynamical and morphological features give independent evidence of the extraneous causes that determine solar and geo-activity. Flares and earthquakes seem to belong to the same class of phenomena and a common method of predicting them is possible.

4. The assumption that solar activity is the manifestation of the dynamical equilibrium of the star in the galaxy is likely.

REFERENCES

- Andis, K. (1977): Heliocentric planetary positions and their effect on sunspots. Cycles, 28:88-95.
- Bagby, J. P. (1973): Further evidence of tidal influence on earthquake incidence. The Moon, 6:398-404.
- Bertaux, J.-L., and J. E. Blamont (1971): Evidence for a source of an extra-terrestrial hydrogen Lyman-alpha emission: The interstellar wind. Astron. Astrophys., 11:200-217.
- Blizard, J. B. (1969): Advance warning of protom emission from the Sun. In: Abstracts of paper of the 130th meeting of Amer. Astron. Soc., Albany, 104.

- Fahr, H. I. (1971): The interplanetary hydrogen cone and its solar cycle variations. Astron. Astrophys., 14:263-274.
- Fehlau, P. E., Chambers, W. H., Fuller, I. C., and Kunz, W. E. (1971): Interplanetary Lyman-alpha: Theory and experiment. Nature, 232:179-180.
- Jose, P. D. (1965): Sun's motion and sunspots. Astron. J., 70:193-200.
- Khlystov, A. I. (1978): Resonance oscillations on the Sun with friction. Astron. Tsirk., 978:1-3.
- Kozelov, V. P., Mingaleva, G. I. (1975): Anisotropy of solar flare activity in the inertial space and resonance ability of the solar system. In: Substorms and disturbances in the magnetosphere. Leningrad, Nauka, 264-274.
- Kropotkin, P. N., Liustikh, A. E. (1974): Seasonal periodicity of earthquakes and Newton-Mach principle. Dokl. Akad. Nauk., 217: 1061-1064.
- Prokudina, V. S. (1973): The application of the planetary configuration's method to the active phenomena on the Sun. Soobshch. Gos. Astron. Inst. Shternberg, 181:11-32.
- Romanchuk, P. R. (1965): To the problem on the nature of solar activity. Soln. Dannye. Byull., 5:65-68.
- Romanchuk, P. R. (1967): To the problem on the nature of solar activity. V. Solar activity and the interaction of planets with corpuscular flows. Soln. Dannye. Byull., 8:86-91.
- Schaten, K. H., and Wilcox, I. M. (1969): Direction of the nearly galactic magnetic field inferred from a cosmic ray diurnal anisotropy. J. Geophys. Res., 74:4157-4161.
- Shpitalnaya, A. A., Vassilyeva, G. Ya., and Petrova, N. S. (1975): On a possibility of gravitational wave action in the solar and Earth activity. In: Dynamic and evolution of stellar system. Moskva-Leningrad, 129-137.
- Svestka, Z. (1968): On long-term forecasts of proton flares. Sol. Phys., 4:18-29.
- Trellis, M. N. (1967): Influence du mouvement du soleil vers l'appex sur la naissance des centres d'activite. Astrophys. Lett., 1:57-58.
- Thomas, G. E., and Krassa, R. F. (1971): OGO-5 measurements of the Lyman-alpha sky background. Astron. Astrophys., 11:218.
- Vassilyeva, G. Ya., Kuznetsov, D. A., Shpitalnaya, A. A., and Petrova, N. S. (1974a): To the problem on annual variations of solar activity. I. A dependence of seasonal variations on the phase of an 11-year cycle. Soln. Dannye. Byull., 4:96-110.

- Vassilyeva, G. Ya., Shpitalnaya, A. A., and Petrova, N. S. (1974b): To the problem of annual variations of solar activity. II. Seasonal variations of solar activity and the structure of interplanetary medium. Soln. Dannye. Byull., 6:99-105.
- Vassilyeva, G. Ya., Shpitalnaya, A. A., and Petrova, N. S. (1975a): Variations of solar activity caused by revolutions of Jupiter, Saturn, and Uranus about the Sun. Soln. Dannye. Byull., 1:84-93.
- Vassilyeva, G. Ya., Shpitalnaya, A. A., and Petrova, N. S. (1975b): Solar activity and the structure of interplanetary medium. Soln. Dannye. Byull., 2:76-84.
- Vassilyeva, G. Ya., Shpitalnaya, A. A., and Petrova, N. S. (1975c): Possibilities of forecasting the solar activity variations. Soln. Dannye. Byull., 3:67-75.
- Vassilyeva, G. Ya., Shpitalnaya, A. A., and Petrova, N. S. (1975d): On the spiral structure of the interplanetary medium. In: Dynamic and evolution of stellar system. Moskva-Leningrad, 108-113.
- Vassilyeva, G. Ya., Shpitalnaya, A. A., and Petrova (1978): IX consultation on solar physics. Wroclaw, 25-30 September.

FORECASTING OF SOLAR AND GEOMAGNETIC ACTIVITY BASED ON THE RELATION BETWEEN GEOMAGNETIC DISTURBANCE AND HIGH-LATITUDE MAGNETIC FIELD OF THE SUN

Y. I. Feldstein, M. A. Livshits, T. E. Valtchuk
Institute of Terrestrial Magnetism,
Ionosphere and Radio-Wave Propagation
U.S.S.R. Academy of Science (IZMIRAN)
P.B. Akademgorodok, Moscow Region, U.S.S.R.

The quantitative relations between a global geomagnetic disturbance and Wolf numbers W for the minima at the ends of even- and odd-numbered cycles of solar activity have been obtained by using geomagnetic aa indices. A considerable difference was revealed in the disturbance level at the ends of even- and odd-numbered cycles of the solar activity during the last century. The data indicated a connection between the geomagnetic activity level and the character of variations of the polar magnetic field of the Sun. Geomagnetic activity on the decreasing branches of the solar cycles depends also on the direction of the solar magnetic field in the polar regions. Based on physical concepts by which the general magnetic field of the Sun is a "material" for producing the active regions in the subsequent cycle, the prediction of W has been made for the 21st cycle together with the diagnostics of the behavior of aa index during this cycle.

1. INTRODUCTION

It appears (see sec. 2) that the high-latitude magnetic field of the Sun is extended far into interplanetary space, filling it up to distances ~ 5 a.u. The fields near the solar poles vary in their values and direction during a period of about 22 years, and reach maximum absolute values near the minima of the 11-year cycles of solar activity. Variability of the polar heliomagnetic field is one of the causes of variations in the intensity of geomagnetic activity, in the course of 22-year cycle, which seems to be related to the appearance of a B_θ component which is antiparallel or parallel to the field on magnetopause, with the maximum field intensity at the ends of even- and odd-numbered 11-year cycles of solar activity. This results first because even-parity control should be included in the studies using the level of solar activity geomagnetic disturbance for forecasting. It is also of great importance that the solar magnetic field extending to the interplanetary space seems to be an indicator for the general level of solar activity during the subsequent 11-year cycle. According to widespread, up-to-date theories, appearance of the large-scale magnetic field near the poles

is related to a transfer (diffusion toward the high latitudes) of the remnants of magnetic dipolar groups (or, more accurately, diffusion of their transformed parts). The general magnetic field of the Sun presents, however, a "material" for a formation of magnetic fluxes in the active regions of the subsequent cycle. These considerations make it possible to apply the physically-argued method to predict solar activity during the subsequent cycle from the intensity in the minimum of the preceding cycle, which seems to be connected with the intensity of the solar general magnetic field.

2. THE RELATION BETWEEN GEOMAGNETIC DISTURBANCE AND POLAR MAGNETIC FIELD OF THE SUN

2.1 Periods of Minima of the 11-Year Cycles

Observations with high resolution from magnetographs reveal an inhomogeneous, ragged structure in the general magnetic field of the Sun. However, when averaged over an extended area (resolution less than tens of seconds), the large-scale field appears to be very homogeneous, and its intensity does not exceed several 0_e . At high-latitudes ($\phi > 55^\circ$) the general field is relatively undisturbed by strong local magnetic fields, and the properties of a high-latitude (polar) field can be considered as known.

The direction and intensity of the high-latitude magnetic field of the Sun vary during a period of about 22 years (Severny, 1966; Howard, 1974). The epochs of maximum solar activity are more or less identical to the epochs of the polarity reversal, whereas the epochs of minima correlate in their phase with the maximum absolute value of the general magnetic field of the Sun. The recurrence of the same magnetic configuration after 22 years is also confirmed by indirect data on the polarity alteration of the leading and following spots in the 11-year cycles. The polar faculae which are identified with the magnetic force tubes coming out onto the surface (Sheeley, 1976) vary simultaneously with the polar field variation. Thus, near the epoch of the 11-year minima, the magnetic field during the last 100 years was such that at the end of the 11-year cycle with an even number the sign of the field was positive (directed away from the Sun) in the northern hemisphere of the Sun and it was negative (toward the Sun) in the southern hemisphere. At the ends of the odd-numbered 11-year cycles, the polarities were reversed.

Some good evidence indicates that the high-latitude magnetic field of the Sun is extended far into interplanetary space. This theory is schematically represented in Figure 1, taken from Valtchuk et al. (1978). Development of this theory was initiated by Rosenberg and Coleman (1969) who revealed the dependence of the observed prevailing polarity of the interplanetary magnetic field (IMF) on the Earth's heliographic latitude (the earth is located at 7° south of the plane of the solar equator from March 5-8 and at the equal absolute value to the north from September 7-10). Figure 2, from the review by Dobrovolsky and Moreno (1976), presents the variations of the numbers of days with a certain polarity IMF at the Earth's orbit for each solar revolution from 1964 to 1972 according to satellite observations. One can see in Figure 2 practically all the sinusoidal variations near the cycle minima, the field reversal between the end of 19th 11-year cycle (1964-1965), and the

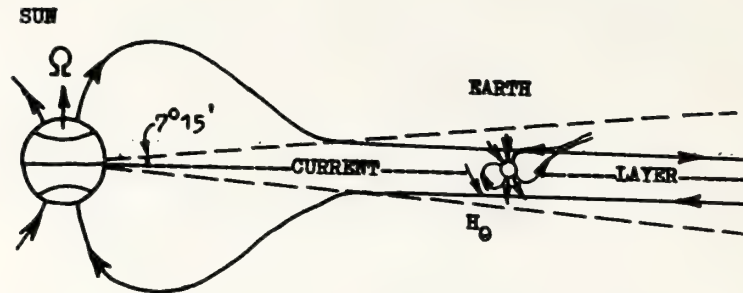


Figure 1. Schematic view of general magnetic field of the Sun in the minima at the ends of even-numbered 11-year cycles with the assumption of a plane current sheet and the Earth with its field in the interplanetary space near the Sun.

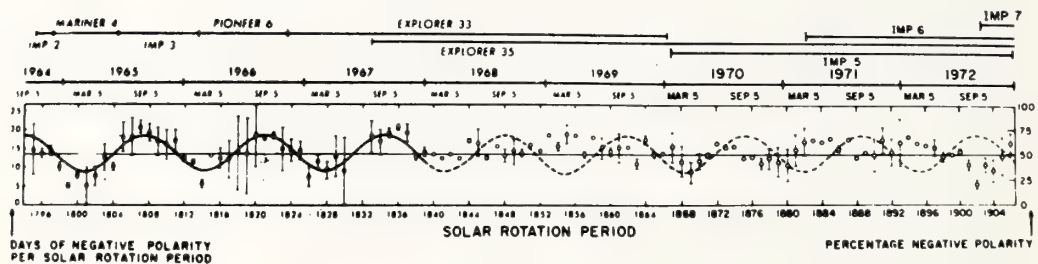


Figure 2. Annual variation of IMF (Dobrovolsky and Moreno, 1976). Number of days (per solar revolution) with the negative IMF polarity (IMF is directed towards the Sun) in the solar wind in 1964-1972.

decreasing branch of the 20th cycle (1971-1972). The prevailing IMF polarity above and below the plane of the solar equator has the same sign as the high-latitude magnetic field in the respective hemisphere of the Sun. The reversal of the field polarity between 1964-1965 and 1971-1972 is also in agreement with the directional variation of the solar magnetic field.

Additional evidence in favor of the conclusion drawn by Rosenberg and Coleman (1969) is presented in Figure 3 based on the sector-structure catalog (Svalgaard, 1976). There is a pronounced period near the cycle minima with the regular field structure and with the reversal of the field sign at the passage from the minimum in 1954-1955 to the minimum in 1964-1965. (Beginning in 1954-1955, the negative ratios $A-C/A+C$ corresponded approximately to the periods of spring and positive ratios to the periods of autumn equinoxes, whereas in 1964-1965 the ratio sign was inverted.) Cyclic variations of the polar magnetic field of the Sun are also confirmed by indirect data on galactic cosmic rays (Svalgaard and Wilcox, 1976), as well as by studies of a relation between geomagnetic disturbance and even parity of a cycle (see below). There is also the direct experimental evidence given by measurements of the Pioneer 11 probe at heliolatitude $+16^\circ$ (Smith et al.



Figure 3. Variation of the ratio of the difference between the number of days in a month with IMF directed away from the Sun (A) and toward the Sun (C) to the sum (A + C).

1978). The regular magnetic field directed continuously away from the Sun with the sign corresponding to the polar magnetic field of the Sun was observed at distances of 3.7 to 5 a.u. during February 1976 (the end of cycle No. 20).

Thus, it appears that a regular magnetic field, which is oppositely directed above and below the plane of the solar equator and varies with the 22-year period, exists in interplanetary space, at least during periods of low activity. If we include that this azimuthal field is twisted into an Archimedean spiral and that the geomagnetic axis is inclined to the axis of the solar "dipole", then, with (Russell and McPherron, 1973), we can conclude that B_θ (the component along the direction of geomagnetic dipole) should exist in interplanetary space at the Earth's orbit at cycle minima. At the end of the even-numbered cycles, this component is antiparallel to the geomagnetic field of the magnetopause (and is parallel at the end of the odd-numbered cycles). Along with this, B_z (the component which is normal to the plane of solar equator and directed to the south) can also be present at the end of even-numbered cycles (see discussion in sec. 2.2). Since the antiparallel directions of the interplanetary and geomagnetic fields on the magnetopause promote intensification of their reconnection process, one should expect a corresponding growth of the magnetic disturbance level at the end of the even-numbered cycles as compared to the odd-numbered cycles.

The variations of geomagnetic activity near the minima of 11-year cycles have been investigated in Livshits et al. (1979). The set of aa indices of geomagnetic activity for the period from 1869 to 1976 (which was introduced by Mayaud (1973) and is quite uniform during the last 100 years) has been used. Figure 4 shows the dependence of the mean annual value of the aa index of geomagnetic activity on the mean annual value of nonsmoothed Wolf numbers W (Vitinsky, 1973) separately for even-numbered and for odd-numbered 11-year cycles in the minima ($W \leq 27$, $aa \leq 20$) and jointly for both in the maxima.

A comparison of mean annual values of aa indices with the Wolf numbers gives the following linear approximations:

$$aa = (0.31 \pm 0.8)W + (6.98 \pm 1.12) \text{ in gammas}$$

$$aa = (0.25 \pm 0.11)W + (12.70 \pm 1.11) \text{ in gammas}$$

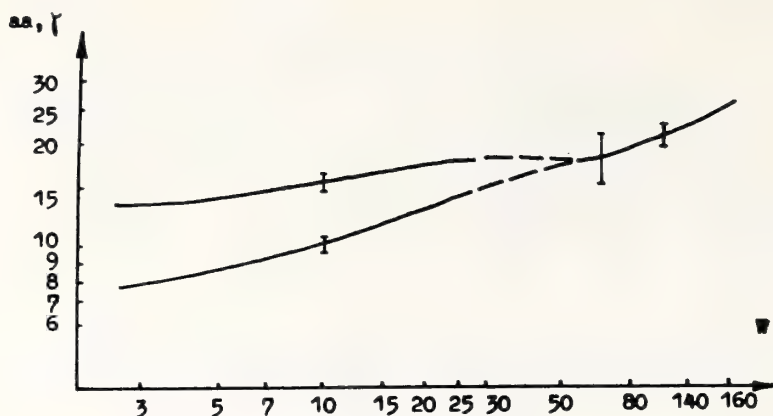


Figure 4. Dependence of mean annual values of geomagnetic activity aa indices on the level of solar activity (Wolf numbers) at the minima of 11-year cycle ($W \leq 27$, $aa \leq 20$). The upper curve corresponds to the ends of even-numbered cycles; the lower curve presents the ends of odd-numbered cycles. The linear dependences of aa on W are presented in the text. For periods near the solar activity maxima ($W > 60$), the even- and odd-numbered cycles are united.

for the minima at the ends of 11-year cycles with odd and even number, respectively. The correlation coefficients are $r = 0.70 \pm 0.14$ and $r = 0.46 \pm 0.18$, respectively. Thus, for odd-numbered cycles the dependence aa on W is closer, and, moreover, aa varies with W more substantially in the minima of odd-numbered cycles than in the minima of even-numbered cycles.

Geomagnetic activity is higher at the ends of even-numbered cycles than at the ends of the odd-numbered ones. When extrapolating the Wolf numbers to zero, the value of aa index remains considerably higher at the ends of the even-numbered cycles; it is approximately 1.8 times higher than at the ends of odd-numbered cycles.

By using the expressions relating the values of aa indices to W , we normalized values of aa to $W = 10$ and $W = 100$ for the minima and the maxima, respectively, of 11-year cycles. These corrected aa values are shown in Figure 5. We can see there a pronounced difference in the level of magnetic activity at the ends of even-numbered and odd-numbered cycles because the activity is increased in the even-numbered cycles as was noted above. A monotonic aa increase for odd-numbered (from cycle No. 13 to cycle No. 19) and for even-numbered cycles (from the cycle No. 14 to the cycle No. 20) can be related to the intensity growth of the general magnetic field of the Sun. In the maxima of the solar cycles, aa values (normalized to $W = 100$) do not vary considerably during the last 100 years and do not undergo a regular variation between odd- and even-numbered cycles. This feature of aa -index behavior may be related to a small, close to zero, value of the general magnetic field of the Sun near the maxima of 11-year cycles. Thus, the above analysis shows that some features of geomagnetic activity variations during the last century are related in a certain way to the regular variations of the general magnetic field of the Sun.

2.2 The Epochs of Decreasing Activity of 11-Year Cycles

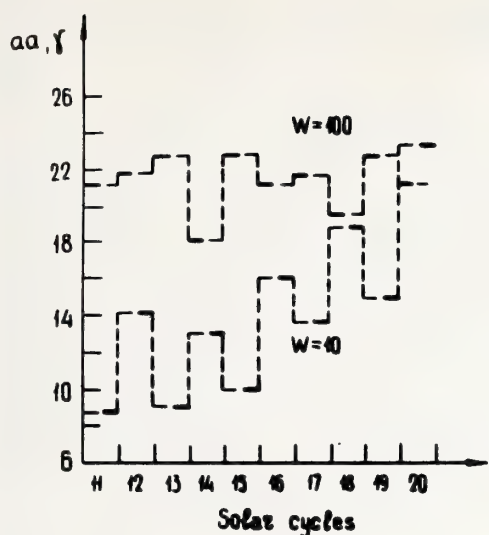


Figure 5. Variations of aa indices normalized to $W = 10$ and $W = 100$ in the minima and maxima of 11-year cycles of solar activity. The intervals of 2-3 years around the cycle extremes were used.

The effect of the high-latitude solar field on phenomena in interplanetary space appears to be substantial, not only for the minimum epochs but also for the periods of decreasing activity after maxima. This also can be seen from the data for $20 \leq W \leq 50$ shown in Figure 4. In Figure 6, the solid lines indicate the variations of aa indices (Figure 6a) and that of W (Figure 6b) during 22-year cycle (starting from even-numbered 11-year cycle and passing to odd-numbered cycle). To obtain the curves, the values of W and aa were averaged in the cycles of the respective even-parity from No. 11 to No. 20. The normalization was carried out to a duration of the growth phase (from the minimum to the maximum of a cycle determined from W according to Vitinsky (1973) and to a duration of the decrease phase (from the maximum to the minimum of W) of the 11-year solar activity cycle. The curves similar to

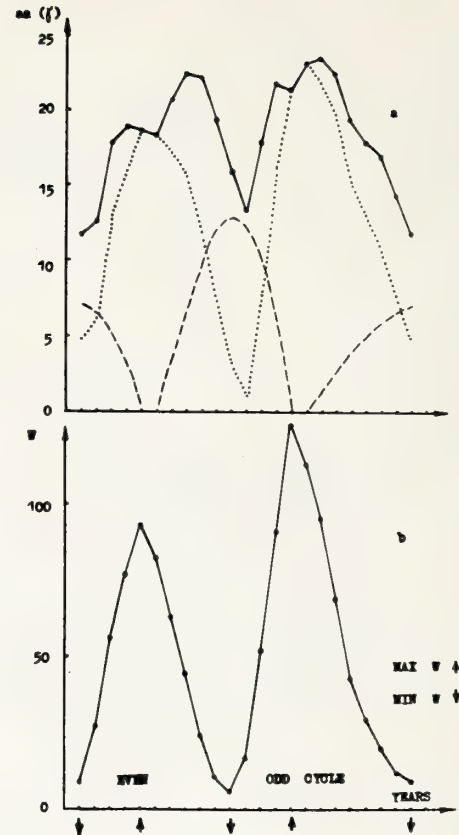
those of Figure 6a but without normalization were presented by Svalgaard (1977).

The cyclic W variations are smooth from the minimal W values in the years of minima to the maximal W values in the years of the cycle maxima. The difference of even- and odd-numbered cycles is only a quantitative one; i.e., W is higher for the maxima of odd-numbered cycles than that for even-numbered cycles.

The cyclic aa variations are substantially different for even- and odd-numbered cycles. The aa value in the maximum of the odd-numbered cycles is higher than its value in the maximum of the even-numbered cycles, and an additional maximum at the decrease phase of the activity is pronounced. The value of this maximum exceeds the values of aa in the maximum of even-numbered solar cycles. In odd-numbered cycles there is one maximum slightly delayed with respect to the solar cycle maximum. The presence of an additional maximum of the aa index at the solar activity decrease during the even-numbered cycles and its absence in the odd-numbered cycles indicate a difference of physical processes resulting in the generation of geomagnetic disturbances. The presence of this maximum can be related to the certain direction of the general magnetic field of the Sun.

The dashed curves in Figure 6a represent the values of the aa index (i.e., geomagnetic disturbance) which is related, according to our theory, with the effects of the high-latitude solar magnetic field. The maxima of dashed curves in the years of solar activity minima are equal to aa values at

Figure 6. Variations of aa indices (top) and W (bottom) in the range from the cycle No. 11 to No. 20 for the even- and odd-numbered cycles, respectively. The cycle duration is normalized to 4 years for the growth phase and to 6 years for the decrease phase of an even-numbered cycle, and to 8 years for the decrease phase of an odd-numbered cycle. The solid line connects the mean annual aa values averaged over the cycles of corresponding type-parity. The dashed line shows aa values related to the effect of high-latitude magnetic field of the Sun. The dotted curve describes aa values related to the active regions on the Sun.



$W = 0$ for the ends of even- and odd-numbered 11-year cycles (see Figure 4). Zero values of the dashed curves correspond to the years of maximum and to the year after the maximum when the general magnetic field of the Sun is assumed to have vanished. The dotted curve corresponding to the differences of aa values on the two curves apparently represents the level of geomagnetic disturbance due to the solar activity, in particular, due to corpuscular fluxes after the solar flares. The maxima of the curves approximately correspond to the maxima of the solar cycles.

The fact that the described characteristics of the cyclic variation are actually caused by the effect of the high-latitude solar field results from the recently obtained experimental data (Rosenberg and Coleman, 1978). The data from a number of spacecraft show the increase of IMF absolute value, i.e., the field compression in the region of interaction between the fast corpuscular flux and the slower solar wind. In this case, the statistical analysis of a direction of B_z component showed that B_z was principally directed to the north in 1964-1965, whereas in 1972-1975 it was directed mainly to the south. The reversal of B_z sign occurred in 1968-1970 immediately after the cycle maximum. Both the sign of B_z and the period of the sign reversal are in agreement with the behavior of the solar high-latitude field (see the scheme in Figure 1 for an even cycle). Thus, the recurrent fluxes in the interplanetary space at the phase of activity decrease result in the increase of the southward solar magnetic field on the Earth's orbit. That is, the solar wind starts to be more effective for generation of geomagnetic disturbances. The appearance of an additional maximum is a result of this effect.

3. SOLAR ACTIVITY FORECASTING FROM THE DATA ON GEOMAGNETIC AA INDEX IN THE PRECEDING MINIMUM OF THE 11-YEAR CYCLE

Ohl (1977) used the data on geomagnetic activity on a decrease branch of the solar activity cycle to predict the parameters of the subsequent cycle. Schatten et al. (1978) and Valtchuk and Feldstein (1979) assumed that there is a physical relation of parameters of the subsequent solar activity cycle with the intensity of the general magnetic field of the Sun in the preceding minimum. Magnetic flux and magnetic energy accumulated in high-latitude regions of the Sun during the minimum are transformed into the magnetic fluxes of active regions at lower latitudes during the maximum of the subsequent cycle. A close correlation of geomagnetic activity with the intensity of the general magnetic field of the Sun is the physical argument for a search for relations between geomagnetic activity in the cycle minimum and the parameters of the subsequent cycle of solar activity.

In Figure 7 the dependence is shown of $\log W_M$ (W_M is mean annual value for the Wolf numbers in the cycle maximum) in the subsequent cycle on $\log aa$ in the minimum of the preceding cycle from the data on the solar cycles from No. 11 to No. 19. Mean annual observed values W_M are taken from Vitinsky (1973); aa is the mean value of the geomagnetic index averaged over 12 months (dots) or over 36 months (crosses) preceding the minimum of W . The data of the minimum (with the accuracy within a quarter) was chosen according to Vitinsky (1973). The values of aa were normalized to $W = 0$ by the correlation expressions obtained above. Both dependences are characterized by the high values of correlation coefficients $r = 0.90 \pm 0.07$ and described by the expressions:

$$\log W_M = (0.76 \pm 0.08)$$

$$\log aa + (1.20 \pm 0.08)$$

$$\log W_M = (1.0 \pm 0.1)$$

$$\log aa + (0.94 \pm 0.11)$$

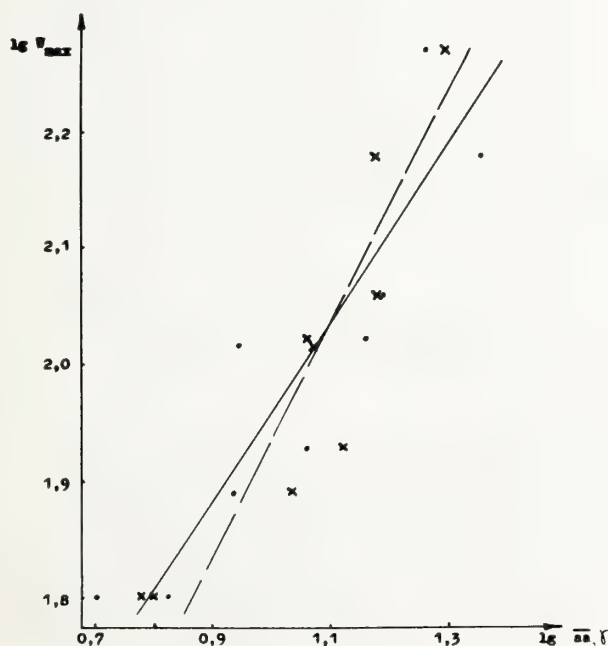


Figure 7. Dependence of mean annual Wolf number values in the maximum of the subsequent activity cycle (W_M) on mean annual aa values in the preceding minimum from the data on solar cycles from No. 11 to No. 19. Dots: aa value is averaged over 12 months (solid curve) preceding the quarter of W minimum; crosses: aa value is averaged over 36 months (dashed line). The straight lines are drawn by least squares method.

for 12 months (solid curve) and for 36 months (dashed curve), respectively. Assuming that the minima of the solar cycle No. 20 occurred in the second quarter of 1976 (Solar-Geophys. Data, 1978) from aa values (Mayaud, 1977a, b) for a year and three years before the minimum, we obtain the predicted W_M^{21} 163 ± 8 and 198 ± 12 , respectively.

Figure 8 shows the dependence of $\log T$ (T is the duration of the growth branch expressed in years) of the subsequent cycle on $\log aa$ in the minimum of the preceding cycle from the data for the cycles from No. 11 to No. 19. The duration of the growth branch with accuracy within a quarter is taken from Vitinsky (1973). The values of aa were reduced to $W = 0$ (dots correspond to aa mean value over 12 months; crosses correspond to 36 months). The dependences are characterized by correlation coefficients $r = 0.75 + 0.15$ and $r = 0.74 + 0.76$ and the regression equations:

$$\log T = - (0.33 \pm 0.08) \log aa + (0.95 \pm 0.09)$$

$$\log T = - (0.43 \pm 0.12) \log aa + (1.06 \pm 0.12)$$

for a year (solid line) and for three years (dashed line), respectively. The predicted T^{21} are equal to 3.2 ± 0.2 and 3.0 ± 0.3 years, respectively. Thus, the prediction of the parameters of the solar activity cycle No. 21 from geomagnetic indices results in $W_M^{21} = 180 \pm 18$ and $T^{21} = 3.1 \pm 0.2$. Correlation between W_M and geomagnetic activity in the subsequent minimum results in $r = 0.53 \pm 0.25$, which is considerably less than the value of r for correlation between W_M with the activity in the preceding minimum. Therefore, some other processes on the Sun besides the diffusion toward the high latitudes of weak magnetic fields which are the remnants of the preceding active forms also affect a formation of that general magnetic field of the Sun.

Table 1 contains various predictions for W_M^{21} and the date of maximum for the cycle No. 21. Our prediction agrees with that presented in Ohl (1977), and we expect very high activity already in 1979. The values of $W = 180$ are on the level of mean annual values in 1957 and 1958 ($W = 189.9$ and $W = 184.8$), i.e., in the maximum of the cycle No. 19 which was the highest during the two-century

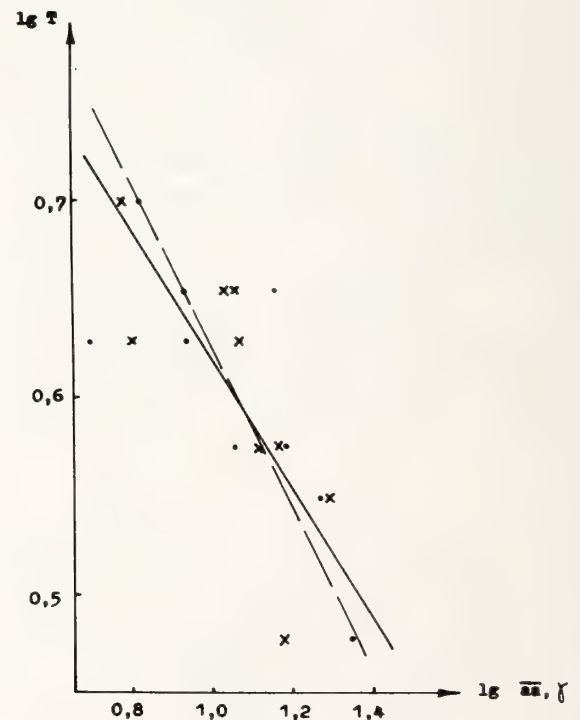


Figure 8. Correlation of the growth-branch duration of a subsequent cycle (T) with mean annual aa values in the preceding minimum from the data of the solar cycles from No. 11 to No. 19. Denotations are identical to those in Figure 7.

Table 1. Forecast for the cycle No. 21.

Author	Years of maximum	W_M^{21}
Vassiljev et al. (1975)	1980.0 - 1980.5	95 ± 15
Bonov (1969, 1970)	1981.1	52
Schove (1955)	1984.5	145
King-Hele (1963, 1966)	1985.3	110
Gleissberg (1971)	1979.5 - 1980.5	$56 + 96$
Henkel (1971)		32 100
Romanchouk (1974)	1980.0	70 105
Besrukova (1959)		82 120
Method Kopetsky's	1980.0	123
Method Xantakis	1980.7 - 1981.2	79 94
Method King-Hele's	1980.7 - 1981.2	80 94
Method Minnis'es	1979.7	$136 + 15$
Odd-even correlation	1979.8	132
Vassiljev et al., 1975		
Ohl (1977)	1979.5	183
Sargent (1977)	1979.5	150
Vitinsky (1976)		82 -152
Sargent, <u>SGD</u> , 1978		152 ± 38
Brown in Schatten et al. (1978)		150 ± 25
Schatten et al. (1978)		140 ± 20
Valtchuk et al. (1978)	1979.6 ± 0.2	180 ± 18
Simon (1978)		235

period of observation of the Wolf numbers (Vitinsky, 1973). Figure 9 gives the observed W values for cycle No. 20; W value averaged over the cycles from No. 8 to No. 20, and the prediction for W in the cycle No. 21 (circles from Solar-Geophys. Data, 1978); solid and dashed lines (Valtchuk and Feldstein (1979)). Crosses correspond to the results of observations at the onset of the growth branch of the cycle No. 21. It can be seen that the prediction for the following year, according to Solar Geophysical Data (1978), is pronouncedly different from our forecast in the second half of 1978. As a rule, all the predictions based on the analytical extension of W sets give W_M^{21} values which are much lower than the prediction based on the certain physical concepts of a relation between the processes in the minimum of solar activity and those in the subsequent maximum.

4. FORECASTING GEOMAGNETIC DISTURBANCE FROM THE WOLF NUMBERS INCLUDING THE EVEN-PARITY OF THE CYCLE

The correlation of geomagnetic disturbance with the general level of solar activity, the existence of the additional aa maximum at the decrease phase of the even-numbered solar cycles (due to recurrent phenomena), and a growth of aa index just in the minima at the ends of even-numbered cycles should be included when forecasting the characteristic geomagnetic activity in the subsequent cycle.

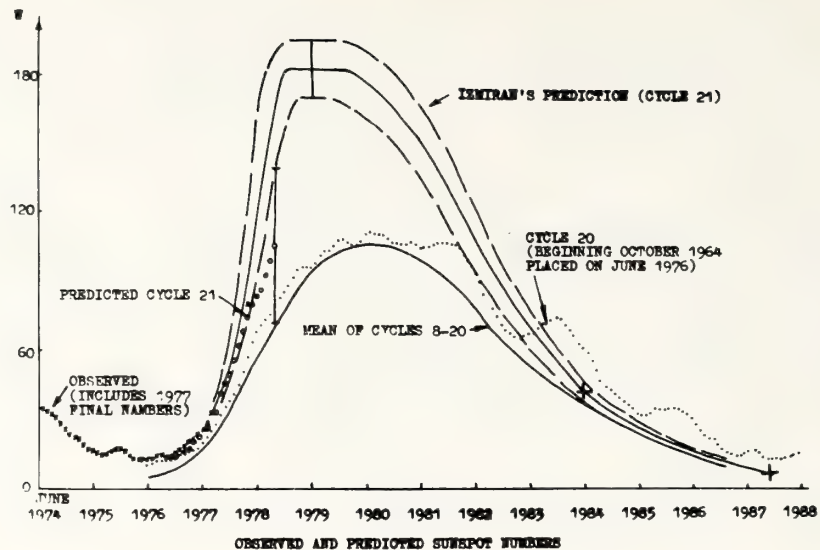


Figure 9. W variations during a cycle of solar activity: solid line corresponds to W averaged over the cycles from No. 8 to No. 20; dotted curve represents cycle No. 20, the onset of which in October, 1964 is superimposed with June, 1976; solid line and two dashed lines represent W forecast of the cycle No. 21 (Valtchuk and Feldstein, 1978) and crosses on the decrease phase W_5 values according to Waldmeier in the book of Vitinsky (1973) and the decrease phase duration; undashed circles correspond to W forecast according to Solar-Geophys. Data (May 1978); crosses are the observed W values on the growth branch in the cycle No. 21.

These factors are used below to predict mean annual aa indices in solar activity cycle No. 21. The predictions of geomagnetic disturbance are based on the Wolf number prediction and on the statistical dependence of aa on W for even- and odd-numbered cycles of solar activity (Figure 4). It was assumed that the dependence of aa on W corresponds to that for the even-numbered cycles in 1976-1977, and it corresponds to the dependence for odd-numbered cycles in 1983-1987. The dependence on even-parity of a cycle vanishes for the years near the solar activity maximum.

Our expected variations of mean annual values of aa index in the cycle No. 21 are presented in Figure 10. At the decrease phase of even-numbered cycles, in contrast to the odd-numbered cycles, it is necessary to include a growth of geomagnetic activity due to the "recurrent" maximum. The more detailed consideration of this problem is outside the scope of the prediction for the solar cycle No. 21.

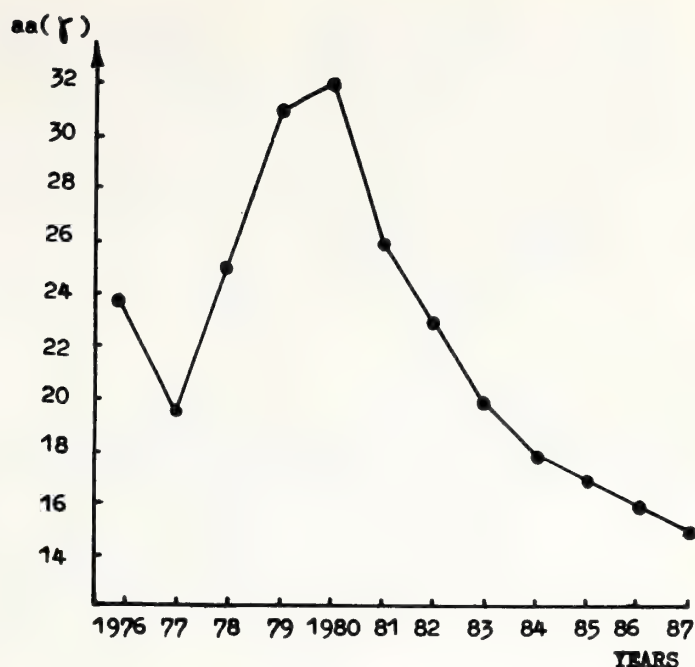


Figure 10. Forecast of aa index variations in the cycle No. 21.

5. REFERENCES

- Besrukova, A. Ya. (1959): Solnechnye Dannye, No. 11, 72-74.
- Bonov, A. D. (1969): Solnechnye Dannye, No. 2, 93-94.
- Bonov, A. D. (1970): Solnechnye Dannye, No. 7, 111-113.
- Dobrovolny, M., and G. Moreno (1976): Space Sci. Rev., 18:685-748.
- Gleissberg, W. (1971): Solar Phys., 21:240-245.
- Henkel, R. (1971): Solar Phys., 20:345-347.
- Howard, R. (1974): Solar Phys., 38:283-299.
- King-Hele, D. J. (1963): Nature, 199:226-227.
- King-Hele, D. J. (1966): Nature, 209:285-286.
- Livshits, M. A., T. E. Valtchuk, and Ya. I. Feldstein (1978): Preprint IZMIRAN, No. 15(214).
- Livshits, M. A., T. E. Valtchuk, and Ya. I. Feldstein (1979): Geomag. and Aeron. (USSR), 19, No. 3.
- Mayaud, P. N. (1973): IAGA Bull., No. 33.
- Mayaud, P. N. (1977a): IAGA Bull., No. 32 g.
- Mayaud, P. N. (1977b): IAGA Bull., No. 39.
- Ohl, A. I. (1977): Solnechnye Dannye, No. 12, 87-89.
- Romanchouk, P. R. (1974): Preprint, Astron. Soc. of Kiev Univ., No. 1.

- Rosenberg, R. L., and P. J. Coleman (1969): J. Geophys. Res., 74(24), 5611-5622.
- Rosenberg, R. L., and P. J. Coleman (1978): Preprint, Inst. of Geophys. and Planetary Phys., March, Publ. No. 1804.
- Russel, C. T., and R. L. McPherron (1973): J. Geophys. Res., 78:92-108.
- Sargent, H. H. (1977): EOS, 58(12):1220.
- Schatten, K. N., P. N. Scherrer, L. Svalgaard, and J. M. Wilcox (1978): Geophys. Res. Lett., 5:411-414.
- Schove, D. J. (1955): J. Geophys. Res., 60:127-146.
- Severny, A. B. (1966): Uspechi Phys. Nauk (USSR), 88:3-50.
- Sheeley, N. R. (1976): J. Geophys. Res., 81(19):3462-3464.
- Simon, P. (1978): private communication, October.
- Smith, E. J., B. T. Tsurutani, and R. L. Rosenberg (1978): J. Geophys. Res., 83, 717-724.
- Solar-Geophysical Data, May 1978, No. 405, Part 1.
- Svalgaard, L. (1976): Interplanetary Sector Structure 1947-1975. SUPR Rpt. No. 648.
- Svalgaard, L., and J. M. Wilcox (1976): Nature, 262(1571):766-768.
- Svalgaard, L. (1977): In: Coronal Holes and High Speed Wind Streams, Ed. J. B. Zirker, Col. Assoc. Univ. Press, p. 371.
- Valtchuk, T. E., and Ya. I. Feldstein (1979): Solnechnye Dannye, No. 2.
- Valtchuk, T. E., M. A. Livshits, and Ya. I. Feldstein (1978): Pis'ma v AJ (USSR), No. 3, 185-189.
- Vassiljev, O. B., Yu. I. Vitinsky, and K. A. Kandaurov (1975): Solnechnye Dannye, No. 10, 55-59.
- Vitinsky, Yu. I. (1973): Cycles and Forecasting of Solar Activity, Nauka, Moscow.
- Vitinsky, Yu. I. (1976): Solnechnye Dannye, No. 11, 59-63.

MODIFICATION OF METHODS OF FORECASTING
MONTHLY AND QUARTERLY WOLF NUMBERS

Yu. I. Vitinsky and B. M. Rubashev
Pulkovo Observatory
Leningrad, U.S.S.R.

Monthly and quarterly Wolf numbers with a forward or backward one-month shift or without any shift are used to forecast monthly and quarterly values 4-6 months in advance. We use here methods proposed earlier by Vitinsky (1973) and show that his techniques give a reliability of prediction with a variance coefficient not greater than 25%. Moreover, the methods generate a forecast that can be improved every month.

The most difficult problem of long-term forecasts of solar activity is prediction of its quarterly and monthly indices. The difficulty is mainly due to fluctuations whose duration are "greater" than 3 months. Although earlier some methods of generating forecasts were elaborated (Vitinsky, 1973) for Wolf numbers, for total sunspot areas, and for solar radio emission flux density, they either were given less than a month in advance or they could be improved only once in 3 months and not every month. For these reasons we began looking for a procedure based on the earlier methods of forecasting quarterly and monthly Wolf numbers which would eliminate the difficulty and permit forecasts to be made for a longer period in advance. Besides, the forecasting formulas (Vitinsky, 1973) were improved using the additional data for solar cycles 19 and 20.

We used Zurich monthly Wolf numbers for 1755-1976 (covering 20 cycles of solar activity) as basic data. Using the data we determined mean Wolf numbers for 3 and 6 months with a month shift. The mean semi-annual values were referred to common* half-years or to so-called specific** half-years (half-years with a 3-month backward shift). All values were marked with superscripts (-1) , (0) and $(+1)$ in accordance with a backward shift, no shift, or a forward shift, respectively--a shift with respect to the middle of a common quarter of a year. As earlier in Vitinsky (1973) we let W_i , W_i' and W_i'' be quarterly, common and specific Wolf numbers respectively. So, in the present paper we use the following values: $W_i^{(-1)}$, $W_i^{(0)}$, $W_i^{(+1)}$; $W_i^{(-1)'}$, $W_i^{(0)'}$, $W_i^{(+1)'}$; $W_i^{(-1)''}$, $W_i^{(0)''}$, $W_i^{(+1)''}$.

*common = semi-annual mean referred to the middle of the half-year.

**specific = 3-month-backward shifted semi-annual mean.

For forecasting smoothed monthly relative sunspot numbers a regression-interpolation method was proposed (Vitinsky, 1973). It uses equations of linear regression between each preceding and following value of the common and specific semi-annular Wolf number (separately for the ascending and descending branch of an 11-year cycle),

$$W_{i+1} = \alpha_i W_i + \beta_i \quad (1)$$

and linear interpolation between the Wolf numbers for the preceding half-year period and that predicted for the following half-year referred to the middle of the half-year. Earlier such equations were obtained only for $W_i^{(o)'}$ and $W_i^{(o)''}$.

Table 1

n	$W_i^{(-1)'}$				$W_i^{(o)'}$				$W_i^{(+1)'}$			
	α_i	β_i	r	σ	α_i	β_i	r	σ	α_i	β_i	r	σ
Ascending Branch												
1					1.48	+ 5	0.62	6	1.19	+ 5	0.56	6
2					1.57	+ 3	0.80	9	1.40	+ 4	0.75	9
3	1.32	+17	0.70	15	1.33	+11	0.78	16	1.45	+11	0.81	14
4	1.39	+ 2	0.89	15	1.26	+18	0.81	31	1.27	+12	0.81	22
5	1.23	- 5	0.90	19	1.09	+ 3	0.95	15	1.01	+13	0.93	16
6	1.04	+24	0.80	10	1.17	+ 8	0.92	20	1.26	0	0.94	18
7	1.20	- 3	0.96	14	1.05	+ 2	0.93	18	0.96	+ 8	0.97	11
8	0.80	+18	0.58	27	1.48	- 7	0.79	20	1.07	+14	0.66	28
Descending Branch												
1	0.86	+ 2	0.96	12	0.84	- 2	0.98	9	0.78	+ 4	0.88	18
2	0.91	+ 4	0.97	10	0.97	+ 4	0.94	14	0.93	+ 7	0.93	15
3	0.86	- 2	0.94	13	0.86	- 2	0.91	16	0.80	+ 4	0.93	13
4	0.86	+ 3	0.90	15	0.88	+ 2	0.93	14	0.93	- 4	0.92	14
5	0.86	0	0.91	14	0.79	+ 4	0.88	15	0.82	+ 2	0.94	10
6	0.77	+ 3	0.87	14	0.77	+ 4	0.86	14	0.71	+ 6	0.87	12
7	0.65	+10	0.84	11	0.65	+ 5	0.92	8	0.81	- 1	0.91	9
8	0.92	- 4	0.92	9	0.99	- 2	0.84	11	0.87	0	0.87	11
9	0.62	+ 5	0.79	11	0.61	+ 4	0.83	9	0.70	+ 5	0.85	10
10	0.84	- 2	0.88	8	0.86	- 1	0.90	7	0.87	- 6	0.91	7
11	0.94	- 3	0.90	7	0.86	- 1	0.91	6	0.70	+ 4	0.89	6
12	0.79	- 1	0.96	4	0.65	+ 1	0.88	6	0.69	0	0.86	6

Tables 1 and 2 give the coefficients α_i and β_i , and corresponding coefficients r and standard deviations σ for all common and specific semi-annual Wolf numbers respectively. n shows a displacement relative to the epoch of minimum and epoch of maximum (in half-years). Gaps in the tables refer to the cases when the value of the correlation coefficient was smaller 0.5. As it follows from Table 1 the equation of

regression for $W_i^{(-1)'}$, $W_i^{(+1)'}$ and $W_i^{(-1)''}$, $W_i^{(+1)''}$ give the same reliability as for $W_i^{(0)'}$ and $W_i^{(0)''}$. Thus, the use of the whole set of common and specific semi-annual Wolf numbers permits to give monthly a forecast of smoothed monthly relative sunspot numbers 4-6 months in advance with a variance coefficient $\pm 5 - 10\%$.

Table 2

n	$W^{(-1)'}$				$W^{(0)''}$				$W^{(+1)''}$			
	α_i	β_i	r	σ	α_i	β_i	r	σ	α_i	β_i	r	σ
Ascending Branch												
1	1.02	+ 4	0.71	3	1.30	+ 5	0.72	4				
2					1.60	- 1	0.89	5	1.07	+ 6	0.71	6
3	1.07	+14	0.53	13	1.82	+ 3	0.86	11	1.82	+ 3	0.82	10
4	1.18	+14	0.73	18	0.79	+32	0.57	24	1.49	+ 8	0.87	15
5	1.31	+ 5	0.90	17	0.80	+28	0.57	34	1.24	+ 7	0.94	14
6	1.01	+12	0.87	22	1.07	+ 9	0.95	15	0.97	+18	0.86	23
7	1.26	-17	0.92	20	1.54	-25	0.89	20	1.36	-13	0.96	14
Descending Branch												
1	0.94	- 8	0.96	12	0.88	-10	0.95	13	0.90	- 8	0.94	14
2	0.88	+ 9	0.93	15	0.99	+ 1	0.97	10	1.02	+ 5	0.95	14
3	0.86	+ 7	0.92	15	0.84	+ 6	0.95	12	0.69	+14	0.77	24
4	0.87	- 3	0.90	16	0.79	+ 7	0.81	20	0.75	+13	0.78	23
5	0.77	+ 7	0.94	10	0.77	+ 3	0.96	8	0.84	0	0.93	12
6	0.85	0	0.88	14	0.86	- 3	0.88	13	0.86	0	0.93	11
7	0.72	+ 5	0.90	10	0.69	+10	0.83	13	0.57	+12	0.82	12
8	0.85	+ 2	0.94	7	0.71	+ 4	0.94	6	0.84	0	0.87	8
9	0.75	+ 1	0.78	13	0.94	- 3	0.85	10	0.77	+ 3	0.84	10
10	0.71	+ 6	0.82	10	0.71	0	0.85	8	0.71	+ 1	0.81	9
11	0.93	- 4	0.89	8	0.91	- 1	0.88	8	0.88	- 1	0.87	6
12	0.85	- 2	0.88	8	0.73	0	0.93	5	0.55	+ 2	0.83	6

Taking into consideration the fact that the mean duration of fluctuations of Wolf numbers is 3 months it is possible to predict accurately enough their quarterly values with a month shift instead of forecasting non-smoothed monthly Wolf numbers. In this connection it would be very convenient to use the method (Vitinsky, 1973) of forecasting relative quarterly sunspot numbers 2 quarters of a year in advance. It consists in using the combination of the predicted by different methods common and specific semi-annual and quarterly Wolf numbers for obtaining the predicted values by the formulas

$$\left. \begin{aligned} W_I &= 2 W_I'' - W_{IV}, W_{II} = 2 W_I' - W_I, \\ W_{III} &= 2 W_{II}'' - W_{II}, W_{IV} = 2 W_{II}' - W_{III} \end{aligned} \right\} \quad (2)$$

or predicted common or specific semi-annual or observed quarterly Wolf numbers by the formulas

$$\left. \begin{aligned} W_I &= 2 W_I'' - 2 W_{II}' + W_{III}^o, & W_{II} &= 2 W_I' - 2 W_I'' + W_{IV}^o, \\ W_{III} &= 2 W_{II}'' - 2 W_I' + W_I^o, & W_{IV} &= 2 W_{II}' - 2 W_{II}'' + W_{II}^o. \end{aligned} \right\} (3)$$

The Roman numerals of the lower indices show the quarters and half-years while the upper index "O" the observed values. For a forecast of semi-annual and quarterly Wolf numbers it is most expedient to use the methods of regression and Mayot (Vitinsky, 1973). The former permits to take into account general peculiarities of cycle curves for various 11-year solar cycles, the latter permits to determine the shape of a current 11-year solar cycle. It can be noted, however, that the modified Mayot method cannot be used in the form it was originally proposed because the peculiarities of the cycle curves for long solar cycles haven't been sufficiently studied.

Applying the method of regression to common and specific semi-annual Wolf numbers formula (1) is used with the coefficients α_i and β_i (Tables 1 and 2). For forecasting relative quarterly sunspot numbers the coefficients α_i and β_i (formula 1) and corresponding correlation coefficients r and standard deviations σ are given in Tables 3 and 4 (similar to Tables 1 and 2) for the ascending and descending branches of the 11-year cycle respectively.

Table 3

n	$W_i^{(-1)}$				$W_i^{(0)}$				$W_i^{(+1)}$			
	α_i	β_i	r	σ	α_i	β_i	r	σ	α_i	β_i	r	σ
1	1.00	+ 3	0.63	3					1.24	+ 3	0.57	4
2					1.36	+ 2	0.71	6	0.99	+ 3	0.57	8
3	0.63	+ 6	0.56	6	0.55	+ 6	0.73	5	0.54	+ 5	0.61	7
4					1.13	+ 1	0.64	9	0.84	+ 8	0.68	7
5	1.28	+ 4	0.87	7	1.36	+ 2	0.91	8	1.51	- 2	0.87	9
6	1.11	+ 1	0.81	11	1.11	+ 7	0.86	12	1.02	+11	0.88	10
7	1.03	+17	0.79	15	1.04	+12	0.82	17	1.24	+ 2	0.87	14
8	1.20	- 1	0.95	10	1.09	+ 4	0.93	13	0.99	+ 7	0.88	16
9	1.05	+14	0.88	17	1.04	+12	0.94	13	1.18	+ 9	0.88	21
10	1.12	+ 1	0.94	15	1.13	- 3	0.93	17	0.81	+16	0.82	24
11	0.99	+ 3	0.97	11	0.98	+ 5	0.94	17	0.93	+ 7	0.87	23
12	1.09	+ 5	0.93	17	1.18	+ 5	0.95	14	1.01	+19	0.78	31
13	1.00	+12	0.81	28	1.12	- 6	0.97	13	1.11	+ 3	0.94	19
14	1.24	- 9	0.91	25	1.15	0	0.97	13	0.96	+ 3	0.96	14
15	1.03	+ 7	0.87	16	0.96	+ 3	0.92	11	1.25	- 9	0.92	10
16	1.35	-11	0.86	20	1.09	+13	0.85	16	1.21	+ 1	0.76	26

For the Mayot method the following equations and their standard deviations σ and variance coefficients $\sigma^2/W \cdot 100\%$ were

Table 4

n	$W_i^{(-1)}$				$W_i^{(0)}$				$W_i^{(+1)}$			
	α_i	β_i	r	σ	α_i	β_i	r	σ	α_i	β_i	r	σ
1	0.86	- 5	0.95	14	0.93	-14	0.99	6	0.93	- 8	0.97	11
2	0.91	+ 1	0.92	18	0.90	- 1	0.99	6	0.77	+10	0.90	17
3	0.76	+26	0.85	21	0.98	+ 5	0.93	15	1.07	- 2	0.92	17
4	0.92	+ 7	0.90	18	0.92	+ 5	0.85	20	0.87	+15	0.89	20
5	0.94	0	0.86	22	0.74	+25	0.83	19	0.82	+12	0.95	12
6	0.70	+18	0.88	17	0.74	+14	0.77	23	0.82	+ 7	0.88	17
7	1.02	- 8	0.92	15	0.93	+ 2	0.92	14	0.82	+11	0.73	27
8	0.86	+ 6	0.90	16	0.86	+ 7	0.95	10	0.73	+14	0.76	24
9	0.84	+10	0.92	13	0.86	+ 1	0.92	11	0.86	+ 7	0.93	13
10	0.94	- 3	0.90	15	0.84	+ 7	0.83	18	0.82	+ 2	0.92	12
11	0.86	+ 7	0.92	13	0.82	+ 7	0.87	15	0.79	+15	0.74	22
12	0.92	- 1	0.93	12	0.85	+ 4	0.88	14	0.69	+ 8	0.82	16
13	0.79	+ 4	0.93	10	0.71	+ 8	0.82	15	0.75	+ 8	0.84	13
14	0.71	+ 5	0.91	8	0.66	+ 9	0.80	12	0.80	+ 5	0.87	11
15	0.88	+ 2	0.87	11	0.71	+ 6	0.81	11	0.74	+ 5	0.89	9
16	0.83	+ 6	0.78	15	0.97	+ 3	0.72	17	1.15	- 5	0.90	10
17	0.85	+ 4	0.92	9	0.76	+ 5	0.84	12	0.80	+ 4	0.86	11
18	0.87	+ 2	0.90	9	0.69	+ 7	0.84	10	0.77	+ 6	0.87	10
19	0.64	+ 2	0.84	9	0.71	0	0.95	5	0.74	+ 3	0.80	11
20	0.87	+ 2	0.79	9	1.02	- 2	0.93	6	0.62	+ 4	0.72	12
21	0.77	+ 5	0.81	9	0.93	0	0.89	8	0.97	0	0.93	6
22	0.84	0	0.89	8	0.80	+ 2	0.87	8	0.89	0	0.91	7
23	0.96	+ 1	0.88	9	0.84	0	0.88	7	0.57	+ 6	0.71	9
24	0.74	0	0.92	6	0.69	+ 1	0.78	8	0.88	- 2	0.83	8
25	0.90	+ 1	0.90	6	0.67	+ 4	0.74	8	0.57	+ 4	0.82	6

were derived on the basis of the data on the semi-annual and quarterly Wolf numbers for 1945-1976 and 1955-1976 respectively

$$\left. \begin{aligned} W_i^{(-1)'} &= 0.70 W_{i-1}^{(-1)'} + 0.28 W_{i-2}^{(-1)'} + 0.09 W_{i-3}^{(-1)'} + 0.01 W_{i-4}^{(-1)'} - 0.31 W_{i-5}^{(-1)'} \\ \sigma &= 20, \sigma/\bar{W} \cdot 100\% = 23\% \\ W_i^{(0)'} &= 0.70 W_{i-1}^{(0)'} + 0.22 W_{i-2}^{(0)'} + 0.17 W_{i-3}^{(0)'} + 0.13 W_{i-4}^{(0)'} - 0.24 W_{i-5}^{(0)'} \\ \sigma &= 17, \sigma/\bar{W} \cdot 100\% = 21\% \end{aligned} \right\} (4)$$

$$\left. \begin{aligned} W_i^{(+1)'} &= 0.88 W_{i-1}^{(+1)'} + 0.13 W_{i-2}^{(+1)'} + 0.02 W_{i-3}^{(+1)'} + 0.06 W_{i-4}^{(+1)'} - 0.29 W_{i-5}^{(+1)'} \\ \sigma &= 16, \sigma/\bar{W} \cdot 100\% = 19\% ; \\ W_i^{(-1)''} &= 0.83 W_{i-1}^{(-1)''} + 0.22 W_{i-2}^{(-1)''} + 0.06 W_{i-3}^{(-1)''} - 0.28 W_{i-4}^{(-1)''} - 0.04 W_{i-5}^{(-1)''} \\ \sigma &= 18, \sigma/\bar{W} \cdot 100\% = 21\% \\ W_i^{(0)''} &= 0.65 W_{i-1}^{(0)''} + 0.41 W_{i-2}^{(0)''} - 0.03 W_{i-3}^{(0)''} - 0.02 W_{i-4}^{(0)''} - 0.24 W_{i-5}^{(0)''} \\ \sigma &= 21, \sigma/\bar{W} \cdot 100\% = 24\% \end{aligned} \right\} (5)$$

$$\left. \begin{aligned} W_i^{(+1)''} &= 0.75 W_{i-1}^{(+1)''} + 0.18 W_{i-2}^{(+1)''} + 0.03 W_{i-3}^{(+1)''} + 0.20 W_{i-4}^{(+1)''} - 0.40 W_{i-5}^{(+1)''} \\ \sigma &= 20, \sigma/\bar{W} \cdot 100\% = 24\% ; \end{aligned} \right\}$$

$$\left. \begin{aligned} W_i^{(-1)} &= 0.84 W_{i-1}^{(-1)} + 0.10 W_{i-2}^{(-1)} + 0.03 W_{i-3}^{(-1)} + 0.23 W_{i-4}^{(-1)} - 0.28 W_{i-5}^{(-1)} \\ W_i^{(0)} &= 0.79 W_{i-1}^{(0)} + 0.10 W_{i-2}^{(0)} + 0.10 W_{i-3}^{(0)} + 0.23 W_{i-4}^{(0)} - 0.29 W_{i-5}^{(0)} \\ W_i^{(+1)} &= 0.96 W_{i-1}^{(+1)} - 0.19 W_{i-2}^{(+1)} + 0.38 W_{i-3}^{(+1)} + 0.02 W_{i-4}^{(+1)} - 0.23 W_{i-5}^{(+1)} \end{aligned} \right\} \begin{aligned} \sigma &= 8, \sigma/\bar{W} \cdot 100\% = 9\% \\ \sigma &= 8, \sigma/\bar{W} \cdot 100\% = 10\% \\ \sigma &= 8, \sigma/\bar{W} \cdot 100\% = 10\% \end{aligned} \quad (6)$$

As is seen from Tables 3 and 4 and formulas (4)-(6) modification of the method of a forecast of quarterly Wolf numbers 2 quarters of a year in advance (Vitinsky, 1973) provides for a satisfactory reliability with the coefficient of variance 20-25%.

While the combination of the two methods of forecasting takes better into account peculiarities of 11-year and long-term variations of Wolf numbers it can be applied to prediction of the non-smoothed monthly Wolf numbers with a variance coefficient 20-25% using quarterly values $W_i^{(-1)}$, $W_i^{(0)}$, $W_i^{(+1)}$.

In conclusion it should be noted that a reliable verification of the described procedure of forecasting monthly and quarterly relative sunspot numbers on the basis of the methods of estimation of the reliability of predictions of solar activity (Vitinsky, Rubashev, 1978) can be only made after the development of the current 11-year solar cycle, including its descending branch. The values given in the paper are based only on the epignosis and comparison of the recent results with those published earlier (Vitinsky, 1973; Vitinsky, Rubashev, 1978).

REFERENCES

- Yu.I. Vitinsky (1973): Tsiklichnost i Prognozy Solnechnoj Aktivnosti. Izd. "Nauka", Leningrad.
 Vitinsky, Yu.I., and Rubashev, B.M. (1978): The Evaluation of the Reliability of Solar Activity Forecasts. Izvestia Glavnoj Astronomicheskoy Observatorii Acad. Nauk U.S.S.R. No. 196, p. 3.

PREDICTION OF THE RADIO EMISSION INDICES OF THE SUN IN THE

FREQUENCY RANGE $1000 \leq F \leq 3750$ MHz

J. N. XANTHAKIS and C. POULAKOS

Research Center for Astronomy and Applied Mathematics

Academy of Athens

14, Anagnostopoulou Street, Athens (136), Greece

Predicted mean annual and mean monthly values of the solar radiation flux at different wavelengths for the 21st solar cycle are presented. The forecast is derived from analytical relations between the relative sunspot numbers, R , and the radio-emission of the sun in the frequency range $1000 \text{ MHz} \leq F \leq 3750 \text{ MHz}$. Two samples of predicted values of the Zürich relative sunspot numbers for the 21st solar cycle are used in this paper. The first is derived with the help of analytical relations between the Zürich relative sunspot numbers and the time of rise, T_R , while the second one is derived from a regression analysis of the cycles $N = 8$ to $N = 20$. The relationship between the Zürich numbers, R , and the radio flux densities at 2800 MHz and 3750 MHz-on a daily basis investigation- is briefly discussed.

1. INTRODUCTION

The effects which solar activity has on the various layers of the earth's atmosphere play an important role in our daily life. For the comparison of solar activity with the different phenomena of the chromosphere, the interplanetary space and particularly the ionosphere, solar activity has been expressed, as a rule, with the help of the Zürich relative sunspot numbers, R . Investigations carried out at the Research Center for Astronomy, Academy of Athens, showed that there is a definite statistical correlation between the Zürich numbers, R , and the solar radio flux in the frequencies 3750 MHz, 2800 MHz, 2000 MHz, 1500 MHz and 1000 MHz (hereafter referred to as F_{3750} , F_{2800} , F_{2000} , F_{1500} , and F_{1000} correspondingly). On the average, this correlation was found equal to $r = 0.98$. The aim of the present investigation is to find out a relation between the Zürich relative sunspot numbers, R , and the solar radio flux at different wavelengths and by using the predicted values of the Zürich numbers to make predictions, as accurate as possible, of the radio frequencies that will be required one or two months or years ahead.

These predictions of the radio-fluxes will, probably, provide advance information months ahead on the probable month-to-month changes in ionospheric characteristics.

2. BASIC EQUATIONS GOVERNING THE PREDICTION OF THE WOLF NUMBERS

Before taking up the main subject we considered that it would be interesting to give the basic equations with which one can predict the mean yearly as well as the highest and the lowest mean monthly values of the Zürich relative sunspot numbers, R , for the present cycle. These predictions are needed since the present forecast of the radio fluxes for the 21st solar cycle is based on the predicted values of R , for the

same cycle.

The studies of Xanthakis (1966 , 1967a) have shown that the mean annual values of the main indices of solar activity such as the areas of the whole sunspots, the faculae, etc. can be satisfactorily represented as functions of the time of rise, T_R , and certain supplementary periodic terms. However, in the case of the relative sunspot numbers, R , and particularly in the case of the 21st cycle if we represent by R_m the mean annual values of , R , during the sunspot maximum and by , T_R the time of rise, then the relationship giving the values of , R_m , is of the form

$$R_m = C + 2 T_o (T_o - T_R)^2 \quad (1)$$

where $C = 66.4$ $T_o = 5.76$ and $T_R = 3.2$ years.

The variation of the mean annual values of R , within the 21st sunspot cycle can be represented by the relation

$$R = R_m \cos^2 \frac{\pi}{2\Omega_{1,2}} t + G_{1,2}(t) \quad t = 0, 1, 2, 3, \dots \quad (2)$$

where $\Omega_1 = T_R$ for the years preceding the sunspot maximum and $\Omega_2 = 11 - T_R$ for the years following the sunspot maximum. Parameter, t , assumes the values $t = 0$ for the year of maximum solar activity and the values $t = 1, 2, 3, \dots$ for the first, second , third ... year preceding (ascending branch) or following (descending branch) the year of maximum. $G_{1,2}(t)$ are periodic terms of the form

$$G_1(t) = 2T_o \sin \frac{\pi}{4} t \cos N\pi \quad (\text{ascending branch}) \quad (3)$$

where $N=21$

$$G_2(t) = - 2T_o \sin \frac{\pi}{4} t \quad (\text{descending branch}) \quad (4)$$

Two additional indices i.e the highest, R_{\max} , and the lowest, R_{\min} , of the monthly relative sunspot numbers during the year of sunspot maximum can also be satisfactorily represented as functions of , T_R , with the help of the relations

$$R_{\max} = a^2 + 2T_1(T_1 - T_R)^2 + 4 T_1 \sin \left[\left(N - \frac{a}{2}\right) \frac{2\pi}{8} \right] \quad (5)$$

$$R_{\min} = T_1^2 + (T_1 + 1) \cdot (T_1 - T_R)^2 \quad (6)$$

$$\text{where } a = 9, \quad T_1 = 6.3 \quad \text{and} \quad N = 21$$

As in the case of the mean yearly values of , R , if we represent by R_{\max}^y and by R_{\min}^y the variation of the highest and the lowest values of the monthly relative sunspot numbers within the cycle $N = 21$ then the relations giving these quantities are of the form

$$R_{\max}^y = R_{\max} \cos^2 \frac{\pi}{2T_R} t + G_1(t) \quad t = 0, 1, 2, 3, \dots$$

$$G_1(t) = 3 T_1 \cos N\pi \sin \frac{\pi}{4} t \quad \text{ascending branch} \quad (7)$$

$$R_{\max}^y = R_{\max} \cos^2 \frac{\pi}{2(11-T_R)} t + G_2(t) \quad t = 0, 1, 2, 3, \dots$$

$$\text{descending branch} \quad (8)$$

$$G_2(t) = -3 T_1 \sin \frac{\pi}{4} t$$

$$R_{\min}^y = R_{\min} \cos^2 \frac{\pi}{2T_R} t + g_1(t) \quad t = 0, 1, 2, 3, \dots$$

$$\text{ascending branch} \quad (9)$$

$$g_1(t) = -T_1 \sin \frac{\pi}{4} t$$

$$R_{\min}^y = R_{\min} \cos^2 \frac{\pi}{2(11-T_R)} t + g_2(t) \quad t = 0, 1, 2, 3, \dots$$

$$\text{descending branch} \quad (10)$$

$$g_2(t) = -2 T_1 \sin \frac{\pi}{6} t$$

It should be noted, however, that although the predictions for the 20th cycle given by Xanthakis (1966), which was derived with the help of equations 1 to 10 and that published in Solar Geophysical Data (Coffey, 1969) (SGD), which was derived from a regression analysis of the cycles $N = 8$ to $N = 19$, were very similar and with an accuracy of about 82% their predictions for the current cycle $N = 21$ differ significantly (Xanthakis and Poulakos, 1978 ; Coffey, 1978). This discrepancy is due to the different values of the time of rise, T_R , used by SGD and by Xanthakis. In fact, Xanthakis (1967b) found that the value of T_R , for the current cycle $N = 21$ will be $T_R = 4.6$ years based on the hypothesis that the curve

representing the variation of the parameter, T_R , reaches its lowest value during the odd cycle $N = 19$. Therefore, the next odd cycle i.e. $N = 21$ ought to lie on the ascending phase of the curve. But it is equally possible, however, that the lowest point of the descending phase of the variation of the parameter T_R not to lie in cycle $N = 19$ but in cycle $N = 21$ and in this case, must have a value of $T_R < 3.3$ years. Thus, from the variation of T_R it is concluded that the time of rise for cycle $N = 21$ can be either $T_R = 3.2$ years or $T_R = 4.6$ years. In the present investigation, if instead of $T_R = 4.6$ years we put in relations 1 to 4 the value $T_R = 3.2$, given by the relevant curve of the SGD'S prediction (Coffey, 1978) then both the SGD prediction and our prediction for the mean annual values of the Zürich numbers, R , for the cycle $N = 21$ appear to be very similar. This is shown in Figure 1 where the small circles represent the SGD prediction while the crosses connected with dashes represent our prediction.

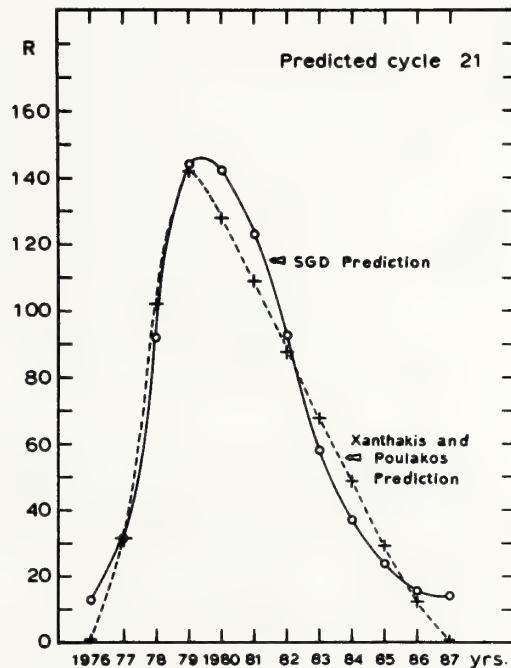


FIGURE 1. PREDICTED MEAN ANNUAL VALUES OF THE WOLF NUMBERS, R , CORRESPONDING TO $T_R = 3.2$. THE SMALL CIRCLES REPRESENT THE PREDICTION GIVEN BY SGD AND THE CROSSES REPRESENT THE VALUES, R , COMPUTED WITH THE HELP OF EQUATIONS (1) TO (4).

3. THE RELATION BETWEEN THE ZURICH RELATIVE SUNSPOT NUMBERS , R , AND THE RADIO EMISSION OF THE SUN , F .

3.1. Correlation Coefficients Between R and F.

The existence of a relationship between the Zürich numbers or the sunspot area and the radio flux values at different wavelengths has been known for a long time (Allen, 1957 ; Covington and Harvey 1960 ; Das Gupta and Basu, 1964; Castelli et al, 1965 ; Covington, 1976). In particular, for the radio emission index F_{2800} , Covington and Harvey (1960) found on a daily basis investigation (154 days - radio data during the year 1952) - that the total flux from the solar disk, F , can be expressed with the help of the equation.

$$F = F_0 + Nf_0 + KA + Mf'_0 \quad (11)$$

where $Nf_0 + KA$ is the flux from N regions with associated sunspot area, f_0 is the area - independent flux contribution of an individual region, F_0 represents the basic disk component and A is the sum of the sunspot areas of the N regions. The flux from M regions which have no associated sunspot area represented by Mf'_0 , where f'_0 is the flux contribution of an individual region. Equation (11) is proposed by Covington and Harvey to be used on a daily basis, while for the mean annual values of the flux they proposed equation (12).

$$F = cg + KA + F_0 \quad (12)$$

where g is the annual mean of sunspot groups, A is the annual mean of sunspot area, F_0 is the annual quiet solar flux, K is the flux per unit sunspot area, and C is the area - independent flux from a single radio region.

No doubt, that both equations (11) and (12) are very interesting and useful for the determination of the radio flux. In practice, equations (11) and (12) cannot be used for prediction for the simple reason that, up to now, no method predicting the sunspot area months or years ahead

exists. In the present investigation we preferred to use the Zürich relative sunspot numbers instead of the sunspot area because the former can be predicted, with a very high approximation, months or years ahead. To this end we calculated the correlation coefficient between the observed mean monthly as well as the observed mean yearly values of R , and the corresponding values of the radio emission indices F_{3750} , F_{2800} , F_{2000} , F_{1500} and F_{1000} for the sunspot cycles for which observational data were available i.e. for cycles $N = 18$ to $N = 20$. The numerical results are shown in Table 1. From the calculations we concluded that the radio emission indices, F , can be expressed as a linear function of the Zürich numbers of the form:

$$F = C + KR \quad (13)$$

where C and K are constants calculated with the help of the least square method. In order to obtain the relation corresponding to each of the radio emission indices F_{3750} to F_{1000} , one should replace the constants, C , and K , with the values given in Table 1. Equation 13 represents the observational values of the quantities F_{3750} , F_{2800} , ..., F_{1000} with a very satisfactory approximation. The accuracy was calculated with the help of the formula $\left(1 - \frac{\epsilon}{F_i}\right) 100\%$. On the average the mean accuracy was found equal to 94% and 91% for the mean annual and the mean monthly values of the radio indices correspondingly. Details for the numerical results for the individual frequencies are tabulated in Table 1.

3.2 The Prediction of Solar Radio Fluxes in the Frequency Range $1000 \text{ MHz} \leq F \leq 3750 \text{ MHz}$

3.2.1 Long - Range Forecast

Using the predicted mean monthly values of the numbers, R , published in SGD (Coffey, 1978) we determined their average annual values for the years 1976-1987. By applying these values of the Zürich numbers to the

T A B L E 1

RELATION BETWEEN THE RELATIVE SUNSPOT NUMBERS AND THE RADIO FLUXES IN THE FREQUENCIES 1000 MHz to 3750 MHz

ANNUAL VALUES				MONTHLY VALUES			
Frequencies (F)	Correlation Coefficient	Equation	Accuracy %	Correlation Coefficient	Equation	Accuracy %	
	$r_{R,F}$			$r_{R,F}$			
1000 MHz	0.96	$F^{pred} = 33.60 + 0.50 R$	92.0	0.95	$F^{pred} = 33.60 + 0.50 R$	89.5	
1500 MHz	0.96	$F^{pred} = 42.28 + 0.75 R$	90.0	0.92	$F^{pred} = 44.66 + 0.71 R$	86.6	
2000 MHz	0.99	$F^{pred} = 41.36 + 0.72 R$	93.4	0.98	$F^{pred} = 44.20 + 0.68 R$	91.7	
2800 MHz	0.99	$F^{pred} = 57.86 + 0.92 R$	95.7	0.98	$F^{pred} = 59.61 + 0.90 R$	91.7	
3750 MHz	1.00	$F^{pred} = 67.51 + 0.85 R$	96.9	0.99	$F^{pred} = 69.18 + 0.83 R$	94.0	

corresponding equations given in Table 1, we calculated the corresponding mean annual values of the radio fluxes. The results are shown in Figures 2 and 3.

2.2.2 Medium - Period Forecast

It is well known that medium - period forecast of solar activity refers to forecast of the monthly and quarterly values of solar indices. Although the equations listed in Table 1 for the prediction of the monthly values are also valid for the quarterly values of the radio fluxes of the sun and the accuracy is about 2 - 3% higher than the accuracy for the mean monthly values, the following discussion will be limited to the prediction only of the monthly values of the radio fluxes in the frequency range $1000 \text{ MHz} \leq F \leq 3750 \text{ MHz}$.

Two samples of predicted values of the wolf numbers , R , were used in the present forecast. The first which was derived from a regression analysis of the cycles $N = 8$ to $N = 20$ was published in SGD (Coffey, 1978). The second sample was derived by means of equations 5 to 10. However, it is well known that the mean monthly relative sunspot numbers present large and anomalous fluctuations during each year. Because of this, the prediction of these numbers is quite difficult, and when fluctuating solar activity is involved, the forecast values usually have considerable error. If we now take into consideration that our proposed equations for forecasting the mean monthly values of the radio fluxes are expressed as functions of the numbers , R , then, our prediction suffers from these errors.

Figures 4 and 5 represent the predicted mean monthly values of the radio - emission indices for the cycle $N = 21$. Our computations were based on the predicted values of R , published in SGD (Coffey, 1978). The up to now published mean monthly values of the radio fluxes in the frequency 2800 MHz, observed during the period January 1976 - June 1978, are represented in Figure 4 by the dashed line.

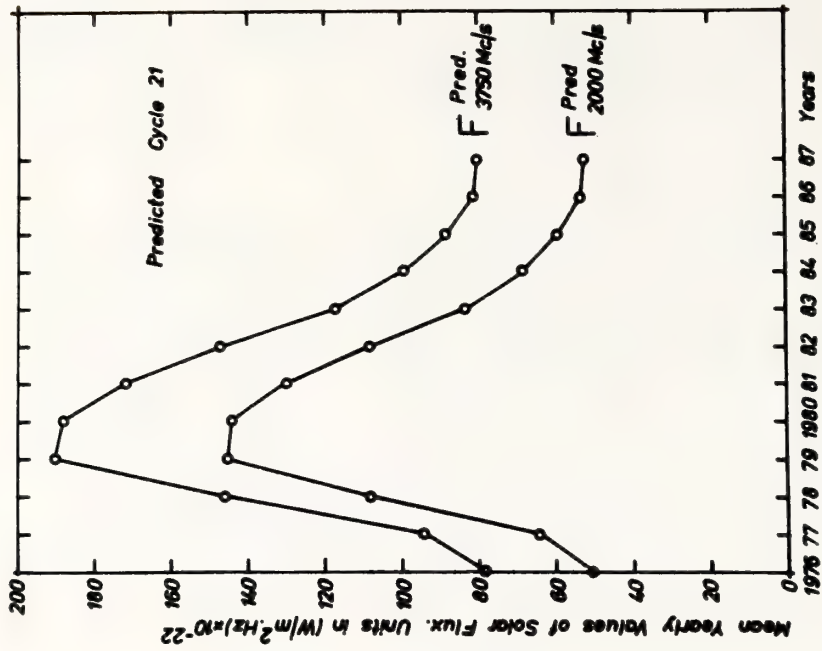


FIGURE 2

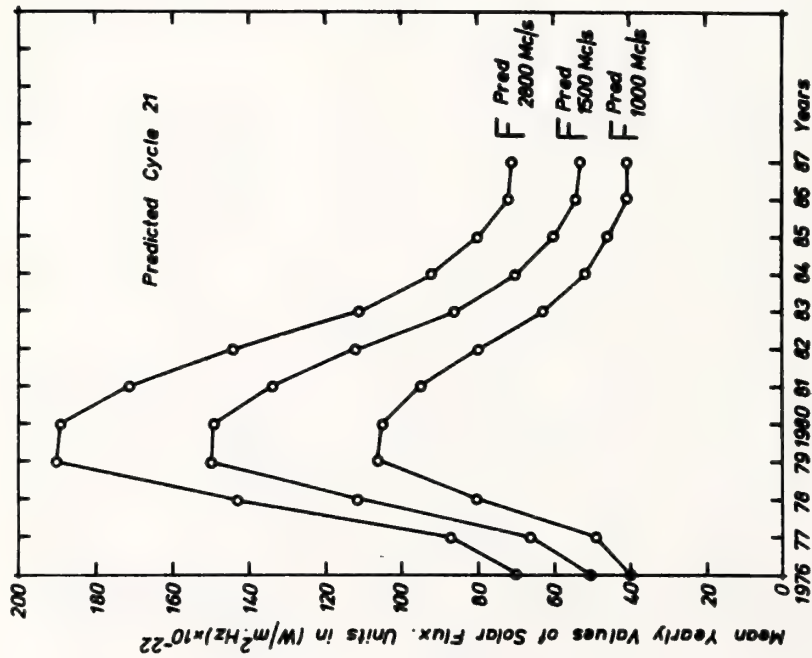


FIGURE 3

FIGURE 2, 3 : PREDICTED VALUES OF THE MEAN ANNUAL RADIO FLUXES IN THE FREQUENCY RANGE $1000 \text{ MHz} \leq F \leq 3750 \text{ Mc/s}$ FOR THE SUCCESSIVE YEARS OF THE CYCLE $N=21$

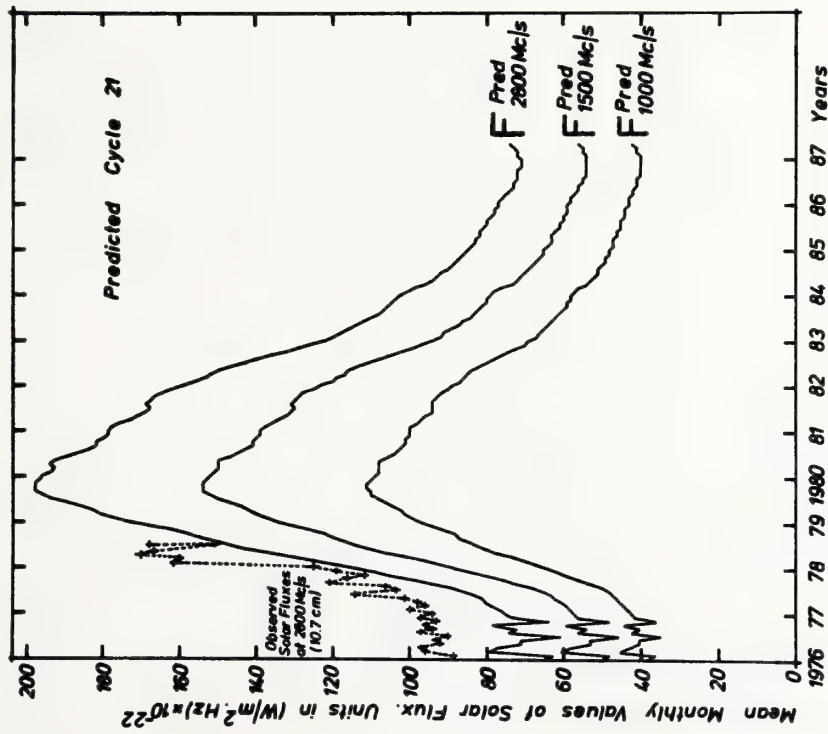


FIGURE 4

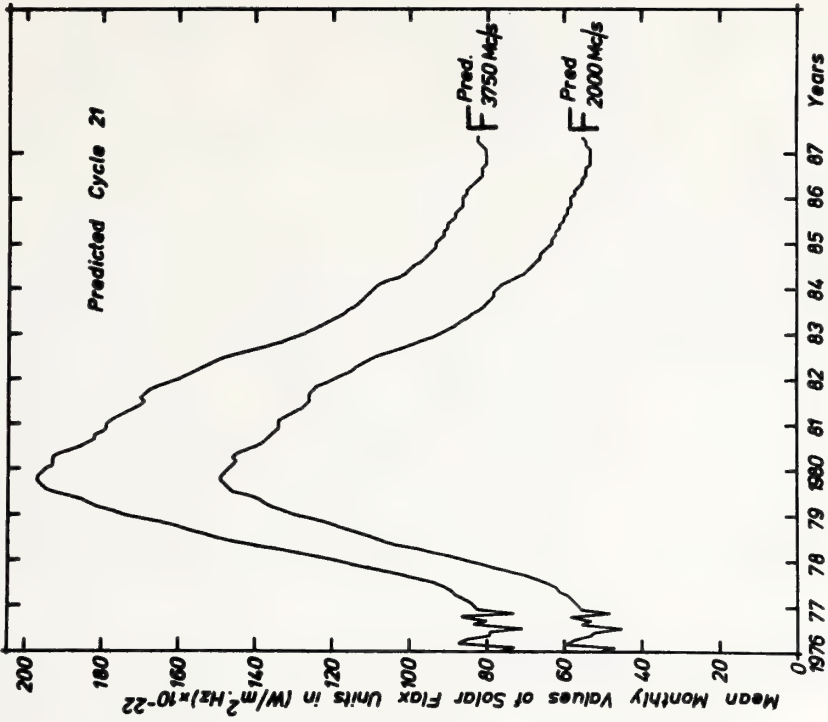


FIGURE 5

FIGURE 4, 5 : PREDICTED VALUES OF THE MEAN MONTHLY RADIO FLUXES IN THE FREQUENCY RANGE 1000 MHz \leq \leq 3750 MHz BASED ON THE PREDICTED VALUES OF THE WOLF NUMBERS GIVEN BY SG D.
THE OBSERVATIONAL DATA IN FIGURE 4 ARE REPRESENTED BY THE DASHED LINE.

There is a slight discrepancy between the observed and computed values of F_{2800} but no doubt both curves in this figure show considerable similarity. According to SGD' prediction of the numbers, R , the epoch of maximum of solar activity will be in the middle of the year 1979 i.e the time of rise is equal to $T_R = 3.2$. Assuming that $T_R = 3.2$ years and based upon our predicted values of the highest and the lowest monthly values of the Zürich relative sunspot numbers, R , we predicted the corresponding highest and lowest mean monthly values of the radio fluxes for cycle $N = 21$. The results of our calculations are shown in Figures 6 to 9. Since it is not possible to predict the exact month of each year during which the values of maximum and minimum will occur, these values have been plotted in these figures for the middle of the corresponding year.

In order to complete the above discussion we should mention that if we use the value of the time of rise $T_R = 4.6$ instead of $T_R = 3.2$ for the calculation of the quantities R_{\max}^y and R_{\min}^y (see equs. 5 and 6) then the predicted highest and lowest values of the radio fluxes during the year of sunspot maximum i.e. for the year 1980 will change as follows:

$F_{1000}^{\max} = 97$, $F_{1500}^{\max} = 138$, $F_{2000}^{\max} = 133$, $F_{2800}^{\max} = 175$ and $F_{3750}^{\max} = 176$ for the highest and $F_{1000}^{\min} = 64$, $F_{1500}^{\min} = 88$, $F_{2000}^{\min} = 85$, $F_{2800}^{\min} = 114$ and $F_{3750}^{\min} = 119$ for the lowest values. All values are in units of $W.m^{-2}.Hz^{-1}.10^{-22}$

4. HOW VALUABLE ARE THE PROPOSED EQUATIONS FOR PREDICTION?

The proposed equations, listed in Table 1, represent the observed mean annual and mean monthly values of the radio fluxes with an accuracy of 94% and 91% respectively. They are highly significant equations. They have also the advantage that they are suitable, probably, for daily predictions provided that the daily value of R is known. The high correlation between the ionospheric parameter f_{F_2} (Monthly median noon critical frequency of the F_2 layer) and the index F_{2800} (10.7cm) argues the use of the predicted values of F_{2800}^{pred} for ionospheric prediction.

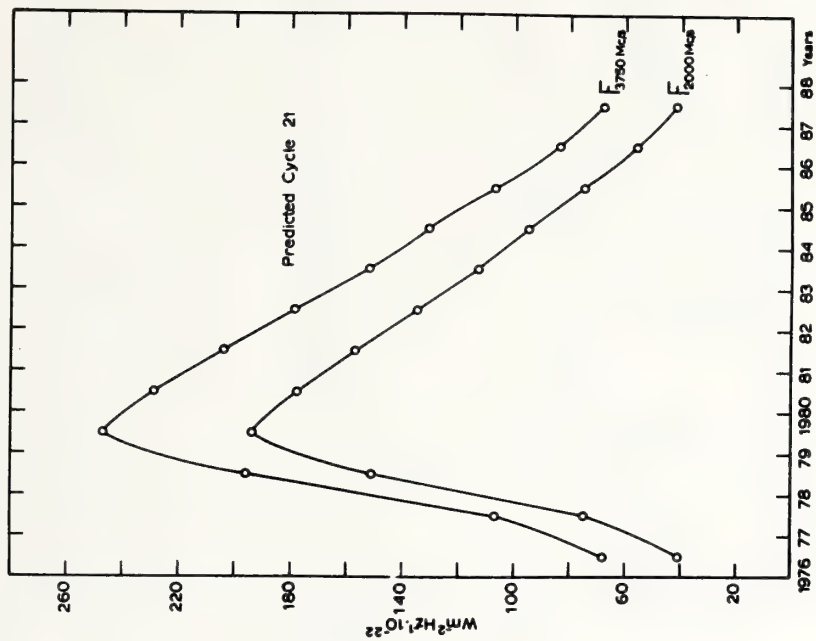


FIGURE 7

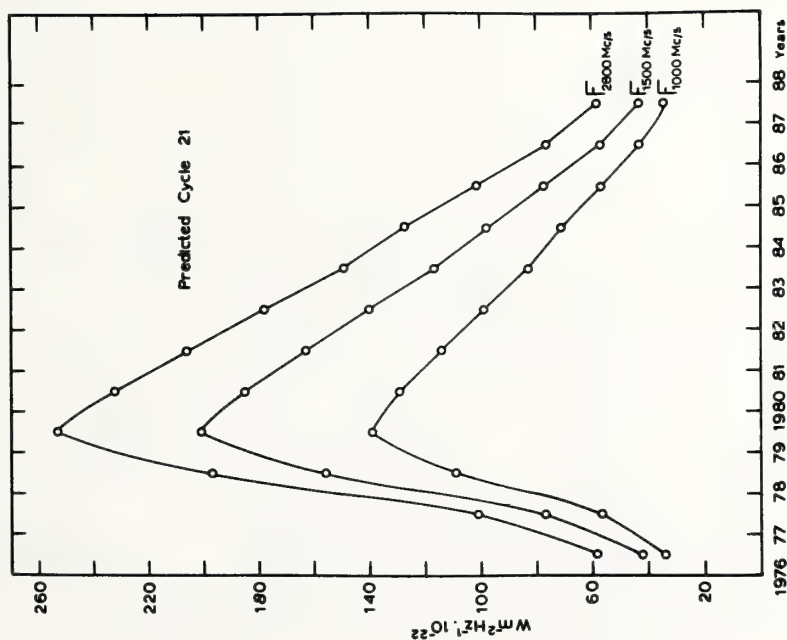


FIGURE 6

FIGURE 6 , 7 : PREDICTED VALUES OF THE HIGHEST MEAN MONTHLY RADIO FLUXES IN THE FREQUENCY RANGE $1000 \text{ MHz} \leq f \leq 3750 \text{ MHz}$. ALL VALUES ARE PLOTTED FOR THE MIDDLE OF THE CORRESPONDING YEAR

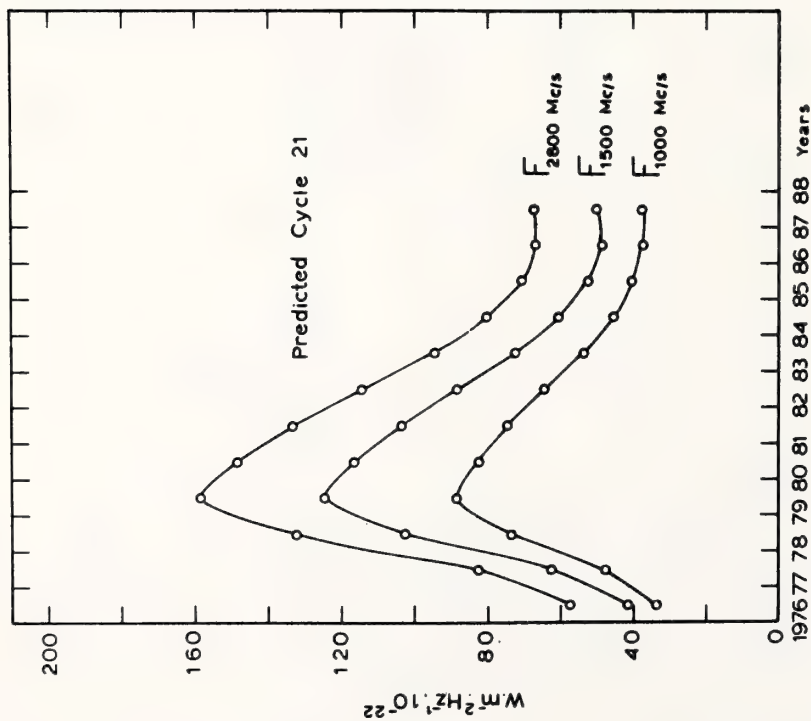


FIGURE 8

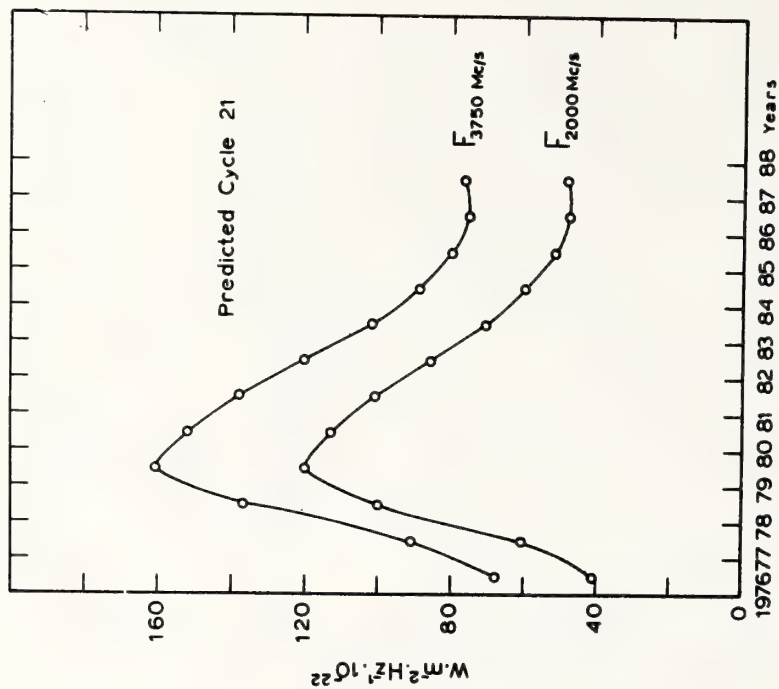


FIGURE 9

FIGURE 8 , 9 : PREDICTED VALUES OF THE LOWEST RADIO FLUXES IN THE FREQUENCY RANGE 1000 MHz $\leq F \leq$ 3750 MHz. ALL VALUES ARE PLOTTED FOR THE MIDDLE OF THE CORRESPONDING YEAR .

A comparison of the mean yearly values of the 2800 MC/S radio flux density, obtained with the help of the equations : a) (12) , given by Covington and Harvey (1960) in which the values F_0 are those determined by Allen (1957) ; b) (13) , given in the present paper and c) the equation proposed by Euler et al (1978) for the period 1948 - 1954, included, shows that they are not significantly different from each other. However, the standard deviation (s.d) values between the observed and computed values of the 10.7cm flux, computed by means of the three cited equations, were found equal to ± 2.4 ; ± 6.3 and ± 9.0 correspondingly. This result, however , should be expected since equation (12) has been defined by using only data from 1948 to 1956, while the latter two methods have been based on data covering a much longer period i.e. 1947 to 1976. Worth mentioning is, also, the fact that the s.d. between the observed mean monthly values of the flux at 10.7 cm and the corresponding predicted values of the flux , computed by means of equation (13) for the period January 1976 to January 1978 was found equal to s.d. = ± 5.7 i.e. a value comparable to that found for the mean yearly values for the period 1948-1954, cited above (see Fig.4).

It would be interesting to examine whether the relations given in Table 1 can be extended also to the case of the total daily flux values. The main difficulty here lies in the fact that for daily values the records are too long to be examined in the present paper which as a matter of fact, deals with long and medium-term prediction of the radio fluxes.

For this reason, in this paper, we will limit ourselves to the study of the correlation between the total daily fluxes of the sun in the frequencies 2800 MC/S and 3750 MC/S and the Zürich relative sunspot numbers for the years 1957, 1958, 1967 - 1969, only. For the same reason we cannot include in the present investigation the methods of segregation of the two components of the radio flux like the methods described by Allen (1957) Covington and Harvey (1960), Covington (1974, 1976). This comprehensive study of the daily radio fluxes at different wavelengths

for the solar cycles Nos. 18, 19 and 20 will have to be postponed to a later time.

The radio data as well as the daily values of the Zürich numbers used for the determination of the correlations were those published in Quarterly Bulletin of Solar Activity.

Figures 10 and 11 show the plot of the daily Zürich numbers against daily flux values at 2800 MC/S and 3750 MC/S correspondingly, for the years 1957, 1958, 1967-1969 included. Both figures show a striking similarity. The linear relation for the two quantities i.e. r.f. and R is evident. A second-degree curve is fitted as well to the points, but the improvement in the correlation coefficient was found negligible. We emphasize here the fact that when the trend is extrapolated to zero sunspot number the trend cuts the frequency index axis between the values 40 and 80 (flux unit : $10^{-22} \text{ W.m}^{-2}(\text{C/S})^{-1}$) which implies that the flux is not zero even at zero sunspot number i.e. even when the sun is considered completely quiet. These results are in accordance with the results obtained by Covington and Harvey (1960) and by Das Gupta and Basu (1964).

To check the reliability of the equations obtained (see Table 1) - on a daily basis investigation - the difference " observed minus computed values " has been determined, and the standard deviation σ of this series calculated. Moreover, the accuracy of the computations has been checked by means of the formula $(1 - \frac{\sigma}{\bar{F}}) 100\%$ where σ represents the s.d. and \bar{F} represents the arithmetic mean of the observed values of the frequencies considered over the periods 1957-1958, 1967 - 1969 included. The results for each of the years as well as the accumulative results for all the five years considered in the present analysis are tabulated in Table 2.

Finally, it should be noted that the equations have the unfair advantage, of being derived from measurements of only 3 solar cycles .

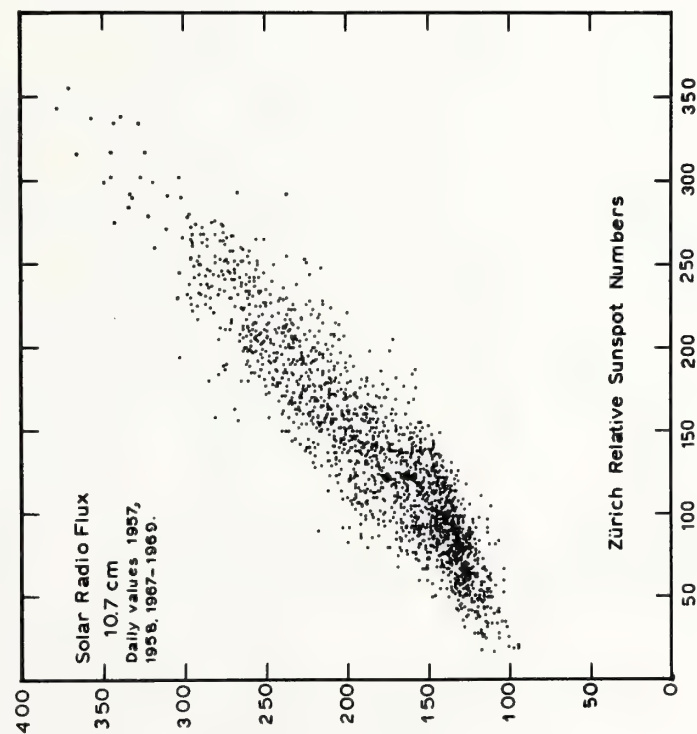


FIGURE 10

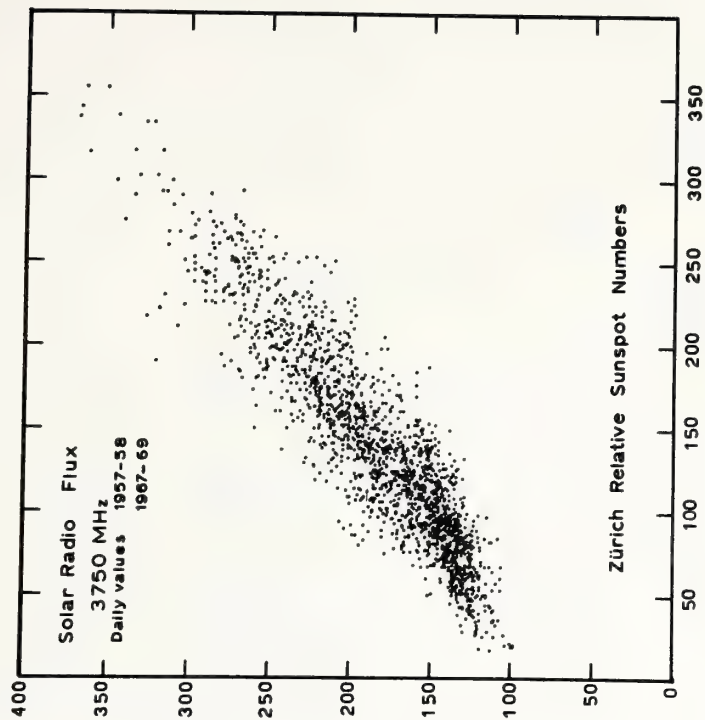


FIGURE 11

FIGURE 10 , 11 : LINEAR RELATION BETWEEN THE SOLAR RADIO FLUX AT FREQUENCIES 2800 Mc/s AND 3750 Mc/s
AND THE DAILY VALUES OF THE ZÜRICH RELATIVE SUNSPOT NUMBERS FOR THE PERIODS 1957-1969 .
(s.d. $\sim \pm 32.0$, $r \sim 0.90$)

T A B L E 2

RELATION BETWEEN THE ZURICH RELATIVE SUNSPOT NUMBERS AND THE FLUX AT 2800 Mc/s AND 3750 Mc/s USING DAILY VALUES. THE ACCURACY OF THE COMPUTED FLUX VALUES IS GIVEN.

	Y E A R S					P E R I O D		
	1957		1958		1967	1968		1969
	frequency		frequency		frequency	frequency	frequency	frequency
$r_{R,F}$	2800	3750	2800	3750	2800	3750	2800	3750
	0.87	0.87	0.83	0.83	0.85	0.84	0.71	0.75
Number of Dates	362	363	361	361	363	360	362	364
MEAN	231.2	229.6	230.4	224.4	143.6	146.1	149.7	151.9
Standard Deviation	± 30.06	± 29.85	± 39.16	± 38.15	± 21.55	± 23.37	± 43.41	± 37.98
Accuracy	0.90	0.90	0.90	0.90	0.88	0.89	0.86	0.88
							0.86	0.87
							± 27.19	± 33.10
							± 32.00	± 32.13
							0.89	0.90
							1812	1806
							0.89	0.90

Of course such a small sample is not sufficient enough to allow accurate predictions to be made, but since no other data exist, it is difficult to see how the accuracy of long and medium period predictions can be improved in the foreseeable future.

REFERENCES

- Allen , C. W. (1957) : Monthly Notices, 117 , 174
- Castelli, J., Basu, S., and Aarons, J. (1965) : Solar radio emission, in " Handbook of Geophysics and Space Environments " ed. by S. L. Valley, p. 16-18, Mc Graw - Hill Book co. N. Y., 1965.
- Coffey, H. (1969) : Solar Geophysical Data, 306 Part 1.
- Coffey, H. (1978) : Solar Geophysical Data, 407 Part 1.
- Covington, A. E., and Harvey, G. A. (1960) : Astrophys. Journal, 132, 435.
- Covington, A. E. (1974) : J. Roy. Astron. Soc. Canada, 68, 31
- Covington, A. E. (1976) : J. Roy. Astron. Soc. Canada, 72, 335
- Eul r, H. C., Lundquist, C. A., and Yaughan, W. W. (1978) : Preprint No. 67 of the Solar - Terrestrial Predictions Proc.
- Das Gupta, M. K., and Basu, D. (1964) : Nature 203, 626
- Xanthakis, J. (1966) : Prakt. de l'Academie d'Athenes, 41
- Xanthakis, J. (1967 a) : Solar Physics ed. by. J. Xanthakis, J. Wiley and Sons Ltd. London.
- Xanthakis, J. (1967 b) : Nature , 215, 1048
- Xanthakis, J., and Poulakos, C. (1978) : Solar Physics, 56, 467

AN ATTEMPT AT PREDICTION OF SOLAR ACTIVITY INDICES
WHICH ARE CLOSELY RELATED TO CLIMATE

TAKIO SUDA
Department of Agriculture
Gifu University
Kakamigahara-shi, Gifu-ken, 504, Japan

The necessity of predicting the C_i or A_p index of geomagnetic activity as well as sunspot number for the prediction of climate is discussed. After summarizing the present author's preceding works, the following results are given.

- (1) Sunspot number is an important factor in the sun-weather relationship regarding meteorological phenomena in the lower latitudes.
- (2) The C_i or A_p index of geomagnetic activity is more important than sunspot number in the higher latitudes.
- (3) The "grand cycles" in solar activity are discussed. The length of individual cycles is from 66 to 86 years. Also a cycle with a period of about 237 years is shown. These cycles have been found in the secular variations of the maximum sunspot number in individual 11-year periods in the recent centuries and the records of the naked-eye sunspot and aurora display in the Far East.
- (4) Long-term prediction utilizing the above-mentioned cycles of sunspot number and the C_i index is discussed.

1. INTRODUCTION

It has been shown in the present author's previous works that sunspot number, which seems to be a good index of solar ultraviolet radiation, has a close correlation with some meteorological phenomena in the lower latitudes. On the other hand, in the higher latitudes, the indices of geomagnetic activity, C_i and A_p which are regarded as a better index of solar corpuscular radiation, are more influential in the sun-weather relationship than sunspot number. Here, a new solar activity index consisting of sunspot number and C_i or A_p is proposed, and it will be shown that this index would be helpful in clarifying the mechanism of sun-weather relationship on a global scale.

In this paper, the author describes some new analyses along the same lines and an attempt at making long-term predictions of general tendencies of sunspot number and the C_i index.

2. A SOLAR ACTIVITY INDEX FOR THE SUN-WEATHER RELATIONSHIP FITTING BETTER IN THE LOWER LATITUDES: SUNSPOT NUMBER

The relationship of the daily values of easterly wind velocity, tropopause height and type of tropopause over Marcus Island (24.3°N, 154.0°E) to the facula area, sunspot area and so on has been investigated by the author (Suda, 1963a), and it is shown that the latter items are positively related to the easterly wind velocity and negatively to the tropopause height. If this is due to the change in heating of ozone layer caused by solar ultraviolet radiation, some correlation might be found between sunspot number and some terrestrial meteorological phenomena. As an example, a good correlation between the behavior of quasi-biennial oscillation (QBO) and sunspot number or the C_i index is shown here.

Year-to-year changes in westerly wind speed (12-month running mean) at the 50-mb level have been shown by Yamamoto (1978) as an illustration of QBO at Singapore. The maximum speed in each westerly phase of QBO, obtained from Yamamoto's figure, is considered to be free from the effect of the seasons of the year.

A good negative correlation is seen between the wind speed maxima and sunspot number (Fig. 1(a)). A small triangle indicates a wind speed which is stronger than that expected from the corresponding sunspot number. Violent volcanic eruptions of Fernandina in 1968 might have disturbed stratospheric conditions and caused this departure in the trend.

On the other hand, there appears to be no correlation between the C_i index and the westerlies (Fig. 1(b)). Therefore, it is considered that the stratospheric westerlies over the tropics are affected more intensively by solar ultraviolet radiation than by corpuscular radiation.

It has been discovered that the period of QBO is better correlated with the C_i index than with sunspot number.

Ebdon's chart (1975) showing year-to-year changes in monthly mean zonal wind components at the 30-mb level over Canton Island indicates that the period of QBO changed from about 20 months to 34 months during 1956-1975. Ebdon considered that the cause of this change might be the volcanic eruptions of Mt. Agung, Bali in 1963, but the author considers it to be the effect of solar activity. The analysis of the relationships among the period of QBO detected by Ebdon, sunspot number and the C_i index indicates that the period is correlated with both indices, and closer to the latter index.

The correlation coefficient between the three-period running means and those of the C_i index is -0.79 (14 pairs, $\alpha < 0.005$) (Fig. 2). The values of C_i at the points of each period have been read from the curve of year-to-year changes in the annual mean.

It is considered that sunspot number may be a key in understanding the effect of solar activity on the weather in the lower latitudes. However, the period of QBO has a better correlation with the C_i index than with sunspot number. This may be explained as in the following.

QBO must be present in the general circulation which is modulated by the atmospheric conditions in the higher latitudes. And those conditions such as the behavior of the polar vortex are better correlated with the C_i index than with sunspot number as described in the next section.

Δ : datum disturbed
by an eruption (a)

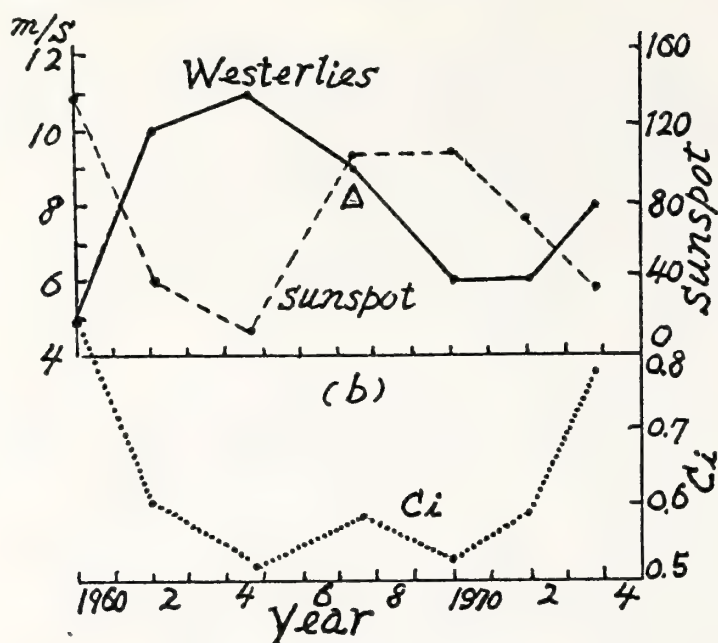


Fig. 1 RELATION BETWEEN WESTERLY WIND SPEED AT THE 50-MB LEVEL. BOTH VALUES ARE OF 12-MONTH RUNNING MEAN.

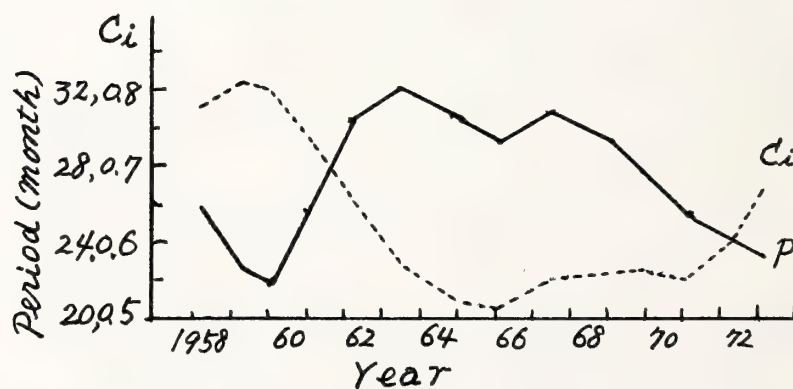


Fig. 2 RELATION BETWEEN THE PERIOD OF 30-MB QBO OVER CANTON ISLAND AND THE Ci INDEX.

3. SOLAR ACTIVITY INDICES FOR THE SUN-WEATHER RELATIONSHIP FITTING BETTER IN THE HIGHER LATITUDES: THE C_i INDEX AND A COMPOSITE INDEX

Sunspot number is, though no better than C_i or A_p , correlated with the polar vortex, the polar night vortex and surface temperature in the higher latitudes in a complex way (Suda, 1976). This will be discussed with respect to the polar vortex. Since the role of A_p in our discussion is qualitatively similar to that of C_i , A_p is omitted in the following.

(1) The C_i value is negatively correlated with the development of the polar vortex.

(2) Sunspot number, S , is positively (negatively) correlated with the vortex development when its value is smaller (larger) than S_r . Here, S_r is the "reversing point" at which the sense of the effect of sunspots on the earth's atmosphere is reversed. The value of S_r varies with the season.

(3) The relation among C_i , S and the degree of expansion of the vortex, E (the mean latitude of the southernmost latitude to which the vortex reaches along each longitude), is expressed as follows.

$$E = a + bC_i \cdot Se^n \quad (1)$$

where Se is the absolute value of $(S - S_r)$.

In the case of analysis of the year-to-year values of mean C_i , S and E at the 500-mb level for December to February during the period from 1949 to 1971 (Fig. 3), constants a , b , and n and S_r are as follows.

$$a = 58.0^\circ, \quad b = 8.0^\circ, \quad n = 0.3, \quad S_r = 120.$$

The correlation coefficient between E and $C_i \cdot Se^{0.3}$ is +0.624 (23 pairs, $\alpha < 0.01$). Hence, accuracy of this empirical formula is fairly good.

Though many researchers, since Duell (1947), paid attention to the effect of solar corpuscular radiation on the weather, nobody has used, to the best of the present author's knowledge, the composite index consisting of sunspot number and C_i .

If the heating effect of corpuscular radiation really reaches the lower atmosphere, the effect should be significant. However, the aspect of the amount of energy alone has been considered so far, and there have been no convincing hypotheses, except that of Markson (1978).

4. THE 237-YEAR PERIOD OF SUNSPOT ACTIVITY

Looking for a longer period in sunspot activity, we have analyzed the secular variation of the maximum sunspot number of each 11-year cycle. The data since 1615 are available. A 237-year period consisting of three grand cycles has been found (Suda, 1975a). The length of the grand cycles, so named for the sake of reference, is from 66 to 86 years, with an average of 79 years. The beginning of each grand cycle can be clearly determined from the secular changes in the maximum sunspot number or the sudden drops by 75 or greater.

Thirteen drops are seen in the secular changes in ΔS which is the difference of the maximum compared with the preceding one, and five of them are larger than 75 (Fig. 4). The values of these large drops are much larger than

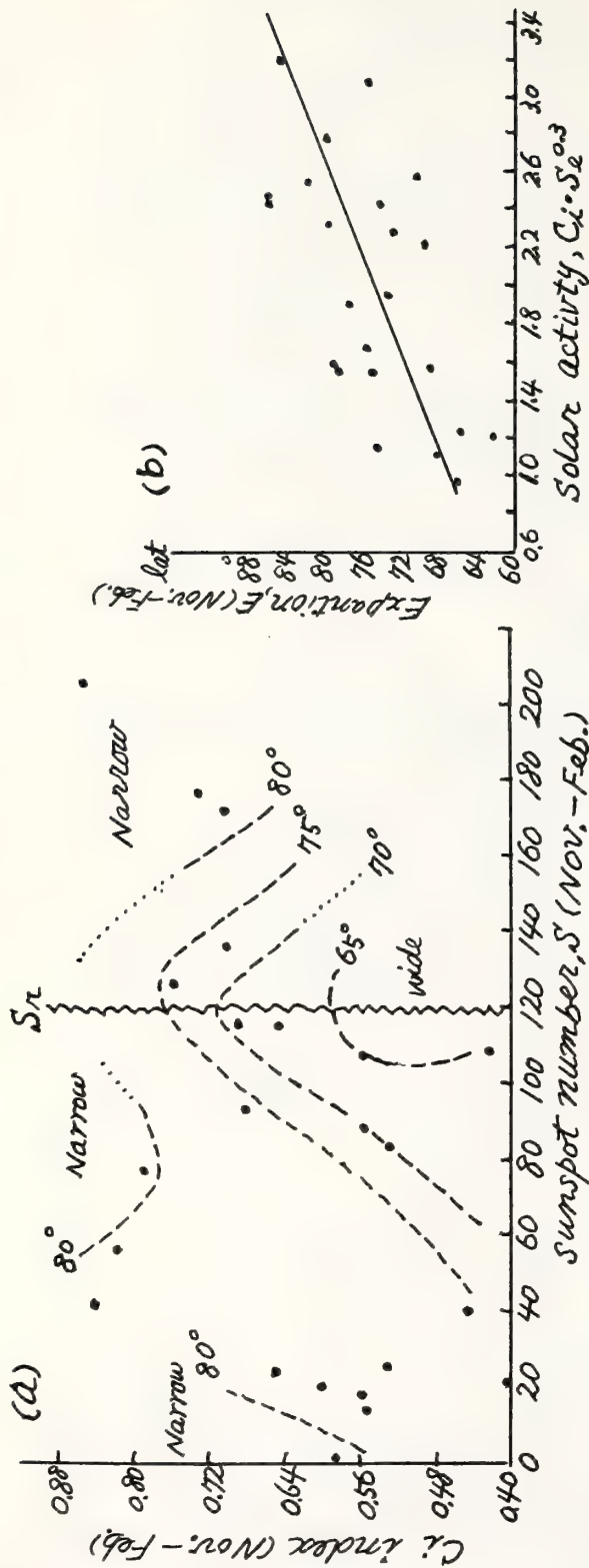


Fig. 3 RELATION AMONG THE EXPANSION OF THE POLAR VORTEX AT THE 500-MB LEVEL, FOR NOV.-FEB., 1949-1971. NUMERALS IN (a) AND THE ORDINATE OF (b) SHOW THE EXPANSION OF THE VORTEX (THE MEAN VALUES OF THE SOUTHERNMOST LATITUDES ALONG EACH LONGITUDE IN EACH YEAR).

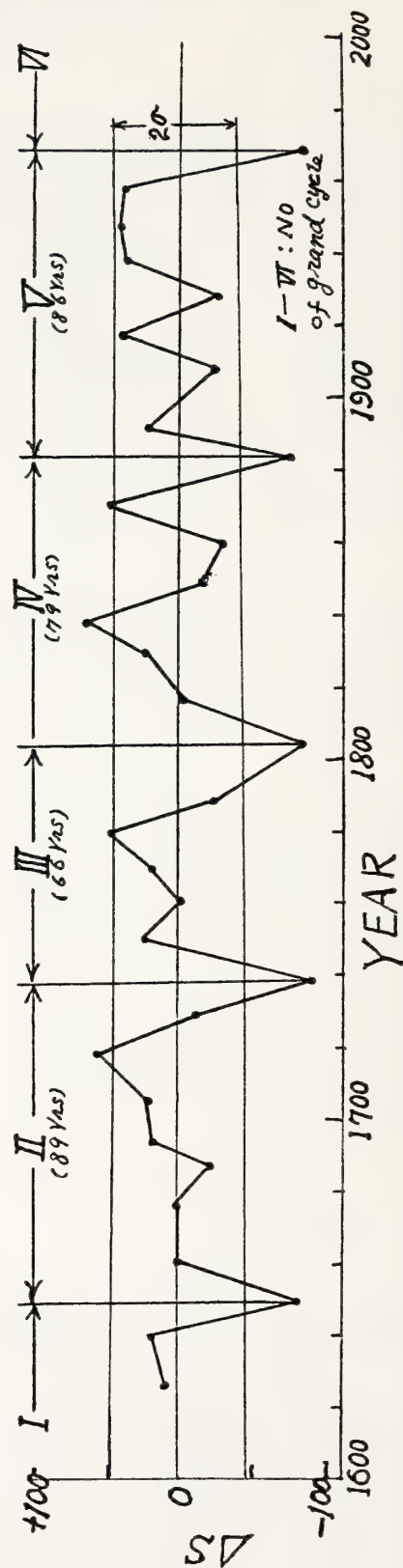


Fig. 4 SECULAR VARIATION OF THE MAXIMUM OF EACH SUNSPOT CYCLE, SHOWING THE GRAND CYCLES; ΔS IS THE DIFFERENCE OF THE MAXIMUM COMPARED WITH THE PRECEDING ONE.

the standard deviation (32.3) of all the drops. And also, these values and other ΔS are separated into two populations (Fig. 5). Thus, these sudden drops are significant. The years of the beginning of grand cycles marked by these peculiar drops of the maximum coincide with the years in which the index for the accumulated energy of sunspot activity becomes minimum. These indices have been obtained from the time series of sunspot number accumulated year by year (Suda, 1975b).

Generally speaking, each grand cycle is of two stages: the inactive, earlier stage and the active, later stage. An inactive stage has from three to five maxima and the mean value of the maxima in all the inactive stages in a grand cycle is about 80. An active stage has three or four maxima (Fig. 6), and mean value of maxima is about 130. Schematic representation of some grand cycles is shown in Fig. 7.

A cycle of about 235 years is seen in the secular variation of the maximum sunspot number of each 11-year cycle (Fig. 8). Namely, the change of the maxima in Zürich number 9 (1948) to number 20 (1969) and that of number -12 (1615) to -2 (1728) resemble each other, and the two series are separated by 235 years. The correlation coefficient between the maxima in the two series is +0.79 (12 pairs, $\alpha < 0.01$). However, the data period is too short to confirm this cyclic change in the sunspot activity. We may require data of 10^3 years or so to verify the existence of this kind of cycle. Although no accurate data of such a long duration is available, ancient records of naked-eye observations of sunspots and aurorae displays in the Far East seem to serve our purposes.

It is said that Turner found cycles of 260 to 280 years in Chinese records of naked-eye sunspots. Kanda (1933) claimed the existence of a cycle of about 1100 years in the variation of sunspot number, from the analysis of Chinese, Korean and Japanese records of naked-eye sunspots.

However, scanty and inhomogeneous data discourage the effort of finding long periods. Especially, missing data for several tens of consecutive years often presented very difficult problem. Now, however, we can ascertain whether such blanks in data reflect the weakened state of solar activity or the lack of interest on the part of record keepers by the deviation in the carbon-14 amount in tree rings.

Fig. 9 shows secular variations, for the interval of about 800 years, in three kinds of phenomena: sunspot, aurora and carbon-14.

(1) Frequency of the years with aurora display in Japan

The records listed by Yamaguchi (1958), as the most reliable ones among others, have been used, excluding the data for the latitudes higher than 40°N and of the recent years to make them comparable to those given in (2) and (3) below.

(2) Frequency of the years with aurora display in Korea

The records introduced by Taguchi (1940) have been used.

(3) Frequency of the years with naked-eye sunspot

The records in China and Korea, including the one in Japan for the year 851, and compiled by Kanda (1932), have been used.

(4) The statistical process

The frequency of a phenomenon is not the number of the records of the relevant phenomenon but the number of the years in which the relevant phenomenon were recorded. Since data are scanty, the frequency for 40-year durations has been obtained at 20-year intervals, and the frequency has been plotted at the mid-point of the relevant term as follows.

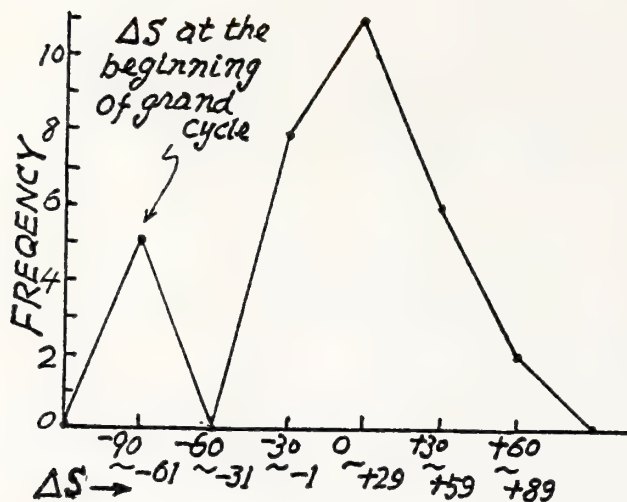


Fig. 5 FREQUENCY DISTRIBUTION OF ΔS WHICH IS THE DIFFERENCE OF EACH MAXIMUM SUNSPOT NUMBER FROM THE PRECEDING ONE, 1615-1969.

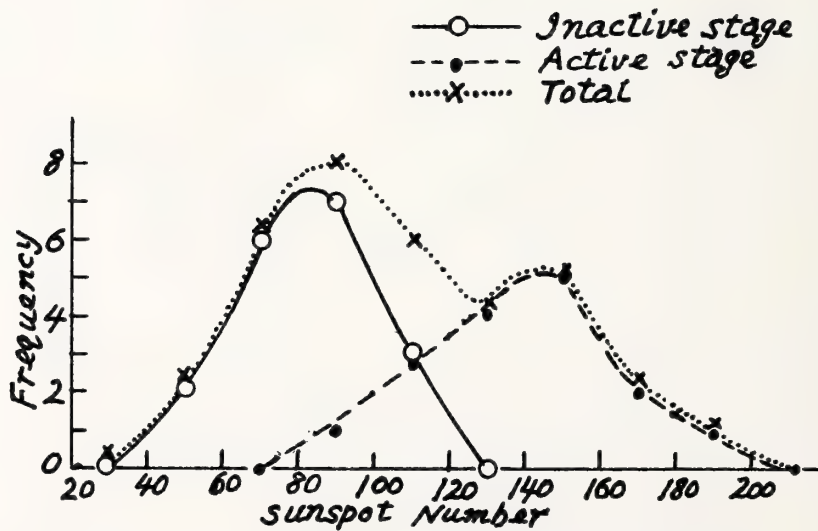


Fig. 6 FREQUENCY DISTRIBUTION OF THE MAXIMUM OF EACH 11-YEAR SUNSPOT CYCLE, 1615-1969.

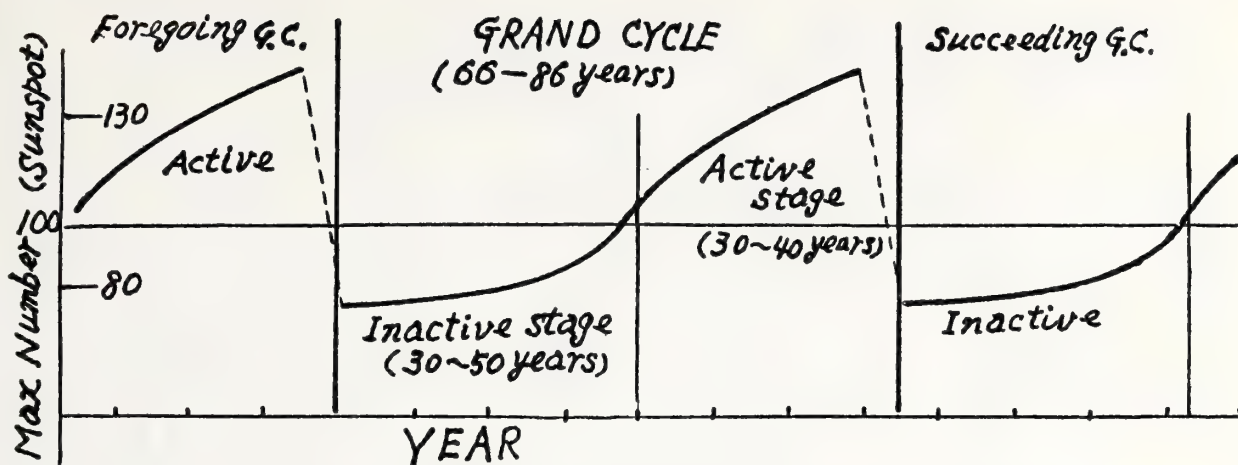


Fig. 7 SCHEMATIC REPRESENTATION OF GRAND CYCLE IN SUNSPOT NUMBER VARIATION.

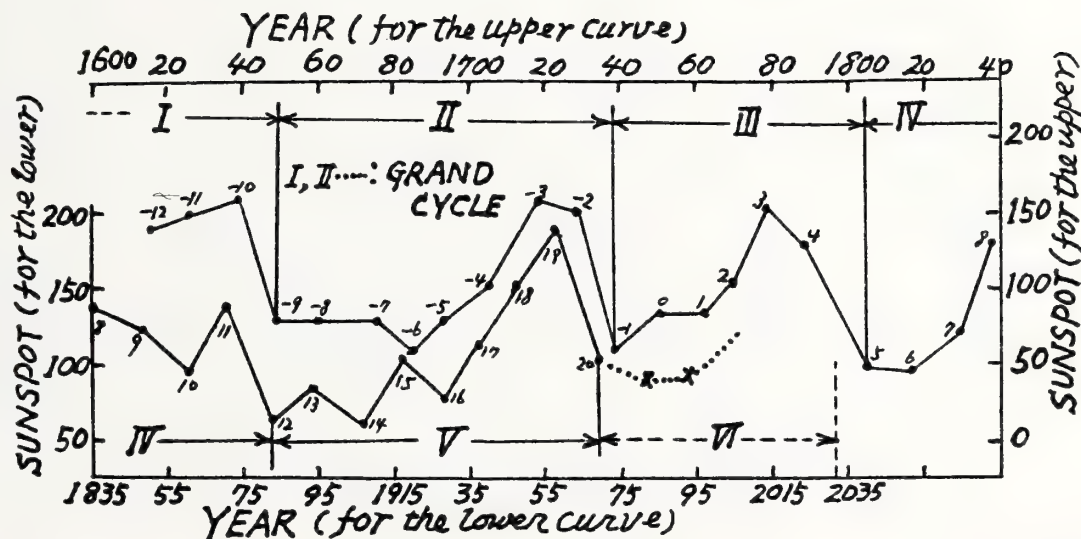


Fig. 8 235-YR PERIOD APPEARED IN THE SECULAR VARIATION OF THE MAXIMUM OF EACH SUNSPOT CYCLE. I - VI: THE NUMBER OF THE GRAND CYCLE. -12 - 0 - 20: THE NUMBER OF THE MAXIMUM.

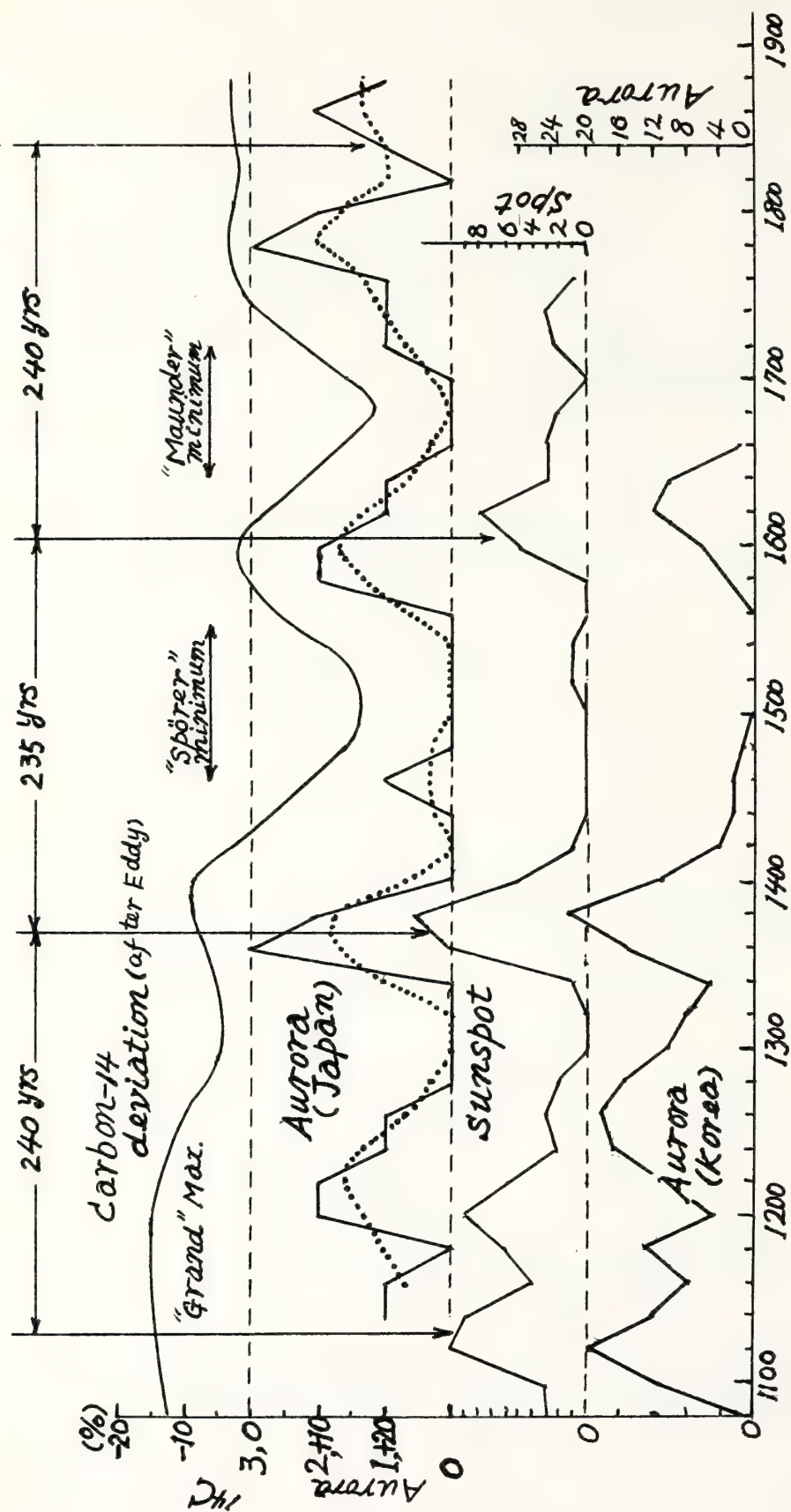


Fig. 9 THE SECULAR VARIATIONS OF THE FREQUENCY OF NAKED-EYE SUNSPOT AND AURORA OBSERVED IN THE FAR EAST, SHOWING THE PERIODICITY OF 235 TO 240 YEARS. FREQUENCY IS THE NUMBER OF THE YEARS WITH SUNSPOT OR AURORA DURING 40 YEARS AT 20-YEAR INTERVAL.

Term	1100-1139,	1120-1159,	1140-1179,
Plot point	1119.5	1139.5	1159.5

It will be seen in Fig. 9 that the bottom three curves, i.e., aurora in Japan, sunspot and aurora in Korea, harmonize very well; for example, the correlation coefficient between aurora and sunspot in Japan during the years 1140 to 1739 is +0.86 (15 pairs, $\alpha \ll 0.01$).

These curves reflect the true features of secular variation of solar activity. Because it was impossible for the people who left the records to exchange information on sunspot appearances or aurora display, and also because they had no knowledge of the relation between these phenomena, these records are completely independent of each other with respect to place, as well as the type of phenomenon.

Four remarkable peaks and three deep troughs are seen in these curves. They coincide very well with those in the curve of carbon-14 deviation given in Eddy's excellent work (1976). The four peaks are around the years 1130, 1370, 1605, and 1840, which suggests that cyclic changes with a period of 235 to 240 years existed in solar activity during the past seven centuries.

To verify statistically this period, a 240-year periodgram analysis has been done for the duration of 960 years (800 to 1759). Here, the analyzed time series is of the number (frequency) of years in a 20-year duration, in which naked-eye sunspot was recorded (Table 1).

Table 1. THE 240-YEAR PERIODGRAM ANALYSIS OF THE SECULAR VARIATION OF THE YEAR WITH NAKED-EYE SUNSPOT.

Phase (20 yrs interval)	1	2	3	4	5	6	7	8	9	10	11	12
Term and Frequency of the years with naked-eye sunspot	800 ~19 1	820 ~39 3	840 ~59 2	3	1	0	1	0	1	1000 ~19 0	1020 ~39 0	
	1040 ~59 0	1060 ~79 3	0	3	7	2	2	4	5	1	1	1260 ~79 2
	1280 ~99 0	0	0	0	1	9	4	1	0	0	0	1500 ~19 0
	1520 ~39 1	0	0	0	5	3	0	2	0	0	2	1740 ~59 1
Sum. of Frequency	2	6	2	7	22	9	4	6	6	1	3	3
mean	0.50	1.50	0.50	1.75	5.50	2.25	1.00	1.50	1.50	0.25	0.75	0.75
	$\sigma = 1.34$, mean 1.48											

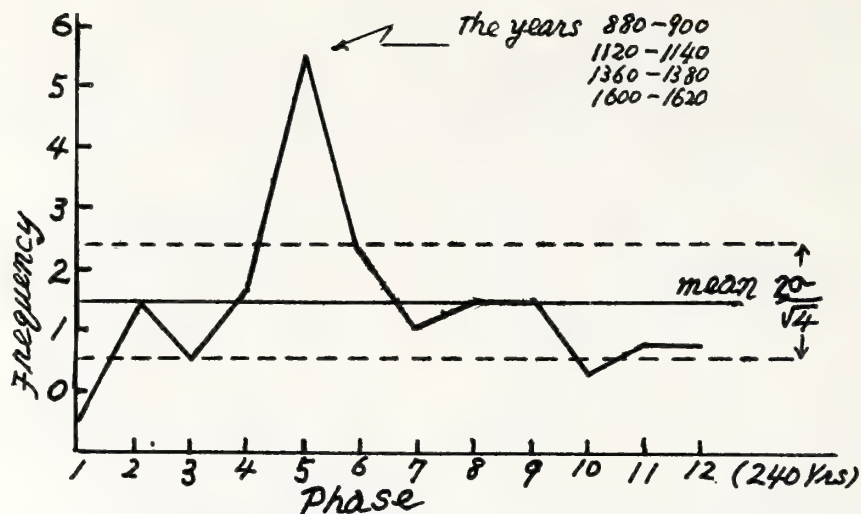


Fig. 10 THE 240-YEAR PERIOD IN THE SECULAR VARIATION OF THE FREQUENCY OF NAKED-EYE SUNSPOT IN THE FAR EAST, 800-1759. THIS IS THE RESULT OF THE PERIODGRAM ANALYSIS. THE MEANING OF FREQUENCY IS THE SAME AS THAT SHOWN IN FIG. 9.

As a result, the 240-year cyclic change with a sharp peak at the fifth phase (the years 890, 1130, 1370 and 1610) has been revealed (Fig. 10). This is statistically significant at a high level as is noted in the following.

The standard deviation of the mean values for each phase, σ_1 , is 1.34 and that of the whole values of series, σ_2 , is 1.94. Here, σ_1 is larger than $\sigma_2 / \sqrt{4} = 0.97$. The χ^2 test shows that this distribution is significant at a high level ($P < 0.01$). On the basis of the above discussion, it is considered that changes with a period of 235 to 240 years existed in sunspot activity during the last 1000 years or so. It is difficult to determine a precise period within the range of 235 to 240 years. However, a 237-year period appears to be the best, due to the following reason. The solar activity may need about 237 ($=79 \times 3$) years to adjust the floats of the 79-year periodic changes (refer to Fig. 8 and Table 2).

Table 2. THE 237-YEAR PERIOD WHICH CONSISTS OF THREE FLOATING GRAND CYCLES.

Grand cycle No.	Interval	Grand cycle No.	Interval
2 nd	89 yrs	5 th	86 yrs
3 rd	66	6 th	66-68 ?
4 th	79	7 th	80 ?
Sum.	234		
Mean	78		

Though general trends of carbon-14 deviation and naked-eye sunspot harmonize well, there are some minor differences. Sunspot activity must have been very weak, as Eddy maintains, during the Maunder minimum and Spörer minimum. We can not believe that the sun was completely free of sunspots during these times, because some naked-eye sunspots were recorded in the above-mentioned two solar minima (recorded in the years 1520, 1660, 1666 and 1720) despite the fact that sunspot recordings are not many, even in the recent centuries in which sunspot activity was stronger.

5. LONG-TERM PREDICTION OF SUNSPOT NUMBER AND THE C_i INDEX

5.1 Sunspot Number

A number of periods have been found, by various methods, in secular variation of sunspot number. By combining some selected periods, a long-term prediction of solar activity may be made, though results have often been disappointing. Here, we will make a different approach utilizing the above-mentioned 237-year period. If solar activity follows this 237-year period, the characteristics of the VI grand cycle (see Fig. 8) may be similar to those of the III grand cycle in which the inactive stage contained three 11-year cycles. On this assumption, we shall attempt to predict the general tendency of sunspot number variations in the following.

5.1.1 The base of prediction

(a) The VI grand cycle has begun in the year 1969. The features of the first half of this cycle will resemble those of the III grand cycle; that is, the inactive stage will have three maxima (one has occurred in 1969 and two will follow).

(b) The maxima in the inactive stages of the III and other grand cycles are similar to each other in value, and none is larger than 110 (Figs. 6-8).

(c) Both the first maximum (in the year 1969) and minimum (1977) were markedly large compared with the corresponding values in the past grand cycles. This is due, presumably, to the change in solar activity having a period longer than 79 years or 237 years. Hence, the coming two maxima will be large despite their being in the inactive stage.

(d) The intervals of two 11-year cycles in the inactive stage of the III grand cycle were both 11.0 years, and those of all grand cycles were 10 to 14 years, with average of 11.8 years.

5.1.2 Prediction of sunspot number maxima

(a) From (a) to (c) of 5.1.1 above, the values of coming two maxima (annual mean) will be from 110 to 120.

(b) From (d) of 5.1.1 above, the occurrence of the coming two maxima will be around 1980 and 1991.

(c) The fourth maxima, which is predicted to appear around the year 2002 will be in the active stage of the VI grand cycle and its value will be about 140.

5.2 The C_i Index

Long-term prediction of the C_i index, a necessity for climatic prediction, is difficult. This is especially true in its detail, because the data period of C_i is too short. The present author's new tack for avoiding this difficulty is as follows. The C_i index dropped suddenly at the beginning of the 1960's as is seen in Fig. 11(a). This is considered to be due to the sudden decay of solar activity, occurring at the beginning of a grand cycle, being reflected more strikingly in the C_i index than in sunspot number (Fig. 11(b)).

On the basis of this idea, long-term variation of the C_i index is predicted as follows: for the coming 30 years, C_i will generally be small, and the upper and the lower limits of the annual mean will be 0.85 and 0.45, respectively. It is desirable to analyze secular variation of the u-measure and other geomagnetic activity indices whose characteristics are similar to those of the C_i index, with data period of considerable lengths.

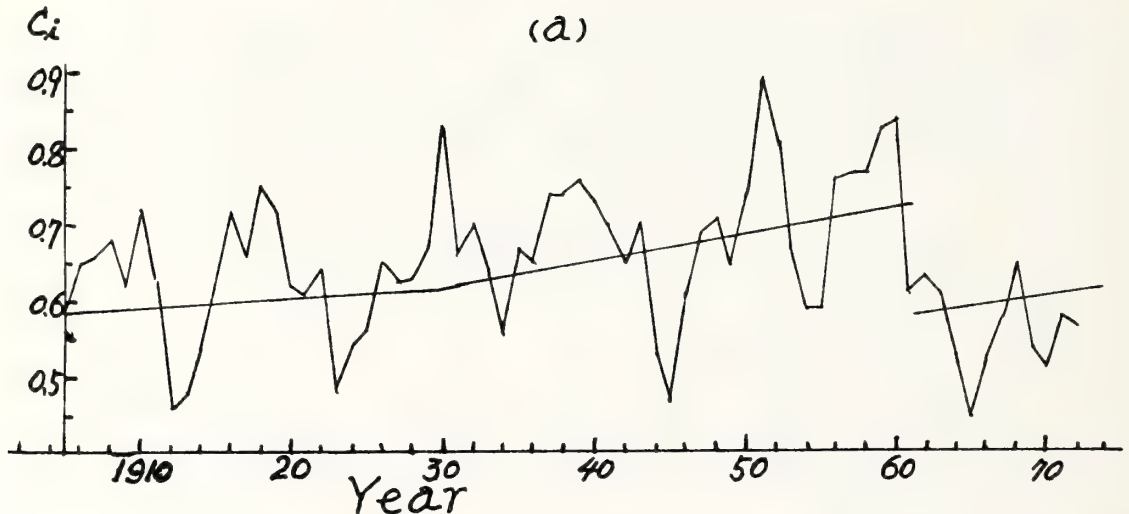


Fig. 11(a) YEAR-TO-YEAR CHANGE OF THE C_i INDEX
SHOWING MARKED DROP IN THE 1960'S (SUDA, 1975).

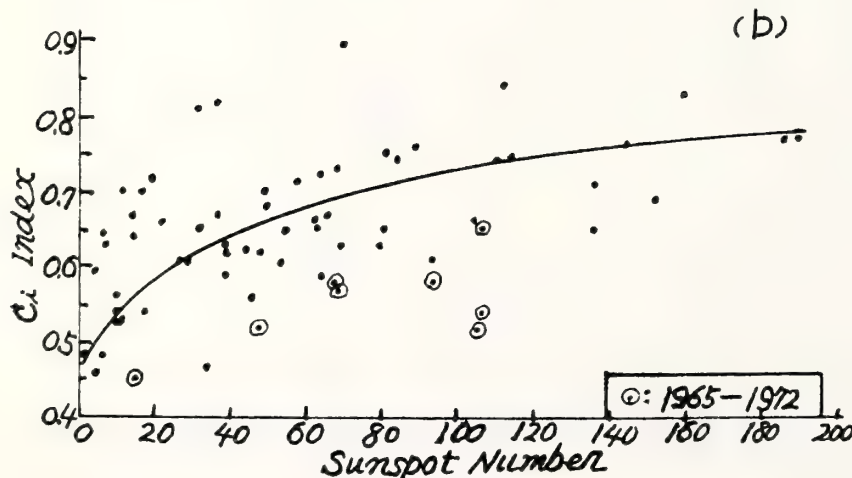


Fig. 11(b) RELATION
BETWEEN SUNSPOT
NUMBER AND THE C_i
INDEX, SHOWING THAT
THE LATTER WAS
REMARKABLY SMALL
COMPARED WITH THE
FORMER IN THE 1960'S,
1965-1972 (SUDA,
1975).

5.3. A Further Discussion

As the recent years happen to be in a trough of the 237-year periodic changes in sunspot activity, the sunspot number since 1969 is expected to be much fewer than that observed. This inconsistency suggests a possibility that a periodicity longer than 237 years might have overlapped on the latter. Another possibility is that the 237-year period might have been decaying in the present century, and the said inconsistency might be reflecting some fluctuations such as those around the fourth peak in Fig. 9.

Acknowledgements

The author wishes to express his most sincere thanks to Dr. R.F. Donnelly of the Space Environment Laboratory for his kind help and encouragement. The author's deep thanks are also due to the reviewers and Mr. T. Yasuda, staff of Planning Division of Japan Meteorological Agency, for their useful suggestions and advice.

References

- Eddy, J.A. (1976): The Maunder Minima. Sci., 192, 4245, 1189-1202.
- Ebdon, R.A. (1975): The quasi-biennial oscillation and its association with tropospheric circulation pattern. Met. Mag., 104, 283.
- Duell, B. (1948): The behavior of barometric pressure during and after particle invasions and solar ultraviolet invasion. Smith. Miss. Coll., 110, 18, 1-31.
- Kanda, S. (1932): On the records of sunspots in the Orient and the period of sunspot (in Japanese). Tokyo Astr. Obs. Report, 1, 37-50.
- Kanda, S. (1933): Ancient records of sunspots and aurorae in the Far East and variation of the period of solar activity. Proc. Imp. Acad. Japan, 9, 293-296.
- Keimatsu, M. (1976): A chronology of aurorae and sunspots observed in China, Korea and Japan. Ann. Sci. Kanazawa University, Japan, 13.
- Markson, R. (1978): Solar modulation of atmospheric electrification and possible implications for the Sun-weather relationship. Nature, 273, 103-109.
- Suda, T. (1962): Some statistical aspects of solar-activity indices. Jour. Met. Soc. Japan, Vol. 40, 5, 287-299.
- Suda, T. (1963a): The effect of solar activity on some meteorological phenomena. Geophy. Mag. JMA, Japan, Vol. 31, 3, 554-579.
- Suda, T. (1975a): On the severe and sudden change of solar activity system occurred in 1966 and its effect on climate (in Japanese). Tenki, Met.

Soc. Japan, Vol. 22, 8, 427-429.

Suda, T. (1975b): *ibid.* 429-430.

Suda, T. (1976): Effect of solar activity on polar vortex and a hypothesis on linking mechanism. Geophys. Mag., JMA, Japan, Vol. 37, 4, 361-369.

Taguchi, T. (1940): Historical data of aurora (in Japanese). Bulletin of Kobe Marine Meteorological Observatory, Vol. 130.

Yamaguchi, K. (1958): Low-latitude aurora observed in Japan (in Japanese). Weather Service Bulletin, Vol. 25, 374-385.

Yamamoto, R. (1978): Volcanic eruption and climatic variability (in Japanese). Tenki, Met. Soc. Japan, Vol. 25, No. 2, 98-99.

SUNSPOT TURNING-POINTS AND AURORAE SINCE A.D. 1510

D. J. Schove
St. David's College, Beckenham, Kent, U. K.

The time of solar maxima and minima extending back to c.1610 were estimated by Wolf and Wolfer at Zurich in the nineteenth century, (Waldmeier, 1961) and those back to c.1710 have been generally accepted. Slight modifications have already been suggested by Schove (1967) for the seventeenth century, although in that century, even the existence of the eleven-year cycle has been questioned (Eddy, 1976). In the course of any sunspot cycle, the pattern of the aurorae in place and time is a characteristic of sunspot cycles of a particular amplitude-class. The precise dates of the Zurich solar maxima and minima since c.1710 can be determined from these patterns by a set of empirical rules. These rules applied to the period c.1510-1710 improve the earlier determination of solar maxima and minima and tend to confirm the dates given by Wolfer for the seventeenth century and by Link (1978) for the late sixteenth century.

1. INTRODUCTION

A table of solar maxima and minima since 649 B.C. has been published (Schove, 1955). Since 1955 many new auroral records have come to light and studies of their chronology and geography for the solar cycles since c. 1710 (see Table 1) have established patterns of auroral observations that can be effectively linked to accepted Zurich solar maxima and minima. These relationships are applied to determine the dates of earlier solar maxima and minima which have not been clearly established.

2. MAXIMA RULES

If the year of Zurich sunspot maximum is counted as zero or year (X), the frequency of auroral displays at a particular geomagnetic latitude normally shows a double peak, a primary peak near the sunspot maximum (year X) and a secondary peak a year or so later (years X+1 to X+4).

Displays later in the cycle are often associated with corpuscular emanations from the sun, and for this reason recurrent aurorae are more frequent at the secondary peak. The pattern of the aurorae frequency depends on the geomagnetic latitude and sunspot number at maximum.

Auroral frequencies are expressed in Table 1 as mean percentages, for each year of the cycle and the for complete cycle of 11 years (from year X-4 to year X+6).

Table 1. Auroral frequencies distributed as percentages of the eleven-year totals in relation to the year of Zurich Maximum (X).

ALL YEARS	-4	-3	-2	-1	X	+1	+2	+3	+4	+5	+6	Total
All Classes												
SUB-TROPICAL	0	0	7	15	20	14	11	11	7	5	9	56
CENTRAL EUROPE	3	3	8	19	24	18	9	9	7	5	4	646
HOLLAND	4	6	11	11	10	14	13	13	8	6	5	391
SCANDINAVIA	6	8	8	10	11	12	12	9	9	9	8	919
Strong Sunspot Cycles, $R > 140$												
CENTRAL EUROPE	4	2	6	19	23	15	9	8	4	6	4	439
SCANDINAVIA	7	9	8	9	10	11	13	10	8	8	7	444
Fairly Strong Sunspot Cycles, $140 > R > 100$												
CENTRAL EUROPE	1	1	7	8	24	19	7	13	13	4	4	151
HOLLAND	10	6	9	5	7	19	16	15	4	4	6	121
SCANDINAVIA	8	7	2	7	10	16	14	7	10	8	10	83
Moderate Sunspot Cycles, $100 > R > 87$												
CENTRAL EUROPE	1	6	13	29	16	12	12	0	8	1	0	75
HOLLAND	2	3	10	15	9	19	15	8	10	6	1	124
SCANDINAVIA	3	5	8	10	9	9	11	9	9	10	9	83
Weak Sunspot Cycles, $R < 87$												
SOUTH OF 46°	0	15	5	10	30	20	0	5	0	10	5	42
CENTRAL EUROPE	6	13	20	9	4	30	4	9	0	2	2	45
EUROPE	9	10	10	8	12	11	7	5	7	4	4	193
SOUTH OF 55°												
HOLLAND	3	9	15	12	7	11	10	13	8	8	5	124

Data based mainly on the standard auroral catalogues of Tromholt, Rubenson, Angot, Visser, Fritz, etc., e.g., Central Europe is based on Switzerland (Wolf), Czechoslovakia (Seydl), and Hungary (Berkcs). (The periods generally range from c.1710 to 1880.)

2.1 An X+2 Lull

In Central Europe and in the Mediterranean (not shown in Table 1), a relative auroral lull--between the main and secondary peaks--occurs two years after the Zurich maximum. In Central Europe this minimum does not occur with moderate cycles.

In Northern Europe this rule applies only when the amplitude of the cycle is strong, in other cycles, the lag is greater than two years (as indicated below).

In Scandinavia this rule does not apply at all, as the maximum, especially in strong cycles, occurs in the X+2 year.

2.2 An X+3 Lull

When solar cycles are only fairly strong, the auroral lull in Scandinavia lags the Zurich maximum by three years. This applies also to moderate cycles in Europe as a whole.

2.3 An X+3 Peak

However, the secondary auroral peak in the Mediterranean occurs in the year X+3. Some of the great displays of aurora tropicalis have occurred three years after the Zurich maximum.

In Holland the late peak is dominant in weak cycles; the aurorae being almost twice as frequent in that year (13%) than at Zurich maximum (7%), which is three years earlier.

2.4 An X+4 Peak

In the Mediterranean, aurorae seldom occur later than three years after the Zurich maximum. In Northern Europe the secondary peak is more pronounced and occurs four years later at (X+4). In Central Europe this secondary maximum has an intermediate date (X+3½) and is, on the average, 3½ years later than the Zurich maximum.

2.5 The Gnevyshev Gap in Sunspots

The above rules are based on the aurora. An additional rule is based on the short lull in large sunspots near the time of a maximum (cf., Wittmann 1978, and Gnevyshev, 1977). Sunspots observed by the Chinese for a given cycle are distributed into two groups, one on each side of the maximum; a feature not noticed in the paper on the fourth century A.D. (Schöve and Ho, 1959). In the seventeenth century when most reported sunspots were large ones, identification of this gap helps to explain the anomalous sunspot distributions of the Maunder Minimum.

3. MINIMA RULES

The auroral zone withdraws towards the pole near sunspot minimum. The date of this withdrawal can be specified from 12- or 13-month running means of high-latitude auroral observations. The auroral minima in Southern Scandinavia between 58°N and 61°N (Zone IV in Tromholt (1892)) almost coincide

with the Zurich sunspot minima. The Southern Scandinavia observations yielded minima in 1724.3, 1734.7, 1766.3, and 1784.3. In Mid-Scandinavia between 65° and $68\frac{1}{2}^{\circ}$ (Tromholt's Zone II) auroral minima occurred in 1810.4, 1824.0, and 1834.3 when the northward withdrawal was greater than usual.

However, in Northern Scandinavia (North of $68\frac{1}{2}^{\circ}$, Tromholt's Zone I), the northward withdrawal leads to a relative maximum (sic) at the time of the Zurich sunspot minimum, e.g., in 1843.7, 1856.7, and 1867.8.

In the period 1740-70, the northward withdrawal was less than in 1840-70 and short relative maxima occurred near the sunspot minimum even south of 65° N. In Zone II such secondary maxima are dated 1745.3, 1755.7, and 1766.3.

In Table 2 this short maximum is shown for the mean results of Tromholt's Zones I and II, with over 5% of the displays occurring in the year of the Zurich minimum.

Table 2. Auroral frequencies distributed as percentages of the eleven-year totals in relation to the year of Zurich Minimum (N)

	-5	-4	-3	-2	-1	N	1	2	3	4	5	Total
N. SCANDINAVIA												
ZONES I & II	11	8	6	5.6	4.2	5.3	4.9	5	7	11	11	550
HOLLAND	11	9	9	5.7	4.8	4.3	4.3	8	12	10	11	438
CENTRAL EUROPE	10	6	7	3.0	4.0	3.2	0.8	8	17	20	11	725

3.1 Auroral Lull near Sunspot Minimum: Northwest Europe and the United States

Observations of aurorae somewhat further south show a lull near sunspot minimum, but it is less well-defined in weak cycles. Considering Fritz's (1873) Zone II as a whole, we find minima in 1723.8 and 1734.2 and in New England in the United States, c. 1745.0, 1755.5, 1766.5, 1776.5, and 1784.5. Dutch observations show characteristic minima at 1733.5 and 1745.0.

4. AURORAL MODES AND SOLAR MINIMA

The dates in particular cases were influenced by gaps in the observations rather than in the aurorae themselves; some of these gaps are due to bad weather. The various results were therefore compared and, instead of the mean date, the modal or "most-frequent date" was selected as the "withdrawal turning-point." These dates together with the Zurich sunspot minima dates are shown in Table 3 and indicate an average high-latitude withdrawal date about three months later.

4.1 The (N+1) Rule in Mid-Latitudes

The above methods of dating minima cannot be applied to the seventeenth century as there were no regular observations in either Canada or Northern

Table 3. Table of auroral modes and sunspot minima.

Auroral Withdrawal (Mode)	Sunspot Minima (Zurich)	Differences in tenths of years
1724.0 \pm 0.3	1723.5	+5
1734.4 \pm 0.3	1734.0	+4
1745.2 \pm 0.1	1745.0	+3
1755.7 \pm 0.1	1755.2	+5
1766.3 \pm 0.1	1766.5	-2
1776.0 \pm 0.2	1775.5	+5
1784.3 \pm 0.1	1784.7	-4
c.1798.5 \pm 0.5	1789.3	(+2)
c.1810.6 \pm 0.4	1810.6	(0)
1823.6 \pm 0.3	1823.3	+3
1834.3 \pm 0.1	1833.9	+4
1843.7 \pm 0.3	1843.5	(+2)
1856.5 \pm 0.2	1856.0	+5
1867.7 \pm 0.1	1867.0	+7

Norway. As noted by Schove (1955), the auroral minimum year is on the average one year after the sunspot minimum in Central Europe (see Table 2).

4.2 The Three-Year Gap in Mid Latitudes (N+1)

The two previous years (N-1 and N) are also almost devoid of displays so that for the British Isles and Northern Europe a more useful form of the rule is therefore to regard the three-year gap as centered at rather than after the sunspot minimum. This method has been applied to a large collection of British aurorae observations for the Maunder Minimum (1645-99, according to this author). In Holland and Central Europe, the gap is nearly 4 years; it is not complete, as 19% and 11% respectively, of the displays occur within the four-year period, but they are mainly of a type too weak to have been noticed in the seventeenth century.

5. REVISED SOLAR MAXIMA AND MINIMA

From these rules, which are more reliable than the five sunspot rules used previously (Schove, 1955, pp. 137-139), the Wolf-Wolfer dates (Waldmeier, 1961) have been revised tentatively as shown in Table 4.

The 1604.4 maxima is a new one, but most of the other dates differ little from the usual Zurich numbers. Some of the discrepancies could be eliminated if more heliographic latitudes could be calculated, but the M-region maxima in the period 1670-90 may have preceded the actual sunspot maxima.

Some other difficulties are as follows:

1608.9 Minimum: The Zurich date is 1610.8 but Abetti (1957, p. 37) has claimed that the large spots noted by Galileo indicate that "a maximum probably occurred in 1611 or 1612"

(sic DJS). The early spots observed by telescope (North, 1974) were indeed mostly high latitude spots of the new cycle. Large spots were seen in March 1611 and September 1611.

- | | | |
|--------|----------|--|
| 1614.0 | MAXIMUM: | The Zurich date is 1615.5 and 1615.0 would be possible. |
| 1620.2 | Minimum: | This slight version of the Zurich minimum (1619.0) is based on the two-and-a-half-year gap in aurorae from November 1618 to September 1621. Sunspots were not recorded between March 1618 and January 9-11, 1621. |
| 1645.5 | Minimum: | The Zurich date of 1645.0 was wrongly assumed to be too <u>late</u> in the earlier attempt at revision (Schove, 1967). The three-year auroral gap occurred 1645-47 so that the Zurich date seems to have been too <u>early</u> . |
| 1650.8 | MAXIMUM: | The Zurich date 1649.0 could be correct as far as the auroral evidence is concerned. Sunspot evidence for this and the next cycle is very scanty and has been discussed by Eddy (1976) and also by Gleissberg and Damboldt (1979). Astronomical diaries in Italy and elsewhere might reveal additional evidence, or the solar maximum could have been later than that given here. |
| 1673.5 | MAXIMUM: | The Zurich date was 1675.0 but Wolf may have been influenced unduly by the well-known recurrent "late" low-latitude spots of 1676. Flamsteed's observations of 1676 show that the spots were heliographically equatorial (3° - 4° in August and 0° - 11° in October-December). In October-November 1672, the latitudes were 10° to 21° (Paris Observatory MSS, Nos. 24, 32, etc.). Even in August 1671, sunspots observed by Sivers at Hamburg were at a fairly low latitude, but higher latitude spots were inhibited in the period 1645-1700 and the Gnevyshev gap may have been unduly long. |
| 1679.5 | Minimum: | The Zurich date is retained, as no spots were recorded between May 1678 and May 1680. An auroral peak nevertheless followed in 1681 (Link, 1978). |
| 1689.5 | Minimum: | The Zurich date is retained although the auroral rules would indicate an earlier date. It is assumed that the sunspots recorded in October 1689 belonged to the old cycle. If not we must accept Link's (1978) revised date of 1687. |
| 1695.0 | MAXIMUM: | The large spots noted by La Hire in 1695 must surely be near the maximum of this cycle, perhaps the weakest cycle since the third century A.D. |
| 1699.0 | Minimum: | This revision, together with that for 1633, was suggested (Schove, 1955, p. 139) originally so that the intervals between adjacent minima would be between 13.6 and 9.0 years. These limits still apply to these minima dated by auroral considerations. |

If these revisions of the Zurich dates are acceptable, a list of annual solar numbers for the seventeenth century can be published. Quantification of some kind is necessary for solar-terrestrial correlation, but such numbers cannot yet be considered reliable or strictly indicative of sunspot activity. Eddy's stimulating paper (1976) suggests that my earlier estimates of sunspot numbers were too high although Gleissberg and Damboldt (1979) and Link (1978) emphasize that the Maunder Minimum was not as lacking in spots as has been supposed.

Table 4. Revised times of solar maxima and minima, 1600-1700 A.D.

Number of Cycle	Maxima	Number of Cycle	
-13	1604.4 \pm 0.5	-12	?1608.9 (1610.8)*
-12	1614.0 (1615.5?)	-11	1620.2 \pm 0.5 (1619.0)
-11	1625.8 \pm 0.5 (1626.0)	-10	1633.7 \pm 0.5 (1634.0)
-10	1639.3 \pm 0.5 (1639.3)	-9	1645.5 \pm 0.8 (1645.0)
-9	1650.8 \pm 1.0 (1649.0)	-8	1655.5 \pm 0.5 (1655.0)
-8	1661.0 \pm 0.5 (1660.0)	-7	1666.5 \pm (?) (1666.0)
-7	1673.5 \pm 1.0 (1675.0)	-6	1679.5 \pm 2.0 (1679.5)
-6	1685.0 \pm 1.0 (1685.0)	-5	1689.5 \pm 0.5 (1689.5)
-5	1695.0 \pm 1.0 (1693.0)	-4	1699.0 \pm 1.0 (1698.0)
	1705.5 (1705.5)		1712.5 (1712.0)

*Zurich dates are shown in parentheses.

6. SIXTEENTH CENTURY

Time of solar maxima and minima based on the auroral rules can be expressed more precisely than was possible previously (Schove, 1955 and 1969, p. 393). See Table 5.

Table 5. Times of solar maxima and minima.

Cycle Number	Minima	Maxima
-22	1501.5 \pm 2.0	1506.5 \pm 1.0
-21	1514.2 \pm 0.3	1517.7 \pm 0.5
-20	1524.7 \pm 0.3	1528.2 \pm 0.3
-19	1534.5 \pm 0.5	1537.4 \pm 0.4
-18	1543.7 \pm 0.5	1547.4 \pm 0.5
-17	1554.5 \pm 0.5	1558.3 \pm 0.5
-16	1567.7 \pm 0.5	1571.3 \pm 0.5
-15	1578.4 \pm 0.5	1581.5 \pm 1.0
-14	1587.2 \pm 0.5	1593.8 \pm 2.0
-13	1598.8 \pm 0.5	1604.4 \pm 0.5

These dates were calculated before Link's (1978) paper, which includes a chart of aurorae from 1540. The auroral maxima and minima revealed by three-

year moving means are given to the nearest year and this often corresponds to the sunspot dates given here. An extra auroral cycle with a maximum in 1555 is due to the over-assiduous search for unusual occurrences by Conrad Lycosthenes who was compiling his catalogue of unusual occurrences at that time in the Far East there is no corresponding maximum.

7. REVISED SUNSPOT NUMBERS, 1700-1751

The original sunspot numbers for this period (Waldmeier, 1961) were based on inadequate information as Waldmeier has pointed out (personal communication). My earlier attempt at increasing them (Schove, 1955, p. 129 and Table 1) was also unsatisfactory, and the various sunspot diagrams and observations (e.g., at Paris Observatory) suggest that a further increase is warranted. The revised figures presented in Table 6 are tentative until they have been fully checked with records of original observers.

Table 6. Revised sunspot numbers, 1700-1751 A.D.

	0	1	2	3	4	5	6	7	8	9	Maximum Value	Maximum Dates Zurich
1700	5	12	22	38	56	68	57	40	35	23	70	1705.5
1710	13	3	0	5	18	35	59	85	84	64	90	1718.2
1720	46	32	23	15	22	54	120	147	134	105	150	1727.5
1730	74	50	24	7	11	45	82	106	132	126	135	1738.7
1740	92	53	29	19	8	15	30	50	71	81	X	
1750	83	66	47								92.6	1750.3

The Wolf-Wolfer solar minima and maxima in this century have been confirmed by the auroral rules in this paper. The only date for which a slight change is suggested is that of the first minimum given as 1712.0 by Wolf and now adjusted to 1712.5.

8. THE 22-YEAR CYCLE

In the period 1841-1940 alternate cycles were usually stronger and, considering the averages over centuries as a whole, they show small persistent differences back to 720 A.D. In the period 200 B.C.-400 A.D. this rule may have been reversed. The phase of the sunspot cycle over long periods can now be determined, given an adequate number of tree-ring and varve-series (cf. Schove, 1978, 1979).

9. LONG-TERM PREDICTIONS

The previous attempt (Schove, 1955) to predict the dates of sunspot minima and maxima from 2025 A.D. was based on a mean cycle of 11.1 years rather than 11.09. Partly for this reason and partly because the sunspot cycles have been even stronger than expected, the dates given have proved slightly too late up to 1978, and this will apply to the next maximum too. Nevertheless, a series of cycles averaging 12 years are likely to begin after the next maximum, which is generally expected in 1980.

10. CONCLUSIONS

Further quantification of solar activity in the period 1500-1700 has been based on empirical rules linking aurorae with the known solar maxima and minima of the period 1710-1950.

The various turning-points given here were tested to check that they belonged to the "same population" (in the statistical sense) as their counterparts since 1749. Thus the time between minimum and maximum is usually a guide to the heights of the maximum, times of 3, 4, 5, 6, and 7 years corresponding respectively to heights of over 130, 100, 75, 60, and 50. This rule suggests that the maxima had amplitudes of the same order as the values tabulated (Schove, 1955, p. 136).

We need to know the precise year of sunspot maxima and minima in order to study solar terrestrial relations. Tree-ring weather (or proxy) data can then be compared separately with an adequate number of sunspot cycles of each amplitude-class. The effects of strong and weak cycles are sometimes opposite, as in the case of the Nile flood (Schove, 1977, figs. 4.8 and 4.6) and associated pressure parameter effects.

The information in the fifteenth century is inadequate, but that in the twelfth is often sufficient for accuracy of ± 0.5 years.

REFERENCES

- Abetti, G. (1957): The Sun. London, Faber, p. 37.
- Eddy, J. (1976): The Maunder Minimum. Science, 192:1189.
- Fritz, H. (1873): Verzeichniss beobachteter Polarlichter. Kaiserlichen Akademie der Wissenschaften, Vienna.
- Gleissberg, W., and T. Damboldt (1979): Reflections on the Maunder Minimum of sunspots. Jour. Brit. Astr. Assn., May.
- Gnevyshev, M. N. (1977): Solar Physics, 51:175.
- Link, F. (1978): Solar cycles between 1540 and 1700. Solar Physics, 59-178.

- North, J. D. (1974): In: J. W. Shirley, ed., Thomas Harriot. London, pl. 4: 118.
- Schove, D. J. (1955): The sunspot cycle, 649 B.C. to A.D. 2000. J. Geophys. Res., 60:136.
- Schove, D. J. (1967): Sunspot cycles. In: R. Fairbridge, ed., Encyclopedia of Atmospheric Sciences and Astrogeology. New York, p. 963-968.
- Schove, D. J. (1969): The biennial oscillation, tree-rings and sunspots. Weather, 24:390-397.
- Schove, D. J. (1977): African droughts and the spectrum of time. In: D. Dalby, R. J. Harrison-Church, and F. Bezzas, eds., Drought in Africa. 2 (Afr. Envir. Spec. Rep. 6).
- Schove, D. J. (1978): Tree-ring and varve scales combined, c. 13500 B.C. to A.D. 1977. Palaeography, Palaeoclimatology, Palaeoecology, 25:209-233.
- Schove, D. J. (1979): In: A. A. Ch. Schluchter, ed., Moraines and varves. Zurich.
- Schove, D. J. (1980): Benchmark Book, Sunspot Cycles. Stroudsburg, Penna., USA, Dowden, Hutchinson and Ross.
- Schove, D. J., and P. Y. Ho (1959): Chinese aurorae L I, A.D. 1048-1070. Jour. Brit. Astr. Assn., 69:295-304.
- Tromholdt, S. (1902): Katalog der in Norwegen bis June 1978 beobachtungen Nordlichter. Oslo, Christiana.
- Waldmeier, M. (1961): The sunspot activity in the years 1610-1960. Zurich, Schulthess & Co.
- Wittman, A. (1978): The sunspot cycle before the Maunder Minimum. Astron. Astrophys. 66:93-97.

A LEVEL OF GEOMAGNETIC DISTURBANCE AND A DISTRIBUTION OF SUPERLARGE-SCALE MAGNETIC FIELDS ON THE SUN

M. I. Pudovkin, D. I. Ponyavin, A. D. Chertkov
Institute of Physics
State University
Leningrad, 199164, U.S.S.R.

By using synoptic charts of a line-of-sight component of the solar photospheric magnetic field (Howard, Bumba and Smith, 1967) the distribution of all three components (B_r , B_θ , B_ψ) of the coronal magnetic field as well as its modulus B are calculated for the period August-December 1965. The magnetic field was assumed to be potential.

The following are shown:

(1) Day-averaged values of K_p and AE indices correlate with B'_θ ($\rho \approx 0.5$ to 0.6) with the time-lag^p with respect to the phenomena on the Sun of 3 to 7 days, where B'_θ is a corrected meridional component of the large-scale solar magnetic field (its distortion while propagating from the Sun is taken into account).

(2) Solar wind velocity on the Earth's orbit positively correlates with B ($\rho \approx 0.5$ to 0.6) with the same time-lag of 3 to 7 days.

In the first case the correlation was the best when B'_θ was calculated in the 40° zone around the equator of the Sun, in the second case when B was calculated directly at the equator.

An index of geoeffectivity of large-scale magnetic fields connected with high-velocity streams in the solar wind is proposed.

Geomagnetic activity is known to have a tendency to recurrent changes with a period of 27 days, which can be understood in terms of long-living high-velocity streams in the solar wind (Snyder et al., 1963). At the same time solar wind velocity (V) is not the only parameter that crucially influences geomagnetic activity. The most geoeffective part of a high-velocity stream is its front, where the variability of the interplanetary magnetic field (σ) is the largest (Bobrov, 1973). Besides that, the level of geomagnetic activity depends on the value and the sign of IMF south component (B_z) averaged in a certain time interval of high-velocity stream (Pudovkin et al., 1979).

Thus, one can expect that the combination of geoeffective parameters v , σ and B_z influences most crucially the level of geomagnetic activity (Garrett et al., 1974). The connection with geomagnetic indices is the largest when they are correlated with the solar wind electric field in the motionless system:

$$E_{sw} = vB_z + kV\sigma,$$

where vB_z = the constant part of the electric field, $V\sigma$ = the alternative part of the electric field, and k = a constant coefficient.

Thus, in order to predict the level of geomagnetic disturbance one must know how to predict the parameters of the solar wind, v , B_z , and σ .

Studies have shown that the parameters of the solar wind are somehow connected with the large-scale solar magnetic fields. Particularly the structure of the large-scale magnetic fields in the lower corona crucially influences the formation and the existence of high-velocity streams (Krieger et al., 1973). The sign of the meridional component of the superlarge-scale magnetic field on the Sun determines the level of geomagnetic disturbance and thus, as one can expect, the sign of B_z in IMF (Pudovkin and Chertkov, 1976).

The relation of σ to the solar magnetic fields has never been directly studied, but one can suppose the existence of indirect relation between them, as it is known that the value of σ is roughly proportional to the value of magnetic field modulus (B) in the solar wind (Hundhausen, 1972).

Thus, one can expect that the large-scale solar magnetic field is decisive in determining the value and the sign of the solar wind electric field on the Earth's orbit and consequently the level of geomagnetic disturbance. This problem will be discussed in our paper.

For our analyses we took four Carrington rotations, 1498-1501, in the year 1965, which was close to the minimum of the solar activity. Strong flares distorting the structure of coronal magnetic fields were practically absent in this period, except for October of 1965. The data on solar wind and IMF were taken from King (1975, 1977). Superlarge-scale magnetic fields in this period were calculated by using synoptic charts of photospheric fields (Howard et al., 1967). Accepting potential approach, Gaussian coefficients of the field were calculated from these data (Altschuler and Newkirk, 1969). The expansion was made up to seven harmonics. This appeared to be sufficient for determining the regular part of the solar wind with the characteristic time-variation of several days.

Unlike Altschuler and Newkirk (1969), we took into account changes of superlarge-scale magnetic fields during a solar rotation. The coefficients were calculated each 1.5 days, which corresponds to the longitudinal displacement by 20° .

The results of the correlation analyses of the relation between superlarge-scale fields with day-averaged values of solar wind velocity (v),

vertical component of IMF (B_z), and geomagnetic activity indices ΣK_p and AE, are plotted in Figs. 1 and 2 (for example, rotation 1498 was chosen). They are presented in the table.

On Fig. 1 cross-correlation functions are shown for the following:

- (a) B and v , where B is modulus of solar magnetic field.
- (b) B_θ and B_z , where B_θ is the meridional component of the solar magnetic field.
- (c) B_θ and ΣK_p .
- (d) B_θ and AE.

The ordinate corresponds to the correlation coefficient (ρ), and the abscissa corresponds to the time-lag in days (τ). Central meridional passage by the magnetic peculiarity on the Sun is marked by vertical line $\tau = 0$. From Fig. 1 one can see the existence of a low but still positive correlation between the value of B_θ on the Sun and the level of geomagnetic activity with the time-lag $\tau \approx 3$ days. This correlation can presumably be explained by the existence of nearly the same (but negative) correlation between B value and day-averaged value of B_z in IMF (Fig. 1b). These data in general

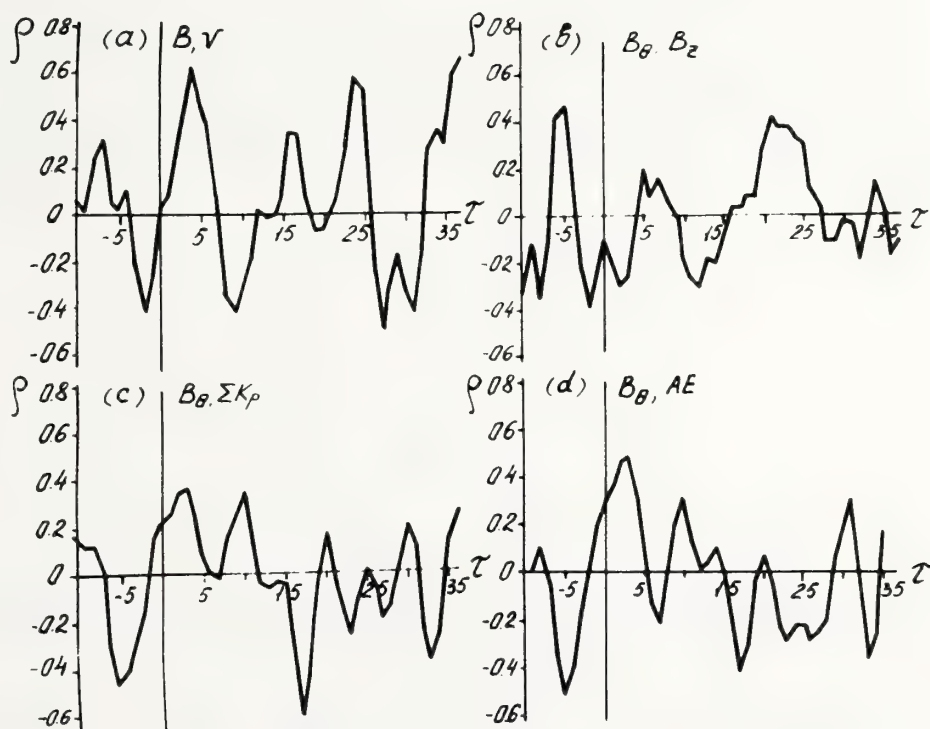


Figure 1.--Cross-correlation functions for magnetic fields calculating on the equator of the sun during 1498 Carrington rotation with parameters of solar wind, IMF and geomagnetic indices.

can prove the supposition that the meridional component of the superlarge-scale solar field is transported by the solar wind up to the Earth's orbit without changing its sign. At the same time one can see from these data that the solar magnetic field, including its vertical component, is substantially distorted on its way from the Sun to the Earth. The latter can be deduced from the fact that the correlation coefficient between the B_θ value and the day-averaged values of geomagnetic activity indices is substantially lower than the correlation coefficients between day-averaged values ΣKp , AE and B_z of solar wind. In addition, the average time-lag between correlated values ($\tau \approx 3$ days) does not correspond to the average solar wind velocity during the period considered; this can be also explained by a substantial distortion of the field B_θ .

One can expect that these distortions are caused by characteristic changes in plasma density and intensity of the frozen-in magnetic field (including its vertical component) in the front part of the high-velocity streams in the solar wind (Hundhausen, 1972; Pudovkin et al., 1979); in this region the values of n , $|B|$, B_z , and σ are approximately proportional to $\partial v / \partial t$. Thus, in order to take into account these distortions, one must know the solar wind velocity as a function of time. Consequently it seems important that, as can be seen from Fig. 1a, solar wind velocity in the Earth's orbit (to say more exactly its day-averaged value) clearly depends on the intensity of superlarge solar magnetic field ($\rho = 0.62$; time-lag between v and B variations ($\tau = 4$ days) corresponds to the average velocity of the solar wind. This result makes it possible to consider, in the first approximation, that solar wind velocity is proportional to the intensity of the superlarge-scale field of the Sun ($v \propto B$). Thus we introduced a value of effective field B'_θ as a value determining the day-averaged value of B_z in IMF:

$$B'_\theta = C_1 B_\theta \left(\frac{\partial \tilde{B}^*}{\partial t} + C_2 \right), \text{ where}$$

$$\frac{\partial \tilde{B}^*}{\partial t} = \begin{cases} \frac{\partial \tilde{B}}{\partial t} & \text{when } \frac{\partial \tilde{B}}{\partial t} > 0 \\ 0 & \text{when } \frac{\partial \tilde{B}}{\partial t} < 0 \end{cases},$$

where \tilde{B} is the smoothed value of B modulus on the Sun and C_2 is chosen to be equal to $1/4$ of the maximum value of $\partial \tilde{B} / \partial t$ for the period considered.

The correlation coefficient between B'_θ and B_z is shown on Fig. 2b; one can see that the correlation between the above-mentioned values in this case is higher than in Fig. 1b, and the time-lag between them ($\tau = 5$ days) corresponds to the transit time of the field propagating from the Sun to the Earth.

The result obtained makes it possible to introduce a combined index of solar wind geoeffectivity, which takes into account predicted value of B_z in

IMF as well as the expected solar wind velocity (v) and the value of IMF variability (σ):

$$G_E \sim (vB_z + kv\sigma) \sim (BB'_\theta + k'B \frac{\partial B^*}{\partial t}), \quad (1)$$

where $k' =$ a coefficient, the value of which ($k' = 1G$) is chosen in such a way that the correlation coefficient between the values discussed is maximum.

Taking into consideration that B value (and according to our hypothesis, the expected value of velocity v) is maximum not necessarily near the equator of the Sun, the v and B'_θ values were calculated in the point where $B = B_{\max}$ in the interval $\pm 20^\circ$ near the equator. The results of the correlation of the introduced index G_E with the level of geomagnetic activity are presented on Fig. 2, c and d. Here one can see that the correlation coefficients between G_E and ΣKp , and G_E and AE , are equal to 0.66 and 0.72, respectively,

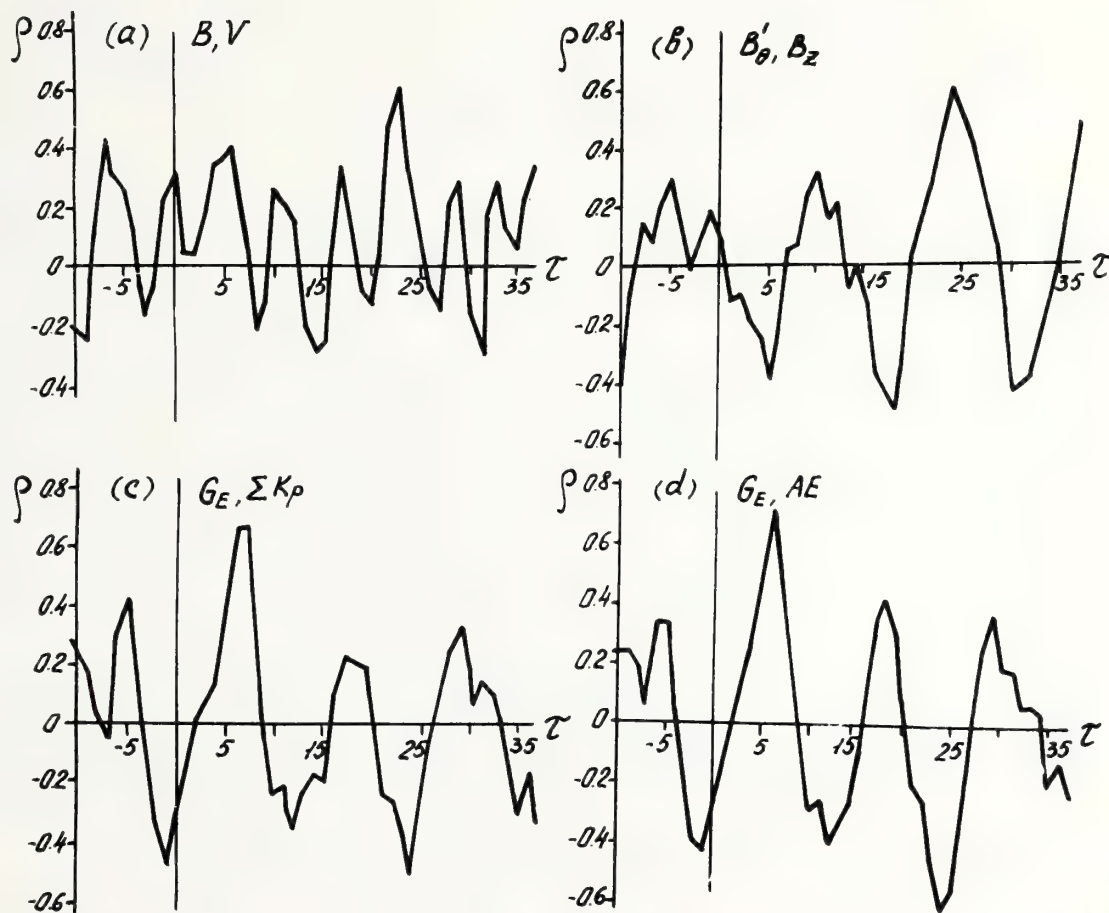


Figure 2.--The same as in Fig. 1 for magnetic fields calculating on the 40° zone near equator.

and are considerably more than in the case shown in Fig. 1, c and d. Time-lag between the variations of the indices of geomagnetic activity on the Earth and the variations of G_E index on the Sun is as much as 6 days. As it was mentioned above, this time-lag corresponds to the transit time of the field from the Sun to the Earth.

At the same time correlation coefficients between solar wind velocity and the value of B on the Sun, chosen by the above mentioned method in the 40° zone around the equator, are a little lower than when B was taken directly at the equator.

These two results can prove the conclusion made by Nolte and Roelof (1977) (who have also considered the data for the year 1965) that high velocity streams are formed in the near-equatorial zone, but the IMF is formed in the middle latitudes. At the same time positive correlation between B and v indicates that high-velocity streams are formed above the areas with the enhanced intensity of the magnetic field.

One can also see in Fig. 1a and Fig. 2, b, c, and d, a characteristic period of $13\frac{1}{2}$ days, which is typical for the curves presented. This period corresponds to a half-period of solar rotation, and its existence can be understood as an independent proof of a close relationship between geomagnetic disturbances and magnetic fields on the Sun.

The values of maximum correlation coefficients in the interval 0-10 days of time-lag for the subsequent 1498-1501 rotations and the corresponding days of delay are presented in the Table. From the data presented one can see that the general behavior of rotations 1500 and 1501 is essentially the same as that of rotation 1498, which was discussed above. Correlation between the level of geomagnetic disturbancy (ΣKp , AE) and the value of the G_E index is about 0.4 to 0.7 with the time-lag of 5 to 7 days. This result can be considered as satisfactory. At the same time one can see that it was unlike the case of rotation 1498; the corrected G index correlates better with the values ΣKp and AE than with the uncorrected value of B_θ . This result can be presumably explained by the fact that in November - December of 1965 (months corresponding to Carrington rotations 1500 and 1501), according to King's data, the high-velocity streams in the solar wind were practically absent and consequently the second term in (1) was relatively small.

In addition one cannot but notice that the correlation of the indices of geoeffectivity of the Sun (B_θ and G_E) with the level of disturbance of the Earth's magnetic field, is better than the indices' correlation with the directly measured parameters of the solar wind. This can presumably be explained by the fact that the data of the direct measurements of solar wind parameters for the period considered are highly irregular and are often lacking (particularly for v in November, and B_z in December).

Rotation 1499 (see table) differs considerably from the three other rotations. The time-lag $\tau \sim 2$ days cannot be explained by the transit of the disturbance by the solar wind, although in the above-mentioned period several intensive flares were registered that could alter considerably the structure of the solar wind.

Table 1.--The maximum correlation coefficients and corresponding time lags between them, the magnetic field intensity at the Sun, and the solar wind parameters and indices of the geomagnetic activity.

Number of Carrington Rotation		Equator				40° zone			
		B,v	B_{θ}, B_z	$B_{\theta}, \Sigma K_p$	B_{θ}, AE	B,v	B'_{θ}, B_z	$G_E, \Sigma K_p$	G_E, AE
1498	ρ	0.62	-0.30	0.36	0.48	0.40	-0.38	0.66	0.72
	τ	4	2	3	3	6	5	6	6
1499	ρ	-0.38/ -0.54	-0.36	0.42	0.42	0.26	-0.14	0.28	0.20
	τ	3/9	4	2	2	5	3	2	2
1500	ρ	0.10	-0.28	0.36	0.32	-0.04	-0.36	0.36	0.38
	τ	6	7	6	6	7	6	7	7
1501	ρ	0.42	0.10	0.52	0.68	0.46	-0.04	0.50	0.70
	τ	5	5	5	5	5	6	5	5

Thus, ignoring the data of the rotation 1499 we can make the following conclusions:

(1) The velocity of the solar wind on the Earth's orbit (day-averaged values) positively correlates with the intensity B of the super-large-scale magnetic field on the Sun ($\rho \approx 0.4$) in the area of the solar equator. The time-delay of the variations in v and B ($\tau \approx 5$ to 6 days) corresponds to the average solar wind velocity.

(2) Day-averaged values B_z of IMF correlate with the value of B'_{θ} on the Sun ($\rho \approx -0.4$) with the same time-lag 5 to 6 days.

(3) The introduced index of solar geoeffectivity,

$$G_E = BB'_{\theta} + k'B \frac{\partial \tilde{B}^*}{\partial t},$$

convincingly correlates with day-averaged values of magnetic activity indices on the Earth ($\rho \approx 0.4$ to 0.7). This correlation takes place when the high-velocity streams are absent (rotations 1500, 1501) as well as when they are present (rotation 1498). This fact gives us hope that the G_E index may be useful for predicting the level of geomagnetic disturbances about 5 days before they occur.

REFERENCES

Altschuler, M. D., and G. Newkirk, Jr. (1969): Magnetic fields and the structure of the solar corona. Solar Phys., 9:131.

- Bobrov, M. S. (1973): K index correlations with solar wind parameters during the first and second stages of a recurrent geomagnetic storm. Planet. Space Sci., 21:2139.
- Garrett, H. B., A. J. Dessler, and T. W. Hill (1974): Influence of solar wind variability on geomagnetic activity. J. Geophys. Res., 79:4603.
- Howard, R., V. Bumba, and S. Smith (1967): Atlas of solar magnetic fields, 1959-1966. Carnegie Inst., Washington, D.C., Publ. No. 626.
- Hundhausen, A. J. (1972): Coronal expansion and solar wind. Springer-Verlag, Heidelberg and New York.
- King, J. H. (1975, 1977): Interplanetary magnetic field data book. National Space Science Data Center.
- Kreiger, A. S., A. F. Timothy, and E. C. Roelof (1973): A coronal hole as the source of a high velocity solar wind stream. Solar Phys., 29:505.
- Nolte, J. T., and E. C. Roelof (1977): Solar wind, energetic particles and coronal magnetic structure: the first year of solar cycle 20. J. Geophys. Res., 82:2175.
- Pudovkin, M. I., and A. D. Chertkov (1976): Magnetic field of the solar wind. Solar Phys., 50:213.
- Pudovkin, M. I., S. A. Zaitzeva, A. D. Chertkov, and E. M. Fomina (1979): The structure and geoefficiency of high velocity solar wind streams, Paper submitted to the Solar-Terrestrial Predictions Proceedings.
- Snyder, C. W., M. Neugebauer, and U. R. Rao (1963): The solar wind velocity and its correlation with cosmic-ray variations and with solar and geomagnetic activity. J. Geophys. Res., 68:6361.

B. INTERPLANETARY MEDIUM PREDICTIONS

INFERENCE OF SECTOR POLARITY OF THE INTERPLANETARY MAGNETIC FIELD FROM THE COSMIC RAY NORTH-SOUTH ASYMMETRY

S. Mori, S. Yasue, Y. Munakata[#], K. Nagashima^{##}

Department of Physics, Faculty of Science, Shinshu University,
Matsumoto 390, Japan

[#]Department of Liberal Arts and Science, Chubu Institute of
Technology,

Kasugai 487, Japan

^{##}Cosmic Ray Research Laboratory, Nagoya University,
Nagoya 464, Japan

Based on ground level cosmic ray observations, inference of sector polarity of the interplanetary magnetic field has been continued for the period 1974-75. A similar high success rate ($\sim 76\%$) is obtained for the present period to that ($\sim 76\%$) for the preceding years of 1971-73.

1. Introduction

Based on data from ground level cosmic ray observations, a great many investigations have been made concerning inference or prediction of various parameters of electromagnetic conditions in interplanetary space. Very recently, Mori and Nagashima (1979; hereafter referred to as Paper I) presented one example; inference of sector polarity of the interplanetary magnetic field (IMF) from the cosmic ray north-south asymmetry (abbreviated as N-S asymmetry). A brief summary of Paper I is as follows. The sector polarity of the IMF has been inferred daily for the period 1971-73, using ground level cosmic ray observations. The method depends on the sector polarity directed towards and away from the Sun being associated with different characteristic variations of the cosmic ray N-S asymmetry. The analysis has a simple basis. The difference between the north and south daily mean intensities of directional telescopes at a single observing

station is determined and its value relative to the 27-day average is calculated. The sign (negative or positive) of the value thus derived corresponds to the sector polarity (away or toward) on a daily basis. Good (~76%) agreement is obtained between polarities inferred indirectly by the present method and those observed directly with spacecraft magnetometers. We therefore suggest that cosmic ray observations can be used with a fair degree of accuracy (~75%) for inferring the sector polarity of the magnetic field in interplanetary space.

The close correlation observed between the cosmic ray N-S asymmetry and the IMF direction follows from the density gradient hypothesis (Swinson, 1969; Gleeson, 1969). The cosmic ray N-S asymmetric flow might be produced from the particle streaming as a result of a positive radial heliocentric cosmic ray density gradient ($\nabla \vec{n}$) in the presence of the IMF (\vec{B}). Thus the direction of the resultant anisotropic flow ($\vec{B} \times \nabla \vec{n}$) alters as the IMF (\vec{B}) direction changes. With the observed fact of the daily association of the sign (negative or positive) of the cosmic ray N-S asymmetry index with the IMF direction (away from or towards the Sun), Paper I has presented a definite support to the above consideration.

In the present report, we continue to examine the correlation between the cosmic ray N-S asymmetry and the IMF direction for the extended period of 1974-75, and to infer the IMF polarity on a daily basis from the cosmic ray N-S asymmetry observed at a single observing station in the same manner as that in Paper I.

2. Prediction Technique

2.1 Method of inferring IMF polarity from cosmic ray N-S asymmetry

The method of inferring the IMF polarity from cosmic ray observations is summarized briefly as: First, the cosmic ray N-S asymmetry is derived on a daily basis at a single observing station. Then its relative value with respect to the 27-day average or the 27-day running mean is calculated to remove the long term variation. Second, from the sign (negative or positive) of the N-S asymmetry thus derived we determine the field polarity (away or toward) on the corresponding day. Inference is made in such a manner that on the day when the N-S asymmetry is negative the IMF polarity points away from the Sun on that day. And on the day when the N-S asymmetry is positive the corresponding IMF is directed towards the Sun.

2.2 Calculation of cosmic ray N-S asymmetry

In order to calculate the cosmic ray N-S asymmetry, we compare the data from two directional telescopes at a single observing station, having each asymptotic direction of the viewing cone towards the north and south respectively. Paper I utilizes the data from the multi-directional muon telescopes at Nagoya (sea level) (Sekido et al., 1975). To extract the N-S asymmetry from the observed intensity variations, the difference is taken between the daily mean directional intensities by following the method proposed by one of the authors (Nagashima et al., 1971).

One of the indices representing the cosmic ray N-S asymmetry, the GG-term is given by the sum of the difference (divided by two) of the counting rates between pairs of telescopes pointing in certain directions at a fixed zenith as defined below,

$$GG = \{(49^\circ N - 49^\circ S) + (49^\circ N - 49^\circ E)\}/2 \quad (1)$$

where each term denotes a directional component having its central direction of the viewing cone pointing towards the zenith angle of 49° in the north (N), the south (S) and the east (E)-direction, respectively. It is noted that because of the second order difference, the GG-term is free from various sources of noise such as the isotropic intensity fluctuations, the contributions from atmospheric effects and the difference in the geomagnetic cut-off rigidity for each direction. It is added to note that since the muon telescopes respond to higher mean primary rigidity than neutron monitors (mean rigidity of response 10^{25} GV); the inclined telescope by 49° to the vertical direction to ~ 80 GV, the intensity measured by these telescopes shows relatively small isotropic intensity fluctuations; less than one-third of that for neutron monitors. This is one of the merits of using the muon component data in comparison with making use of the nucleonic component data. For a median primary rigidity of 80 GV, the GG-term represents the intensity difference between $\sim 45^\circ$ north and $\sim 15^\circ$ south in the asymptotic latitudes in the hemispheres. In the present report, the GG-term at Nagoya (Sekido et al., 1979) is exclusively utilized as is done in Paper I.

3. Basis for Technique

3.1 Basis for technique for inferring IMF polarity from cosmic rays

So far a great many investigations have been performed to examine and establish the relationship between the cosmic ray N-S anisotropic flow and the IMF conditions (e.g., Yoshida et al., 1973). The N-S anisotropic flow might be produced from a particle drift due to a positive radial density gradient in the presence of the IMF (Swinson, 1969; Gleeson, 1969). The resul-

tant anisotropic flow could be perpendicular to the ecliptic plane (Yasue, 1979). Thus it may be expected that this flow vector can be resolved into two components, and these also may be observed on the Earth as, at least, two components of the anisotropy; the N-S asymmetry and the associated sidereal diurnal anisotropy. Fig. 1 shows schematically the anisotropic flow and

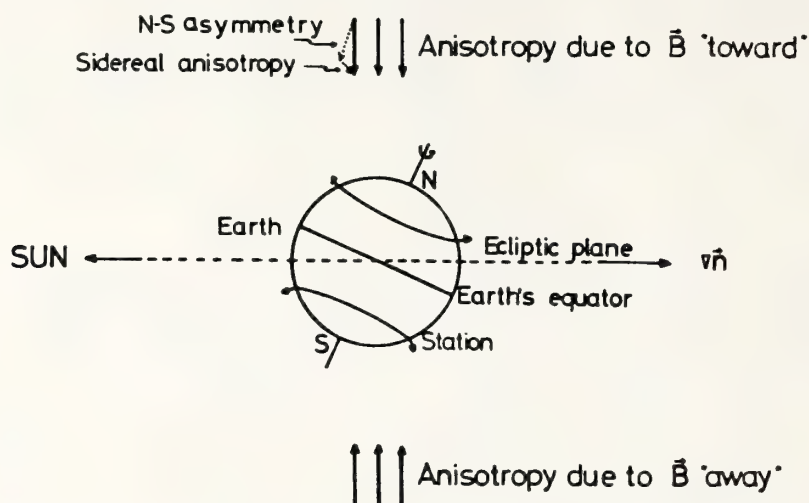


Fig. 1

its dependence on the direction sense of the prevailing IMF, together with the observable two components on the Earth mentioned above. As is seen in the diagram, it might be possible to infer the IMF direction sense from the observed cosmic ray N-S anisotropy or also from either of the N-S asymmetry or the associated sidereal diurnal anisotropy (Bercovitch, 1969, 1971; Iucci and Storini, 1972; Swinson, 1969, 1971). Also we can see that from a simple geometrical consideration the amplitude-ratio between two components; the N-S asymmetry and the sidereal diurnal variation observed on the Earth, may be about 3:1 ($=\cos 23.5^\circ : \sin 23.5^\circ$). This can be understood based on the fact that the former component could be the parallel flow and the latter is the normal flow to the Earth's rotational axis, which has a tilt by 23.5° to the ecliptic north-pole. Thus the N-S asymmetry is probably preferable for inferring the direction sense of IMF.

Alternately the N-S asymmetry can be derived by comparing the observations obtained at sites in the northern and southern hemispheres. Comparison of data from polar neutron monitor stations at Arctic and Antarctic has usually been performed. Each station has each asymptotic cone of viewing of nearly 90° in the north and south latitudes and is almost opposite to each other. In the data of neutron monitors, however, large isotropic intensity fluctuations ($\sim 1\%$) are often observed to perturb greatly the small N-S asymmetric term ($\sim 0.1\%$) in the variations. Thus this method is unsatisfactory for deriving the N-S asymmetry on a daily basis, but is applied to the data averaged over a month or a

yearly basis (Bercovitch, 1969, 1971; Iucci and Storini, 1972; Kudo and Wada, 1977), or during disturbed periods when the asymmetry is large ($>2.0\%$) (Duggal and Pomerantz, 1976).

Also note that theory predicts and the observations verify (Yoshida et al., 1973; Kondo et al., 1975; Mori et al., 1975; Yasue, 1979) that the yearly averaged amplitude of the N-S asymmetry is approximately 0.1% for quiet periods when the solar wind velocity $\sim 400\text{km/s}$ and the prevailing IMF $\sim 5\gamma$. In order to determine such a small N-S asymmetry on a daily basis the statistical uncertainty in the data should be quite small, so the counting rate of the telescopes should be high. For example, Nagoya high-counting, multi-directional muon telescopes meet these requirements as shown in Table 1. The counting-rate error

Component	Average counts($\times 10^6/\text{h}$)	Geomagnetic cut-off(GV)
Vertical	2.76	11.5
49°North	0.49	12.9
49°South	0.48	10.9
49°East	0.46	21.0

Table 1 Some sub-telescope of Nagoya multi-directional telescope

for the GG-term is $\sim 0.07\%$ for the daily mean value.

One example showing the above close relationship between the cosmic ray N-S asymmetry and the IMF polarity, is plotted in Fig. 2 (cited from Paper I). In the figure relative daily values with respect to the 27-day average are shown on Bartels 27-day solar rotation period for 1971. The field polarities are also plotted in the figure, which are referred to the data from direct measurements (Wilcox et al., 1975; Fairfield and Ness, 1974). In comparison between the GG-term (Nagoya) and the IMF polarity in Fig. 2, it is clear that on the day when the IMF points away from the Sun almost all the GG-values lie below the 27-day average, i.e., the relative GG-values are negative. And on the day when the field is directed towards the Sun, the corresponding GG-values are almost always greater than the 27-day average, i.e., the relative GG-values are positive.

The success rate of our prediction is examined by comparing the signs (negative or positive) of these GG-values with the corresponding IMF polarity (away or toward) obtained by the direct measurements. The rate of agreement is approximately 79% for the year 1971.

Another illustration of above correspondence is shown in Fig. 3, which compares among inferred IMF polarities from cosmic rays (GG-term) by the present method, those observed directly by the spacecrafts (I) and those inferred based on the geomagnetic field observations made by Svalgaard (SVL) (1975). It is evident that these three sets of observations agree very well among them-

selves. A quantitative comparison is made between GG and I, and

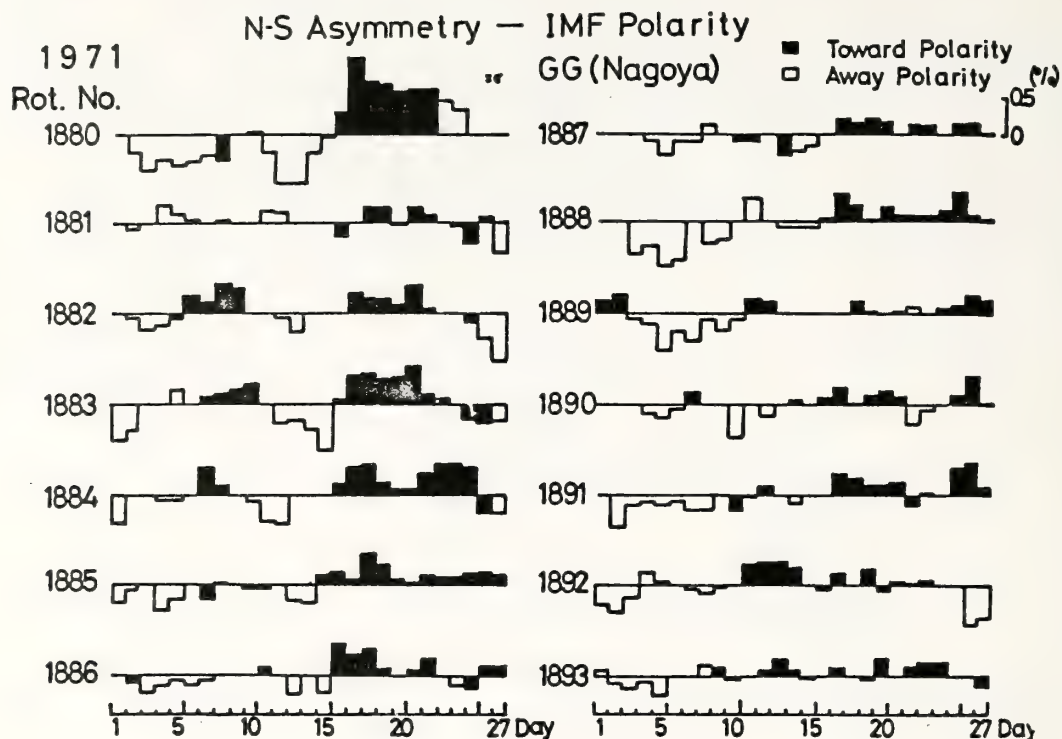


Fig. 2 Relative daily values of cosmic ray N-S asymmetry for 1971

is given in Tables 2(a), 2(b) and 2(c) for each year 1971, 1972 and 1973, respectively. The number of days of occurrence of each of the nine possibilities for the polarities inferred from cosmic ray data and those of the direct measurements are listed. In these tables, a term 'mixed' is used when $GG = 0.0\%$. Table 3 summarizes these success rates for each, in which 'mixed' is counted for 50% agreement (A) and 50% disagreement (D) for both cases of the field polarities.

Inferred polarities	Observed polarities		
	Toward	Away	Mixed
Toward	132	17	14
Away	25	101	16
Mixed	20	7	2

Table 2(a) Number of days of occurrence of each of the nine possibilities for the polarities inferred and observed for 1971

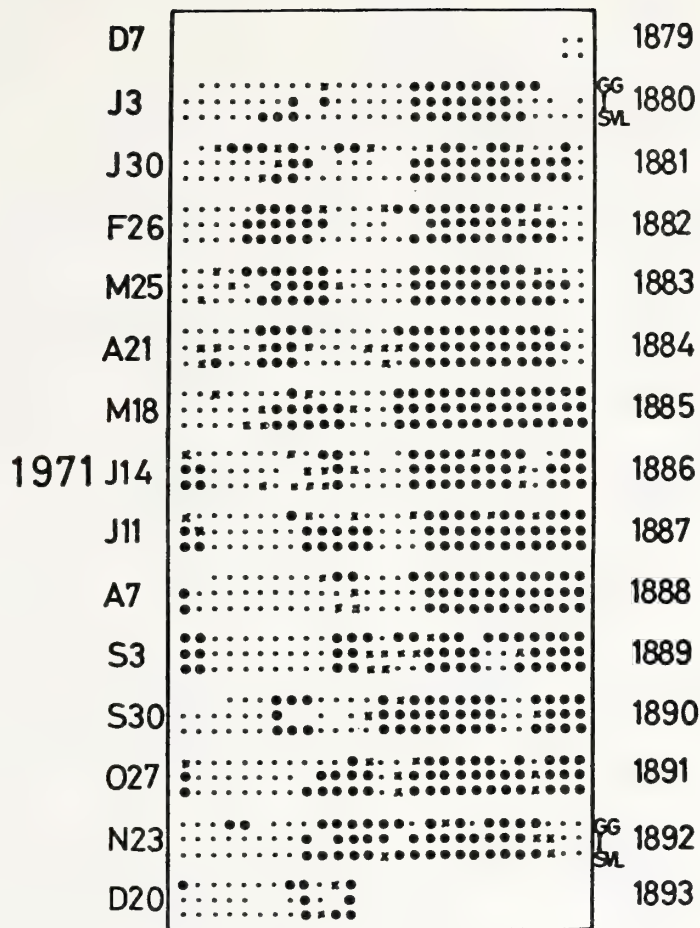


Fig. 3 Comparison among inferred IMF polarities from cosmic ray data and those observed directly with the spacecrafts for 1971. The inferred ones from geomagnetic field data are also given. Bartels rotation numbers are given on the right and the starting day of each rotation is indicated on the left. The top line (GG) of each triple represents the field polarity inferred from cosmic ray data (GG-term), the middle line (I) of each represents the field polarity obtained directly with the spacecrafts and the bottom line (SVL) of each represents the inferred field polarity from geomagnetic field data given by Svalgaard. A small dot (•) represents a day with the field polarity directs away from the Sun, a large dot (●) represents a day with the field polarity directs toward the sun, a cross (×) represents an uncertain or ambiguous day and a blank represents a day of lack of data or a gap in the observations.

Inferred Polarities	Observed polarities		
	Toward	Away	Mixed
Toward	118	26	13
Away	28	100	12
Mixed	20	11	8

Table 2(b) Same format as that of Table 2(a) but for 1972

Inferred polarities	Observed polarities		
	Toward	Away	Mixed
Toward	102	28	28
Away	27	104	21
Mixed	10	10	3

Table 2(c) Same format as that of Table 2(a) but for 1973

Year	Success rate (=A/A+D) (%)
1971	79
1972	76
1973	73

Table 3 Success rate of agreement between the polarities inferred from cosmic ray data and those observed directly with the spacecrafts for each year, 1971, 1972 and 1973

4. Present examination and inference of IMF polarity

Using the GG-term at Nagoya, we continue to examine the relationship between the cosmic ray N-S asymmetry and the IMF polarity, and inference is made by means of the method described earlier and in Paper I. Fig. 4 displays the daily values of the GG-term for 1974 and in Fig. 5 those for 1975 in the same format as in Fig. 2 for 1971. The IMF polarities are also indicated in the figure. The IMF polarities are determined with our calculations with the data prepared by NASA (1976). 'Away' polarity is defined as the IMF direction (the daily vectorial mean angle) lying between 45° and 225° in longitude measured eastwardly from the Sun-Earth line and 'toward' polarity as the IMF direction between 225° and 45° . In the calculation, data

points less than 6 hours are not included. In Figs. 4 and 5, a day with a lack of data for either observation of the GG-term or of direct measurements of IMF, is not displayed.

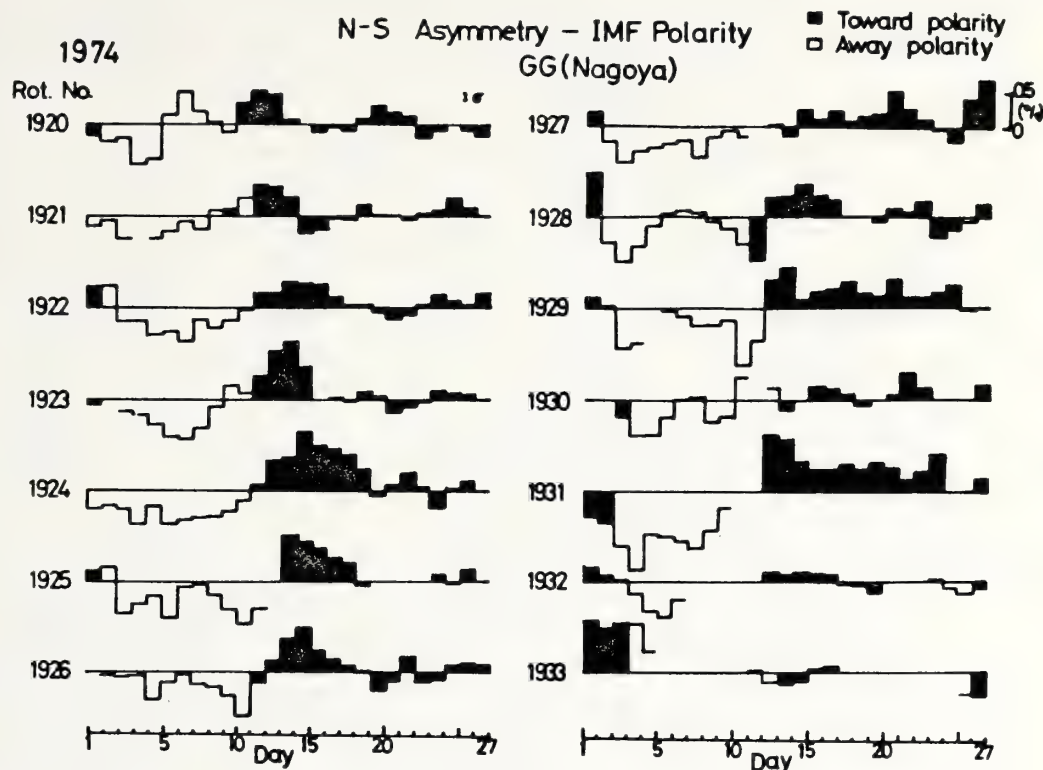


Fig. 4 Relative daily values of cosmic ray N-S asymmetry (GG-term) with respect to the 27-day average for 1974

From Figs. 4 and 5 the same conclusion about the relationship between the cosmic ray N-S asymmetry and the IMF direction can be definitely deduced as that in Paper I. A quantitative comparison is also evaluated in the same manner as in Table 2, and given in Tables 4(a) for 1974 and 4(b) for 1975 (until October 23). Table 5 summarizes those success rates for each year, 1974 and 1975.

Inferred polarities	Observed polarities	
	Toward	Away
Toward	140	19
Away	54	100

4(a)

Inferred polarities	Observed polarities	
	Toward	Away
Toward	63	26
Away	20	74

4(b)

Table 4 Number of days of occurrence of each of the four possibilities for the polarities inferred from cosmic ray data and from direct measurements; 4(a) for 1974 and 4(b) for 1975

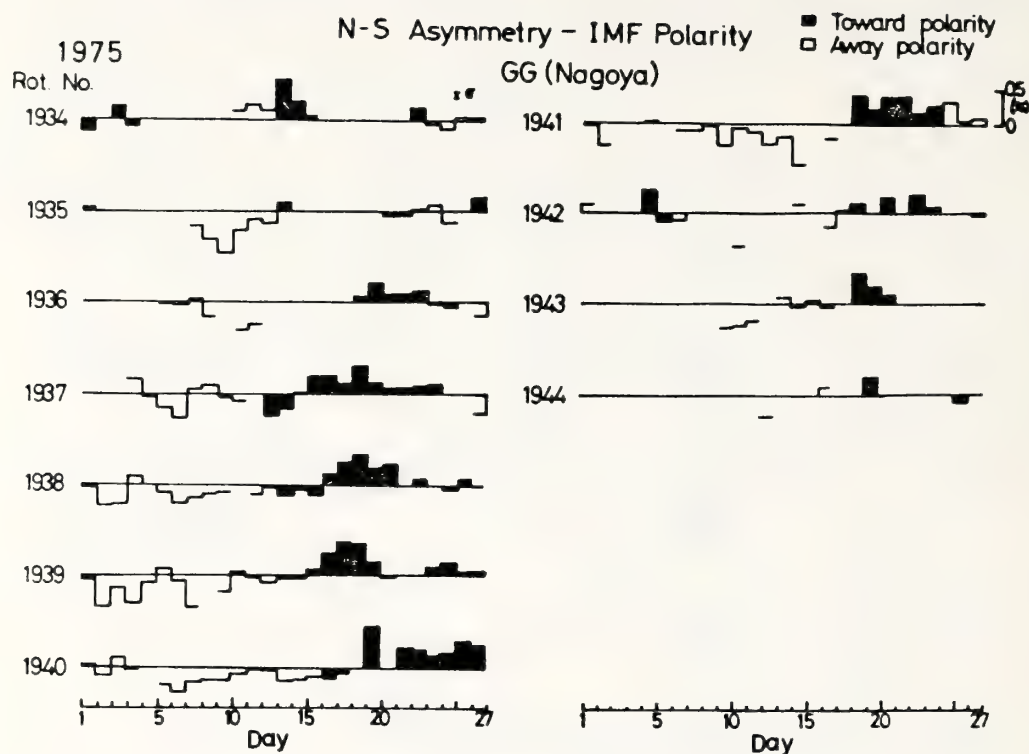


Fig. 5 Same format as that in Fig. 4 but for 1975

Year	Success rate (A/A+D) (%)
1974	77
1975	75

Table 5 Success rate of agreement between the polarities from cosmic ray data and from direct measurements for each year of 1974 and 1975

5. Summary

The present success rate for 1974 and 1975 is obtained as high as those for the preceding years of 1971-73 (see Table 3 and 5). Therefore, we can strongly suggest that the cosmic ray observations, particularly the cosmic ray N-S asymmetry may be used with a fair degree of accuracy ($\sim 75\%$) for inferring the sector polarity of the magnetic field in interplanetary space.

References

- Bercovitch, M. (1969): Determination of the heliocentric gradient using neutron monitor data. Proc. Int. Conf. Cosmic rays (Budapest), Supp. 2, 29-169.
- Bercovitch, M. (1971): The heliocentric radial gradient of relativistic cosmic rays in 1969-1968. Proc. Int. Conf. Cosmic Rays (Hobart), 2-579.
- Duggal, S. P., and M. A. Pomerantz (1976): Origin of transient north-south anisotropy of cosmic rays. J. geophys. Res., 81-5032.
- Fairfield, D. H., and N. Ness (1975): Interplanetary sector structure: 1970-1972. J. geophys. Res., 79-5089.
- Gleeson, L. J. (1969): The equations describing the cosmic ray gas in the interplanetary region. Plane. Space sci., 17-31
- Iucci, N., and M. Storini (1972): The north-south anisotropy and the cosmic-ray radial gradient in the vicinity of the Earth. Nuovo Cim., 10-325.
- Kondo, I., Z. Fujii, and K. Nagashima (1975): North-south asymmetry of cosmic ray flux and polarity of interplanetary magnetic field. Proc. Int. Conf. Cosmic Rays (Munich), 4-1182.
- Kudo, S., and M. Wada (1977): Field dependent north-south anisotropy of cosmic rays in rigidities 10 GV to 300 GV. Proc. Int. Conf. Cosmic Rays (Plovdiv), 3--158.
- Mori, S., S. Yasue, and M. Ichinose (1975): Three-dimensional anisotropy of high energy cosmic rays and its relation to the interplanetary magnetic field. Tech. Rep. DPSU 76-01, Shinshu Univ., Matsumoto, Japan.
- Nagashima, K., K. Fujimoto, Z. Fujii, H. Ueno, and I. Kondo (1971): Three-dimensional cosmic ray anisotropy in interplanetary space-Origin of solar semi-diurnal variation. Rep. Ionos. Space Res., Japan. 26-31.
- NASA-NSSDC (1976): Interplanetary magnetic field data. NASA-NSSDC, 76- .
- Sekido, Y., K. Nagashima, I. Kondo, H. Ueno, K. Fujimoto, and Z. Fujii (1975): Rep. of Cosmic-Ray Res. Lab. No. 1, 1970-1973, Nagoya Univ., Nagoya, Japan.
- Sekido, Y., K. Nagashima, I. Kondo, H. Ueno, K. Fujimoto, and

- Z. Fujii (1978): Rep. of Cosmic-Ray Res. Lab., No.3,
1974-1976, Nagoya Univ., Nagoya, Japan.
- Svalgaard, L. (1975): An atlas of interplanetary sector structure 1957-1974. SUIPR, Rep. No. 629, Stanford Univ., Stanford, U. S. A.
- Swinson, D. B. (1969): 'Sidereal' cosmic-ray diurnal variations. J. geophys. Res., 74-5591.
- Swinson, D. B. (1971): Solar modulation origin of 'sidereal' cosmic ray anisotropy. J. geophys. Res., 76-4217.
- Wilcox, J., Svalgaard, L., and P. Hedgecock (1975): Comparison of inferred and observed interplanetary magnetic field polarities, 1970-1972. J. geophys. Res., 80-3585.
- Yasue, S. (1979): North-south anisotropy and radial density gradient of galactic cosmic rays. To be submitted to J. Geomagn. Geoelectr., Japan.
- Yoshida, S., N. Ogita, S-I. Akasofu, and L. Gleeson (1973): Variations of three-dimensional anisotropy of cosmic rays during Forbush decreases. J. geophys. Res., 78-6409.

COSMIC RAY ANISOTROPY AND THE GROSS STRUCTURE OF THE INTERPLANETARY MAGNETIC FIELD

H.S. Ahluwalia
Department of Physics and Astronomy
The University of New Mexico
Albuquerque, New Mexico 87131

In this paper we describe a promising prediction technique based on the observed long term changes in the parameters applicable to the cosmic ray anisotropy in solar time. Solar daily variation of cosmic rays consists of three components. They are the diurnal, the semidiurnal and the tridiurnal variations. We have shown elsewhere (Ahluwalia and Singh, 1973a) that these three components are worldwide and therefore have an extra-terrestrial origin. We have also shown that harmonics higher than third do not exist in the cosmic ray data (Ahluwalia and Singh, 1973b). In this paper we examine the year-to-year change in the nature of the diurnal variation during the solar activity cycle 20. Neutron monitor data from Deep River and vertical muon data obtained underground at Embudo are used in our analyses. The results obtained by us lead us to believe that it might be possible to predict long term changes in the solar activity, with periods of 11- and 22-years. We are presently testing models which if successful are sufficiently flexible to provide us with a capability to make predictions about the electromagnetic states of the interplanetary medium over much shorter periods of time.

1. INTRODUCTION

It is a well-known fact that most of the information regarding the electromagnetic states of the interplanetary medium, prior to the space probe era, was derived from the careful analyses of the cosmic ray intensity variations. These variations were observed with a global network of cosmic ray detectors (such as neutron monitors and muon telescopes) deployed over a variety of observing sites ranging from mountain tops to deep underground. Alfven (1950) pioneered this approach by postulating the existence of magnetized solar beams in the interplanetary medium. He (Alfven, 1954) and his co-workers (Brunberg and Dattner, 1954) showed that such beams modulate the cosmic ray intensity in the interplanetary space, in a characteristic manner. Notable pioneers who contributed to this area of research are: Davis (1955), Nagashima (1955), Morrison (1956), Dorman (1957), Gold (1959), Elliot (1960),

Parker (1958, 1960, 1961, 1964), McCracken (1962), Ahluwalia and Dessler (1962), and Axford (1965). It is indeed a tribute to the patience and the scientific wisdom of these and several other workers that when direct measurements were finally made in the free space, broad notions regarding the meteorology of the interplanetary medium were found to be essentially correct. The advent of the space probe era has in no way minimized, at least thus far, the importance of the technique of continuous monitoring of cosmic ray intensity as a means of deriving information about the broad features of the interplanetary magnetic field. By no means do I wish to minimize the importance of the spacecraft observations in free space. The fact is that observations in the free space have provided us with a lot of details as to the fine structure and the temporal changes in the state of the interplanetary medium. But by and large there have not been too many surprises. One should note here the fact that spacecraft observations have essentially been confined to low energies, close to the plane of the ecliptic, at isolated points in space, for a limited amount of time. Most of these limitations are not likely to be overcome, at least in the near future, even when the spacecrafts begin to probe areas far away from the ecliptic plane, inside the heliosphere.

Recently (Ahluwalia, 1977a,b) it has become apparent that it might be possible to make inferences regarding the large-scale features of the interplanetary magnetic field through the use of the cosmic ray technique. Also it should be noted that research workers exploring the nature of the solar magnetism are just now beginning to speculate about the overall structure of the interplanetary magnetic field (Svalgaard et al., 1974). It is possible therefore that the two independent lines of investigations might produce an acceptable internally consistent model of the solar magnetism with details being filled-in by well planned scientific experiments aboard the future space probe missions. An important aspect of the models should be to provide us at least with a reliable method of forecasting solar activity on a long term basis. Moreover depending upon the completeness of the models it is conceivable that we might even acquire capability of making reliable short-term predictions. Some suggestions are made in this paper as to how to achieve these highly desirable objectives.

2. SOLAR DIURNAL ANISOTROPY OF COSMIC RAYS

The large-scale characteristics of the interplanetary magnetic field may in principle be related to the temporal characteristics of the cosmic ray solar diurnal anisotropy. A commonly accepted model for this phenomenon emerged from the efforts made by Ahluwalia and Dessler (1962), Parker (1964), and Axford (1965). The model is illustrated in Figure 1. Cosmic rays tend to diffuse into the heliosphere along the interplanetary magnetic field lines, which on the average are inclined at an angle of 45° west of the earth-sun line, as indicated in the diagram. The cosmic ray flux along the field is indicated by the vector \vec{F} . However cosmic rays are also swept radially outwards by the Alfvén magnetized beams (commonly called the solar wind). It turns out that the radial flux of cosmic rays (\vec{C}) outwards is exactly balanced on the average by the radial component of \vec{F} , resulting in no net radial streaming of cosmic rays within the heliosphere. A cosmic ray wind

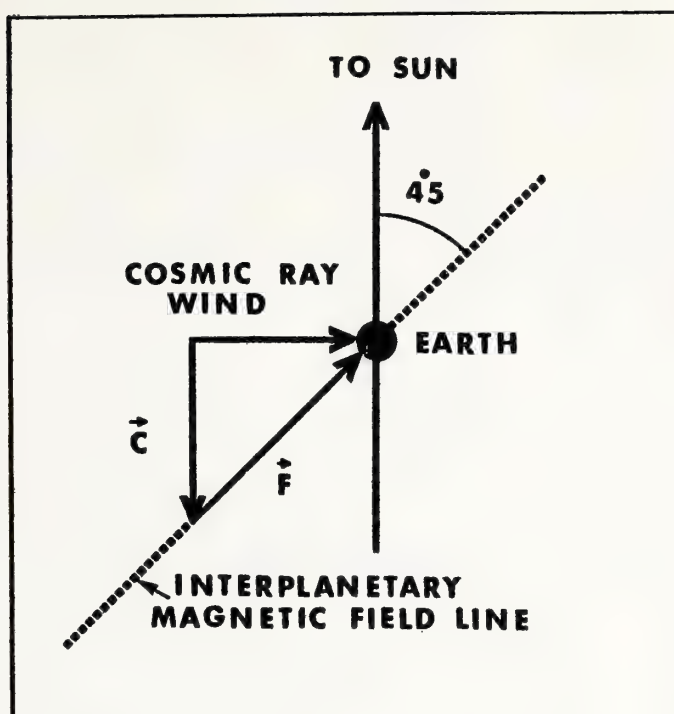


Figure 1

then naturally appears in the model. This is shown in the diagram. The net streaming is tangential to the orbit of the earth, i.e. the cosmic rays appear to corotate with the sun. A detector on the rotating earth therefore sees a slight excess of cosmic rays arriving from the local dusk direction. This effect is commonly called Corotational Anisotropy of Cosmic Rays. It has a period of 24 hours in local solar time. It is a small effect. The amplitude of the sinusoidal variation is about 0.5%.

When cosmic ray data, obtained at a given observing site, are averaged over a long period of time and subjected to a Fourier analysis three periodicities stand out. Figure 2 shows the power spectral density estimate (in arbitrary units) made from ten years (1962-71) of data obtained at Deep River with a super neutron monitor (Hatton, 1971). Clearly there are well-defined peaks at 1-cpd, 2-cpd, and 3-cpd. As can be seen the peaks are highly significant. Note that cosmic ray diurnal variation (1-cpd) is by far the largest effect (the power spectral densities at 1-cpd, 2-cpd, 3-cpd are approximately in the ratio of 800:20:1, respectively). We might point out that semidiurnal variation (2-cpd) is perhaps on the threshold of being understood. The tridiurnal variation was discovered only five years ago (Ahluwalia and Singh, 1973a). At the present time no consensus exists as to its origin.

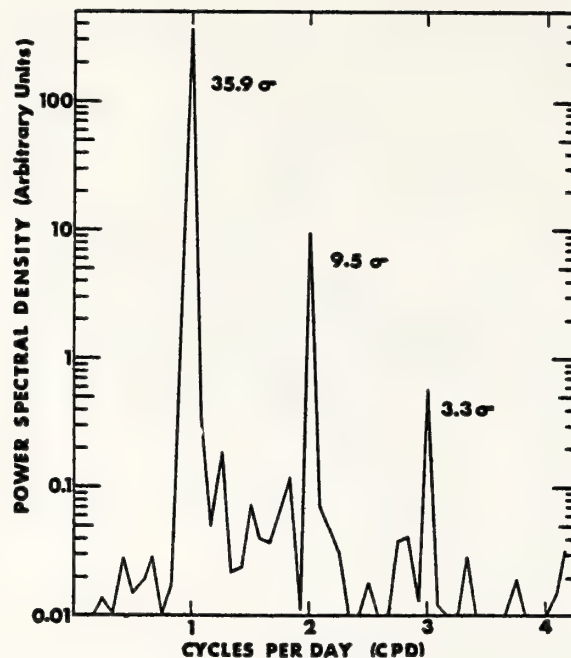


Figure 2

3. SOLAR ACTIVITY AND THE AMPLITUDE OF DIURNAL ANISOTROPY OF COSMIC RAYS

The function that controls the amplitude of the diurnal variation (the so called variational spectrum) is given by,

$$\frac{\delta D(R)}{D(R)} = \begin{cases} A R^{\beta} \cos \bar{\lambda}, & \text{if } R \leq R_c \\ 0, & \text{if } R > R_c \end{cases}$$

where

R = magnetic rigidity of primary cosmic rays. R is a measure of total energy of a primary cosmic ray particle per unit of its electrical charge,

$D(R)$ = isotropic differential rigidity spectrum of the primaries,

$\delta D(R)$ = modulated primary rigidity spectrum,

A = free space amplitude of solar diurnal anisotropy,

$\beta = 0.0$ (Ahluwalia and Ericksen, 1970),

$\bar{\lambda}$ = mean asymptotic latitude of response of the detector calculated by using suitable weights (coupling functions) for primaries of different rigidities which contribute to the counting rate of the detector (Dorman, 1957),

R_c = upper cut-off rigidity in the primary spectrum above which the modulation process is ineffective.

It appears that the parameter R_c relates the amplitude of the annual mean diurnal variation to the level of the solar activity, as measured by the intensity of the coronal green line (5303 Å) at low heliolatitudes (Ahluwalia and Ericksen, 1970, 1971; Ahluwalia, 1971). The values of R_c apparently range from (43 ± 2) GV in 1965 to 100 GV in 1969. From Figure 3 the reader can get some feel for the solar cycle dependence of R_c . Partially filled-in circles give quarterly mean coronal green line intensity observed at Kislovodsk (USSR) at low heliolatitudes ($\lambda = \pm 5^\circ$) during the period 1957-69. Also plotted are monthly mean Zurich sunspot numbers (solid dots). The annual mean sunspot numbers are indicated by "-x-" and are joined by the dotted line. The periods of maxima and minima in the sunspot activity are indicated by arrows near the abscissa. The values of R_c determined by Jacklyn and Humble (1965) and by Ahluwalia and Ericksen^c (1970, 1971) during this period are also indicated in Figure 3. Positive correlation between R_c and 5303 Å line intensity is apparent. One can also see that no correlation exists between R_c and Zurich sunspot numbers. We believe that we are now beginning to understand and appreciate the underlying physical process responsible for the observed correlation between R_c and the intensity of 5303 Å line. This is discussed in section 5.

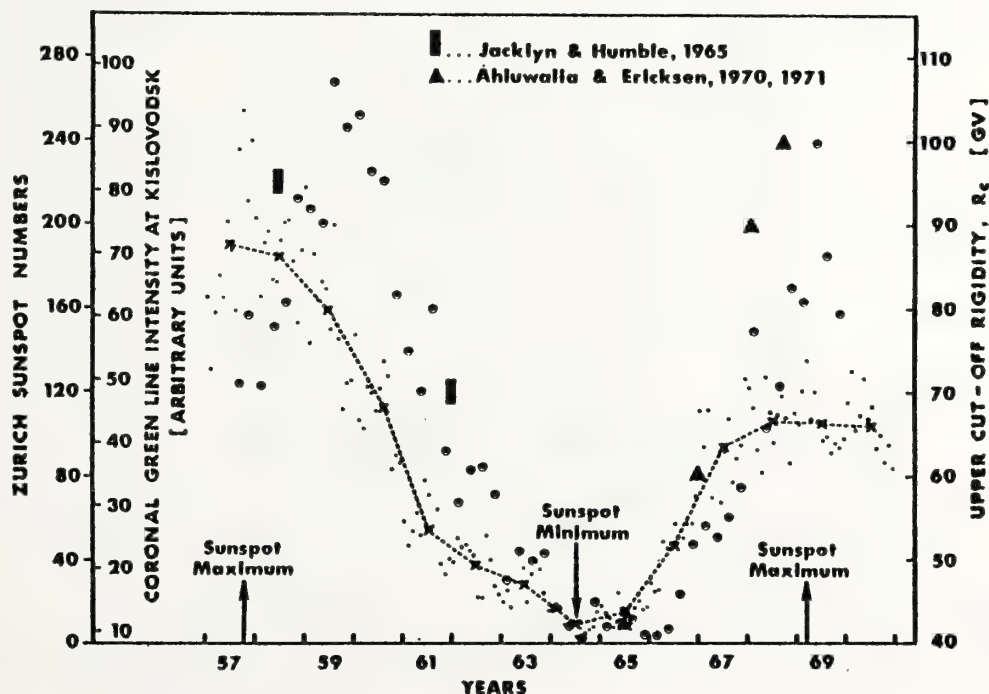


Figure 3

4. LONG TERM CHANGES IN THE TIMES OF MAXIMUM OF SOLAR ANISOTROPIES OF COSMIC RAYS

Figure 4 shows the year to year change in the times of maximum of the diurnal, the semidiurnal and the tri-diurnal variations for the Deep River neutron monitor (black dots) and the University of New Mexico Vertical Muon telescope located underground at Embudo, New Mexico (circles with crosses). The two detectors respond to different median magnetic rigidities (R_m) of the primary cosmic rays. For Deep River neutron monitor, $R_m \approx 10$ GV. For the muon telescope underground at Embudo, $R_m \approx 100$ GV. It follows therefore that the neutron monitor at Deep River responds to low energy primary cosmic rays and the muon detector at Embudo responds to high energy primary cosmic rays.

Let us consider the time of maximum of the diurnal variation only. It is clear that the diurnal time of maximum (uncorrected for the bending of the primaries by the geomagnetic field) remains nearly constant from 1962 to 1970, at about 15 hours LT. Slight shift to early hours of the time of maximum in 1965 is understood in terms of lower value of R_m obtainable during that time (Ahluwalia and Ericksen, 1970). This situation is upset in 1971 when an anomalous shift towards early hours is observed. It appears that this shift has continued at least up to 1976. Such a drastic change was last observed during the deep solar minimum of 1954. The effect remains unexplained. Note however that 1971 was not the year of solar activity minimum.

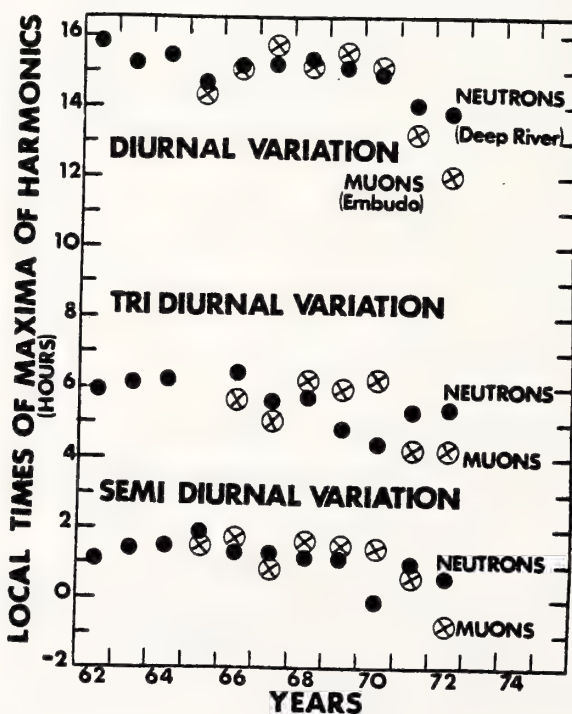


Figure 4

5. CORONAL HOLES, FAST STREAMS, AND SOLAR DIURNAL ANISOTROPY OF COSMIC RAYS

Figure 5 illustrates one possible way in which our results might be understood. It is known that during 1970-72 period solar wind was undergoing a drastic transition. A pattern of high speed streams, corotating with the sun, was beginning to emerge. They are probably related to the coronal holes. It turns out that coronal holes located at low heliolatitudes are bounded on both sides by regions of high coronal green line intensity (Bohlin, 1976). It is possible therefore that the close correlation observed by us and discussed in section 3 between R_c and the intensity of 5303 Å line is indicative of the control exercised by the coronal holes on the electromagnetic weather in the interplanetary medium.

Also the holes often extend over a wide range of heliolatitudes (Timothy et al., 1975). It follows that on such occasions a large-scale structure of unidirectional magnetic fields must exist in space over a large enough range, normal to the ecliptic plane. A similar inference has been reached independently by Svalgaard et al. (1974). They studied the long-term changes in the observed solar sector structure pattern of the interplanetary magnetic field. It appears to us therefore that off-ecliptic cosmic rays must make a significant contribution to the cosmic ray solar diurnal anisotropy. Figure 5 shows the streaming patterns of off-ecliptic cosmic rays under four different configurations of the large-scale, well-ordered, interplanetary magnetic field, far away from the ecliptic plane. The suggested streaming is driven by a symmetrical cosmic ray particle density gradient ($\vec{V}n$) normal to the ecliptic plane, as shown in the diagram. Off-ecliptic cosmic ray contributions to the solar anisotropy are illustrated in Figure 6. Clearly a great deal of flexibility is available in accomodating departures of amplitude and times of maximum from those pertaining to the Corotational Anisotropy discussed in

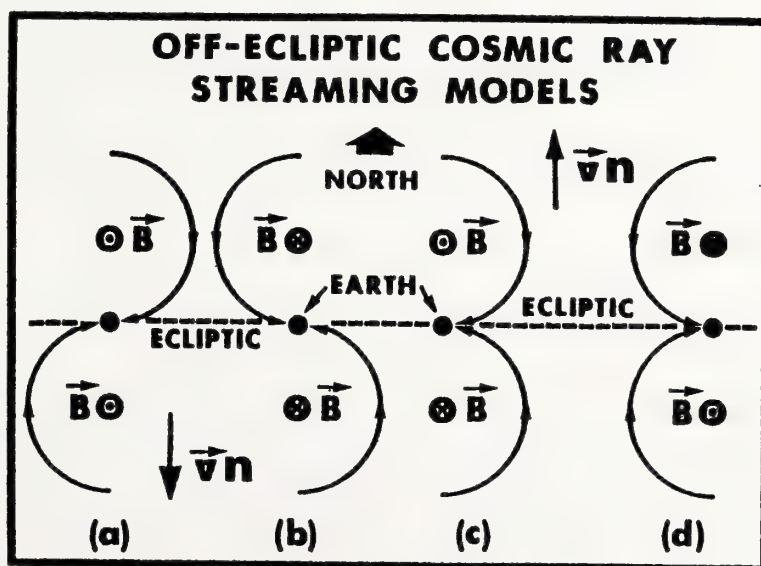


Figure 5

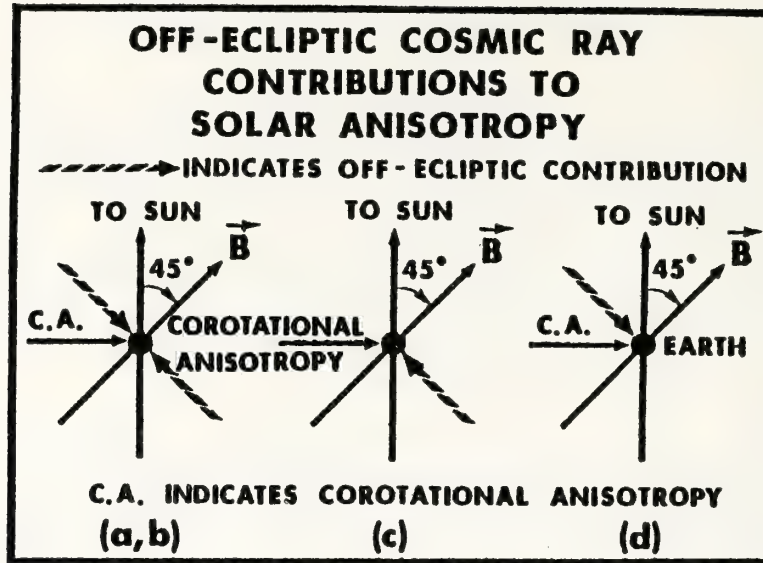


Figure 6

section 2. Streaming models 6a,b give rise to semidiurnal variation of cosmic rays, as discussed by Subramanian and Sarabhai (1967) and Quenby and Leitti (1968). The models shown have the potential of explaining the observed features of the day-to-day, as well as year-to-year changes in the solar diurnal variation of cosmic rays. But the most important feature of these models is that one may also be able to derive information regarding the mean interplanetary magnetic field far away from the ecliptic plane, using data obtained with the muon telescopes located deep underground. Moreover one may be able to obtain information regarding the off-ecliptic scattering processes which affect cosmic rays, by comparing data obtained with muon telescopes located underground with data obtained with surface level muon and neutron detectors. Thereby one can get some feel for the "roughness" of the off-ecliptic interplanetary magnetic field. In passing one also notes that at very high energies off-ecliptic cosmic rays might carry information about the characteristics of the boundary between the heliomagnetosphere and the interstellar medium. Space at such large distances is unlikely to be sampled in depth by the spacecrafts, at least in the present century.

6. SUMMARY

We have presented a detailed discussion of the present capability of cosmic ray technique to forecast solar activity on a long-term basis. The technique is in an evolutionary state. It is clear however that if we are successful in interpreting the results presented in this paper in terms of quantitative models, we would acquire a very powerful tool which would enable us to predict the electromagnetic states of the interplanetary medium on a long-term as well as on a short-term basis in regions of space not likely to become easily accessible in the near future. The contribution of this paper

therefore lies in its attempt to draw attention to an alternate promising technique which is in an advanced stage of development. We might also point out that this technique relies heavily on continued availability of observations obtained from a global network of neutron and muon detectors. Due to financial crunch vital elements of this network are disappearing at an alarming rate. A way must therefore be found to keep alive the remaining relics of the network to ensure that data of high quality continue to be available to the scientific community for variety of uses.

ACKNOWLEDGEMENT

This research was supported in part by the Atmospheric Sciences Section of the National Science Foundation under grants # ATM 74-16328 and ATM 78-10727. This support is gratefully acknowledged.

REFERENCES

- Ahluwalia, H.S., and Dessler, A.J. (1962): Planet. Space Sci., 9, 195.
- Ahluwalia, H.S., and Ericksen, J.H. (1970): Acta Phys. Acad. Scient. Hung., 29, Suppl. 2, 139.
- Ahluwalia, H.S., and Ericksen, J.H. (1971): Geophys. Res., 76, 6613.
- Ahluwalia, H.S. (1971): Twelfth Intern. Conf. Cosmic Rays, Hobart. Conference Papers (University of Tasmania), 2, 641.
- Ahluwalia, H.S., and Singh, S. (1973a): Thirteenth Intern. Conf. Cosmic Rays, Denver. Conference Papers (University of Denver), 2, 948.
- Ahluwalia, H.S., and Singh, S. (1973b): Thirteenth Intern. Conf. Cosmic Rays, Denver. Conference Papers (University of Denver), 2, 3129.
- Ahluwalia, H.S. (1977a): Fifteenth Intern. Conf. Cosmic Rays, Plovdiv. Conference Papers (Bulgarian Academy of Sciences), 4, 24.
- Ahluwalia, H.S. (1977b): Fifteenth Intern. Conf. Cosmic Rays, Plovdiv. Conference Papers (Bulgarian Academy of Sciences), 4, 25.
- Alfven, H. (1950): Cosmical Electrodynamics. Clarendon Press, Oxford.
- Alfven, H. (1954): Tellus, 6, 232.
- Axford, W.I. (1965): Planet. Space Sci., 13, 115.
- Bohlin, J.D. (1976): Physics of Solar Planetary Environments (Proc. Intern. Symposium on Solar-Terrestrial Physics), 1, 47.
- Brunberg, E.A., and Dattner, A. (1954): Tellus, 6, 254.

- Davis, L. (1955): Phys. Rev., 100, 1440.
- Dorman, L.I. (1957): Cosmic Ray Variations. State Publishing House for Technical and Theoretical Literature, Moscow.
- Elliot, H. (1960): Phil. Mag., 5, 601.
- Gold, T. (1959): J. Geophys. Res., 64, 1665.
- Hatton, C.J. (1971): Progress in Elementary Particle and Cosmic Ray Physics, 10, 3. Eds. J.G. Wilson and S.A. Wouthuysen. North-Holland Publishing Co., Amsterdam.
- Jacklyn, R.M., and Humble, J.E. (1965): Austr. J. Phys., 18, 451.
- McCracken, K.G. (1962): J. Geophys. Res., 67, 447.
- Morrison, P. (1956): Phys. Rev., 101, 1397.
- Nagashima, K. (1955): J. Geomag. Geoelectr., 7, 51.
- Parker, E.N. (1958): Astrophys. J., 128, 664.
- Parker, E.N. (1960): Astrophys. J., 132, 821.
- Parker, E.N. (1961): Astrophys. J., 133, 1014.
- Parker, E.N. (1964): Planet. Space Sci., 12, 735.
- Quenby, J.J., and Lietti, B. (1968): Planet. Space Sci., 16, 1209.
- Subramanian, G., and Sarabhai, V. (1967): Astrophys. J., 169, 417.
- Svalgaard, L., Wilcox, J., and Duvall, T.L. (1974): Solar Phys., 37, 157.
- Timothy, A.F., Krieger, A.S., and Viana, G. (1975): Solar Phys., 42, 135.

ON THE DIAGNOSIS OF IMF PARAMETERS BY THE VERTICAL
IONOSONDE DATA FROM VOSTOK STATION, ANTARCTICA

A. S. Besprozvannaya, A. V. Shirochkov, T. I. Shchuka
The Arctic and Antarctic Research Institute
Leningrad, USSR

The results of extensive analysis of the probability of Es occurrence at Vostok Station, Antarctica from local ionosonde data are reported. A close relationship has been found between the two main maxima in the Es diurnal variations at Vostok Station and various IMF parameters. The magnitude of the evening maximum in Es occurrence depends strongly on the sign of the azimuthal component of the IMF (B_y), while for the noon maximum in Es occurrence there is a similar dependence on the sign of the vertical component of the IMF (B_z). These allow us to construct a rather simple but efficient method of sign determination of B_y and B_z by the ionosonde data.

Data on the distribution of sporadic E ionization within the polar caps reveal a strong dependence of the Es occurrence on the B_y component of the IMF (Besprozvannaya and Shirochkov, 1976). It has been found that in the north polar cap area, the Es layers occur predominantly when B_y is positive ($B_y > 0$), whereas in the south polar cap this is true when B_y is negative ($B_y < 0$). This effect of the IMF influence on the Es occurrence can be seen in the evening hours basically; hence, a real possibility exists of using the Es data for the diagnosis of a B_y value.

The present paper is an attempt to elaborate on a quantitative criterion for such a diagnosis by the ionosonde data from Vostok Station ($\phi = 84^{\circ}3'S$). The polar diagrams were made where the probability of Es ($f_o E_s \geq 3.0$ MHz) occurrence is a function of different values of both azimuthal ($B_y > 0$ and $B_y < 0$) and vertical ($B_z > 1$ and $B_z < -1$) components of the IMF. The ionosonde data presented are taken for the period from 1965 to 1969. For the IMF data, the results of satellite measurements were used (King, 1977). These polar diagrams are shown for summer (October - March) and winter (April - September) months (See Figures 1 and 2).

One can see from these that the probability of Es occurrence at Vostok Station in the evening hours never falls below 25 per cent when B_y is negative and never exceeds this value when it is positive. A rather simple method can be suggested for the determination of a B_y sign for any particular day. It is only necessary to calculate the probability of Es occurrence from 16 to 23 hours GLT from f-plot data of an ionosonde (the geomagnetic local

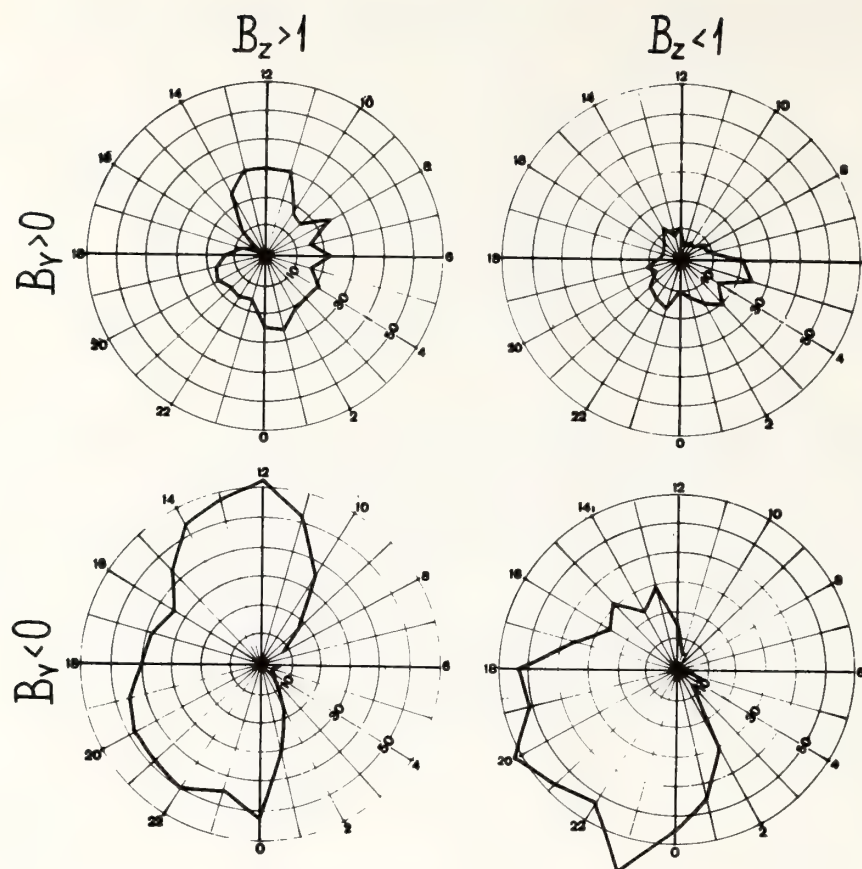


Figure 1. Histograms of the diurnal variations of the occurrence probability of the sporadic E layer at frequencies larger than 3.0 MHz at Vostok Station for summer months (October-March) of 1966-69 with different parameters of the IMF.

time at Vostok Station corresponding to those in UT). If this probability is higher than 25 per cent, we would know that the B_y value is less than zero, and with the probability of Es occurrence being less than 25 per cent, it is larger than zero.

An evaluation of the reliability of this method gives us an accuracy of 78-82 per cent for both summer and winter months. It is important to note that this accuracy is higher than the corresponding degree of reliability of the Mansurov-Svalgaard method of the determination of the B_y sign from the ground-based magnetometer data (Mansurov, 1969, and Svalgaard, 1968). Besides, the proposed method seems to have another advantage: it can be used with equal success both in summer and in winter, while the Mansurov-Svalgaard effect is inefficient in winter.

Some results of the comparison between the determination of a sign of the azimuthal IMF component by direct satellite measurements and by the suggested method are given in Table 1. There are different tables for summer and winter months for the period of 1967-1970. The data presented demonstrate

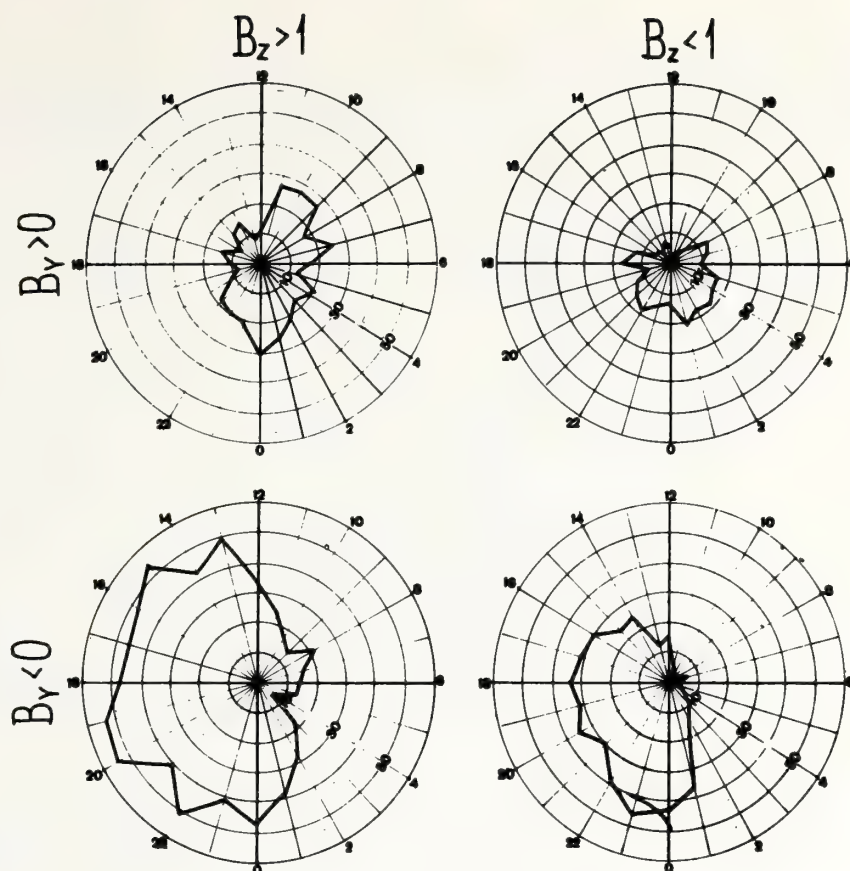


Figure 2. The histograms of the diurnal variations of the occurrence probability of sporadic E layer at frequencies larger than 3.0 MHz at Vostok Station in winter months (April-September) of 1966-69 with different parameters of the IMF.

Table 1. The B_y sign, derived from both ionosonde and satellite data.

<u>winter</u>			<u>summer</u>		
	<u>ionosonde</u>			<u>ionosonde</u>	
<u>satellite</u>	<u>$B_y < 0$</u>	<u>$B_y > 0$</u>	<u>satellite</u>	<u>$B_y < 0$</u>	<u>$B_y > 0$</u>
$B_y < 0$	241	49	$B_y < 0$	257	44
$B_y > 0$	54	148	$B_y > 0$	51	204

a rather high degree of reliability of the suggested method, being 79.6% for winter and 82.9% for summer, and its independence from the season of observation.

The data in Figures 1 and 2 reveal another intriguing aspect of the relationship between the IMF parameters and the Es occurrence within the polar cap. Besprozvannaya and Shirochkov (1976) have shown that the diurnal variations of Es occurrence at Vostok Station have an additional maximum near the local geomagnetic noon in addition to the main one, located at the premidnight hours. In summer this additional maximum of Es occurrence is particularly distinct. Besprozvannaya and Shirochkov (1976) claim that the nature of this noon maximum of Es occurrence is due to the effects of the processes in the polar cusp in the polar ionosphere. It is established now that the position of the polar cusp is primarily determined by a value of the vertical component of the IMF (B_z) (Burch, 1973; Zaitzeva and Pudovkin, 1976). When B_z is large enough, the position of the polar cusp in summer can be as high as $82-84^\circ$ of invariant latitude, i.e. very near to Vostok Station ($\phi' = 84.3^\circ$). So it is natural to expect that a noon maximum of Es occurrence at Vostok Station would depend on a sign of B_z if it is indeed due to the influence of the polar cusp. Actually one can see from Figures 1 and 2 that Es occurrence at Vostok Station does depend on the B_z sign in summer, particularly with $B_y < 0$ when the most favourable conditions existed for Es formation in the south polar cap. It is worthwhile noting that the magnitude of the noon maximum in Es occurrence with $B_z > 1$ becomes even greater than the premidnight one; it disappears, however, almost completely when $B_z < -1$.

Such a remarkable dependence of the diurnal variations of Es occurrence on the B_z sign gives us an opportunity for using Es data for the diagnosis of the sign of the vertical IMF component. The quantitative criterion for such diagnosis can be the same as for the B_y sign described above. From the ionosonde f-plots, the Es occurrence for the period from 10 to 15 hours of GLT is calculated and then compared with the corresponding hourly mean B_z values from satellite measurements. Results of this comparison for summer months of 1966 and 1967 are shown in Figure 3. The data shown in Figure 3 demonstrate that if we have the probability of Es occurrence less than 15%, we can expect the southward-oriented vertical component of the IMF with more than 80 per cent accuracy, while for Es occurrence higher than 45%, we can claim the northward orientation of B_z with the same accuracy. This relationship proved to be valid for other years.

Similarly to the B_y case (Table 1), the reliability of this method of the diagnosis of a B_z sign using Es data was tested by means of comparing it with the results of direct satellite measurements of B_z sign (Table 2). It is seen that the reliability of the suggested method equals to 75% roughly, which is very encouraging.

It is necessary to note that Table 2 includes only extreme cases when the Es occurrence is less than 15% or is higher than 45%. At the same time, data in Figure 3 clearly show that there are a lot of cases when Es occurrence is more than 15% and less than 45%. Thorough study of these cases reveals the fact that for the considered period (from 10 to 14 GLT), Es took place either at prenoon hours or during the afternoon hours only. Consequently, all cases with Es probability less than 45% but more than 15% were divided into two groups, i.e. for prenoon hours (10-12 GLT) and for afternoon hours (12-14 GLT). For each of these groups of data, a mean value of B_z from satellite measurements was calculated (Figure 4). The upper

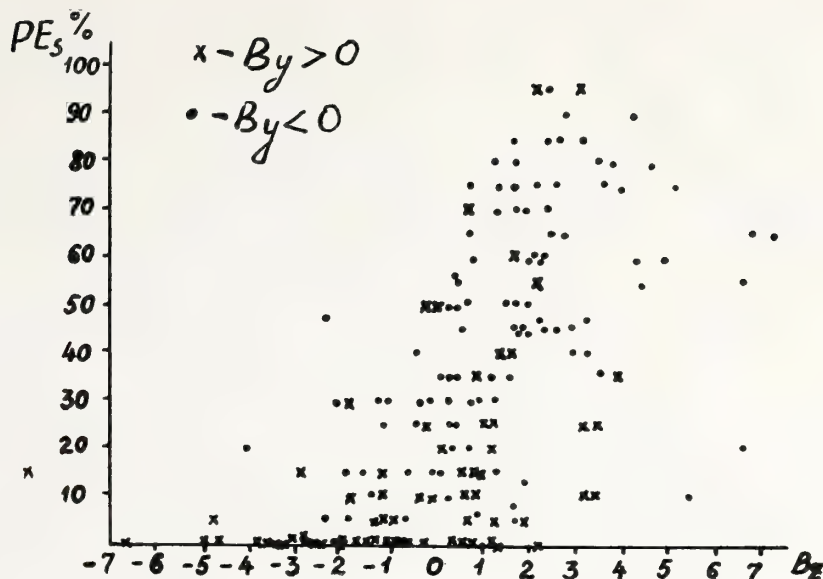


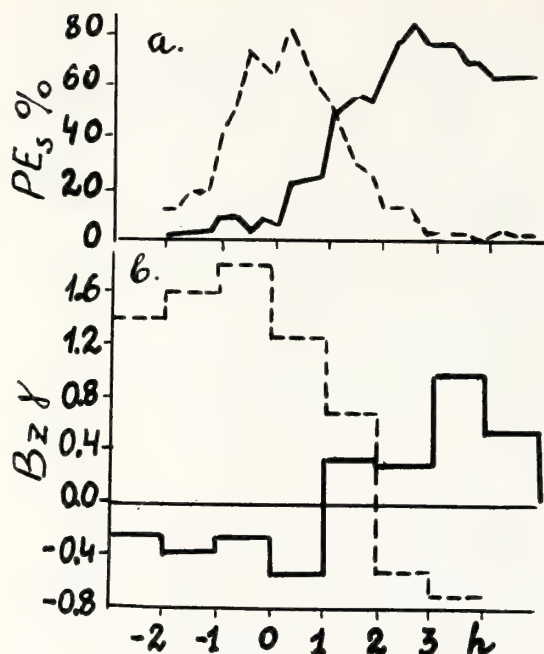
Figure 3. The relationship of the Es occurrence for the period of 10-15 GLT and the Bz sign for summer months of 1966 and 1967.

Table 2. The Bz sign, derived from ionosonde and satellite data.

	<u>Ionosonde</u>	
<u>Satellite</u>	<u>Bz > 0</u>	<u>Bz < 0</u>
Bz > 0	134	51
Bz < 0	28	172

portion of the Figure shows Es occurrence (prenoon data by the solid line, the afternoon data by the dashed line). The mean values of Bz are shown in the lower portion of Figure 4. The evident order can be traced in the Es distribution presented, which is undoubtedly related to a sign change of Bz, during the period of time considered (10-14 GLT). The transition from the northward to southward orientation in Bz appears to be the most essential feature because such transition manifests the start of a magnetospheric substorm in most cases. Such a case corresponds to the situation with a predominant Es appearance at prenoon hours (solid line in Figure 4). The analysis of these data for the period from 1966 to 1970 shows that in 78 per cent of all cases the prenoon appearance of Es precedes the substorm development at 13-16 hours UT (which corresponds to 13-16 GLT at Vostok Station).

We can conclude that the Es distribution data for Vostok Station in summer have allowed us not only to determine the orientation of the vertical component of the IMF but to use this information for predicting substorm development on the night side of the auroral oval with a high degree of



accuracy. Unfortunately, due to a large variability of the magnitude and orientation of B_z , the determination of the B_z sign from the Es data of the single point of observation is limited by a comparatively narrow period of time. If we have at least three ionosondes located at invariant latitudes $82-85^\circ$ spaced in longitude properly, it will be possible to do the diurnal monitoring of B_z orientation using the ionosonde data only.

Figure 4. The comparison of the Es occurrence (a) and the mean values of B_z (b); dashed line for the prenoon data, solid line for the afternoon data. (0 means local geomagnetic midday.)

REFERENCES

- Besprozvannaya, A. S. and A. V. Shirochkov (1976): On the relationship of the near Pole Es to the parameters of the space magnetic field. (In Russian). Geomagn. and Aeronomy, 16:84.
- Burch, J. L. (1973): Rate of erosion of dayside magnetic flux based on a quantitative study of the dependence of polar cap latitude on the interplanetary magnetic field. Radio Sci., 8:955.
- King, J. H. (1977): Interplanetary medium data book. NSSDS, Rep. 77.04, Nat. Space Sci. Data Center, Greenbelt, Md.
- Mansurov, S. M. (1969): New evidence on the relationship of the interplanetary magnetic field and geomagnetic field. (In Russian). Geomagn. and Aeronomy, 9:768.
- Svalgaard, L. S. (1968): Geophysical Paper R-6, Dan. Meteorol. Data.
- Zaitzeva, S. A. and M. I. Pudovkin (1976): On the longitudinal extent of the polar cusp. Planet. Space Sci., 24:588.

PREDICTION OF ACTIVE PROCESSES IN THE SOLAR SPACE

N. N. Kontor and G. P. Lyubimov
Nuclear Physics Institute Moscow State University
Moscow, 117234, USSR

The technique of predicting strong active region evolution, the moments of strong solar flares, and proton event profiles are described. An example of prediction is made for the active region 14943 during 6-28 September 1977. Prediction of year-averaged strong flare numbers and proton fluxes with energies more than 1 MeV and 10 MeV is made for solar cycle 21.

1. INTRODUCTION

In previous studies we introduced (Kontor, 1976) and developed (Kontor et al., 1975, 1976; Vernov et al., 1977a; Kontor et al., 1979) a concept of an active process in the solar space (APS). The characteristics of APS are shown in Figure 1. According to this model the strong active regions (SAR), for which the maximum index of active region $J_{AR} > 1$ (Kontor et al., 1979), are sources of APS. Strong solar flares (SF) occur in SAR when the current index $J_{AR} > 1$. Energetic particles and shocks are generated in the solar atmosphere at the moment of SF. They propagate in the solar space (corona and interplanetary space) interacting between themselves.

From the APS model point of view the forecast of some solar phenomena consists of predicting the main characteristics of the following sequence of phenomena: SAR \rightarrow SF \rightarrow PE (proton event in the interplanetary space).

If the series of homogeneous data is long enough, the forecast reliability usually increases. Such data are available for the sunspot numbers R_z only. As far as APS is concerned, data are available mainly for the period of the 20th solar cycle. In this connection, the APS prediction technique described is based upon the limited study of solar phenomena in this period.

2. SHORT TERM APS PREDICTION

2.1 SAR Prediction

SAR prediction consists of predicting the evolution of the strong active region; that is, in predicting the time dependent changes of the J_{AR} -index. Such prediction comes from initial data about SAR evolution. For this the

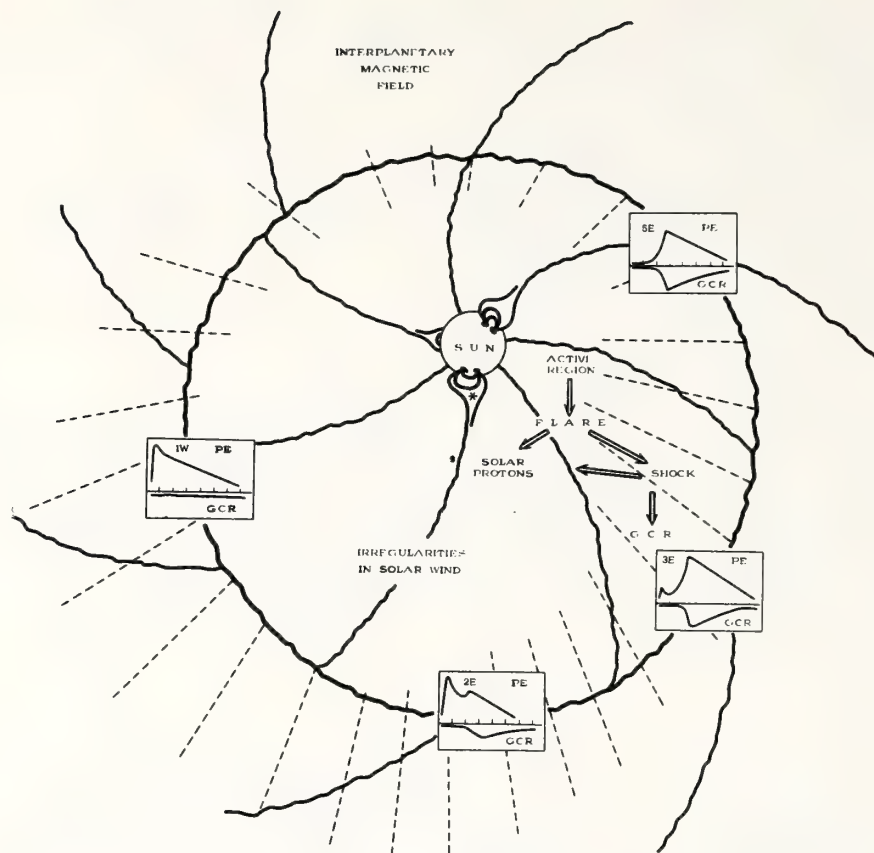


Figure 1. The scheme of APS.

current index $(JAR)_i$ is calculated for every active region appearing on the sun, by the relation

$$(JAR)_i = \frac{1}{3} \left(\frac{S_i}{30} + \frac{M_i}{100} + \frac{f_i}{3} \right) \quad (1)$$

In equation (1), S_i , M_i and f_i are, respectively, area (in units of 10^{-4} hemisphere), power (in relative units of $S \times B$, where B is the brightness), and number of flares that occurred in some active region on the i th day of its existence. If $(JAR)_i < 1$ for any i , evolution prediction does not take place since the active region is weak and is therefore rejected from the APS forecast. If at some moment $(JAR)_i$ happens to be greater than 1, a prediction algorithm of $JAR(t)$ is involved. This algorithm works as follows. From the data of $(JAR)_1, (JAR)_2, \dots, (JAR)_i$, the parameters D , μ and σ of the function

$$JAR(t) = \frac{D}{\sqrt{2\pi \cdot \sigma \cdot t}} \exp \left[-\frac{(\ln t - \mu)^2}{2\sigma^2} \right] \quad (2)$$

are determined. This function approximates the profile JAR for some strong active region. Then $JAR(t)$ is calculated for $t \geq 1$, where $t=1$ corresponds to the first day of existence of SAR. According to the 20th solar cycle data analysis the first strong flare occurs in SAR not earlier than five days

after its appearance, i.e., the first prediction of $JAR(t)$ can be derived on the basis of the first five values of $(JAR)_i$. Then this prediction is specified and corrected. If SAR occurs behind the limb the prediction is complicated, as we do not know the date of its appearance. In this case the following estimations take place. If SAR occurs on the east limb with $(JAR)_x < 1$ or $(JAR)_{x+1} < 1$, then $x=5$; if $(JAR)_x > 1$ or $(JAR)_{x+1} > 1$ then $x=10$; if $(JAR)_x > 2$ or $(JAR)_{x+1} > 2$, then $x=15$. An example of the approximation of $JAR(t)$ is given in Figure 2 (upper part) for SAR 14943. The parameters of $JAR(t)$ in equation (2) are the following: $D=51$, $\mu=3.1$, $\sigma=0.6$.

2.2 SF Prediction

Suppose that the first prediction of $JAR(t)$ based on data from $(JAR)_1$ up to $(JAR)_i=1$ is obtained on this i th day the first strong flare can occur. If SAR has $JAR > 1$ on the east limb then SF prediction begins from this very day. The period of time ΔT during which the strong flares can occur in SAR is determined and then specified. ΔT is taken equal to the time interval when

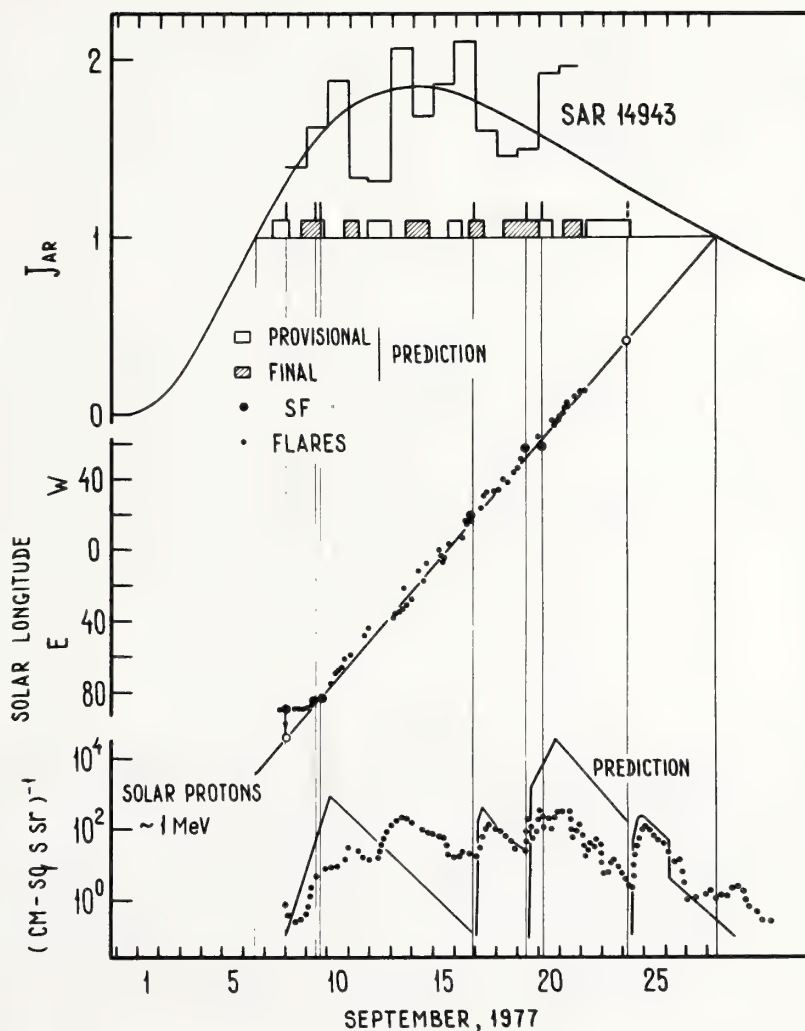


Figure 2. An example of short-term prediction.

$JAR(t) > 1$. The final ΔT given in Figure 2 turned out to be equal to 22 days from 6 to 28 September 1977.

The number of SF in SAR followed by the proton events in the interplanetary space is supposed to be equal to the whole part of JAR (maximum of JAR). In other words the number of APS occurring in some SAR is equal to $[JAR]$. As can be seen from Figure 2, the real number of APS in some SAR can significantly differ from the supposed number of APS. This fact, in turn, can influence the long-term APS prediction.

Together with the prediction of ΔT , the moments, coordinates, and importances of flares in SAR should be fixed. Flares occur in the separate centers of quasigomological flares (CGF, Kontor, 1976). The middle part of Figure 2 shows that flares in SAR 14943 take place mainly in one CGF. Data analysis shows that before SF the frequency of flares ν in some CGF usually increases as $\nu = 1/\Delta t$, where Δt is average time interval between the consequent flares, determined from five consequent flares. The most probable time interval of SF appearance is taken equal to $t_2 - t_1$, where t_1 is the moment of fifth flare and $t_2 = t_1 + 10 \cdot \Delta t$. Prediction begins from the second flare and ends when time interval between two consequent flares is more than 12 hours. Then prediction is restored. Rectangles in the upper part of Figure 2 represent predicted time intervals of SF occurrence and SF moments. SF strength in our analysis is determined by three parameters: optical importance, chromospheric radio burst, and spectral type two of radio burst. The latter parameter indicates shock generation in that SF. These parameters define both the number of protons A injected during SF and the PE time profile.

2.3 PE Prediction

Prediction of the PE time profile is based on the Lupton and Stone (1973) model. It is done for protons with energies about 1 MeV. The number of injected protons A is determined from Table 1. To predict the PE profile more quickly, the PE profiles are calculated beforehand for all heliolongitudes (through every 10 degrees) and for averaged parameters of interplanetary medium (Kontor et al., 1979). The energetic proton spectrum is supposed to have a parabolic form (Lyubimov and Kontor, 1973, Kontor et al., 1979) with density

$$\frac{dJ}{dE} = a_0 \left(\frac{1}{E} \right)^{2+0.3 \ln E} \quad (3)$$

To predict the PE profile for some SF it is only necessary to choose A (Table 1) and reproduce the PE profile for a given longitude. This prediction will reproduce a situation when SF is not accompanied by the shock (e.g., a similar situation took place for SF on September 16; see Figure 2). If the shock is not too strong, the PE profile varies as shown in Figure 2 for SF on September 24. If the shock is strong enough, the PE profile varies as shown in Figure 2 for SF on September 7 and 19. This rough model to describe the effects of shock on the PE profile is based on the results of Vernov et al. (1977a). Experimental data were taken from SGD (1977, 1978a).

Table 1. Predictions of PE profile, given A and SF importance.

SF optical importance	A Amplitude of chromospheric radio burst on frequencies > 2800MHz in units 10^{-22} W/sq-m Hz			
	< 10^{-2}	10^{-2} - 10^{-3}	10^{-3} - 10^{-4}	> 10^{-4}
1N, -B	10^{31}	10^{32}	10^{33}	10^{34}
2N, 1B	10^{32}	10^{33}	10^{34}	10^{35}
3N, 2B	10^{33}	10^{34}	10^{35}	10^{36}
4N, 3B, 4B	10^{34}	10^{35}	10^{36}	10^{37}

3. LONG-TERM APS PREDICTION

The aim of long-term APS prediction consists of predicting the SAR distribution as a function of \hat{J}_{AR} during the solar cycle and hence prediction of SF frequency F_s and proton fluxes in the interplanetary medium. This prediction is based on the prediction of 11-year cycle of sunspot numbers R_z (SGD, 1978b) and on analysis of APS during the 20th solar cycle.

3.1 SAR Prediction

As a result of analysis of active region statistics during the 20th solar cycle (Kontor and Khotilovskaja, 1975), the distributions of long-lived active regions as functions of maximum area S_m were determined for every year from 1965 to 1974. These distributions are described by a log-normal distribution analogous to equation (2). The distributions have three parameters: N_{AR} = number of long-lived active regions in a given year; S_μ = median value of S_m ; and σ = a value characterizing the distribution form. For the 20th solar cycle the following relations between N_{AR} , S_μ , σ , and R_z were determined:

$$N_{AR} = 11\sqrt{R_z} \quad (4a)$$

$$S_\mu = 3.7\sqrt{R_z} \text{ (on the upward branch of a cycle)} \quad (4b)$$

$$S_\mu = 2.7\sqrt{R_z} \text{ (on the downward branch of a cycle)} \quad (4c)$$

$$\sigma = 0.59 \text{ (has a weak dependence on } R_z) \quad (4d)$$

These relations enable us to determine the distributions of long-lived active regions as a function of S_m from R_z predictions, supposing that the relations in equation (4) remained correct during the 21st solar cycle. Using results of correlation studies of active region parameters (Kontor and Khotilovskaja, 1975), when

$$M_m = 3.81 S_m - 8.7 \quad (5a)$$

$$f_m = 0.093 S_m - 0.06 \quad (5b)$$

one can calculate \hat{J}_{AR} as a function of S_m :

$$\hat{J}_{AR} = \frac{1}{3} \left(\frac{S_m}{30} + \frac{M_m}{100} + \frac{f_m}{3} \right) \approx \frac{S_m}{30} \quad (6)$$

Table 2 gives the data of R_Z prediction (SGD, 1978b) and parameters N_{AR} , S_μ and σ for every year from 1976 to 1986.

3.2 SF Prediction

Assuming that the number of SF in SAR is equal to $[\hat{J}_{AR}]$ where \hat{J}_{AR} distributions are received from long-term SAR prediction, the number of SF for every year N_i (see Table 2) can be estimated.

Table 2. R_Z prediction and parameters for 1976-86.

Year	R_Z	N_{AR}	S_μ	N_i	F_s	C_1	C_{10}
1976	13.4	40	13.6	5	0.42	54	1.9
1977	31.5	62	20.8	18	1.50	195	6.9
1978	91.0	105	35.3	93	7.75	1008	35.7
1979	142.7	131	44.2	162	13.50	1755	62.1
1980	141.9	131	32.2	97	8.08	1051	37.2
1981	122.3	122	29.9	81	6.75	878	31.0
1982	92.8	106	26.0	53	4.42	574	20.3
1983	57.8	84	20.5	25	2.08	271	9.6
1984	37.0	67	16.4	11	0.92	119	4.2
1985	23.7	54	13.1	4	0.33	43	1.5
1986	15.1	43	10.5	2	0.17	22	0.8

3.3 PE Prediction

Long term PE prediction consists of estimating year-averaged proton fluxes using the technique described by Vernov et al. (1977b). According to this technique, every SF gives the same averaged proton flux. Averaged monthly intensity from one SF was estimated by the value $J_1=260 \text{ (cm-sq s sr)}^{-1}$ for the 19th solar cycle and $65 \text{ (cm-sq s sr)}^{-1}$ for the 20th solar cycle for protons with energies more than 1 MeV and $J_{10}=8.7 \text{ (cm-sq s sr)}^{-1}$ for the 19th solar cycle and $2.4 \text{ (cm-sq s sr)}^{-1}$ for the 20th solar cycle for protons with energies more than 10 MeV. R_Z prediction shows that the 21st solar cycle must be something intermediate between the 20th and 19th solar cycles; therefore, averaged intensity from one SF in that cycle may be estimated as a geometrical mean of the corresponding values of J_1 and J_{10} . Then $J_1=130 \text{ (cm-sq s sr)}^{-1}$ and $J_{10}=4.6 \text{ (cm-sq s sr)}^{-1}$ will be obtained for the 21st cycle. Year-averaged intensities $C_1=J_1 \cdot N_i/12$ and $C_{10}=J_{10} \cdot N_i/12$ as well SF frequency $F_s=N_i/12$ are shown in Table 2 and Figure 3.

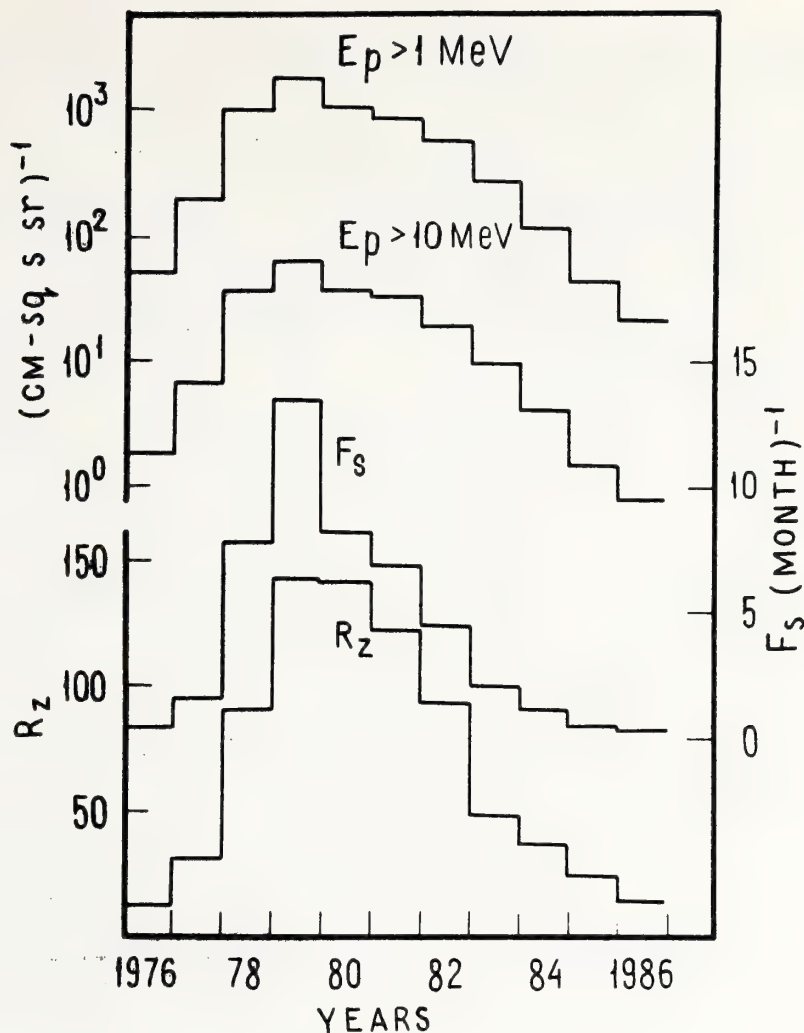


Figure 3. Long term prediction of F_s and proton fluxes.

4. CONCLUSION

The APS prediction described in this paper is an attempt to predict some sequence of interconnected phenomena occurring in the solar atmosphere and interplanetary medium. It comprises a definite prediction technique for active regions, flares, and proton fluxes. Attention is drawn only to strong active regions, for which the period of SF occurrence is predicted. SAR prediction allows one "to look behind the limb". For example, from Figure 2 one can see that the most active period of SAR 14943 began on September 6, when it had a longitude of about 176°W . SF prediction does not include the estimations of flare strength; therefore it is desirable to complete it with the synoptic methods of SF prediction (Steshenko, 1973; Pick and Simon, 1973; Syrovatskij, 1977).

Today much attention is paid to PE prediction (see Roelof and Gold, 1975, 1976; Akin'yan et al., 1977; Smart and Shea, 1978a, 1978b). If details

are not taken into account we may hope that systematic comparison of different PE predictions with the observed profiles will help to specify our knowledge of the physical processes on the Sun and in the interplanetary medium as well as our choice of the most adequate methods of PE prediction. The same can be said about other aspects of APS prediction.

As for a long-term APS prediction, its accuracy depends on both the accuracy of the R_z prediction and correctness of the estimates that were assumed in our analysis. In particular, it concerns the relations of equation (4), the average number of SF in SAR and intensities J and J_0 . A considerable change of any of these parameters may appreciably effect the 21st solar cycle prediction.

REFERENCES

- Akin'yan, S. T., V. V. Fomichev, and I. M. Chertok (1977): Definition of the parameters of solar protons in the vicinity of the earth from radio bursts. Geomagn. Aehron., 17:10, :177, :596.
- Kontor, N. N. (1976): Strong active regions on the sun as sources of solar protons and cosmic ray modulation effects. Thesis, Nucl. Phys. Institute Moscow State University.
- Kontor, N. N., G. P. Lyubimov, A. G. Nikolaev, N. V. Pereslegina, B. A. Tverskoj, and T. G. Khotilovskaya (1975): Solar activity and streams of cosmic ray protons in March-July 1972. Geomagn. Aehron., 15:777.
- Kontor, N. N., and T. G. Khotilovskaya (1975): Active region statistics in the 20th solar cycle. Report of Nucl. Phys. Inst. Moscow State University, December 1975.
- Kontor, N. N., G. P. Lyubimov, T. G. Khotilovskaya, and E. P. Zaborova (1976): Strong active regions and disturbances of the interplanetary medium. Izv. Acad. Nauk SSSR, ser. fiz., 40:477
- Kontor, N. N., G. P. Lyubimov, and T. G. Khotilovskaya (1979): Cosmic ray data analysis based on the model of active process in the solar space. Cosmic rays, No. 20, Nauka, Moscow (in press).
- Lupton, J. E., and E. C. Stone (1973): Solar flare particle propagation: comparison of a new analytic solution with spacecraft measurements. JGR, 78:1007
- Lyubimov, G. P., and N. N. Kontor (1973): Forbush decreases of solar cosmic rays. Astron. Tsirk., No. 781:5.
- Pick, M., and P. Simon (1973): Solar activity and its forecast. Proc. IEEE, 61:1303.
- Roelof, E. C., and R. E. Gold (1975): Evaluation of a prediction technique for low energy solar particle events. AFCRL-TR-75-0503, November 1975.

Roelof, E. C., and R. E. Gold (1976): Prediction of solar energetic particle event histories using real-time particle and solar wind measurements. AFGL-TR-76-0136, 25 June 1976.

Smart, D. F., and M. A. Shea (1978a): Prediction of the solar proton time-intensity profiles for the 30 April 1976 event. COSPAR: Space Research, 18:373.

Smart, D. F., and M. A. Shea (1978b): Current status of short-term solar proton predictions., preprint.

SGD: Solar-Geophysical Data (1977), No. 399-part 1, November 1977, Department of Commerce (Boulder, Colorado, USA 80302).

SGD: Solar-Geophysical Data (1978a), No. 403-part 2, March 1978, Department of Commerce (Boulder, Colorado, USA 80302).

SGD: Solar-Geophysical Data (1978b), No. 408-part 1, August 1978, Department of Commerce (Boulder, Colorado, USA 80302).

Steshenko, N. V. (1973): Research on conditions of solar flare appearance. Vestn. AN SSSR, No. 3:42.

Syrovatskij, S. I. (1977): About problem of solar flare forecast. Solar activity problems and "Prognoz" cosmic system, Nauka, p. 5-22.

Vernov, S. N., N. N. Kontor, G. P. Lyubimov, B. A. Tverskoy, and T. G. Khotilovskaya (1977a): Proton fluxes in interplanetary space relevant to the active processes on the sun. 15th Intl. Cosmic Ray Conference, Plovdiv, Bulgaria, 3:142.

Vernov, S. N., S. I. Ermakov, N. N. Kontor, G. P. Lyubimov, B. A. Tverskoy, and E. A. Chuchkov (1977b): 11-year variations of the low energy solar proton fluxes. 15th Intl. Cosmic Ray Conference, Plovdiv, Bulgaria, 3:133.

SOLAR-TERRESTRIAL PREDICTIONS USING IPS TECHNIQUE

Takashi Watanabe*

Space Environment Laboratory, NOAA/ERL
Boulder, Colorado 80303

A capability of the multi-site IPS observations for solar-terrestrial predictions is discussed. It is essential to know the accurate arrival time of a flare-generated disturbance at a line of sight to a radio source to give a reliable prediction at a point farther from the sun. Arrival of the shock front at the line of sight is identified by sudden increase in the flow speed accompanied with rather weak increase in the level of scintillations. In this case, we can estimate the arrival time of the shock front at the Earth with considerable accuracy assuming a suitable dynamical characteristic. The arrival of the piston plasma of the disturbance is identified by the big increases both in the flow speed and the level of the scintillations. When the piston plasma is observed by at least two sets of a multi-site IPS group (such as La Jolla and Toyokawa) with suitable time intervals, we can estimate the dynamical characteristics of the disturbance to improve the accuracy of the prediction. Some provisional method to make the prediction using only one IPS observation of the disturbance is also proposed.

1. INTRODUCTION

One of the most fundamental problems in scientifically-based field of solar-terrestrial predictions is the arrival time prediction of a flare-generated disturbance at the Earth. This prediction has very important meaning because the principal phase of the solar-terrestrial events is triggered by the arrival of the disturbance at the Earth. Since the dynamical characteristics of the disturbance will depend on the various initial and boundary conditions, such as the amount of the energy input from the solar flare and the physical conditions of the ambient solar wind, its prediction will be quite difficult without the observation of the disturbance prior to its arrival at the Earth. Interplanetary scintillation (IPS) technique provides a means to detect the disturbance in the region inside the Earth's orbit. When solar wind data obtained by spacecraft orbiting inside the Earth's orbit are not available, only the IPS technique will supply reliable data of the disturbance for the prediction. Cronyn et al. (1975) first treated this

*NRC Post-Doctoral Research Associate. On leave from the Research Institute of Atmospherics, Nagoya University, Japan

problem, depending on the increases in the scintillation indices of a number of radio sources detected by a large radio telescope. Roelof et al. (1977) also proposed a method of prediction depending on the change in characteristic of the power spectrum of the scintillations observed by a single radio telescope. According to these observations, we will have an approximate geometry of the disturbance prior, say one day before, to its arrival at the Earth.

The three-site IPS observations (e.g. Coles, 1978) enable us to measure the flow speed of the solar wind in addition to the scintillation index. At present, three-site IPS observations are carried out by IPS groups at the University of California, San Diego (UCSD) and at Nagoya University, Toyokawa (TYKW). Three-site IPS stations are also presently under construction by the Physical Research Laboratory (PRL) in India. It seems that, although the 'existence' of the disturbance on the line of sight will be frequently identified by the IPS observations, the chance to detect the 'arrival' of the disturbance at the line of sight will be rare because present IPS observation for each radio source is made only for 10 minutes to 2 hours in a day by each presently-operational IPS group. Nevertheless, since the observational time at TYKW for a given radio source is made about seven hours after the observation of the same source at UCSD, there exist several possibilities to determine the structure and the dynamical characteristics of the disturbance. In this paper, provisional methods to make solar-terrestrial predictions using the multi-site IPS observations will be proposed.

2. IPS OBSERVATIONS OF FLARE-GENERATED DISTURBANCES

It will be convenient to examine a typical example of the IPS observation of a flare-generated disturbance to grasp the general idea of the IPS technique. A series of flare-generated disturbances were detected by the IPS observations during early August 1972 (e.g. Kakinuma and Watanabe, 1976). Among them, the disturbance generated by the solar flare which occurred at 1515 UT on August 7, 1972, was recognized as showing a feature typical of a flare-generated disturbance. Figure 1 shows the flow speeds obtained by the IPS groups of UCSD (Rickett, 1975) and TYKW (Watanabe, 1977) by the IPS observations of 3C144. The scintillation indices of 3C144 which were estimated by Rickett (1975) of UCSD and by Ward (1975) of Adelaide University, Australia, are also plotted (as bars) in Figure 1. The observational time of 3C144 at Adelaide was very close to that at TYKW. Daily IPS index obtained at UCSD is halved to adjust the base levels of both observations (Watanabe, 1977). TYKW group did not estimate the scintillation index; instead, the RMS of the scintillations, which corresponds to the unnormalized scintillation index, was estimated. The heliocentric distance of the closest approach to the sun of the line of sight to 3C144 was about 0.8 AU. As shown in Figure 1, the IPS group of UCSD observed a very high speed flow of 1220 km/sec at about 16 UT on August 8. It is very remarkable to note that the UCSD group detected only a rather small increase in the scintillation index (Rickett, 1975). The amount of increase was within 20% as compared with that of the previous day. On the other hand, the IPS observations at Adelaide and TYKW which were made about seven hours after the observation at UCSD on August 8 showed a very sharp rise in IPS index of more than 200% of the value of the

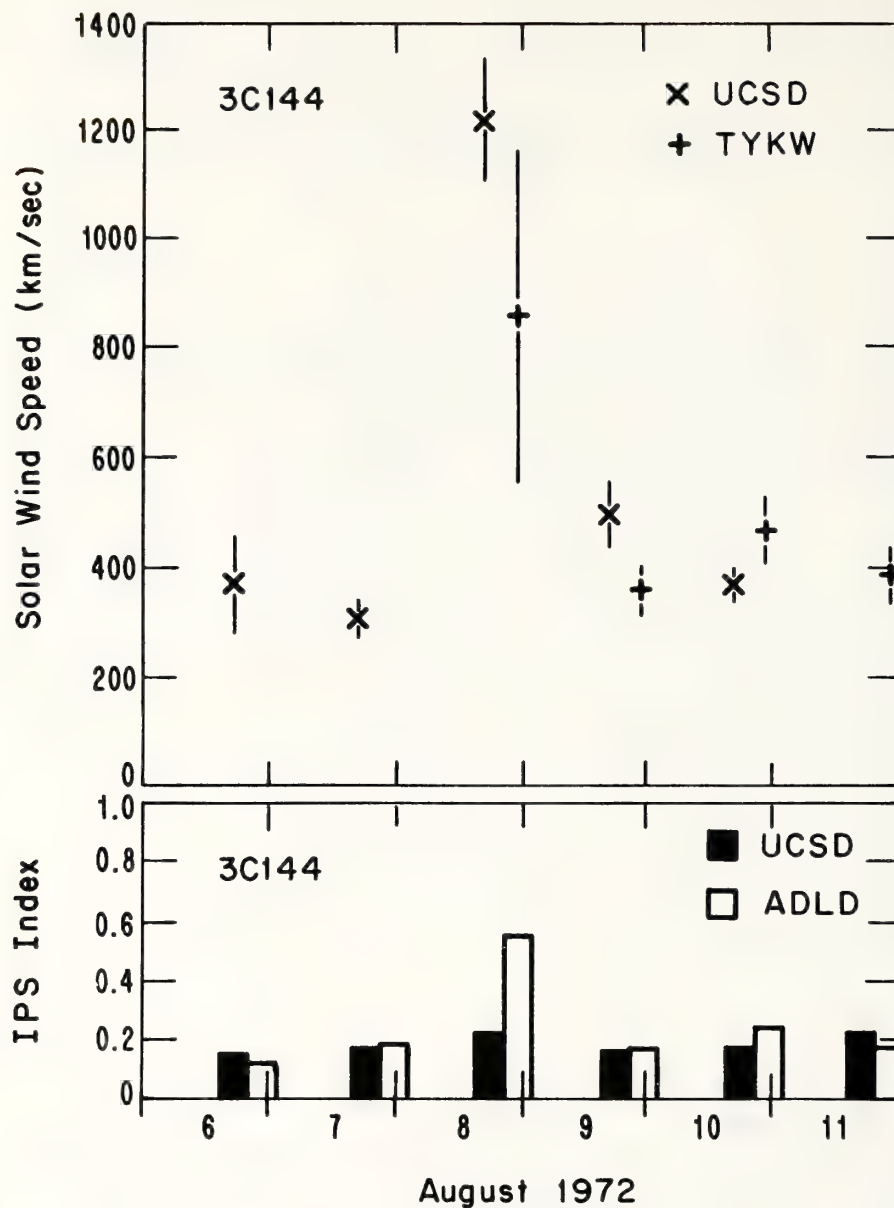


Fig. 1 Solar wind speeds and scintillation indices obtained by the IPS observations of 3C144 in early August 1972. The marks \times and $+$ with error bars represent the solar wind flow speeds obtained at the University of California, San Diego (UCSD) and at Nagoya University (TYKW) respectively. The filled and open bars represent the magnitudes of the scintillation indices of 3C144 observed at UCSD and at Adelaide University (ADLD) respectively (see text).

previous day. The observed flow speed at TYKW was about 870 km/sec. These observations seem to show the spatial structure of the post-shock plasma of the flare-generated disturbance. That is, we interpret this coordinated set of observations as showing the flow speed immediately behind the shock front to be very high, but the level of the turbulence is not so enhanced. Instead, the turbulence level reaches its maximum a few hours after the shock front passage.

This special feature of the post-shock plasma has been confirmed for two events, including the above-mentioned disturbance, through the comparison between the IPS observations and the in situ solar wind data obtained by spacecraft during early August 1972 (Watanabe, 1977). According to these analyses, the post-shock plasma associated with the turbulence of the highest level seems to correspond to the region with the highest density. This region follows the shock front with the time interval of 4 ~ 6 hours when we observe it (via enhanced scintillation indices) in the vicinity of 1 AU from the sun. The MHD theory of flare-generated disturbances (e.g. Dryer, 1972) suggests that the density of the post-shock plasma will reach its maximum in the vicinity of the contact surface (or 'piston'). The highly turbulent region detected by the IPS method seems, thereby, to correspond to the 'piston' (Watanabe, 1977). Therefore, it is considered in the present case that the IPS observation at UCSD on August 8 was made immediately after the arrival of the shock front at the line of sight to 3C144 and that the IPS groups at TYKW and Adelaide detected the highly turbulent piston following the shock front.

We will now try to predict the arrival time of the shock front at the Earth using the above-mentioned IPS observations. The dynamical characteristic of the disturbance will be expressed by the following formula:

$$V_R = V_O (R/R_O)^{-k} \quad (1)$$

where;

- R : heliocentric distance of the disturbance
- V_R : speed of the disturbance at R from the sun
- R_O : heliocentric distance of the reference point
- V_O : speed of the disturbance at R_O
- k : deceleration coefficient.

When the value of ' k ' is given, the arrival time of the disturbance at the Earth is estimated through the integration of Eq. (1) for an isotropically expanding disturbance:

$$T_E = \frac{R_O}{V_O(k+1)} ((R_E/R_O)^{k+1} - 1) \quad (2)$$

where:

- T_E : the time interval between the arrival times of the disturbance at R_O and at the Earth
- R_E : heliocentric distance of the Earth.

Several examples of the IPS observations of the disturbances show that the deceleration coefficient is distributed between 0 to 1.3. In the case of the disturbance generated by the solar flare on August 7, 1972, the degree of deceleration in the region between the sun and the line of sight to 3C144 seems to have been medium because the observed flow speed (1220 km/sec) is somewhat slower than the minimum mean speed of the disturbance (1350 km/sec) which is estimated from the heliocentric distance of the closest approach to the sun on the line of sight to 3C144 and the time interval between the onset of the relevant solar flare and the IPS observation of 3C144 at UCSD on August 8, 1972. The predicted time of the onset of SSC due to this disturbance is 23 UT on August 8 for $k=0$ (non-deceleration) and 24 UT on August 8 for $k=0.7$ (medium deceleration). For simplicity, we set the value of V_0 to be equal to the observed flow speed at UCSD (1220 km/sec) because we cannot estimate the intrinsic speed of the shock front by IPS observations. Since the actual shock speed will be faster than that of the post-shock plasma, this choice will produce another ambiguity. The second prediction ($k=0.7$) seems to be quite successful because the actual SSC was reported at 2354 UT on August 8, 1972. It is seen that the small change in k does not affect the prediction very much. This is caused by the high speed of the disturbance and the small difference (0.2 AU) in the radial distances between the Earth and the closest approach to the sun on the line of sight to 3C144. The high accuracy of this prediction mainly depends on the small ambiguity in determination of the arrival time of the shock front at the line of sight. The IPS observations of 3C144 will be useful for prediction work because the line of sight to 3C144 is always very close to the ecliptic plane. This condition excludes the ambiguity caused by possible anisotropic expansion of the disturbance in the latitudinal direction.

A very similar event was observed in early March 1978. A solar flare of importance 3B occurred at 1135 UT on March 6, 1978 (Solar-Geophysical Data, No. 404-Part 1). The IPS group of UCSD (Solar-Geophysical Data, No. 404, Part 1) detected high speed flow of 830 km/sec at 23 UT on March 7 by the IPS observation of 3C48. The IPS group of TYKW also detected high speed flow of about 700 km/sec at seven hours after the UCSD observation of the same radio source. The IPS activity of 3C48 on March 7, as observed by the IPS group of UCSD, was slightly increased (within 20%) as compared with that on the previous day, March 6 (Coles, private communication). On the other hand, the IPS group at TYKW observed the increase in the IPS activity of more than 40% as compared with that of the previous day. It seems that these observations demonstrate a situation similar to the case of the above-mentioned disturbance generated by the solar flare on August 7, 1972. We will apply above-mentioned procedure to this disturbance. The deceleration of this disturbance in the region between the sun and the line of sight to 3C48 (0.8 AU from the sun) seems to have been medium ($0 < k < 1.3$) because the observed flow speed (830 km/sec) is somewhat slower than the minimum mean velocity between the sun and the line of sight to 3C48 (940 km/sec). The predicted time of SSC is about 1120 UT on March 8, 1978 when we assume the value of k as 0.7 for the case of medium deceleration. The actual SSC due to this disturbance was reported at 1439 UT on March 8, 1978 (Solar-Geophysical Data, No. 405, Part 1). The error of prediction is about 3 hours in this case. This error will be partially due to the possible ambiguity of a few hours in the arrival time of the disturbance at the line of sight. In addition, an anisotropic nature

of the expansion in the latitudinal direction is also suggested because the line of sight to 3C48 has an angle of 21 degrees to the ecliptic plane and the flare occurred at 25 degrees north of the solar equator. Hence, the portion of the asymmetrical shock which moved through the ecliptic plane apparently moved slower than the portion directly above the flare.

We have seen that when we can identify the existence of the postshock plasma distributed immediately behind the shock front by the IPS observation, the prediction can be made with considerable accuracy. To determine the dynamical characteristic of the disturbance, it is required to make the observations of the piston plasma at least twice with a suitable time interval. This method depends on an idea that the observed flow speed will decrease with time because of the following three effects: deceleration of the piston plasma, the projection effect, and the anisotropic expansion. The second effect means that we can only observe the transverse component of the flow vector by the multi-site IPS observations and that the projection angle increases as the piston plasma expands outward from the sun. The geometry is shown in Figure 2. The value of 'k' can be estimated through the comparison between the observed flow speeds and the predicted values for various 'k' using equations similar to Eqs. (1) and (2) and the consideration of the projection effect. Sometimes we must take into account the anisotropic expansion. In this stage, we have no example which can be used for the trial of the prediction. The applications of this method to find the dynamical characteristics of the disturbance are given by Watanabe (1977).

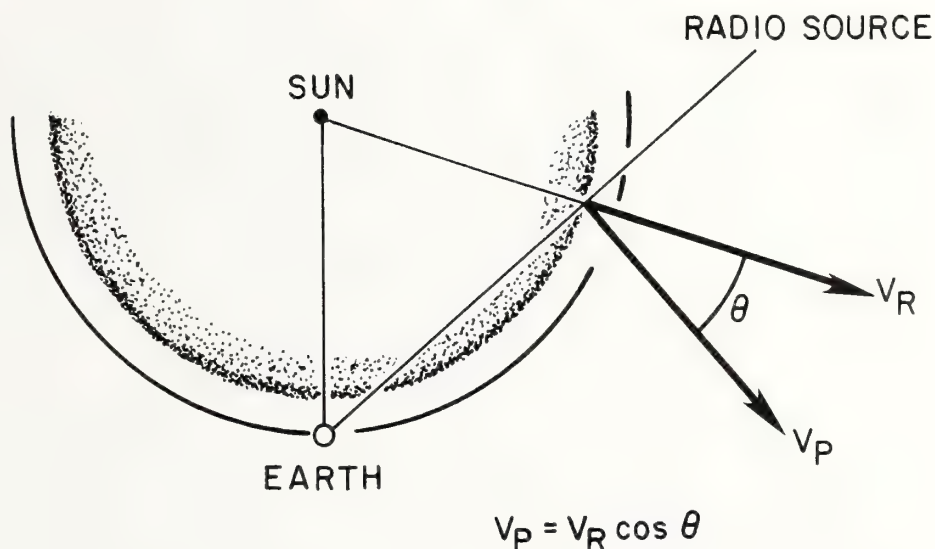


Fig. 2 Schematic geometry of the IPS observation of an isotropic flare-generated disturbance. Observed flow speed V_P is the transverse component of the radial flow vector V_R . The projection angle is θ . Consideration of the scintillation closest to earth (along the line of sight) may be precluded due to the Fresnel filtering effect in the example shown here.

3. PREDICTION USING ONLY ONE MULTI-SITE IPS OBSERVATION

If we can identify the existence of the post-shock plasma immediately behind the shock front by some methods, the second observation is not necessary for the rough prediction. But the detection of the high speed solar wind with rather low turbulence level is not sufficient to identify the post-shock plasma because the corotating high-speed stream also shows very similar tendency. Rickett (1975) showed that the skewness coefficient (Bourgois, 1972) presented a sharp rise on August 8, 1972 while the increase in scintillation index is small (see Fig. 1). The increase in skewness coefficient will be a criterion to identify the post-shock plasma as suggested by Rickett (1975). However, the chance of the detection of the post-shock plasma immediately behind the shock front will be rare because the highly turbulent piston plasma will shortly arrive at the line of sight a few hours after the arrival of the shock front at the line of sight. Beside this, when the longitudinal extent of the piston plasma is large, it will still exist on the line of sight for one or two days. The somewhat weak IPS caused by the post-shock plasma immediately behind the shock front will be easily masked by the intense IPS due to the highly turbulent piston plasma. Thus it is expected that the chance to observe the piston plasma will be frequent as compared with that of the post-shock plasma immediately behind the shock front. In this section we will propose a convenient method to predict the solar-terrestrial events depending only on a single multi-site IPS observation of piston plasma.

There exist several cases wherein the observed flow speed of the piston plasma was very similar to the minimum mean speed of the disturbance in the region between the sun and the line of sight. In these cases, it is expected that the ambiguity in the arrival time of the disturbance at the line of sight is very small; it is also expected that the deceleration of the disturbance is very weak. We can predict the arrival time of the shock front at the Earth with considerable accuracy, assuming the possible time separation (~ 4 hrs) between the shock front and the piston. Two examples are shown in Table 1 (Nos. 1 and 2). It is very interesting to note that, in the case of No. 2, it was the Forbush decrease (F.D.) of galactic cosmic rays, and not the SSC, which was reported near the predicted time.

In many cases, the observed flow speed may be considerably slower than the minimum mean speed of the disturbance. In these cases it is necessary to distinguish whether the reduction of the observed flow speed is caused by the projection effect (see Fig. 2) or the deceleration of the disturbance itself. Since we cannot know the arrival time of the piston at the line of sight only on the basis of the single multi-site IPS observation, it will be impossible to give an unambiguous decision. Nevertheless, the following situations may be imagined. When the heliocentric distance of the line of sight is small (0.3 to 0.5 AU), the reduction of the observed flow speed will be caused mainly by the projection effect rather than the deceleration because of the following two reasons. Firstly, several analyses of the IPS observations of flare-generated disturbances show that the deceleration in the region close to the sun will be small. Secondly, the projection effect sensitively affects the observation because the rate of the increase in the

No.	Solar Flare (UT)	IPS Obs. (UT)	V_{obs} (km/s)	\bar{V}_{min} (km/s)	k	Prediction (UT)	Event (UT)	Error (hrs)
1	April 30/21h, '76	May 02/06h 3C144, 0.7 AU	835	841	0	May 02/19h	May 02/18h (SSC)	1
2	Sept. 07/23h, '77	Sept. 10/06h 3C298, 0.8 AU	550	572	0	Sept. 10/20h	Sept. 11/00h (F.D.)	4
3	June 19/23h, '74	June 22/22h 3C48, 0.9 AU	451	507	0.7	June 23/07h	June 23/09h (SSC)	2
4	Sept. 19/11h, '77	Sept. 20/00h 3C225, 0.6 AU	570	1700	1.3	Sept. 21/22h	Sept. 21/21h (SSC)	1

Table 1. Examples of solar-terrestrial predictions using single multi-site IPS observations. In the third column, the distance in AU is the heliocentric distance of the line of sight to the observed radio source. V_{obs} is the observed flow speed. \bar{V}_{min} is the mean speed of the disturbance which is estimated from the distance of the line of sight and the time interval between the relevant solar flare and the observational time. The deceleration coefficient is represented by k (see text).

porjection angle (θ in Fig. 2) with a given time delay is larger than that in the cases of the lines of sight with larger heliocentric distances.

On the other hand, when the heliocentric distance of the line of sight is large (0.6-0.9 AU), the reduction of the observed flow speed will mainly be caused by the deceleration of the piston. Otherwise, in many cases, we must assume that the disturbance will propagate far beyond the Earth at the observational time to attribute the reduction of the flow speed to the projection effect. Two examples of the predictions are shown in Table 1 (Nos. 3 and 4). We tentatively assume the deceleration coefficient according to the amount of the reduction of the observed flow speed from the minimum mean speed. Since we select the T_0 in Eq. (2) as the observational time, the accuracy of the prediction will somewhat depend on 'chance'. We have no IPS observational examples of disturbances in the vicinity of the sun at present because it is difficult to identify the flare-generated disturbance by the increase in the scintillation index. Even when the highly turbulent piston exists on the line of sight, the amplitude of the scintillation is suppressed by the strong scattering effect which is caused by the ambient solar wind with a high degree of electron density fluctuations distributed in the vicinity of the sun. This effect becomes important when the line of sight is closer than about 0.5 AU from the sun for the observing frequency of about 70 MHz (e.g. Coles et al., 1974).

Observations of type II radio burst will supplement the IPS observations of interplanetary disturbances because a linear relationship between drift velocities of type II bursts and initial velocities of interplanetary disturbances was suggested by Pinter (1973). Among examples given in Table 1, type II radio burst of 1250 km/sec was observed (Pintér, 1977) for event No. 1. If we assume that this disturbance propagated from the solar corona to the line of sight of 3C144 (0.7 AU) with uniform deceleration, the estimated deceleration coefficient of this disturbance is less than 0.1. This value is fairly consistent with that given in Table 1 ($k=0$) for event No. 1, depending on small difference between V_{obs} and V_{min} .

4. CONCLUDING REMARKS

We have seen in the previous two sections that solar-terrestrial predictions can be made by IPS observations with considerable accuracy when the ambiguity of the arrival time of the flare-generated disturbance at the line of sight is small. However, such a chance will not occur frequently because of the poor time resolution of the present IPS observations. To improve this situation, it is quite desirable to set up a world-wide coordination of the IPS observations.

Acknowledgements

The author is grateful to Dr. M. Dryer for encouragement and comments on the manuscript. His thanks are especially due to Prof. W. A. Coles and Dr. J. J. Kaufman of University of California, San Diego for kindly providing their unpublished IPS data. Thanks are also due to Prof. T. Kakinuma, Dr. H. Washimi, and Mr. M. Kojima of Nagoya University for their contributions in IPS observations.

REFERENCES

- Bourgois, G. (1972): A theoretical study of the higher moments of the interplanetary scintillations. Astorn. and Astrophys., 21:33.
- Coles, W. A. (1978): Interplanetary scintillation. Space Sci. Rev., 21:411.
- Coles, W. A., B. J. Rickett, and V. H. Rumsey (1974): Interplanetary scintillations. In Solar Wind Three (C. T. Russell, Ed.), pp. 351, Institute of Geophysics and Planetary Physics, University of California, Los Angeles, Calif.
- Cronyn, W. M., F. Erskine, S. D. Shawhan, B. L. Gotwols, and E. C. Roelof (1975): Prediction of ionospheric effects associated with solar wind disturbances using interplanetary scintillation observations at 34.3 MHz. The Johns Hopkins University-Applied Physics Laboratory preprint series January 1975.
- Dryer, M. (1972): Interplanetary double-shock ensembles with anomalous electrical conductivity. In Solar Wind, (C. P. Sonett, P. J. Coleman, Jr., and J. M. Wilcox, Eds.) pp. 453, NASA SP-308.
- Kakinuma, T., and T. Watanabe (1976): Interplanetary scintillation of radio sources during August 1972. Space Sci. Rev., 19:611.
- Pintér, S. (1973): Close connexion between flare-generated coronal and interplanetary shock waves, Nature Phys. Sci., 243:96.
- Pintér, S. (1977): Velocities of propagation of March/April 1976 coronal and interplanetary shock waves, in Collected Data Reports for stip Interval II, 20 March - 5 May 1976 (H. E. Coffey and J. A. McKinnon, Eds.), p. 127, WDC-A for Solar Terrestrial Physics, NOAA, Boulder, Colo.
- Rickett, B. J. (1975): Disturbances in the solar wind from IPS measurements in August 1972. Solar Phys., 43:237.
- Roelof, E. C., B. L. Gotwols, D. G. Mitchell, W. M. Cronyn, and S. D. Shawhan (1977): Use of interplanetary radio scintillation power spectra in predicting geomagnetic disturbances. AFGL-TR-77-0244, U.S. Air Force Geophysics Laboratory.
- Ward, B. D. (1975): Ph.D. Dissertation, The University of Adelaide, South Australia, Australia.
- Watanabe, T. (1977): IPS observations of flare-associated shock waves. In 1972-1974. In Contributed Papers to the Study of Travelling Interplanetary Phenomana/1977 (Proceedings of COSPAR Symposium B, Tel Aviv, Israel, June 1977, M. A. Shea, D. F. Smart, and S. T. Wu, Eds.), p. 139.

SPACE PLASMA MONITORING: TWO NEW CAPABILITIES FOR THE COMING DECADE

D. P. Cauffman
Solar-Terrestrial Division
NASA Headquarters
Washington, DC 20546
USA

Two powerful capabilities for monitoring solar-induced influences on the terrestrial environment are becoming available for the first time:

(1) in-situ monitoring of the solar wind from the sunward libration point, and (2) multi-spectral imaging of the auroral oval and polar cap. These capabilities are expected to be intermittently available throughout the next decade. They are important because they will provide detailed quantitative data that can be used to test hypotheses concerning how solar wind variations influence fluctuations in the terrestrial space environment, including those expected to operate on sunspot-cycle time scales.

1. SOLAR WIND MONITORING

Until the present, data describing the solar wind have been limited to brief glimpses from exploratory spacecraft destined for other planets, those parameters that can be usefully measured from the ground by radio techniques, or measurements from spacecraft near the earth. To date there has been no capability to monitor, continuously, many parameters of that part of the solar wind which intercepts the earth, far enough upwind to be free of the earth's perturbations. This capability now exists.

On November 20, 1978, the heliocentric International Sun-Earth Explorer-3 (ISEE-3) spacecraft was injected into a halo orbit about the libration point $\sim 240 R_E$ sunward of the earth. The instrument complement is summarized in Table 1 and is described by Ogilvie, et al (1978). Note that many parameters germane to solar-terrestrial

TABLE 1
ISEE-C INSTRUMENTS

<u>TITLE/PARAMETERS</u>	<u>PRINCIPAL INVESTIGATOR</u> <u>AFFILIATION</u>
<u>X-rays and Electrons</u> X-rays 8-72 keV Electrons 2 - 1000 keV	K. A. Anderson <u>U./Cal., Berkeley</u>
<u>Solar Wind Plasma</u> Ions 150 eV - 7 keV Electrons 5 eV - 2.5 keV	S. J. Bame <u>LASL</u>
<u>High Energy Cosmic Rays</u> Nuclei 20-500 MeV/nucleon (H-Ni)	H.H. Heckman <u>U./Cal., Berkeley</u>
<u>Low Energy Cosmic Rays</u> Nuclei \leq 20 MeV/nucleon	D. Hovestadt <u>Max Planck Inst., Garching</u>
<u>Energetic Protons</u> Protons 30 keV to 1.4 MeV Alphas 1.4 MeV to 6 MeV	R. J. Hynds <u>Imperial Col., London</u>
<u>Cosmic Ray Electrons & Nuclei</u> Electrons 5 - 400 MeV Protons 36 - 13000 MeV	P. Meyer <u>U./Chicago</u>
Helium-sulfur 60 - 13000 MeV/nuc Iron Group 150 - 13000 MeV/nuc	
<u>Plasma Composition</u> Ions 470 eV/Z to 10.5 keV/Z (M/Z 1-5.6)	K.W. Ogilvie <u>GSFC</u>
<u>Plasma Waves</u> Magnetic fields 20 Hz - 1 kHz Electric fields 20 Hz - 100 kHz	F. L. Scarf <u>TRW</u>
<u>Radio Mapping</u> 3-D tracing of Type III burst paths in 20 kHz to 3MHz band	J. L. Steinberg <u>Paris Obs.</u>
<u>Helium Vector Magnetometer</u> 3 components 0-3 Hz	E. J. Smith <u>JPL</u>
<u>High Energy Cosmic Rays</u> Nuclei 2-200 MeV/nucleon (Li-Ni)	E. C. Stone <u>CIT</u>
<u>Medium Energy Cosmic Rays</u> Nuclei 1 - 500 MeV/nucleon (Z 1 - 26) Electrons 2 - 12 MeV	T. T. von Rosenvinge <u>GSFC</u>
<u>Ground Based Solar Studies</u> Solar spectral observations	J. M. Wilcox <u>Stanford U.</u>

predictions are measured, including solar wind magnetic field magnitude and direction, bulk velocity, and composition. ISEE-3 is currently planned to be operated through 1981; its propulsion capability will allow continuation if the spacecraft and instruments are healthy.

A spacecraft to continue observations in halo orbit about the sunward libration point after the projected lifetime of ISEE-3 is currently in the planning stage as an element of the Origins of Plasma in the Earth's Neighborhood (OPEN) program, described in the Appendix. Planned for a 1985 launch, the OPEN-A spacecraft will have improved instrumentation and is expected to operate through the late 1980's. Together, ISEE-3 and OPEN-A are intended to provide almost continuous in-situ solar wind data upwind from the Earth during nearly a full 11-year sunspot cycle.

2. AURORAL MONITORING

Auroral images from the Defense Meteorological Satellite Program (DMSP) satellites have recently demonstrated the usefulness of such data for monitoring the state of the magnetosphere and studying magnetosphere-ionosphere coupling (Pike, 1975; Mizera, et al, 1978). These images, acquired in low Earth orbit, scan the same local time and longitude only on successive orbits, an interval of about two hours. To exploit fully the possibility of using auroral images as monitors (a) they should cover the whole polar cap, since different latitudes and longitudes map to very different parts of the magnetosphere; (b) they should repeat on the time scales that significant changes occur in the magnetosphere (e.g. minutes, in the case of substorm phenomena); (c) they must be continuously available for periods as long as major magnetospheric cycles (e.g. many hours in the case of substorms); and (d) they should be acquired simultaneously at several selected wavelengths in order to deduce the incident particle fluxes from the auroral spectra (Luhman and Blake, 1977). To date it is not possible to survey emissions from the entire polar cap with repetition intervals of minutes for periods of hours.

In early 1981 a multi-spectral auroral imaging instrument built by L. A. Frank of the University of Iowa will be launched on the Dynamics Explorer-A (DE-A) satellite into a 90° inclination, 4.75 R_E apogee, 600 km perigee orbit. This orbit has a period of 420 minutes, allowing a continuous viewing time nearly as long, although the drift of the latitude of apogee (0.36 degrees/day, or 16.5 months pole-to-pole) will prevent imaging of either entire polar cap during some intermediate periods. The DE-A imaging

instrument employs a stepping mirror and satellite spin for aiming, and imaging photometers for photon collection. Each image is built up from signals in 144 look directions, called "pixels", in each of 144 scan lines. Table 2 lists the detailed instrument characteristics. Careful tradeoffs in sensitivity, aperture, and temporal resolution result in limited temporal resolution in the multi-spectral mode (14.4 minutes for a full picture from each of three photometers). However, this can be cut to 7.2 minutes by combining signals from the two visible wavelength photometers for a single wavelength, and further improved to 2.4 minutes by, in addition, scanning only one-third of the pixels constituting a full frame. The planned operational lifetime of DE-A is 13 months, but it can be operated longer if it remains healthy.

OPEN-C, another of the four spacecraft planned for the OPEN program (see Appendix), will follow DE-A into orbit four years later and will carry improved auroral zone and polar cap multispectral imaging instruments. OPEN-C will initially be injected into a 15 R_E apogee polar orbit, and later, using on-board propulsion, be dropped back into a 4 R_E apogee orbit. Details about the OPEN program will be contained in a Science Definition Working Group report available in June 1979. This Working Group will be disbanded and an Announcement of Opportunity (AO) for scientific participation in the OPEN program released in summer, 1979. Proposals will be considered for imaging or scanning at X-ray wavelengths as well as at visible and ultraviolet wavelengths.

3. DATA AVAILABILITY

It is NASA's policy to make data from these missions available to members of the scientific community for use that complements the primary mission objectives for which the Principal Investigators were selected.

ISEE-3 solar wind summary data are obtainable through the National Space Science Data Center (NSSDC) at Goddard Space Flight Center. A description of the data available in this form will be available soon (von Rosenvinge, 1979). Plans are under consideration by NASA and NOAA to make some ISEE-3 data available in real-time through the NOAA Space Environment Laboratory Data Acquisition and Display System (SELDADS), described by Williams (1976). Additional data may, of course, be obtained through direct contact with the Principal Investigators. The NASA Headquarters Space Plasma Physics Program Office periodically funds small unsolicited proposals for "guest investigations" on ISEE (Hinnners, 1978).

TABLE 2

DYNAMICS EXPLORER MULTISPECTRAL
IMAGING INSTRUMENT CHARACTERISTICS*

Frame Size	360 x 360
Pixels Per Frame	20,736 (1442)
Pixel Angular Resolution	0.250 (4.4 Milliradians)
Spatial Resolution	28 km at 1 RE altitude 84 km at 3 RE altitude
Dynamic Range	2,000
Number of Photometers	3 (two visible wave- length and one vacuum ultraviolet wavelength)
Temporal Resolution Per Frame for Each Photometer (Up to Three Wavelengths)	864 sec. (14.4 min.)
Maximum Temporal Resolution (one wavelength, one-third- frame picture size)	144 sec. (2.4 min.)

Wavelengths and Sensitivities:

<u>Photometer No.</u>	<u>Wavelength</u>	<u>Sensitivity</u>
1 or 2	391.4 nm	370 Rayleighs per count per pixel
1 or 2	557.7	390
1 or 2	630.0	530
3	140.0-170.0	240
3	128.0-140.0	400
3	117.0-127.0	650

*Data provided courtesy of L. A. Frank, University
of Iowa, Principal Investigator

DE-A images and OPEN data will be widely distributed to scientists outside the Investigator Working Groups. How these will be handled is currently being worked out. Presently there are no plans for these data to be available in real-time. Persons or institutions with needs for real-time data should make these needs known to NASA Headquarters.

4. CONCLUSION

This report has described sources of two new kinds of data for solar-terrestrial research. These capabilities will be available for the greater part of the next decade and will provide quantitative measures of solar wind characteristics and of energy deposition from the magnetosphere into the polar cap. This information will be necessary to test the predictive power of hypotheses suggesting how solar wind variations induce fluctuations in the terrestrial space environment.

5. APPENDIX

ORIGINS OF PLASMA IN THE EARTH'S NEIGHBORHOOD (OPEN) PROGRAM

Exploration of the Earth's nearby space environment has revealed an elaborate and dynamic system of interacting plasmas, magnetic fields, and electrical currents surrounding the planet. Energy from matter expelled by the Sun flows through this system into the Earth's environment, constituting a small but highly variable part of the planet's total solar sustenance.

The purpose of the OPEN program is to understand how the parts of this closely coupled, highly time-dependent system work together; to trace the flow of matter and energy through the system from input by the solar wind to ultimate deposition into the atmosphere; to understand the physical processes controlling the origins, entry, transport, storage, acceleration and loss of plasma in the Earth's neighborhood; and to determine the role of these processes in the delicately balanced terrestrial environment. The OPEN program includes:

(1) observing laboratory spacecraft shuttle-launched into each of the two principal plasma source and two principal energy storage regions of the magnetosphere (Table 3 lists these spacecraft);

TABLE 3
ORIGINS OF PLASMA IN THE EARTH'S NEIGHBORHOOD (OPEN)
SPACECRAFT

<u>NAME</u>	<u>PHYSICAL LOCATION</u>	<u>ORBIT</u>
A. Interplanetary Physics Laboratory (IPL)	Solar Wind	Halo Orbit (radius ≥ 15 R_E) About Libration Point 240 R_E Sunward
B. Geomagnetic Tail Laboratory (GTL)	Magnetotail Distant Plasma Sheet	Lunar-Cranked With 240 R_E Anti-Sunward Apogee
C. Polar Plasma Laboratory (PPL)	Polar Cusp Plasma Mantle Polar Cap	Polar Orbit with 15 R_E Apogee, Later Dropped to 4 R_E Apogee
D. Equatorial Magnet- osphere Laboratory (EML)	Near-Earth Plasma Sheet Ring Current	2 x 12 R_E Equa- torial Orbit

(2) complementary ground-based radar and magnetometer observations;

(3) a fully integrated program of theoretical studies and modelling; and

(4) a modern network of computers and terminals in order to accomplish the required data intercomparison and analysis.

Approval is being sought for a FY 1981 or FY 1982 start with launches planned to occur in 1985. The spacecraft will be designed to operate reliably through 1988. A brief description of the OPEN program has been prepared by Goddard Space Flight Center (Alexander, 1979).

6. ACKNOWLEDGMENTS

The author is grateful to L. A. Frank for providing details of his instrument on DE-A. He and T. von Rosenvinge made helpful comments on the manuscript, but the responsibility for errors is the author's.

This work was prepared as part of the author's official duties as an employee of the U.S. Government and, in accordance with 17 USC 105, is not available for copyright protection in the United States.

7. REFERENCES

- Alexander, J. (1979): Origins of Plasma in the Earth's Neighborhood, A Mission Synopsis. NASA/Goddard Space Flight Center, Greenbelt, MD 20771.
- Hinners, N. W. (1978): Space Science Notice, November 6. NASA Headquarters, Washington, DC 20546.
- Luhmann, J. G. and J. B. Blake (1977): Calculations of soft auroral bremsstrahlung and K α line emission at satellite altitude. J. Atmos. and Terrestrial Phys., Vol. 39: 913-919.
- Mizera, P. G., J. G. Luhmann, W. A. Kolasinski, and J.B. Blake (1978): Correlated observations of auroral arcs, electrons, and X-rays from a DMSP satellite, J. Geophys. Res., accepted for publication.
- Ogilvie, K. W., A. Durney, and T. von Rosenvinge, Eds. (1978): Special issue on instrumentation for the International Sun-Earth Explorer Spacecraft. IEEE Trans. Geoscience Electronics, Vol. GE-16.3: 151-280.
- Pike, C. P., Ed. (1975): Defense Meteorological Satellite Program Auroral-Ionospheric Interpretation Guide. AFCRL-TR-75-0191, Hanscom AFB, MA 01731.
- von Rosenvinge, T. (1979): Notes on the ISEE-3 data pool tape. Code 661, Goddard Space Flight Center, Greenbelt, MD 20771, in preparation.
- Williams, D. J. (1976): SELDADS; An operational real-time solar-terrestrial monitoring system. NOAA Technical Report, ERL-357-SEL-37, Environmental Research Laboratories, Boulder, CO 80302.

THE STRUCTURE AND GEOEFFICIENCY OF HIGH VELOCITY SOLAR WIND STREAMS

M. I. Pudovkin; S. A. Zaitzeva; A. D. Chertkov; E. M. Fomina
Institute of Physics, State University
Leningrad, 199164, USSR

The structure of high velocity streams in the solar wind is considered and their geoefficiency is shown to be determined by the vertical component of the interplanetary magnetic field, by the variability of it and by the wind velocity.

The vertical component of the interplanetary magnetic field within the main body of the flare stream is shown to be determined by the meridional component of the large scale solar magnetic field at the flare region. This fact being taken into account, an index of the geoefficiency of solar flares has been proposed.

Some examples are presented to show the vertical component of the IMF within the recurrent streams to be also determined by configuration of super large scale solar magnetic field at the region of the origin of the streams.

Carrington (1859) was the first who had noticed that some intensive solar flares could produce magnetic disturbances on the Earth. By now the interrelation between those two phenomena has been investigated in detail and at present there is no doubt that the geomagnetic disturbances are most often associated with high velocity streams of the magnetized solar plasma ejected by solar flares or by quasi-stationary M-regions, although the nature of the latter is not clear as yet.

So the problem of the prediction of the geomagnetic disturbances seems to be reduced to the problem of the prediction of the high velocity streams in the solar wind, which is not difficult, for example, in case of the flare streams.

However, the real problem proved to be much more complicated. The fact is that, as the direct observations show, not every high velocity stream produces a magnetic storm on the Earth; in particular, only 50 percent of all the flares of the importance 2 are followed by intense geomagnetic disturbances.

What may be the cause of such a complicated behavior of the flare streams? To make this question clear, let us look at Figure 1, where the

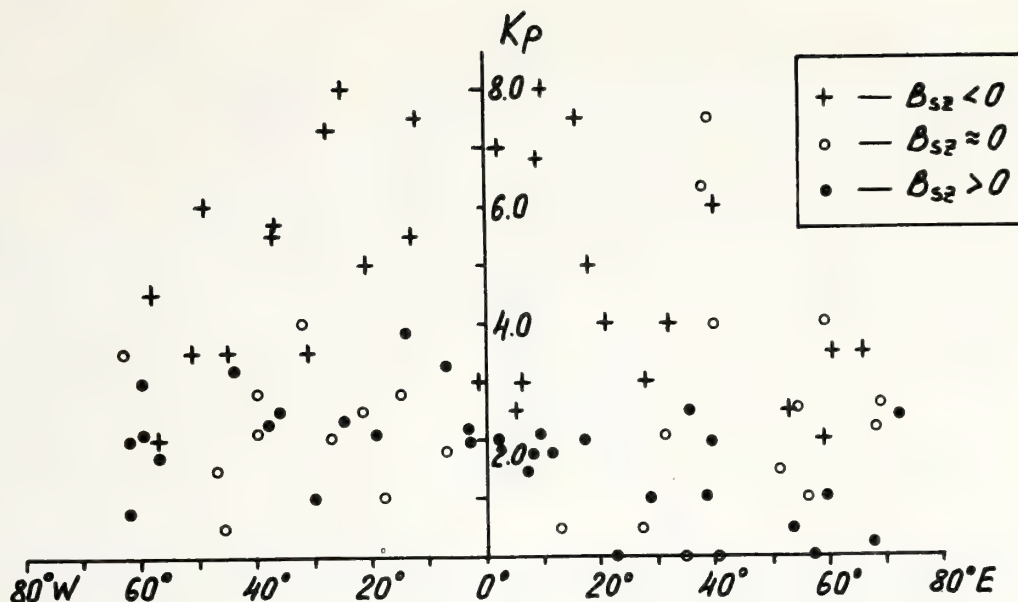


Figure 1: The daily mean value of the K_p-index of the days when flare streams are passing by the Earth as a function of the longitude of the flares.

geomagnetic effect is shown (the daily mean value of the K_p-index on the day when the flare stream is passing the Earth) of 84 flares of the importance 2 for the period May, 1967 - August, 1972; along the X-axis of the figure the heliocentric longitude of the flares is plotted.

Having neglected the difference of the symbols which mark various flares (the sense of those symbols will be discussed some later), one can see in the figure that:

1. Approximately equivalent flares can produce significantly various effects on the Earth (the daily mean values of the K_p indices vary from 0 to 8).

2. The effect of a flare distinctly depends on the heliocentric longitude of the flare, the most intensive geomagnetic storms being associated with the central flares.

This experimental fact makes those who want to predict the effect of a certain flare take into account the location of the flare on the solar disc. However, even with that location being taken into account, the problem is still far from being solved. Indeed, one can see in the figure that even the central flares ($20^\circ > \lambda > -20^\circ$) produce intensive geomagnetic storms in less than 50 percent of all the cases.

In this connection it is worth remembering that geoefficiency of the solar wind is determined by the intensity and orientation of the interplanetary magnetic field (Fairfield and Cahill, 1966; Pudovkin et al., 1970;

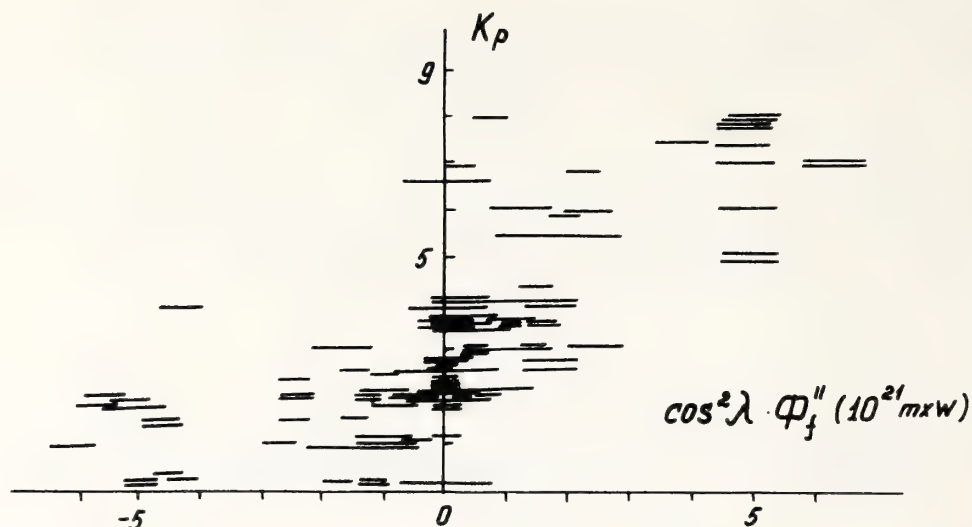


Figure 2: Geoefficiency of the flares in dependence of the value of the magnetic flux at the flare region.

Arnoldy, 1971). Accordingly, Pudovkin and Chertkov (1971, 1976) have suggested that the geoefficiency of the flare streams may be determined by the orientation of the large-scale magnetic field at the Sun. So, all the flares shown in Figure 1 were separated into three groups:

1. The flares which took place in the regions where the large-scale solar magnetic field B_s was directed southwards (are marked by the crosses).
2. The flare which took place in the regions where B_s was northward (are marked by solid circles).
3. The flares which took place in the regions where the B_s -field was directed along the heliographic parallel (open circles).

Results of such a separation are obvious: almost all the intensive geomagnetic disturbances proved to be associated with the flares of the first group, while the flares of two other groups produce only weak or moderate disturbances.

This result allowed Pudovkin and Chertkov (1976) to propose an index of the geoefficiency of the flares:

$$G_f = \phi_{||} \cos^2 \lambda,$$

where $\phi_{||}$ is the flux of the solar magnetic field component parallel to the Earth's rotation axis, close above the flare region. The procedure of the calculation of the value of $\phi_{||}$ is described in detail in paper by Pudovkin and Chertkov (1976).

The geomagnetic effect of all the flares given in Figure 1 is shown in dependence of the value of G_f -index in Figure 2 (Pudovkin and Chertkov, 1976); the correlation between the two quantities is obvious (the coefficient of correlation between them equals to 0.6).

Table 1. The probability of the geomagnetic disturbances of various intensities in dependence of the value of G_f .

K_p	$G_f (10^{21} \text{Mxw})$	<-5	<-4	<-2	<-1	-1++!	>1	>1	>2	>3
<2		1.0	0.9	0.9	0.9	0.7	0.3	0	0	0
<3		1.0	0.9	0.9	0.9	0.9	0.6	0.2	0	0
>3			0.1	0.1	0.05	0.05	0.3	0.8	1.0	1.0
>4.5				0	0	0	0.05	0.5	0.9	1.0

In a form more convenient for practice, the data shown in Figure 1 are presented in Table 1 where the probability (more strictly, the normalized frequency of appearance) of a geomagnetic disturbance with a certain intensity is given in dependence of the value of G_f -index.

From the data given in Table 1 one can see that when, for example, $G_f < -2 \times 10^{21} \text{ Mxw}$ at a flare's region, such a flare may be expected to produce a strong geomagnetic disturbance with the probability not more than 0.1; on the other hand, when $G_f > 1 \times 10^{21} \text{ Mxw}$, the probability for a sufficiently strong geomagnetic storm to appear is not less than 0.8. And, at last, when G_f value lies in the range $\pm 1 \times 10^{21} \text{ Mxw}$, the probability for the flare to produce or not to produce a geomagnetic storm is approximately the same, and some other parameters of the flares have to be used to predict their effect.

The correlation between the values of G_f and the intensity of the geomagnetic disturbances suggests that the large scale magnetic field of the Sun extended by the high velocity flare stream does not change the sign of its vertical component on the whole way from the Sun to the Earth. This supposition may be confirmed by the direct measurements of the solar wind magnetic field. In Figure 3 (Pudovkin et al., 1977) there are shown according to the data by King (1975) the average time variations of the scalar intensity of the interplanetary magnetic field and that of the vertical component of the latter for 12 flares of the first group (i.e. B_{sz} is southward) and for 10 flares of the second group (i.e. B_{sz} is northward), the moment of the arrival of the flare stream to the Earth having been chosen as the moment $t = 0$.

One can see in the figure that two characteristic periods may be distinguished in those time variations:

1. $0 \leq t \leq 12$ hours; the IMF intensity is extremely high in this region; the vertical component of IMF is very changeable there and does not correlate with the value of the B_{sz} in the flare region at the Sun. This period seems to correspond to the region of the compressed solar wind in the flare streams model by Hundhausen (1972).

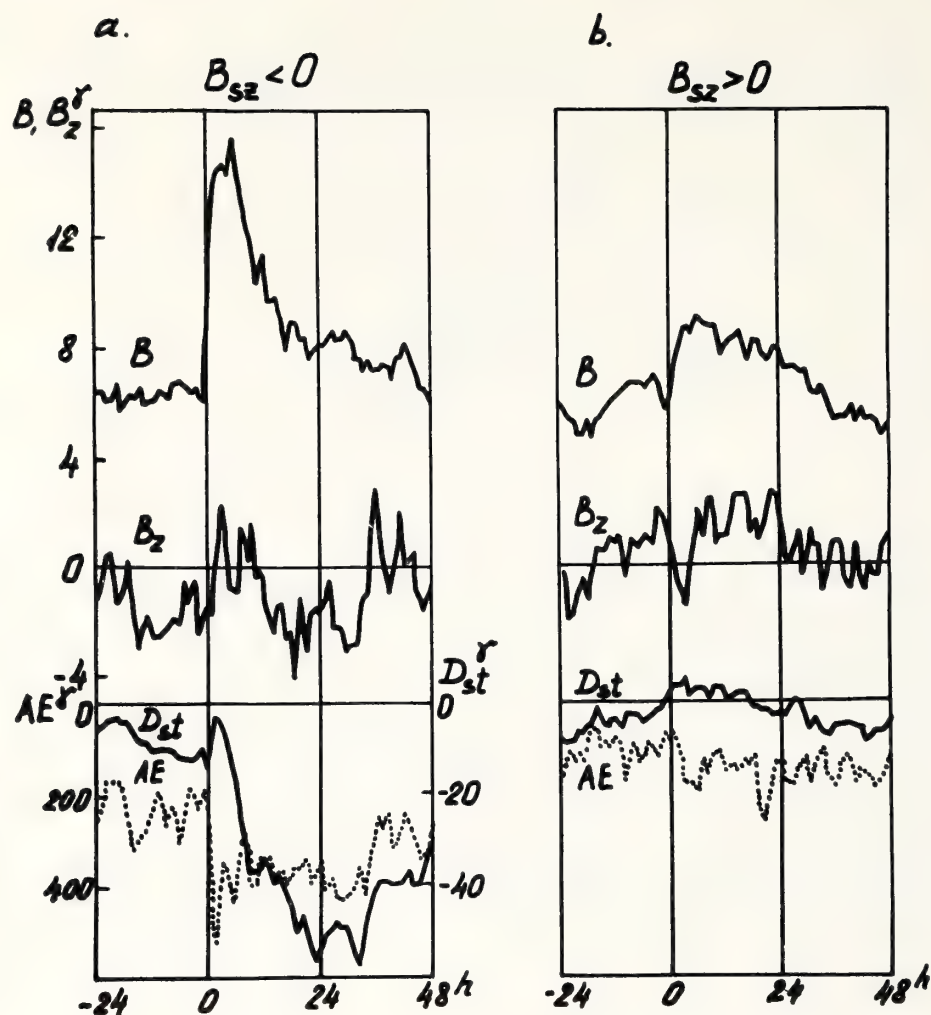


Figure 3: The variation of the mean parameters of the flare streams and of the geomagnetic activity indices. a - the flares with the B_{sz} -field directed southwards ($B_{sz} < 0$). b - the flares with the B_{sz} -field directed northwards ($B_{sz} > 0$).

2. $12 < t < 36$ hours; in this region the sign of the vertical component of the IMF corresponds to the sign of the meridional component of the large scale solar magnetic field at the flare region, and the coefficient of correlation between them equals to 0.55.

Thus, the above relation of the level of the geomagnetic disturbancy to the intensity and orientation of the solar magnetic field at the flare region may be really explained as the result of the extension of the solar magnetic field by the flare stream into the space up to at least the Earth's orbit.

We have considered the structure and geoefficiency of the flare streams responsible for the sporadic geomagnetic storms. On the other hand, it is well known that at the epochs of low solar activity, geomagnetic disturbances are predominantly associated with another type of streams, known as quasi-stationary high velocity streams (Hundhausen, 1972) or with the leading parts

of them (Bobrov, 1975). However, these models do not involve consideration for the interplanetary magnetic field and because of that need some correction.

The necessary analysis of the experimental data has been carried out by Burlaga and Lepping (1977) and by Pudovkin et al. (1978). Figure 4 shows the variations of the intensity of the geomagnetic disturbance (AE and D_{st} -indices) as well as those of the intensity of the interplanetary magnetic field (B) and of the vertical component of the latter (B_z), of the variability of B (or the standard deviation of IMF (σ), of the solar wind velocity (V), of the number density of the solar wind plasma (n) and of the product ($V \times B_z$), obtained by averaging the data for 6 recurrent storms; the moment $t = 0$ corresponds to the moment of rapid intensification of the AE-indices.

The data shown in the figure confirm the supposition that the recurrent storms are usually caused by the recurrent high velocity streams of the solar wind. Besides, one can see in the figure that geoeffective recurrent streams are also characterized by a sufficiently distinct variation of the B-field, and rapid intensification of the geomagnetic activity is associated with the appearance of the southward (negative) component of the IMF, and the southward component of the IMF goes on existing for the whole period of the recurrent magnetic storm.

Besides the recurrent periods of the enhanced geomagnetic activity there also exist the periods of geomagnetic calmness. Analysis of the available data has shown that such periods may be related to two quite different situations within the solar wind. The first of them is peculiar to the quiet solar wind

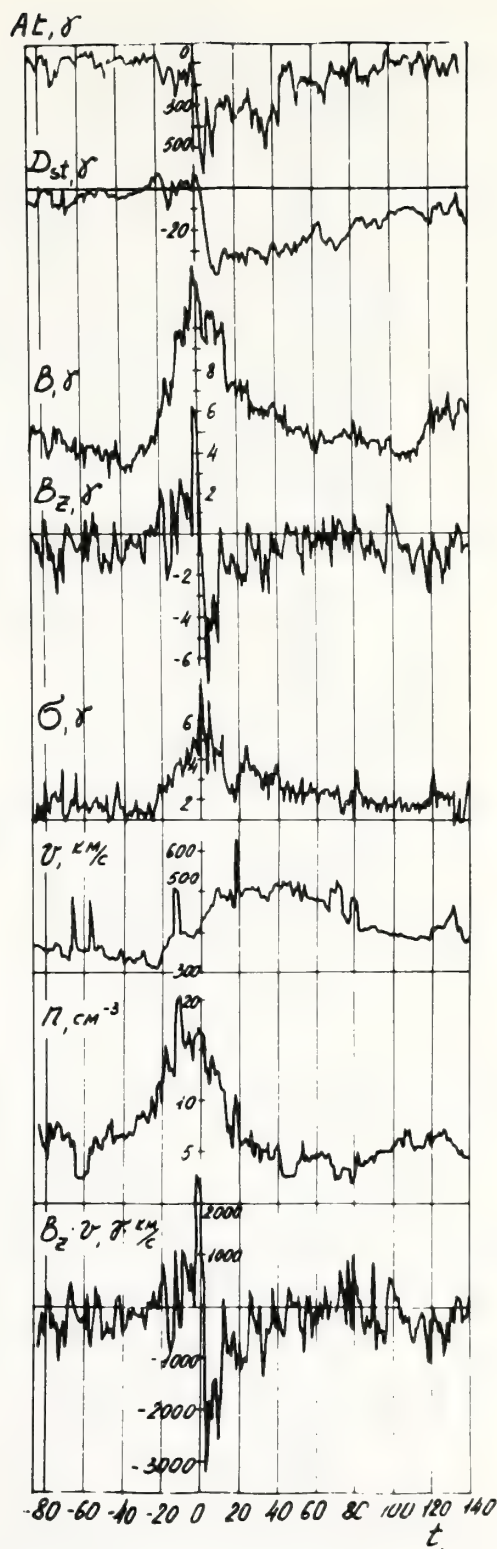


Figure 4: The mean variation of the solar wind parameters and geomagnetic activity within the geoeffective recurrent streams.

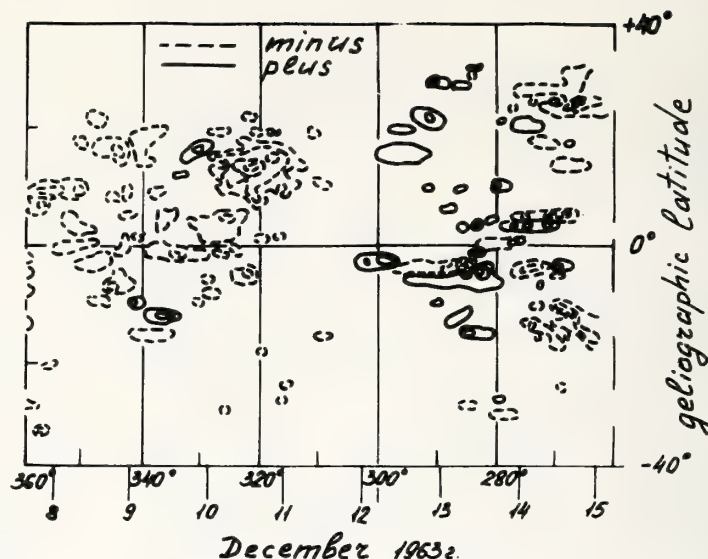
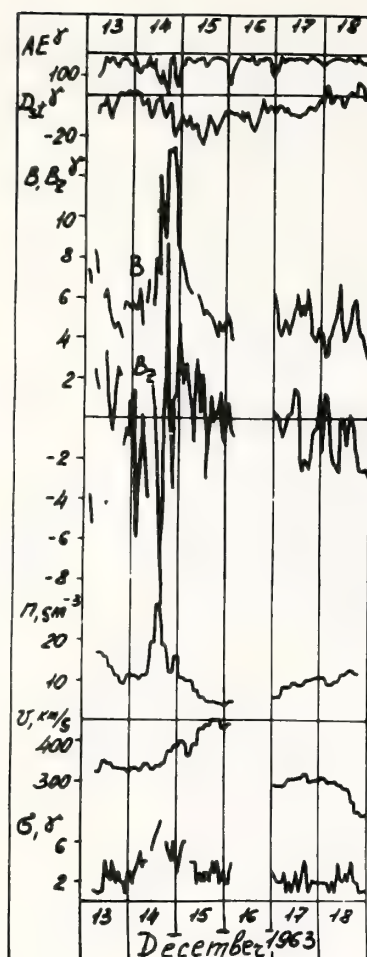


Figure 5: The variation of the solar wind parameters and of the geomagnetic activity within a ineffective high velocity recurrent stream (a) and the distribution of the large scale solar magnetic field (b).

without any high velocity streams or at the gap between them and is characterized by relatively low velocity ($V \leq 400 \text{ km/sec}$), low intensity of the IMF ($B \leq 5\gamma$) and $B_z \approx 0$.

The second situation corresponds to high velocity streams characterized by the northward component of the IMF ($B_z > 0$). In Figure 5 there is shown an example of such a stream which was observed on December 13-16, 1963. As can be seen in the figure, the variations of the magnetic field intensity, of the solar wind velocity and plasma density are similar to those within the typical high velocity streams, and nevertheless the geomagnetic activity was relatively low at the whole period, which seems to be due to the northward direction of the B_z at that time.

Thus, to predict the Earth's effect of a certain high velocity stream, it is necessary to know how to predict the B_z -field within it (as well as some other parameters such as the wind velocity and variability of the magnetic field). An attempt to do this is presented in Figures 5 and 6, in which the synoptic maps of the solar magnetic field are given for the regions from which the considered high velocity streams might have come.

In Figure 5 one can see a large region of negative (i.e. sunward) magnetic field located at the longitudes 320° - 340° , the center of weight of which

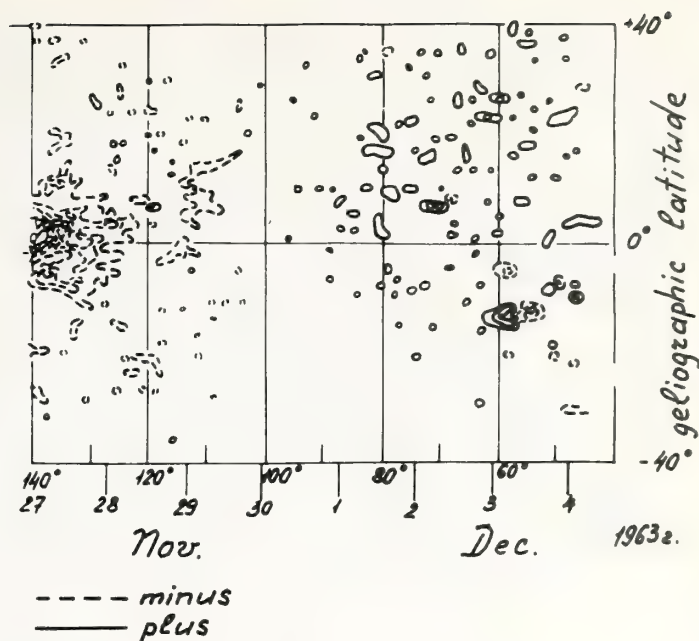
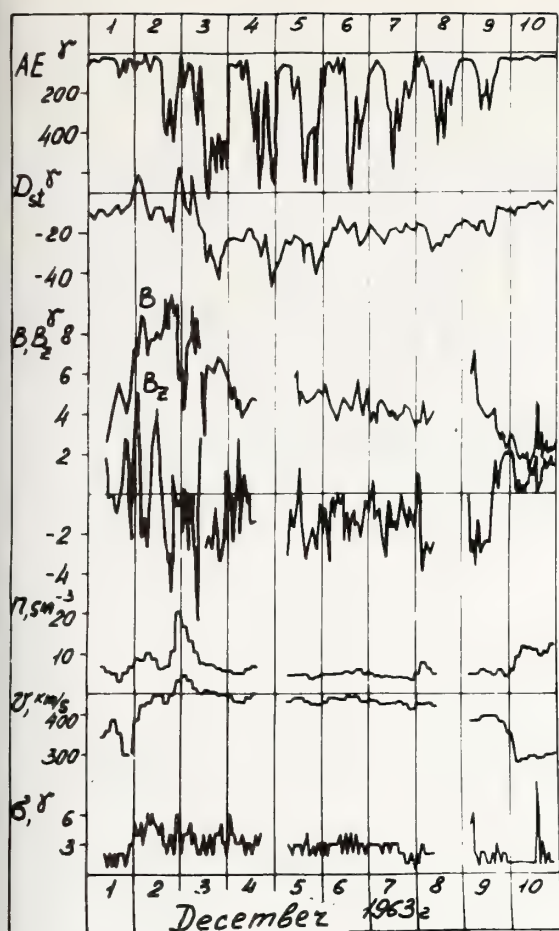


Figure 6: The same as in Figure 5 for a geoeffective stream.

locates in the northern hemisphere, i.e. above the equator; to the west of that region a region exists with positive magnetic field with the center of weight located at the equator or even to the South of it. So one can suppose the meridional component of the solar magnetic field to be directed northwards at the region under consideration. Consequently, the interplanetary magnetic field has to also be northward in 4-5 days after the Central Meridian Passing by this region, that is on the 15-16 of December, which agrees with the experimental data.

Analogous consideration of Figure 6 shows that the meridional component of the large scale solar magnetic field has to be southward at the equator at the longitudes 70° - 130° , and as a consequence, the vertical component of the IMF must be negative on the 3-7 of December, which also agrees with the experimental data.

So one may believe that the vertical component of the IMF within the high velocity streams of the solar wind is determined by the meridional component of the large scale magnetic field of the Sun at the region of origin of those streams. The method of calculation of the magnetic field within the high velocity streams and index of geoefficiency of the latters are discussed in the paper by Pudovkin et al. (1979).

CONCLUSIONS

1. Intensity of the geomagnetic disturbances caused by a flare stream is determined by the location of the flare on the solar disc and by the orientation and the intensity of the large-scale solar magnetic field at the flare region.

2. An index of geoefficiency of the flares is proposed and the coefficient of correlation of that index with the daily mean value of the K_p -index in two days after the flare is equal to 0.6.

3. The geoefficiency of the recurrent high velocity stream is determined by the velocity of the stream and by the intensity of the southward component of the IMF, the latter being associated with the distribution of the large scale magnetic field at the Sun.

REFERENCES

- Arnoldy, R. L. (1971): Signature in the interplanetary medium for substorms. J. Geophys. Res. 76: 5189-5201.
- Bobrov, M. S. (1975): Geoactive zones in the solar wind. Planet. Space Sci., 23: 627-636.
- Burlaga, L. F., R. P. Lepping (1977): The causes of recurrent geomagnetic storms. Planet. Space Sci., 25: 1151-1160.
- Carrington, R. C. (1859): Description of a singular appearance seen in the Sun on September, 1859. Mon. Not. Roy. Astron. Soc. 20: 13.
- Fairfield, D. H. and L. J. Cahill (1966): Transition region magnetic field and polar magnetic disturbance. J. Geophys. Res. 71: 155-169.
- Howard, R., Bumba, V., and S. Smith (1967): Atlas of solar magnetic fields, 1959-1966. Carnegie Inst., Wash., Publ. No. 626.
- Hundhausen, A. J. (1972): Coronal expansion and solar wind. Springer-Verlag, Heidelberg-New York.
- King, J. H. (1975): Interplanetary magnetic field data book. National Space Sci. Data Center.
- Pudovkin, M. I., O. M. Raspopov, L. A. Dmitrieva, V. A. Troitskaya, and R. V. Shepetnov (1970): The interrelation between parameters of the solar wind and the state of the geomagnetic field. Ann. Géophys. 26, N 2, 389-396.

- Pudovkin, M. I., and A. D. Chertkov (1971) (In Russian): Efficiency of solar flares. Doklady of AN SSSR, T.201, No. 1: 75-77.
- Pudovkin, M. I., and A. D. Chertkov (1976): Magnetic field of the solar wind. Solar Phys., 50; 213-229.
- Pudovkin, M. I., S. A. Zaitzeva, I. P. Oleferenko, and A. D. Chertkov (1977): The structure of the solar flare stream magnetic field. Solar Phys., 54: 155-164.
- Pudovkin, M. I., D. I. Ponyavin and A. D. Chertkov (1979): Level of geomagnetic disturbance and distribution of large-scale magnetic field at the Sun Paper submitted to Solar-Terrestrial Prediction Proceedings.

THE POSSIBILITY OF FORECASTING MAGNETIC ACTIVITY
FROM OBSERVATIONS OF INTERPLANETARY SPACE AND SUN

N. I. Dvinskikh
Institute of Automation
Irkutsk, U.S.S.R.

B. G. Dolgoarshinnyh
SibIZMIR. U.S.S.R.

V. V. Mihnevitch, Yu. V. Pisanko
N. M. Rudneva, P. M. Svidsky
Institute of Applied Geophysics, Goscomhydromet
Moscow, U.S.S.R.

Results are given for the comparison of the vertical components of the interplanetary magnetic field in the Earth's orbit with the meridional component of the coronal magnetic field and for investigations of the geoefficiency of large-scale structures of the solar wind. Rules are suggested for identifying space parameters of quiet and disturbed geomagnetic intervals.

The existence of a relationship between solar activity and geomagnetic variations is not in doubt. But the attempts to relate geomagnetic storms to specific phenomena on the Sun are not sufficiently successful to provide highly reliable forecasts of geomagnetic disturbances (Mead, 1972). Satellite measurements in the interplanetary medium have made it possible to detect geoefficient parameters of the solar wind. Simultaneous observations of the solar wind, magnetic field, and coronal solar radiation have shown that the interaction between the plasma and magnetic field in the solar corona plays an important role in the formation of large-scale structure of the solar wind (Hundhausen, 1972).

The following results concern both comparison of the vertical components (B_z) of the interplanetary magnetic field (IMF) in the Earth's orbit with the meridional component (B_θ) of the coronal magnetic field and investigations of the geoefficiency of large-scale structures of the solar wind: quiet and disturbed intervals of the prescribed duration and high-speed streams in the solar wind. Methods of compiling forecasts of magnetic activity on the basis of the satellite interplanetary space observations are suggested.

1. COMPARISON OF THE VERTICAL COMPONENT OF THE INTERPLANETARY MAGNETIC FIELD WITH THE SOLAR MAGNETIC FIELD

The southern component of the interplanetary magnetic field (IMF) is known as the most geoefficient parameter of interplanetary space (Arnoldy, 1971; Foster et al., 1971; Tsurutani and Meng, 1972; Meng et al., 1973, Murayama and Hakamada, 1975). The ability to detect the IMF component in the Earth's orbit from solar observations could significantly improve the forecasting of magnetic activity. Pudovkin and Chertkov (1976) obtained some promising results when they compared geomagnetic activity with a large-scale photosphere field. We analysed the experimental data on solar and interplanetary magnetic fields for the period from July 30 to December 13, 1965 (1497-1501 solar rotations). From the solar photosphere magnetic fields observed by Howard et al., (1967) coronal magnetic fields were calculated using the techniques proposed by Altschuler and Newkirk (1969). The field was made up in 2916 points on the photosphere surface. To accomplish this the synoptic charts were divided into areas of 5° latitude and 7° longitude. The average field of each area referred to its center; the field at latitudes 45° was supposed to equal zero. The field potential is represented by series of six spherical harmonics. The calculated values of B_θ (the component of the coronal magnetic field) and B_z (the IMF component with time) are shown in Figs. 1, 2, and 3. B_z is plotted with a lead of 4.5 days. The B_θ value is plotted using 12-h averages. The solid curves give smoothed pictures of the B_z variation obtained by adding the first six harmonics of Fourier resolution of these data. The mean B_z values were calculated from data of King (1975). The B_θ dependence on time is given for the different latitudes shown on the right side near each curve for the distance of 1.75 solar radii. It is shown in the figures that the coronal magnetic field changes significantly with latitude. At the same longitude with the same latitude difference of several degrees B_θ can have opposite signs. It is also seen that both the coronal and interplanetary magnetic fields have different temporal variations. The large-scale structure, which is characterized by variations with periods of 14 and 27 days, is more distinctly pronounced in the coronal field. In B_z resolution the harmonic wave amplitudes with several-day periods do not exceed 0.5γ , and the sum of the first six harmonic waves gives a value of $B_z \approx 1\gamma$. At the same time, at certain time intervals of several hours, B_z reaches $10-15\gamma$. Only on the 1499th rotation is the smoothed B_z curve similar to the B_θ curve at latitude 12° , but B_z and B_θ change out of phase.

Since large B_z values averaged over 12 h are observed relatively seldom (44 intervals for the period considered), it is of interest to analyze the solar wind conditions similar to cases with $|B_z| > 1.5\gamma$ and $|B_z| < 1.5\gamma$. With this aim we calculated mean values of the solar wind parameters for two groups of intervals. Forty-four intervals with $|B_z| > 1.5\gamma$ were included in the first group. Thirty-two intervals with $|B_z| < 1.5\gamma$ were selected for the second group. The mean values of the following solar wind parameters are given below: B --the IMF module, $|B_x|$, $|B_y|$, $|B_z|$, --modules of the IMF components in the solar-ecliptic system of coordinates; σB_x , σB_y , σB_z --root-mean-square deviations of B_x , B_y , B_z , hour values, V and n --solar wind velocity and density.

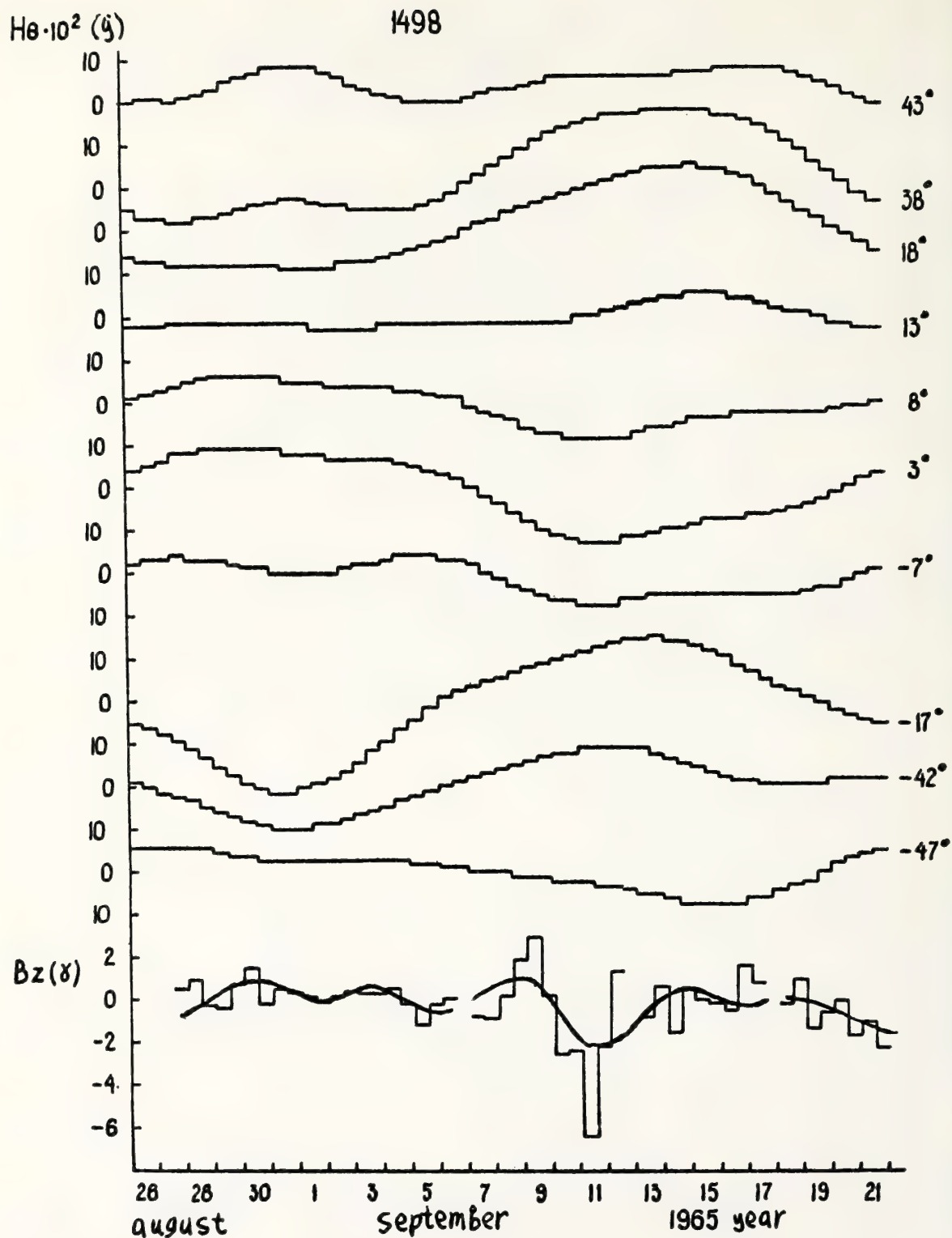


Figure 1. Calculated values of B_θ -component of the coronal magnetic field for different heliolatitudes and B_z -component of the interplanetary magnetic field for the 1498th solar rotation. B_z is 4.5 days ahead.

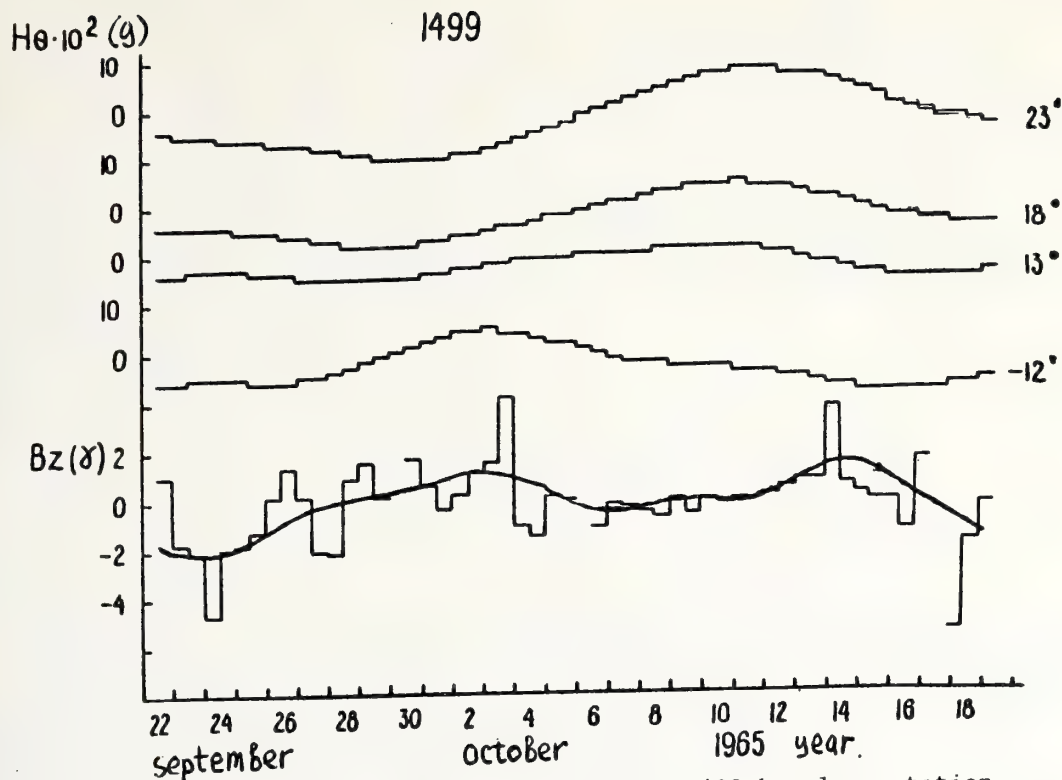


Figure 2. The same as in Fig. 1, but for the 1499th solar rotation.

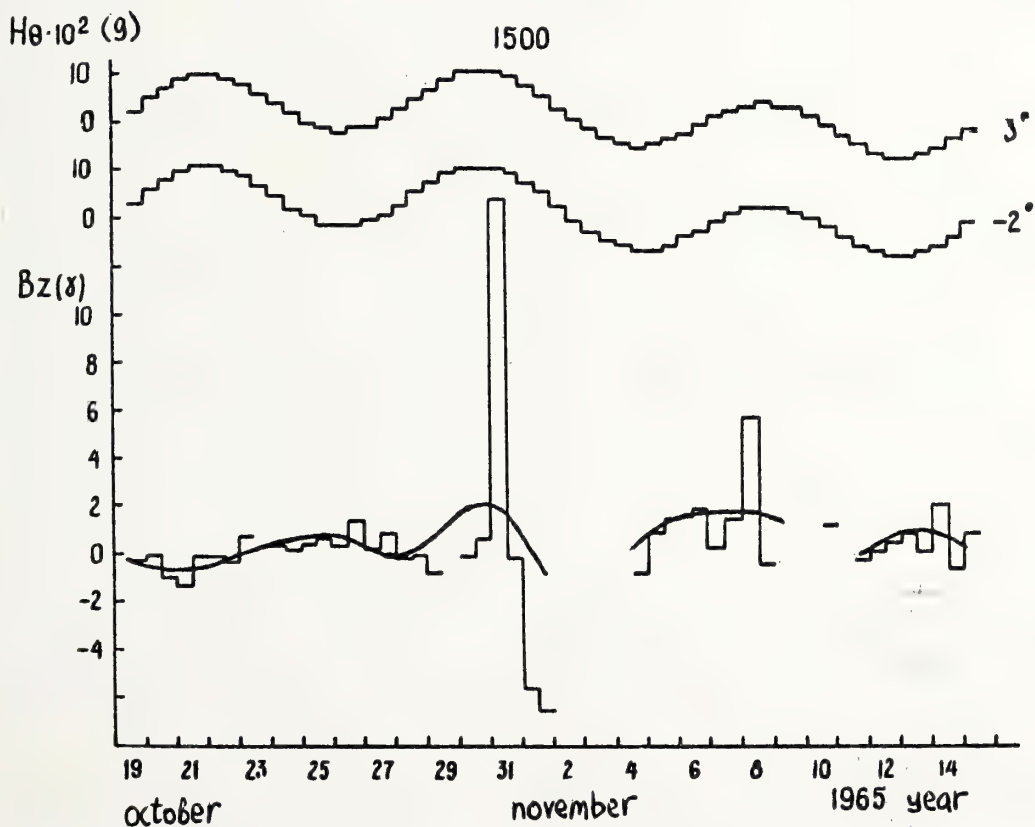


Figure 3. The same as in Fig. 1, but for the 1500th solar rotation.

	B	B _x	B _y	B _z	σB_x	σB_y	σB_z	V	n
1 group	6.6	2.6	2.5	2.8	1.0	1.3	1.4	390	8.6
2 group	3.8	1.8	1.8	0.2	0.9	1.0	1.1	413	6.7

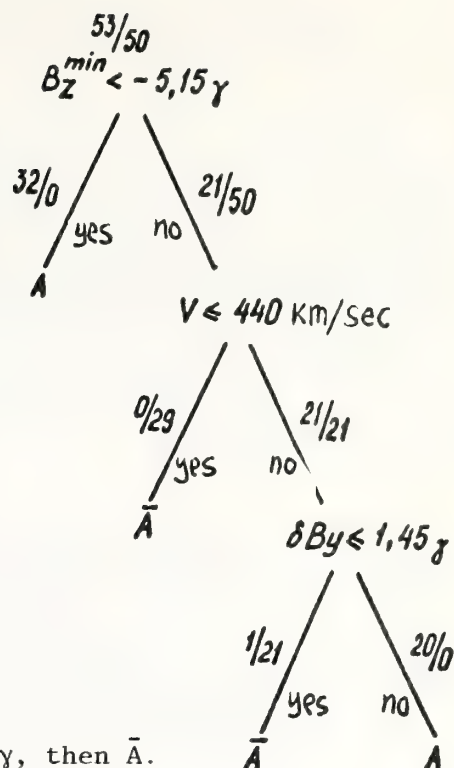
The increased values of the solar wind density and the complete IMF vector are characteristic of the first group intervals ($|B_z| > 1.5\gamma$). This appears to indicate that large $|B_z|$ values are observed under conditions of the compressed solar wind.

2. IDENTIFICATION OF QUIET AND DISTURBED GEOMAGNETIC INTERVALS BY INTERPLANETARY SPACE PARAMETERS

The quiet and disturbed intervals were identified with the following parameters of interplanetary space averaged over the interval: B , B_x , B_y , B_z , σB_x , σB_y , σB_z , V , n . Furthermore for the purpose of the analysis there was used parameter σB_z^- -- a sum of negative values of B_z for an interval B_{\min}^z -- a minimum value of B_z in the interval, and the difference of the maximum and minimum V and n for an interval. The problem of identification was solved by logical resolving functions (Dolgoarshinnyh, 1976) for 12- and 6-hour intervals. The essence of the method is the sequential dissection of the original set of objects into two classes. Each step is characteristic of the best dissection, that is, errors of classification are minimized by scanning various dissections with all prescribed intervals of the input characteristic values. The dissection sequence is shown as a logic tree. The values of the characters that determine the corresponding dissection are written in the knots. The extreme tops of the tree form the class that can be reached with the given branch of the tree. The process of dissection stops when all the objects at the extreme tops belong to the same class or when further dissection does not give significant improvement in the classification accuracy. To solve the problem with 12-h intervals (Dvinskikh et al., 1978) 50 quiet and 53 disturbed intervals were chosen for the training selection and 24 quiet and 24 disturbed intervals for the examination selection. In the task with 6-h intervals the training selection included 110 quiet and 115 disturbed intervals; examination selection contained 45 and 36 intervals. The magnetic activity index inside the quiet intervals (the \bar{A} class objects) $Ap < 15$, and inside the disturbed interval (the A class objects) $Ap \geq 15$.

The information content of each solar wind parameter (characteristic) was studied, i.e., the accuracy of index separation for each individual parameter was determined. The quality criterion of the dissection into two classes was the minimum of the largest of the errors in 1 and 2 classes. When the solving rule was designed on the basis of one characteristic the following parameters appeared to have maximum information content: B , B_{\min}^z , σB_z^- , σB_y , σB_z . The solving rules for separating quiet and disturbed 12-h intervals for each of these parameters are as follows:

Figure 4. Logic tree illustrating the sequential dissection of 12-hour intervals into two classes: the A class objects (intervals $A_p \geq 15$) and the A class objects (intervals with $A_p < 15$).



On the basis of B_z : if $B_z > 6.35\gamma$, then A, if $B_z < 6.35\gamma$, then \bar{A} .

On the basis of B_z^{\min} : if $B_z^{\min} < -3.6\gamma$, then A, if $B_z^{\min} > -3.6\gamma$, then \bar{A} .

On the basis of $\sigma B_z^{(-)}$: if $\sigma B_z^{(-)} < -13\gamma$, then A, if $\sigma B_z^{(-)} > -13\gamma$, then \bar{A} .

On the basis of σB_y : if $\sigma B_y > 1.4\gamma$, then A, if $\sigma B_y < 1.4\gamma$, then \bar{A} .

On the basis of σB_z : if $\sigma B_z > 1.75\gamma$, then A, if $\sigma B_z < 1.75\gamma$, then \bar{A} .

The accuracy of identification by each of the first three parameters calculated from the training selection is 89% for the A class and 88% for \bar{A} . The accuracy of identification by σB_y for A - 81%, for \bar{A} - 98%, by σB_z for A - 77% and for \bar{A} - 94%. In designing the rule by totality of characteristics the group of three characteristics appeared to be the best: B_z^{\min} , V and σB_y . The solving rule designed on their basis is shown as a logic tree in Fig. 4. Figures separated with a line show the number of objects of the A class over the line and the \bar{A} class under the line that are taken into consideration at each step in the process of dissection. The rule can be formulated as follows: if $B_z^{\min} < -5.15\gamma$ or $V > 440$ km/s and $\sigma B_y > 1.45\gamma$, then A; otherwise \bar{A} . The accuracy of identification on the basis of the three above parameters with the training selection was 98% for the A class and 100% for the \bar{A} class. The check of the solving rule with the examination selection gave 87.5% and 96% correspondingly. It is worth noting that if to exclude the B_z^{\min} parameter its place is occupied by the $\sigma B_z^{(-)}$ parameter, the accuracy of identification will not change; i.e., these two parameters carry the same information.

The solving rules obtained for the task with 6-h intervals use the same totality of characteristics and differ only in threshold values of the solar wind parameters. The accuracy of separation of 6-h intervals is somewhat lower than that for 12-h intervals and is $\approx 90\%$ for both classes.

3. GEOEFFICIENCY OF HIGH-SPEED STREAMS IN THE SOLAR WIND

At present, there are several ideas on geoefficient parameters of high-speed streams. Burgala and Lepping (1977) believe that geomagnetic activity is caused by the increase of the interplanetary electric field $\vec{E} = \vec{V} \times \vec{B}$ during high-speed streams. In the first phase of the stream E increases (the region of the solar wind compression) because of increased B_z fluctuations and increases in the tail part of the stream because of increased velocity. Bobrov (1973 and 1975) pointed to the role played by IMF variability in the maintenance of the magnetic disturbance in the tail part of the stream. According to Pudovkin and Chertkov (1976) the geoefficiency of the high-speed streams depends on the value and direction of B_z -- the IMF component in the second phase of the stream.

Data for 26 high-speed streams (not connected with the solar flares) from July 1965 to December 1968 are analyzed below using the solar wind parameters and magnetic activity indices. All of the examined streams caused geomagnetic variations, but their intensity was variable: the least geoefficient stream caused the maximum values $A \approx 8-10$, maximum AE, 500-600 γ , while the maximum geoefficient stream led to the A increase up to 30-50, AE more than 1000 γ . In some streams the Dst variation reaches -100 γ ; in others it is practically absent. It is noteworthy that geoefficiency of the streams is practically determined by the first phase of the stream: in 22 streams the compression region caused more intensive geomagnetic variations than are characterized by three indices of the magnetic activity.

The mean values of the solar wind parameters are calculated for each phase of the stream: B , B_z , σB_x , σB_y , σB_z . The maximum values of V and n , the maximum values of B_z , and σB_z are determined. The maximum given phase values of A depending on the value of the B_z , σB_y , V parameters are given in the circles in Figs. 5, 6, 7. The same diagrams of the distribution of the A , AE magnetic activity indices were built in relation to mean values of each of the solar wind parameters. They illustrate that it is impossible to divide the stream into geoefficient and nongeoefficient using only one solar wind parameter. For dividing the phases of the given high-speed streams into two classes by their maximum value A_p , the following rule based on the totality of three characteristics can be suggested: if $B_z^{\min} < -6.6$ or $V > 400$ km/sec and $\sigma B_y > 1.3\gamma$, then $A_p \geq 15$; otherwise $A_p < 15$. The accuracy of dissection when this rule is used is 89%. The threshold values in the rule for dividing high-speed streams into two classes differ from the threshold values in rules obtained for the intervals of the fixed duration, and that may be attributed to different durations of high-speed streams. It is worth noting that the rule to identify streams by the extent of geoefficiency was formulated on the basis of limited data and should be further verified. However our analysis showed that the totality of the solar wind parameters is responsible for the geoefficiency of both phases of the streams: the southern IMF component, variability of the IMF components perpendicular to the solar wind velocity, and the solar wind velocity.

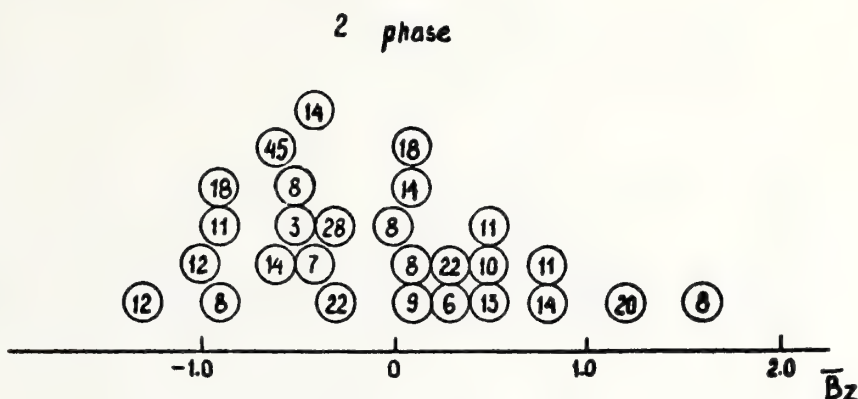
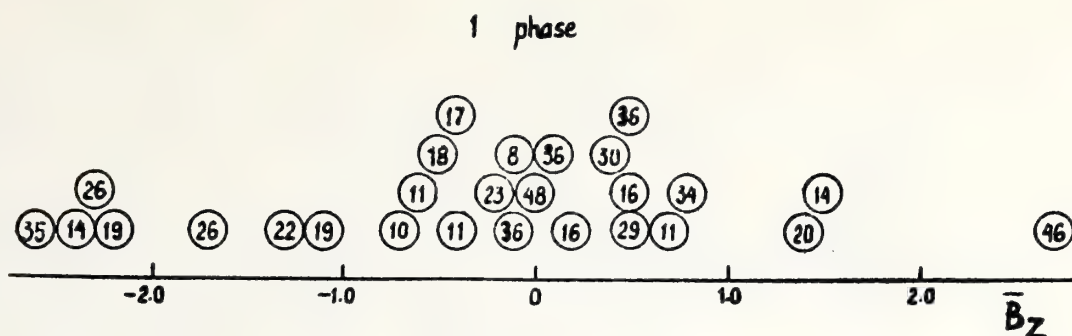


Figure 5. The diagrams of the Ap distribution in dependence on the average over a phase \bar{B}_Z value. The maximum for the given phase value of Ap is shown in circles.

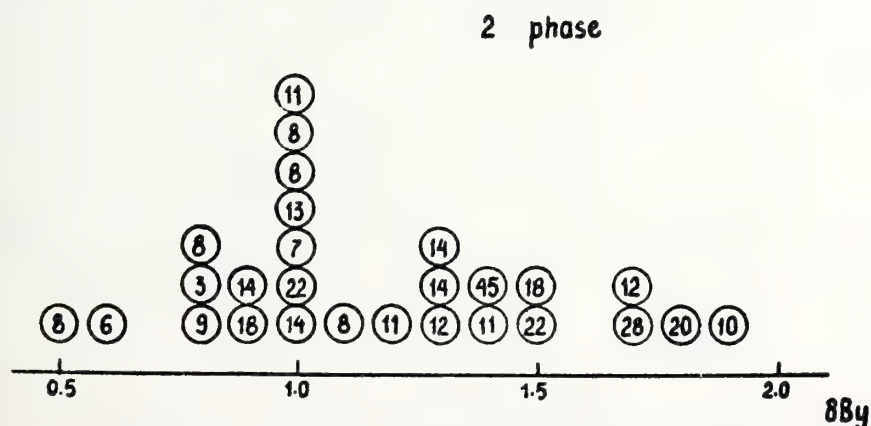
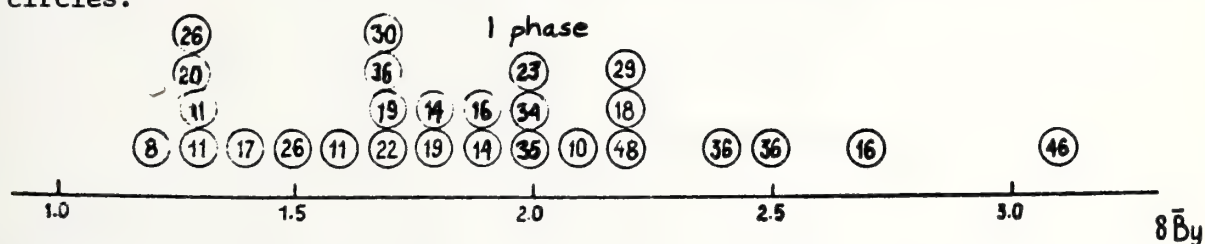


Figure 6. The same as in Fig. 5 depending on the average $\sigma \bar{B}_y$.

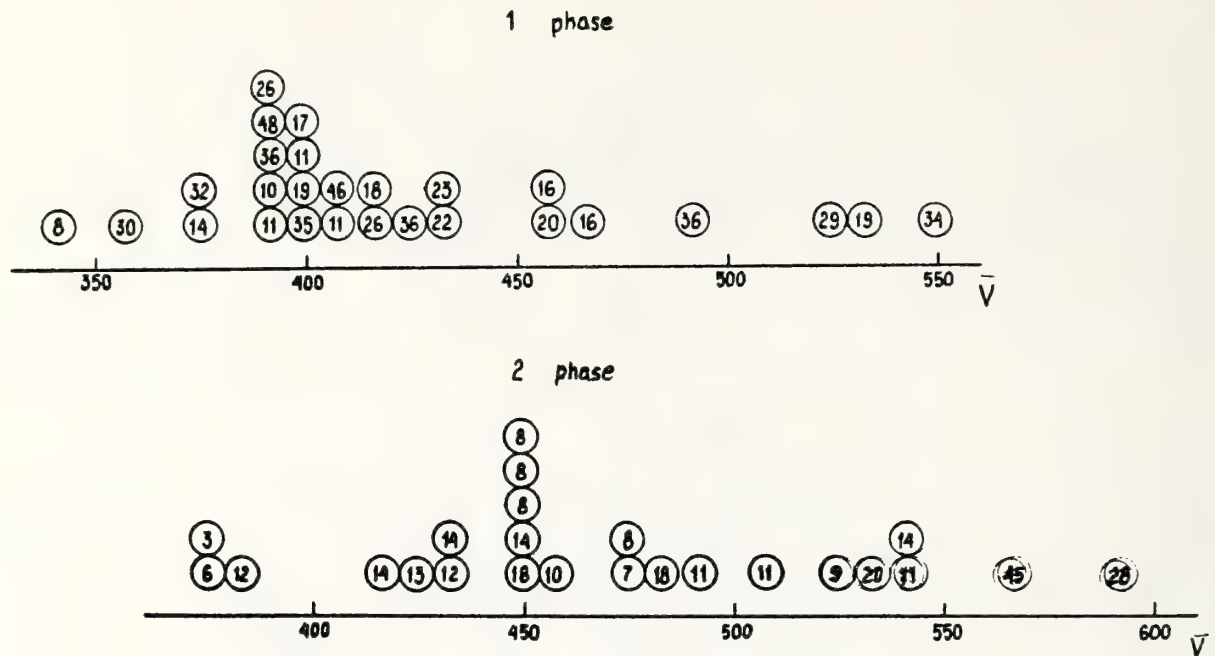


Figure 7. The same as in Figure 5 depending on the average \bar{V} .

4. PRINCIPAL CONCLUSIONS

(1) The major part of geomagnetic disturbances is related to the disturbed region of the solar wind impacting on the Earth's magnetosphere. These regions of high fields are characterized with high values of modules and with the IMF fluctuations that occur as a result of interaction between streams with different velocities.

(2) Forecasting of magnetic activity with sufficient reliability seems to be possible using interplanetary observations in the Sun-Earth line or east from the Earth. It is necessary to provide observations of B_z and B_y , the IMF components with high discrepancy in time and velocity of solar wind. One may hope that rules established to identify quiet and disturbed geomagnetic intervals by the parameters described above will be used in forecasting without significant changes after they are tested against solar wind parameters at a sufficient distance from the Earth.

(3) To forecast magnetic disturbances on the basis of the solar observational data one should be able to get from these data the information both on magnetic fields and on the solar wind streaming velocity. One should also be able to detect the magnetic field and the solar wind velocity in the interplanetary space on the basis of the magnetic field and the solar wind velocity on the corona.

REFERENCES

- Altschuler, M. D. and G. Newkirk (1969): Sol. Phys., 9:131.
- Arnoldy, R. L. (1971): J. Geophys. Res., 76:5189.
- Bobrov, M. S. (1973): Planet. Space Sci., 21:2139.
- Bobrov, M. S. (1975): Planet. Space Sci., 23:619.
- Burlaga, L. F., and R. P. Lepping (1977): Planet. Space Sci., 25:1151.
- Dolgoarshinnyh, B. C. (1976): Issledovania po geometnetizmu, Sb. Nauka, 39:198.
- Dvinskikh, N. I., B. G. Dolgoarshinnyh, and N. M. Rudneva (1978): Geom. i Aer., 4:680.
- Foster, J. G., D. H. Fairfield, K. W. Ogilvie, and T. J. Rosenberg (1971): J. Geophys. Res., 6971.
- Howard, R., V. Bumba, and S. F. Smith (1967): Atlas of Solar Magnetic Fields. Washington, D.C. 20005.
- Hundhausen, A. J. (1972): Coronal Expansion and Solar Wind. N. York.
- Mead, G. D. (1972): Solar Activity Observations and Predictions. Massachusetts Institute of Technology, 242 pp.
- Meng, C.-I., B. Tsurutani, K. Kawasaki, and S.-I. Akasofu (1973): J. Geophys. Res., 73(4):617.
- Murayma, T., and Hakamada (1975): Planet. Space Sci., 23:75.
- Pudovkin, M. I., and A. D. Chertkov (1976): Sol. Phys. 50:213.
- Tsurutani, B. T. and C.-J. Meng (1972): J. Geophys. Res., 77:2964.

C. ACTIVE REGION AND FLARE PREDICTIONS

PREDICTION OF SOME GREAT FLARES BASED ON THE MAGNETIC FIELD CONFIGURATION AND EVOLUTION OF SUNSPOT GROUPS

Katsuo Tanaka
Tokyo Astronomical Observatory
Mitaka, Tokyo, Japan

The possibilities of predicting great activity by means of the white light observation of sunspots are considered. First we performed an experiment using past sunspot data (1917-1974) to determine whether a δ -group with inverted polarity has actually produced a great flare or not. It is found that this happened with high probability (90%), which demonstrates the usefulness of this criterion for detecting great activity. Some general relations between the occurrence of a great flare and the evolutionary characteristics of sunspot groups are described. Using an example of how the accumulated energy available for flares can be estimated from the sunspot shear motion in the real time, and based on an empirical rule that the accumulated energy is always about twice the radiated energy in the soft x-ray region, we propose a method for predicting the flare energy in sunspot groups associated with continued proton flare activity.

1. INTRODUCTION

Recent morphological studies of active regions that are rich in proton flares have revealed that these regions show characteristic magnetic field configurations and evolution (cf. Zirin and Tanaka, 1973; Tanaka, 1976). For example, the great activity of August 1972 showed the following properties found from $H\alpha$ and white light morphologies:

(1) the sunspot group is rather compact and has a δ -configuration in which several umbrae of opposite polarity lie closely embedded in a single penumbra and the relative orientations of the sunspots are much deviated from the Hale's law, i.e., the polarity is inverted.

(2) the spot group evolves very rapidly while the activity continues. Rapid growth or decay of spots are accompanied by a lateral displacement of spots relative to the opposite polarity spot in proximity, i.e., shear motion. A large two-ribbon flare occurs over the sunspot group after one to two days of continued relative motion of the spots.

(3) horizontal magnetic structures such as penumbral filaments and $H\alpha$ fibrils are highly sheared at the neutral line, i.e., these structures are parallel to the neutral line which divides the two spots; spiral or

vortex structure develops near the edges of these structures to surround the two spots.

These properties indicate a stressed magnetic configuration in which the fluxtube is sharply buckled and twisted. Since flare instabilities can be considered as a relaxation from stressed to unstressed, i.e., potential configurations (Tanaka and Nakagawa, 1973), the association of this configuration with flare activity is conceivable. Hence, this geometry may be useful in some techniques for predicting great activity. From this point of view, we performed an experimental prediction of great flare activity using past sunspot data (Section 2). The particular evolutionary nature, i.e., shear motion and development of the sheared configuration, has been interpreted as an energy storage process by Tanaka and Nakagawa (1973) and Tanaka, Smith and Dryer (1978). In Section 3, we show a simple formula for deriving an increase of the stored energy and give an example comparing the stored and released energies. This example gives a basis for predicting flare energy based on the real time observations of sunspot groups and soft x-ray flux.

2. EXPERIMENTAL PREDICTION OF GREAT ACTIVITY USING PAST SUNSPOT DATA

To detect stressed magnetic configurations, we need high resolution vector magnetograms. However, for proton flare activity which occurs right on the sunspot group in which sunspots are closely packed, we can use sunspot photographs supplemented by magnetic field data and $H\alpha$ data to detect polarity inversion, shear motion of the magnetic fields, and sheared magnetic structures. We have performed a test to determine whether past spot groups with stressed configurations actually produced great activity or not. For this we selected from the Mt. Wilson daily sunspot pictures those spot groups which have δ -configuration with inverted polarity as a whole group. We compared them with a list of the great activity regions which was made after this selection to avoid biased selection. The δ -configuration indicates a close distance between the two polarities, an important criterion of stressed configuration. Generally, a δ -group is a mixture of multiple spots of both polarities. Some 80% of the δ -groups we studied, however, showed basically bipolar structure in which two groups of spots of opposite polarity are rather clearly separated by a single neutral line within the group. In these bipolar δ -groups the bipolar axis, with high probability, deviates from the normal direction by more than 45° , a condition which we defined as inverted polarity. We considered that other complex δ -groups are also polarity inverted and included them in our selection. Our data selection extended back to 1917 when the visual determination of spot fields was started by Hale and Nicholson (1938) although there was a gap of no magnetic field data between 1925 and 1934. Over the 46 years we examined, 136 such groups have been detected.

To obtain a list of great activity regions independent of this selection, we classified all the active regions according to the number of great flares produced in each region. After some trials to get a homogeneous classification among different periods, three ranks of the activity class (B,A,AA) of an active region were defined as shown in Table 1. For the

regions before 1935, since no homogeneous flare records exist, we defined the great activity regions as those producing great or small geomagnetic storms which were compiled by Spencer Jones (1955).

Table 1. Definition of Activity Classes of an Active Region.

<u>Years</u>	<u>class B</u>	<u>class A</u>	<u>class AA</u>
1935-1955	more than one Imp.2* flare	more than four Imp.2* flares	class A with great geomagnetic storm
1956-1974	more than one Imp.2 flare with CFI** ≥ 10	more than three CFI ≥ 10 or four Imp.2 flares	class A with more than two CFI ≥ 14 flares

*Imp.2 flare with reported duration more than one hour

**Comprehensive Flare Index (Dodson and Hedeman, 1971; 1975)

The number distribution of the active regions which can be classified into three classes in each of recent four cycles are shown in Table 2. (Note that the population of this classification is restricted to those regions that produced more than ten flares during its disk transit as reported in the Quarterly Bulletin of Solar Activity.)

Table 2. Number of Active Regions in Three Activity Classes.

	<u>class B</u>	<u>class A+AA</u>	<u>class AA</u>
1935-1943	51	7	3
1944-1955	48	10	4
1956-1965	67	18	5
1966-1974	41	14	3
total	207(51%)	49(12%)	15(4%)

Comparing the list of the selected δ -group with the above list of the great activity regions, we find as shown in Table 3 that 94.5% of the selected δ -groups proved to belong to the activity class higher than B for the data after 1935, and that 76% of the selected groups before 1935 actually produced geomagnetic storms. In the last three columns of Table 3 are shown ratios of the number of the selected δ -groups which belong to each activity class, to the total number of the active regions which belong to that class. One can see that about one-third of the class B regions and two-thirds of the class A regions have been selected in the present survey with a criterion of inverted and δ -configurations only. These results may indicate the effectiveness of judging the high activity from the characteristic appearance of the sunspot configuration. In particular, the capability of detecting super activities (class AA) appears quite high (14 out of 16 class AA regions have been detected). In our experiment we restricted our selection only to those groups showing the δ -configuration as a whole near the disk center. Inclusions of other groups showing the δ -configuration only locally and other δ -groups which developed only near the limb would increase the detection probability.

Table 3. Results of Great Activity Prediction by δ -and Inverted Configurations.

	number of selected groups	number of selected groups higher than B class activity	ratio of selected number to total number		
			class B	A	AA
1917-1924	25	19(76%)	--	--	--
1935-1955	36	34(94.5%)	24%	47%	88%
1956-1974	75	69(94.5%)	42%	75%	88%
total	136	122(90%)			

Although we have considered only the overall correspondence between the stressed configuration and great activity, the approximate time of occurrence of a great flare can also be predicted by watching the evolutionary changes. Examples of the evolution of selected δ -groups are shown in Figure 1. Most of the inverted, bipolar δ -groups appear with their bipolar axis being oriented north south, and, together with rapid growth, gradually evolve to become more east west oriented. This change of configuration is characterized as a shear motion of one polarity spot to the other. Large flares occur generally when the gross tilt of the bipolar axis becomes apparent, usually one to two days from the start of the shear motion. It should be noted that the two spots showing the shear motion often decrease their distance at the initial growth associated with rapid development of sheared, curled filamentary structure in the penumbra dividing the two spots. In some cases, large flares continue to occur with an interval of one to two days while the whole group shows a steady shear motion (e.g. Figure 1, 1959 July 14). In general, the shear motion occurs in two different modes: one is a real movement of the spot, and the other is an apparent shift of the spot position due to rapid appearance and growth of new spots adjacent to the older spots, which tend to decay. As a modification of the latter, there are often cases which show parallel extensions of two polarities along the neutral line. In the complex δ -group other than bipolar ones there can be observed continuous structural changes (e.g. Figure 1, 1951 May 16).

3. QUANTITATIVE RELATION OF THE SPOT SHEAR MOTION WITH FLARES AND ITS APPLICATION TO THE PREDICTION OF FLARE ENERGY

Using an example, we show below how the spot shear motion is correlated with flares, how to evaluate the increase of flare energy quickly and how to predict the flare energy. Figure 2 shows the whole spot evolution of McMath 13043 (1974 June 28-July 10), which produced numerous flares (58) and an unprecedentedly large number (28) of major flares (Dodson and Hedeman, 1975). Flares occurred almost continuously inside the δ -configuration in close association with the spot shear motion (shown by arrows in Figures 2 and 3). The shear motion occurred three times in succession in different parts of the group. While these motions continuously changed the magnetic configuration of the group, flares always started at the sides of the neutral line which underwent the shear motion from one side. See Figure 3 for the correspondence of flare positions to shear motions. So the flare position

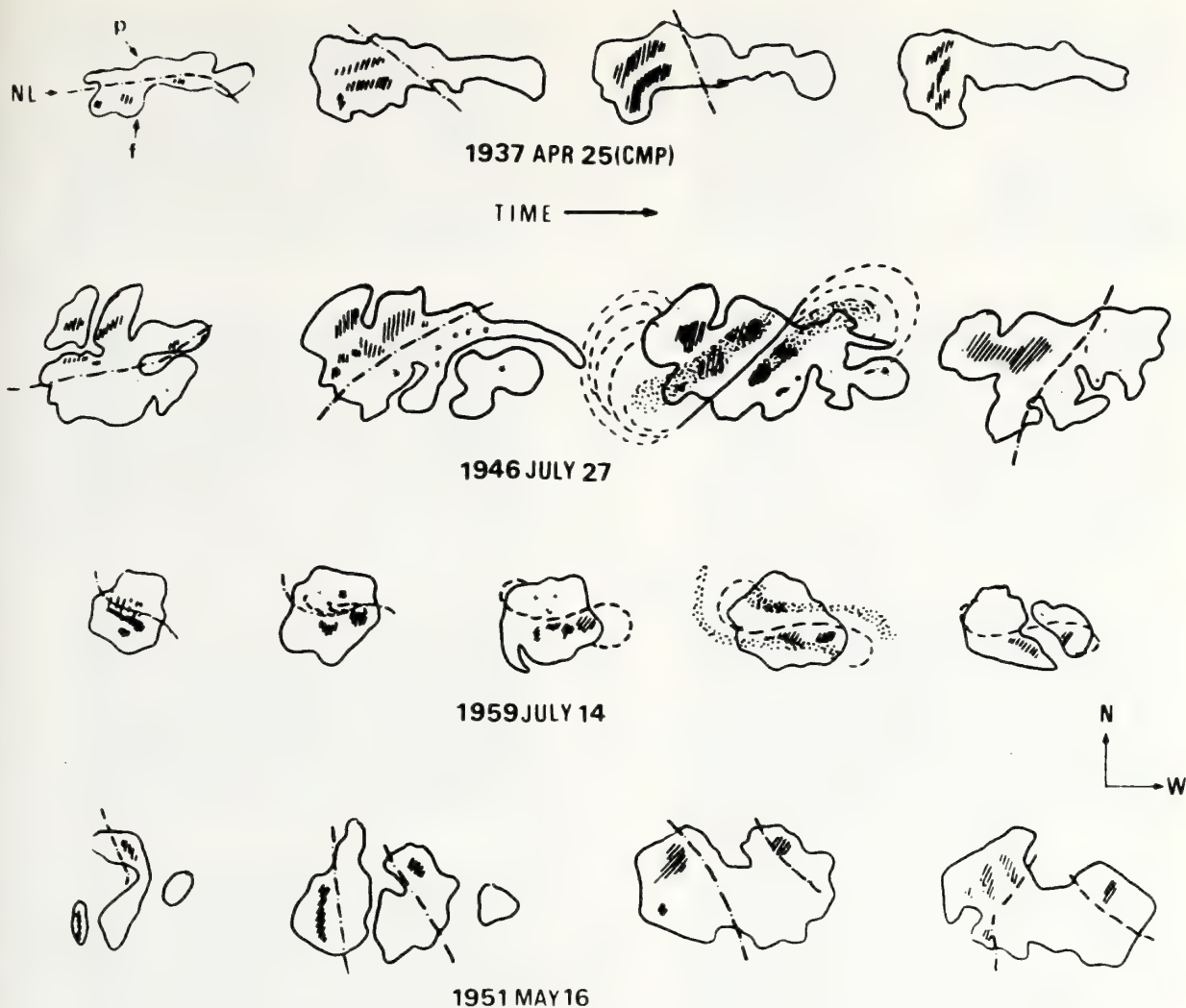


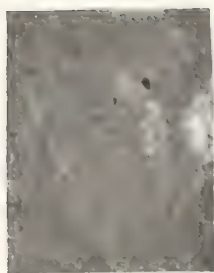
Figure 1. Examples of δ -group evolution. The neutral line is shown by a dash-dot line, flare by dots, filament by dashed lines, umbrae of following polarity by hashed lines and leading polarity by solid areas.

shifted successively while the continued spot motion changed the shape of the local neutral line. In addition, the activity was switched quickly to a new place when a new motion started. When no motion occurred (July 3), no flare occurred. This example tells how honestly flare occurrence reflects shear motion inside a δ -configuration.

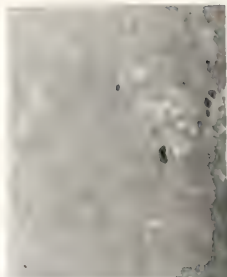
Based on the theory of the energy integral (Tanaka and Nakagawa, 1973), the amount of energy provided into the closed magnetic field above the photospheric surface by the motion's work at the surface can be represented as (Tanaka et al., 1978):

$$M(t) - M(t_0) = 8.96 \times 10^{-3} \int_{t_0}^t B^2 A V dt \text{ ergs} , \quad (1)$$

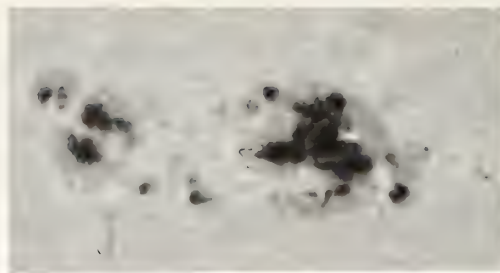
where $M(t)$ is magnetic energy content at time t , B and A are the peak



10



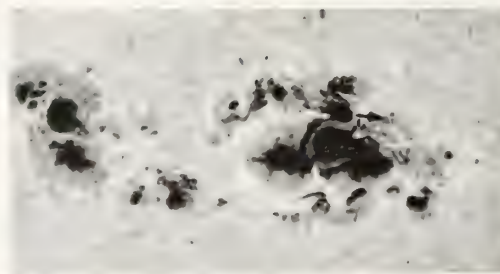
6/28
22 UT



7/4
7 UT



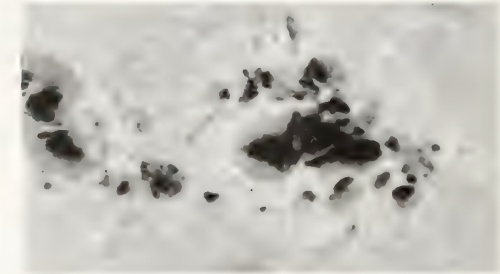
6/30
21



7/4
17



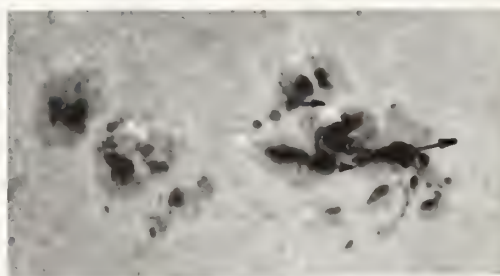
7/1
18



7/4
21



7/2
18



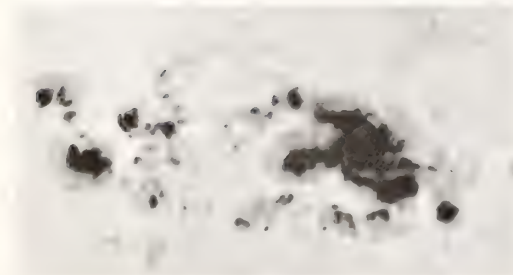
7/5
21



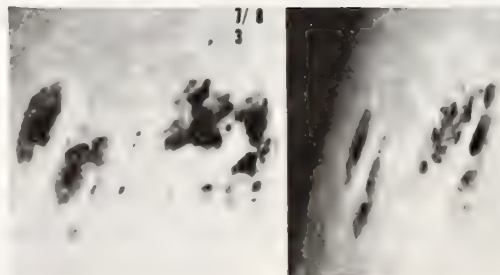
7/3
7



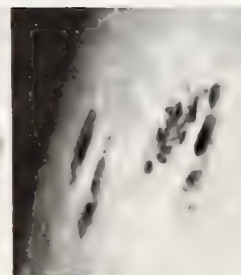
7/6
18



7/3
19



7/8
3



7/8
2

Figure 2. Sunspot evolution of McMath 13043 from June 28 to July 9, 1974. Shear motions are shown by arrows. (Pictures from Big Bear Observatory).

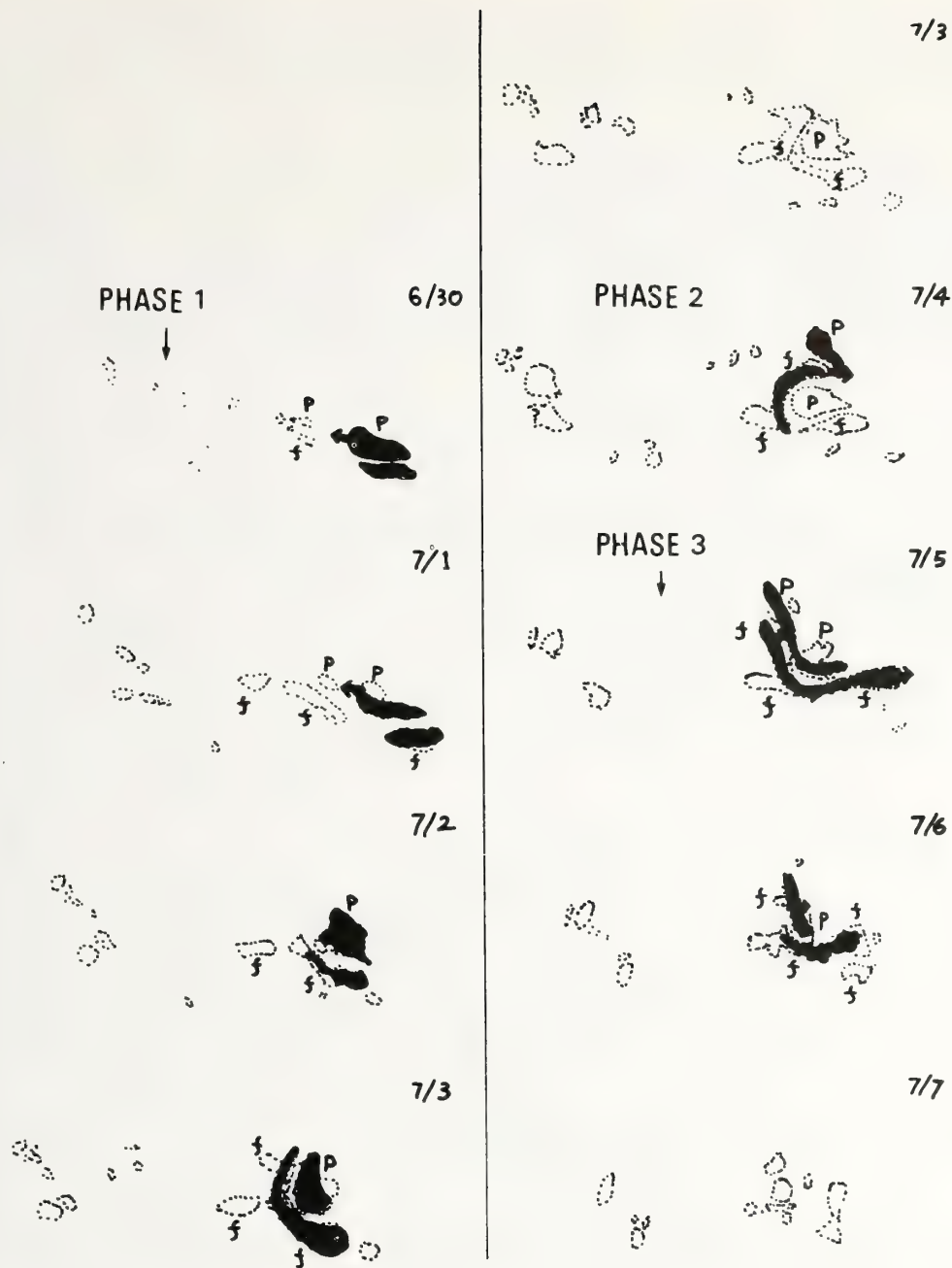


Figure 3. Flare positions (shaded), polarity distribution in McMath 13043 shown in Figure 2. Note the correlations between spot shear motions and flare sites.

longitudinal field (gauss) and area (cm^2) of a moving spot, and V is a velocity component (cm s^{-1}) parallel to the neutral line. To apply this formula we need the condition that the moving spot constitutes a bipolar connection with the opposite polarity spot (by $\text{H}\alpha$ or penumbral filaments) as well as that the two spots are almost in contact with each other and

separated by a narrow penumbral area where filamentary structures lie parallel to the neutral line. These conditions are generally satisfied in the bipolar δ -group, like this case.

The evaluated increase of the magnetic energy content in the above example is shown by the solid line in Figure 4. We find that the energy content increases in each shear motion almost linearly with time with an average rate of 3.9×10^{26} ergs s^{-1} . Note that there is no increase of the energy on July 3 and that this corresponds to the absence of motion. In Figure 4 we have also plotted the time increase of twice the total radiated energy ($E(t)$) (dotted line) which is derived from the soft x-ray flux $F(1-8A)$,

$$E(t) - E(t_0) = 6.7 \int_{t_0}^t F(1-8A) dt \text{ ergs} , \quad (2)$$

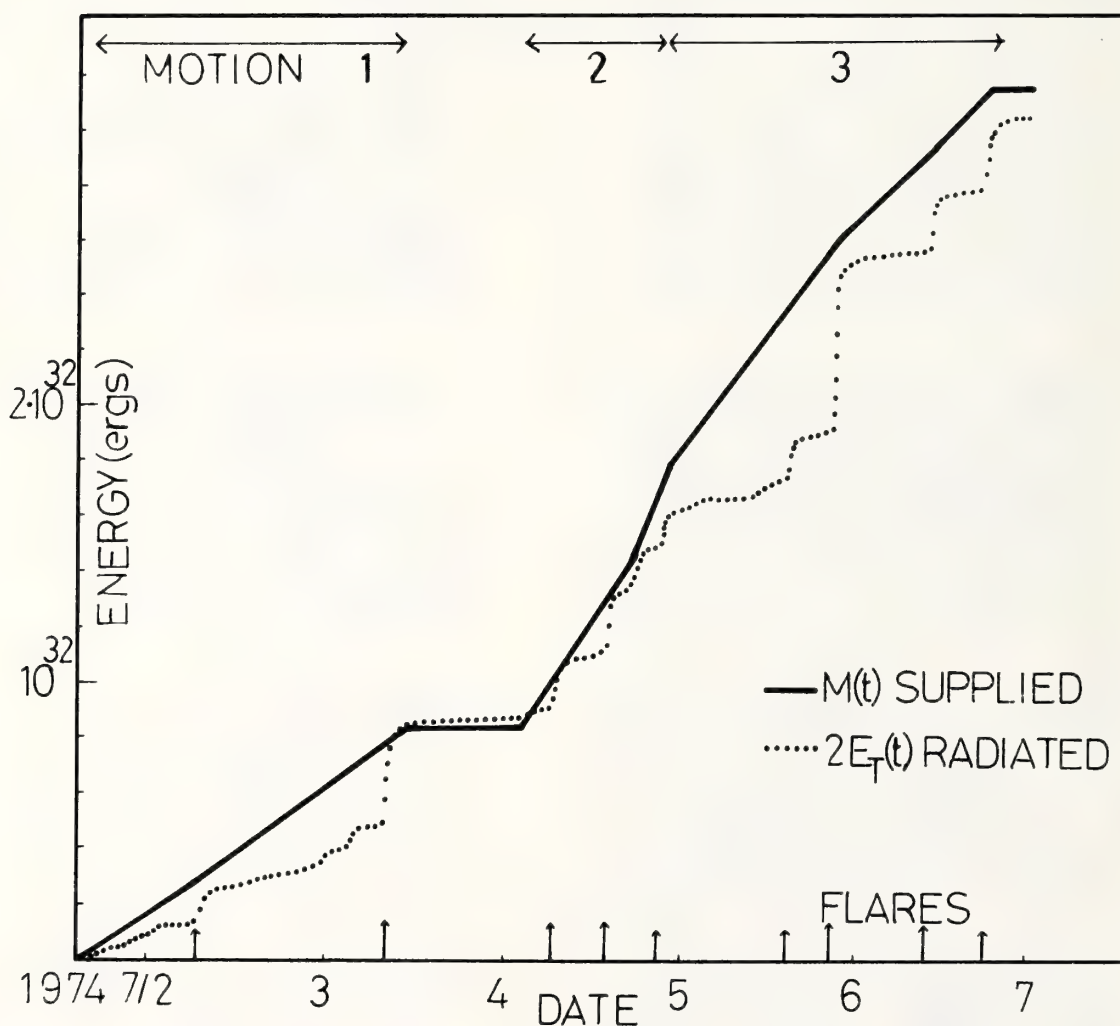


Figure 4. Increases of the accumulated energy ($M(t)$ solid line) as derived from eq. (1) and twice the radiated energy: $E(t)$ in the x-ray region (dotted line) throughout the activity in McMath 13043 (Figures 2 and 3). Note that $2E(t)$ is precisely enveloped by $M(t)$.

where a factor of 6.7 is used to convert the radiated flux in the 1-8A band to the total radiated flux (Tucker and Koren, 1971). We have subtracted the background flux $E(t_0)$ in evaluating (2). In this figure big flares are represented by sharp rises in $2E(t)$ and indicated by arrows at the bottom, while gradual increases in $E(t)$ are due to frequent occurrences of small flares. One can see a remarkable correlation between the linearly increased energy content, $M(t)$, and the energy released in big flares. Thus, stepwise increases (i.e. big flares) of the radiated energy are closely enveloped by the energy accumulation curve. Looking into time behaviours of $M(t)$ and $E(t)$, we find two modes of the energy release: in one case the linear increase of $M(t)$ is cleared frequently by small size flares as in the case of July 4, while in other cases, like the activity after July 5, $M(t)$ is released only after a prolonged energy accumulation so that the flare energy is large. The mode by which the energy release occurs seems to depend on the magnetic configuration. Equation (1) indicates that the energy available for flares is proportional to B^2AVt , where t is a time in which energy is accumulated without drastic release. In this example, because the size of the region is rather small and the accumulation time is not longer than one day, individual flare energies are not very large. Since V (about 100ms^{-1}) and B (typically 2500G) differ little among various groups, flare energy depends mainly on At . The large amount of released energy in the 1972 August flares is therefore due to the large area of a moving spot and prolonged shear motion without causing a flare instability (one to two days). The huge flare on 1946 July 25 (Figure 1) can also be understood as due to displacement of a huge spot.

As can be seen in Figure 4, the constant scaling between the accumulated energy and radiated energy is remarkable. In Table 4 we show, for the eight big flares in our present example and three large flares in the 1972 activity, the accumulated energy (M) between two successive major flares and the radiated energy (E) in the same period. The amount of radiated energy turns out to occupy a half of the accumulated energy to within small scatter ($49\% \pm 9\%$ for the 1974 activity, and $62\% \pm 20\%$ for the 1972 activity).

Table 4. Comparison of Accumulated Energy (M) and Radiated Energy (E) in Big Flares (unit of 10^{30} ergs).

1974	<u>July 2 6UT</u> 1n	<u>July 3 8UT</u> 1b-2b	<u>July 4 6UT</u> 1b	<u>July 4 13UT</u> 1b-2b
M	13.5	28	11	14
E	7.2(53%)	15.8(56%)	5.0(45%)	6.2(44%)
1974	<u>July 4 17-21UT</u> 1n-1n	<u>July 5 15+21</u> 1b 2b	<u>July 6 11UT</u> 1b	<u>July 6 18UT</u> 1b
M	17	49	16	11
E	7.7(45%)	23(47%)	5.9(37%)	7.4(67%)
1972	<u>Aug. 2</u> 2b+2b	<u>Aug. 4</u> 3b	<u>Aug. 7</u> 3b	
M	140	60	130	
E	61(44%)	50(83%)	75(58%)	

Physically this would mean that a half of the available energy is released in the form of thermal energy which is radiated, and the rest is released probably in the form of kinetic energy of shock waves. If the shock wave originates from thermal expansion of the hot plasma as in the case of the solar wind, its energy cannot exceed the thermal energy of the hot plasma, and equipartition of the energies may be reasonable (see Tanaka et al., 1978). In any case, this empirical rule may provide us with a technique for predicting the flare energy. From the real time observations of sunspot evolution of δ -groups and x-ray flux, we may plot $M(t)$ and $2E(t)$, like in Figure 4. When $M(t)$ greatly exceeds $2E(t)$, the probability of occurrence of a large flare will be high. When $M(t)$ is overtaken by $2E(t)$, no big flare will be expected.

For the actual application of this technique, however, we will need high resolution sunspot pictures taken at intervals of a few hours. In a recent example of the 1978 July activity (Figure 5), we started to take enlarged spot pictures in the white light from July 10 at a rate of one picture per day. The sunspot on July 10 showed a δ -configuration with north-south inversion and an $H\alpha$ filament divided the two components with an indication of curled structure. Comparison of pictures at 2UT July 11 and 5UT July 12 (Figure 5) revealed that the f-spot approached the p-spot showing shear motion and spiralled penumbral filaments developed in between them. At this time we expected a large flare to occur, but actually a large x15 flare took place on July 11, 1054 UT between these times. A rough estimate

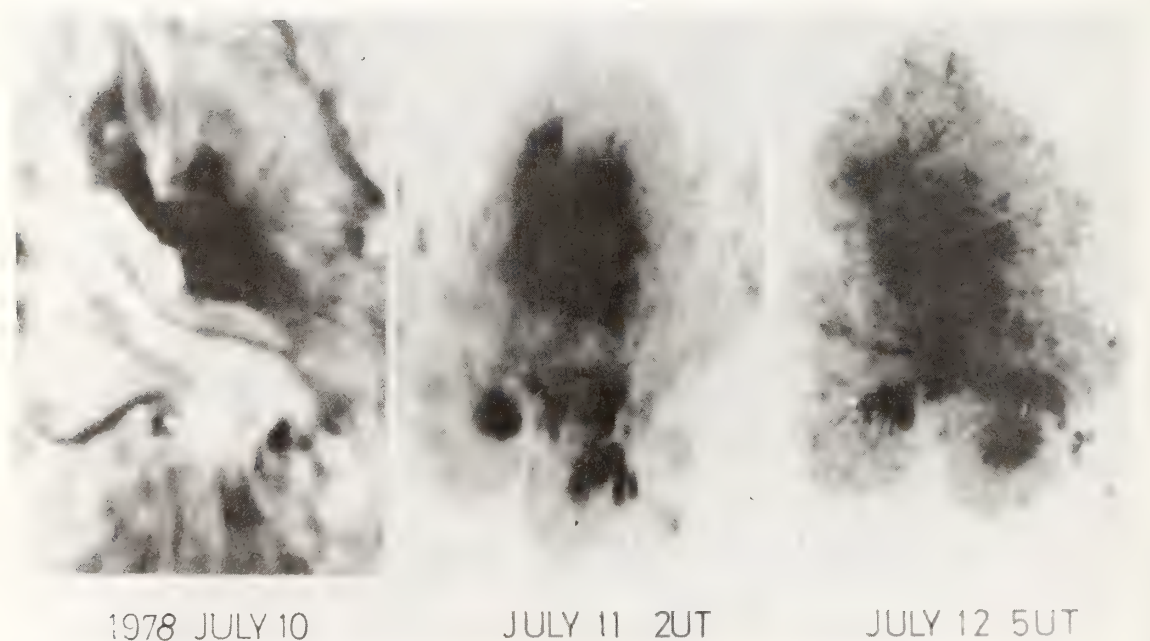


Figure 5. An example of flare conditions using white light and $H\alpha$ photographs.

of the energy accumulation rate (1.7×10^{27} ergs s^{-1}) suggested an energy supply equal to 1.5×10^{32} erg by the time of flare occurrence.

We have considered the flare prediction problem from the viewpoint of the magnetic configuration. So far only the δ -configuration has been examined for evolutionary changes of magnetic configuration at the flare sites that can be readily detected by examining the sunspot structure. Further application of this kind of analysis to groups other than the δ -group would be possible by extensive observations using magnetograph, H α and white light photographs and x-ray filtergrams showing loop structures.

We thank Dr. Donnelly for providing soft x-ray data, Dr. Howard for providing old sunspot pictures and sketches, and Dr. Zirin for providing the BBSO data.

REFERENCES

- Dodson, H. W., and E. R. Hedeman (1971): An experimental comprehensive flare index and its derivation for "major" flares 1955-1969. World Data Center A Rep. UAG-14.
- Dodson, H. W., and E. R. Hedeman (1975): Experimental comprehensive solar flare indices for certain flares 1970-1974. World Data Center A Rep. UAG-52.
- Hale, G. E., and S. B. Nicholson (1938): Magnetic observation of sunspots, 1917-1924. Washington: Carnegie Institution of Washington, Publ. No. 498.
- Jones, H. Spencer (1955): Sunspot and geomagnetic storm data 1874-1954. London: Her Majesty's Stationery Office.
- Tanaka, K. (1976): Evolution of fibrils with special references to flare activity. Solar Phys., 47:247.
- Tanaka, K. (1978): Stressed magnetic configuration in the great activities and a model of an emerging twisted fluxtube. in preparation.
- Tanaka, K., Z. Smith and M. Dryer (1978): An energy storage process and energy budget of solar flares; IAU Symp. 91, D. Reidel in press.
- Tanaka, K., and Y. Nakagawa (1973): Force-free magnetic fields and flares of August 1972. Solar Phys., 33:187.
- Tucker, W. H., and M. Koren (1971): Radiation from a high-temperature low-density plasma. Astrophys. J., 168:283.
- Zirin, H., and K. Tanaka (1973): The flares of August 1972. Solar Phys., 32:173.

SHORT-TERM PREDICTION OF THE POTENTIAL OF AN ACTIVE REGION TO PRODUCE RECURRENT PROTON FLARES

Susan M.P. McKenna Lawlor
Physics Department,
St. Patrick's College,
Maynooth,
Co. Kildare,
Ireland.

Three homologous proton flares in McMath Plage 5265 commenced above Mt. Wilson Group 14284 in intervals, spanning each flash phase, of ≤ 10 h (an upper limit determined by the availability of white light pictures) within which directly underlying umbrae either disappeared or diminished in area. A new proton flare was produced when the previously degraded umbra had waxed again. It is suggested that the localized recovery of magnetic field strength beneath a known "trigger" area may indicate the renewed potential of a region to produce energetic particles. A particularly likely situation for proton production may be one in which an energetic flare is triggered above a satellite umbra, at the perimeter of a variable sunspot having field strength at least > 2000 G. Enduring magnetic patterns within active regions lead to Homologous Flaring so that it is feasible in such situations to predict the morphology of ensuing major events.

1. INTRODUCTION

McMath Plage 5265 which crossed the central meridian of the Sun at latitude N. 15° on 14 July 1959, represents one of only five "unusual" solar regions identified by Dodson et al. (1973) as developing, during Cycle 19, at least four "major" flares with Comprehensive Indices ≥ 11 .^{*} Among the five "unusual" regions thus defined, only one other was associated with the generation of somewhat comparable particle radiation. Indeed, although cosmic rays have been recorded with ground-based detectors for almost 40 years, only that cosmic ray storm associated with the transit of McMath Plage 11976 in August 1972 ever exceeded in magnitude that associated with the disk passage of Plage 5265 in July 1959.

It will be shown in Section 3 that three successive proton flares in McMath Plage 5265 commenced above the same part of underlying spot group Mt. Wilson 14284. These commencements always occurred within intervals (in no case exceeding 10 h ^{**}) bridging the flare flash phase within which directly underlying spot

* The Statistics for the Comprehensive Flare Index were limited to flares that were major in the sense that at least one of the following circumstances was satisfied: $SID \geq 3$, $H\alpha_{imp} \geq 3$, 10 cm flux $\geq 500 \times 10^{-22} \text{ W m}^{-2} \text{ Hz}^{-1}$, Type 11 burst, Type 1V radio emission, duration > 10 min (Dodson and Hedeman 1971).

** This time interval represents an upper limit determined by the availability of white light pictures of the region.

umbrae either disappeared or diminished in area. A "new" proton flare was produced when the previously degraded umbra was seen to have waxed again. These observations suggest that localized recoveries of magnetic field strength beneath a known "trigger" area indicate the renewed ability of a region to produce an energetic event. It is thus suggested that, given the presence of a solar center displaying those characteristics generally associated with the occurrence of proton flaring, and the production there on a previous occasion of a particle-producing event, the potential of the region to produce further energetic particles may be assessed by monitoring the re-growth of spots in the photosphere directly underlying that part of the chromosphere at which the first flare was observed to flash.

In the case of McMath region 5265, it will further be shown that the development of bright flare filaments extending outside the ambience of Mt. Wilson spot group 14284 during major optical events was strongly influenced by circumstances relating to the positions on the Sun of outlying satellite spot groups. In particular, the enduring stability of the magnetic pattern formed by Mt. Wilson 14284 and its satellites resulted, when conditions appropriate to the triggering of proton flares on July 10, 14 and 16 had been established, in the production of three "Homologous"* events, the first and third more than 163 h apart. It is consequently suggested that observations of the deposition of satellite sunspot groups above a major active center may enable us to predict the morphology of ensuing major flares.

2. SOURCES AND KINDS OF SOLAR DATA USED

The monochromatic data used in this study were based primarily on spectroheliograms secured by the staff of the McMath-Hulbert Observatory, the University of Michigan, during the sunlit hours 07-21 July 1959. These records were of two main types: (a) H α spectroheliograms obtained at 30-s intervals with the McMath SECASI telescope for the international flare patrol (solar diameter 1.45 cm); (b) concomitant swept wavelength observations centered on H α and the K-line of Ca⁺, obtained with the McMath Observatory Tower telescope at focal lengths of 6.1 m and 12.2 m (solar diameters 5.6 and 11.2 cm) respectively. These latter comprised numerous sweeps or series of 17 spectroheliograms recorded with systematic changes of wavelengths from 3 Å or more on the violet to 3 Å or more on the red side of the H α line and corresponding sweeps to 1.5 Å or more on either side of the K-line of Ca⁺. Observations at H α were made with slit widths corresponding to a spectral band 0.36 Å wide. Observations at the Ca II, K-line were made with the spectral band 0.18 Å wide. Each series required 2 to 4 min observing time to complete.

In addition to the Michigan data, H α spectroheliograms taken at 1-min intervals over the period 06-20 July 1959 were available, contained in a copy of the

* Homologous flares are defined by Ellison et al. (1960) as "those which occur successively in the same active region, correspond in position relative to the local sunspots and show a common pattern of structure and development".

Continuous Solar Movie, originally compiled from world-wide Lyot Heliographic records by Dr. Henry Smith (Smith 1963).

White-light pictures of the sunspot group were kindly provided for days 08-20 July 1959 by Mrs. Ogir (Crimean Astrophysical Observatory, Russia), for days 09-15 July by Dr. R. Howard (Mt. Wilson Observatory, U.S.A.) and for days 09-10 and 13-14 July by W.M. Baxter (Private Observatory, Acton, England).

Details of the arrival at the earth in July 1959 of high and intermediate energy protons associated with flaring in McMath 5265 were taken mainly from the Proceedings of the "Symposium on the July 1959 Events and Associated Phenomena", Helsinki (1960) and the "Catalog of Solar Particle Events 1955-1969" (Ed. by Švestaka and Simon 1975).

4. OBSERVATIONS ON WHICH THE PREDICTED POTENTIAL OF A REGION TO PRODUCE PROTONS IS BASED.

Center of activity, McMath 5265, mentioned in Section 1 as associated with the production of three homologous proton flares, crossed the central meridian of the Sun at latitude N. 15° on 14 July 1959. As seen on white-light pictures, it consisted of an aggregate of groups of sunspots, and Table 1 summarizes information concerning their individual magnetic classes, field strengths and life-times.

TABLE 1

THE MAGNETIC CLASSES, FIELD STRENGTHS AND LIFE TIMES OF SUNSPOT GROUPS IDENTIFIED AT THE MT. WILSON OBSERVATORY IN ASSOCIATION WITH MCMATH PLAGE 5265 DURING ITS JULY 1959 DISK PASSAGE.

Mt. Wilson No.	Mag.* class	Intensity (100 G)	Days seen
14280	d β d	(7)	07-14
14282	d α p d	(2)	08-14
14284	l γ l	27	08-20
14285	d β p l	13	09-20
14292	d α d	(2)	12-16
14297	d χ d	(2)	14-15

*Mount Wilson sunspot classification and notation as given by Hale and Nicholson (1938).

Principal spot group Mt. Wilson 14284 displayed all the usually recognized attributes of a solar region especially associated with the production of proton

flares. It was (a) of Zürich class E; (b) of magnetic class γ ; (c) it showed reversed polarity; and (d) the gradient of the longitudinal component of the magnetic field near the "neutral line" was high. Properties of the group indicating its potential to be associated with proton flares included: (a) the presence of a δ configuration; (b) the presence of an A configuration; (c) the counter-clockwise rotation of the group axis and (e) the presence of neighbouring "satellite" spot groups.

Flare activity, as observed on H α and Ca spectroheliograms during the disk transit (07-21 July 1959) of this complex center, tended to occur in favoured locations that could be recognized unambiguously from day to day. Fig. 1 comprises a set of composite drawings showing the relative positions in the active region on days July 09, 10, 13, 14, 16 and 17 respectively of sunspot umbrae and penumbrae, bright structures in the calcium network and well-defined elevated dark filaments. The positions of certain of the recurrently flaring areas observed are designated by lower case letters; roman subscripts and superscripts are sometimes added to these letters to describe areas that flared in close proximity to one another.

Table 2 lists (cf. column 2) the commencement times of three major proton-producing flares that occurred in the active region on 10, 14 and 16 July respectively. The onset of the flash phase in each instance was coincident with the time of onset (cf. column 4) of a "very strong" radio burst (here defined to consist of very broad band >9000 MHz bursts in the centimeter range, smoothed peak flux density at centimeter wavelengths $>1000 \times 10^{-22} \text{ W m}^{-2} \text{ Hz}^{-1}$ and duration >1 h).

From data showing the anomalous increase in the soft-component cosmic rays observed by Brown and d'Arcy in balloon flights over College, Alaska, Nagata et al. (1960) estimated that the energy of the incoming protons on 10 and 14 July was ≤ 200 MeV and ≤ 500 MeV respectively. Also, from an analysis of cut-off rigidity for anomalous increases in the neutron component of cosmic rays reported by Nagata and Kodama (1960), it was estimated that, on 16 July, the energy of the incoming solar protons was ≤ 1200 MeV. Also, the world-wide array of neutron monitors (with sensitivity to protons with energies of the order of 10 BeV) recorded a cosmic ray event at ground level from 22^h 50^m UT, 16 July, with maximum at about 05^h 00^m UT, on 17 July (McCracken and Palmeira 1960). For additional measurements and references see the "Catalog of Solar Particle Events 1955-1969" (Ed. by Švestka and Simon 1975).

Common to each flare event during its flash phase was the brightening of flare-sensitive area d. This part of the chromosphere (diameter ~ 5000 km) was not only the single most flare active area in the entire complex but also that most frequently associated at its brightening with the generation of time-associated (within ± 1 m) centimeter-wave and/or Type III bursts (McKenna-Lawlor 1978a).

Careful study of the spot data contained in McMath λ -sweep spectroheliograms and of complimentary white-light pictures of the spot group reveals that, on 09 July, area d was located above a "satellite spot" of unknown polarity flanking

RELATIONSHIP BETWEEN THE COMMENCEMENT OF PROTON FLARING IN MC MATH 5265, THE ONSET OF "VERY STRONG" RADIO BURSTS AND OBSERVED CHANGES IN THE CONSTITUENTS OF MT. WILSON GROUP 14284

Date	Times of onset (UT) of proton flares and ("very strong" radio bursts)	Flare sensitive areas** involved in flash phase	Changes in components of Mt. Wilson Group 14284	Intervals within which the ob- served magnetic changes occurred
10	^h 02 ^m 05 ^m (02 ^h 06 ^m) ^h 02 ^m 06 ^m ^h 02 ^m 09 ^m	c, d a-b-c-d-d ^I a-b-c-d-d ^I -e-f-g-h	Disappearance of N21 between c and d and possibly of minor umbrae and penumbral structure underlying b and c ⁺ , apparent merging and southward motion of umbrae underlying f and g; distension westwards of western penumbral boundary.	^h 21 ^m 38 ^m July 09- ^h 06 ^m 02 ^m July 10 (^h <8.4 h).
14	^h 03 ^m 27 ^m (03 ^h 30 ^m) ^h 03 ^m 33 ^m	c, d ^I c-c-d-d ^{IV} ^I e, ^I o	Umbra N26 between d and d ^{IV} shows a reduction in area; separation of south polar umbrae and growth of a new umbra between S23 and fragmenting main group.	^h 19 ^m 14 ^m July 13- ^h 05 ^m 14 ^m July 14 (^h <10.0 h).
16	^h 21 ^m 14 ^m -21 ^h 16 ^m (21 ^h 18 ^m) 21 ^h 18 ^m	^{IV} d, d ^I , e ^I -e ^I (^{IV} d, ^{IV} d ^{IV})(e ^I -e ^I) (^{IV} k ^{III}) ^I c-c-d-d ^{IV} -d ^I e ^I -e ^I ^{IV} k ^{III} -k-k ^{II} -f ^I ^{VII} x	Umbra N28 between d and d ^{IV} shows a reduction in area; also umbrae located immediately to the north and south of S28 disappeared and those underlying e ^I and e ^I faded. Two minor umbrae waxed somewhat to the west of this latter pair. A large island of penumbra containing S28 as well as a waxing south polar umbra underlying k ^{IV} separated from the main body of group 14284.	^h 21 ^m 30 ^m July 16- ^h 04 ^m 42 ^m July 17 (^h <9.4 h).

* >9000 MHz in cm-m range, smoothed p.f.d. $>1000 \times 10^{-22} \text{ W m}^{-2} \text{ Hz}^{-1}$ at cm wavelengths, duration > 1 h.

**For the locations of these areas within the active region see the drawings of Figure 1.

†Minor umbrae and ambient penumbral structure underlying b and c certainly disappeared between 18^h00^m July 09 and 06^h02^m July 10. Since minor umbrae are difficult to identify unambiguously on the swept wavelength records it is not certain if these magnetic features were present on the spectroheliogram 21^h38^m July 09 when umbra N21 was still clearly visible.

the eastern rim of a large north polar umbra of field strength >2000 G.* A proton flare began at 0205 UT on 10 July with a sudden flash in intensity in areas c and d (cf. Fig. 1) accompanied from 0206 UT by a "very strong" radio burst. Emission thereafter rapidly spread. Between 2138 UT 09 July-0602 UT 10 July, that is within an <8.4 h interval spanning the flash phase of this flare, the large north polar umbra mentioned above substantially disappeared (see Plate 1, which reproduces two high-quality photographs of the region - taken on 09 July at 0915 UT and on 10 July at 0945 UT respectively).

Over the next several days a north polar umbra gradually formed in the general position from which N21 had previously disappeared. On 14 July, when this spot showed a field strength of >2000 G, a second proton flare commenced in region 5265. Observations of the beginning of this event are incomplete, but the flash phase, with onset time at 0330 UT (as deduced from the time of commencement of an associated "very strong" radio burst) included the brightening of flare-sensitive areas d and d^{lv}, individually situated above satellite spots to the east and west respectively of the newly grown umbra. Between 1914 UT 13 July and 0514 UT 14 July, that is within a <10 h interval spanning the major flare, this latter umbra showed a marked reduction in area (compare the drawings of 13 and 14 July in Figure 1).

By 16 July, the previously reduced north polar umbra had again aggrandized and showed a measured field strength of 2800 G. The third and last proton flare of the series commenced on this day at 2114 UT, with flash phase at 2118 UT, and flare onset again included brightenings in d and d^{lv} above satellite umbrae to the east and west of the newly waxed spot. Over the interval 2120 UT 16 July to 0442 UT 17 July (that is within a <7.4 h interval spanning the major flare) this same large umbra suffered again a reduction in area; compare the drawings of 16 and 17 July in Figure 1.

Within that 8.4 h interval spanning the flare of 10 July, changes also took place among the south polar umbrae in the spot group (cf. column 4, Table 1). An impression is given either that certain south polar umbrae disappeared or else that they moved southwards and merged. In either instance, those south polar umbrae present on 10 July following the major flare appeared to be further apart than were those present prior to flare onset, thereby indicating that a change had taken place in the magnetic gradient in this part of the spot group. Again on 14 and 16 July, a general separation between major south polar umbrae (with small superposed variations due to the waning and/or waxing of certain minor umbrae at positions between these fragmenting features) resulted in the development within the spot group of associated changes in magnetic gradient within individual <10 h intervals spanning each major flare.

* Note that "small localized enhancements of magnetic field of both polarities around the perimeter of a sunspot" are defined by Smith (1971) to comprise "satellite spots". This definition does not quite correspond with that given by Rust (1968), who describes satellite spots as "polarity reversals in B₁₁ near the edges of large-spot penumbrae". In the case of McMath region 5265 it is not possible to determine if minor umbrae, such as that mentioned above underlying d, displayed contrasting polarities or not, and in what follows such features will be referred to as "satellite spots" in the sense defined by Smith.

The observation that all of the three flares discussed were associated with situations where (taking an overall view) underlying umbrae of one polarity (north) were merging and/or waxing while umbrae of the opposite polarity (south) were declining and/or fragmenting is in accord with the law of Evolving Magnetic Features (EMFs) derived by Martres et al. (1968a, 1968b) and Ribes (1969), who showed that flaring occurs where two adjacent EMFs of opposite polarities evolve in opposite senses.

It may be noted that two magnetographic studies have been made of McMath 5265 over a period spanning the 16 July proton flare, one at the Mt. Wilson Observatory by Howard and Babcock (1960) and the other at the Crimean Astrophysical Observatory by Howard and Severny (1963). The first analysis indicates that no changes occurred with time in the strength and configuration of the measured magnetic fields other than certain minor effects attributable to seeing and imperfections in scanning. The second investigation however shows that, within an interval between 1500 UT 16 July and 0600 UT 17 July the higher magnetic fields near and inside certain associated sunspots decreased by nearly a factor of 3. The resulting loss of magnetic energy amounted to about 10^{32} ergs. It is noted by Howard (1964) with reference to these observations that the magnetic measurements which were obtained at Mt. Wilson would not have shown changes in fields which always remained greater than 40 G, and in consequence the Mt. Wilson observers could not have recorded those changes in the spot fields which were detected at the Crimea. Magnetic changes preceding or occurring during the opening minutes of the flare in the 5-40 G fields would also have been missed at Mt. Wilson.

In each of the three events discussed, bright flare filaments developed so as to cross and obscure those umbrae of high field strength within the group that showed magnetic change. This may be related to a report by Ellison et al. (1961) that flares emitting GLE protons cover partially or completely those underlying umbrae displaying highest field strength and with observations by Dodson and Hedeman (1961) that the extension of a flare to cover at least one spot umbra is "significant" with respect to its association with PCA protons.

On 10 July, following the proton flare, there was a conspicuous drop in activity above Mt. Wilson group 14284, that is to say above that group from which umbra N21 had disappeared. Recovery on 11 July appeared to be associated with the emergence in the region of new magnetic flux. Similarly, on 14 July, there was, following the proton flare, again a depression in activity directly above that group where a spot had suffered a rapid diminution in area. The fact that important flaring meanwhile took place along the "distant" southern border of 14284 and in other parts of the active center meant that the overall level of flaring in McMath 5265 (as reported in such international lists as the Quarterly Bulletin) remained high on this day and masked the localized effect. Following the outstanding proton flare of 16 July there was no further significant flaring above Group 14284 and, during the remainder of the July transit (up until 21 July), the bulk of activity observed took place above Group 14285.

These observations suggest that there was a localized exhaustion of the energy supply in Group 14284 after each proton flare and a period of recovery was required before another energetic event could be produced at the same trigger

point. Conditions favourable for producing proton flares were re-established between 10 and 14 July in ~ 97 h 28 min and between 14 and 16 July in ~ 65 h 45 min. The marked difference in time scale may have been associated with the fact that the magnitude of the magnetic change associated with the flare of 10 July (disappearance of a major north polar umbra) was much greater than that associated with the flare of 14 July (partial disappearance of such an umbra). Following the threefold decrease in umbral field strength in the group associated with the 16 July event no further proton flare was produced before McMath 5265 transited the west limb on 21 July (that is for > 122 h).

4. DISCUSSION OF THE SIGNIFICANCE OF THE OBSERVATIONS

Although, as shown above, three successive proton flares were triggered above positions within a spot group where substantial magnetic changes occurred in intervals that never exceeded 10 h bridging each optical event (and in at least one case was known to be < 8.4 h), it is not possible to definitely say if the observed magnetic changes were sudden and flare-associated or if they rather represent progressive variations produced by the "independent" comings and goings of spots.

Some indications however suggest that the observed correlation between magnetic field change and flaring is significant. In this connection it was found that intensity enhancements in McMath 5265 which were time-associated (within ± 1 min) with five individual "Strong" * radio bursts were, as in the case of those events accompanied by "Very Strong" bursts, associated with changes in directly underlying sunspots within intervals spanning the flare flash phase. These intervals in no case exceeded 12.7 h (as defined by data availability) and showed a lower limit of < 7.4 h. Similarly, brightenings accompanying 14 "Moderate" * radio bursts were associated with directly underlying magnetic field changes within intervals having an upper limit of < 24.1 h and a lower limit of < 7.4 h. The kinds of magnetic field change referred to included: (a) the emergence of new flux; (b) local variations in magnetic gradient due to sunspot proper motions; and (c) magnetic waxings and wanings due to processes such as aggrandizing due to merging and degradation due to fragmentation of individual spots. No burst-associated brightenings were observed to occur at locations characterized by an absence of underlying magnetic field change.

Again, although correlations are incomplete owing to lack of telescopic coverage, there was a close spatial association between localized filament activations in McMath 5265 and the trigger points of energetically important

*"Strong" radio bursts are here defined as broad-band > 1000 MHz events in the centimeter to meter-wave range, smoothed peak flux density at centimeter wavelengths < 1000 units, duration ≤ 1 h. Similarly "Moderate" radio bursts are defined as broad-band ≥ 1000 MHz or single-frequency events in the centimeter-wave range only, smoothed peak flux density at centimeter wave-lengths < 1000 units, duration < 1 h (1 solar flux unit = 10^{-22} W m $^{-2}$ Hz $^{-1}$).

flaring. The presence of such adjacent active dark material provides an indication that those parts of the active region within which magnetic changes occurred over intervals spanning the flare flash phase were already in a state of instability up to 30 min prior to and at the onsets of the flares concerned. These observations are complementary to reports by Smith and Ramsey (1964), Hyder (1967a, 1967b), Martin and Ramsey (1972) and McKenna-Lawlor (1978b) on pre-flare filament activity.

It is notable that impulsive brightenings in the active region, whether burst-associated or not, appeared to break out directly above minor umbrae. Steshenko (1967) has shown that sunspots can develop only when their field strengths exceed approximately 1100 G and we can conclude that the relevant flare-associated umbrae had individual field strengths in excess of this value. In the case of the most energetic events flaring additionally spread to cross and obscure umbrae of high field strength (>2000 G) within the group.

No brightenings occurred at flare-active sites previous to the interval within which minor underlying umbrae appeared and when they had vanished impulsive activity ceased. The umbrae concerned were usually too small to be clearly visible on λ sweep records but could be clearly identified on white-light pictures. Interestingly, these features either (a) constituted satellite umbrae located at the perimeters of major spots and within 10" of a magnetic "neutral line" or (b) directly bordered lengths of dark absorption material traversing individual spot groups making up the active center (i.e. were positioned along the locus of zero or of very low values of the longitudinal magnetic field).

These various observations appear to provide confirmatory evidence that local variations in magnetic fields underlying McMath 5265 were closely associated with flaring and support indications that there was indeed a causal relationship between the disappearance, or alteration in the appearance of, major umbrae (located beneath the common trigger region) and the occurrence of proton flares on 10, 14 and 16 July 1959. This interpretation is in accord with a report by Howard (1963) of a time-associated diminution in the total areas of various spot groups that produced cosmic-ray flares. Sawyer (1968) also discussed specific cases where a decline in sunspot area set in suddenly and immediately after certain flares. Among exceptions to these observations she notes that the sunspot group that produced the event of 2114 UT 16 July (after PCE flares on 10 and 14 July) reached its maximum area within a day after this GLE flare, declining thereafter. In the present text the parameter of change relevant to the 16 July event is individual sunspot rather than overall group area so that these reports are not in conflict.

5. APPLICATION OF THE PREDICTION TECHNIQUE

If the "recovery" of sunspots temporarily degraded during major proton flares, is to be used as a monitor in short-term forecasting of further proton events, then high-quality white-light pictures of the photosphere from a network of observatories throughout the world should be readily available for comparison with spectroheliographic data. When a proton flare occurs,

experienced solar astronomers at the station from which it is observed should make a composite drawing showing the positions of spots relative to important H α features so that the trigger region and its underlying spots can be identified. Information concerning this spot group, sent by standard encoded messages to observers in downstream time zones, would then advise that changes in relevant umbrae should be specially monitored. Situations where (within time scales probably of the order of hours to days) spots had aggrandized to their original condition should be considered particularly indicative of a "danger" situation for proton flaring, and under these conditions a special "alert" statement might be issued. It is the opinion of the author, based on observing many proton flares, that a particularly pregnant situation for proton production is one in which (as in the case of the 10, 14 and 16 July events) a satellite umbra underlying an especially flare active area is located close to the perimeter of a large variable sunspot with field strength at least >2000 G. This concurs with reports by Gopasyuk et al. (1965) and Rust (1968) of a general association between flaring and satellite sunspots.

The securing of white-light pictures at sufficiently close intervals to determine if spot changes begin before, during or after the flash phases of energetic flares is of course of enormous theoretical interest and it is strongly recommended that white-light photographs at a cadence sufficient to allow the relevant sequence to be determined should be taken by observers as a matter of standard procedure when filament activations, adjacent to known "trigger" regions, signal the build-up of magnetic instability within an active center.

6. MAJOR FLARE MORPHOLOGY AND ITS PREDICTION

It is of interest to note that the development of bright flare filaments extending outside the ambience of Mt. Wilson 14284 during the three proton flares described in Section 3 did not take place at random but was strongly influenced by circumstances relating to previously existing magnetic features. A close correlation is known to exist between the K plage and longitudinal fields of 20-200 G (Howard 1967; Bumba and Godoli 1968) while H α plages are identified as regions where the photospheric field strength is >80 G (Nakagawa et al. 1974). It consequently appears that the spread of extensive flaring in McMath 5265 was intimately associated with locations on the Sun where "moderate" solar magnetic fields were already present.

Also, individual flare filaments extended only towards the positions of outlying "satellite" sunspot groups. The three proton flares appeared to occur at times when these outlying satellite groups were changing. This may indicate that these events were associated with large-scale sub-photospheric disturbances. However, in no instance did emission spread from an outlying group towards the position of Mt. Wilson 14284 during the course of flaring and activity could take place "alone" in a distant group without apparently involving 14284 itself.

Emission appeared to spread during each flare to the positions of distant spot groups according to the following sequence: Group 14284 (initial flash); Group 14285, Group 14297; umbrae underlying chromospheric chain V* and Group 14292. These three events were "Homologous" as defined by Ellison et al. (1960), and the repeating sequence of flares, the first and third of which were 163.2 h apart, appears to have been a consequence of the enduring nature of the relationship between Mt. Wilson 14284 and its outlying "satellite" spot groups.** Owing to cloud gaps in the relevant records, it is not possible to establish if the times required to carry out the repeating sequence were similar in each case.

Interestingly, when less energetic events than the three proton flares mentioned were triggered in the same part of the active region, only the initial steps in the sequence were followed. This suggests that, rather than reflecting the presence of a large-scale sub-photospheric disturbance linking different parts of the active center, the development of bright filaments comprised a response to the occurrence of localized energy releases, the magnitude of which determined (according to a well-defined hierarchy) which bright filaments might form.

The observations further suggest that, in instances where individual magnetic elements within an active center maintain their relative strengths and positions over long periods, Homologous Flaring is possible and in such situations it is feasible (in principle) to anticipate the morphology of ensuing major events. It should however be noted that, in certain instances, even subflares in active regions may be associated with the occurrence of major solar energy releases (McKenna-Lawlor 1978b) so that the primary event in a series of energetic flares need not necessarily be one producing extensive bright filaments.

ACKNOWLEDGEMENTS

I am deeply indebted to Professor Helen Dodson Prince and to Professor Orren Mohler of the Astronomy Department, the University of Michigan for generously providing me with McMath-Hulbert spectroheliographic records of Region 5265, and to Dr. R. Howard (Mt. Wilson Observatory), Mrs. Ogir (Crimean Astrophysical Observatory) and the late William Baxter (Acton, London) for their individual gifts of white-light pictures of the underlying spot group.

* Cf. the drawings of Fig. 1 where this chromospheric feature is illustrated—underlying umbrae were not assigned a special group number by the Mt. Wilson observers.

** The longest time between Homologous Events previously known to the author is a 54 h interval between two 2b flares reported by White and Janssens (1970).

BIBLIOGRAPHY

- Bumba, V., and G. Godoli (1968): Correlation between calcium plages and longitudinal magnetic fields of the CSSAR active regions. Proc. I.A.U. Symp. No. 35, Ed. K.O. Kiepenheuer, D. Reidel Publ. Co., Dordrecht-Holland, p. 338.
- Bumba, V., L. Krivský, M.J. Martres, and I. Soru-Iscovi (1968): Flare activity and spotgroup development. Proc. I.A.U. Symp. No. 35, Ed. K.O. Kiepenheuer, D. Reidel Publ. Co., Dordrecht-Holland, p. 311.
- "Catalog of Solar Particle Events 1955-1969" (1975): Ed. Z. Švestka and P. Simon, Astrophysics and Space Science Library, Vol. 49, Publ. D. Reidel, Dordrecht-Holland.
- Dodson H.W., and E.R. Hedeman (1961): Photographic observations of certain flares associated with Polar Cap Absorption. Arkiv. Geofysik, 3, 469.
- Dodson, H.W., and E.R. Hedeman (1971): "An experimental Comprehensive Flare Index and its Derivation for 'Major' Flares 1955-1969". Report UAG-14, Solar World Data Centre A, NOAA, Boulder, Colorado, p. 25.
- Dodson, H.W., E.R. Hedeman, and O.C. Mohler (1973): "Comparison of activity in Solar Cycles 18, 19 and 20". Invited paper presented at the Symposium on Solar-Terrestrial Phenomena for Cycles 18-20. AGU Fall Annual Meeting, December 12, 1973 (private communication).
- Ellison, M.A., S.M.P. McKenna, and J.H. Reid (1960): "Light curves of 30 Solar Flares in relation to Sudden Ionospheric Disturbances". Dunsink Observatory Publications, 1, No. 1, p. 3.
- Ellison, M.A., S.M.P. McKenna, and J.H. Reid (1961): "Cosmic Ray Flares". Dunsink Observatory Publications, 1, No. 3, p. 54.
- Gopasyuk, S.I., M.B. Ogir, A.B. Severny, and E.F. Shaposhnikova (1963): The structure of magnetic fields and its variations in flare regions. Publ. Crimean Astrophys. Obs., 30. 15.
- Hale, G.E., and S.B. Nicholson (1938): Magnetic Observations of Sunspots. Carnegie Inst. Wash. Publ. No. 498, p. 692.
- Howard, R. (1963): On the relation of major flares with changes in sunspot areas, Astrophys. J., 138, 1312.
- Howard, R. (1964): Magnetic observations relating to Solar Flares. Proc. AAS-NASA Symp. on the Physics of Solar Flares. Ed. W.N. Hess, National Aeronautics and Space Administration, Washington, D.C., p. 89.
- Howard, R. (1967): Magnetic field of the Sun (observational). Ann. Rev. Astron. Astrophys., 5, 1.

- Howard, R., and H.W. Babcock (1960): Magnetic fields associated with the solar flare of July 16, 1959. Astrophys. J., 132, 218.
- Howard, R., and A. Severny (1963): Solar magnetic fields and the great flare of July 16, 1959. Astrophys. J., 137, 1242.
- Hyder, C.L. (1967a): A phenomenological model for Disparitions Brusques followed by flare like chromospheric brightenings, 1. Solar Phys., 2, 49.
- Hyder, C.L. (1967b): A phenomenological model for Disparitions Brusques followed by flare like chromospheric brightenings, 11. Solar Phys., 2, 267.
- Martres, M.J., R. Michard, I. Soru-Iscovisci, and T. Tsap (1968a): A study of the localization of flares in selected active regions. Proc. I.A.U. Symp. No. 35, Ed. K.O. Kiepenheuer, D. Reidel Publ. Co., Dordrecht-Holland, p. 318.
- Martres, M.J., R. Michard, I. Soru-Iscovisci, and T. Tsap (1968b): Étude de la localisation des éruptions dans la structure magnétique évolutive des régions actives solaires. Solar Phys., 5, 187.
- Martin, S.F., and H.E. Ramsey (1972): Early recognition of major solar flares in H α . Progress in Astronautics and Aeronautics, Vol. 30, Ed. P.S. McIntosh and M. Dryer, M.I.T. Press, Cambridge, Mass., p. 371.
- McCracken, K.G., and R.A.R. Palmeira (1960): Comparison of solar cosmic rays injection including July 17, 1959 and May 4, 1960. J. Geophys. Res., 65, 2673.
- McKenna-Lawlor, S.M.P. (1978a): "Chromospheric and Photospheric evolution of an extremely active solar active region in Cycle 19". (Accepted for publication as a special report by the National Oceanic and Atmospheric Administration, Boulder, Colorado.)
- McKenna-Lawlor, S.M.P. (1978b): Mass ejections accompanying the Flare of September 05, 1973. Report to the Skylab Flare Workshop.
- Nakagawa, Y., M.A. Raadu, and J.W. Harvey (1973): The topological association of H α structures and magnetic fields. Solar Phys., 30, 421.
- Nagata, T., Hakura, and T. Goh (1960): Ionospheric Black Out in the Polar Regions during July 1959 events. Proc. Symp. on the July 1959 events and associated phenomena, Helsinki, Union Géodésique et Géophysique Internationale, Monographie No. 7 (Imprimé par l'Institut Géographique National Paris), p.135.
- Nagata, T., and M. Kodama (1960): Cosmic Ray increases on July 16-17, 1959. Proc. Symp. on the July 1959 events and associated phenomena, Helsinki, Union Géodésique et Géophysique Internationale, Monographie No. 7 (Imprimé par l'Institut Géographique National, Paris), p. 28.
- Ribes, E. (1969): Study of the correlation between flares and the evolution of magnetic field. Astron. Astrophys., 2, 316.

- Rust, D.M. (1968): Chromospheric explosions and satellite sunspots. Proc. I.A.U. Symp. No. 35, Ed. K.O. Kiepenheuer, D. Reidel Publ. Co., Dordrecht-Holland, p. 77.
- Sawyer, C. (1968). Sunspot changes following proton flares. Proc. I.A.U. Symp. No. 35, Ed. K.O. Kiepenheuer, D. Reidel Publ. Co., Dordrecht-Holland, p. 543.
- Smith, H.J. (1963): A continuous solar movie. Sky and Telescope, Vol. XXV, No. 1, p. 19.
- Smith, S.F. (1971): $H\alpha$ structures and small-scale magnetic field configurations. Proc. I.A.U. Symp. No. 43, Ed. R. Howard, D. Reidel Publ. Co., Dordrecht-Holland, p. 323.
- Smith, S.F. and H.E. Ramsey (1964): The flare associated filament disappearance. Z. Astrophys., 60, 1.
- Steshenko, N.V. (1967): Magnetic fields of small sunspots and pores. Izv. Krym. Astrofiz. Obs., 37, 21.
- "Symposium on the July 1959 events and associated phenomena", Helsinki, Union Géodésique et Géophysique Internationale, Monographie No. 7 (Imprimé par l'Institut Géographique National, Paris).
- White, K.P. III, and T.J. Janssens (1970): An example of radio and optical homologous flares. Solar Phys., 11, 291.

LEGEND TO FIG. 1(a-c)

Series of composite drawings made from $H\alpha$ and K spectroheliograms showing spot groups, chromospheric chains, flare sensitive areas and dark absorption material pertaining to McMath Region 5265 on days 9, 10, 13, 14, 16 and 17 July 1959. North is at the top and East is at the left of the diagram.

Spot groups and regions of bright emission in the chromospheric network are drawn as they appeared on K spectroheliograms. Filamentary material was generally more clearly visible on $H\alpha$ than on K spectroheliograms and is thus drawn as it appeared on such pictures.

Spot Umbrae are shown in black and penumbral borders are indicated by a "fringed" continuous line.

Regions of bright emission in the chromospheric network are shown enclosed within a continuous line interspersed with black circles. Individual lengths of the network are designated by roman numerals.

The positions of individual flare sensitive areas are indicated by lower-case letters with added roman subscripts and/or superscripts.

Faint dark filaments are shown enclosed within a continuous line. Well-defined dark filaments are shown enclosed within a continuous line and stippled.

Amorphous dark material is hatched diagonally.

Polarities and magnetic field strengths in units of 100 G as determined at Potsdam or Mt. Wilson are shown for individual umbrae (10, 13, 14 July Potsdam measures; 16, 17 July Mt. Wilson measures).

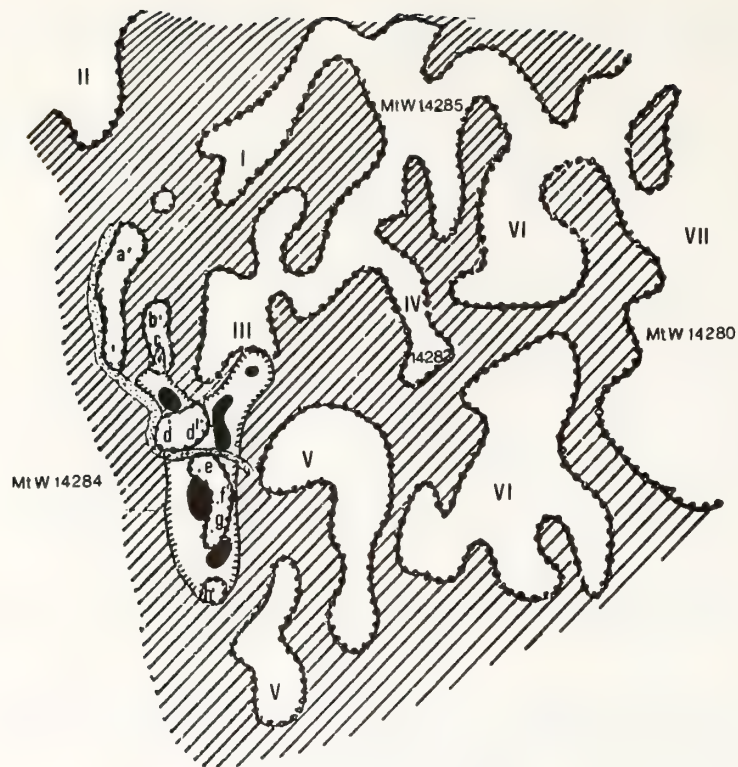


FIG. 1a - COMPOSITE DRAWINGS OF McMATH REGION 5265 FOR 09 JULY (TOP) AND 10 JULY (BOTTOM) 1959.

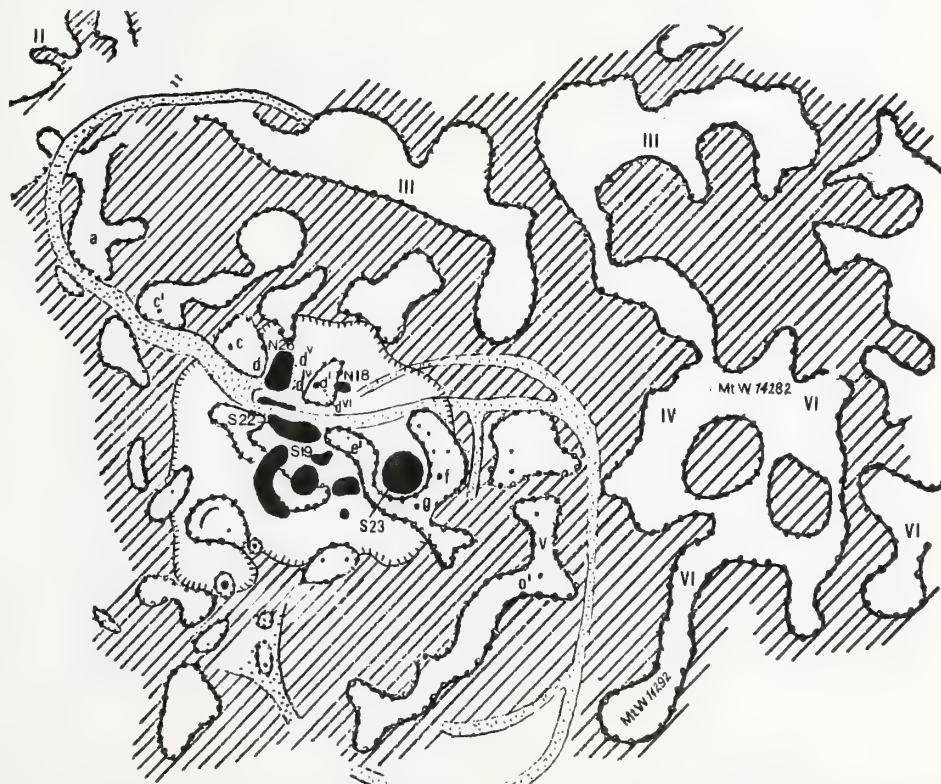


FIG. 1b - COMPOSITE DRAWING OF McMATH REGION 5265 FOR 13 JULY (TOP) AND 14 JULY (BOTTOM) 1959.

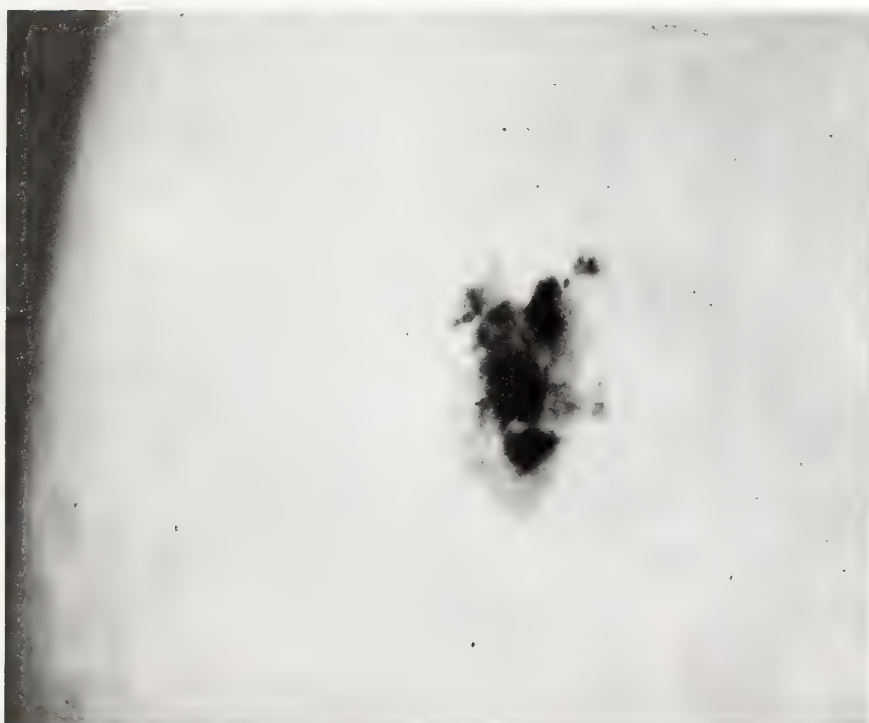


PLATE 1. WHITE LIGHT PHOTOGRAPHS OF MT. WILSON GROUP 14284 TAKEN BY
W.M. BAXTER AT 09^h15^m UT 09 JULY (TOP) AND AT 09^h45^m UT
10 JULY (BOTTOM) 1959.
C - 29

FORECASTING OF SOLAR FLARES
BASED ON MAGNETIC FIELD CONFIGURATIONS

Karen L. Harvey*
Solar Physics Research Corporation
4720 Calle Desecada
Tucson, Arizona 85718 USA

and

Sara F. Martin
San Fernando Observatory
California State University, Northridge
14031 San Fernando Road
Sylmar, California 91342 USA

Magnetic field configurations observed in the daily Kitt Peak magnetograms were used in making *ex post facto* predictions of intervals of solar flare activity during a three-month period in 1973 coinciding with ATM observations. The predictions consisted of specifying the locations within active regions where flares were anticipated for intervals of one or more days. Using this approach, we failed to predict 16% of the 466 subflares and 41% of 17 of the major flares (importance 1 or greater) occurred. We overspecified flaring intervals by 35%.

After the prediction phase of this study, we reviewed the number of times that various magnetic field configurations did and did not produce flares and defined a "relative flaring index" for given magnetic field configurations. The relative flaring index is the ratio of flares produced to the total number of times a given pattern or change was noted in the three-month interval of this study. Confirming the work of previous authors we found that the types of magnetic field configurations that yield the highest flaring index are reversed polarity regions, satellite poles around sunspots and new regions interacting with old regions. All types of emerging flux regions yielded a high flaring index only if the rate and duration of the emergent flux was great. Location of the emergent flux in relation to pre-existing flux also seemed to be an important factor in flare occurrence.

We further examined the magnetic field configurations where flares occurred and were not predicted. In a significant number of these situations,

*Consultant, California State University, Northridge and Visiting Astronomer, Kitt Peak National Observatory, operated by the Association of Universities for Research in Astronomy, Inc., under contract with the National Science Foundation.

significant emerging flux in neighboring areas was observed. This suggests that the evolution of interacting flux regions is an important factor in flare occurrence, over larger areas and involving older fields than we had anticipated at the outset of this study.

1. INTRODUCTION

If a build-up of magnetic energy precedes flares and if this build-up results in the development of identifiable photospheric magnetic field configurations, then it is reasonable to anticipate that solar flares may become predictable hours to days in advance of their occurrence. Many photospheric magnetic field configurations and parameters are already known to be correlated with flares, as discussed in reviews by McIntosh and Dryer (1972), Rust (1973), 1976a, b), Svestka (1976), Neidig (1977), and Martin (1979). This investigation was an attempt to learn more about the preflare state by testing our ability to forecast flares "*ex post facto*" based upon the known correlations between flares and magnetic field configurations. Our specific goals were: (1) to ascertain how well the positions and times of flares could be predicted *ex post facto*, (2) to identify the magnetic field configurations most frequently associated with flares during an interval in 1973, (3) to search for additional magnetic field parameters useful in future forecasting, (4) to test the utility of the Kitt Peak daily magnetograms in flare forecasting, and (5) to define preflare magnetic field conditions which need additional study.

This investigation proceeded in three consecutive steps: (1) A detailed study of the magnetic field configuration and evolution of active regions was made by one of us independent of knowledge of the flare activity which occurred in the regions. Predictions were made of the locations where flares would occur within active regions and of the days on which flares would occur. For two and one-half of the three months the predictions also specified whether only subflares were expected or whether flares equal to or greater than importance 1 would also occur. (2) A comparison was made of the observed flare data with the magnetic field data to determine the successfulness of the predictions and to learn what configurations and changes of the field were characteristic at the flare locations in the study. (3) The magnetic field data was reexamined to determine how often these magnetic field configurations and changes, associated with flares, are observed without flares.

2. OBSERVATIONS

The magnetic field data used in this study were the full-disk observations of the longitudinal-component of the photospheric magnetic field of the sun taken daily at Kitt Peak National Observatory using the 40-channel magnetograph. The spatial resolution of the magnetograms is 5 arc-sec with a noise level of about 10 G per resolution element. The magnetic field data is

displayed in pictorial form, with intensity proportional to magnetic field strength. From a grey level equalling zero gauss, increasing field strengths of the opposite polarities approach black and white.

The H α photographic observations of the sun used in our analysis are the flare patrol films from the Observatory Network of the NOAA Space Environment Services Center operated jointly with the Air Force Air Weather Service. Thirty-five mm copies of the H α films, borrowed from the Space Physics Laboratory at Aerospace, were used to identify flares with the aid of a list of flares reported during this period (Hirman et al., 1977). The H α films were used to determine the flare configurations, their precise locations in the active regions, and the nature of associated activity, information not available from the flare list. The films also allowed us to confirm the occurrence, times, and importance ratings of flares reported in the flare list. All reported subflares were included in this study. Flare drawings were made to the same scale as the full-disk magnetograms. Comparison of the flare data with the magnetic field was easily made by superimposing these two sets of data.

The flare forecast and analyses were made for the period from 14 June 1973 to 11 September 1973. Because of strong geometric effects in the magnetic field data as the regions neared the limb, the analysis was restricted to regions located within 60° of central meridian. The final data sample included a total of 501 flares which occurred in 48 of the 57 active regions observed and studied during this three-month period. Of the 501 flares, six (6) were of importance 2 or greater, 29 were of importance 1, and the remaining 466 were subflares. Based on the Skylab flare reports by Hirman et al. (1977), only 256 of the 501 flares in our data sample were associated with reported X-ray bursts. Only one (1) event was classed as X, 11 were of magnitude M, 9 events were of magnitude C5-C9 and the remaining 225 events C0-C4.

3. *EX POST FACTO* PREDICTIONS AND ANALYSIS

The parameters used in the predictions are listed in Figure 1 and Table 1. These constitute all of the identifiable configurations in the line-of-sight components of the photospheric magnetic fields of active regions which are known by us to be correlated with flares. Evolutionary patterns related to flare occurrence (Martres et al., 1971) could not be considered without having better time resolution than afforded by one magnetogram per day.

For each region studied, a graphical representation was made indicating the periods of time, shown by bars, that any of the flare-related configurations were present, as in the example in Figure 1. The development or decay of a particular configuration was indicated by an increase or decrease in the width of the bar. If more than one configuration parameter was present at a site, a bar was drawn for each parameter observed. The predictions were made by underlining the periods of time for the specific configurations (locations) where flares were anticipated. Subsequent to making the predictions of flare

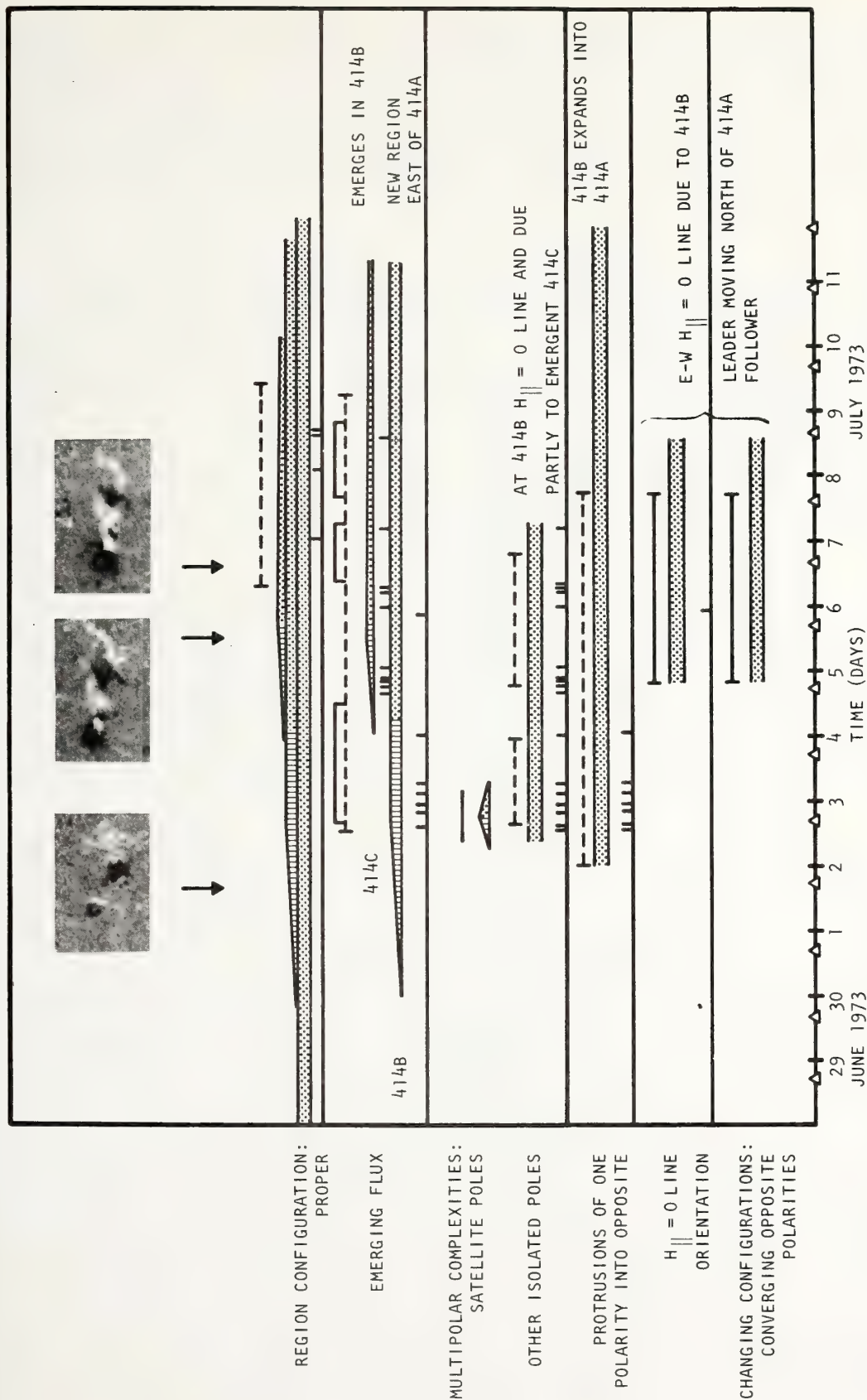


Figure 1. Graphic representation of the magnetic field analysis of McMath Region 12414. The bracketed dashed lines seen above the designated field configurations found in the region indicate periods of predicted flare activity. The solid lines indicate a prediction of the occurrence of flares of importance 1 or greater. The vertical lines (subflares, short; importance 1 or greater, longer) indicate the occurrence of a flare.

periods and locations, the times and locations of all observed flares were added to the graphs.

We predicted flaring (one or more flares) to be restricted to 80 areas located within 36 active regions. Sixty-nine (86%) of the predicted areas flared, while 11 (14%) did not. The 11 areas that did not flare were generally small-scaled anomalies in the magnetic field such as the eruption of new (and a relatively small amount of) flux at the periphery of a decaying active region.

In addition to the 69 flaring sites which we predicted, 23 areas were observed to flare where we failed to predict any flare activity. Five of these areas were at a location on the solar disk where geometrical effects allowed no meaningful interpretation of the magnetic field data and one area occurred in a sunspot umbra. The magnetic field characteristics of the remaining 17 areas of flare activity fall into four categories: (1) old region fields where, in some cases, the flares occurred at the time of rapid growth of newer regions in their vicinity (7 cases), (2) the close approach of weak network flux (3 cases), (3) no observable magnetic field anomaly; we generally found only one polarity at these locations (4 cases), and (4) the failure to identify a flare-associated configuration (3 cases).

For two and one-half months (14 June-31 August) of the three months covered by this study, the predictions specified whether major flares (importance 1 or greater) were anticipated in addition to subflares. During the interval, 8 of 40 regions were predicted to have flares equal to or greater than importance 1. Four (50%) of these regions had major flares within three days of the start of the predicted interval. The other four regions had no major flares although they were characterized by substantial numbers of subflares and X-ray events.

Five regions produced seven major flares that were not predicted. All of these flares occurred in decaying magnetic regions and were associated with the sudden disappearance (presumed eruption) of a filament.

Because of the time resolution of the magnetic field data (one map per day), we made no attempt to predict the occurrence of individual flares but instead we defined periods of days when we felt flares (one or more) were likely to occur. Of the 417 flares which occurred in the 80 predicted flaring areas, 408 (98%) occurred within the predicted periods of activity. Five flares occurred ± 1 day outside the predicted intervals; three flares occurred ± 2 days outside of the predicted interval and one occurred at greater than two days outside the predicted period. While these statistics seem very good it must be kept in mind that we failed to predict the occurrence of 84 of the 501 flares in our original flare sample and 7 of these 84 flares were of importance 1 or greater. Although we apparently can predict flare sites over 85% of the time and periods of flare activity within those sites over 95% of the time, we cannot yet ascertain in advance when and where all flares will occur.

A comparison has also been made of the start and end of observed flaring with the start and end, respectively, of the predicted period of flaring. In

Figure 2 is a histogram showing the distributions of this comparison. It is apparent from the graph that we can predict quite well to within one day when flare activity may start. In only 14 of 69 (20%) flaring intervals, did we anticipate the start of flaring too early by 1 to 3 days. The end of the flaring interval was more difficult to predict than its start. In about 1/3 (36%) of the cases we have over-estimated the end of the flaring interval and in another 8% of the intervals have we under-estimated the end of the interval of flaring by 1 to 3 days.

Another way to evaluate the accuracy of our predictions of intervals of flare activity is to compare the total number of days on which flares did and did not occur in the predicted intervals. Counting each prediction within

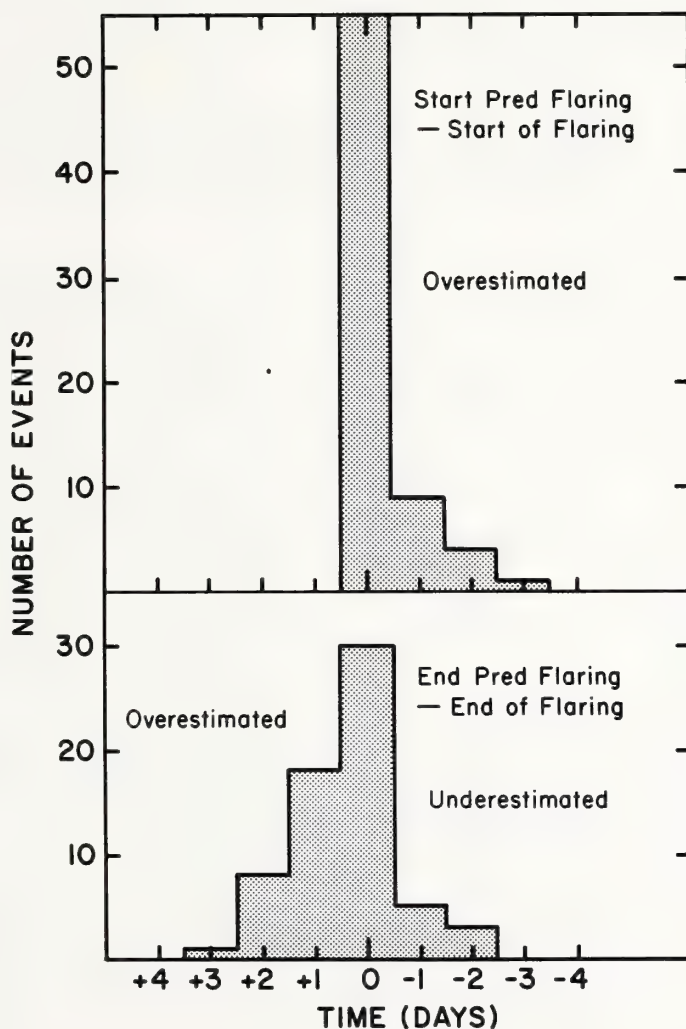


Figure 2. Comparison of the start and end of predicted periods of flaring with the start and end of periods of observed flaring.

each active region separately, there was a total of 208 flare prediction days. Flares actually occurred on 135 (65%) of the flare prediction days, while on 75 (35%) of the flare prediction days, no flares occurred.

4. FLARE OCCURRENCE IN RELATION TO MAGNETIC FIELD CONFIGURATION AND EVOLUTION

For each flare, predicted or not, the characteristics of the field were noted. The results of this analysis are shown in column 1 of Table 1. A single flare or active region may be tallied under more than one category if more than one flare-correlated characteristic is present at a flare site. A flare, for example may be located in an active region exhibiting strong gradients and an area of emerging flux.

We subsequently re-examined the magnetic field data looking for the same magnetic field configurations and changes as listed in Table 1, but which were not associated with flares. These results are listed in column 2 of Table 1.

Column 3 in Table 1 gives the total number of flares observed in the active regions during the interval of time covered by our study. The last column labeled "Relative Flaring Index" is the number of flares in column 3 divided by the sum of the numbers in each row in columns 1 and 2. This index is a measure of the relative frequency that flares will occur in relation to the number of times that a particular magnetic field characteristic is observed. It is clear that reversed polarity regions and highly inclined regions have a much higher flare index than all other configurations. (Reversed regions are those in which the dominant areas of opposite polarity are reversed east for west from the pattern known as the Hale Law of Sunspot Polarities, and represent the dominant orientations existing for the majority of regions for each solar cycle and hemisphere. "High inclination" regions are those in which a line drawn between the centroid of the opposite polarities is highly inclined ($> 45^\circ$) relative to parallels of latitude.) Although our sample of reversed and highly inclined regions is small (6 regions), this result is in complete agreement with the finding of Smith and Howard (1966) that reversed polarity regions were the most flare productive of all of their magnetic classes of active regions.

Because we have studied to date only a relatively small sample of data, we have not yet performed statistical analyses to determine the probability of flare occurrence given a particular magnetic field configuration or change. However, the data reveals a number of interesting facets. Next in flare production to reversed polarity or highly inclined regions are the satellite fields around sunspots, interacting active regions, and simply the emergence of some new regions. The latter requires some interpretative comments since it is clear that not all emerging flux is related to high flare incidence. It appears that just the emergence of new flux, either as a new region or a new region within an existing active region, is not a sufficient condition for flare production. Seven of the 25 new regions produced no flares and

TABLE I

Magnetic Field Characteristics	No. of Occurrences		No. of flares	relative† flaring index
	with flares	without flares		
1. Emerging Flux				
1.1 New active region	18	7	105	4.2
1.2 New region in existing region	20	7	145	5.4
2. Multipolar Complexities				
2.1 Satellite poles	14	6	71	3.6
2.2 Other isolated poles	59	0	119	13.2
3. Interacting Regions				
3.1 Old region near a new region	3	0	10	3.3
3.2 Other interacting regions	7	0	20	2.9
4. Protrusions of One Polarity into Opposite				
4.1 Minor protrusions	7	0	25	3.6
4.2 Major protrusions	3	0	10	3.3
5. $H_{ } = 0$ Line Orientation: east-west sections or abrupt changes in direction	12	1	47	3.6
6. Obviously Changing Configurations				
6.1 Steepening gradients*	10	0	61	6.1
6.2 Relative motion of opposite polarities*	7	0	29	4.1
7. Reversed or Highly Inclined Configurations	6	1	119	17.0
8. Old, Relatively Static Regions	7	7	17	1.3

$$\dagger \text{Relative Flaring Index} = \frac{\text{Number of flares}}{\text{Number of occurrences with flares} + \text{occurrences without flares}}$$

*Excludes normal evolutionary changes observed in regions.

similarly seven of the 27 eruptions of new flux within active regions resulted in no flares. All of these flux eruptions were small and persisted 1-2 days. Conversely, all of the flux eruptions positionally associated with flares were larger and were observed over much longer periods of time. The amount of flux erupting and the rate of flux emergence definitely seem to be important factors in whether or not a flare will occur.

The position of the emerging flux within an existing region also appears to be a significant factor in flare production. The eruption of flux at the $H_{||} = 0$ line or near a sunspot is more likely to result in flare activity than when the flux emergence takes place elsewhere in the region. Satellite sunspots or areas of opposite polarity adjacent to sunspots, for example, are strong producers of flares. Seventy-one flares were observed in 14 satellite sunspots noted during our observations. And those were always associated with surge activity. Similarly, the appearance of a complex magnetic field with the presence of isolated opposite polarity poles near an $H_{||} = 0$ line (9 cases), often the result of newly emerging flux, is related to high flare incidence (119 flares).

A particularly significant finding is that the eruption of a new active region in close proximity of another region also appeared to result in increases in flare productivity. In our 3 month data sample, there were 11 cases of new regions developing near existing regions. In 4 of the 11 cases, the pre-existing region was relatively old while in the other 7 cases, the earlier formed active regions were near or only slightly past their maximum development. During the developing phase of the new regions in 10 of these 11 cases, 30 flares occurred in the adjacent regions (category 3 in Table I). Only one of the pre-existing older regions, failed to produce any flares within the growth phase of the adjacent new region.

Some of the larger flares observed during our period of study occurred in regions having magnetic characteristics of regions which typically do not flare very often (category 8 in Table I), such as simple bipolar or old active regions. Three such simple bipolar regions were among the 4 mentioned in the preceding paragraph as being relatively old regions in the vicinity of new active regions. Ten flares occurred in these 3 old active regions within 1 or 2 days after the birth of the new regions (3.1 in Table I). Six of the 10 flares were known to be associated with "disposition brusques". All of the 10 flares were "two-ribbon" flares. These associations suggest to us that the interaction of active regions noted to be significant in Table I for closely spaced regions may also be important to flare occurrence even when one of the interacting fields is an old active region. From new knowledge of the apparent reconnecting field lines in the solar corona associated with developing active regions (Sheeley et al., 1975), we suggest that magnetic field reconnection is a mechanism which may be related to the triggering of flares in neighboring magnetic regions. Consequently, with further research many of the types of flares that we failed to predict in this study could become predictable in the future. EUV and X-ray images of the solar corona also may be particularly useful in future forecasting of flares in weak field regions.

5. CONCLUSIONS

We have found the Kitt Peak daily magnetograms to be very useful in defining the intervals of time and locations where flares may be predicted *ex post facto*. We overestimated the start of flaring intervals by 1 to 3

days less than 20% of the time, although we mis-estimated the end of flaring intervals by 1 to 3 days about 36% of the time. In some of the cases where we failed to predict flares, we found evidence that substantial emerging flux regions in neighboring areas may be associated with these flares. This appears to be a promising subject for further research on preflare conditions.

The magnetic field characteristics most frequently associated with flares were reversed polarity or highly inclined regions, satellite fields around sunspots, strong isolated poles near an $H_{\parallel} = 0$ line, interacting active regions, and regions with a substantial amount of emerging flux. Since these results are based only on the configurations and changes evident in daily magnetograms, we suggest that further research on the relationship of flares to all of these configurations would be profitable using magnetograms of higher time and spatial resolution.

6. ACKNOWLEDGMENTS

We wish to thank Dr. J. Harvey and the Kitt Peak National Observatory for making available to us the 1973 full disk magnetograms. We also thank R. Broussard at the Aerospace Corporation for the loan of the 35 mm copies of ATM ground based H_{α} observations used in this study and L. Hermans for assisting in the flare reduction. This work was supported in whole by the Air Force Office of Scientific Research under grant number 76-3068 and subsequent AFOSR Contract F49620-78-C0025.

REFERENCES

- Hirman, J., Losey, R., and Heckman, G. (1977): A compilation of solar flares reported during the skylab mission. NOAA Memorandum, August, 1977.
- Martin, S. F. (1979): Preflare conditions, changes and events. Solar Phys. in press.
- Martres, M. J., Soru-Escout, I. and Rayrole, J. (1971): An attempt to associate observed photospheric motions with the magnetic field structure and flare occurrence in an action region. In: Solar Magnetic Fields, R. Howard (ed.). IAU Symp. 43:435.
- McIntosh, P. S. and Dyer, M., eds. (1972): Solar activity observations and predictions. Progress in Astronautics and Aeronautics, Vol. 30.
- Neidig, D. F. (1977): Parameters used in the prediction and evaluation of flares. Preprint.

- Rust, D. M. (1973): Estimating the flare-production potential of solar active regions from analysis of real-time magnetic field data. AFCRL Environment Research Paper No. 440.
- Rust, D. M. (1976a): Flares, observations of flare-associated magnetic field changes. Phil. Trans. Royal Soc. London, Series A, 281:427.
- Rust, D. M. (1976b): An active role for magnetic fields in solar flares. Solar Phys. 47:21.
- Sheeley, N. R., Bohlin, J. D., Brueckner, G. E., Purcell, J. D., Scherrer, V. E., and Tousey, R. (1975): The reconnection of magnetic field lines in the solar corona. Astrophys. J. 196:L129.
- Smith, S. F. and Howard, R. (1966): Magnetic classification of active regions. In: Structure and Development of Solar Active Regions, K. O. Kiepenheuer (ed.). IAU Symp. 35:33.
- Svestka, Z. (1976): Solar Flares, D. Reidel Publ. Co., p. 18.

PHOTOSPHERIC VELOCITY FIELDS AS INDICATORS OF FLARE ACTIVITY

K. Harvey*
Solar Physics Research Corporation
4720 Calle Desecada
Tucson, Arizona 85718 USA
and
J. Harvey
Kitt Peak National Observatory**
950 N. Cherry Avenue
Tucson, Arizona 85726 USA

The photospheric line-of-sight velocity field of 24 active regions was examined in relation to the flare activity of the regions. There is a good correlation between the complexity of the velocity field and the level of flare activity in the active region within ± 12 hours. Specific velocity patterns could be recognized at 55 of 73 flare sites. Failure to detect patterns at all but one of the remaining flare sites can be understood as due to unfavorable geometry for the detection of the patterns. The specific velocity patterns found at flare sites consist of anomalous Evershed flow patterns in sunspot penumbras (12 of 55 sites); small-scale, multipolar velocity structures (15 of 55 sites), and apparent horizontal shears of the velocity field (48 of 55 sites). The shears are frequently but not necessarily associated with magnetic polarity reversal lines. There appears to be a better relation between flare activity and the spatial extent of a velocity shear line than with the strength of the shear. As an aid to predicting the level of flare activity, the velocity complexity of an active region appears to be a practical and valuable parameter. Observations of velocity shears appear to be useful in locating potential flare sites and in estimating the potential size of the flares.

1. INTRODUCTION

Velocity fields are generally considered to be important in the process of energy buildup leading to flares, but little observational work has been done on this possible relationship. In a previous study of a single active region (Harvey and Harvey, 1976), we found that flares tended to occur where

*Visiting Astronomer, Kitt Peak National Observatory.

**Operated by the Association of Universities for Research in Astronomy, Inc., under contract with the National Science Foundation.

both the velocity and magnetic fields were unusually complex. In particular, flares were found to begin close to locations with inferred strong horizontal velocity shears at the magnetic neutral line. Flare sites and shapes conformed to areas with low line-of-sight velocity surrounded by higher velocities.

In similar but more comprehensive studies, Martres et al. (1971, 1974, 1977) concluded that flares occur at locations where lines separating opposite line-of-sight velocity and magnetic components ($V_{11} = 0$, $H_{11} = 0$) cross. They also inferred that a horizontal vortex motion, concurrent with a magnetic field change at or near the $H_{11} = 0$ line, is a necessary condition for flares to occur.

This study is aimed partly at verifying the conclusions of earlier investigations with superior observations but mainly to address three specific questions: 1. Are there any significant differences in the velocity patterns of active regions with and without flare activity? 2. Do locations of anomalous velocity patterns correlate well with flare locations? 3. Can observations of velocity fields be used to improve predictions of flare activity? We provisionally conclude that the results of previous studies require some modifications and that the answer to all the specific questions is yes.

2. OBSERVATIONS

Observations of 24 flaring and non-flaring active regions for periods of 1 to 4 days were made with the 512-channel magnetograph (Livingston et al., 1976) at the 70-cm Vacuum Telescope of the Kitt Peak National Observatory. The observations consisted of digital photoelectric recordings of the intensity, Doppler shift, and longitudinal Zeeman effect of the photospheric 8688 Å Fe I line with a spatial element of 1 arc second, a spatial extent of between 512 by 512 arc seconds and 512 by 240 arc seconds, and a time cadence of from 75 to 150 seconds.

As usual, the observed Doppler shift is interpreted as representing the average line-of-sight velocity field in a resolution element although we recognize that line profile variations and line-of-sight integration effects make this simple interpretation somewhat suspect. Similarly, we interpreted the longitudinal Zeeman effect as directly indicating the line-of-sight component of the magnetic field although line-profile variations also complicate this simple interpretation. In our opinion, the errors caused by simple interpretations do not compromise the results of this study.

Although most of the observations were made away from the disc center, the 5-minute photospheric oscillation was still a major source of noise which must be suppressed. Several techniques for suppressing the 5-minute oscillation were tried. The simplest technique was to average observations made 150 seconds apart in time. This method is far from optimum but does reduce the effects of the oscillation to a considerably smaller level. The technique finally developed consists of taking observations at approximately 75 second intervals and producing weighted averages of groups of 8 such observations.

The weights are chosen to approximate a sinc function in time such that the response to temporal variations is essentially zero for variations with periods less than about 6 minutes. This technique removes virtually all traces of the 5-minute oscillations. The magnetic and intensity data were also processed by the same averaging techniques to preserve comparability with the velocity data. The averaging process generally reduced spatial resolution to several arc seconds although seeing was good enough in a few cases to preserve 2 arc second resolution.

Pertinent observational information is collected in Table I. We have included both the McMath and Boulder region numbers and note that many of the McMath regions are identified by Boulder as complexes of two or more regions.

A preliminary list of flares associated with each active region was compiled from reports to the NOAA Space Environment Laboratory and from the weekly NOAA Preliminary Report of Solar Geophysical Data. This list was augmented by examination of H α patrol films generously lent by NOAA, Boulder, and the Big Bear Solar Observatory. For three of the regions, high-resolution H α films were lent by Big Bear Solar Observatory and San Fernando Observatory. When possible, published data were compared with the films and found to be generally consistent which gives us confidence in the quality of the published data. A major defect in this study is the inadequate flare patrol coverage available and the resulting uncertainty about exact levels of flare activity and flare locations. Nevertheless, the results should be significant in relative and statistical senses. No efforts were made to correct for incomplete flare data.

3. RESULTS

3.1 Velocity Complexity and Flare Activity

As shown in Table I, we arbitrarily selected time intervals of 24 hours centered on each series of velocity observations to establish flare activity levels. Within these time intervals a total of 232 flares, from subflare class to importance 4B, occurred at 73 sites in 18 of the 24 active regions. The remaining 6 regions were old active regions and produced no flares within ± 12 hours of the velocity observations.

Classification of the velocity field is a more subjective procedure which requires elaboration. The simplest velocity patterns we observed in active regions (after suppressing the 5-minute oscillation) consisted of only normal Evershed effect in the sunspot penumbras (if sunspots were present); otherwise the active region was indistinguishable from the quiet sun. Next in complexity is an active region which shows normal Evershed velocities in penumbras and additional structure outside sunspots, but the additional structure is significantly weaker in magnitude than the Evershed velocities. The most complex regions show abnormal Evershed velocities in sunspots and velocities outside sunspots which can rival or exceed the Evershed velocity magnitude. This classification is illustrated in Figure 1.

TABLE I
Ledger of observations

McMath	Region Boulder	Date Observed (1978)	Time Observed (UT)	Region Position	Mag Class ¹	Vel Class ²	Flaring Level	Number of Flares		Major > IMP 2
								±12 Hrs	±3 Hrs	
15266	1092	4-28	2319-22	N25E37	δ+βp	C	High	11	4	4B 1308+
15403	1203	7-11	1734-1821	N18E41	δ	C	High	20	8*	2B 1049 & 2215
15525	1284	7-13	1549-1846	E16	δ	C	Moderate	23	14*	
		7-14	1808-2103	E03	δ	C	Moderate	23	13*	
		9-7	1704-07	N33E55	β	A	Moderate	9	5	
		9-8	1604-07	E46	β	A	Low	4	3	
		9-9	1740-43	E34	β	Q	Quiet	1	1	
15509	1272	9-10	1548-51	E25	β	Q	Low	3	0	
		9-7	1713-16	S32W28	β	A	Low	10	3	
		9-8	1620-23	W42	β	A	Low	7	5*	
		9-9	1749-51	W55	β	A	Moderate	10	3	
		9-10	1554-57	W65	β	Q	Low	2	2	
15526	1282	9-7	1713-16	S23W32	β	A	Low	11	6	
		9-8	1620-23	W44	β	A	Moderate	7	5*	
		9-9	1749-51	W56	β	Q	Quiet	1	0	
		9-10	1554-57	W69	β	A	Low	3	3*	
		9-21	1901-16	N36W29	βγ	A	Moderate	16	9*	
15543	1294	9-22	1754-1809	W43	βγ	A	Low	5	3*	
		9-23	1613-28	W53	β	A	High	9	0	
		9-21	1901-16	N28W38	αp	Q	Quiet	0	0	
		9-22	1754-1809	W58	αp	Q	Quiet	3	0	
		9-23	1613-28	W67	αp	Q	Quiet	2	0	
15532	1287	9-21	1901-16	N37W43	αp	Q	Quiet	0	0	
		9-22	1754-1809	W59	αp	Q	Low	2	2	
		9-23	1613-28	W72	αp	Q	Quiet	0	0	
		10-17	1538-49	N31E40	β	A	Low	3	1	
		10-18	1637-48	E24	βγ	A	Low	2	0	
15598	1351	10-17	1538-49	N20E32	αp	Q	Low	2	0	
		10-18	1637-48	E17	αp	Q	Quiet	0	0	
		10-17	1551-1601	S22W10	β	Q	Quiet	1	0	
		10-18	1650-1700	W23	β	Q	Low	5	0	
		10-18								

3B 0947+

TABLE 1 - continued

Region		Date Observed (1978)	Time Observed (UT)	Region Position	Mag Class ¹	Vel Class ²	Flaring Level	Number of Flares	
McMath	Boulder							±12 Hrs	±3 Hrs
									Major > IMP 2
15587	1346	10-17	1605-17	S20W50	β	A	Low	7	4
		10-18	1703-13	W65	β	Q	Quiet	0	0
15587	1344	10-17	1605-17	S24W52	α	Q	Quiet	0	0
		10-18	1703-13	W67	-	Q	Quiet	0	0
15587	1335	10-17	1605-17	S20W62	αp	Q	Quiet	1	0
		10-18	1703-13	W77	αp	Q	Quiet	0	0
15587	1352	10-17	1605-17	S21W57	-	Q	Quiet	0	0
		10-18	1703-13	W73	-	Q	Quiet	0	0
15586	1336	10-17	1605-17	S31W62	-	Q	Quiet	0	0
		10-18	1703-13	W75	-	Q	Quiet	0	0
15631	1371	10-26	1834-1921	S13E81	β	Q	Quiet	0	0
		10-27	1734-43	E65	αp	Q	Quiet	0	0
		10-28	1531-40	E54	αp	Q	Quiet	0	0
15619	1365	10-28	1745-1852	N20E05	βγ	Q	Moderate	4	1
15619	1370	10-28	1745-1852	N24W01	β	Q	Low	0	0
15620	1366	10-28	1907-16	S19E13	αp	Q	Low	1	0
15621	1367	10-28	1907-16	S24E03	-	Q	Low	1	1
15641	1382	11- 4	2039-2108	S11E38	β	A	Low	8	4
		11- 5	1957-2006	E25	βγ	A	Low	7	5*
15642	1374	11- 4	2116-34	S26E01	β	Q	Quiet	2	1
		11- 5	2009-35	W11	β	Q	Quiet	2	0
15642	1381	11- 4	2116-34	S18W10	β	Q	Quiet	0	0
		11- 5	2009-35	W24	β	Q	Low	4	2

1. Mt. Wilson magnetic classification.

2. C = complex, A = active, Q = quiet. See Section 3.1 for definition of velocity complexity.

* Flare or flares occurred during velocity observations.

+ Proton flare.

Flaring Level { High: 1-3 IMP > 2 flares per day with M/X level X-rays.
 Moderate: 7-15 flares per day with > 1 IMP 1 flare, C/M level X-rays.
 Low: 1-8 subflares per day, C level X-rays.
 Quiet: ≤ 1 subflare per day, no X-ray events.

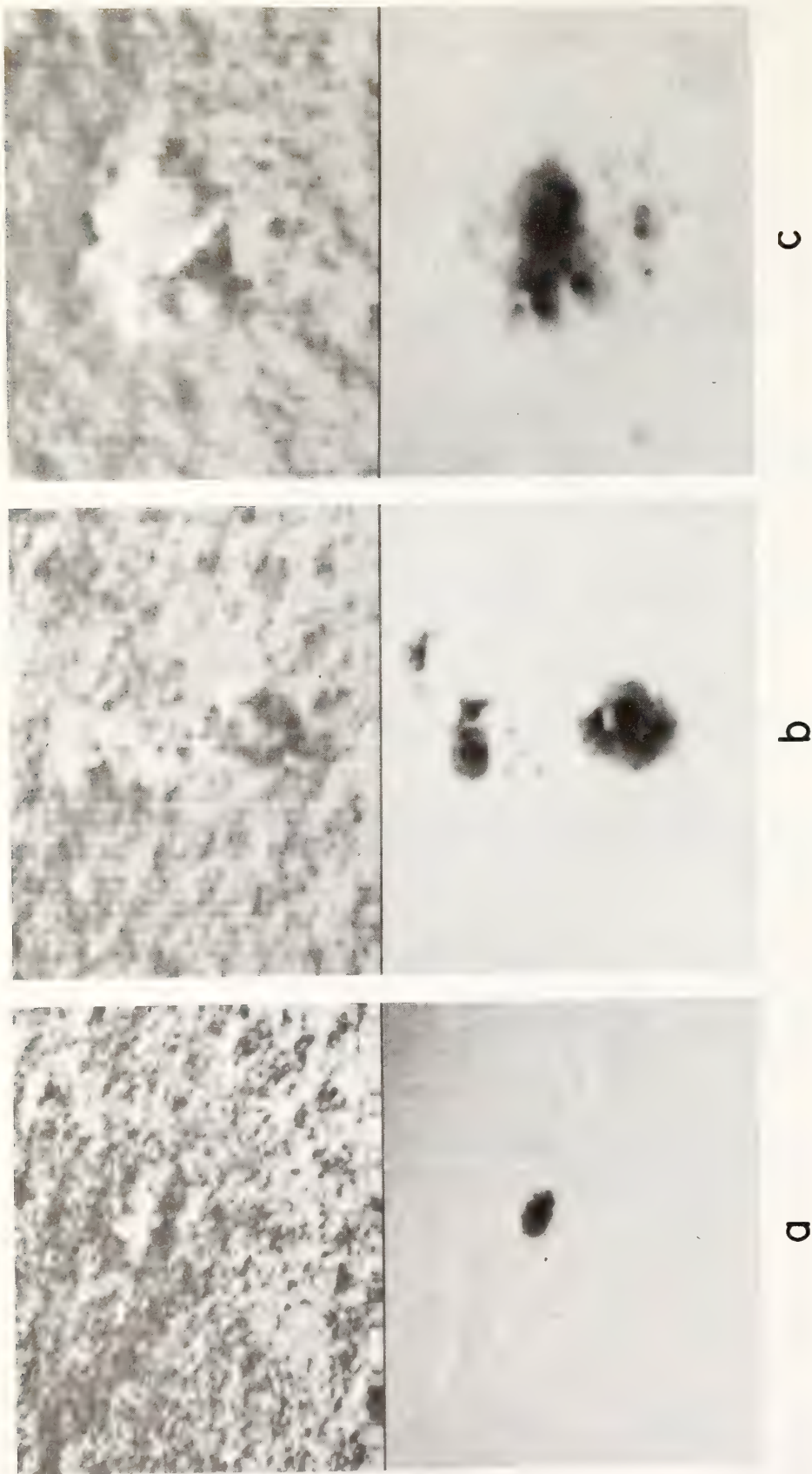


Figure 1. Examples of velocity field complexity classification. (Top) Velocity field with black representing approach and white recession. (Bottom) Intensity images in exact register with velocity images. The extent of the observations is 207 arc seconds east-west by 256 arc seconds north-south. North is to the left and east to the top. (a) A quiet velocity pattern (Boulder region 1371 on October 28, 1978). (b) An active velocity pattern (Boulder region 1382 on November 4, 1978). (c) A complex velocity pattern (Boulder region 1203 on July 11, 1978).

We can now address the first question posed earlier, and we conclude that there is a significant difference between the photospheric velocity fields of flaring and non-flaring regions. The basis for this conclusion is condensed in Table II. The conclusion holds not only for the entire sample of 24 active regions but also for individual active regions as they evolve.

TABLE II
Distribution of 54 determinations of velocity complexity and flare activity within ± 12 hours.

Velocity	Flare Level			
Complexity	Quiet	Low	Moderate	High
Complex	0	0	2	2
Active	0	11	4	1
Quiet	24 ^a	9	1	0

3.2 Velocity Patterns at Flare Sites

A more detailed comparison of the velocity pattern at flare sites is complicated by the fact that we can observe only one component of a three-dimensional velocity vector pattern. To some extent this problem can be resolved by comparing observations at various distances from disc center. With few exceptions we find no correlation between flare sites and velocity patterns when a region is observed near disc center ($\theta < 20^\circ$). Very close to the limb ($\theta > 70^\circ$), foreshortening so degrades the effective spatial resolution that velocity patterns are hard to detect. Specific velocity patterns have been identified at 55 of the total of 73 flare sites with the best correlation observed at disc center distance $\theta > 30^\circ$. This confirms our earlier result (Harvey and Harvey, 1976) that specific flare activity is related to at least one component of the horizontal velocity field. We discern three types of velocity patterns at flare locations which are now discussed in detail.

3.2.1 Anomalies in Sunspot Evershed Velocity

The normal Evershed velocity pattern of a sunspot penumbra appears as a blue-shifted, non-uniform velocity on the disc center side of a spot and a red-shifted velocity on the limbward side. Departures from this pattern were observed at 12 flare sites. The types of anomalies observed are: (i) An oppositely-directed velocity structure (5-10 arc seconds in size) imbedded in the otherwise normal surrounding velocity pattern (2 cases). (ii) The presence of a velocity pattern having the opposite sense of a normal Evershed velocity pattern and associated with smaller, rapidly growing spots (7 cases). (iii) A strong Evershed velocity pattern on one side of the spot (flare-site) but a much weaker or non-existent pattern on the other side of the spot (3 cases). Such spots were often rapidly developing or showed large proper motions.

3.2.2 Small-Scale Velocity Structures

At 15 of the 55 velocity-associated flare sites, the velocity pattern consisted of at least two, adjacent, oppositely-directed velocity elements of 3 to 10 arc seconds size. This multipolar velocity structure is observed both in areas without spots and in areas with smaller, rapidly-changing or growing spots. The magnetic field associated with these structures was not necessarily complex and was often unipolar.

3.2.3 Shears

The predominant velocity pattern found at flare sites is a velocity shear. We define this as oppositely-directed velocity features in close proximity with an extent in at least one dimension in excess of 10 arc seconds. To detect velocity shears we computed the derivative of the velocity observation in a direction parallel to the limb. This technique largely suppresses the normal Evershed velocity pattern in sunspots but unfortunately only reveals one component of a (presumably) two-dimensional, horizontal shear pattern.

Velocity shears were identified at 48 of the 55 velocity-associated flare sites. There appears to be a much better correlation between the spatial extent of a velocity shear and the associated level of flare activity (Table III) than between the strength of a shear and associated flare activity. An example of a long shear line is shown in Figure 2. In most cases the velocity shear is closely related to the $H_{11} = 0$ line (see below) but in 19 of the 48 shear examples there is no such association. In these cases the shears appear to be the result of (i) the combined Evershed velocity pattern of several sunspots in close proximity or multiple umbrae within a single penumbra, (ii) anomalous small-scale velocity structure within the normal Evershed pattern or, (iii) multipolar velocity structures located in an area of unipolar magnetic flux.

TABLE III

Flare activity related to length of velocity shear (corrected for foreshortening).

Number of flares (± 12 hrs.)	Length of shear (arc seconds)					
	≤ 5	5-10	10-15	15-25	25-45	> 45
IMP ≥ 2	0	1	0	0	0	3
(all classes)						
> 10	0	0	0	0	1	1
6-10	0	1	1	0	1	0
3-6	0	4	7	3	0	2
2-3	1	8	4	1	0	0
≤ 1	7	9	3	2	0	0

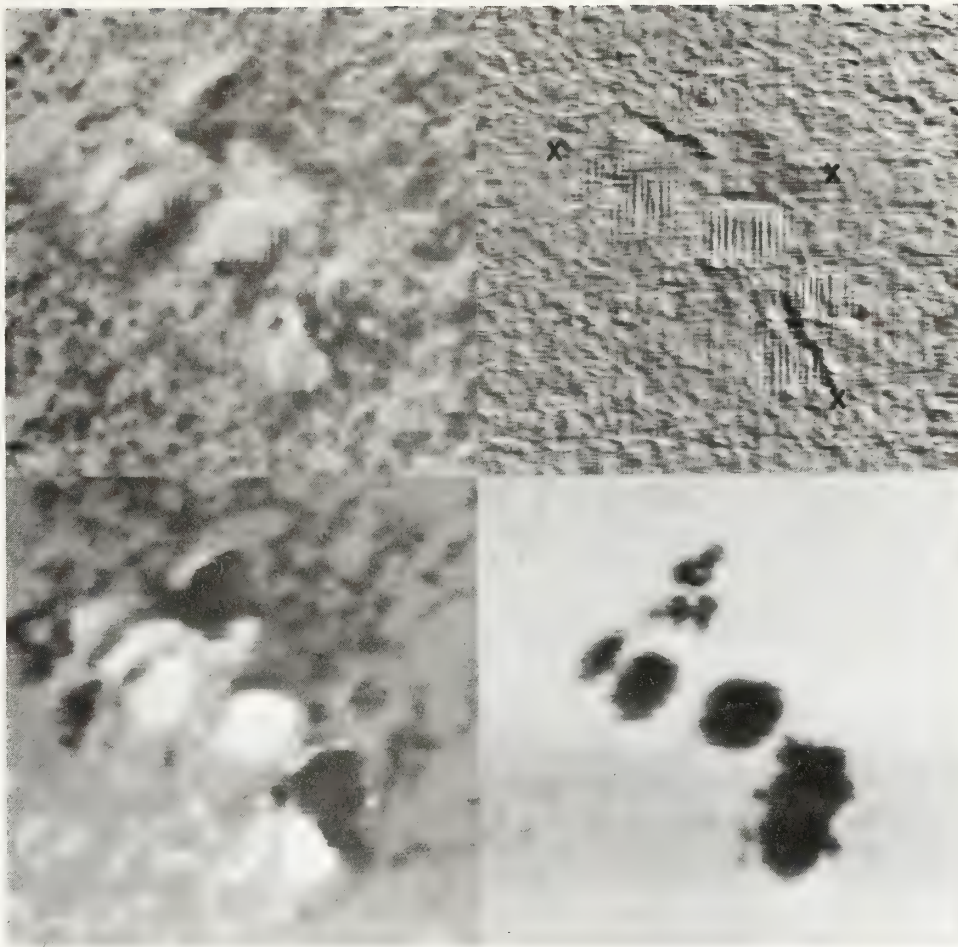


Figure 2. Boulder region 1092 on April 28, 1978. Each frame covers an area of 256 by 256 arc seconds with north to the left and east to the top. (top left) Velocity image with black representing approach and white recession. (top right) Velocity shear image with x's indicating flare sites. (bottom left) Magnetic field with white representing a field toward the observer and black away from the observer. (bottom right) Intensity image.

3.2.4 Flares without Velocity Pattern

For 18 of the 73 flare sites studied, no identifiable velocity pattern could be found. Geometric considerations explain most of this lack of correlation. Ten of the flare sites were located in regions within 20° of the disc center. If the velocity field associated with flares is horizontal, the poor sensitivity to such fields near disc center explains these cases. The remaining 8 flare sites were in 5 regions observed away from disc center ($\theta > 30^\circ$). In 4 regions the $H_{11} = 0$ line was parallel to the limb and if a

velocity shear was present and parallel to the $H_{11} = 0$ line, as is usually the case, we would be unable to detect it in these cases. The one remaining flare site was located between two active regions and the lack of an associated velocity pattern currently cannot be explained.

3.3 Association of Velocity and Magnetic Patterns

We examined the magnetic pattern at the 48 flare sites which were associated with velocity shears. It was generally possible to construct $H_{11} = 0$ lines as well as $V_{11} = 0$ and shear lines. In 29 of the 48 cases an $H_{11} = 0$ line was located near the flare site (and $V_{11} = 0$ and velocity shear line). In some of these cases, the $H_{11} = 0$ and $V_{11} = 0$ lines crossed in agreement with the results of Martres et al. (1971, 1974, 1977). However, in most of the 29 cases, the velocity shear, $V_{11} = 0$ and $H_{11} = 0$ lines were roughly parallel. There was frequently a 3 to 8 arc second displacement of the $H_{11} = 0$ line. Thus the requirement of Martres et al. is not confirmed for all of the events in our sample.

In the 7 cases of distinctive velocity patterns at flare sites without shear patterns, the magnetic field was either unipolar and undistinguished or so complicated by small-scale structure as to defy construction of $H_{11} = 0$ lines.

In Figure 3 we treated the magnetic pattern the same way as the velocity pattern to obtain a magnetic "shear" pattern. This illustrates the similarity between the $H_{11} = 0$, $V_{11} = 0$, and shear lines. It also shows a complexity of the magnetic "shear" picture which is greater than in the velocity shear picture with several features unrelated to flare activity.

3.4 Time Changes in the Velocity Field and Flare Association

Long time series of observations suitable for a study of velocity variations in association with flares were not generally taken during this study. For one region (Boulder, 1203), however, a time sequence was available for a few hours on each of three days. On one of the days, changes in the velocity pattern were observed which suggested an association with subsequent flares. In one case, a blue-shifted velocity element appeared 90 minutes prior to the onset of a flare, and in the second case, an existing blue-shifted feature strengthened 100 minutes prior to a flare. In both areas flare activity and an increase in $H\alpha$ plage intensity was observed only after the onset of the velocity change. No corresponding magnetic or photospheric intensity changes were noted. This is hardly compelling evidence but is consistent with pre-flare blue shifts reported by Harvey and Harvey (1976) and others on previous occasions (Yoshimura et al., 1971; Rust, 1973; Zirin and Tanaka, 1973).

3.5 Velocity Fields as an Aid to Predicting Flares

The velocity field pattern is not a perfect guide to predicting flare activity, size, or location. A suitable blind test was not conducted during

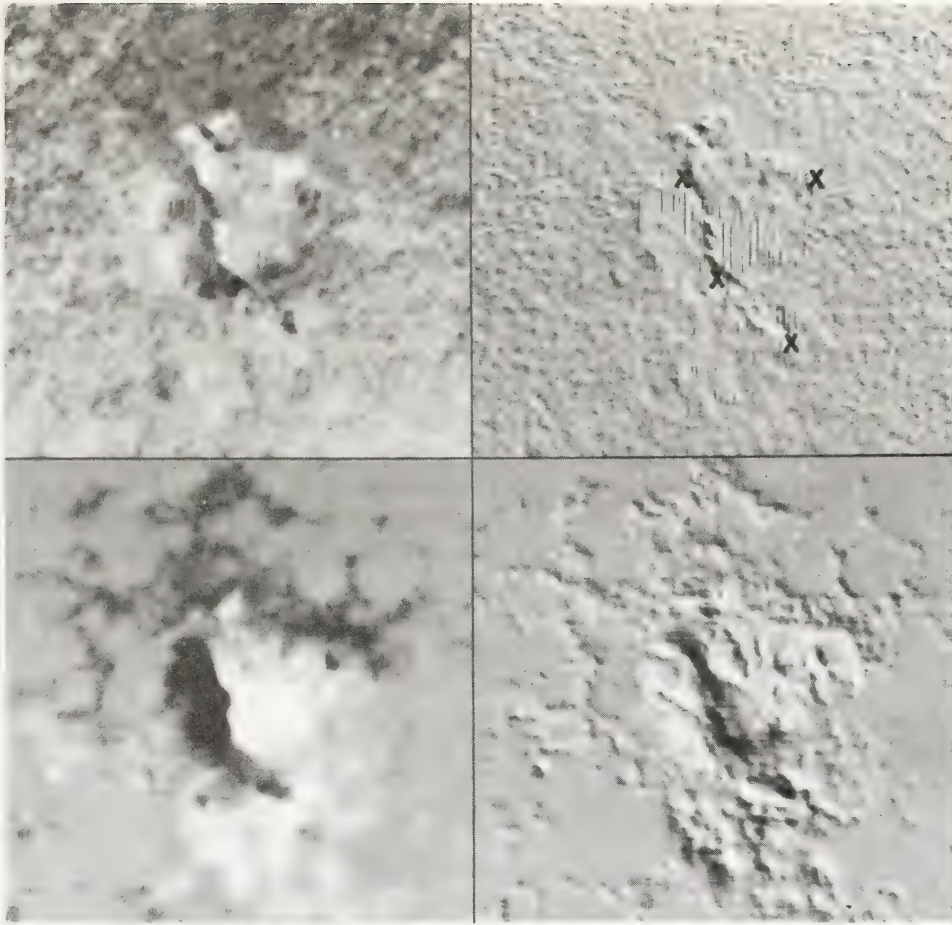


Figure 3. Boulder region 1203 on July 13, 1978. Each frame covers an area of 256 by 256 arc seconds with north to the left and east to the top. (top left) Velocity image with black representing approach and white recession. (top right) Velocity shear image with x's indicating flare sites. (bottom left) Magnetic field with white representing a field toward the observer and black away from the observer. (bottom right) A magnetic field "shear" image produced in the same way as the velocity shear image but from the magnetic data rather than the velocity data. Strong features are present which have no relation to flare activity.

this study, but some results look promising for further investigation. On the positive side, there is a very good correlation between flare activity and velocity complexity. Anomalies of the Evershed pattern, if associated with shears of the velocity pattern, were invariably the site of flare activity within ± 12 hours. Large-scale velocity shears were associated with flare sites in every case. Evidence that a photospheric blue shift precedes flares was strengthened. Velocity shear patterns are relatively easier to interpret than magnetic field patterns.

On the negative side, no significant velocity pattern was found at nearly 1/4 of the flare sites studies. The fact that this can be explained as due to geometry does not make the failure any less significant. Velocity shears were identified at 8 locations at which no flares were reported. These shears were weak and small in extent and possibly unreported flares did occur at these sites, but, based on available data, these shears represent a failure of the shear pattern as a flare-site predictor. We suspect that photospheric blue-shifted features appear and disappear all the time, and some additional criterion is required if such features are to be useful as flare precursors.

Fourier transforms of the velocity pattern of several of the active regions were computed in the hope that some distinctive signature of a flare-rich active region could be found. The transforms were dominated by the Evershed effect and the spacing of sunspots in the active regions and yielded nothing in the way of a clear signature representing flare activity. We believe that the shear pattern is much more useful, and it is certainly easier to compute. It is possible that some simple parameter of shear map such as RMS shear could be an effective single parameter to characterize the flare potential of an active region, but a more extensive investigation is required.

4. CONCLUSIONS

We conclude from this limited study that the complexity of the photospheric velocity field is closely associated with the level of flare activity in the active region. Further, the sites of flare activity are closely associated with specific velocity patterns, especially with apparent horizontal velocity shears. The spatial extent of such shears appears to be related to the magnitude of flare activity. Finally, although geometric problems are a limiting factor, observations of the velocity field are practical and can provide valuable additional information to help predict the flare potential of active regions.

5. ACKNOWLEDGMENTS

This study was supported in part by the Air Force Geophysics Laboratory project order ESD 8-0927 through NOAA Purchase Order 01-8-B01-3883.

We are grateful to G. Heckman of the Space Environment Laboratory of NOAA for his personal interest in supporting this study and to F. Recely of NOAA for making many of the observations and to B. Gillespie for taking most of the remaining observations. The operation of the Vacuum Telescope at Kitt Peak National Observatory is partially supported by NOAA. Flare and H α film data were kindly provided by M. Pierce and M. Losleben of the Space Environment Laboratory, F. Tang and H. Zirin of Big Bear Solar Observatory, and S. Martin of San Fernando Observatory.

REFERENCES

- Harvey, K. L. and Harvey, J. W. (1976): A study of the magnetic and velocity fields in an active region. Solar Phys. 47:233.
- Livingston, W. C., Harvey, J., Slaughter, C., and Trumbo, D. (1976): Solar magnetograph employing integrated diode arrays. Appl. Opt. 15:40.
- Martres, M. -J., Soru-Escaut, I. and Rayrole, J. (1971): An attempt to associate observed photospheric motions with the magnetic field structure and flare occurrence in an active region. In: Solar Magnetic Fields, R. Howard (ed.), IAU Symposium 43, p. 435.
- Martres, M. -J., Rayrole, J., Ribes, E., Semel, M., and Soru-Escaut, I. (1974): On the importance of photospheric velocities in relation to flares. In: Flare-Related Magnetic Field Dynamics Conference, Boulder, Colorado, p. 333.
- Martres, M. -J. and Soru-Escaut, I. (1977): The relation of flares to 'newly emerging flux' and 'evolving magnetic features'. Solar Phys. 53:225.
- Rust, D. M. (1973): Analysis of the August 7, 1972 white light flare: changes in the magnetic and velocity fields. Solar Phys. 33: 205.
- Yoshimure, H., Tanaka, K., Simizu, M., and Hiei, E. (1971): Photospheric mass motions associated with a flare. Publ. Astron. Soc. Japan 23:443.
- Zirin, H. and Tanaka, K. (1973): The flares of August 1972. Solar Phys. 32:173.

SHORT-TERM FLARE PREDICTIONS AND THEIR STATIONARITY DURING THE 11-YEAR CYCLE

M.Jakimiec and J.Wasiucionek
Astronomical Institute, Wrocław University
Wrocław, Poland

Non-linear multiple regression analysis has been used to work out algorithms for prediction of the number of solar flares of various importances. The investigations have been made for sunspot groups of various Zurich classes (D,E,F,H) separately. It has been found that the following parameters of active region are most effective for the predictions: the magnetic classification of a sunspot group, the sunspot-group area, the calcium plage intensity, numbers of flares of various importance and a new index, MFI, of complexity of magnetic field in the sunspot group.

Value of the informativity index has been calculated for each parameter used in the predictions. From detailed analysis of these values it has been found that the following conclusions are true for all the considered sunspot group classes: 1. the following parameters: the magnetic classification, the sunspot group area and the calcium plage intensity play more important role in the predictions of subflares than in the predictions of higher importance flares, 2. the role of MFI index strongly increases for large flares, 3. flare activity in the preceding day is significant for the predictions of flares of all importances, 4. sets of parameters being most important for the flare predictions are different for different flare importances.

Flare predicting algorithms have been worked out separately for a period of higher (1971-72) and lower (1973-75) solar activity. It has been found that the respective equations of regression are significantly different for these two periods. In particular the multiple correlation coefficients as well as the role of various parameters for the predictions change with the phase of the 11-year cycle.

The obtained prediction algorithms were tested using a set of data not included when deriving the algorithms.

1. Introduction

The aim of the present investigation is to work out an optimum method of flare prediction using the active region characteristics, which are currently available on daily basis. The predictions are made for individual active regions and here we consider the predictions for the next day only.

The commonly used Zurich classification of sunspot groups pro-

vides an important characteristic of the stage of development of the group in an active region. This classification is however purely qualitative and it is very difficult to include it into regression analysis in a quantitative way. Therefore we have carried out our analysis for sunspot groups of individual Zurich classes separately. In the present paper we have investigated groups of class D, H and E together with F. Observational data used in the analysis cover the period 1971-75 and have been taken from Solar Geophysical Data.

2. The prediction technique

We have used a non-linear multiple regression analysis as a basis method of our investigation. The non-linear analysis has been used because there are some observational and theoretical indications that simultaneous occurrence of some active region features may be important for the flare activity of the region. The number of terms in the non-linear regression equations strongly increases with the number of independent variables and therefore it is not recommended to make the analysis for a large number of the variables. Our computations were carried out with seven (or less) independent variables, i.e. the active region characteristics used in the investigation (see Table 1) were analysed in sets comprising seven (or less) characteristics - the sets are denoted: S1, S2, ..., S5 in the table.

The following three characteristics have been predicted for the next day:

1. the number of subflares, $N(s)$
2. the number of importance 1 flares, $N(1)$
3. the number of flares of importance 2 and higher, $N(2)$.

Some of the characteristics listed in Table 1 need additional explanation:

The Neutral Line Index, NLI is a characteristic of the run of the magnetic neutral line in a group and characterizes the inclination of the neutral line to the solar meridian and complexity of its shape. The values of NLI were determined from the Mt Wilson magnetograms in the 8-step scale:

0 - an unipolar magnetic region

1 - a bipolar magnetic region in which the neutral line is roughly parallel ($\pm 30^\circ$) to the solar meridian and the distribution of polarities is normal for a given hemisphere in the given solar cycle

2 - a bipolar magnetic region in which the neutral line is inclined between 30° and 60° to the solar meridian and the distribution of polarities is normal

3 - a bipolar magnetic region in which the neutral line has a several points of inflexion and the distribution of polarities is normal

4 - a bipolar magnetic region in which the neutral line is roughly parallel to the solar equator or the distribution of polarities is inversed in relation to normal to the hemisphere and solar cycle

Table 1

Active region characteristics used as predictors

No	Characteristic	Sets of characteristics used in the computation					Variables in the equations
		S1	S2	S3	S4	S5	
1	The strength of sunspot magnetic field, h	o					
2	The Neutral Line Index, NLI	o					
3	The distance between the maximums of the strength of the magnetic field, d	o					
4	The Flare Activity Index, FAI	o	o				
5	The magnetic classification of sunspot group	o	o	o	o	o	x1
6	The sunspot group area	o	o	o	o	o	x2
7	The calcium plage intensity	o	o	o	o	o	x3
8	The Magnetic Field Index, MFI		o	o	o	o	x4
9	The number of faint flares			o			
10	The number of normal flares			o			
11	The number of bright flares			o			
12	The number of subflares				o		
13	The number of imp.1 flares				o		
14	The number of flares of imp.2 and higher				o	o	x7
15	The number of sn and sb flares					o	x5
16	The number of 1n and 1b flares					o	x6

5 - a bipolar magnetic region but within the limits of one polarity are observed small areas of the opposite polarity (independently of the run of the neutral line)

6 - a multipolar magnetic region, i.e. the polarities are distributed in a more complicated pattern than in a typical bipolar region

7 - a magnetic region in which the polarities are completely mixed and the run of the neutral line is very complicated.

It should be noted that the spatial resolution of the Mt Wilson magnetograms changed from 17.5" to 14.2" in October 1974 and this introduces some unhomogeneity into the data from which the

NLI is determined. However, this cannot have any significant effect on the analysis presented in the following sections, because the change of the spatial resolution is rather small and does not significantly changed the errors of determination of the shape of the neutral line.

The Flare Activity Index, FAI, is a weighted sum of numbers of flares of various importances.

The magnetic classifications of a sunspot group was introduced as a zero-one variable in the following way: for sunspot group D, E and F:

$x_1 = 0$ if the magnetic classification is β , β_p or β_f and

$x_1 = 1$ if the classification is $\beta\gamma$ or δ ,

for sunspot groups H:

$x_1 = 1$ if the classification is β , β_p or β_f and

$x_1 = 0$ if the classification is α .

The characteristic MFI was used in the investigation instead of the three separate characteristics: h, d and NLI, as an alternative, compact description of the sunspot group magnetic field. The strength of sunspot magnetic field, h, was taken from the Mt Wilson sunspot magnetic field measurements. The distance between the maximums of the strength of the magnetic field, d, was measured on the Mt Wilson magnetograms and corrected for geometric foreshortening. The Magnetic Field Index was defined as follows:

$$MFI = \frac{h}{d} NLI. \quad [1]$$

For each set of variables: S1, S2, ..., S5, the regression equations have been calculated and for each equation a value of the multiple correlation coefficient, R, has been computed as a characteristic of the quality of the regression.

By comparing the results of computation for sets S1 and S2 (see Table 1) we wanted to investigate which way of characterizing the magnetic field structure of a sunspot group is more effective for the predictions:

a. by introducing the three separate characteristics: h, d and NLI or

b. by introducing one MFI parameter.

It has been found by comparing the values of R, that the latter variant is more effective for our purpose.

Sets S2, S3, S4 and S5 were introduced in order to investigate what manner of introducing the information about present flare activity is most effective for predictions:

a. by means of one flare index, FAI - set S2,

b. by introducing separately the numbers of flares of various importances - set S4,

c. by introducing separately the numbers of flares of various brightness characteristics, independently of their importances - set S3 or

d. by introducing separately the numbers of flares of various importances excluding sf and 1f flares - set S5.

It has been found that the last manner of introducing the present flares is the most effective for our purpose, i.e. the value of multiple regression coefficient, R, is the highest for this case.

In the regression analysis significance of each term in a regression equation was investigated by means of t-Student statistics (cf. Bartkowiakowa, 1976), assuming the significance level equal to 0.05 and only the significant terms were retained in the equations. In the computations the regression analysis program worked out by Bartkowiakowa (1978) was used. The regression equations obtained for the class E and F sunspot groups from the period 1971-72, are given in Table 2 as an example.

Table 2

Examples of the regression equations for class E and F from the period 1971-72

Prediction equation	error of the prediction
$N(s) = 3.364 + 0.225 x_3 x_5 + 0.0724 x_2 x_3$	4.54
$N(1) = 0.237 + 0.0262 x_4 x_6 + 0.0120 x_4 x_5 +$ $- 0.00394 x_2^2$	0.58
$N(2) = 0.0427 - 0.0846 x_4 x_7 - 0.00390 x_2 x_4 +$ $+ 0.272 x_7^2 + 0.00137 x_5^2 +$ $+ 0.0117 x_4^2 - 0.0504 x_4$	0.23

3. Test of the flare predictions

Flare predictions given by the regression equations have been tested using data for some, randomly chosen, active regions, which were not included in the above regression analysis. In Table 3 is shown the correlation between the predicted and actually observed numbers of flares of various importances.

The agreement between the predicted and observed numbers of flares has been also characterized by values of the skill-score index, proposed by Heidke:

$$s = \frac{r - e}{n - e} \quad [2]$$

where r is the number of correct predictions (the sum of the diagonal terms in the table), n is the whole number of cases in the table and e is the number of correct predictions which is expected in the case if the predicted and observed numbers of flares were independent variables (cf. Brier and Allen, 1952).

It is seen from Table 3 that the application of the prediction technique provides very promising results. It is worth-while to note that these results have been obtained using only the basic characteristics of active regions including standard magnetic observations. Introduction of more sophisticated data, such as active

Table 3

The correlation between predicted and observed numbers of flares

		The predicted number of flares				skill-score s	
The observed number of flares	subflares	subflares				0.52	
			0-1	2-5	6-9		≥10
		0-1	27	12	1		0
		2-5	3	30	10		0
		6-9	1	2	10		1
	10	1	4	5	10		
	importance 1	importance 1				0.52	
			0	1	2		≥3
		0	75	10	0		0
		1	10	17	1		0
		2	0	0	2		1
	3	1	0	0	0		
	importance ≥2	importance 2				0.79	
			0	1	2		
		0	71	0	1		
		1	0	2	0		
		2	0	0	0		

region X-ray intensity and fluxes at centimeter wavelengths will probably give further improvement of the predictions.

4. Linear and non-linear regression

In order to evaluate an improvement in the regression analysis obtained by introducing non-linear terms, all the calculations were carried out in two variants: using non-linear (quadratic) and linear regression. In Figure 1 is shown a comparison of values of the multiple correlation coefficients, which have been obtained in the linear and non-linear regression. The correlation coefficients have been calculated for individual flare importances and they are averaged over various classes of sunspot groups. It is seen that the introduction of the non-linear terms into the regres-

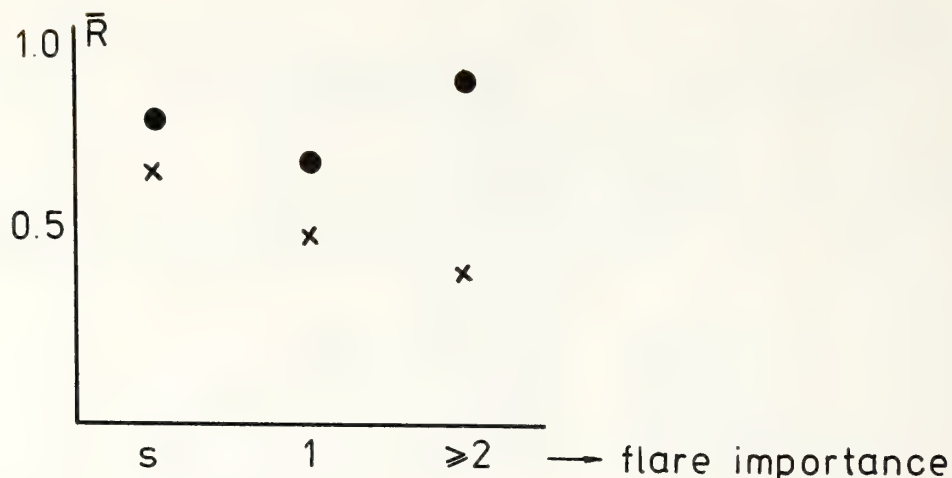


Fig. 1. Values of the multiple correlation coefficient obtained for linear (x) and non-linear (●) regression analysis.

sion analysis is most important for the largest flares.

5. The role of individual characteristics in the flare predictions

The role of individual characteristics in a regression equation has been characterized by the informativity index:

$$INF x_k = \frac{t_k + t_{kk} + 0.5 \sum_j t_{jk}}{\sum_k (t_k + t_{kk} + 0.5 \sum_j t_{jk})} R^2 \cdot 100\% \quad [3]$$

where t_k , t_{kk} and t_{jk} are values of the t-Students statistics for individual terms in a regression equation containing variable x_k (cf. Section 2), t_k relates to linear term (x_k), t_{kk} relates to square term (x_k^2), t_{jk} relates to cross-products ($x_j x_k$), and R is the multiple correlation coefficient.

The index $INF x_k$ indicates what part of the total variance of the given predicted variable is due to variation of the predictor x_k . Values of the informativity index for individual predictors in the obtained prediction equations are given in Table 4. The values are averaged over various classes of sunspot groups.

From Table 4 it is seen that for the prediction of subflares number the most important characteristic is the number of subflares (excluding faint subflares) on the previous day, x_5 . For the predictions of number of the importance 1 flares and importance ≥ 2 the most important is the Magnetic Field Index, x_4 . But for the largest flares (imp. ≥ 2) prediction the observed number of large flares, x_7 is also of great importance.

It is worth-while to note that the role of the MFI clearly in-

Table 4

Values of the informativity index

importance of flares	predictor						
	x1	x2	x3	x4	x5	x6	x7
subflares	5.95	4.20	7.85	7.53	18.95	1.26	1.06
imp.1	1.02	5.65	5.34	12.41	6.41	6.28	3.22
imp. ≥ 2	0.36	2.92	3.53	18.60	4.46	9.44	16.42

creases with increasing importance of the predicted flares and that such basic characteristics of active regions as magnetic classification, x1, the sunspot group area, x2, and the calcium plage intensity, x3, are of very low importance for the predictions of large flares.

6. Stationarity of the flare predictions during the 11-year solar cycle

In order to investigate the stationarity of the flare predictions during the 11-year solar cycle, the regression equations have been calculated separately for the period of higher solar activity (1971-72) and for the period of lower activity (1973-75). The regression equations significantly differ for these two periods, showing that the role of various characteristics for the flare predictions changes with the phase of the 11-year cycle.

In Table 5 values of the multiple correlation coefficients, R, for various classes of sunspot groups and various flare importances are given.

Table 5

Values of the multiple correlation coefficient for high and low solar activity

Zurich class	E + F			D			H	
importance of flares	sub	1	≥ 2	sub	1	≥ 2	sub	1
1971-72	.69	.61	.77	.60	.54	.18	.56	.50
1973-75	.77	.80	.98	.65	.66	.84	.83	.71

From Table 5 it is seen that:

1. The values of the multiple correlation coefficient, R, are high ($R \geq 0.5$) for all the cases except the case of regression for large flares (imp. ≥ 2) in sunspot groups of class D, for the period of higher solar activity. The investigation suggests that the low qua-

lity of the regression for large flares in the class D sunspot groups is due to strong inhomogeneity of this class of groups: among the D groups we have fast developing groups, relatively stable groups at their maximum development, as well as quiet decaying groups, previously classified as class G.

2. In all the cases the quality of the regression, as characterized by the values of the multiple correlation coefficient is significantly better for the period of lower solar activity. This indicates that the flare predictions are significantly better, when the solar activity is lower. This is most probably the result of the fact that during periods of higher solar activity active regions are crowded, they often occur in complexes of activity. The influence of adjacent active regions on the flare activity of a given region was not considered in the present paper, thus it introduces an additional "noise" (increase of the random variance) into our regression analysis, i.e. decrease of the value of the correlation coefficient during the periods of higher activity. Some additional noise arises also from the fact that during the periods of high activity flares more often occur near the boundaries between adjacent active regions in a complex of activity and therefore their attribution to a particular active region is not univocal. The occurrence of the flares at the boundaries between active regions is clearly also a result of physical interaction of the active regions.

7. Concluding remarks

Our analysis clearly shows that regression equations obtained during high solar activity cannot be used during low solar activity and vice versa. It has been shown, however, that if the regression equations calculated for a given time interval (of about two-year duration) are used to predict numbers of flares in other active regions appearing during the same time period, the results of the predictions are very good (Section 3).

All our analysis relates to the decreasing phase of the solar cycle. It is very probable that the regression equations obtained will not be valid for increasing phase of the solar cycle at similar level of solar activity and also their applicability at decreasing phase of another solar cycle needs additional investigation. This is why we intend to carry out the regression analysis successively for short time intervals (of 1-2 year duration) during the development of the present solar cycle and to use the obtained regression equations for flare predictions within a short time intervals next to the analysed one.

Acknowledgements

The authors express their sincere thanks to Dr. Jerzy Jakimiec for many helpful conversations and to Dr. Anna Bartkowiakowa of the

Wrocław University Computing Center for help in adopting her program to their needs.

References

- Bartkowiakowa, A. (1976): Algorytmy analizy regresji. Roczniki Polskiego Towarzystwa Matematycznego. Seria III. Matematyka Stosowana VII, 101.
- Bartkowiakowa, A. (1978): Opis merytoryczny programów statystycznych. Uniwersytet Wrocławski, Wrocław, 87.
- Brier, G. W. and R. A. Allen (1952): Verification of Weather Forecasts. Compendium of Meteorology, American Meteorological Society, Boston Massachusetts, 841.

THE APPLICATION OF MULTIVARIATE DISCRIMINANT ANALYSIS TO SOLAR FLARE FORECASTING

Joseph W. Hirman¹, Donald F. Neidig²,
Paul H. Seagraves³, William E. Flowers¹,
and Philip H. Wiborg²

- ¹ Space Environment Services Center, National Oceanic and Atmospheric Administration,
Boulder, Colorado 80303, USA
- ² Air Force Geophysics Laboratory, Sacramento Peak Observatory*,
Sunspot, New Mexico 88349, USA
- ³ High Altitude Observatory, National Center for Atmospheric Research,
Boulder, Colorado 80307, USA

Solar parameters derived from the daily region analysis program at the Space Environment Services Center (SESC) are submitted to a multivariate discriminant analysis (MVDA) in which the parameters relevant to flare incidence are identified and formulated in probability equations for flare occurrence. The analysis uses one year of data (1977), half of which is used as a training set, while half is used to test a daily prediction formula for the occurrence of the largest solar flare. The MVDA forecast is compared with a subjective forecast derived from the forecast issued by the SESC during the same period. The MVDA technique is discussed in terms of its value as an objective forecasting tool.

1. INTRODUCTION

The present techniques for producing daily forecasts for solar flare activity utilize actual solar observations but also depend to a significant degree on human judgment. An objective forecast, that is, a prediction formula based solely on solar data, is certainly desirable in setting a quantitative base from which a final forecast could be developed. The utility of such a procedure, simply as a means of coping with the flow of real-time data, would enable forecasters to concentrate their efforts on producing the actual forecast. In fact, it appears that a prediction formula may even be able to generate forecasts superior to those produced by conventional techniques.

* Operated by the Association of Universities for Research in Astronomy, Inc., under contract with the National Science Foundation

Previous efforts in deriving objective prediction methods are summarized in a series of United States Air Force publications (e.g. Enger et al., 1966; Reilly and Enger, 1967; Reilly et al., 1969; Podsiadlo, 1973; Moschandreas et al., 1974). These methods were based on regression analysis, and while they appear to have been successful we are unable to compare their results with those of this study due to the different formats and types of solar data existing then and now. Moreover, the accuracy of any forecast is dependent upon the level of solar activity; this creates an additional difficulty in comparing the successes of forecasts made during different times. An important feature of the analysis here is the comparison of the objective forecast with a conventional forecast made during the same period.

2. PROCEDURE

2.1 Summary

In this study we have used a multivariate discriminant analysis (MVDA) in a computer program which is described briefly in Appendix A. The essential feature of the program is the comparison between a number of input variables and a number of output classes, in which the discrimination between the classes in terms of the given variables is maximized by constructing appropriate classification functions. In the application to flare prediction the input variables are observed daily solar parameters for each active region on the solar disk, and the output classes are the levels of flare activity occurring on the following day within each active region. There is no limit to the number of records (active region-days) which can be analyzed during one run of the program. In this study we have used approximately a half-year of data (750 records) to derive the classification functions. The latter are then extrapolated forward in time to produce a true forecast.

2.2 Data

We have used data for the entire year 1977, obtained from the region analysis program at the Space Environment Services Center (SESC) in Boulder. The region analysis program evolved from lists of solar parameters which the SESC forecasters considered vital to the preparation of a 24-hour flare forecast for a particular active region. The present form of the list is given in Appendix B, where the solar characteristics pertaining to each parameter are arbitrarily prioritized and weighted. For all parameters except sunspot class the given priority scale has been based upon qualitative association between flare activity and solar active region characteristics. Larger scale numbers indicate conditions characteristic of greater activity. In the case of the sunspot parameter the priority scale was derived from an actual investigation of spot class vs flare incidence (McIntosh, 1977).

The daily parameter values are derived from observations which stream into the SESC from various solar observatories furnishing raw data, coded and plain language reports. Included are calcium plage data from McMath, magnetograms from Mt. Wilson, east-west radio drift scans from Ottawa, and radio flux measurements from Ottawa, Sagamore Hill, Manila, Athens, and Palehua. In addition, the SESC operates a Razdow $H\alpha$ telescope, monitors the GOES II and III satellites, as well as several radio frequencies and a magnetometer. The Air Force Solar Observing Optical Network (SOON) contributes most of the optical data, and will soon be able to provide 24-hour observational coverage. A description of the collection, organization, decoding and display of the near real-time flow into the SESC is given by Williams (1976).

Subjectivity is inescapable in any analysis scheme and the region analysis program is no exception. An interpretation is required for many of the incoming data in order to assign values to the daily parameters. $H\alpha$ data are usually specified in general terms and the forecaster must then determine, for example, the existence of arch filament systems, bright points, or active filaments in the region. The parameter with the least amount of subjectivity is the sunspot class. Familiarity with the normal life cycle of spots, combined with universal procedures for measuring and classifying spots, keeps subjectivity to a minimum for this parameter. For all parameters considerable emphasis is placed on consistency in the priority assignments.

The region analysis is completed daily before 2200 UT, in time for the forecast to be issued for the 24-hour period beginning 0 UT the following day. An individual forecast is made for each of the active regions on the solar disk. The forecasts utilize all available information but rely heavily on the judgment of the forecaster. No objective formulas are used in their preparation. The SESC forecasts will be used in the following section to derive a forecast for comparison with the MVDA forecast.

2.3 Application of the MVDA Program

The region analysis parameters in Appendix B are independent of any information on flare activity occurring the following day. Therefore, these parameters can be used today to produce a flare forecast for tomorrow, assuming that some of the parameters actually contain predictive information. For input variables we used all parameters of the region analysis program except No. 23 (full disk radio flux) which does not apply to individual active regions. The three-letter sunspot class (parameter No. 1) was broken down into three separate parameters each prioritized according to observed flaring rates (McIntosh, 1977). Thus, the first letter, with possible designations of A, B, C, D, E, F, or H was assigned respective values of 1, 2, 4, 5, 6, 7, or 3. Similarly, the second letter, r/x, s, a, h, or k was assigned 1, 2, 3, 4, 5; the third, x, o, i, or c was assigned 1, 2, 3, 4. The largest magnetic field strength in the active

region (parameter No. 3) was separated into two parameters, one giving the polarity of the field in binary code and the other giving the field strength in hundreds of gauss. In cases where data were missing for any particular parameter the average value of that parameter for all records available was substituted.

In addition to the 24 individual parameters, six Boolean combinations or sums of Boolean combinations were entered as input variables. These are listed in Appendix C. There was no systematic procedure involved in the derivation of these; rather, they were constructed on the basis of intuitions about the form in which predictive information might be contained in the data and about physical quantities (e.g. energy stored in sheared magnetic fields) presumed relatable to the origin of flares. Obviously, the supply of Boolean combinations is virtually inexhaustible and there is no reason to suppose that the examples used here are the most significant.

Four mutually exclusive classes were used in the MVDA program: no flare occurred in the region, largest flare was X-ray class C, largest flare was class M, or largest flare was class X. These X-ray classes are roughly equivalent to H α importance classes 1, 2, and 3, respectively, and are defined in terms of the 1-8 Å peak flux ($\text{erg cm}^{-2}\text{sec}^{-1}$) at 1 AU according to the following: C($1-9 \times 10^{-3}$); M($1-9 \times 10^{-2}$); X($\geq 1 \times 10^{-1}$).

A collection of records containing both the input variables (30 parameters) and the class of the largest flare occurring on the following day, constitutes a training set. We selected an initial training set of the first 750 records from a total of 1483 for the year 1977. The classification functions computed from these were then applied to a test set consisting of records 751-850 for which only the 30 input variables were given. The result of the classification performed on the latter was taken as the MVDA forecast for records 751-850. The data base was then moved forward in time in steps of 100 records, maintaining a training set of 750 records immediately previous to the test set. In this manner a total of 733 predictions were made during the last half of 1977.

The sliding data base described above is a technique which is readily adaptable to the operation of a forecast center. The program is trained on recent solar data and may even be retrained on a daily basis. The use of a small test set (records for one day in an actual forecast operation) minimizes the effects of secular trends, either of observational or solar origin, which might be present in the data.

3. RESULTS AND DISCUSSION

The MVDA program was trained on the X-ray class of the largest event (none, C, M, or X) occurring in the region, and therefore the format for the MVDA forecast is a probability that the largest event will be in one

of these classes. Since the outcomes in this format are mutually exclusive the sum of the probabilities for each class must be unity. The SESC forecast, however, is given in terms of the probability for the occurrence of each class of event, which is a non-exclusive format. In order to measure the relative success of the MVDA predictions we therefore derived a comparison forecast using the "exclusive" format by selecting the largest event class in the SESC forecast which was assigned a probability greater than or equal to 0.50.

The performances of both the MVDA and the comparison forecasts are given together in Table 1. In Table 1 the numbers in parentheses on the diagonals are the percentages of forecasts correct. Numbers in parentheses on the row labeled Total Events are climatological probabilities (percent) for the four classes, obtained by dividing the number of events entered there by the total number of events in all classes. The higher scores for the MVDA forecast are not very significant statistically (significant only at about the 1 σ level for classes C and M), but certainly suggest that the technique has merit as a forecasting tool. This is especially true in view of the objectivity of the procedure. Both forecasts show considerable skill in predicting flares, as can be seen by comparing the forecast accuracies with the climatological probabilities in each class (For a discussion of forecast evaluations see Simon and McIntosh, 1972). From the data in Table 1 the reader may verify that by combining the event classes C, M, and X, forming a flare/no-flare format, the MVDA forecast obtains 59 correct predictions from a total of 94 made for the occurrence of a flare - an accuracy of 63 percent. The comparison forecast produced 59 correct from 95, or 62 percent. Thus, the two forecasts are equally good in predicting the occurrence of flares of unspecified magnitude.

It is noteworthy that the erroneous predictions of both forecasts are nearly evenly distributed on both sides of the diagonals in Table 1. The MVDA forecast is slightly biased toward underprediction while the comparison forecast shows a tendency for overprediction.

The MVDA program performs a significance test on the input variables, listing the significant variables and the statistical probability of their significance in classifying the training set. Table 2 summarizes those solar parameters which exceed a probability of 0.99. Of course, the actual level of significance of any given parameter varied somewhat from one training set to another.

Unfortunately, the derived classification functions in terms of the significant variables are not simple equations which can be written in a form tractable enough to present here. Furthermore, the functions vary somewhat from one data set to another.

Table 1.

MVDA Forecast and Comparison Forecast vs Observed Class of the Largest Event for the Last 733 Active Region-Days in 1977.

Largest Event Forecasted	Largest Event Observed				Total Forecasts
MVDA	None	C	M	X	
None	608 (95)	24	6	1	639
C	33	35 (43)	11	3	82
M	2	5	5 (42)	0	12
X	0	0	0	0	0
Total Events	643 (88)	64 (9)	22 (3)	4 ($\frac{1}{2}$)	733
COMPARISON	None	C	M	X	
None	607 (95)	28	2	1	638
C	26	22 (37)	10	1	59
M	9	13	9 (27)	2	33
X	1	1	1	0 (0)	3
Total Events	643 (88)	64 (9)	22 (3)	4 ($\frac{1}{2}$)	733

Table 2.

Significant Parameters in the MVDA Training Sets.

(Parameter Numbers)

22 in Appendix B	15 in Appendix B	5 in Appendix C
1 in Appendix C	20 in Appendix B	4 in Appendix B
3 in Appendix C	6 in Appendix C	16 in Appendix B
4 in Appendix C	2 in Appendix C	17 in Appendix B
5 in Appendix B	6 in Appendix B	

It must be emphasized that statistically significant is not necessarily equated to physically significant in terms of the conditions required to produce flares. Consistency in the recording of a particular solar parameter undoubtedly has much to do with its selection as "significant". Similarly, it is no surprise that the sunspot parameters are significant because their priority scales were the only ones determined empirically. On the other hand, in a controlled experiment where the input variables are objectively determined, physical associations involving the significant variables may be suspected.

The MVDA forecast could be improved through several refinements. The data contained in the region analysis program could be based on quantitative measurements and objective criteria. New parameters could be added to the data base, and the MVDA program would quickly determine whether any of these were worthy of continued collection. The optimum size for the training set, while not determined here, will be a compromise between a sample of records statistically large enough to train the program yet small enough to avoid secular trends in the data. Consistency in the input data is of utmost importance.

A noteworthy feature of the MVDA program is that it enables the researcher to monitor the interrelation of the input variables from one data set to another. This capability suggests additional uses of the program in the study of various solar activity characteristics as a function of time.

In the future we plan to incorporate the refinements mentioned above. Additional data will soon be available which will increase the size of the test set by a factor of three.

APPENDIX A

The MVDA Computer Program

The computer program, called BMD07M, was originally written at UCLA and was obtainable as one of a package of statistics program (Dixon, 1968). The particular version used here was obtained from the University of British Columbia where Seagraves (1972) had further developed the program to include the Cooley and Lohnes (1962) classification procedure and the Lachenbruch (N-1) technique. The Cooley and Lohnes procedure does not assume uniformity of variance, and this sometimes results in better classification scores. The computational burden, however, is increased because linear classification functions are not possible. In this case, canonical variables, constructed from the original input variables, are used as a

transformation to reduce the matrix dimension in the classification formulas. The Lachenbruch (1968) technique removes bias when the program classifies its own data base.

The basic references for the body of the program are Rao (1952) and Anderson (1958). Chapter 6 of Anderson has an excellent and brief description of multivariate discriminant analysis.

APPENDIX B

Parameters in the SESC Region Analysis Program

<u>Parameter</u>	<u>Characteristics</u>	<u>Priority Scale</u>
1. Spot Class	None observed	0
	Enter spot class three letter code	---
	No data	9
2. Magnetic Class	No spots	0
	Alpha	1
	Beta	2
	Beta-gamma	3
	Gamma	4
	Delta	5
	No data	9
3. Magnetic Field Strengths (largest)	No spots	0
	Enter letter (R/V) and two digit value (if same use leader polarity)	---
	No data	9
4. Magnetic Gradients in gamma/km	No spots or unipolar region	0
	Enter the gradient as N.NN	---
	No data	9
5. Sunspot Dynamics	No spots or not applicable	0
	Coalescing of spots	1
	Spot rotation	2
	Relative spot motion (opposite polarity spots)	3
	No data	9
6. Interaction with Another Region	None occurred	0
	Strong spots of opposite polarity converge (from less than 2 degrees apart)	1
	No data	9

7. Stage of Development	No spots	0
	Mature group (stable)	1
	Decaying	2
	Growing	3
	Rapid decay (spot or area decrease by > 50%)..	4
	Rapid growth (spot or area increase by > 50%)..	5
	Rapid growth (spot or area increase by > 100%)	6
	No data	9
8. Leader Emerged in Leader or Trailer Polarity Fields (from previous synoptic map)	Structure not definite	0
	Returning region - enter region number	---
	< 5 deg of NL and out-of-phase with NL	2
	> 5 deg of NL and in leader polarity fields ..	3
	> 5 deg of NL and in trailer polarity fields .	4
	< 5 deg of NL and in-phase with NL	5
9. Relationship with Nearest Sector Boundary (Hale = region polarity matches the boundary)	No data	9
	Sector structure not definite	0
	Region is > 30 degrees from nearest boundary .	1
	Non-Hale and 10 to 30 deg west of boundary ...	2
	Non-Hale and 10 to 30 deg east of boundary ...	3
	Non-Hale and < 10 deg of boundary	4
	Hale and 10 to 30 deg west of boundary	5
	Hale and 10 to 30 deg east of boundary	6
10. Plage Compactness and Embedded Filament (compact = NL corridor > 2 degrees wide)	Hale and < 10 deg of boundary	7
	No data	9
	Non-compact plage and no filament	0
	Non-compact plage with filament	1
	Non-compact plage with active filament	2
	Compact plage without embedded filament	3
	Compact plage with embedded filament	4
	Compact plage with active embedded filament ..	5
11. Main NL Orientation within Plage	No data	9
	Weak structure	0
	North-south (+/- 45 degrees to NS)	1
	East-west	2
	Hairpin (E-W)	3
	Mostly circular	4
	Reverse polarity region	5
	No data	9
12. Neutral Line Complexity	No kinks or weak structure	0
	1-3 kinks (very simple region)	1
	4-6 kinks (simple region)	2
	7-12 kinks (intermediate region)	3
	> 12 kinks (very complex)	4
	No data	9

13. Neutral Line Temporal Changes	No definite trend	0
	Neutral line becoming simple	1
	Neutral line becoming complex	2
	No data	9
14. Associated Filament (external to region but along common neutral line)	No associated filament	0
	Filament unchanged	1
	Filament growing	2
	Filament disappeared within past 24 hours	3
	Filament darkens or is active	4
	No data	9
15. Bright Points and/or Plage Fluctuations	None occurred	0
	Occurred but not along neutral line	1
	Occurred along the neutral line	2
	Plage fluctuations	3
	No data	9
16. Emerging Flux and/or AFS	None occurred or region is new	0
	Isolated pole in region	1
	New EFR emerges within existing spot group ...	2
	New EFR emerges near region (within 5 degrees of existing spot group)	3
	AFS present in region	4
	No data	9
17. Radio Burst and/or sweep	None occurred or small events	0
	> 250 flux units at 10 cm	1
	> 1000 flux units at 10 cm	2
	Type III sweep	3
	Type IV sweep	4
	Type II followed by type IV sweep	5
	U burst	6
	Major and complex 10 cm burst	7
	No data	9
18. Largest Flare Since Region Appeared	None occurred or first day observed	0
	C class flares have occurred	1
	M class flares have occurred	2
	X class flares have occurred	3
	No data or region appeared on east limb	9
19. Region First Appeared	Formed on disk	0
	Came around east limb - first transit	1
	Second transit	2
	Third transit (and etc)	3
	No data	9
20. Proton Event (this transit)	No particle event	0
	Proton-10 event = $10 \text{ cm}^{-2} \text{sec}^{-1} \text{ster}^{-1}$ @ >10 MeV	1
	Ground level event	2
	No data	9

21. (conventional forecast)		
22. Largest Flare	None occurred or < C	0
for the Past	Class C	1
24 Hours	Class M	2
	Class X	3
	Proton event	4
	No data	9
23. 10 cm	10 cm flux value for today	---

APPENDIX C

Boolean Combination Parameters
(Numbers refer to parameter numbers in Appendix B).

1. Product of three sunspot parameters (see Section 2.3).
2. Product of three sunspot parameters and (2)
3. Product of three sunspot parameters and (16)
4. (3) (4) (5 + 11)
5. (2) (5) (12)
6. (5) (11 + 12 + 13)

REFERENCES

- Anderson, T.W. (1958): An Introduction to Multivariate Statistical Analysis, Wiley.
- Cooley, W.W., and Lohnes, P.R. (1962): Multivariate Procedures for the Behavioral Sciences, Wiley.
- Dixon, W.J.(ed.) (1968): Biomedical Computer Programs, University of California Publications in Automatic Computations, No. 2, University of California Press. p. 214a.
- Enger, I., Padsiadlo, R.T., Jensen, D.C., and Ward, F. (1966): Solar Flare Occurrence as a Function of Sunspot Size, AFCRL-66-29, Hanscom Air Force Base.
- Lachenbruch, P.A., and Mickey, M.R. (1968): Estimation of Error Rates in Discriminant Analysis, Technometrics, 10:1.
- McIntosh, P.S. (1977): Solar Flare Predictions with a Revised Sunspot Classification, Bul. Amer. Astron. Soc., 9: 330.
- Moschandreas, D.J., Enger, I., and Hwang, P.H.-J. (1974): Space Forecast Techniques, AFCRL-TR-74-0299, Hanscom Air Force Base.

- Podsiadlo, R.T. (1973): An Objective Baseline for Flare Prediction, in M.J. Rycroft and S.K. Runcorn (eds.), COSPAR Symposium 15, Akademie-Verlag, Berlin, p. 817.
- Rao, C.R. (1962): Advanced Statistical Methods in Biometric Research, Wiley.
- Reilly, A.E., and Enger, I. (1967): The Influence of Radio Brightness Temperature on Solar Flare Prediction, AFCRL-67-0670, Hanscom Air Force Base.
- Reilly, A.E., Enger, I., and Pavlowitz, A. (1969): Flare Occurrence Tomorrow as a Function of Area and Flariness of Sunspot Today, AFCRL-69-0148, Hanscom Air Force Base.
- Seagraves, P.H. (1972); UBC BMD07M Stepwise Discriminant Analysis, University of British Columbia Computing Centre Documentation.
- Simon, P. and McIntosh, P.S. (1972): Survey of Current Solar Forecast Centers, in P.S. McIntosh and M. Dryer (eds.), Solar Activity Observations and Predictions, Progress in Astronautics and Aeronautics 30, MIT Press, p. 343.
- Williams, D.J. (1976): National Oceanic and Atmospheric Administration Report ERL 357-SEL 37, U.S. Dept. of Commerce.

LOGISTIC REGRESSION FOR SOLAR FLARE PROBABILITY FORECASTING

D. F. Vecchia, G. A. Caldwell and P. V. Tryon
Statistical Engineering Division
Center for Applied Mathematics
National Bureau of Standards
Boulder, CO 80303 (U.S.A.)

and

R. H. Jones
Department of Biometrics, Box B-119
University of Colorado Medical Center
Denver, CO 80262 (U.S.A.)

An objective statistical technique has been proposed for 24-hour forecasting of solar flares by region. This technique is founded on a logistic response function model for conditional probabilities in the general classification problem. The logistic regression model is demonstrated to provide a reasonable framework to forecast the occurrence or nonoccurrence of solar flares, but the extension of the technique to discriminate among X-ray classes involves, primarily, the proper selection of a training sample to determine a model relevant to the specific probability to be forecast. Objective scoring procedures are used for intercomparison of logistic regression, multivariate discriminant analysis, and subjective forecasts provided by the Space Environment Services Center (SESC) of the National Oceanic and Atmospheric Administration, Boulder, Colorado.

1. INTRODUCTION

Historically, solar flare forecasting methods have been subjectively formulated, relying heavily on forecaster insight. This paper addresses the desire for an objective technique for solar flare probability forecasting, in light of the importance of accurate forecasts to the scientific community and the general public.

The Space Environment Services Center (SESC), a part of the NOAA Space Environment Laboratory in Boulder, Colorado, provides 24-hour probability forecasts of regional solar flare disturbances (Heckman (1979)). Variables comprising predictive information for this subjective method are those found or conjectured to be useful by SESC forecasters over a period of years (Hirman and Flowers (1979)). The "region analysis" variables thought essential to flare occurrence serve, as well, for our development of an objective technique.

Solar flare forecasts made by the SESC predict both the occurrence and magnitude of flares. Four classes, denoting the largest event in a 24-hour period, can be identified: (1) no flare, (2) class C flare, (3) class M flare, and (4) class X flare. It is the moderate class M flare and the major class X flare which are of greatest consequence to near-earth environmental disciplines.

If we let z represent a random variable such that $z = 0, 1, 2,$ or 3 corresponding to the largest event (flare) which occurs in the next 24 hours in a selected region, then estimates are provided by the SESC for the following conditional probabilities:

- (i) $\Pr[z = 0 \mid x]$
- (ii) $\Pr[z \geq 1 \mid x]$
- (iii) $\Pr[z \geq 2 \mid x]$
- (iv) $\Pr[z = 3 \mid x]$

where x denotes an observed vector of prediction variables associated with the selected region.[†]

Objective prediction of probabilities (i)-(iv), or variants of these, has been accomplished with some success by Hirman, et al. (1979) using the technique of multivariate discriminant analysis. These results demonstrate potential improvement on subjective forecasts and, together with our preliminary forecast model performance, indicate that, perhaps, the time has arrived for an expanded effort to develop an objective technique. This would enable forecasters to attach quantitative significance to the many (interrelated) variables comprising the inputs to any forecasting method.

We propose the technique of logistic regression for prediction of (i)-(iv). Empirical evaluation of the technique extends only to (i) and (ii) at present. We suggest, however, that an extension of the method to forecast (iii) and (iv) or other desired probabilities will be apparent from the general description of the logistic analysis procedure. Though we undertake

[†]The notation " $z = 0 \mid x$ " is read " $z = 0$ given x ." For example, (iii) is the probability that an M or X flare occurs **given** the predictors x .

to examine only 24-hour forecasts, with continued development and understanding the procedure can be applied to other time frames. It should be emphasized that a complete evaluation of any proposed technique can result only from comparison to the baseline measure provided by the subjective forecasting system. For the example, we provide scores for intercomparison of logistic regression, discriminant analysis, and the SESC forecasts, based on the measures of section 4.

2. THE LOGISTIC MODEL

All information regarding z given by an observed x is contained in the conditional probability distribution $F(z | x)$. We therefore define a probability estimate to be an estimate $F(z | x)$ of the conditional probability distribution. This paper considers only estimation for a dichotomous random variable where $z = 1$ corresponds to the occurrence of a class C, M or X flare in the next 24 hours and $z = 0$ indicates no flare activity. Extension of logistic regression to polychotomous z is discussed in Jones (1968) and (1975). The latter case corresponds to probability forecasts by Hirman et al. (1979).

The general problem is to relate a qualitative, or discrete, dependent variable to one or more predictor variables, which may or may not be qualitative. Suppose that region-day observations belong to two distinct populations. For example, π_1 , might denote the set (population) of region-day occasions which produce at least a class C flare in the next 24 hours, and π_0 the set of occasions producing no flare. Let the probabilities that observations belong to π_1 and π_0 be p_1 and $p_0 = 1 - p_1$, respectively. Also, let the population membership of an occasion be given by a random variable z , where $z = 1$ if the region-day observation belongs to π_1 and $z = 0$ otherwise. A random vector x is observed on each region and, on the basis of x , a decision or forecast is to be made about which population the region belongs to, that is, about z .

It is usually assumed that for both π_0 and π_1 , the random vector x has a multivariate normal distribution with different mean vectors μ_0 and μ_1 , but common covariance matrix Σ . In this case it can be shown that:

$$\Pr[z = 1 \mid x] =$$

$$\left\{ 1 + \frac{p_0}{p_1} \exp\left[-x - \frac{1}{2} (\mu_0 + \mu_1)'\right] \Sigma^{-1} [\mu_1 - \mu_0] \right\}^{-1}, \quad (2.0.1)$$

which is of the form

$$p(x) \equiv \Pr[z = 1 \mid x] = 1/[1 + \exp\{-\alpha - x'\beta\}]. \quad (2.0.2)$$

This is the logistic regression model, where (α, β) are unknown parameters to be estimated from the data. It appears to be a reasonable model since, as a smooth function of x , $p(x)$ is bounded between 0 and 1 and approaches these values as limits as $x_j \rightarrow \pm\infty$ for any j .

2.1 Estimation of (α, β)

We will mean by **logistic regression (LR)** the procedure by which statistical maximum likelihood estimators (MLEs) of (α, β) are obtained for the logistic regression model. Other estimation methods lead to competing probability estimators. The most common alternative formulation of the problem leads to discriminant function estimators (DFEs) of (α, β) for the logistic response function. The latter technique is the basis for the multivariate **discriminant analysis (DA)** used by Hirman, et al. (1979) and has been computed for comparison in the example. Brelsford and Jones (1967) discuss the differences between MLE and DFE procedures.

2.2 Discussion

Press and Wilson (1978) note that:

"Discriminant function estimators have often been used in logistic regression, in both theory and applications. When such estimators were compared empirically with maximum likelihood estimators for logistic regression problems, however, they were found to be generally inferior, although not always by substantial amounts...

The rationale for a logistic formulation of the relationship between qualitative and other variables ... has been discussed extensively in the literature ...".

We suggest consideration of the logistic formulation for the solar flare forecasting problem for many of the reasons alluded to indirectly in the

above statement. In particular, the logistic response function (2.0.2) was demonstrated to result if the explanatory variable x is multivariate normal for each population. However, many types of underlying assumptions about x lead also to a prediction equation of the logistic form. For example, the logistic results if some predictor variables are multivariate normal and others are qualitative, so that LR estimation is appropriate for more general distributions of x in addition to multivariate normal. The DA approach, however, is strictly applicable only when x is multivariate normal. For the present application most of the explanatory variables are qualitative. In such cases, the differences in solutions for the two approaches can be substantial.

We do not provide additional support for the logistic approach here. The important comparisons can be found in Brelsford and Jones (1967) or Press and Wilson (1978). However, we remark that in a similar application, LR is used by the National Weather Service to forecast conditional probabilities of frozen precipitation (Glahn, et al. (1973)).

3. SELECTION OF PREDICTORS

3.1 Transformation of Variables

At this time, we consider neither the transformation of individual variables nor the addition of explanatory "functions" of given variables as new predictors. Both of these considerations could serve to relate the physical mechanism which produces flares. Conversely, a thorough examination of interactions among variables may enhance understanding of the solar flare process. These issues will be central in any continuation of this work.

3.2 Stepwise Variable Selection

A question of fundamental interest centers around the identification of information essential to prediction of flare occurrence. Furthermore, we would like to identify the relevant explanatory variables in order of importance to a purely objective prediction method.

We have adapted a logistic regression computer program written by the fourth author to allow stepwise, one-at-a-time deletion of least informative variables from the total explanatory set. The deletion criterion is a statistical test of hypothesis concerning the additional explanatory information provided by a selected variable, after account is taken of information provided by all other predictors. This is analogous to the

(backward) stepwise regression procedure for objective variable selection. A logistic regression program has recently become available in the UCLA Biomedical Computer Programs P-series (BMDP).

4. EVALUATION OF OBJECTIVE METHOD

The objective flare forecast techniques will be tested by comparing probability estimates from the models to the baseline subjective forecasts. Two scoring procedures discussed by Brelsford and Jones (1967) are considered.

The Brier Score used in meteorology is essentially mean square error. It assigns a loss of

$$\sum_{j=0}^1 (z_{ij} - \hat{z}_{ij})^2$$

to the i -th trial, where we have used \hat{z}_{ij} to denote an estimate of $\Pr[z_j = j | x_i]$, and where $z_{i0} = 1$ if the i -th region-day occasion produced no flare, $z_{i0} = 0$ if a flare resulted, and $z_{i0} + z_{i1} = 1$. Given a set of N trials, the Brier Score for a forecast method M is:

$$\text{Brier}(M) = \frac{1}{N} \sum_{i=1}^N \sum_{j=0}^1 (z_{ij} - \hat{z}_{ij}^{(M)})^2.$$

Another natural scoring function derived from information theory assigns a loss of $-\log \hat{z}_{i(m)}$ to the i -th trial, where m is the event which occurred. For forecast method M , the Information Loss Score is given by:

$$\text{Info}(M) = -\frac{1}{N} \sum_{i=1}^N \log \hat{z}_{i(m)}^{(M)}.$$

This loss function is minimized by maximum likelihood estimation of the parameters.

For both scoring measures it is desirable to achieve a minimum score. Three forecasts are considered for the example: the SESC subjective forecasts, LR estimates, and DA forecasts. The Information Loss Score may be preferred since probability estimates are constrained to the range $0 < \hat{z} < 1$. A probability prediction of zero is unacceptable if the event occurs, since the loss would be $+\infty$.

5. EXAMPLE

To illustrate the ideas of section 2-4, we consider the estimation of $p(x) \equiv \Pr[z = 1 | x]$ where, for a given region, $z = 1$ if the region produces a class C, M, or X flare in 24 hours and $z = 0$ otherwise.

5.1 Data Record

The empirical data result from a data collection and analysis scheme initiated by the SESC on January 1, 1977. Our example is based on 1495 region-day records collected through December 31, 1977. This record was further reduced to 949 cases by the elimination of records indicating the absence of sunspots, since such regions rarely result in flares.

The explanatory variables for this study were mixed -- continuous and discrete -- and some were dichotomous. A priori, a few of the variables provided by the SESC were withdrawn from the analysis based on an observed high number of missing values among the 949 cases. These variables were exempted since the high missing value rate indicates a frequent loss of predictive information and because it was desired to utilize the maximum number of cases over the limited period of record.

A list of available variables is presented in Table 1. Fifteen explanatory variables, selected with the above considerations in mind, are denoted by "*". We have indicated if a variable is continuous or discrete and, if discrete, the number of distinct levels assumed. Some variables are recoded and/or reordered versions of the original SESC counterparts. For the most part, this recoding was based on a reassessment by staff forecasters of the relation of the variables to solar flare activity. Additional information in Table 1 reflects the fact that variables range from completely objective measurements to highly subjective forecaster observations, such as visual evaluation of photographic maps. This range has been informally coded into three categories by SESC forecasters.

1. EXPLANATORY VARIABLES.[†]

Number	Name	Type	Description
1	*SPOTCLAS	D-8	Coded sunspot class (2)
2	*MAGCLAS	D-7	Magnetic class (2)
3	MAGSTR	D-9	Magnetic field strength (3)
4	MAGGRAD	C	Magnetic gradients in gamma/km (3)
5	*SSDYNAM	D-3	Sunspot dynamics (1)
6	*SSINTER	D-2	Interaction with another region (1)
7	*STGDEV	D-6	Stage of development (2)
8	*LEADTRAI	D-6	Leader emerged in leader or trailer polarity fields (3)
9	*SECTEOW	D-8	Relation with nearest sector boundary (3)
10	PLAGFIL	D-6	Plage compactness and embedded filament (1)
11	NEUTLOR	D-5	Main NL orientation within plage (1)
12	*REVPOL	D-2	Orientation within plage (3)
13	NEUTLCOM	D-5	Neutral line complexity (1)
14	NEUTLCHG	D-3	Neutral line temporal changes (1)
15	ASSOCFIL	D-5	Associated filament (2)
16	*BRTPTS	D-3	Bright points (3)
17	*PLAGFLUX	D-2	Plage fluctuations (3)
18	*ISOPOLE	D-2	Isolated pole (2)
19	*EFR	D-3	Emerging flux (2)
20	*AFS	D-2	AFS present (3)
21	FLAREHIS	D-4	Largest flare since appearance (3)
22	FIRSTAPP	D-6	Region first appeared (3)
23	PROTHIS	D-3	Proton event history (3)
24 [†]	FLARER	D-4	Largest flare in next 24 hours (3)
25	*FLUX	C	10 cm flux (3)
26	*FLARERT	D-4	Largest flare today (3)

[†]Variable type codes are: C = continuous and D-n = discrete-number levels. Description parenthetic codes denote level of objectivity for the response (1 = least objective, 2 = moderately objective, 3 = most objective).

[‡]Denotes dependent variable -- not a predictor.

5.2 Model Estimation

The observations analyzed were 881 region-day cases for which no data were missing on the selected variables. Cases were divided into two groups. The first group of 612 cases was used as a training set for the estimation of the parameters (α, β) in (2.0.2). The remaining group of 269 cases, called a hold-out sample, was used to cross-validate the probability forecast function estimated from the first group. Division of cases was achieved by first including all M and X event observations in the hold-out sample, and then randomly selecting some no flare and C flare cases to be held out.

Remaining no flare and C flare observations served to estimate (α, β) . M and X events were arbitrarily held out since such observations may introduce a bias in the procedure for predicting **at least** a class C flare. The training and validation sets remained fixed for both the LR and DA estimation procedures.

To select a subset of explanatory variables to be used for probability prediction, we employed the (backward) stepwise procedure described in section 3.2. At stage k the maximum likelihood estimators (α_k, β_k) were obtained and then, for $z = 1$ corresponding to the occurrence of a class C, M, or X flare, the LR regression forecast for case j is given by:

$$\hat{p}(x_j^{(k)}) \equiv \hat{\Pr}[z_j = 1 \mid x_j^{(k)}] = 1/[1 + \exp\{-\hat{\alpha}_k - \hat{\beta}_k' x_j^{(k)}\}]. \quad (5.2.1)$$

Here we have used $x_j^{(k)}$ to denote the set of observed variables in the equation at stage k for case j . The dimension of x is reduced by one at successive stepdown stages. DA forecasts obtain from (5.2.1) when corresponding discriminant function estimators of (α, β) are computed.

Two stopping criteria were considered by the authors to determine the final prediction model. The two methods are: chi-square tests based on the change in $-2 (\log_e \text{likelihood})$ when deleting parameters, and Akaike's Information Criterion (AIC) (Akaike (1973) and (1974)), which is:

$$\text{AIC} = -2 (\log_e \text{likelihood}) + 2 (\text{no. of estimated coefficients}).$$

AIC is an objective method for selecting the "best" model from a number of alternatives by choosing the model for which AIC is a minimum. This method is subjectively adjusted by deleting an insignificant predictor in the "best" model if there is one, and backing off to the next model as long as AIC does not increase by more than 1 or 2. We have elected to be conservative in deleting variables for the example since a more thorough examination is desirable.

Associations of the explanatory variables with flare incidence may be studied by inspection of the estimated prediction equations. Table 2 displays the chosen set of variables and the estimated parameters (α, β) to be used for probability prediction in (5.2.1).

2. ESTIMATED PARAMETERS.

Variable	Parameter	Parameter Estimates	
		Discriminant Analysis	Logistic Analysis
Constant	α	7.491	5.483
SPOTCLAS(1)	β_1	- .388	- .267
MAGCLAS(2)	β_2	- .649	- .280
SSDYNAM(5)	β_3	- .085	- .111
SECTEOW(9)	β_4	-2.856	-1.325
REVPOL(12)	β_5	- .872	- .690
BRTPTS(16)	β_6	-1.831	-1.540
PLAGFLUX(17)	β_7	- .724	- .573
EFR(19)	β_8	-1.015	- .800
AFS(20)	β_9	- .013	- .011
FLUX(25)	β_{10}	-2.490	-1.179
FLARERT(26)	β_{11}	- .457	- .167

It is not surprising that the estimates of β_i 's are negative since the scales for most variables are based on a subjective association between flare activity and region measurements. From (5.2.1) it can be observed that a negative β_i is consistent with a positive correlation of the corresponding x_i to flare incidence.

5.3 Probability Forecasts

We are particularly interested in a comparison of actual predictions by the objective and subjective procedures. In the appendix SESC, LR, and DA forecasts for the validation set of region-day occasions are tabulated. We remark here that it is reasonable to suspect that some cases for which large discrepancies between SESC and objective methods exist could be the result of data tabulation or keypunch errors. This would not, in principle, be a problem if a computer model for online probability forecasts was implemented. Existence of such outliers would, however, disrupt the methods of comparison in the next section.

5.4 Model Evaluation

Observations in both the training and validations sets were classified into the two event classes (no flare vs. C, M, or X flare) using estimated prediction functions (see Tables 4 and 5). Classifications for the SESC forecasts are given in Table 3.

3. SUMMARY OF CLASSIFICATIONS BY SESC.

	Event Observed	Percent Correct	Event Predicted	
			No Flare	C Flare or Greater
Training Set	No Flare	90.6	484	50
	C Flare	60.3	31	47
Validation Set	No Flare	90.7	194	20
	C Flare	52.2	11	12
	M Flare	89.7	3	26
	X Flare	66.7	1	2
C,M or X Flare		72.7	15	40

4. SUMMARY OF CLASSIFICATIONS BY LR.

	Event Observed	Percent Correct	Event Predicted	
			No Flare	C Flare or Greater
Training Set	No Flare	96.6	516	18
	C Flare	42.3	45	33
Validation Set	No Flare	97.2	208	6
	C Flare	34.8	15	8
	M Flare	65.5	10	19
	X Flare	66.7	1	2
C,M or X Flare		52.7	26	29

5. SUMMARY OF CLASSIFICATIONS BY DA.

	Event Observed	Percent Correct	Event Predicted	
			No Flare	C Flare or Greater
Training Set	No Flare	89.5	478	56
	C Flare	69.2	24	54
Validation Set	No Flare	90.7	194	20
	C Flare	69.6	7	16
	M Flare	89.7	3	26
	X Flare	100.0	0	3
C,M or X Flare		81.8	10	45

The SESC classified 531(484+47) of the 612 cases in the training set correctly, for an 86.8 percent correct classification rate. In the validation set 234(194+40) of the 269 cases were classified correctly, for a success rate of 87.0 percent.

Corresponding results for the logistic analysis are in Table 4. For the training set, 549(516+33) of the 612 cases were correctly forecast, for an 89.7 percent correct classification. In the validation set, 237(208+29) of the 269 cases, or 88.1 percent, were classified correctly.

The discriminant analysis (Table 5) classified 532(478+54) cases, or 86.9 percent, correctly in the training set. For the validation set, 239(194+45) of the 269 cases were correct, for a rate of 88.8 percent correct.

A strict comparison of overall classification rates for the validation set would seem to favor the DA predictions, though all methods demonstrate considerable skill in classifying regions. The most striking feature of the results, however, becomes apparent from examination of success rates on a finer partition of event classes. What is indicated by this example is that LR may have a minimum error rate for classification of no flare events and DA may be superior for correctly predicting the occurrence of flares. It is possible that apparent differences are the result of an offset in the forecasts, which perhaps could be removed by adjusting α for one of the methods.

The Brier and Information Loss Scores of section 4 are more informative measures of forecast method performance because they are indicative of the "average" discrepancy between the probability estimate for the event which occurred and the aposteriori probability for the event (viz. 1). Both the Brier Scores (Table 6) and the Information Loss Scores (Table 7) are, for the

most part, consistent with the comments and conjectures made with respect to classification rates.

6. BRIER SCORES FOR ALL FORECAST METHODS.

	Event Observed	Number Cases	SESC	Logistic Analysis	Discriminant Analysis
Training Set	No Flare	534	.128	.045	.167
	C Flare	78	.633	.863	.474
	All	612	.192	.149	.206
Validation Set	No Flare	214	.130	.045	.156
	C Flare	23	.701	.974	.476
	M Flare	29	.159	.496	.179
	X Flare	3	.436	.459	.036
	No + C	237	.186	.135	.187
	C + M + X	55	.401	.694	.296
	M + X	32	.185	.493	.166
	All	269	.186	.178	.185
All Data		881	.190	.158	.200

7. INFORMATION LOSS SCORES FOR ALL FORECAST METHODS.

	Event Observed	Number Cases	SESC	Logistic Analysis	Discriminant Analysis
Training Set	No Flare	534	.224	.101	.306
	C Flare	78	1.015	1.326	.747
	No + C	612	.325	.257	.362
Validation Set	No Flare	214	.226	.105	.296
	C Flare	23	1.064	1.450	.755
	M Flare	29	.269	.756	.286
	X Flare	3	.592	.642	.101
	No + C	237	.308	.236	.340
	C + M + X	55	.619	1.040	.472
	M + X	32	.299	.746	.268
	All	269	.307	.296	.332
All Data		881	.319	.269	.353

Individual or combined scores for the training and validation sets showed LR to be better than both the SESC and DA methods. For the validation set, DA and SESC Brier Scores were nearly equal. It is apparent that LR scored uniformly better than the SESC and DA on no flare cases and

uniformly worse on region-day observations producing 24-hour flares. Also, DA was better for this example than the SESC on cases producing flares excepting M flare events, where the SESC forecasts were slightly better.

6. SUMMARY AND SUGGESTIONS

The objective techniques of (LR) and discriminant analysis (DA) have been demonstrated to be somewhat successful for probability forecasting of solar flares. For the example, LR showed an apparent bias toward underprediction, while DA may overpredict flares. As a result, LR scores better than DA and the SESC on no flare cases, and DA performs best on cases producing flares. Because the appendix shows that DA forecasts are usually higher than LR forecasts, the possibility of an offset, which could be removed by adjusting α 's, requires further investigation.

This paper has considered the prediction of $\Pr[C, M \text{ or } X \text{ Flare} | x]$. The extension to other forecasts will involve the proper selection of subsets of cases to estimate a hierarchy of prediction models, not all (necessarily) depending on the same set of explanatory variables. Developing the full potential of objective forecast techniques will demand great effort and cooperation on a broad front. We have identified the central considerations for continuation of this work to include: (1) transformed and rate of change variables, including physically relevant "interactions;" (2) conditional models to account for persistence--an approach would be to fit distinct models, conditional on flare occurrence or nonoccurrence during the 24-hour period when the prediction is made; (3) adaptive models to follow secular variation in the solar cycle; and (4) spatial and time correlation, possibly accounted for by inclusion of lagged variables.

ACKNOWLEDGMENTS

The work reported here was supported by the U.S. Department of Commerce, NOAA Space Environment Laboratory (SEL). The authors would like to thank G. R. Heckman (SEL) for the opportunity to investigate the use of logistic regression for solar flare forecasting. Numerous discussions with W. E. Flowers, J. W. Hirman and T. G. Clark of the SEL provided both understanding and encouragement for the study. We also thank T. G. Clark for assistance in preparation of the data, and J. E. Koontz and J. R. Donaldson of the Statistical Engineering Laboratory, National Bureau of Standards, for computational assistance.

APPENDIX

Below are tabulated probability forecasts for the 269 cases of the validation data set. Presented are SESC, logistic regression (LR), and discriminant analysis (DA) predictions of $100 \cdot \Pr[C, M \text{ or } M \text{ Flare} | x]$. The actual event is noted in column two.

No.	Event	SESC	LR	DA	No.	Event	SESC	LR	DA
1	No Flare	1	3	4	44	No Flare	89	43	91
2	No Flare	1	3	4	45	No Flare	10	4	6
3	No Flare	1	3	4	46	No Flare	20	5	9
4	No Flare	1	4	6	47	No Flare	10	2	4
5	No Flare	1	3	4	48	No Flare	5	2	3
6	No Flare	1	3	4	49	No Flare	5	3	4
7	No Flare	1	4	7	50	No Flare	1	4	4
8	No Flare	50	33	89	51	No Flare	15	12	23
9	No Flare	10	8	19	52	No Flare	10	2	3
10	No Flare	10	10	21	53	No Flare	30	12	36
11	No Flare	50	20	52	54	No Flare	30	15	57
12	No Flare	10	3	5	55	No Flare	1	4	4
13	No Flare	50	3	5	56	No Flare	80	10	22
14	No Flare	1	2	3	57	No Flare	94	30	83
15	No Flare	10	6	19	58	No Flare	40	6	15
16	No Flare	1	3	4	58	No Flare	40	3	6
17	No Flare	30	15	51	60	No Flare	30	3	4
18	No Flare	1	2	2	61	No Flare	10	3	6
19	No Flare	50	3	4	62	No Flare	10	2	4
20	No Flare	1	3	6	63	No Flare	30	8	13
21	No Flare	1	3	6	64	No Flare	20	3	4
22	No Flare	10	25	76	65	No Flare	20	5	6
23	No Flare	1	3	4	66	No Flare	30	5	10
24	No Flare	20	2	3	67	No Flare	20	5	10
25	No Flare	20	2	3	68	No Flare	1	2	3
26	No Flare	75	6	26	69	No Flare	20	2	3
27	No Flare	1	2	3	70	No Flare	60	25	71
28	No Flare	5	2	2	71	No Flare	40	5	7
29	No Flare	10	2	3	72	No Flare	69	36	94
30	No Flare	5	2	3	73	No Flare	60	4	8
31	No Flare	10	2	3	74	No Flare	10	6	21
32	No Flare	10	2	3	75	No Flare	10	6	20
33	No Flare	1	2	2	76	No Flare	40	6	11
34	No Flare	10	8	15	77	No Flare	1	3	3
35	No Flare	3	3	4	78	No Flare	5	3	4
36	No Flare	1	2	2	79	No Flare	10	8	12
37	No Flare	10	4	5	80	No Flare	1	2	2
38	No Flare	15	4	5	81	No Flare	10	6	10
39	No Flare	1	2	3	82	No Flare	30	3	5
40	No Flare	25	42	88	83	No Flare	5	3	5
41	No Flare	5	1	1	84	No Flare	40	6	24
42	No Flare	5	3	3	85	No Flare	30	2	2
43	No Flare	10	3	3	86	No Flare	20	2	2

No.	Event	SESC	LR	DA
87	No Flare	20	2	2
88	No Flare	1	2	4
89	No Flare	1	2	2
90	No Flare	5	2	2
91	No Flare	40	3	4
92	No Flare	20	3	4
93	No Flare	1	2	4
94	No Flare	10	2	2
95	No Flare	10	2	3
96	No Flare	1	3	4
97	No Flare	1	2	2
98	No Flare	1	2	4
99	No Flare	69	21	49
100	No Flare	1	2	3
101	No Flare	10	2	2
102	No Flare	10	3	4
103	No Flare	30	6	19
104	No Flare	10	3	6
105	No Flare	20	3	4
106	No Flare	1	2	3
107	No Flare	1	2	3
108	No Flare	1	2	3
109	No Flare	10	2	3
110	No Flare	1	2	2
111	No Flare	1	5	9
112	No Flare	30	5	13
113	No Flare	20	6	12
114	No Flare	60	5	17
115	No Flare	30	6	18
116	No Flare	10	5	8
117	No Flare	1	3	4
118	No Flare	1	4	5
119	No Flare	5	10	23
120	No Flare	1	5	7
121	No Flare	50	10	22
122	No Flare	10	6	11
123	No Flare	10	6	12
124	No Flare	1	2	3
125	No Flare	10	3	7
126	No Flare	94	53	97
127	No Flare	40	17	75
128	No Flare	25	5	14
129	No Flare	1	3	4
130	No Flare	1	3	4
131	No Flare	30	4	6
132	No Flare	1	10	38
133	No Flare	30	12	32
134	No Flare	1	5	7
135	No Flare	40	55	97
136	No Flare	1	4	6

No.	Event	SESC	LR	DA
137	No Flare	10	6	16
138	No Flare	1	6	11
139	No Flare	1	2	3
140	No Flare	1	2	3
141	No Flare	1	3	5
142	No Flare	1	2	3
143	No Flare	1	2	3
144	No Flare	1	3	5
145	No Flare	1	3	4
146	No Flare	1	2	3
147	No Flare	1	2	3
148	No Flare	1	2	3
149	No Flare	1	2	3
150	No Flare	1	4	11
151	No Flare	1	3	5
152	No Flare	1	5	8
153	No Flare	1	2	3
154	No Flare	1	2	3
155	No Flare	10	5	8
156	No Flare	20	6	16
157	No Flare	10	12	25
158	No Flare	10	26	58
159	No Flare	50	13	36
160	No Flare	20	6	17
161	No Flare	1	3	4
162	No Flare	10	3	5
163	No Flare	1	8	16
164	No Flare	10	3	4
165	No Flare	1	10	16
166	No Flare	5	3	4
167	No Flare	1	6	11
168	No Flare	1	2	3
169	No Flare	1	2	3
170	No Flare	1	3	4
171	No Flare	40	19	41
172	No Flare	10	4	4
173	No Flare	1	8	17
174	No Flare	10	5	9
175	No Flare	69	10	22
176	No Flare	20	6	12
177	No Flare	10	2	3
178	No Flare	10	6	11
179	No Flare	20	15	34
180	No Flare	10	6	17
181	No Flare	1	2	3
182	No Flare	10	5	8
183	No Flare	5	8	16
184	No Flare	1	2	3
185	No Flare	60	82	98
186	No Flare	1	3	4

No.	Event	SESC	LR	DA
187	No Flare	1	4	4
188	No Flare	1	3	4
189	No Flare	1	3	4
190	No Flare	1	3	4
191	No Flare	10	2	3
192	No Flare	30	96	98
193	No Flare	20	8	15
194	No Flare	1	4	5
195	No Flare	20	6	13
196	No Flare	10	10	22
197	No Flare	1	3	5
198	No Flare	10	10	22
199	No Flare	20	19	36
200	No Flare	1	2	3
201	No Flare	10	24	56
202	No Flare	1	6	12
203	No Flare	1	3	4
204	No Flare	1	3	4
205	No Flare	20	3	5
206	No Flare	25	4	6
207	No Flare	10	33	79
208	No Flare	80	71	98
209	No Flare	30	12	27
210	No Flare	10	25	47
211	No Flare	10	16	31
212	No Flare	20	16	31
213	No Flare	89	51	98
214	No Flare	1	4	5

1	C Flare	10	4	8
2	C Flare	50	33	89
3	C Flare	94	32	90
4	C Flare	89	64	98
5	C Flare	5	5	10
6	C Flare	80	25	79
7	C Flare	20	2	4
8	C Flare	85	15	57
9	C Flare	50	16	59
10	C Flare	25	13	26
11	C Flare	40	20	48
12	C Flare	89	96	98
13	C Flare	94	64	98
14	C Flare	94	85	98
15	C Flare	30	25	73
16	C Flare	30	51	96
17	C Flare	80	60	93
18	C Flare	20	25	57
19	C Flare	30	17	49

No.	Event	SESC	LR	DA
20	C Flare	98	87	98
21	C Flare	10	3	4
22	C Flare	1	32	54
23	C Flare	50	55	95
1	M Flare	80	12	39
2	M Flare	89	66	98
3	M Flare	89	85	98
4	M Flare	98	87	98
5	M Flare	25	4	6
6	M Flare	89	49	97
7	M Flare	89	87	98
8	M Flare	89	92	98
9	M Flare	89	85	98
10	M Flare	60	55	98
11	M Flare	89	94	98
12	M Flare	98	87	98
13	M Flare	89	87	98
14	M Flare	98	98	98
15	M Flare	40	36	87
16	M Flare	50	51	92
17	M Flare	80	24	69
18	M Flare	98	92	98
19	M Flare	98	98	98
20	M Flare	98	80	98
21	M Flare	80	66	96
22	M Flare	60	55	97
23	M Flare	80	35	86
24	M Flare	89	60	98
25	M Flare	89	82	98
26	M Flare	85	13	58
27	M Flare	30	4	12
28	M Flare	89	20	51
29	M Flare	89	48	98

1	X Flare	94	91	98
2	X Flare	60	80	98
3	X Flare	30	20	77

REFERENCES

- Akaike, H. (1973): Information theory and an extension of the maximum likelihood principle. Second International Symposium on Information Theory (B. N. Petrov and F. Csaki, Eds.), Budapest, Akademia Kaido, 267-281.
- Akaike, H. (1974): A new look at the statistical model indentification. IEEE Trans. Automat. Contr., AC-19:716-723.
- Brelsford, M. W., and R. H. Jones (1967): Estimating probabilities. Monthly Weather Review, 95:570-576.
- Glahn, H. R., J. R. Brocchieri, and R. H. Jones (1973): Forecasting the conditional probability of frozen precipitation. In: Proceedings from the Third Conference on Probability and Statistics in Atmospheric Science, June 19-22, 1973, Boulder, Colorado, American Meteorological Society.
- Heckman, G. R. (1979): Verification of solar flare forecasts at the space environment services center for the years 1969-1974. Technical report (to appear), U.S. Department of Commerce, National Oceanic and Atmospheric Administration.
- Hirman J. W. and W. E. Flowers, (1979): An objective approach to region analysis for flare forecasting. Technical report (to appear), U.S. Department of Commerce, National Oceanic and Atmospheric Administration.
- Hirman, J. W., D. F. Neidig, P. H. Seagraves, W. E. Flowers, and P. H. Wiborg (1979): The application of multivariate discriminant analysis to solar flare forecasting. To appear in: Solar-Terrestrial Prediction Proceedings, April 23-27, 1979, U.S. Department of Commerce, National Oceanic and Atmospheric Administration, Space Environment Laboratory, Boulder, Colorado.
- Jones, R. H. (1968): A nonlinear model for estimating probabilities of k events. Monthly Weather Review, 96:383-384.
- Jones, R. H. (1975): Probability estimation using a multinomial logistic function. J. Statis. Comput. Simul., 3:315-329.
- Press, S. J., and S. Wilson (1978): Choosing between logistic regression and discriminant analysis. Journal of the American Statistical Association, 73:699-705.

FORECASTING PARAMETERS OF ENERGY BUILD-UP IN THE CHROMOSPHERIC ACTIVE REGION

V.V.Kasinsky

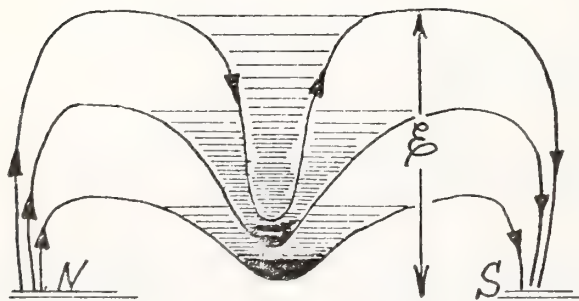
Siberian Institute of Terrestrial Magnetism, Ionosphere and
Radio Wave Propagation, Academy of Sciences
Irkutsk 664033 p/b 4 USSR

An essential drawback of available forecasting schemes is their local character. The analysis of global sequence (550) of flares reveals its "associativity" and interaction of distant active regions. The typical feature of proton flares is the new satellite group emergence. The energy build-up factors is the magnetic gradients and flux near neutral line and the filament depression depth.

1. General considerations

1.1 Flare's time prediction

Forecasts achieve their goal whenever the probability, location, and time and importance of event (flare) are indicated at an accuracy as great as possible. In practice the problem reduces to the pre-calculation of flares of at least 1-class importance as the most geoeffective ones which may be accompanied by protons with fluxes no less than $1 \text{ prot. cm}^{-2}/\text{s ster.}$ (Pereyaslova et al., 1978). The simplest model of a flare region which geometrically corresponds to some observable structure of an active region can be as follows. The quasi-Horizonta magnetic field fixed at the ends in sunspot systems of opposite polarity retains in its central part in the region of the "magnetic canyon", a mass of matter which grows continuously. This model resembles the model of (Kiepenhahn and Schluter, 1957). as being one of several possible models. The concentration of the mass of matter and the "precipitation" of the field lines downward leads to a gradual formation of a dark "neutral filament" designating the $H_{\parallel} = 0$ line of field (fig. 1).



If the initial load (mass of the filament) is lacking at the time $t_0 = 0$ the magnetic field possessing a definite "break" solidity will decay with possible falling of the filament on the two sides of the neutral line producing two flare's ribbons at the time :

$$t_0 = Q_0 / (dQ / dt) \quad (1)$$

Here Q_0 is a certain limit load or tension of the magnetic field leading to a disruption, dQ / dt is the rate of load increase. The formulae (1) is in accordance with the Hyder (1966) mechanism of winking filaments and prominence. In (1) Q_0 can involve all the static characteristics of the system such as gradient, the magnetic moment, the field flux etc., and dQ/dt implies taking into account the dynamics of the same characteristics. From (1) it follows that if static parameters: -configuration, compactness index (Kasinsky et.al., 1976) and gradient etc. can be determined once a day, the determination of the dynamical parameters actually imposes the flare "expectance" time. Since the inverse time of the flare development $1/t \sim 1/\mathcal{T} - 1/T$, \mathcal{T} - is a duration of flash phase, corresponds to the frequencies $3 \cdot 10^{-3} - 10^{-4} \text{ s}^{-1}$ then for a successful forecasting of the same order must be the frequency of observation of the corresponding parameters. Here $\mathcal{T} = 5 \text{ min}$ is the time of the flash phase and $T = 60 \text{ min}$ is the time of prolonged energy input. The routine solar service does not provide such a resolution. Therefore on the basis of the investigation of parameters describing the state of the groups once a day one may forecast to within 1-3 day accuracy (Severny and Steshenko, 1969).

Let us note that if the rate of load is associated with some kind wave or oscillation process $Q = \xi = a \cos(\omega t)$ where a - is an amplitude of winking of filament's depth, ω is Hyder frequency, then $t_0 \approx \xi_0 / a\omega$. This case the characteristic "expectance" time of the flare is the less the greater is the amplitude and the frequency of the periodical process involved. It is noticeable that one of the pronounced manifestation of the pre-flare activity is the growth of the amplitudes of quasi-periodical pulsations of solar radio emission in the "cm" range with 20 - 30 min (Bachyrin et. al., 1978). In the phenomenological scheme of the flare mechanism suggested by Mogilevsky (1978) the low-frequency joint oscillations of the force-free magnetic field and the velocity field on the photospheric level (macromagnetic perturbation) are an important factor in the energy and mass release process in the flare.

Assuming the frequency of the characteristic "pre-flare" oscillations 1-6 cycle per hrs after Hyder (1966) the static magnetic field in the filament region $Q_0 \sim 100 \text{ gs}$ and the amplitude of oscillation about 5 gs we get the mean expectance time of flare for the developed oscillations

$$t_0 \approx 100 \text{ gs} / (5 \text{ gs} \cdot 2,7 \cdot 10^{-3} \text{ s}^{-1}) \approx 5-10 \text{ hrs}$$

Such simple calculations based on phenomenological models illustrates the idea advanced in (Mogilevsky, 1973) that, for the goals of forecasting, important is the knowledge of changes of the characteristic parameters in the pre-flare situation. Thus merely static criteria are insufficient.

1.2 Non-randomness of temporal relationships of flares - far distant interconnections

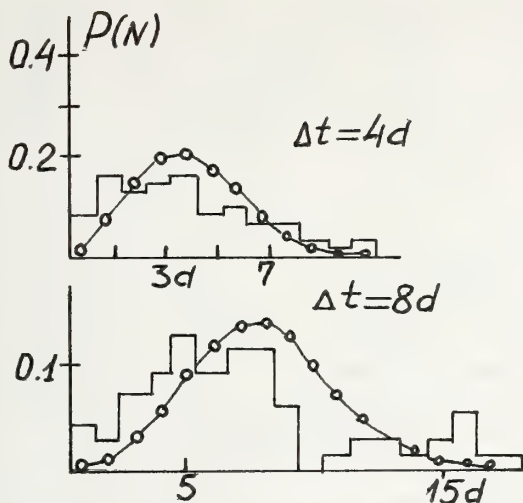
One of the drawbacks of the above mentioned schemes of forecasting is taking into account of only local parameters of groups and the neglecting of the interaction of a given group with the surrounding ones in the process of flaring. Nevertheless long ago has been known a series of phenomena and factors indicating the interaction of spatially distant flares. Here pertains the fact of the existence of sympathetic or mutually - induced flares and the phenomena of Moreton waves (Smith and Smith, 1966) the recent finding of the accompaniment of strong group by distant satellite groups which "stimulate" the flare productivity of the main one (Kasinsky, 1972) and the rare phenomena of "magnetic pulsations" - field enhancement developing immediately alongside of chromospheric flares in several active regions (Chistiakov, 1970).

In this connection is the question of whether the real global sequence of flares will be an accidental series or whether there are "related" associations or corteges of flares (Kasinsky, 1971). The material on No. 19 solar cycle maximum (1958 - 1959) has been used (IGY maps ed. Ellison, 1961). The reality of sympathetic flares can be verified readily via comparison of the observed occurrence of "simultaneous flares with the frequency of Poisson theoretical distribution:

$$P(N) = (\lambda \Delta t)^N \exp(-\lambda \Delta t) / N! \quad (2)$$

which yields the probability of the number N of flares in the time interval Δt if the sequence is random and stationary. The mean occurrence of strong flares for the selected interval was 1.01/day. The probability for finding this or that number $P(N)$ within the Δt -d interval is given in (2). The comparison of the real and theoretical distributions shows an apparent divergence as the flares are being grouped in still longer time intervals: 1, 2, 4, 64 days. And the probability of the multiple birth of flares - the far terms in the Poisson distribution (2) is significantly different from zero. Thus for the intervals of 8 and 16 days a clear secondary maximum on the distribution, Fig. 2 is observed which is completely inconsistent with the theoretical random one. A general conclusion is as follows: at least two flares may be associated through some signal but there is possible an associative relationship of three and more flares. This supports the sympathetic flares concept globally.

The probable number of flares in the association can be revealed using the χ^2 criterion. The diagram χ^2 shows the saturation of the curve within 16-32 days with the mean number of flares in an association being 3-4 . This means that flares



in distant active regions are not independent which agrees with other data (Kasinsky, 1971a). A nice illustration of the associativity of flares are the well known proton events on the Sun in August 1972 where from 1 to 4 August three large flares were observed and other two from 7 to 11 August (Kasinsky, 1976 a).

Fig 2. A comparison of global probability of flares (histograms) and the Poisson random distribution (smoothed) for different time intervals.

1.3 The interaction of flare and satellite-groups

Non-occasional links between active regions may in the general way be accomplished through common systems of magnetic fields or individual field tubes as shown by observations on the "Skylab" (Chase et al., 1975). A triggering interaction between the newly emerging sunspot groups and groups which have signs of proton predictors is also possible. In this connection the question of interest is the large-scale spatial interaction between the satellite and flare groups inside one proton complex (Kasinsky, 1973). The problem was studied on the material of 134 strong flares irrelative to their "protonity" (Kasinsky, 1972). It is typical that out of 134 selected events of flare groups 70% showed the presence of pronounced satellites. Than if a flare of 1+ and 2 classes gives 67% of accompaniments by satellites while the flares of 3 class give 92% of such accompaniments. This implies that strong flares almost always require the presence of a satellite as it was on 30 April 1976 when a day before the proton flare a satellite had appeared whose area was greater than the area of a main sunspot (Kasinsky et al., 1977). As shown by Kasinsky (1972) the satellite pertain as a rule to a rapid dynamical type of development: 1) emerging groups of A and B class; 2) submerging group of class H or J; 3) short-lived (1-3 days) impulsive group; 4) group of a later class C, D, E but with a strong growth phase of the area.

Very important for understanding the satellite-main group relationship is the space correlation observed between the direction to the satellite or azimuth and the azimuth of the main knots of the flare with respect to the group-generator. The correlation proved to be very high 0.8 - 0.9. We have selected 30 proton events on the Earth to which corresponded a flares on the Sun (1957-1958). For those events 40 satellite were identified accompanying proton groups. The correlation degree flare azimuth - spatial location of the flare was found to be + 0.58.

The investigation has shown that in 47% of cases satellites appeared before the flare and in 39% overlapped the time of a flare to within ± 6 hrs. Only in 14% of cases time delay of the satellite appearance with respect to the time of the flare was observed (Kasinsky, 1973). Consequently satellites may be called precursors of strong flares at the photospheric level.

2. Phase of energy accumulation

2.1 Forecasting parameters in the chromosphere of the region

We have described some phenomena and parameters of the active regions taking into account of which is essential in determining the external influence upon the pre-flare situation. However about 30% groups generating flares according to our statistics do not show clearly pronounced a satellites whereas energy accumulation in them does occur undoubtedly. For this purpose one should consider the internal parameters of the group determining the magnitude of the energy build-up.

As it is well known the potential magnetic energy can be stored in various ways e.g. in current systems in the corona (Syrovatsky, 1972). However this way of accumulation is not unique but from the experimental point of view it is questionable (Mogilevsky, 1978). It is known that the magnetic force can be divided into two components (Cowling, 1959):

$$[\mathbf{j} \times \mu \mathbf{H}] = -\text{grad } \mu H^2 / 8 + \text{div } \mu \mathbf{H} \mathbf{H} / 4 \quad (3)$$

and the first term for a slow evolutionary development of the region is nearly always compensated for by the hydrostatic pressure of the environment and does not work. An exception is probably the transient phenomena in which the magnetic field under the special conditions may accelerate the gas before it (Uralov and Kasinsky, 1976). The changes of magnetic energy may take place only on account of the second term (3). Whenever the line of force deviates from the equilibrium, for example under the gravity of the mass which it supports, work is accomplished and energy is accumulated. Thus dark active filament on the neutral line $H_{\parallel} = 0$ can be produced in the magnetic cavity, Fig. 1. Let us calculate the order of energy build-up. For sinusoidally curved line of force with the length λ and depression ξ the volume force will be: $\pi \mu H^2 \xi / \lambda^2$, where H is the field strength. The work on the path $d\xi$ will be $\pi \mu H^2 / \lambda^2 \xi d\xi$, or going over from one field line to the full tube with cross section $S = \pi R^2$ length $2\pi \lambda / 2$ and volume $\pi^2 R^2 \lambda / 2$ we will get integrally the work over the tube volume after integrating from 0 to ξ (Kasinsky, 1978):

$$E \approx \pi^2 \mu / 4 \cdot (\text{grad } H) \cdot F \xi^2 \text{ erg} \quad (4)$$

Here $F = \int R^2 H$ is the magnetic flux and $\text{grad} H \sim H/\lambda$. Thus the magnetic energy accumulated by the filamentary depression, Fig 1 is proportional to the field gradient and magnetic flux supporting the filament and square of deviation of line of force from dipole position. The expression for magnetic energy build-up (4) shows that the magnetic flux is as important as the gradient is (Severny and Steshenko, 1969). Therefore the new magnetic flux eruptions into the surroundings of the "neutral line" as indicated by Rust's (1974) observation are important forecasting factor together with the magnetic gradients.

Formula (4) can be rewritten if we put $F = H \int dl$ where dl is the length element along the filament. Note that in the vicinity of the filament $H_{//} = 0$, $H_{\perp} \neq 0$. Then integrating the magnetic flux of the transversal component along the filament we shall get for the magnetic energy build-up content the formula :

$$E \approx \frac{\pi^2 \mu}{4} \int H_{\perp}^2 (\text{grad } H_{//}) \xi^3 \cdot dl \quad (5)$$

This last expression shows that the energy is proportional also to the length of a dark filament lying on the neutral line. This agrees with such a parameter of evaluation of magnetic complexity as the number of points of curvature -N which is used for forecasting of flare activity.

2.3 Estimation of energy from observable parameters

Of practical interest for forecasting is the calculation of energy build-up of the active region before and after the flare. For calculations we have chosen magnetographic maps of Mt. Wilson NO. 18594 group in isogauss obtained at the Sac. Peak Observatory on 18-23 October 1971 by Rust (1973). A flare of 1B class occurred on 19.X. at 13 04UT. The result of estimation of forecasting parameters of the group and calculation from them of energy from (5) are shown in the Table.

Energetic parameters of Mt. Wilson 18594 group

Date 1971	Magnetic basic gs/ km	gradient local gs/ km	Magnetic flux $\times 10^{22}$ mxw	Zero line length $\times 10^4$ km	Magnetic field H gs	Energy content erg $\times 10^{30}$
18.X	0.084	-	3.3	6.0	160-320	1.6
19.	0.055	0.099	8.6	8.2	80-160	0.7-0.3
20.	0.048	0.119	6.6	10.4	80-160	0.6
21.	0.045	0.074	9.6	7.0	80	0.4
22.	0.038	0.054	11.5	5.6	40-80	0.13
23.X	0.037	0.038	10.1	8.3	80	0.06

For all calculations the value of depression ξ of the filament is assumed to be of the order 1000 km. As shown by the

Table the Mt. Wilson No. 18594 region possessed moderate magnetic gradients not more than 0.15 gs /km. The maximal basic gradient is between the main components of the group not more than 0.085 gs/km one day before the flare. In contrast to this the magnetic flux increased approximately three times by the day of the flare in comparison with preceding day and was 8.6×10^{22} mxw. The zero line length was increasing in the period 18-20 .X. 1971. The maximal energy build-up was observed one day before the flare and was $1.6 \cdot 10^{30}$ erg. From calculation it is seen that after the flare of class 1B the energy in the region dropped nearly two orders.

3. Summary, conclusions

At the present time on the basis of the body of observational data and synoptic information one can carry out a qualitative forecast of solar flares with 70% reliability. For the developing a quantitative forecast (Mogilevsky, 1973) the most promising are the phenomenological models of flares taking account of the internal (oscillations) and external (satellites group) dynamics of magnetic field and considerations based on the physical-statistical analogies for example the "earthquakes - flare" analogy.

1. An essential drawback of the presently available forecasting schemes is their "local" character because the magnetic gradients, δ -configuration and the shape of the zero line etc. bear no information about the phenomena in other regions and about the global interaction of active centers.

2. The statistical analysis of a global sequence of 550 flares (1958-59) has shown that the typical feature of large flares is their "associativity" and homology which is manifested in a strong deviation of their momenta from the random Poisson sequence. The latter indicative of the role of "impulsive" processes covering the size of several active regions on the Sun.

3. The typical feature of most proton flares is the emergence of a new magnetic flux on the periphery of the complex namely the "satellite" sunspot groups separated from the main one. The relationship satellite - flare is manifested in spatial 0,6-0,9 and temporal (0,7) correlation of the mentioned entity.

4. In the phase of preliminary energy build-up the decisive role is played by two parameters - the magnetic gradient and the flux of transversal field penetrating the filament in the region of depression ($H_{\perp} = 0$). The value of energy involves also linear parameters: the magnetic canyon depth (depression) and the filament neutral line length.

Acknowledgments

The author expresses his gratitude and respect to Prof. V. A. Krat for discussions and Prof. V. E. Stepanov for support. The author is indebted to S. I. Syrovatsky, E. I. Mogilevsky as well as

V.F.Chistyakov and V.M.Tomozov for repeated attention and interest to this work. Special thanks to Mr.V.G.Mikhalkovsky for his help in the manuscript preparing.

REFERENCES

- Bot,M.O.(1968): On problem of earthquakes forecast.In:
Earthquakes Forecasting,Moscow,Mir.
- Bachyrin,A.F.,Dvoriashin A.S.,Eryishev N.N.,Cvetkov L.I.(1978):
Pre-burst behaviour of the local source on the Sun on
wavelenth 1.9, 2.5,and 3.7 cm. Report to section of council
"Solar Radioemission",Oct.,Kislovodsk.
- Chase R.C.,Krieger A.S.,Svestka Z.,and Vaiana G.S.(1975):
Skylab observation of X-ray loops connecting separate
active regions. Report to COSPAR Meeting XVII,Varna .
- Chistiakov,V.F.(1970): Some features of short-periodic pulsa -
tions of the magnetic strength of sunspots .In:Res.Geom.
Aeron.Sol.Phys.,Vol.10,Moscow.
- Hyder,Ch.L.(1966):Winking filaments and prominence and coronal
magnetic fields.Z.Astrophys.,Vol.66,No.2,78-84 pp.
- Kasinsky,V.V.(1971):About flare assosiations as the sympathetic
feature of flares on the daily time intervals.Solnechnye
dannie, No.4,104 pp.
- Kasinsky,V.V. (1971a):Solar flare recurrence and energetic
interpretation of the importance scale.Res.Geom.Aeron.Sol.
Phys.,Vol.20,63 -72.
- Kasinsky,V.V. (1972): On the large scale interrelation between
the chromospheric flare generating sunspots and the
satellite groups. Solar-Terrestrial Physics,3,Moscow,296pp.
- Kasinsky,V.V. (1973): On role of the satellite groups as the
proton flare predecessors.Res.Geom.Aeron.Sol.Phys.Vol.26,
118 pp.
- Kasinsky,V.V.,and V.A.Krat (1973a):On solar tsunamy.Solar Phys.
Vol.31,219 pp
- Kasinsky,V.V. (1976):On the mutual influence of space remoute
groups united into the flare active complexses.Report to
7 th Region.Consult.Solar Phys.,Vol VI,ed.by Sykora,
VEDA,Bratislava.
- Kasinsky,V.V.,E.V.Ivanov,V.N.Obridko (1976a): Compactness index
of sunspots and proton flare characteristics.Res.Geom.Aeron.
Sol.Phys. Vol.37,9 pp.

Kasinsky, V.V., V.I. Polyakov, V.G. Zandanov (1977): Observations of the satellite-type sunspots complex region of 26 Apr. - 3 May 1976 at Mt. Sayan Observatory. Report UAG - 61, WDCA, Collect. Data Report for STIP Inter. II, August 1977, 26 - 29 .

Kasinsky, V.V. (1978): Energy build-up and magneto-hydrostatic instability of filament before large flares. Report to IX th Consultation on Solar Physics, Wroclav, 24 pp.

Kippenhahn, R., Schluter A., (1957): Zeits. Astrophys. Vol. 43, 36 pp.

Mogilevsky, I.I. (1973): The qualitative short range forecasting. Vestnic Acad. Sci., No. 3.

Mogilevsky, I.I. (1978) : Phenomenological model of solar flares and pre-flare phenomena. Report to IX th Consultation on Solar Physics, Wroclav, Poland.

Pereyaslova, N.K., L.A. Kolesnikova, M.N. Nazarova, I.E. Petrenko (1978) : Some features of the active region development connected with the proton flares. Report to section of council "Solar Radio emission", Oct., Kislovodsk.

Rust, D.M. (1974): Observation on flare associated magnetic field changes. In: Flare-related magnetic field dynamics. NSAR, Boulder, Colorado, 243 pp.

Rust, D.M. (1973) : Estimation of flare production potential of solar active region from analysis of real time magnetic field data. Preprint Sac. Peak Observatory, ERP, No. 440.

Severny, A.B. and Steshenko N.V. (1969): Magnetic field and problem of flare forecasting. Solar-Terrestrial Physics, Vol. 1, Moscow, 3 pp.

Smith, G. and E. Smith. (1966). Solar flares. ed. Severny, Mir, Moscow.

Syrovatsky, S.I. (1972): Three phase of solar flares. Solar-Terrestrial Physics, Vol. 3, Moscow, 109 pp.

Uralov, A.M. and Kasinsky V.V. (1976): To the problem acceleration transient phenomena on the Sun. Astr. Zhurnal. Vol. 53, 6, 1204 pp.

"Solar activity maps" DI, DII. Annals of IGY. Vol. 21, ed. Ellison, Pergam. Press. Oxford-London-New-York-Paris (1961).

PREDICTION OF SUNSPOT GROUP FLARE ACTIVITY 1-10 DAYS IN ADVANCE

V. B. Gumanitsky, V. I. Efimenko, V. M. Efimenko,
and V. V. Telnyuk-Adamchuk

Kiev University Astronomical Observatory
Kiev, USSR

From the data of sunspot groups, flare activity of spot groups, and sector structure of the interplanetary magnetic field for the period 1956-65, the possibility of predicting flares in a spot group 1-10 days in advance is analyzed. Two problems are solved: the prediction of flares in a spot group 1-10 days in advance from the observations for the first several days; and the prediction of flares of importance 3 and more in a spot group for the period of its passage across the solar disk, from the observations for the first three days of its existence in this revolution. Algorithms used for prediction are described. Verification of forecasts is 70 to 80 percent.

1. INTRODUCTION

Prediction of solar flares is one of the fundamental problems in forecasting solar activity in view of the consequences they cause in the interplanetary space and on the Earth. The present report is a review of some work at Kiev University Astronomical Observatory on short-term predictions of solar flares.

The possibility of predicting flares in sunspot groups with methods related to the theory of image identification was studied. For the parameters characterizing the state of a spot group, the data of the group and development of surrounding ones, the group's flare activity, and also some data of the sector structure of the interplanetary magnetic field (IMF) and of the magnetic field structure in a spot group were used.

To perform this task, analyses were conducted for two different approaches: (1) from the parameters characterizing the state of a spot group for a certain prehistory period, the appearance of flares of different importance is predicted one to two days in advance (Efimenko et al., 1976; and Efimenko et al., 1977); and (2) from the parameters characterizing the state of a spot group--the sector structure of IMF for the first three days of observations from the moment of its appearance--it is possible to predict whether only one flare of importance 3 and more will appear for the period of the group's passage across the solar disk (Gumanitsky, 1979). As forecasting

values, the number of flares and flare index were taken, the latter characterizing the energy release in the group in terms of flares one or two days in advance (in the first case) and the existence or absence of the importance 3 flares for the period of the group passage across the solar disk (in the second case).

2. INITIAL DATA

The observed data of solar activity for cycle 19 published in catalogues were used in the investigations. In view of the fact that different approaches were used, the initial data had to be properly selected.

In the first case the material for 1959 was used. The initial data taken were daily data of solar protosphere and chromosphere observations, namely: the area of a spot group (S), the area of the largest spot in it (S_0), the number of spots in the group (K), group class according to Zurich classification, the number of flares having appeared in the group for a day, duration, importance and area of each flare. The data of spot groups located in the vicinity up to 20° were included in the list of initial data.

Observational material for spot groups is given (Gnevysheva, 1965) and that for the flares as well (Warwick, 1966). To eliminate the distortions in determining the area of the group and the number of spots in it on the limb, the time it was outside 70° from the solar disk center was not considered. Ignoring this time, the spot groups that existed for not less than six days, for a single passage across the disk, were chosen for investigation. About 200 spot groups satisfy these conditions.

In the second case, from the published data for cycle 19, 140 spot groups with areas more than 200 millionths of the sun's visible hemisphere (m.s.h.) were chosen for analysis. From these, 71 groups produced flares of importance 3; the other 69 groups produced no flares. From the groups that produced large flares, 9 appeared on the disk; the other 62 appeared from behind the limb (for the groups of comparison: 7 and 62, respectively).

It is known that flare activity of the group correlates with its area, especially for energetic groups. Nevertheless, most of the groups with large areas still do not initiate the flares of importance 3, although 70% of the groups that produced such flares have an area more than 200 m.s.h. If one chooses the groups of comparison by chance, the groups with small areas will form the great bulk of them (about 80% of the groups will have areas less than 200 m.s.h.) and the area factor will dominate, creating certain disadvantages at utilizing the method because the groups with large areas will be automatically assigned to potentially active ones. For this reason, the distribution of the basic groups and those of the comparison groups had to be similar in area (Table 1). This specified the task of choosing between groups similar in area to those that generated energetic flares.

The initial data taken were: area of the group (S); area of its largest spot (S_0); the number of spots in the group (K); Zurich classification of groups, area, the number of spots and the class of near spot groups; frequency of the group appearance and the rough orientation of the group magnetic axis; and group location relative to the IMF sector boundary.

Table 1. Distribution of sunspot groups by areas.

Groups \ Area in m.s.h.	200-399	400-599	600-799	800-999	1000-1399	1400	Sum
Basic	16	17	8	12	10	8	71
Comparison	16	16	20	6	8	3	69
All groups	32	33	28	18	18	11	140

The data of spot groups are taken from Gnevysheva (1960, 1962, 1964, 1965, 1967), and Waldmeier (1957-1966); the magnetic group orientation was defined approximately from the maps of Waldmeier (1957-1966); IMF sector structure from Mansurov (1975) and Svalgaard (1972); and flare data from Solar Geophysical Data (1957-1965).

3. PARAMETERS

From the initial data, parameters were obtained which included the values of both the very initial data and the secondary ones. A set of parameters characterizing the state of an object for a prior period has been made to correspond to each of the predicted values for a given day of the existence of a spot group.

In the first case, 28 parameters were obtained from the initial data. A four-day prior period was chosen. Altogether there were 600 such sets from the spot groups treated during 1959.

The parameters obtained can be divided, conditionally, into three groups. The first group consists of the parameters characterizing flare activity of spot groups:

- P₁ is the mean number of flares;
- P₂ is the mean flare index;
- P₃ is the mean number of large flares (having an index greater than that of the mean flare of importance 1);
- P₄ is the mean index of large flares;
- P₅ is the dispersion of flare number;
- P₆ is the dispersion of mean flare index;
- P₇ is the dispersion of mean number;
- P₈ is the dispersion of a mean index of large flares;
- P₉ is the difference in number; and
- P₁₀ is the difference in flare index for the last two days before the forecast.

The second group consists of parameters characterizing the development of a spot group:

- P₁₁ is the group area for the last day before the forecast;
- P₁₂ is the maximum group area for the prior period;
- P₁₃ is the number of days from the day with maximum area to the last day before the forecast;
- P₁₄ is the mean fraction of area of a single spot in the group;
- P₁₅ is the mean splitting of the group;

- P₁₆ is the mean area of a single spot in the group;
- P₁₇ is the mean number of spots in the group;
- P₁₈ is the mean rate of variations in the group area;
- P₁₉ is the dispersion of the mean fraction of a single spot in the group;
- P₂₀ is the dispersion of group splitting;
- P₂₁ is the dispersion of the mean area of a spot in the group; and
- P₂₂ is the Zurich group classification for the last day in relative units.

The group splitting characterizing the irregularity in the group area distribution on single spots similar to Brailovsky et al. (1971) was calculated from the formula

$$S_e = - \frac{S - S_0}{S} \ln \frac{S - S_0}{(k-1)S} - \frac{S}{S_0} \ln \frac{S}{S_0} \quad (1)$$

The characteristics of spot groups surrounding the group constitute the third group:

- P₂₃ is the mean area of a single spot of neighboring groups;
- P₂₄ is the mean rate of variation in the areas of the neighboring groups;
- P₂₅ is the number of neighboring groups;
- P₂₆ is the area of neighboring groups;
- P₂₇ is the number of spots in the neighboring groups; and
- P₂₈ is the distance to the nearest neighboring group on the last day before the forecast.

The parameters for all of the mean values were calculated for the prehistory period; i.e., for four days in advance.

To check the quality of the material used, the dependence of the predicted values on each of the parameters was examined. Graphs were drawn of the predicted values versus the parameters. For a more complete determination of this relationship, a reverse procedure was carried out; i.e., the graphs were drawn of the parameters versus the predicted values. The degree of correlation may be judged by the angle between the direct and inverse relationships. Good correlation with the number of flares is displayed by the parameters: P₁, P₅, P₇, P₉, P₁₁, P₁₂, P₁₃, P₁₅, and P₁₈; good correlation with the index of flares is displayed by the parameters: P₁, P₃, P₅, P₇, P₁₁, P₁₂, and P₁₇.

An examination of the parameters utilized enabled us to reduce the number of parameters from 28 to 15. The remaining parameters are now:

- P₁ is the mean area of a group;
 - P₂ is the mean area of the largest spot in the group;
 - P₃ is the mean number of spots in the group;
 - P₄ is the mean flare index of the group;
 - P₅ is the flare index of the group;
 - P₆ is the mean index of large flares;
 - P₇ is the index of large flares;
 - P₈ is the area of the group;
 - P₉ is the number of spots in the group;
 - P₁₀ is the number of flares in the group;
 - P₁₁ is the flare index in the group on the last day before the forecast;
 - P₁₂ is the area of adjacent groups;
 - P₁₃ is the number of spots in adjacent groups on the last day before the forecast;
 - P₁₄ is the mean splitting of the group; and
 - P₁₅ is the rate of the group area variation for the prehistory period.
- Along with the reduction of the number of parameters, the dependence of

the prediction results on the prehistory period considered was investigated (Efimenko, 1976). To estimate the quality of the predictions, the mean-square deviations of the calculated values from the true values were defined. In Figure 1 is given the dependence of the mean-square deviation σ_N upon the prehistory interval T for the number of flares. The minimum corresponds to a two-day optimal prehistory interval. This result was used for further investigations.

In order to predict large flares from observations of a spot group for the first three days of existence in a particular revolution, a set of 14 parameters has been produced. The sign ϵ is set equal to 1 for the case that a flare occurred and equal to 0 for no flare. The set of parameters was as follows for this case:

- P_1 is the group area;
- P_2 is the area of the largest spot in the group;
- P_3 is the number of spots in the group;
- P_4 is the splitting of the spot group;
- P_5 is the area of the adjacent spot groups in the vicinity up to 20° ;
- P_6 is the number of spots in the adjacent groups;
- P_7 is the number of adjacent groups;
- P_8 is the rate of the group area variations;
- P_9 is the class of the group;
- P_{10} is the class of the most developed adjacent group;
- P_{11} is the frequency of the group appearance;
- P_{12} characterizes the group location relative to the IMF sector boundary projected on the solar surface with a 4.5-day time delay. This parameter is given the value 1 if the group was located at a distance less than 13° from the boundary; the value 0 in the case it was inside the sector of arbitrary polarization; and the value 0.5 when it was impossible to state the group location relative to the boundary for some reason.
- P_{13} is the rough orientation of the group's magnetic axis. This parameter is given the values of 0 in the case of a single spot; 2 if the magnetic axis deviated severely from the parallel; and 1 in intermediate cases.

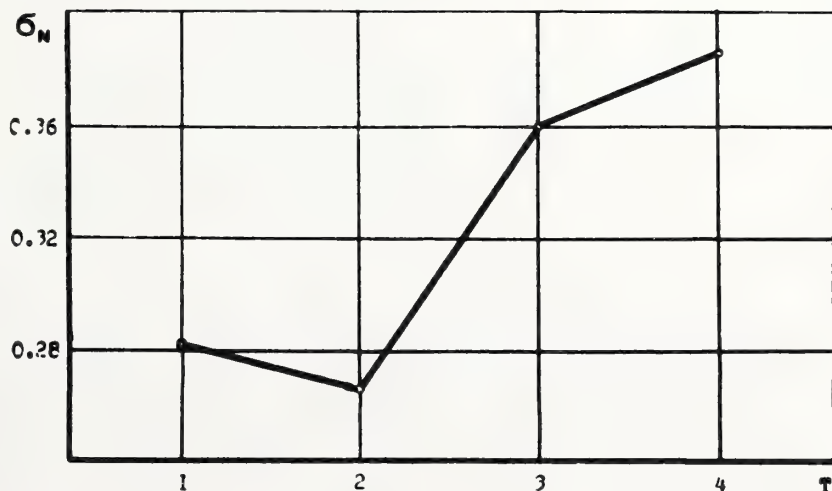


Figure 1. Dependence of σ_N mean-square deviation upon the prehistory interval T for the number of flares.

P_{14} was arrived at by considering some investigations indicating the relation between the flare activity and sector boundary character (Dittmer, 1975). This parameter is given the value 0 if the group is in the North hemisphere near the sector boundary where the polarity changes from + to -; 1 in the inner part of the sector or near the +/- boundary in the South hemisphere; and 2 at the +/- boundary in the South hemisphere.

Parameters P_1 to P_6 and P_8 were averaged for the first three days of observations after the group appeared from behind the eastern limb or after its appearance on the disk (there were about 10% of such groups). The class of a group, as in the first approach, was parameterized on the basis of the Zurich classification: classes A and B were set equal to 1; C and D = 2; E and F = 3; and G, H, and J = 4.

From the correlations between the reduced parameters, closed, isolated groups of parameters can be distinguished. By choosing the most typical members from the group of parameters and without losing information, the analysis can proceed with a smaller number of parameters. To distinguish such groups, a factor analysis may be conducted by building the "correlation pleiads," the analysis of a belonging factor and so on.

Table 2 gives the correlation matrix of all the parameters. The second column contains correlation factors with the sign (predicted value).

Table 2. Correlation matrix of initial parameters (in 0.01 units)

P	ϵ	1	2	3	4	5	6	7	8	9	10	11	12	13
1	16													
2	02	74												
3	50	56	22											
4	46	46	-11	78										
5	20	02	-08	15	14									
6	28	-06	-10	12	10	77								
7	27	08	0	15	16	45	56							
8	-09	35	27	29	28	04	0	-02						
9	-34	-09	17	-40	-52	-14	-13	-16	-16					
10	12	01	-07	12	11	52	40	68	-06	-13				
11	14	-01	-05	-09	-08	04	05	07	-12	10	05			
12	-08	09	-01	-05	02	11	08	-01	04	04	07	02		
13	34	35	10	50	55	10	08	26	18	-49	16	05	02	
14	-02	07	11	0	-06	03	07	02	10	01	-01	07	14	-01

Figure 2a presents the "correlation pleiads." Circles contain the parameter numbers; corresponding correlation factors are below the lines connecting them. Figure 2b gives the diagrams, with the same designations, for two combinations of parameters (minimum correlation level is 30%).

Thus, two combinations can be distinguished: the first, connected with the basic spot group, and the second, connected with the adjacent groups. Furthermore, three individual parameters do not join either of them. These are P_{12} , P_{14} (connected with a sector structure), and P_{11} .

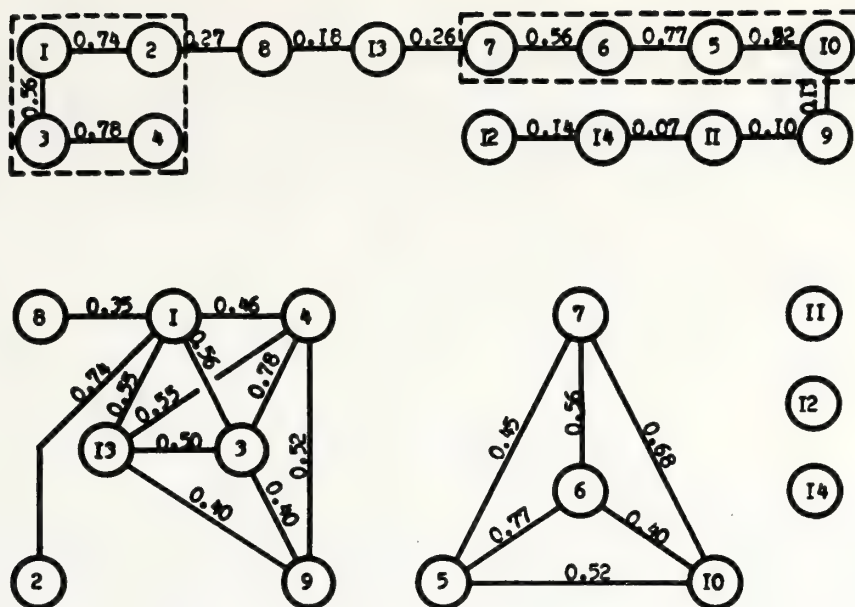


Figure 2. (a) "Correlation pleiads" of the system of parameters, and (b) Groups of closely related parameters.

4. CALCULATION TECHNIQUE

To investigate the possibility of predicting the flares in a spot group, the methods used related to those of the theory of image identification. In particular, the method of building a prediction function as the function of several variables was used in the first case, and the method of potential functions (MPF) and the method of group consideration of arguments (MGCA) were used in the second case.

4.1 The Method of Building a Prediction Function as the Function of Several Variables

A prediction function similar to that of Brailovsky et al. (1971) is built by means of successive approximations

$$F = \sum_{m=1}^s f_m(P_{i_m}, P_{j_m}); \quad i_m, j_m \in \{1, 2, \dots, n\} \quad (2)$$

where s is the number of approximations and n is the number of parameters characterizing the state of an object. Each approximation depends on the pair of parameters built in terms of

$$f_m(P_{i_m}, P_{j_m}) = \alpha_m + \beta_m P_{i_m} + \gamma_m P_{j_m} + \delta_m P_{i_m} P_{j_m} \quad (3)$$

Coefficients α_m , β_m , γ_m , and δ are defined by means of the least-square method (LSM). For a first approximation, by successively selecting all possible combinations of parameters, an approximation of F is built and from the condition that the sum of the squares of the residuals is a minimum, the best pair of parameters is chosen. Then the procedure is repeated for the residual

$$\Delta_1 = F - f_1(P_{i_1}, P_{j_1}) \quad (4)$$

Similarly, $f_2(P_{i_2}, P_{j_2})$ is built, and so on.

4.2 The Method of Potential Functions

If there are two standard points from two opposite classes, then some unidentified point should be assigned to the class the standard of which will prove to be nearer in a certain sense. As a measure of such proximity of point s to standard x^* , it is suggested that the function value be chosen of the type of the potential (Aizerman et al., 1970) at this point (standard being a "source" of potential). Then assuming the function

$$f(x^*, x) = [1 + \alpha \rho^\beta(x^*, x)]^{-1} \quad (5)$$

as a basis where $\rho(x^*, x)$ is the distance between two points in multidimensional space, α and β are the function parameters, and assuming all the points of the initial sample to be standard ones we may build the prediction function

$$F_N(x) = \sum_{i=1}^N \tau_i f(x_i^*, x); \quad \tau_i = i^{-\gamma} [F_{i-1}(x_i^*) - \varepsilon_i] \quad (6)$$

Here, N is the number of objects; ε_i is the value of the possibility of prediction for the i th object of the sample. The coefficients τ_i are determined in the process and characterize the standardization of the i th point of the initial sample; α , β , and γ are determined in the process of machine experiment.

4.3 The Method of Group Consideration of Arguments

The idea of the method (Ivakhnenko, 1975) that reproduces the scheme of a mass selection is as follows. As a basis, a function of two variables, P_i and P_j , is assumed.

$$x_k^{(1)} = f(P_i, P_j) \quad (7)$$

From the variables of the zero level (a set of primary parameters), the variables of the first level (step) are formed as follows. From the sample l_1 , the LSM coefficients for f are found that satisfy, in the best way, a number of values of ε . For the check sample l_2 , from the set $x_k^{(1)}$, the most regular ones are selected by identifying those that provide the extreme value for the regularity index chosen beforehand (correlation factor between ε and $x_k^{(1)}$, mean square deviation, and so on). Thus we obtain n_i variables of the first level: $x_1^{(1)}, x_2^{(1)}, \dots, x_{n_i}^{(1)}$. Then the variables of the second level are formed, and so on:

$$x_2 = f(x_i^{(1)}, x_j^{(1)}) \quad (8)$$

Usually the number of variables at each subsequent level is reduced, and thus, in the final step, a "particular" description is obtained from two variables, $x_1^{(s)}$ and $x_2^{(s)}$,

$$\hat{\varepsilon} = f(x_1^{(s)}, x_2^{(s)}) \quad (9)$$

which contains all or some of the primary variables P_i . The selection levels should be built up until the regularity increases considerably.

5. RESULTS OF CALCULATIONS

Some calculations are made to investigate the possibility of predicting the flares in a spot group one to two days in advance using a prediction function as a function of several variables (the first case). The coefficients α , β , γ , and δ are defined from the calculations and the best parameters are found in each approximation for one or the other of the predicted values (the flare number or index). The correlation between a number of the calculated and real predicting values is within 70-75%. The mean number of flares in a spot group and the rate of variation in the group area appeared to be the most informative factors. The optimal number of approximations is three.

To investigate the possibility of predicting energetic flares (the second case) by the method of potential functions, five parameters were selected: P_3 and P_9 from the first combination of parameters, P_6 from the second combination, and P_{11} and P_{12} . The identifications obtained from a reduced system differed insignificantly from those obtained with fourteen parameters and are about 75% correlated.

This method of considering a group of arguments was realized on a full system of parameters. Figure 3 presents the prediction results of the existence or absence of energetic flares obtained by MGCA for the initial (I), check (II), and an independent (III) sample. The forecast verification was determined as the relation of correct forecasts to all of them. For the MGCA scheme, number 3 appeared to be optimal for the selection levels. It is precisely at the third step where the quality of independent forecast is the highest. Most often (with MGCA) the parameters P_3 , P_4 , P_6 , P_8 , P_9 , and P_{12} were used; those of P_2 , P_{10} , P_{14} , P_1 , P_{11} , and P_{13} were used more rarely; and P_5 and P_7 were usually not applied at all.

6. PRACTICAL FORECASTING

The results obtained from predicting flares in a spot group (the first case, and in a lesser degree the second one) were used for practical forecasting.

In the preliminary investigation, the relationship was stated between the importance and the flare index. Table 3 lists mean flare indices for the flares of different importances. Considering that the flare indices for

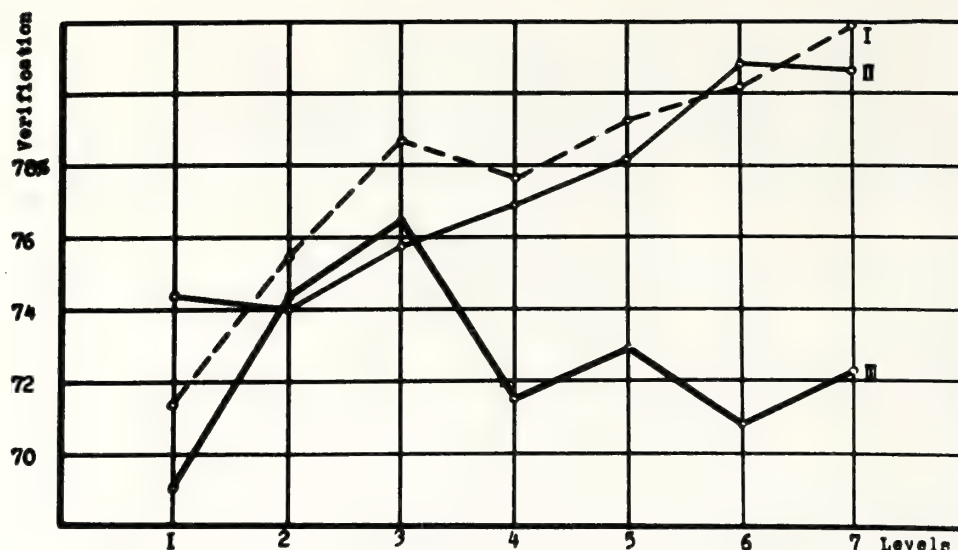


Figure 3. Verification of predictions of importance 3 (and greater) flares by MGCA. I is the initial sample; II is the check sample; and III is an independent identification.

each successive class differ nearly by an order, one may predict the flares in a spot group from the calculated values of the flare number and index.

The technique described was used for predicting flares in a spot group since 1974. Prediction was made for the spot groups observed after their appearance or coming from behind the limb for four days, and since 1976 for two days and more.

Table 3. Mean flare indices for the flares of different importances.

Importance	Index value
subflare	10
1	70
2	470
3	3650

For the period from 1974 to 1977 predictions were made for the appearance of flares in 154 spot groups one to two days in advance. The following categories of predictions were produced:

- no flares are expected in the group
- subflares are expected in the group
- flares of importance 1 and lower are expected in the group
- flares of importance 2 and lower are expected in the group.

Table 4 gives the results of predictions and observations of flares for a given period. [Categories (b) and (c) are combined in the table as there is no complete set of corresponding observational data.]

Verification of forecasts is 72%; 21% appeared to be overestimated and 8% to be underestimated.

Table 4. Results of predictions and observations of flares for 1974-1977.

Issued forecasts		Observations		
Category	Number	no	subflare, 1	2
no	312	285	26	1
subflare, 1	287	117	149	21
2	14	1	8	5
Total	613	403	183	27

The results obtained from the method of predicting energetic flares are used for practical forecasting as well. Because of the lack of data it is impossible, however, to summarize the results of this category.

7. CONCLUSION

From the work performed it follows that:

1. The method developed here predicts flares in a spot group one to two days in advance with a probability not more than 70% (the first case).
2. The method developed predicts the appearance of flares of importance 3 and more for groups of area not less than 200 m.s.h. for the period of the passage across the disk (the second case).
3. A further improvement of the verification of forecasts may be achieved by improving the system of parameters utilized and a more detailed investigation of them. The prediction results depend to a lesser degree on the method of calculation. This has been confirmed by Burov et al. (1976) and Gumenitsky et al. (1977) in solving the task of forecasting the appearance of flocculi at the next revolution on the solar disk.

REFERENCES

- Aizerman, M. L., E. M. Braverman, and L. I. Rozonoer (1970): Method of potential functions in the theory of machine teaching. Nauka, Moscow.
- Brailovsky, V. L., and Yu. I. Brailovskaya (1971): Method of building solar flare predictions as the function of many variables. Doklady Akademii SSSR, 198:319-322.
- Burov, V. A., G. V. Kuklin, T. L. Slutskaya, and N. N. Stepanyan (1976): The comparison of various methods of forecasting of flocculi appearance at the limb. In: The appearance and evolution of active regions on the Sun, Nauka, Moscow, 150-156.
- Dittmer, P. H. (1975): The relationship between solar flares and solar sector boundaries. Solar Physics, 41:227-231.

- Efimenko, V. M. (1976): On the optimum interval of the prehistory for flare forecasting. Solnechnyje Dannya, 11:63-67.
- Efimenko, V. M., V. I. Efimenko, and V. V. Telnyuk-Adamchuk (1976): Short-term forecast of spot group flare. In: The appearance and evolution of active regions on the sun, Nauka, Moscow, 182-185.
- Efimenko, V. M., V. I. Efimenko, and V. V. Telnyuk-Adamchuk (1977): On the short-term forecast of the chromospheric flares on the base of sunspot group characteristics. Vestnik Kievskogo Universiteta. Astronomiya, 19: 19-29.
- Gnevysheva, R. S. (1960, 1962, 1964, 1965, 1967): Catalogues of solar activity. Trudy GAO v Pulkovo, Nauka, Leningrad.
- Gumanitsky, V. B., V. M. Efimenko, and V. V. Telnyuk-Adamchuk (1977): On the prediction of the recurrent flocculi appearance at the solar limb. Solnechnyje Dannya, 11:58-62.
- Gumanitsky, V. B., and V. V. Telnyuk-Adamchuk (1979): On the forecasting of powerful flares in the sunspot groups by the potential function and group consideration of argument methods. Vestnik Kievskogo Universiteta. Astronomiya, 21. (In press.)
- Ivakhnenko, A. T. (1975): Long-term forecasting and the control by complex systems, Tekhnika, Kiev.
- Mansurov, S. M., G. S. Mansurov, and L. G. Mansurova (1975): Catalogue of interplanetary magnetic field sector polarity determinations for 1957-1974, IZMIRAN, Preprint No. 8 (123), Moscow.
- Solar Geophysical Data (1957-1965): Nat. Geophys. and Solar-Terr. Data Center, Boulder, Colorado.
- Svalgaard, L. (1972): Interplanetary magnetic-sector structure, 1926-1971. J. Geophys. Res., 77:4027-4034.
- Waldmeier, M. (1957-1966): Heliographische Karten der Photosphäre für das Jahr 1957-1965. Publikationen der Eidgenössischen Sternwarten, Zürich.
- Warwick, C. (1966): Standardized solar flare data 1959 through 1961. IGY Solar Report Series, No. 33.

NEW ASPECTS OF SOLAR ACTIVITY FOUND WITH HIGH TIME RESOLUTION AND HIGH SENSITIVITY OBSERVATIONS AT CM- AND MM-WAVELENGTHS

P. KAUFMANN, F.M. STRAUSS, J.C. RAFFAELLI, and R. OPHER*
CRAAM**/ON/CNPq-Conselho Nacional de Desenvolvimento Científico e
Tecnológico, R. Pará 277, 01243 - São Paulo, SP, Brazil.

Preliminary results on some novel features associated with solar activity at 7 GHz, 22 GHz and 43 GHz are presented. A summary of these features is as follows: 1) Simple isolated fast spikes, with half duration times τ of several seconds, occur in large numbers; their spectrum peaks somewhere between 7 and 43 GHz; 2) There are impulsive bursts consisting of a "fast" repetitive component made up of spikes with a τ on the order of a second or less superimposed on a "slow" component with a τ of tens of seconds; 3) The spectral index α ($S \propto f^\alpha$), of the slow component in the impulsive burst is negative in the frequency range 7-22 GHz while the fast component has a positive spectral index in the same range; 4) The characteristic time scale τ of the fast repetitive component in the impulsive burst decreases with increasing intensity; 5) Fast impulsive spikes ($\tau \lesssim$ seconds) have been observed superimposed on the slow gradual events ($\tau \sim$ tens of minutes) which have previously been believed to have a purely thermal origin; 6) Major 7 GHz impulsive structures are often delayed about 2 seconds with respect to the 22 GHz time structures; 7) Undamped 5.6 minute oscillations were observed for a time interval of two hours, starting at the time of a burst. These oscillations were not observed at any other time during over 50 hours of tracking McMath plage 15403 at 22 GHz.

Implications of the above phenomena are commented upon; in particular, we note that spike-like bursts may be an important indicator of the properties of the active center and its ability to produce large events. The repetition rate R of the fast spike-like components of complex bursts increases with an increase of mean flux S and we infer $R > 30 \text{ s}^{-1}$ for large bursts ($S > 1000 \text{ s.f.u.}$).

1. OBSERVATIONS

During the period 9-21 July 1978 we observed solar activity at 7 GHz, 22 GHz and 43 GHz at the Itapetinga Radio Observatory. At 7 GHz we used a standard solar patrol polarimeter (whose beam width is larger than the sun).

* On sabbatical leave from Technion, Haifa, Israel.

** Formerly "Centro de Rádio-Astronomia e Astrofísica Mackenzie" now absorbed by CNPq

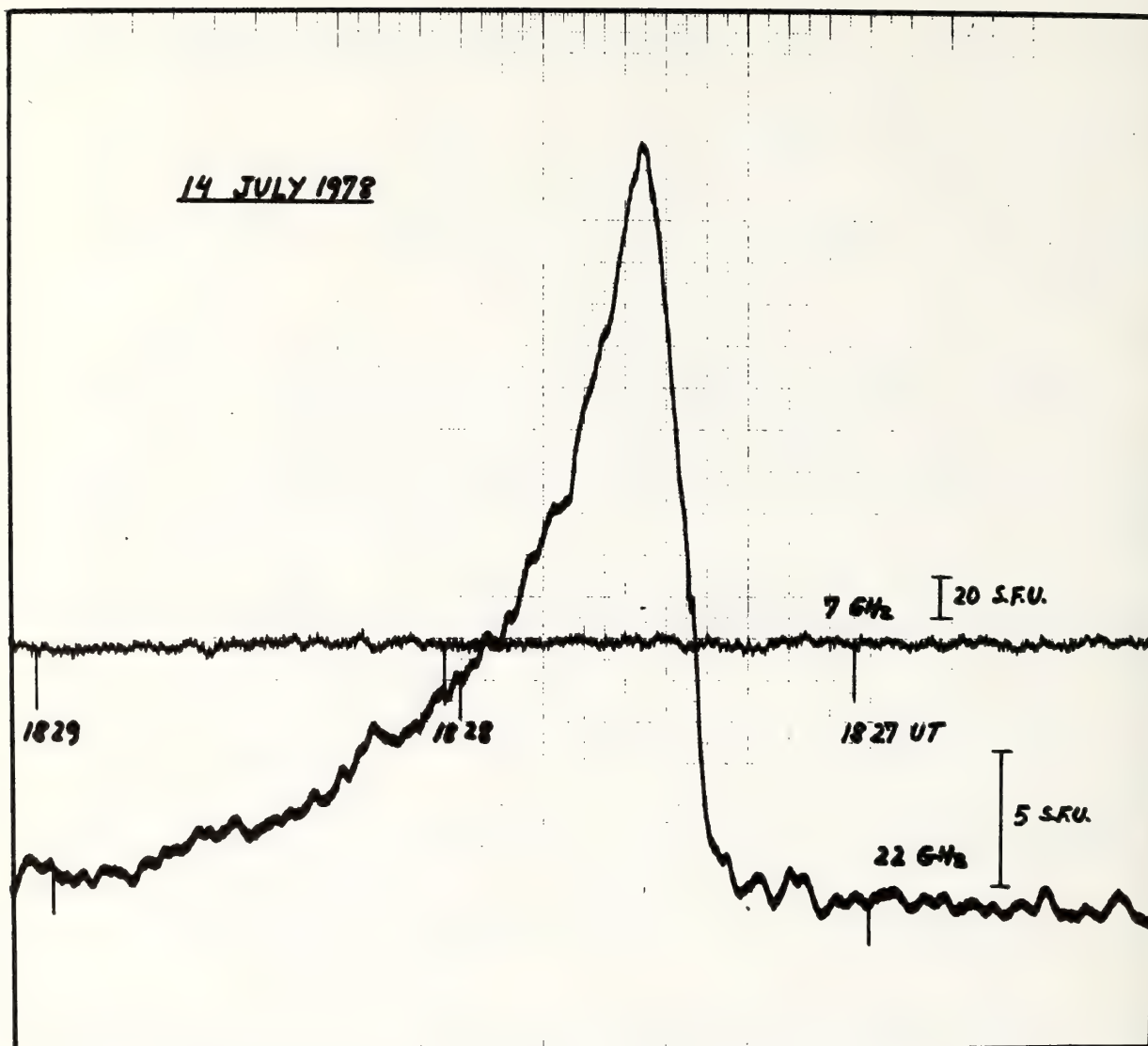


Fig. 1: EXAMPLE OF A 22 GHz ISOLATED LARGE SPIKE, WITH NO MEASURABLE RESPONSE AT 7 GHz (MIDDLE RECORD).

Simultaneous measurements with the 7 GHz polarimeter were made at either 22 GHz or 43 GHz with the Itapetinga 45 ft dish having a beam width of 4.5' arc or 2' arc, respectively, and a sensitivity nearly two orders of magnitude better than standard patrol instruments. The time constant was about 100 milliseconds at 7 GHz, and less than about 50 milliseconds at 22 GHz or 43 GHz. The radiometers' bandwidths were 20 MHz at 7 GHz and 1 MHz at 22 GHz or 43 GHz. The data were recorded on magnetic tape for later processing. During the period of observations the solar activity was largely dominated by McMath plage 15403 (NOAA, 1978) which was continuously tracked at 22 GHz or 43 GHz with an accuracy of better than 10" arc. Polarization time features at 7 GHz with time scales equal to or larger than 100 milliseconds, were not considered in the present study (earlier results are treated in a separate study, Kaufmann, 1978).

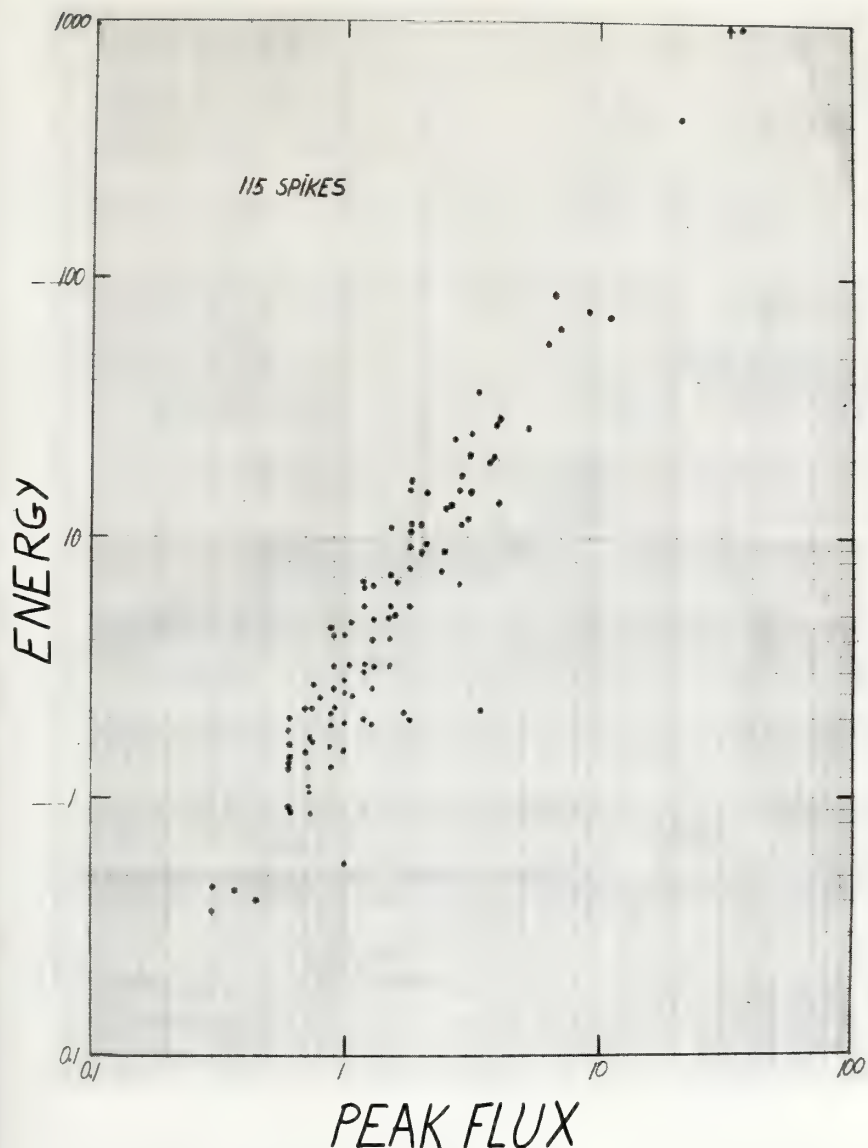


Fig. 2: THE RELATIONSHIP BETWEEN SPIKE ENERGY (S.F.U. X SEC) AND PEAK FLUX (S.F.U.).

Tracking with the large antenna was on the active centers. The sun, in general, shows one or more radio peaks. A particular peak was chosen and the large antenna tracked the maximum of this peak. Flux scales were established assuming burst sources small compared with the antenna beamsizes (i.e., point sources). A calibrated noise tube source was used as a reference. The antenna temperatures were corrected for atmospheric and radome absorption.

2. ISOLATED SPIKES

The occurrence of the simplest impulsive feature, isolated spikes, was clearly identified at 22 GHz. During certain periods they would appear at a rate of 10-30 spikes per hour. Their half duration times τ ranged from 1-10 seconds, with a sharp peak in occurrence at about 2.5 seconds. Few examples were obtained at 43 GHz, where their occurrence was rare. An example of a 22 GHz spike is shown in figure 1. Alternate one-hour tracking of McMath 15403 at 22 GHz and at 43 GHz has indicated that moderate intensity spikes (i.e., less than about 10 solar flux units, s.f.u.) occurring frequently at 22 GHz, had intensities smaller than the noise threshold at 43 GHz (i.e., smaller than about 0.1 s.f.u.). On the other hand, larger spikes at 22 GHz (up to 30 s.f.u.) had no corresponding events at 7 GHz (i.e., larger than the 2-3 s.f.u. noise threshold). We can infer qualitatively that the spike spectrum peaks somewhere between 7 and 43 GHz, with spectral indices

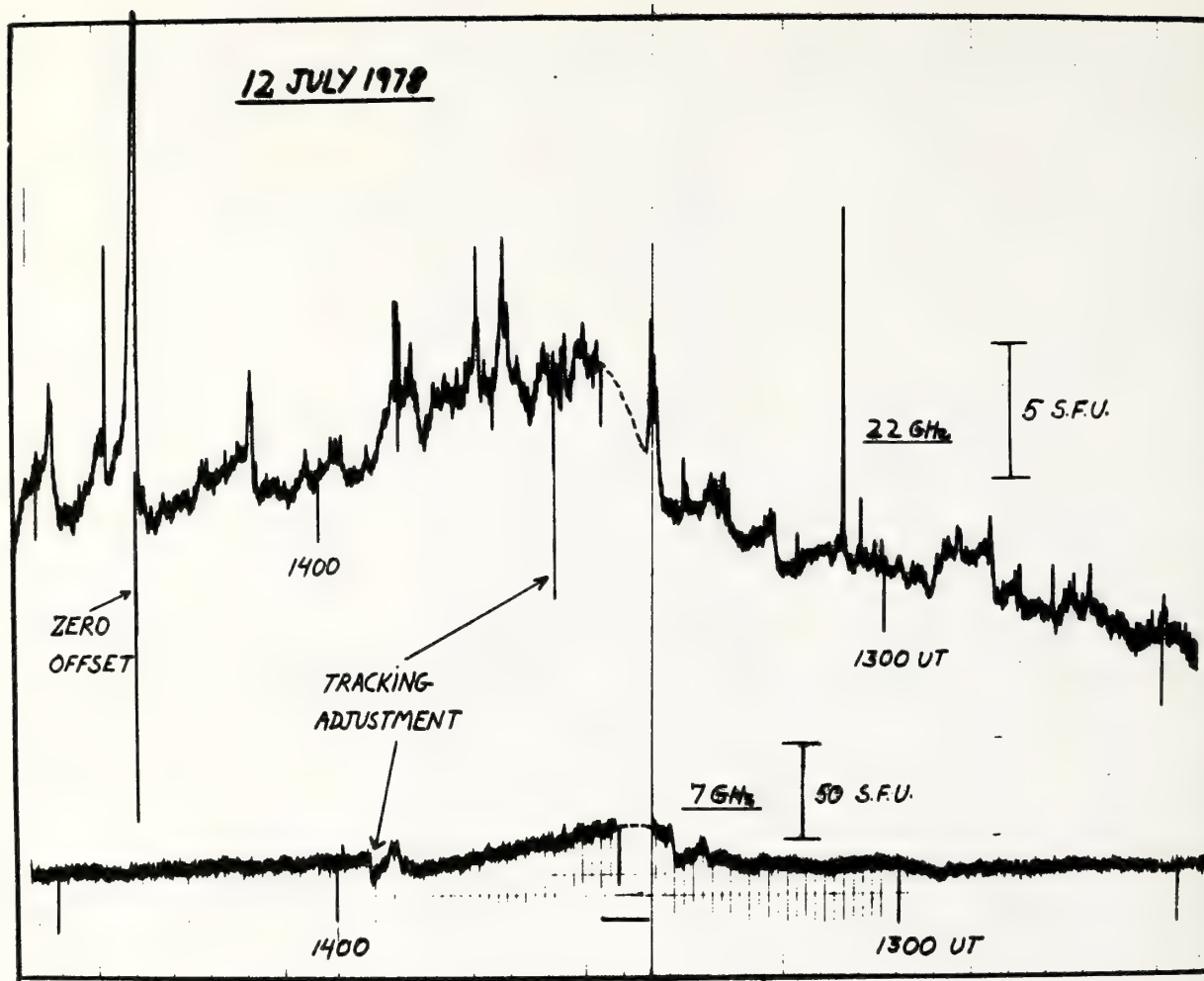


Fig. 3: A LARGE NUMBER OF SPIKES ARE SUPERIMPOSED ON A 22 GHz GRADUAL EVENT. AT 7 GHz THERE IS A COMMON SIMPLE 3F BURST, DISPLAYING ONLY SLOW TIME STRUCTURES.

(defined by $S \propto f^\alpha$) ranged conservatively as $\alpha > 2.5$ in 7-22 GHz range, and $\alpha < -2.5$ in the 22-43 GHz range.

A characteristic boundary condition relating the spikes energy (ϵ) (integral of the flux of the spike over time) and the peak flux of the spike (S_p) can be obtained from figure 2. It follows that $\Delta\epsilon/\Delta S_p \propto \epsilon/S_p$. This condition, which appears to hold for simple spikes, was found also in a large collection of soft X-ray bursts (Kaufmann et al., 1978), for time structures of microwave bursts (Kaufmann and Iacomo Jr., 1978), and as a trend in large collections of microwave events (Wefer, 1973).

3. SPIKES ASSOCIATED WITH GRADUAL EVENTS

Gradual events ($\tau \sim$ tens of minutes) with or without superimposed structures as defined by the 7 GHz observations (i.e., a standard patrol

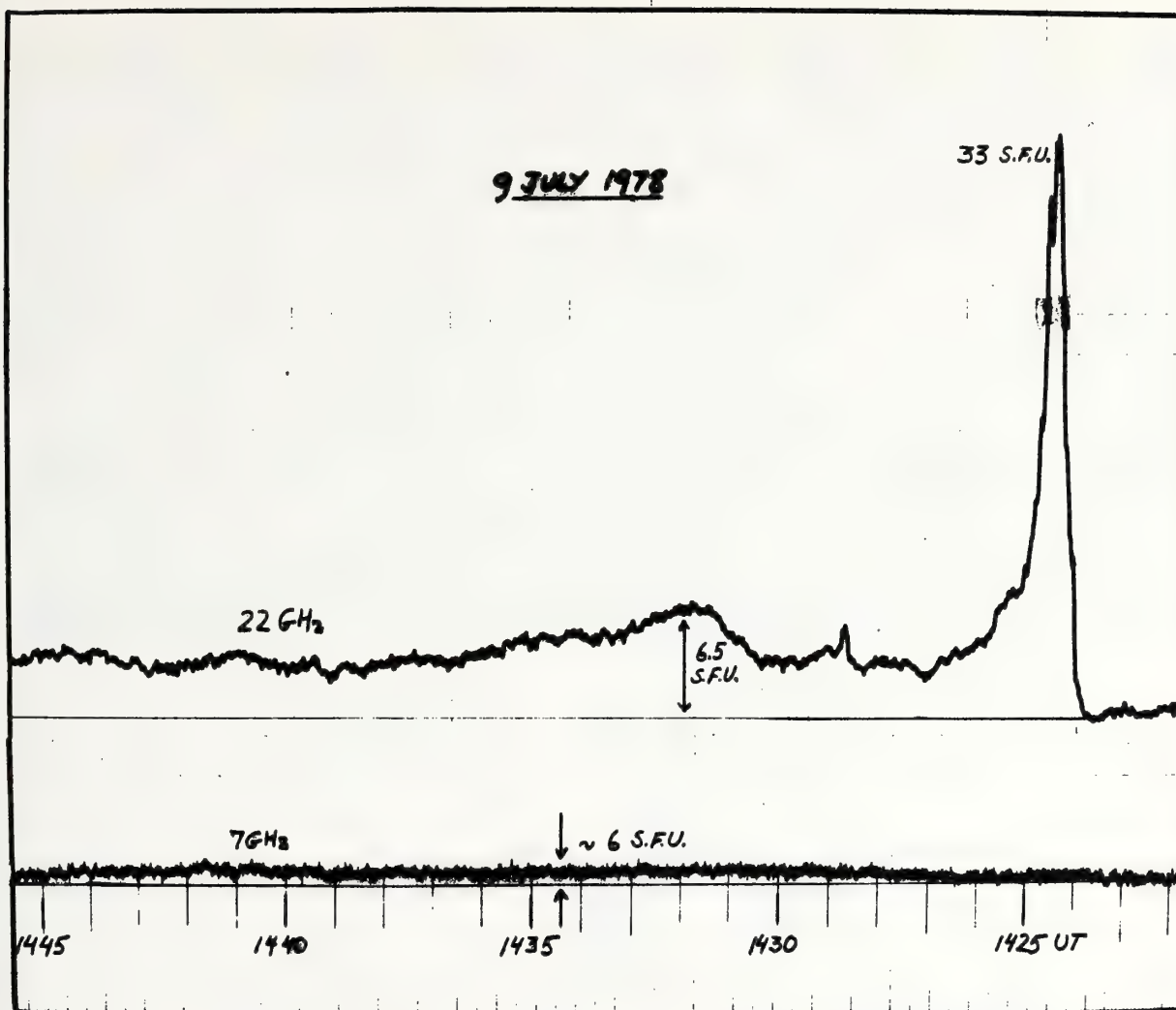


Fig. 4: A SPIKE AT 22 GHz PRECEDES A P.B.I.-AT 7 GHz THERE IS A WEAK GRADUAL RISE-AND-FALL EVENT.

microwave telescope), appeared to be always associated with spike activity as observed with high sensitivity at 22 GHz (see figures 3 and 4). The baseline is not always well defined at 22 GHz but some examples indicate that the slow gradual rises and falls are likely to have nearly flat spectra (i.e., optically thin thermal plasma in the 7-22 GHz range). The associated spikes have the same characteristics described in the previous section ($\tau \approx 1-10$ seconds).

4. TIME STRUCTURE OF IMPULSIVE BURSTS

In many impulsive bursts ($\tau \sim$ tens of seconds) observed simultaneously at 7 GHz and at 22 GHz it was possible to distinguish the presence at 22 GHz of a superimposed repetitive fast "super-impulsive" component ($\tau < \text{second}$). The corresponding fast super-impulsive component at 7 GHz either does not

exist or is below the noise level. A typical example is shown in figure 5, whose maximum is shown in an "exploded time scale" in figure 6. As the impulsive burst grows at 22 GHz the super-impulsive component increases in amplitude with a decreasing τ . The 7 GHz slow impulsive component is delayed by about a second with respect to the 22 GHz slow underlying component. The spectra for the impulsive and super-impulsive components, for different phases of the burst, are shown in figure 7. If the slow and fast components of figure 7 can be inferred to come from the same region, the presence of two electron populations is clearly evident. The fast component, with $\alpha > 0.9$ in 7-22 GHz range, have a spectral trend comparable to the fast spikes analysed previously. Data for the 22-43 GHz range were not obtained for these phenomena.

The major time structures at 7 GHz and at 22 GHz (which we may call the "slow impulsive components") were found usually delayed at 7 GHz with respect to 22 GHz. This was the case of the event shown in figures 5 and 6. Another example is shown in figure 8. Cross-correlation analysis has indicated a delay of about 2 seconds (figure 9). The spectral development with time in the range 7-22 GHz is shown in figure 10. A negative spectral index for the

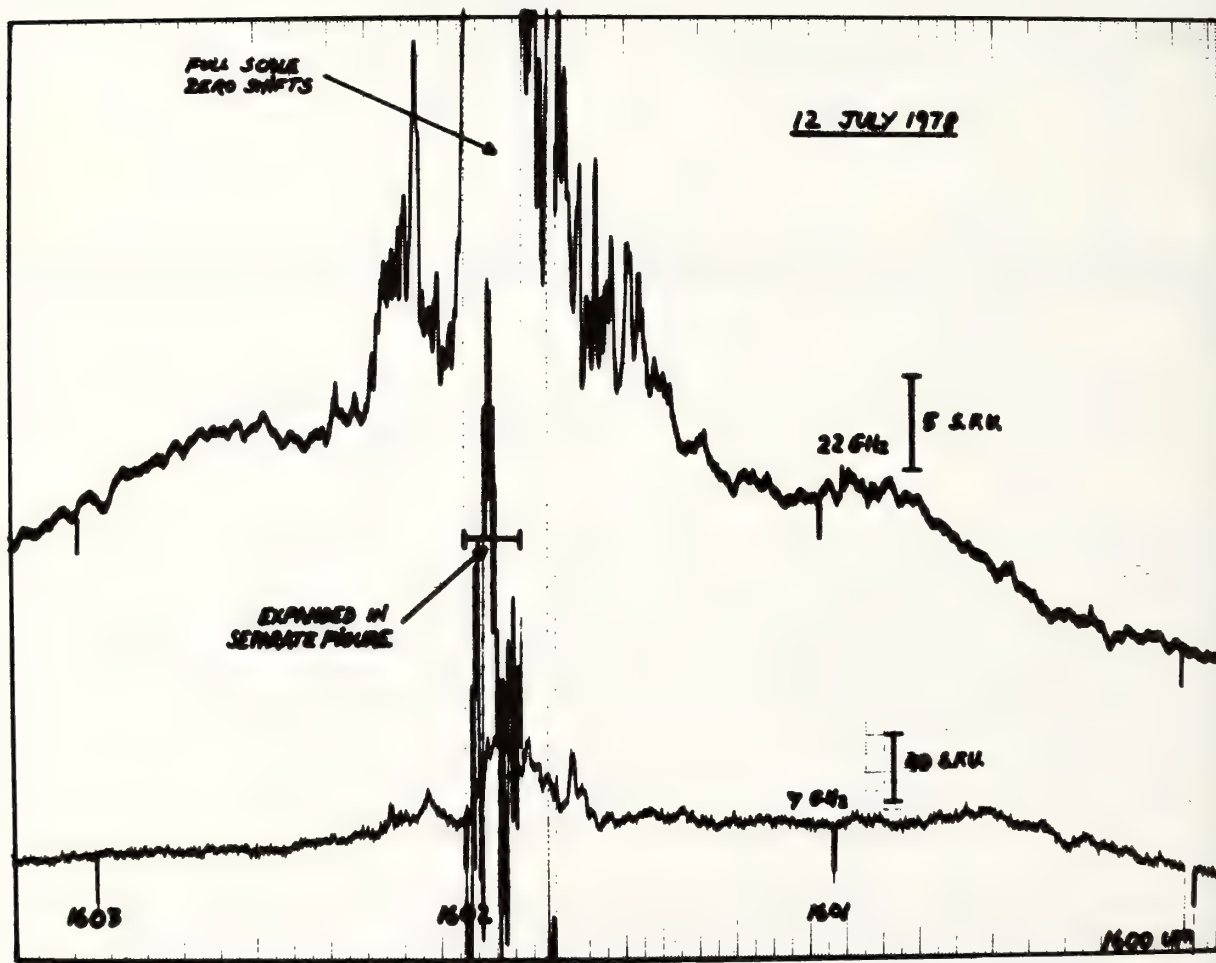


Fig. 5: A CHARACTERISTIC EXAMPLE OF A COMPLEX IMPULSIVE EVENT, WITH FAST REPETITIVE "SUPER-IMPULSIVE" SUPERIMPOSED COMPONENT. AN 8 SEC. INTERVAL AT THE MAXIMUM IS SHOWN EXPANDED IN FIGURE 6.

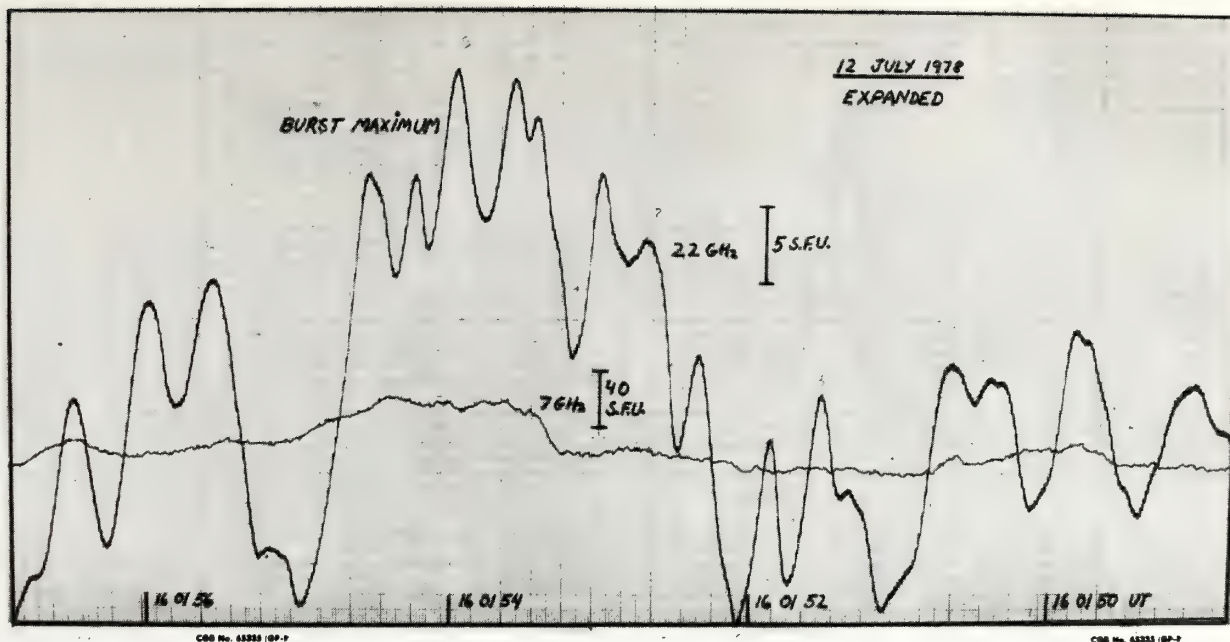
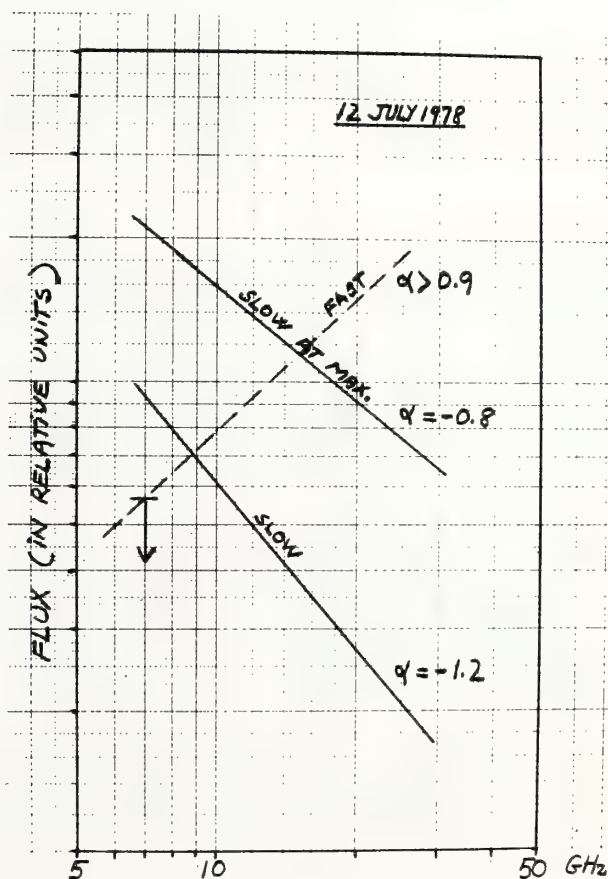


Fig. 6: "EXPLODED VIEW" OF MAXIMUM OF THE BURST OF FIGURE 5. FAST REPETITIVE SUPER-IMPULSIVE COMPONENT SHOWS OVERLAPPING EFFECTS AS WELL AS SOME SMOOTHING PRODUCED BY INSTRUMENTAL TIME CONSTANT LIMITATIONS (I.E., OF ABOUT 50 MSEC).

Fig. 7: TWO-FREQUENCY SPECTRAL INDICES FOR THE IMPULSIVE AND SUPER-IMPULSIVE COMPONENT OF THE BURST SHOWN IN FIGURES 5 AND 6 (12 JULY 1978, APPROX. 1600 UT). TWO SUPERIMPOSED ELECTRON POPULATIONS ARE INDICATED.



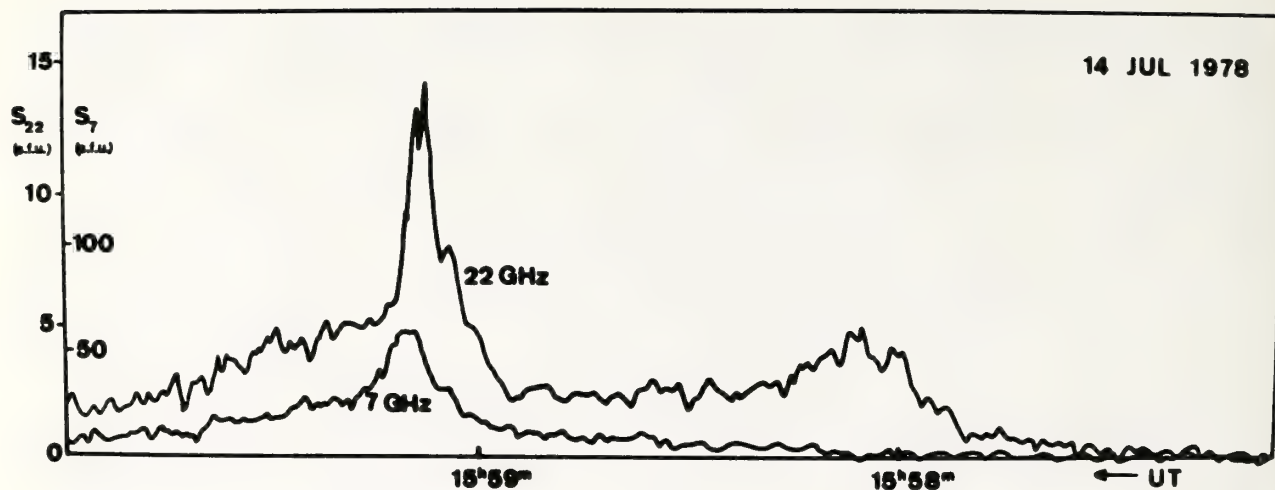


Fig. 8: MAJOR IMPULSIVE TIME STRUCTURES FOR THE EVENT OF 14 JULY 1978 (AT ABOUT 1557.5 UT), AT 7 GHz AND AT 22 GHz.

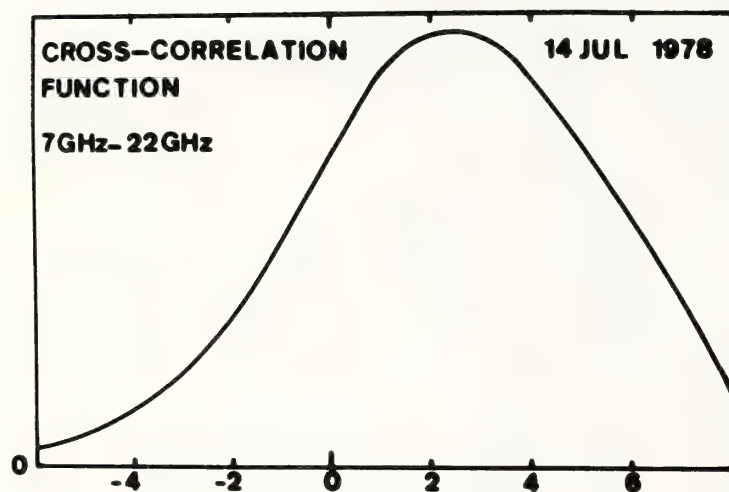


Fig. 9: THE CROSS-CORRELATION 7-22 GHz FOR THE TIME STRUCTURES OF THE EVENT OF FIGURE 8 IN THE INTERVAL 15 59 00 TO 15 50 30 UT. (THE ABCISSA IS IN SECONDS). THE 22 GHz TIME STRUCTURES LEAD THE 7 GHz STRUCTURES BY ABOUT 2.3 SEC.

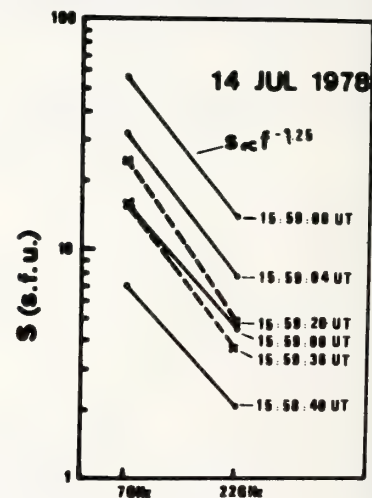


Fig. 10: FLUXES IN THE RANGE 7-22 GHz DURING THE EVENT SHOWN IN FIGURE 8 AND THE INDICATED SPECTRAL INDICES.

"slow" impulsive component in the 7-22 GHz range appears to be common to all impulsive bursts observed simultaneously at the two frequencies.

5. 5.6-MINUTE OSCILLATIONS

A 5.6-min. oscillation at 22 GHz was remarkably well defined for about 120 minutes on 10 July 1978, starting with a burst at about 1729 UT and

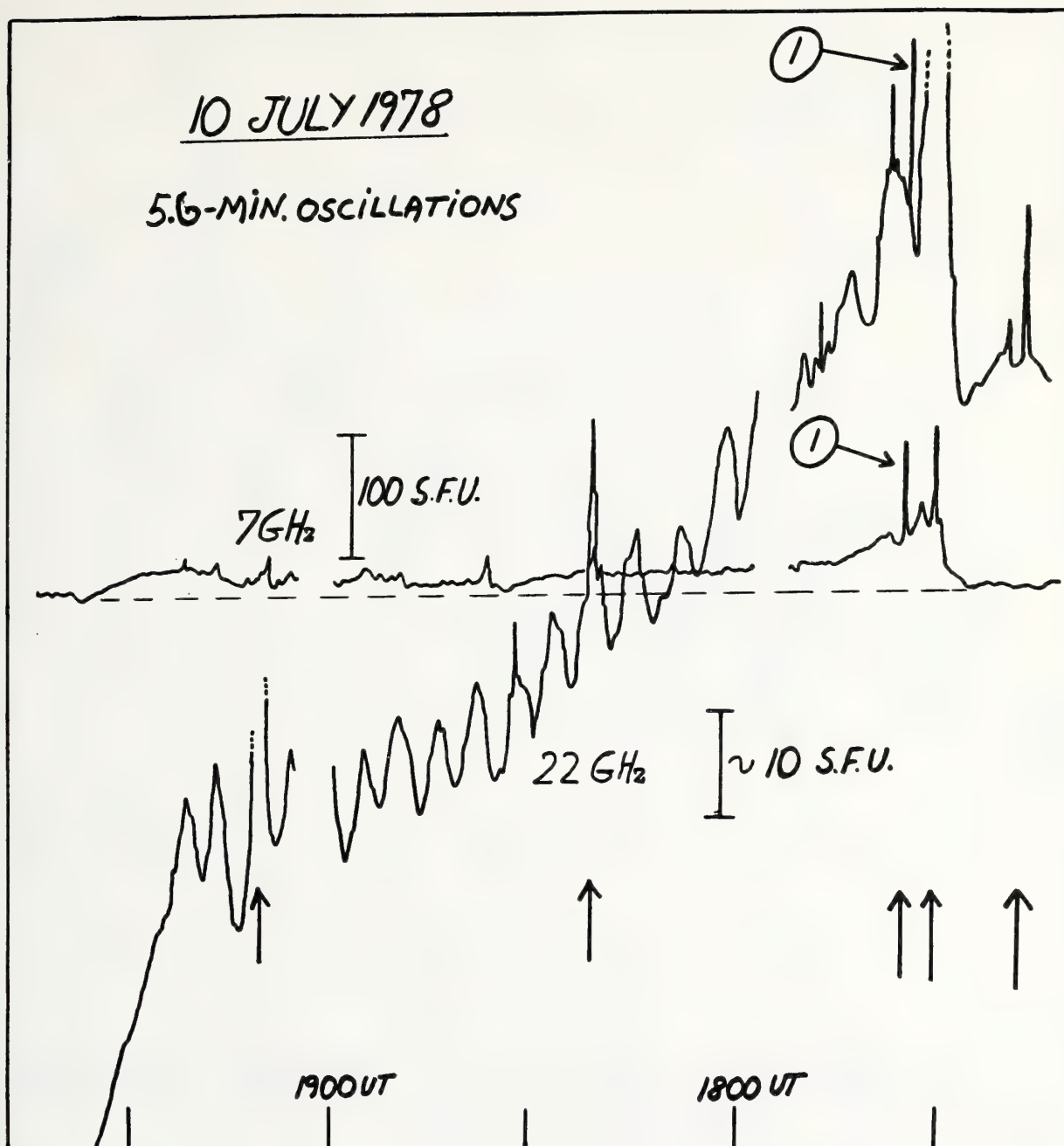


Fig. 11: 5.6-MINUTE OSCILLATIONS OBSERVED AT 22 GHz STARTED SUDDENLY WITH A BURST AT 1729 UT ON 10 JULY 1978. BURSTS ARE INDICATED BY ARROWS. OTHER MAJOR BURSTS OCCURRED AT ABOUT 1820 UT AND AT 1919 UT. THE OSCILLATIONS ENDED ABRUPTLY AT 1925 UT WITHOUT SHOWING ANY DAMPING. AT 7 GHz THE BASELINE REMAINED HIGH, RECOVERING ONLY AT THE END OF THE PHENOMENON. THE SPIKE-LIKE EVENT 1 (IN THE PRESENT COMPRESSED TIME SCALE) IS EXPANDED IN FIGURE 13.

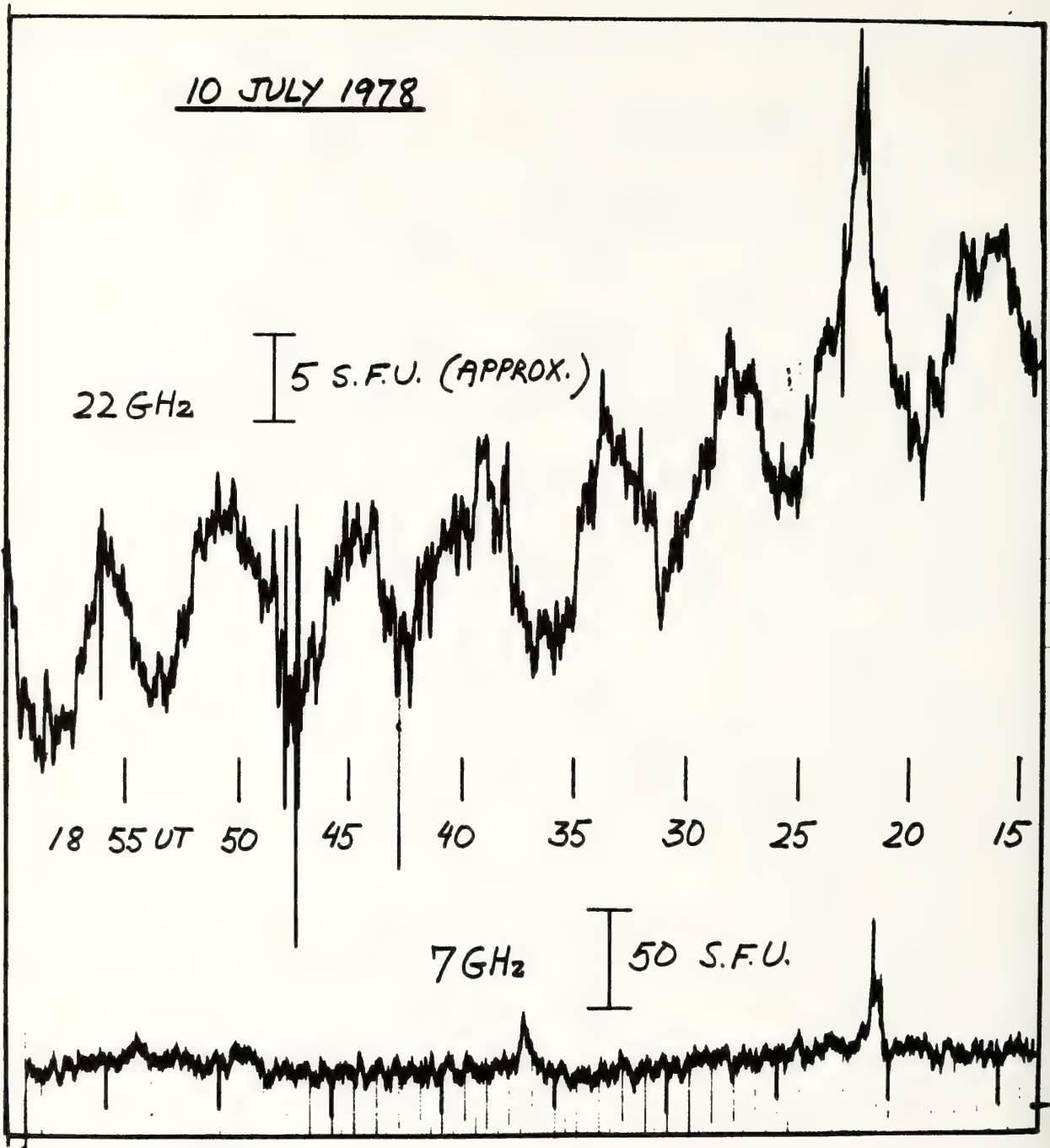


Fig. 12: SAMPLE OF THE ACTUAL RECORD OF THE 5.6 MIN. OSCILLATION OBSERVED ON 10 JULY 1978.

lasting until 1925 UT. The 7 GHz level recovered only after the series of oscillations stopped (see figure 11). Another detailed illustration of the actual recording is shown in figure 12.

Five minute microwave oscillations have previously been observed all across the solar disk by interferometric measurements (Lang, 1974).

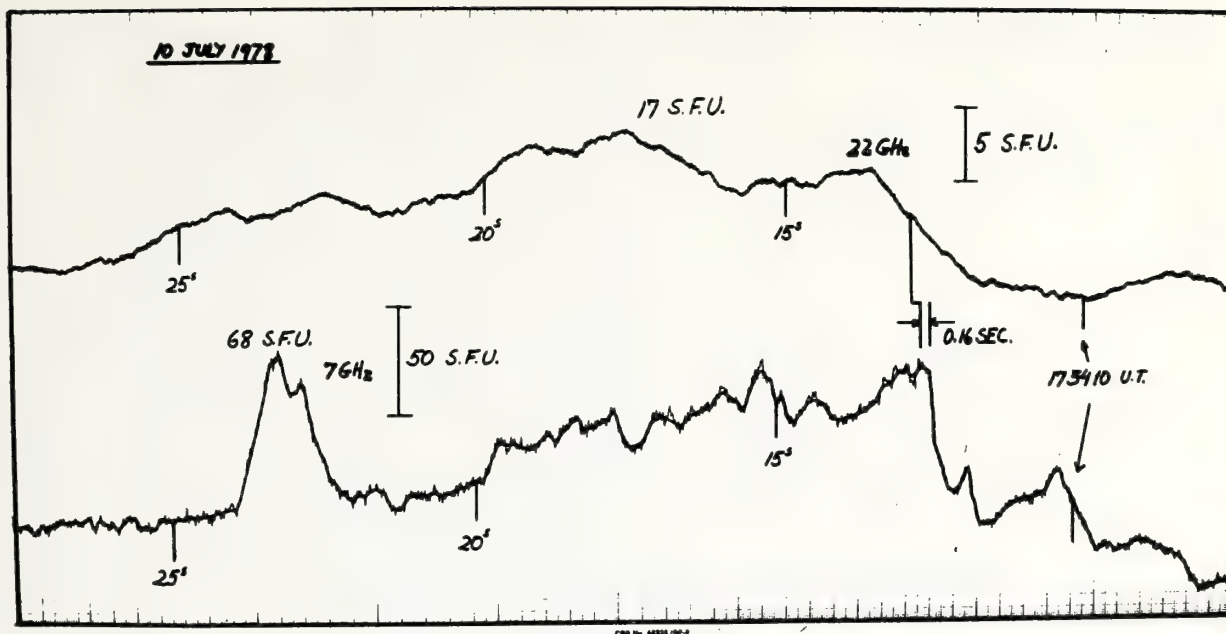


Fig. 13: AN "EXPLODED VIEW" OF THE IMPULSIVE EVENT SUPERIMPOSED ON THE 5.6-OSCILLATION WHICH OCCURRED AT 1734 UT. IT SHOWS IN PARTICULAR THE 7 GHZ TIME STRUCTURES LEADING BY ABOUT 0.16 SEC THE 22 GHZ TIME STRUCTURES, WHICH APPEAR RATHER SMOOTHED OUT. THE OTHER BURSTS ASSOCIATED WITH THE 5.6-MIN. OSCILLATION PERIOD SHOWED SIMILAR TRENDS.

This result was questioned by Kundu and Alissandrakis (1975) and recently by Zirin et al. (1978), who claim that interferometric data do not provide evidence for unique periodicities.

The bursts occurring during the duration of the 5.6-min. oscillations had features different from the other events considered in this study. The negative spectral index in the 7-22 GHz range for these bursts is particularly pronounced. In figure 13 the "complex" spike occurring at 173410 UT is shown as an example of this on an expanded time scale. The 7 GHz time structures are faster and larger than the 22 GHz structures and lead slightly in time. The 7 GHz level also remained high with respect to the baseline. This might be understood if the bursts occur higher in the solar atmosphere during the period that the 5.6-min. oscillations were observed. It is significant to note however, that the "complex" spike that occurred at about 1717 UT (i.e., just before the start of the 5.6-min. oscillations) had characteristics comparable to the other impulsives analysed in this work.

These 5.6-min. oscillations and the association with an active center seems to be a rather rare phenomenon, deserving further investigation. It was not observed during many hours of observations possessing a wide range of weather conditions: twenty hours in July 1974, fifty hours in July 1978 and fifty hours in December 1978.

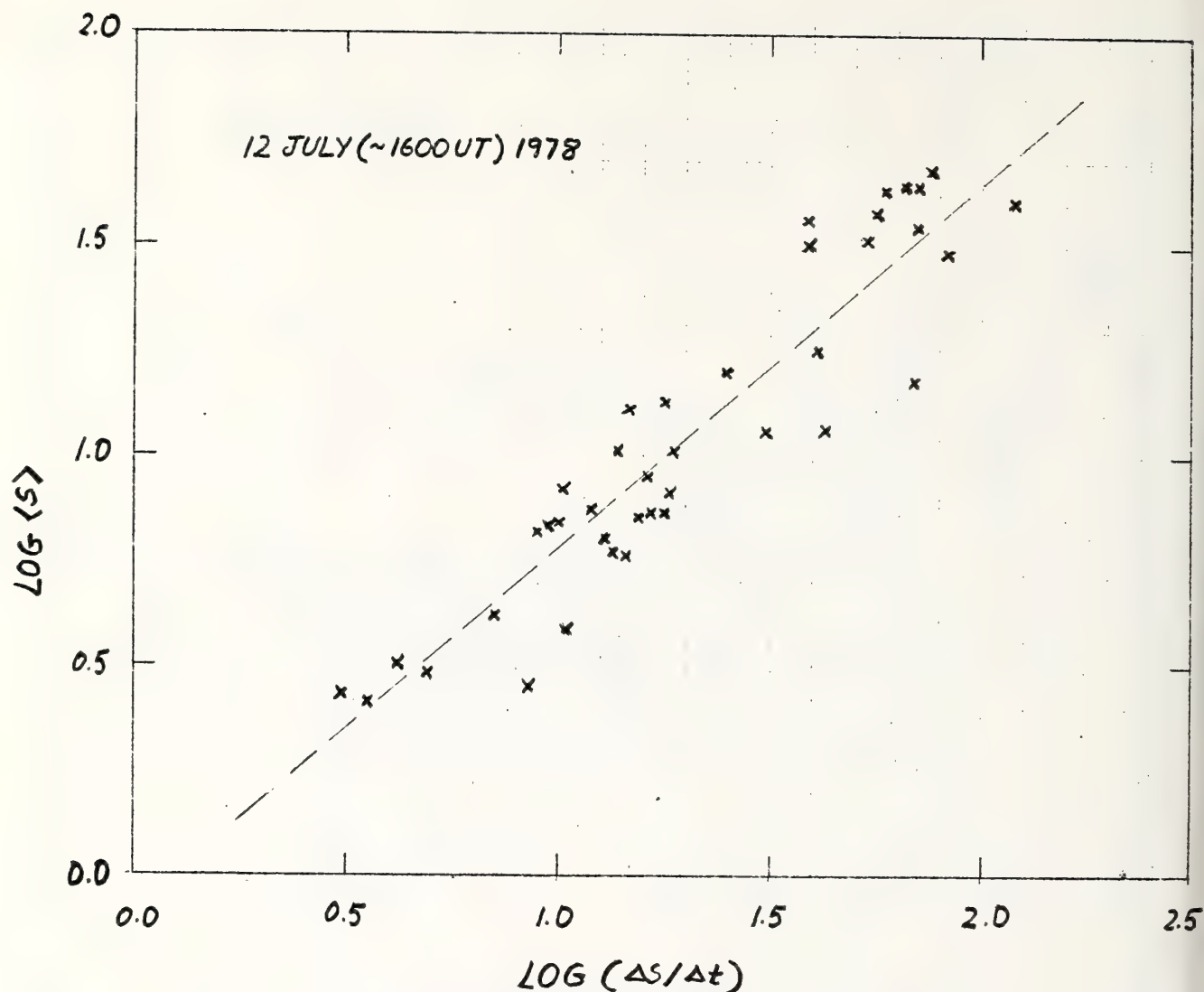


Fig. 14: THE 22 GHz MEAN FLUX $\langle S \rangle$ FOR THE BURST OF 12 JULY 1978 (~ 1600 UT) VARIATION AS A FUNCTION OF IMPULSIVITY ($\Delta S / \Delta t$) OF THE SUPERIMPOSED ULTRA-FAST STRUCTURES.

6. DISCUSSION

(a) The "micro-activity" at active centers

The observation of solar active centers with high sensitivity and high time resolution at 22 GHz uncovers a large number of transient phenomena which were totally unknown in the data of standard patrol instruments. The presence of "micro-activity" (spike-like bursts in great numbers, and other low level oscillatory phenomena - which will be further investigated), do not seem to be common to all active centers. This is a tentative qualitative indication which can be inferred from our tracking of active centers other than McMath 15403 (for short periods), and several attempts made in the past

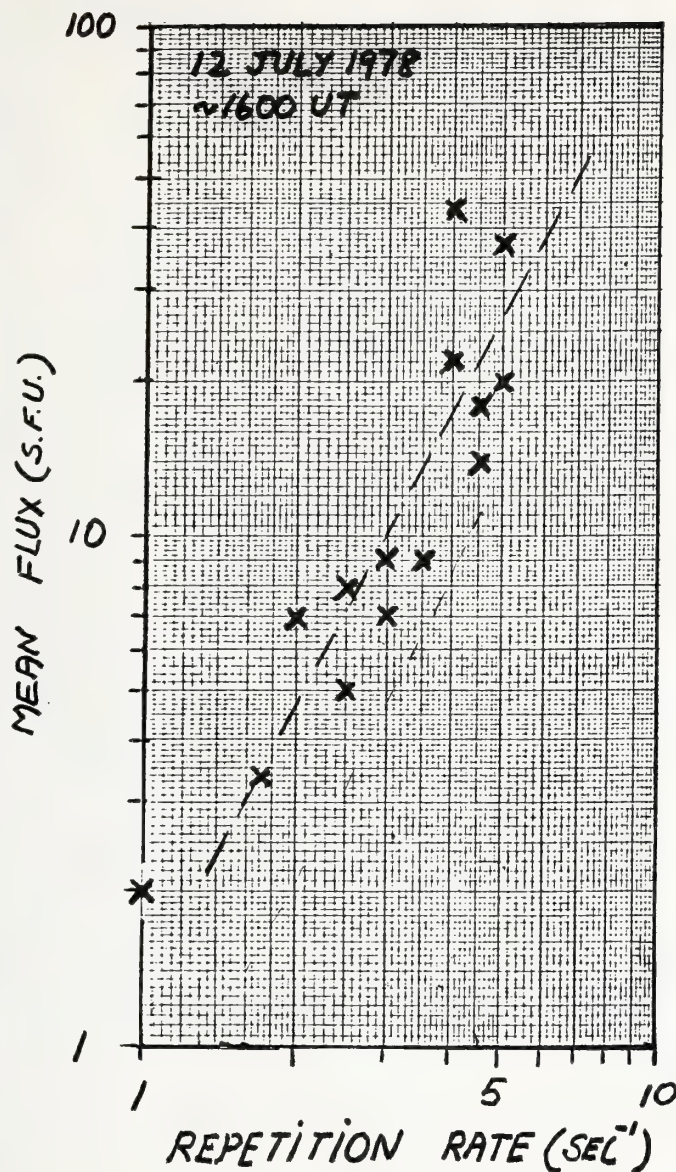


Fig. 15: 22 GHz MEAN FLUX
DEPENDENCE ON THE
REPETITION RATE OF ULTRA
FAST STRUCTURES
SUPERIMPOSED TO THE
12 JULY 1978 (~ 1600 UT)
IMPULSIVE EVENT.

(including those referred by Kaufmann et al., 1975; Blakey, 1976). The presence of such kind of activity may be an important indicator of very unstable and critical regimes occurring in an active center under certain conditions. The establishment of such a regime and the ability of the active center to produce great bursts is suggested as an important topic for further investigations.

(b) Ultra-fast spikes in
impulsive bursts

Very fast time structures are distinguishable in impulsive bursts, being much faster than the characteristic time scales which were believed typical in such bursts. We may suggest that the "visibility" of the "super-impulsive" components in impulsive bursts is not a necessary condition for their presence. The very fast component can be easily smoothed out in traversing a dense plasma and/or by instrumentation.

A number of trends are readily distinguishable in several moderate to small impulsive bursts. The example of figure 5, 6 and 7 can be taken as rather typical. As the total mean flux $\langle S \rangle$ increases the impulsivity ($\Delta S/\Delta t$) increases and the time scale between ultra-fast structures decreases; the sequence reverses in the decay phase (or phases). This was observed as a trend for several events in the July 1978 observations. Analyzing in more detail the burst of 12 July (~ 1600 UT) we show in figure 14 a plot of $\log \langle S \rangle$ (i.e., the mean flux) vs $\log (\Delta S/\Delta t)$ (i.e., the impulsivity). The linear correlation coefficient for 40 data points for $\log \langle S \rangle$ vs $\log (\Delta S/\Delta t)$ was found to be 93%, and a function of the form $\langle S \rangle \approx A (\Delta S/\Delta t)^B$ can be fitted with $A \approx 0.8$ and $B \approx 0.9$. It is to be noted

that since B is approximately unity, time integrated flux (energy increments $< S > \Delta t$) is nearly proportional to flux, and the data in figure 14 have the same qualitative information as those of figure 2 for isolated spikes. Finally, we find for the repetition rate of ultra-fast structures vs mean flux, the relationship shown in figure 15 for the event of 12 July 1978 (~ 1600 UT).

The trends of the results are clear taking due consideration of all possible sources of inaccuracy (e.g. estimates of weak fluxes, faster time structures which are smoothed out by instrumental resolution, etc.) These observational trends, although preliminary, are consistent with a suggestion made previously in the analysis of a large collection of soft X-ray bursts that energetic integrated flare by - products may be treated as the response of a quantisable magnitude (Kaufmann et al., 1978).

A radio burst at mm-wavelengths is probably the response of energetic injections. The radio emission observed comes from direct emission of these energetic injections plus the response of the plasma to these injections. The ultra-fast components are a closer representation of the energetic injections than the slow components and the repetition rate of the ultra-fast component is an important parameter to take into consideration (figure 15). From figure 15 we can infer that for very intense bursts, for example $S > 1000$ s.f.u., one may obtain repetition rates $R > 30 \text{ s}^{-1}$ or time scales $R^{-1} < 30$ msec. Indeed, time structures faster than 20 msec. have been found in strong bursts at decimetric wavelengths (Dröge, 1977; Slottje, 1978) which were suggested to be associated with elementary flare processes. This concept was also suggested from the results obtained from hard X-ray bursts with moderately good time resolution (Frost, 1969; van Beek et al., 1974). Detailed investigations of the very preliminary results presented here are being prepared separately by the authors. More data with higher time resolution, higher sensitivity, and simultaneous measurements at more than one mm-wavelength, and especially at hard-X-rays, will provide crucial tests for the understanding of the wave-associated phenomena connected with solar flares.

7. ACKNOWLEDGEMENTS

We are grateful to Centro Tecnológico de Hidráulica from EPUSP for the loan of a magnetic tape recorder. One of the authors (RO) received support from FAPESP and Technion. This research was supported partially by FINEP. In data handling and reduction we received help from several students, and in particular from Y.R.Hadano, O.Bertolani Neto, L.Buzzeli, C.R.S.Cuellar, T.Orlando and O.Negrini Neto.

NOTE ADDED IN PROOF: A new observational run was carried during 18-25 February 1979, with simultaneous observations at 23.2 GHz and 44.3 GHz. Several impulsive bursts were recorded, and the results presented here on ultra-fast components were essentially confirmed. However, in nearly thirty hours of observations, no evidence on the slow 5.6 min. oscillation was found.

Note added in proof: Another observational run carried 18-25 February 1979, at 23.2GHz and 44.3GHz, simultaneously, confirmed the phenomena described here (except for the 5-min oscillations which seem to be rare). We recently became aware that similar results are being obtained by K. Tapping (private communication) at 10.7GHz using the 150ft antenna of Algonquin Radio Observatory, Canada.

LATE COMMENT ON 5.6-MIN OSCILLATIONS OBSERVED AT 22GHz

The 5.6 min oscillations observed at 22GHz, reported above in the present Proceedings is a very rare effect. It was only observed for 120 minutes in more than 250 hours of tracking of various active centers, at various positions in the solar disc (including the limb) during runs performed in 1974, 1978 and 1979.

In a recent 22GHz observation with the same instrument (6-9 September 1979) an instrumental oscillation of 4-10 min was identified. It always occurred for limb observations. This was not the case for the July 1978 observations when the 5.6 min oscillations were observed. The presently identified instrumental effect is probably a new one.

Although this effect is peculiar, it is being understood and we expect correct it in the near future. We do not believe that it was present in 10 July 1978, although this possibility cannot be entirely eliminated. Some arguments against the observed 5.6 minute oscillation in 10 July 1978 being instrumental are: 1) They only appeared for 120 minutes during hundreds of hours of observation, 2) The active region size at 22GHz during the 120 minutes had probably grown to dimensions comparable to the beamsize, which would be a necessary condition to notice the experimental effect, and 3) The period 1729UT-1925UT was coincident and dominated by a strong 1B-2B class flare with very large X-ray emission level (NOAA, 1978). The above mentioned effect, and its correction, is now under investigation.

REFERENCES

- Blakey, J.R. (1976): Solar micro-bursts at 22.2 GHz and their relationship to events observed at lower frequencies. Solar Phys., 46:241.
- Dröge, F. (1977): Millisecond fine-structures of Solar Burst radiation in the range 0.2-1.4 GHz. Astron. Astrophys., 57:285
- Frost, K.J. (1969): Rapid fine structure in a burst of hard solar X-rays observed by OSO 5. Astrophys. J., 158:L159.
- Kaufmann, P., P. Iacomo Jr., E.H. Koppe, P. Marques dos Santos, R.E. Schaal, and J.R. Blakey (1975): The July 1974 solar events: a possible lower limit for microwave activity. Solar Phys., 45:189.
- Kaufmann, P., L. Rizzo Piazza, R.E. Schaal, and P. Iacomo Jr. (1978): A statistical analysis of soft X-ray effects in the low terrestrial ionosphere and some inferences on the nature of solar flares. Ann. Geophys., 34:105.
- Kaufmann, P. (1978): Fast time structures superimposed to impulsive solar microwave bursts with slowly varying or stationary polarization degree. Submitted to Solar Phys.
- Kaufmann, P., and P. Iacomo Jr. (1978): Some preliminary results on time structures of solar microwave bursts and apparent boundary conditions regulating the burst energy release with time. Accepted by Rev. Bras. Física.
- Kundu, M.R., and C.E. Alissandrakis (1975): A search for periodic variations of solar radio emission at 3.7- and 11.1- cm wavelengths. M.N.R.A.S., 173:65.
- NOAA (1978): Solar-Geophysical Data, prompt reports, Report n° 408, Part 1, August 1978, Environmental Data and Information Service, Boulder, Colorado, USA.
- Lang, K.R. (1974): The small-scale, quasi-periodic, disc component of solar radiation. Astrophys. J., 192:777.
- Slottje, C., (1978): Millisecond microwave spikes in a solar flare. Nature, 275:520.
- van Beek, H.F., L.D. de Feiter, and C. de Jager (1974): Hard X-ray observations of elementary flare bursts, and their interpretation. Space Research XIV:447.
- Wefer, F.L. (1973): A catalog of matrix diagram for simple and complex microwave solar radio event morphological parameters, Scientific Report n° 027, Dept. of Astronomy, The Pennsylvania State University, USA.
- Zirin, H., G.J. Hurford, and K.A. Marsh (1978): The small scale source of quiet-sun centimeter-wave radio emission. Astrophys.J., 224:1043.

SOLAR FLARE PREDICTION USING RADIO WAVELENGTH INTERFEROMETERS

Kenneth R. Lang
Department of Physics
Tufts University
Medford, MA 02155

Observations of solar active regions with interferometers at centimeter and millimeter wavelengths indicate that the regions always exhibit intense small-scale sources which are a few seconds of arc in size and which are about 50% circularly polarized. These small-scale sources dominate solar emission at these wavelengths. As long as the active regions are quiescent and not emitting solar flares, the intensity, angular sizes, and degree of circular polarization of the small-scale sources remain constant for intervals as long as days. This stability allows the construction of synthesis maps at two circular polarizations with second of arc resolution. Magnetic field configurations in the solar chromosphere and corona can therefore be compared with those in the lower lying photosphere with the same angular resolution. Immediately prior to and during the eruption of solar flares the small-scale sources exhibit dramatic changes in circular polarization of up to 80%. These changes occur at times between a few minutes and one hour before flare eruption. The polarization changes are due to changes in the magnetic field configuration. Changes in the magnetic field configuration may trigger subsequent flare eruption, whereas interferometric observations of the circularly polarized sources may lead to a reliable flare prediction technique. A comparison of radio wavelength synthesis maps with Doppler-Zeeman observations at optical wavelengths can lead to a description of flare related changes in magnetic field configurations at different levels in the solar atmosphere.

1. INTRODUCTION

Interferometric observations of solar active regions indicate that solar emission at centimeter and millimeter wavelengths is dominated by a few small-scale sources which are only a few seconds of arc in size (one second of arc is equivalent to 700 kilometers on the solar surface), and which are highly circularly polarized. The circular polarization of these small-scale features indicates a direct connection with the intense magnetic fields in sunspots, whereas changes in circular polarization reflect moving or emerging magnetic fields. As long as solar active regions are not emitting solar flares, the small-scale sources are remarkably stable with angular sizes, intensities, and

degrees of circular polarization which remain constant for days. This stability allows us to construct synthesis maps of the small-scale sources. In Section 2 we present Very Large Array (V.L.A.) synthesis maps of active regions at 6 cm wavelength for both left hand (L.C.P.) and right hand (R.C.P.) circularly polarized radiation. These maps specify coronal magnetic field structures whose shape, orientation and dipolar structure agree with similar features seen in optical wavelength magnetograms of the photospheric magnetic field. This agreement supports our interpretation of the circularly polarized emission in terms of coronal magnetic field structures. It is changes in these structures which may provide the source of energy for solar flares, and which may forecast subsequent flare eruption. In Section 3 we discuss flare prediction using changes in the circular polarization of the small-scale sources. Radio wavelength interferometric observations of the sources prior to, during, and following the emission of solar flares are discussed. In marked contrast to their stability during quiescent solar periods, the small-scale sources exhibit dramatic changes in circular polarization of up to 80% immediately prior to and during the eruption of solar flares. The polarization changes occur tens of minutes before the eruption of solar flares seen at H α wavelengths, and they suggest that changing magnetic fields trigger subsequent flare emission. Magnetic field changes in the flare trigger sources are also related to similar changes during the eruption of the flares themselves.

2. RADIO WAVELENGTH MAPS OF SOLAR ACTIVE REGIONS WITH SECOND OF ARC ANGULAR RESOLUTION

2.1 Observation Techniques

The solar active regions 1046 and 1056 were respectively observed with the National Radio Astronomy Observatory's Very Large Array (V.L.A.) on March 30 and April 1, 1978. During this period no flare activity was reported at any optical or radio observatory. A signal wavelength of 6 cm was used and both the right circularly polarized (RCP) and the left circularly polarized (LCP) signals were sampled every 30 seconds using eleven 25 m diameter paraboloids which provided individual beamwidths of 8.6 minutes of arc. The intermediate frequency signals (bandwidth 12 MHz) for the two different polarizations received at each of eleven antennae were sent to a central location, where they were multiplied together to give the correlated flux for a total of 55 antenna pairs with antenna separations ranging between 70 meters and 10.43 kilometers and effective angular resolutions ranging between one and two hundred seconds of arc.

For each antenna pair the gain, phase and polarization of the correlator outputs were calibrated by observing 3C 84 or CTA 102 for five minutes every twenty minutes. The solar active region was observed during the other fifteen minutes of each twenty-minute period. The levels of the two i.f. signals being fed into each multiplier from each antenna were kept at a fixed value using an automatic level control (a.l.c.) loop which automatically compensates for the variation in gain magnitude caused by the introduction of an extra i.f. attenuator when observing the Sun. The correlated flux when observing the Sun for each polarization with each antenna pair (m,n) was determined from the equation

$$S_{mn}(\text{sun}) = \frac{R_{mn}(\text{sun})}{R_{mn}(\text{cal})} \frac{[T_{sm}(\text{sun})T_{sn}(\text{sun})]^{\frac{1}{2}}}{[T_{sm}(\text{cal})T_{sn}(\text{cal})]^{\frac{1}{2}}} S_{mn}(\text{cal}) \exp[i(\phi_m^* - \phi_m) - i(\phi_n^* - \phi_n)] \quad (1)$$

where R_{mn} denotes the correlated power for one polarization of the antenna pair (m,n) .

$$R_{mn}(\text{cal}) = [G_m G_n]^{\frac{1}{2}} \frac{S_{mn}(\text{cal})}{[T_{sm}(\text{cal}) T_{sn}(\text{cal})]^{\frac{1}{2}}} \exp[i(\phi_m - \phi_n)], \quad (2)$$

where G_m and ϕ_m respectively denote the magnitude and phase of the complex gain of the detection system of antenna, m , the $S_{mn}(\text{cal})$ is the correlated flux when observing the calibration source with one polarization of the antenna pair (m,n) , and $T_{sm}(\text{cal})$ denotes the system noise temperature when observing the calibrator source with one polarization of antenna, m . Similarly when observing the solar active region the correlated power, $R_{mn}(\text{sun})$, for one polarization of the antenna pair (m,n) is given by

$$R_{mn}(\text{sun}) = [G_m^* G_n^*]^{\frac{1}{2}} \frac{S_{mn}(\text{sun})}{[T_{sm}(\text{sun}) T_{sn}(\text{sun})]^{\frac{1}{2}}} \exp[i(\phi_m^* - \phi_n^*)]. \quad (3)$$

The levels of the two i.f. signals being fed into each multiplier from each antenna were kept at a fixed value using the automatic level control (a.l.c.) loop in which the sampled signal level controls an attenuator in the final i.f. amplifier. This meant that we could assume that the gain magnitudes are the same when observing the calibrator and the sun ($G_m = G_m^*$). The gain phase difference $\phi_m^* - \phi_m$ introduced by the extra i.f. attenuation when observing the Sun was measured for each antenna by observing 3C 84 with the attenuator in and out. The system noise temperatures, $T_{sm}(\text{cal})$, when observing the calibrator were measured for each antenna using a switched noise source whose temperature of 3K was accurately calibrated by observing the Moon. The system noise temperature, $T_{sm}(\text{sun})$, when observing the active region was measured for each antenna by determining the differences in the total power detected when observing the active region and a quiet sun region whose temperature was assumed to be 10^4 K. Even at these high temperatures the front end amplifiers were in their linear, unsaturated regions.

The correlated flux of the calibration source, $S_{mn}(\text{cal})$, was taken to be 49 Jy and 34 Jy, respectively, when observing 3C 84 and CTA 102. The gain and polarization were calibrated by adjusting the digitized output of the correlators to give the same values of $R_{mn}(\text{cal})$ for every baseline pair and both polarizations. This is essentially because the calibrator sources can be assumed to be unpolarized point sources. These instrumental adjustments were also applied to the solar data.

2.2 Mapping Techniques

For each polarization of each antenna pair the corrected amplitude, $S_{mn}(\text{sun})$, and the corrected phase $(\phi_m^* - \phi_m) - (\phi_n^* - \phi_n)$ were determined for every 30 seconds of each 15 minute period of solar observation. These amplitudes and phases were taken to be the amplitude and phase of the visibility function, $V(u,v)$. Because corrections for solar rotation and horizontal parallax were incorporated in the computer program which determined the pointing of each antenna, the changing values of the visibility function could then be used to measure the brightness distribution of the active region $I(x,y)$, through the fundamental Fourier transform relation

$$V(u,v) = I(x,y) \exp[-2\pi i (ux + vy)] dx dy, \quad (4)$$

where the visibility function and the brightness distribution are determined separately for the two circular polarizations, u and v are the projections of the baseline vector in the direction of increasing right ascension and declination, respectively; and x and y are, respectively, coordinates in the direction parallel to increasing right ascension and declination. These quantities, defined in radians, are given by

$$u = \frac{B}{\lambda} [\cos \delta_b \sin (LHA - BHA)] \quad (5)$$

$$v = \frac{B}{\lambda} [\sin \delta_b \cos \delta_s - \cos \delta_b \sin \delta_s \cos(LHA - BHA)],$$

where δ_b and δ_s are the declination of the baseline vector and of the source, respectively, LHA and BHA are the local hour angle of the source and the baseline, and B and λ are the magnitude of the baseline vector and the wavelength of observation. The baseline declination and hour angle depend on the geocentric components, B_x , B_y , and B_z of the baseline vector, for each antenna pair.

$$\delta_b = \text{Arctan} \left[\frac{B_z}{(B_x^2 + B_y^2)^{1/2}} \right] \quad (6)$$

$$BHA = \text{Arctan} \left(\frac{B_y}{B_x} \right). \quad (7)$$

As the earth rotates, and the local hour angle of the source changes, the projected baseline describes an ellipse in the u - v plane. The ellipse is centered at $u = 0$, $v = \frac{B}{\lambda} \sin \delta_b \cos \delta_s$, has eccentricity $\cos \delta_s$ and semimajor axis equal to equatorial component of the baseline. If the u - v plane were sufficiently sampled then one could take the inverse transform of equation (4) to obtain the brightness distribution. If the source had a maximum angular extent Δx and Δy in right ascension and declination, then one need only make observations at intervals of $u \sim \frac{1}{\Delta x}$ and $v \sim \frac{1}{\Delta y}$, to obtain a

unique map of the source. Since the source brightness is a real function, it follows from Equation (4), that $V(u,v) = V^*(-u,-v)$, so we need only measure $V(u,v)$ on one half of the $u-v$ plane. In practice, however, there are never enough interferometer pairs to satisfy the sampling criterion, and so one must resort to using some other technique for obtaining a map.

The procedure we have implemented involves a direct synthesis of a "dirty" map

$$D(x,y) = \frac{1}{N} \sum A_i \cos \phi_i + 2\pi(ux + vy), \quad (8)$$

where A_i and ϕ_i are the amplitude and phase of observation i , N is the number of observations, and x and y are positions located on a grid of coordinates of the sky. Since the visibility function is symmetric, only the real (cosine) part of the transform need be calculated. The dirty map is the convolution of the true brightness distribution with the response function of a point source. This response function or "dirty beam" is the Fourier transform of the sampling function and is given by

$$B(x,y) = \frac{1}{N} \sum \cos (u_i x + v_i y) w_i, \quad (9)$$

where w_i is the weight given to each data point. Figure 1 shows the dirty VLA beam pattern at 6 centimeters constructed from observations during the daylight hours on April 1, 1978 with uniform weighting $w_i = 1$. The half power width is 1 second of arc x 3 seconds of arc and the highest sidelobe is 14% of the maximum response. One could alter the beam pattern by adjusting the weights. If the outer spacings were more heavily weighted, the beamwidth would become smaller, but at the expense of higher sidelobes. Weighting the inner spacings more heavily would broaden the main beam but decrease the inner sidelobes.

A deconvolution was then performed by means of the "clean" procedure in which the brightness distribution was decomposed into a sum of beam patterns. The dirty map was searched for the maximum and a point source is fit to the map at that point

$$\text{Amp} = \frac{\sum_{j=1}^n \sum_{i=1}^m \frac{D_{ij}}{B_{ij}} (B_{ij})^2}{\sum_{j=1}^n \sum_{i=1}^m B_{ij}^2} \quad (10)$$

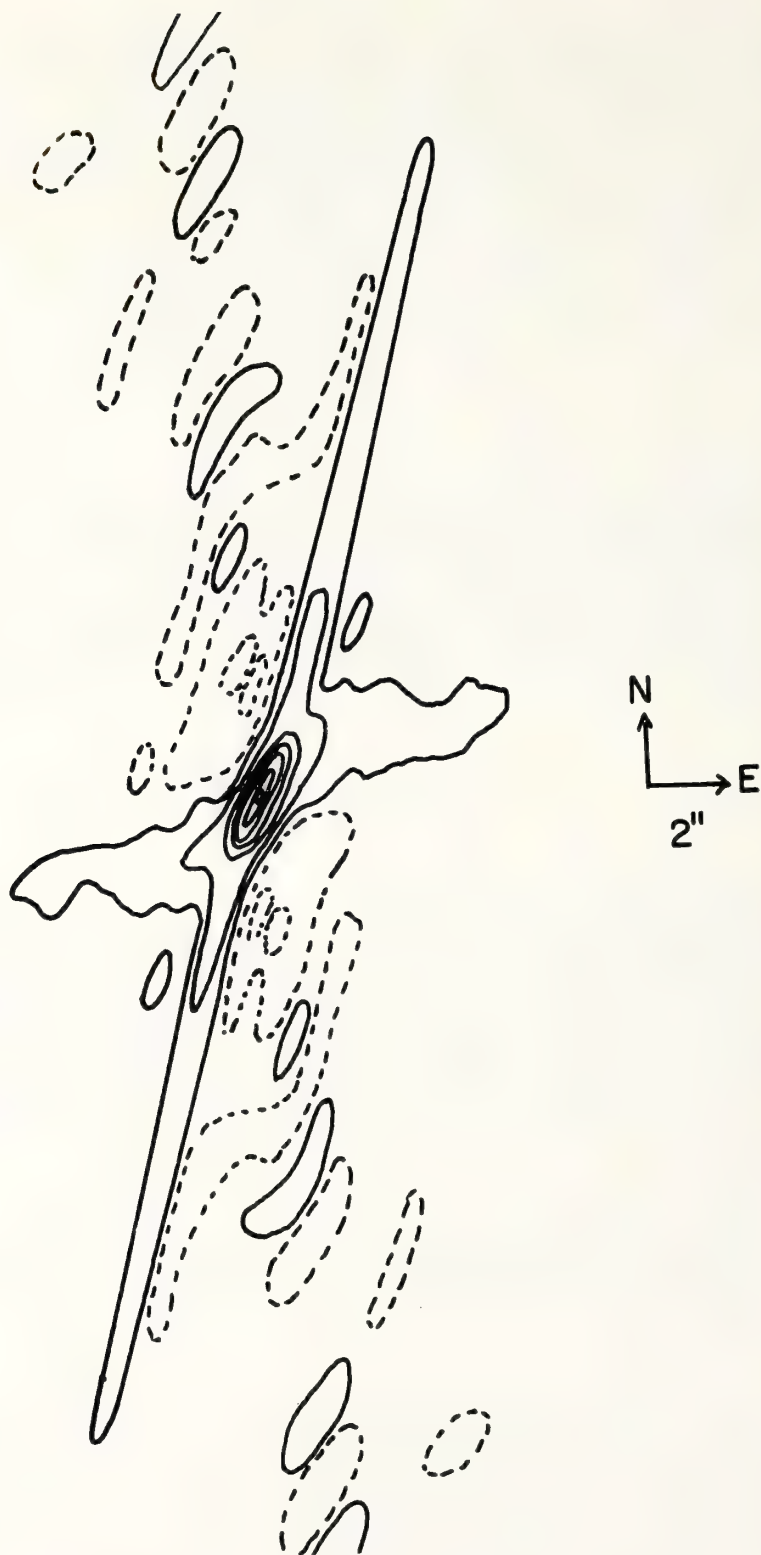


Figure 1. The V.L.A. beam pattern at 6 cm wavelength.

Here i and j correspond to positions on the grid which contained 40 by 40 points for our program.

Because both active regions were resolved for angular resolutions larger than 15 seconds of arc, we deleted those data having fringe spacings less than this value. The resulting synthesized beam, shown on the clean maps, had a half power width of 7 seconds of arc by 20 seconds of arc. The clean maps for both senses of circular polarization for the two regions are shown in Figures 2 and 3, respectively. The contours are in units of flux units per square arc second with the outermost contour drawn at 2. The most striking aspect of these maps is that the small-scale sources shown in the LCP and RCP maps are not spatially coincident. They suggest the feet of small dipole magnetic fields with positive magnetic polarity corresponding to the regions with strong right circular polarization. McMath region 15205, for example, contains two sources $\sim 30'' \times 30''$ in size which are $\sim 80\%$ left circularly polarized with one source of similar angular size and $\sim 60\%$ right circular polarization located between them. Assuming a source size of $30'' \times 30''$ an intensity of 100 Jy per synthesized beam area ($7'' \times 20''$) and a beam efficiency of 80%, we obtain a source brightness of $\sim 10^{-11}$ erg sec $^{-1}$ cm $^{-2}$ Hz $^{-1}$ rad $^{-2}$. Using the Rayleigh-Jeans law with a wavelength of 6 cm and this value of brightness we obtain a brightness temperature of $\sim 10^6$ K. Thus the small-scale sources and the magnetic structures which give rise to their circular polarization belong to the higher, hotter, coronal regions of the solar atmosphere. Assuming that the radio emission is at the first few harmonics of the gyrofrequency, magnetic field strengths on the order of a few hundred gauss are inferred.

Our interpretation of the circularly polarized radio wavelength emission in terms of coronal magnetic field structures may be confirmed by comparisons with photospheric magnetic field structures inferred from optical wavelength magnetograms. In fact, comparisons of W.S.R.T. synthesis maps of active regions at 6 cm wavelength with magnetograms indicated that the radio wavelength emission comes from regions of strong magnetic fields (M.R. Kundu, C.E. Alissandrakis, J.D. Bregman and A.C. Hin, *Astrophysical Journal*, 213, 278 (1977)). We have compared the V.L.A. maps shown in Figures 2 and 3 with Kitt Peak (K.P.N.O.) magnetograms, and shown that the general shape, orientation and bipolar configurations of the coronal magnetic structures (V.L.A.) are similar to those seen in the photosphere (with right circular polarization corresponding to positive magnetic polarity in magnetograms). (See K.R. Lang and R.F. Willson, *Nature*, 278, 24 (1979)).

In summary, V.L.A. observations provide information on coronal magnetic field structures with angular resolutions comparable to those obtainable at optical wavelengths in the photosphere. Future V.L.A. maps can give new information on the evolution of coronal magnetic fields, and on the distribution of magnetic field structures in height.

3. FLARE PREDICTION USING CHANGES IN THE CIRCULAR POLARIZATION OF THE SMALL-SCALE SOURCES

Solar active regions were observed with the N.R.A.O. three element interferometer in November, 1975, November, 1976 and May, 1978. A dual channel

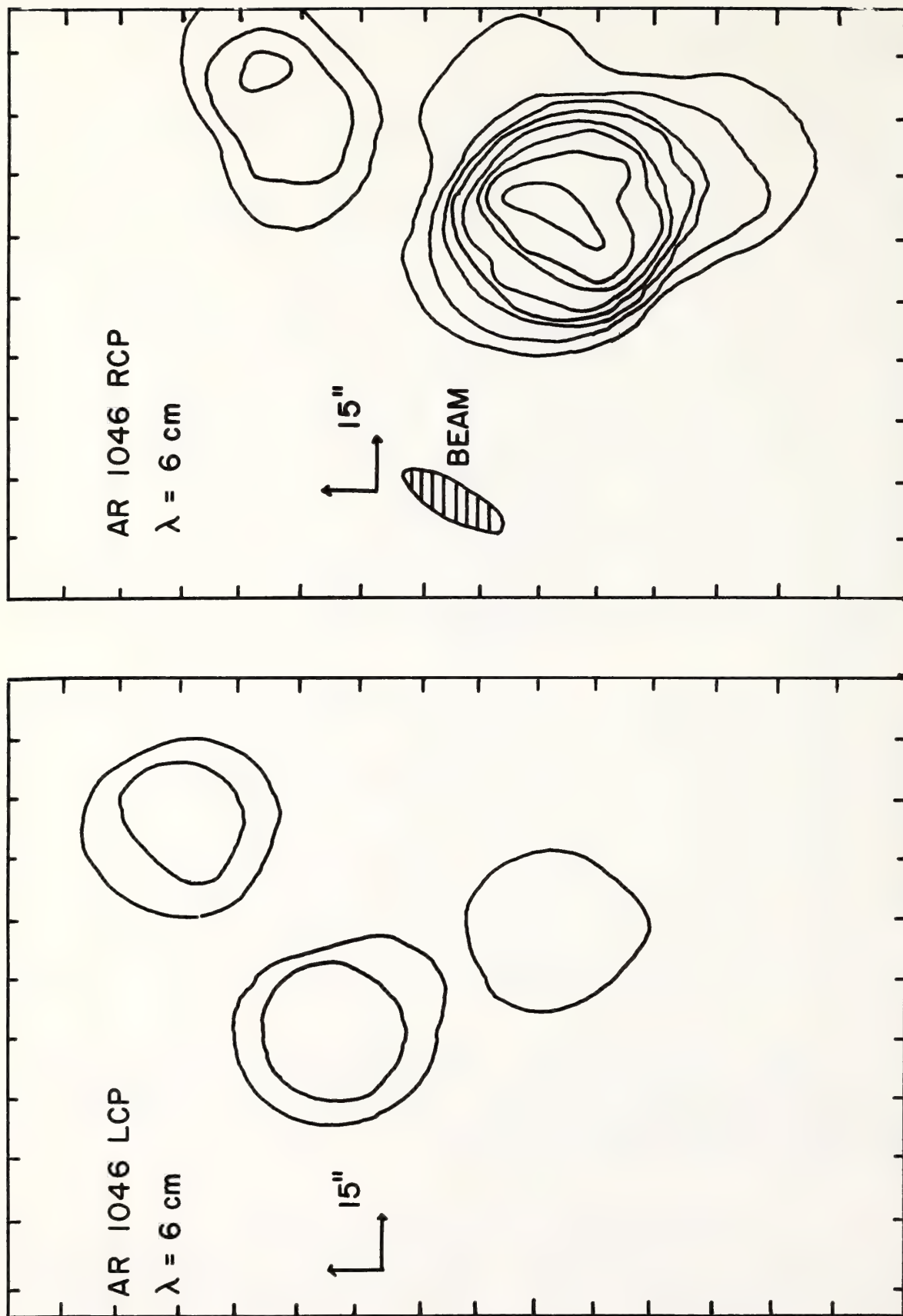


Figure 2. V.L.A. synthesis maps of active region 1046 obtained with left (LCP) and right (RCP) circularly polarized radiation at 6 cm wavelength on March 30, 1978. McMath region 15205

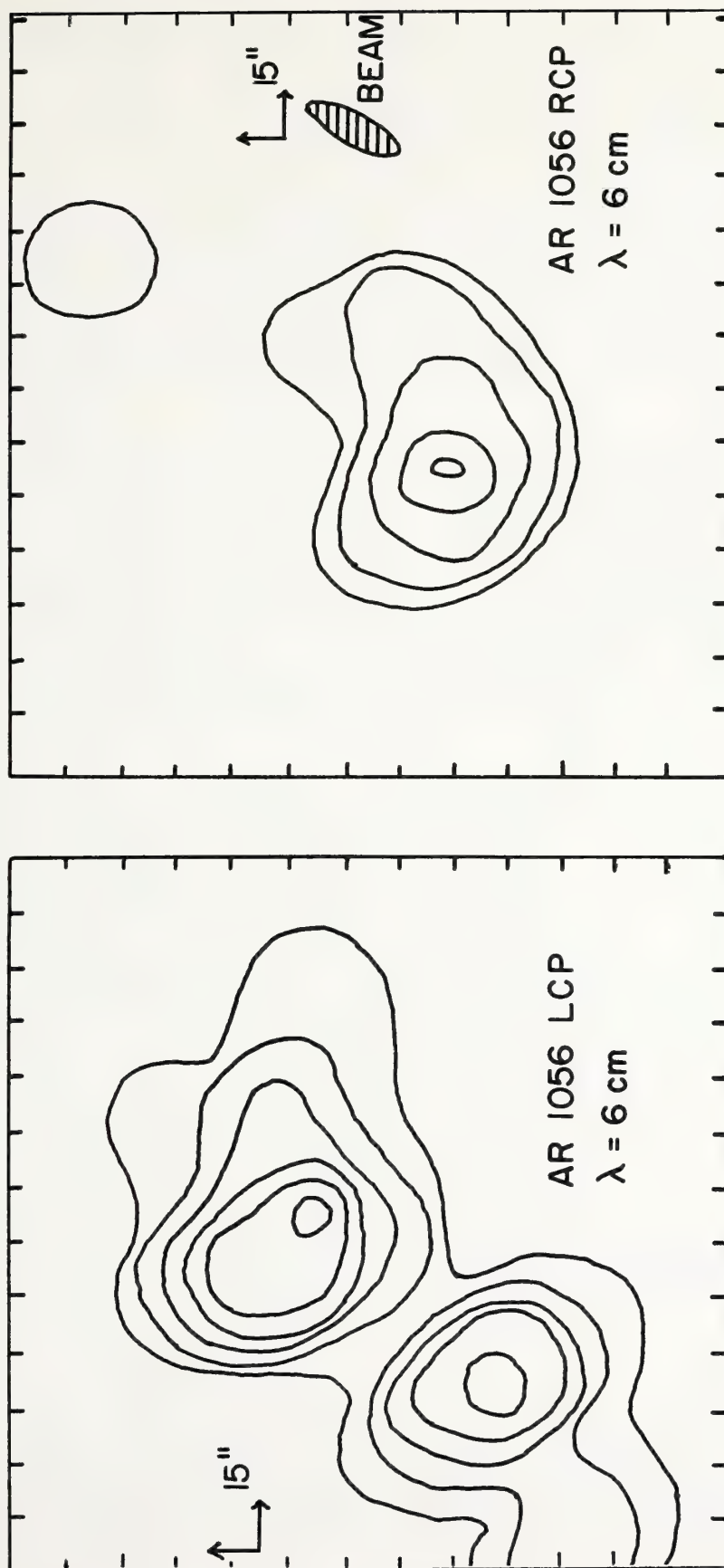


Figure 3. V.L.A. synthesis maps of active region 1056 obtained with left (LCP) and right (RCP) circularly polarized radiation at 6 cm wavelength on April 1, 1978. McMath region 15220

system was used at signal wavelengths of 3.7 cm and 11 cm, and both right circularly polarized (R.C.P.) and left circularly polarized (L.C.P.) signals were sampled every 30 seconds at alternate wavelengths. Three 25.9-m diameter paraboloids were placed on a skewed baseline with linear phase center displacements of 600, 1200, and 1800 m. These baselines provided maximum angular resolutions of 12.3, 6.2, and 4.1 seconds of arc at 3.7 cm and 36.7, 18.3 and 12.2 seconds of arc at 11 cm. The half-power beamwidths of the component antennae were ≈ 4 minutes of arc at 3.7 cm and ≈ 12 minutes of arc at 11 cm. The parametric amplifiers were bypassed, and the system-noise temperature was completely dominated by the solar brightness temperature of $\approx 2 \times 10^4$ K. For our 30 MHz intermediate frequency bandwidth and 30 second integration time, this system noise temperature resulted in a r.m.s. noise fluctuation in the fringe amplitude of 10 Jy, where $1 \text{ Jy} = 10^{-23} \text{ erg s}^{-1} \text{ cm}^{-2} \text{ Hz}^{-1}$.

The fringe amplitudes and phases and the circular polarization were calibrated by observing the radio source 3C 84. The gain of the system was adjusted so that the intermediate frequency signals were the same when observing the calibrator and the Sun. The fringe amplitudes obtained while observing the Sun were calibrated in Jy by multiplying them by GS/A , where G denotes the attenuation required to adjust the intermediate frequency signals to the same level, A denotes the fringe amplitude of the calibrator, and the flux density, S , of 3C 84 was assumed to be 27.8 Jy at 11 cm and 55.3 Jy at 3.7 cm. The circular polarization was calibrated by assuring that the fringe amplitudes of the two circularly polarized signals were equal when observing 3C 84 with a given interferometer pair.

After the observations were completed we plotted the left circularly polarized (LCP) and right circularly polarized (RCP) fringe amplitudes and phases as a function of time for all three baselines and both wavelengths. We also plotted the percentage circular polarization $V = (LCP - RCP)/(LCP + RCP)$ at the same times. For any given day between November 5 and November 9 of 1975, the degree of circular polarization of the active region (Mc Math No. 13926) remained constant within 10% during the 12 daylight observing hours. For all wavelengths and baselines used the degree of circular polarization was below 30% for all four days. Although the degree of circular polarization remained low (less than 30%) and constant (within 10%) for the 50-hour observing period between November 5 and 9, the active region suddenly exhibited dramatic changes in circular polarization about one hour prior to the emission of a flare. As illustrated in Figure 4, similar changes in circular polarization were observed about 30 minutes and 15 minutes before the flare emission as well. In view of the fact that no similar changes were observed in the 50 hours prior to flare emission, we believe the observed changes in circular polarization reflect emerging magnetic fields which triggered the flare emission. The implications for predictions of flare emission are clearly evident.

The degree of circular polarization observed while tracking active region 757 between November 18 and 22, 1976 remained constant at about 40% for all five days, and during this period no flare activity was reported by any optical or radio observatory. The fact that no changes in circular polarization were observed when no flares were emitted is valuable statistical evidence which supports the view that changes in circular polarization may

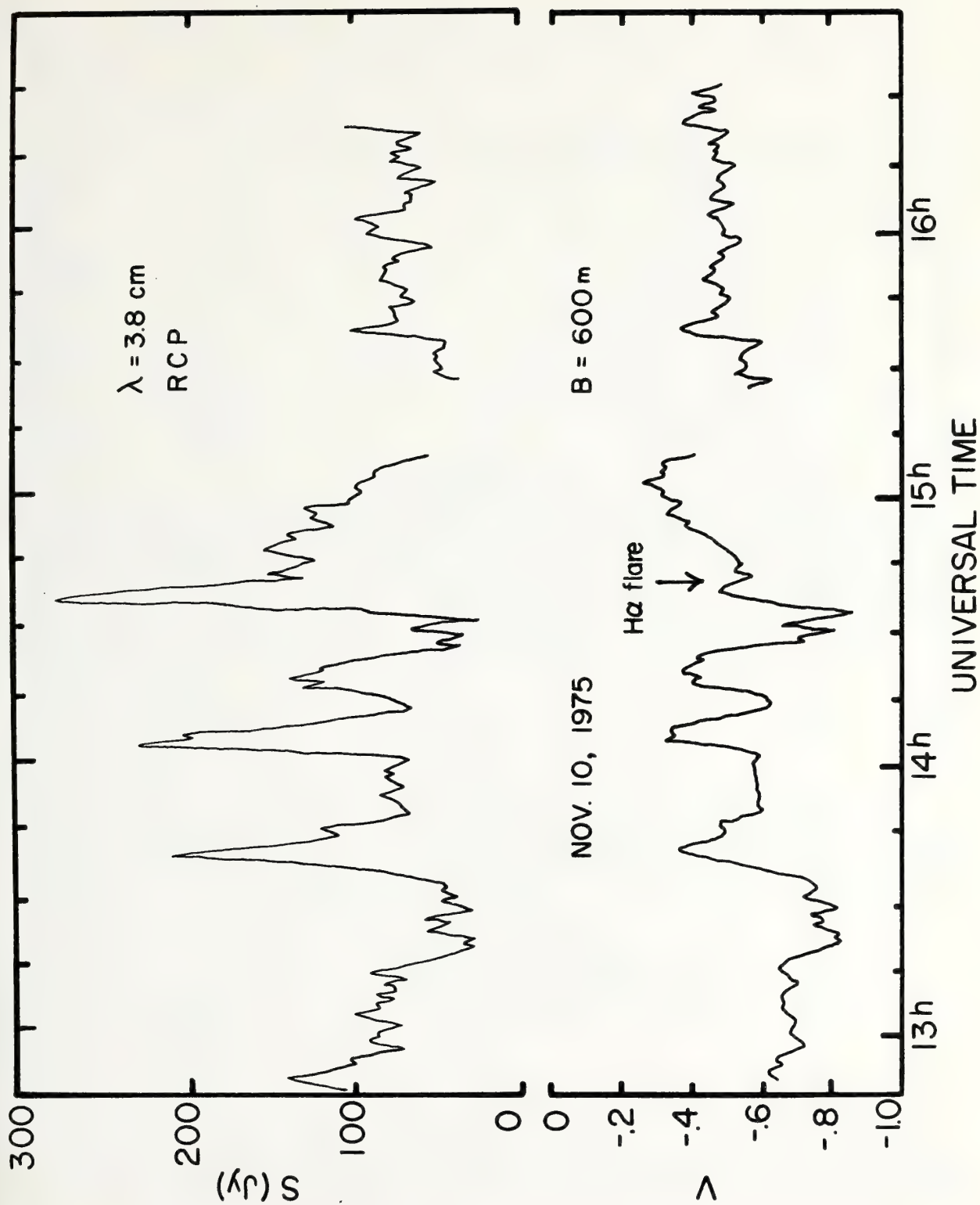


Figure 4. Interferometric observations of an active region (McMath No. 13926) showing large changes in the right circularly polarized (RCP) signal and the degree of circular polarization, V , prior to the eruption of a solar flare (denoted by vertical arrow).

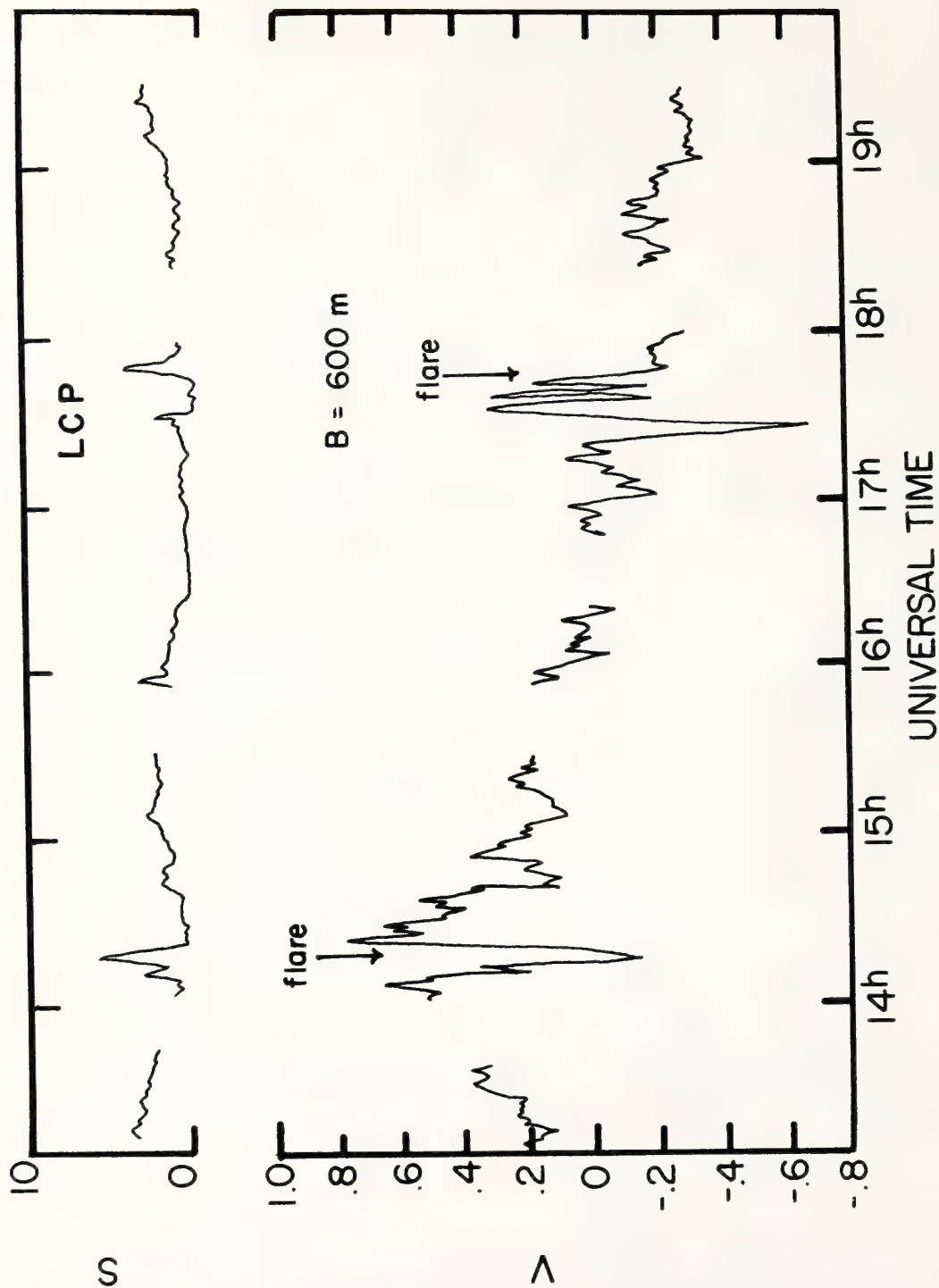


Figure 5. Two examples of interferometric observations of an active region (No. 1110) showing large changes in circular polarization, V, prior to the emission of solar flares (denoted by vertical arrows).

reflect emerging magnetic fields which trigger flares.

Active region No. 1110 was observed between May 10 and 13, 1978 while active region No. 1112 was observed between May 14 and 16, 1978. As illustrated in Figure 5, on May 12 we resolved structure at 3.7 cm whose angular size is ≈ 12 seconds of arc, and which undergoes dramatic changes in V which occur before and during the flares illustrated in the top plot of the LCP signal. We also obtained a second example of a multiple circularly polarized burst which was best seen at the highest angular resolution ($B = 1800$ m, $\lambda = 3.7$ cm and 4 seconds of arc resolution). These changes in circular polarization occurred on May 14 and lasted about 40 minutes. In our previous example of this type of long multiple burst, the flare observed at $H\alpha$ wavelengths only occurred during the last phase after the two radio wavelength precursors had already gone off (see Figure 4). The data shown in Figures 4 and 5 represent examples in which dramatic changes in the circular polarization of small-scale sources occur immediately prior to and during solar flares; whereas no similar changes were observed during the long intervals between solar flares.

In summary, analysis of interferometric data taken at centimeter wavelengths illustrate the presence of small-scale (≈ 10 seconds of arc), circularly polarized ($\gtrsim 40\%$) sources which emit intense circularly polarized emission (up to 80%) prior to and during the eruption of the solar flares seen at $H\alpha$ wavelengths and at other radio wavelengths with coarser angular resolution. The circularly polarized precursors probably trigger subsequent flare emission and may serve as reliable flare predictors.

4. ACKNOWLEDGMENTS

Radio interferometric studies of the Sun at Tufts University are supported under Contract No. F 19628-79-0010 with the Air Force Geophysics Laboratory. The National Radio Astronomy Observatory is operated by Associated Universities, Inc., under contract with the National Science Foundation.

SOFT X-RAY EMISSION FROM THE NON-FLARING SUN AS A PRECURSOR TO FLARE ACTIVITY

D. M. Horan, R. W. Kreplin and K. P. Dere
E. O. Hulburt Center for Space Research
Naval Research Laboratory
Washington, D. C. 20375

Ratios of the soft X-ray energy flux from the non-flaring Sun are formed using the 1-8Å, 2-10Å, and 8-16Å sensors aboard the SOLRAD 11B satellite. Values of these ratios are used as the basis for predictions of daily solar flare activity which are compared to predictions based on the 1-8Å flux level. The comparison shows that the use of the flux ratio provides no advantage over the use of the 1-8Å flux. The predictions of daily solar flare activity are approximately 50% accurate. Predictions of solar quiet are over 90% accurate.

INTRODUCTION

During the period 1966 to 1973, the Naval Research Laboratory made informal predictions of solar flare activity based entirely on changes in the full disk solar X-ray emission measured by broadband detectors. Specifically, when the X-ray energy flux in the 0.5-3Å, 1-8Å, and 8-20Å bands exceeded certain levels while no flares were in progress, a forecast of imminent solar flare activity was made. The predictions were sufficiently accurate to indicate that some relationship existed between the increase in broadband energy fluxes and ensuing flare activity.

During the same period, a technique using the ratio of flux levels in adjacent X-ray bands to calculate the temperature and emission measure of the emitting coronal plasma was demonstrated (Horan, 1971). Initially the technique assumed that all of the X-ray emission was continuum emission caused by free-free and free-bound electron transitions in the thermal plasma. Later the contribution of line emission was included (Dere, et al., 1974).

This technique has frequently been applied to flare emission to obtain temperature and emission measure variations during the course of flares. Application of this analysis technique to measurements made while no flares were in progress suggested itself as a more accurate and useful forecasting tool than the individual broadband energy flux levels.

DATA SOURCE

Ionization chambers sensitive to the 1-8Å, 2-10Å and 8-16Å bands and carried aboard the Naval Research Laboratory's SOLRAD 11 satellites provided X-ray energy flux levels used in this study. The two Earth satellites were launched on 15 March 1976 into a circular orbit with a radius of approximately 125,000 km and a period of approximately five days. A single ground station has primary responsibility for acquiring telemetry from the satellites. The length of time each SOLRAD 11 satellite is in sight of the ground station is determined more by the Earth's rotation than by the satellite's motion and a single pass over the ground station lasts between nine and eighteen hours. The SOLRAD 11A satellite provided good data in the bands of interest from launch until June 1977. SOLRAD 11B has also provided good data in the bands of interest since launch, and continues to do so. Since the data base from SOLRAD 11B is larger and increasing, it became the data source for this study.

FLUX RATIOS

The initial approach was to form the ratios of the 1-8Å to 8-20Å, the 1-8Å to 2-10Å, and the 2-10Å to 8-20Å energy fluxes. The energy fluxes are calculated by multiplying the current generated in an ionization chamber by a constant determined by the detector window area, the detector sensitivity as a function of wavelength, and a solar emission spectrum assumed to be a dilute blackbody at 2×10^6 K (Kreplin, 1961). Therefore, each ratio formed is actually a ratio of the currents generated in the ionization chambers multiplied by the ratio of the current-to-flux conversion constants. The response of the ionization chamber sensitive to X-rays in the 8-16Å band is converted to an energy flux over the larger 8-20Å band through the extension of the assumed solar emission spectrum to the wider band. Values of the ratios were formed at seven minute intervals throughout periods when data from SOLRAD 11B was available. Data collected by NASA stations when SOLRAD 11B was out of sight of the primary ground station helped to fill some of the data gaps. All three ratios were formed even though only two are unique because the most convenient presentation of the information was also being sought.

The initial approach was modified to amplify changes in the ratios as solar conditions changed. It was assumed that minimum values for the energy fluxes in each band could be associated with a quiet Sun having near zero probability of flaring. Minimum values were sought in the available data and were observed on 23 April 1976. The minimum values for each band were:

$$\begin{aligned} 1-8\text{\AA}: & \quad 2.0 \times 10^{-5} \text{ ergs/cm}^2 \text{ sec} \\ 2-10\text{\AA}: & \quad 9.0 \times 10^{-5} \text{ ergs/cm}^2 \text{ sec} \\ 8-20\text{\AA}: & \quad 9.4 \times 10^{-4} \text{ ergs/cm}^2 \text{ sec} \end{aligned}$$

These flux values and their ratios correspond to a solar plasma at $2.5 \times 10^6 \text{ K}$ with an emission measure of $3 \times 10^{48} \text{ cm}^{-3}$.

Ratios of the difference between the observed and minimum flux levels for each pair of bands were then formed at seven minute intervals. The values for each pair of bands were then plotted and the plots were scanned visually to determine if the ratio value for each day generally exceeded, was equal to, or less than certain reference levels. In most cases it was quite easy to determine how the ratios related to the reference levels. In some cases a subjective determination had to be made. If the data for a day was insufficient or too variable to make a reasonable assessment, that day was excluded.

The ratio of the modified 1-8 \AA to 8-20 \AA fluxes ranged between 0.01 and 0.10. The reference level used for that ratio was 0.03 to 0.04. The ratio of the modified 1-8 \AA to 2-10 \AA fluxes ranged between 0.05 and 0.50. The reference level used was 0.30. The ratio of the modified 2-10 \AA to 8-20 \AA fluxes ranged between 0.02 and 0.20. Its reference level was 0.10. The reference levels were selected by examining the behavior of the ratio values during a few days of known solar flare activity and a few days known to be free of flare activity. The reference levels selected appeared to have significance as precursors during these short periods.

SOLAR ACTIVITY

Solar flares in Baker Class M or X (Baker, 1970) were the standard used to evaluate the three ratios as forecasting tools. This level was selected because the X-rays of a Class M or larger event are considered capable of significant geophysical effects. The occurrence of one or more flares with X-ray emission in the 1-8 \AA band exceeding $1 \times 10^{-2} \text{ ergs/cm}^2 \text{ sec}$ (Class M) on a given day caused that day to be listed in the active category. No distinction was made between days having single or multiple Class M or greater flares. If no flares with 1-8 \AA X-ray emission exceeding $1 \times 10^{-2} \text{ ergs/cm}^2 \text{ sec}$ occurred on a day, that day was

listed in the quiet category. The source of information for Class M or greater flare occurrence was NOAA's weekly Preliminary Report and Forecast of Solar Geophysical Data. Although this document warns that it is preliminary and not to be referenced in publications it was found to be sufficiently accurate for this study because flare sizes and occurrence times within broad limits were sought and exact X-ray levels and time information were not needed.

COMPARISONS OF RATIOS AND SOLAR ACTIVITY

Day by day comparisons were made between the relationship of each of the three ratios of modified flux levels to its reference level and the classification of each day as active or quiet. The comparisons were carried out in two ways. Each daily ratio relationship was compared to the solar activity classification for that same day, and independently to the solar activity classification for the next day. Most of the days for which comparisons were made were in the period 20 June 1977 to 3 June 1978. All of the days compared fell within the period 24 March 1976 to 31 August 1978. Results of these comparisons are given in Table 1 which shows the number of days in the active and quiet Sun categories and the percentage of days in the active Sun category on and following a day when the ratio value was above, at, or below its reference level.

Table 1(a)

Relationship of modified $1-8\text{\AA}$ to $8-20\text{\AA}$ energy flux ratio to its reference level.

Ratio Value	Same Day's Sun			Next Day's Sun		
	Active	Quiet	%Active	Active	Quiet	%Active
High	56	77	42	51	82	38
Reference	5	76	6	7	73	9
Low	2	108	2	3	108	3

Table 1(b)

Relationship of modified $2-10\text{\AA}$ to $8-20\text{\AA}$ energy flux ratio to its reference level.

Ratio Value	Same Day's Sun			Next Day's Sun		
	Active	Quiet	%Active	Active	Quiet	%Active
High	60	139	30	58	140	29
Reference	0	59	0	3	56	5
Low	4	68	6	1	70	1

Table 1(c)

Relationship of modified 1-8Å to 2-10Å energy flux ratio to its reference level.

Ratio Value	Same Day's Sun			Next Day's Sun		
	Active	Quiet	%Active	Active	Quiet	%Active
High	62	127	33	57	132	30
Reference	1	31	3	0	30	0
Low	0	103	0	2	101	2

No significant differences appeared in the comparison to the same day's versus the next day's solar activity for any of the three modified flux ratios. This result was expected due to the common occurrence of flare activity over several days in sequence rather than on isolated days. The reference level used with the modified 1-8Å to 8-20Å flux ratio yielded the most accurate activity predictions in that the Sun produced one or more Class M or larger flares on 40% of the days on or following days when the ratio exceeded the reference level. An active Sun occurred for about 30% of the active Sun forecasts based on the reference levels used with the other two ratios. All three sets of ratios and reference levels produced quiet Sun forecasts which were better than 90% accurate but this is typical of many forecasting techniques.

COMPARISON OF FLUX AND SOLAR ACTIVITY

In order to compare the accuracy and usefulness of the ratios of energy fluxes as a forecasting tool with that of the energy flux level alone, the average level of the 1-8Å energy flux over a given day was also compared to reference levels. Two reference levels were used for the 1-8Å energy flux, 1×10^{-3} ergs/cm² sec and 5×10^{-4} ergs/cm² sec. The relationship of the 1-8Å energy flux for a given day to each reference level was determined by a visual scan of the plotted flux levels. The day by day comparison of the relationship of the 1-8Å flux level to each reference level and the classification of each day as active or quiet was made in the same way as for the ratios. The results of these comparisons are given in Table 2.

Table 2(a)

Comparison of $1-8\text{\AA}$ energy flux to the 1×10^{-3} ergs/cm² sec reference level

Flux Level	Same Day's Sun			Next Day's Sun		
	Active	Quiet	%Active	Active	Quiet	%Active
Higher	38	31	55	31	33	48
Equal	10	13	43	6	17	26
Lower	14	218	6	21	210	9

Table 2(b)

Comparison of $1-8\text{\AA}$ energy flux to the 5×10^{-4} ergs/cm² sec reference level.

Flux Level	Same Day's Sun			Next Day's Sun		
	Active	Quiet	%Active	Active	Quiet	%Active
Higher	51	67	43	49	69	42
Equal	4	11	27	3	12	20
Lower	2	185	1	9	173	5

Use of the higher reference level appears to provide a more accurate prediction of the same day's solar activity than of the next day's solar activity. This may be due to a greater possibility of incorrectly interpreting flare activity as a high background level. In such cases the result would not be a prediction of flare activity, but a confirmation of flare activity already occurring. Use of the lower reference level produced no significant difference in the accuracy of predicting the same day's versus the next day's solar activity. Use of the higher reference level yielded the more accurate solar activity predictions. An active Sun occurred for about 50% of the active Sun forecasts based on the higher reference level in contrast to slightly greater than 40% accuracy in the case of the lower reference level. Both reference levels produced quiet Sun forecasts which were better than 90% accurate, but the lower reference level was superior by a few percentage points.

CONCLUSION

The data presented in Tables 1 and 2 show that soft X-ray emission from the non-flaring Sun contains information which can be useful in assessing the probability of solar flare activity. A comparison of Table 1 and Table 2 shows that there is no advantage obtained by using the ratios of flux levels in different

bands. The use of different reference levels with the ratios would probably provide more accurate active Sun or quiet Sun forecasts. Possibly, a series of reference levels could be used with the ratios to generate forecasts of solar activity within probability bands such as is done by NOAA's Space Environment Services Center. However, the use of two reference levels with the 1-8Å flux clearly demonstrates the same potential without adding the complication of forming a ratio.

Table 3 shows why forming the ratio of fluxes doesn't provide a better forecasting tool than the use of flux levels alone. The table is derived from a daily comparison of the modified 1-8Å to 8-20Å flux ratio related to its reference level and the 1-8Å energy flux referenced to 5×10^{-4} ergs/cm² sec. These parameters were selected for comparison because each produced forecasts of solar activity which were approximately 40% accurate.

Table 3

Comparison of 1-8Å to 8-20Å ratio relationship and the 1-8Å energy flux referenced to 5×10^{-4} ergs/cm² sec.

1-8Å Flux	Ratio Compared to Reference Level		
	High	Reference	Low
Higher	99	7	18
Equal	17	6	56
Lower	0	1	107

Higher values of the ratio indicate the presence of high temperature solar plasma. However, high 1-8Å flux levels could be caused by the presence of higher temperature solar plasma, a larger emission measure, or a combination of the two. The top row in Table 3 shows that on 99 days the high 1-8Å flux levels occurred in conjunction with the presence of higher temperature plasma. However, the higher 1-8Å flux levels were observed in the absence of higher temperature plasma on only 18 days. Therefore, 80% of the forecasts of solar activity made using high flux levels are accidentally based on the same high temperature plasma information which is obtainable only by means of the flux ratios.

TECHNIQUE REFINEMENT

The refinement of soft X-ray emission as a forecasting tool can only be done by, or in close association with, a forecast center which needs it. Reference levels could be identified which would enhance the accuracy of forecasting solar activity or solar quiet. Sets of reference levels could be identified to forecast solar activity within different probability bands.

The basic time unit of one day could be changed. However, identification of more useful reference levels and time units would depend upon the specific needs of a forecast center and the source of its solar X-ray data.

REFERENCES

- Baker, D. (1970): Flare classification based upon X-ray intensity. AIAA Paper 70-1370, Huntsville, Ala.
- Dere, K. P., D. M. Horan, and R. W. Kreplin (1974): The spectral dependence of solar soft X-ray flux values obtained by SOLRAD 9. Journal of Atmospheric and Terrestrial Physics, 36, 989.
- Horan, D. M. (1971): Electron temperature and emission measure variations during solar X-ray flares. Solar Physics, 21, 188.
- Kreplin, R. W. (1961): Solar X-rays. Annales de Geophysique, 17:2, 151.

RELATIONS BETWEEN SOLAR X-RAY BURSTS, SUDDEN ENHANCEMENTS OF ATMOSPHERICS AND REGIONS OF SOLAR ACTIVITY.

B. LEROY

(Chercheur I.R.S.I.A.)

Institut d'Astronomie et d'Astrophysique.
Université Libre de Bruxelles-Belgique.

The statistical analysis of S.E.A.'s, solar X-ray flux and solar active regions shows some correlations between several parameters which describe these phenomena. The results are different according to the wavelength of the X radiation and the correlations appear to be more significant for short wavelengths. On the other hand, there seems to be a relation between the production of S.E.A.'s by an active region of the solar disc and the maximal evolution of the most developed group of sunspots in this region. The observation of S.E.A.'s can lead to predictions of characteristics of solar activity, as well as to information on solar X-ray bursts which reach the terrestrial atmosphere.

1. INTRODUCTION

The solar activity influences considerably the terrestrial atmosphere and, in particular, it produces disturbances in the ionospheric medium. These disturbances can be observed indirectly through their influence on the propagation of the radio waves. At the level of the D layer, they can be studied by means of long waves ($\lambda \approx 10$ km) and, among other methods, by observing the atmospheric noise emitted mainly by distant tropical storms. The solar activity results in a sudden enhancement of the level of distant atmospherics (S.E.A.), and a relation can be found between the slope at onset on the recording and some physical solar phenomena [Coutrez et al., 1963]. We have made a statistical analysis of the S.E.A.'s recorded in 1970 by the Royal Observatory of Belgium and the corresponding X-ray flux between 0.5 Å and 16 Å (from 0.8 to 25 keV) detected by Explorer 37.

Relationships between the production of S.E.A. by an active region of the solar disc and characteristics of this region have also been sought.

2. DATA

2.1 S.E.A.

During 1970 recordings of distant atmospherics have been made by the Royal Observatory of Belgium at Uccle and Humain-Rochefort.

The tuning frequencies of the two receivers are respectively 26.8 and 27.2 kHz, and the time constant of the recorders is 4 s. For a complete description of the equipment, see Coutrez et al. (1963) and Leroy (1976). A relative calibration of the receivers is achieved by using a noise source (thyatron 2D21) followed by an amplifier and a step attenuator. When the receiver is calibrated, the noise signal is applied to the input of the receiver and by varying the attenuation from 32 dB (reference level) to 59 dB (3 dB steps), a relative calibration scale is obtained.

In order to obtain a linear scale, the results of the measurements in dB are converted into percentage of the reference level using the following formula

$$n \text{ (dB)} = 20 \log_{10} \frac{100}{N(\%)}$$

The simultaneous use of two receivers with bordering frequencies, located 100 km from each other, and comparisons with the data published in "Solar-Geophysical Data" [1] enable us to eliminate the uncertainty, due to local noise, concerning the real character of some S.E.A.'s. In order to describe the observations, the following characteristics of the occurrences have been computed : time of beginning and time of maximum level ; level of atmospherics immediately before the beginning and at maximum enhancement (NI and NS) ; importance ($= 1 - NI/NS$); slope at onset (in % of enhancement per minute).

A typical S.E.A. recorded at Uccle is given in Figure 1.

2.2 X-ray flux.

The data used are those recorded by the Explorer 37 satellite and published in "Solar-Geophysical Data" [2] in the form of graphs giving for each day three curves corresponding to the 0.5 - 3 Å, 1 - 8 Å and 8 - 16 Å ranges. Sudden outbursts in the X-ray flux occurring simultaneously with S.E.A.'s have been sought whenever possible (the gaps due to the occultation of the satellite result in a lack of information). The X-ray flux is given in $\text{erg.cm}^{-2}.\text{s}^{-1}$ in a logarithmic scale and the importance is determined as for the S.E.A.'s. The time of the beginning and maximum are read on the graph and determined with a precision similar to that obtained for the S.E.A.'s.

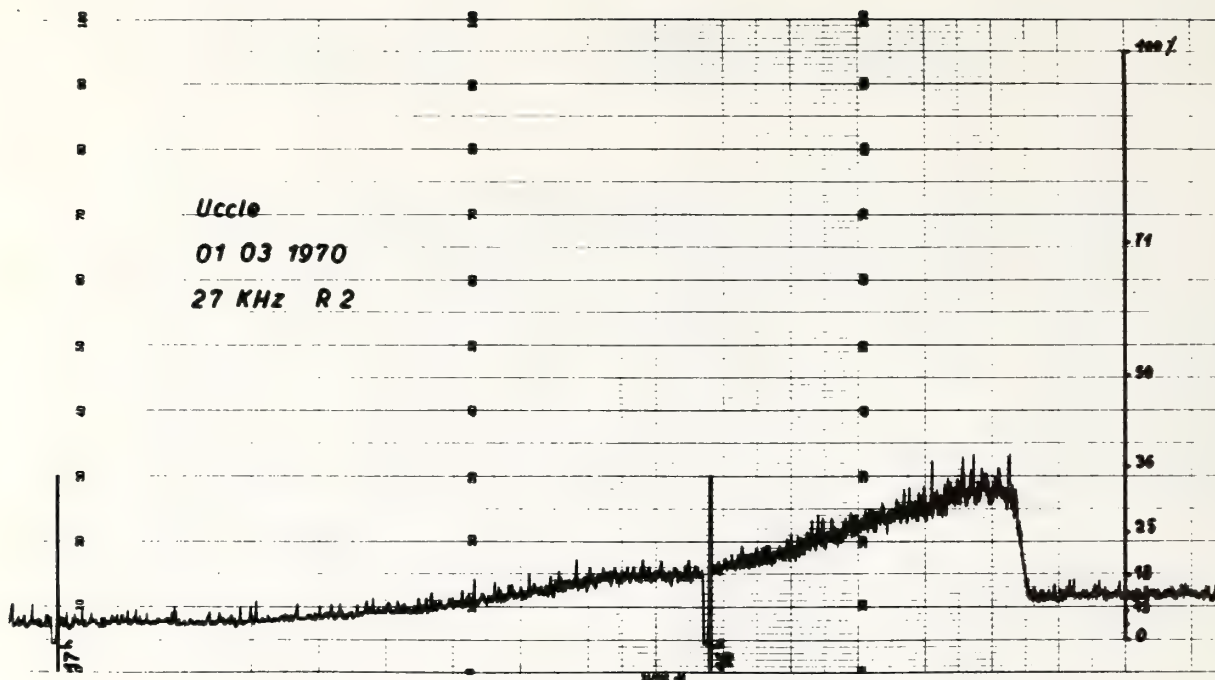


Figure 1 : Typical S.E.A. recorded at Uccle.

Time is running from the right to the left ; the vertical scale give the enhancement in % from a reference level.

3. RESULTS

3.1 Correlations between the characteristics of the S.E.A. and of the X-ray bursts.

301 S.E.A.'s have been observed on recordings of distant atmospherics but the final number of events (N) taken into account for the computation of the correlation coefficients (r) is less, due to various reasons (local noise, missing data, etc.). Moreover, saturation effects of the 0.5 - 3 Å receiver cause a supplementary loss of information in this range. The correlation coefficient r has been determined by means of the normal mathematical process, for example Kendall (1948), and the validity of the correlations is ensured by Δ , the confidence interval (95 %) about the estimate. Various parameters describing the X-ray phenomena and S.E.A.'s have been used : delay between the beginning and the maximum of the S.E.A. (del. S.E.A.), delay between the beginning and the maximum of the X-ray burst (del.X), importance of the X-ray burst (imp. X), maximum level of the X-ray burst (max.lev.X), slope at onset of the S.E.A. (slope S.E.A.), slope at onset of the X-ray burst (slope X), importance of the S.E.A. (imp. S.E.A.).

Table I : Correlation between various parameters describing
the X phenomena and the S.E.A.
(for explanation, see the text)

Correlation between ...	r	$\pm \Delta$	N
1. del. S.E.A. and del. X			
range 1 (0.5 Å - 3 Å)	0.42	0.25	61
range 2 (1 Å - 8 Å)	0.61	0.19	103
range 3 (8 Å - 16 Å)	0.60	0.20	101
2. imp. S.E.A. and imp. X			
range 1	0.29	0.21	85
range 2	0.43	0.18	118
range 3	0.47	0.18	116
3. imp. S.E.A. and max. lev. X			
range 1	0.50	0.21	86
range 2	0.26	0.18	121
range 3	0.28	0.18	118
4. slope S.E.A. and max. lev. X			
range 1	0.37	0.21	86
range 2	0.36	0.18	122
range 3	0.32	0.18	119
5. slope S.E.A. and slope X			
range 1	0.45	0.26	59
range 2	0.55	0.20	98
range 3	0.36	0.20	97

The main results obtained with the Uccle recordings are given in Table I. The results from the Humain-Rochefort station are similar.

The correlation between the two first characteristics (result 1.) appears clearly ; during the ascending phase, the time profiles of both the S.E.A. and the sudden increase in X-ray flux are similar. The X rays produce disturbances in the ionospheric D layer. The results given in Table I show that the high energy range differs from the lower ranges ; in (2.), the correlation coefficient for range 1 is lower than for ranges 2 and 3 while in (3.), the situation is inverted. The importance of the S.E.A. seems to be linked to different characteristics of the X-ray burst according to the energy range considered.

The results in (4.) show that the slope at onset of the S.E.A. is correlated with the peak level of the X-ray burst but that the wavelength does not influence the correlation coefficients.

The last series of results gives the highest correlation coefficients which vary according to the energy range considered. It appears that the correlation is better when the shorter components of the solar X radiation are taken into consideration. The same result is achieved by a study made using another method of indirect observation of the ionosphere (S.P.A.) [Kimpapa, 1975].

A further correlation, between the importance and the lower level of the same S.E.A. is negative : $r = -0.23$, $N = 217$, $\Delta = 0.13$. The recordings of S.E.A.'s where there was some uncertainty (due, for example, to interference, local storms, etc.) have been rejected. This correlation would indeed reflect a saturation effect in the ionospheric D layer, the ionizing radiation being less effective when the ionization of this layer is already high.

3.2 Influence on the production of S.E.A.'s by an active region of the solar disc.

Possible relations between the production of S.E.A.'s by an active region of the solar disc and some of its characteristics have been sought and, in particular, the development of the associated sunspots groups as given by "Solar Geophysical Data" [3].

We have distinguished between three types of regions :

- (a) regions which give rise to a single S.E.A. during their transit across the disc (28 regions concerned) ;
- (b) regions which produce 2 to 6 S.E.A.'s (26 regions concerned) ;
- (c) regions which give rise to more than 6 S.E.A.'s (7 regions concerned).

The study reveals that the number of S.E.A.'s which can be associated with a given region is higher when the groups of sunspots which this region produces attain a more developed type [Leroy, 1977]. The largest area reached by the sunspots of the region, and the maximum number of spots in this region influences in the same way the production of S.E.A. On the other hand the largest magnetic field strength measured in the region, that is a parameter in relation with the Brunner classification [Koeckelenbergh, 1975], does not seem to influence so markedly the production of S.E.A. by the region concerned. This parameter is meanwhile obtained with less precision.

The present analysis shows that further studies would be of some interest, e.g. : identification within each region of the sunspots group responsible for the S.E.A.; determination of the local configuration of the magnetic field ; study of non productive regions and sunspot groups ; extension of this study to a full solar cycle.

4. POSSIBILITIES OF PREDICTIONS

Paragraph 3.2 shows the relations between the effectiveness of a region on the solar disk in producing S.E.A.'s, and certain of its characteristics. The observation of these could, therefore, make it possible to predict the number of detectable S.E.A.'s. However, this

study was led to an examination of the characteristics of a region as a whole and a search for more detailed data (sunspot really responsible for the S.E.A., use of the radio spectrum, local configuration of the magnetic field, ...) would allow to precise the relations and the resulting predictions. This refinement would inversely, permit the deduction of the precise characteristics of solar activity from the number of detectable S.E.A.'s.

This point of view seems preferable and paragraph 3.1 shows the interest. At the present time a rough prediction of the characteristics of X-ray bursts reaching the terrestrial atmosphere can be made using the characteristics of the S.E.A.'s. In fact, the correlations tend to show that the importance of the S.E.A., and perhaps its slope at onset, make it possible to deduce the profile of the associated X-ray burst, in the wavelength band considered here.

In conclusion, the observation of S.E.A.'s can lead to predictions of certain characteristics of solar activity, as well as to information on solar X-ray bursts which reach the earth's atmosphere. A supplementary remark is necessary concerning active regions (see above) and X-ray flux (problems due to saturation in range 1, use of wide bandwidth,...)

These matters are at present under investigation.

Acknowledgements

We are deeply indebted to Prof. R. Coutrez, Director of the Institute of Astronomy and Astrophysics of the University of Brussels, who has initiated and guided this work. We thank Mmes C. Gonze-Delys and G. Evrard and Drs P. Cugnon, R. Gonze, A. Koeckelenbergh and M. A. Van Hauwaert, members of the Royal Observatory of Belgium for their help.

References.

- Coutrez, R., R. Gonze, A. Koeckelenbergh, E. Pourbaix and R. Roquigny (1963) : Contribution to the study of sudden enhancement of atmospherics (S.E.A.'s) and associated events. In : Radio Astronomical Studies of the Atmosphere, North-Holland Publishing, Amsterdam, 476.
- Kendall, M.G. (1948) : The Advanced Theory of Statistics, Ch. Griffin C^o Ltd., London.
- Kimpara, A. (1975) : Relations entre les anomalies brusques de phase en ondes très longues et les sursauts du rayonnement X solaire. Comptes rendus Acad. Sc. Paris, série B, vol. 280, 323-324.
- Koeckelenbergh, A. (1975) : Etude statistique des associations entre le champ magnétique des groupes de taches solaires et la morphologie des éruptions solaires et des sursauts associés sur ondes décimétriques. Ciel et Terre, vol. 91, n^o 2, 119-133.
- Leroy, B. (1976) : Contribution à l'étude des relations solaires-géophysiques : corrélations entre les renforcements soudains d'atmosphériques (S.E.A.) et la radiation X solaire. Ph. Thesis, Université Libre de Bruxelles.
- Leroy, B. (1977) : Etude statistique des relations entre la radiation X solaire, les renforcements soudains d'atmosphériques et les plages d'activité solaire. Ciel et Terre, vol. 93, n^o 4, 215-223.
- Solar-Geophysical Data [1] (1970-1971) : Prompt Reports, 307 I - 318 I U.S. Dept. of Commerce, Boulder, Colorado, U.S.A.
- Solar-Geophysical Data [2] (1970-1971) : Comprehensive Reports, 311 II-322 II, U.S. Dept. of Commerce, Boulder, Colorado, U.S.A.
- Solar-Geophysical Data [3] (1970-1971) : Prompt Reports, 306 I - 317 I, U.S. Dept. of Commerce, Boulder, Colorado, U.S.A.

PREDICTION OF SOLAR X-RAY FLUXES BASED ON SUNSPOT STRUCTURE

J. M. Mosher

Lockheed Palo Alto Research Laboratory
Palo Alto, California 94304

A comparison is made between the sunspot structure and the slowly-varying x-ray output from individual solar active regions. Using data from the Lockheed Mapping X-Ray Heliometer experiment on OSO-8, it is found that the 1-8 Å x-ray intensity is approximately proportional to either sunspot area or count. If the product of these two parameters is used, the correlation improves and two-thirds of all regions lie within a factor of two of the average trend. An additional class of sources producing x-ray fluxes up to about 10^{-7} W/m² is associated with spot-free regions.

1. Introduction

Monitoring the flux of soft x-rays incident on the earth's atmosphere has been an important scientific objective of experiments on rockets and satellites for more than twenty-five years. As a result of the research which has been done, it is now well appreciated that nearly all of this radiation comes from solar active regions, but relatively little attention seems to have been directed towards the problem of defining or attempting to predict the typical level of emission from an individual region. Because of the limitations of most earlier instruments, what interest has been expressed has focussed primarily on the comparison of full disk fluxes with total spot areas (Michard and Ribes, 1968) or Zurich sunspot numbers (Teske, 1969; Parkinson and Pounds, 1971). In the present study, two and one half years of data from the Lockheed x-ray experiment on OSO-8 are examined in an attempt to determine within what limits the x-ray flux from an individual active region can be anticipated on the basis of the underlying sunspot structure.

2. X-ray Data

This study is based on results generated during the quick-look analysis of data from the Lockheed Mapping X-Ray Heliometer (MXRH) experiment onboard OSO-8. The MXRH, which is capable of assigning individual intensities to each of several solar active regions approximately once every 40 seconds, has been described in detail by Wolfson et al. (1975; 1977).

As a part of the quick-look analysis, a map is constructed showing the 'typical' appearance of the x-ray sun for each day. Since the x-ray fluxes are highly variable, the decision as to what constitutes 'typical', based on the examination of about four hours worth of solar data, is obviously rather arbitrary; yet, avoiding obvious flare peaks as much as possible, the objective has been to choose an interval of five to ten minutes which seems representative of the available sample-- that is, neither the quietest nor the most active time.

The intensities of the sources on the daily map are then evaluated in counts per second summed over the spectral range of the detectors, which is nominally 1.5-15 keV. Data from as many as three independent detector systems may be used in making the intensity evaluation. For the purposes of the

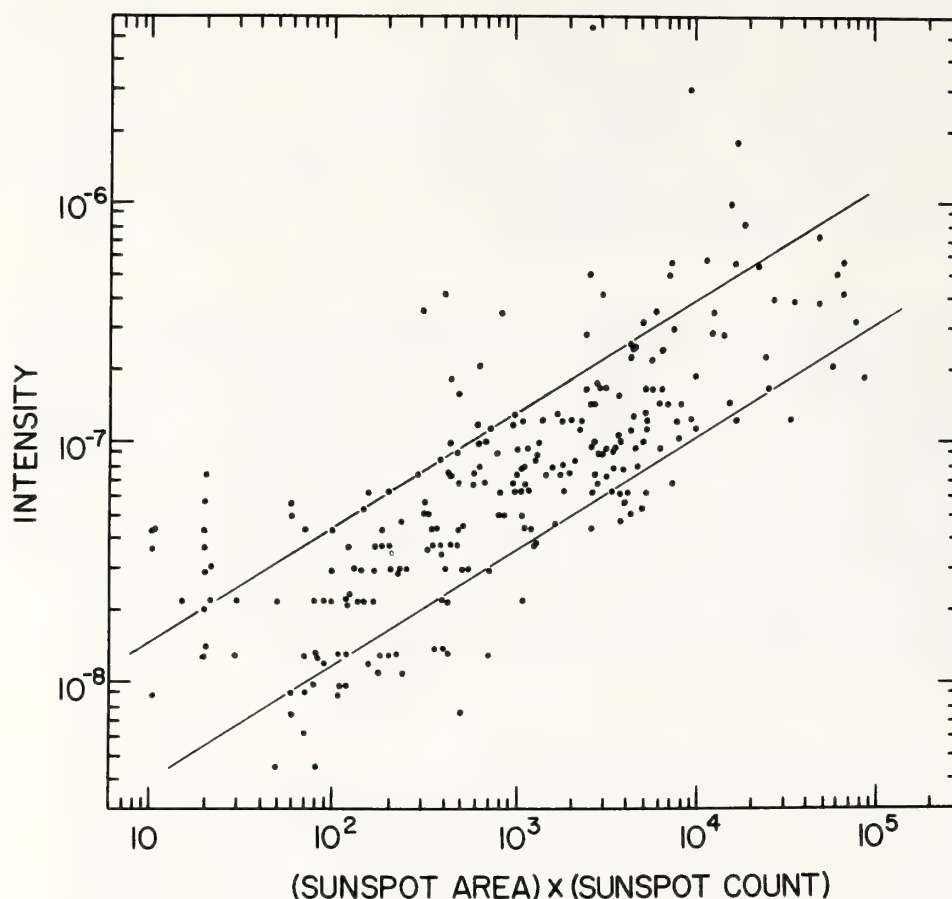


Fig. 2. Scatter plot of I vs. AxC with same format as Fig. 1. In a few instances a single McMath region contained more than one sunspot group. In these cases an average was made between the values of AxC obtained using separate and combined parameters.

of the data as determined by eye. The trends used were:

$$I = 1.34 \times 10^{-9} A^{0.84} \text{ W/m}^2 \quad (1)$$

$$I = 8.33 \times 10^{-9} C^{0.96} \text{ W/m} \quad (2)$$

$$\text{and} \quad I = 2.57 \times 10^{-9} (AxC)^{0.47} \text{ W/m} \quad (3)$$

The difference in the thickness of the 1σ scatter bands (which depends somewhat on the choice of slope) is not significantly different when the x-ray data are plotted against area, as opposed to count: a factor of ± 2.45 in the former case, and ± 2.34 in the latter. The 1σ scatter is reduced to a factor of ± 1.9 when the product AxC is used.

The scatter in the plots arises from several sources:

- (a) There are random errors in the choice of a 'typical' x-ray intensity whenever the region in question is variable (which is almost always) .
- (b) There are genuine variations in the temperature of regions at any given level of intensity, so that the conversion from counts per second to W/m^2 cannot be uniformly accurate for all regions.
- (c) There are random errors of unknown magnitude in the reported values of A and C.
- (d) There is undoubtedly an intrinsic scatter in the true relationship between I and A or C or $A \times C$.

The precise amount of the total scatter due to the last source is not entirely clear since we do not have accurate estimates of the contributions due to the other three, but the next section will indicate that at least some of the deviations from the average trend are real.

To within the accuracy of the present data, it would be fair to say that for regions with reported sunspot structure, the 1-8 Å x-ray flux is observed to be proportional to either the sunspot area or count separately, or alternatively, and with somewhat less scatter, to the square root of the product of area times count.

6. Exceptional Regions

It seems useful to attempt to identify the origin of points lying unusually far either above or below the average trend. Regions with unusually high x-ray outputs are almost always found to have been in a flaring or semi-flaring state at the time of the daily map. As an example, the highest intensity shown is $I = 5.3 \times 10^{-6} \text{ W/m}^2$ for McMath 14607 at 1934 UT on January 12, 1977. This young, growing region with $A = 130$ and $C = 21$ happened to be near a flare peak at the time of the map. Earlier the flux had been as low as $5 \times 10^{-8} \text{ W/m}^2$, and a typical 'quiescent' value for the day, based on the full 24 hours of data, would be something like $1.5 \times 10^{-7} \text{ W/m}^2$.

Anomalously low x-ray intensities, on the other hand, are almost always associated with decayed regions, which tend to be relatively stable. McMath 14564, for example, which had $A = 130$ and $C = 4$ on December 21, 1976, had an x-ray output of only about $7.5 \times 10^{-9} \text{ W/m}^2$ -- a factor of 5 to 10 lower than would normally be expected for a group of its size. The pictures in Solar-Geophysical Data indicate an extremely simple region magnetically, consisting almost entirely of a single spot which is at least one, and perhaps nearly two rotations old.

7. X-rays from Spotless Regions

A logical extension of the last category is the x-ray sources associated with totally spot-free regions. Of the weak sources which could be studied with 1-8 Å x-ray outputs in the range 1×10^{-8} to $5 \times 10^{-8} \text{ W/m}^2$, nearly one-third were of this variety, and invariably the spotless region represented the decayed remnant of a region which had or appeared previously to have had spots (possibly on the backside). The highest flux encountered in association with a spotless region during the course of this study was $I = 1.5 \times 10^{-7} \text{ W/m}^2$ for

McMath 14616 at 0800 UT on January 26, 1977. In retrospect, this unusually high flux was associated with a very gradual flare-like enhancement (possibly of the type described by Webb et al., 1976). In the absence of this transient event, the region would probably have been at or near the threshold of detectability for the MXRH.

8. Conclusions

A quantitative comparison of MXRH daily x-ray intensities with sunspot areas and counts indicates that the 1-8 Å x-ray flux from individual solar active regions can be roughly anticipated on the basis of the underlying sunspot structure. To within the accuracy of the present data, the x-ray intensity appears to be proportional to either the area or spot count considered separately, or, alternatively, to the square root of their product. In the latter case, the scatter of individual regions around the average trend is by a factor of about 2. In addition to the sources which obey this proportionality, there is a class of x-ray sources (typically with intensities below 5×10^{-8} W/m²) associated with decayed and apparently spotless regions.

The implication of this study is that rough estimates of solar x-ray intensities incident at earth can be made even at times when direct measurements are not available simply by examining the sunspot structure. It should be noted, however, that the present results apply only to the slowly-varying component of the x-ray signal, and that the bulk of the integrated x-ray output from a region will usually be produced by flares. A separate study would be required to determine if the flare contribution can also be anticipated on the basis of sunspot structure.

Acknowledgements

Dr. L.W. Acton is principal investigator for the MXRH experiment. The great majority of the daily quick-look analysis has been performed by K.L. Smith. This work is supported by NASA Contract NAS5-22411 and by grants from the Lockheed Independent Research Program.

REFERENCES

- Michard, R. and E. Ribes (1968): La Composante Lentement Variable des Rayons X Solaires en Relation Avec la Structure des Centres d'Active. In Kiepenheuer (ed.) Structure and Development of Solar Active Regions, 420.
- Parkinson, J.H. and K.A. Pounds (1971): X-ray Observations of Solar Active Regions from OSO-5. Solar Physics, 17:146.
- Solar-Geophysical Data: National Geophysical and Solar Terrestrial Data Center, U.S. Department of Commerce, Boulder, Colorado.
- Teske, R.G. (1969): Observations of the Solar Soft X-ray Component: Study of Its Relation to Transient and Slowly Varying Phenomena Observed at Other Wavelengths. Solar Physics, 6:193.
- Webb, D.F., A.S. Krieger, and D.M. Rust (1976): Coronal Enhancements Associated with H-alpha Filament Disappearances. Solar Physics, 48:159.

Wolfson, C.J., L.W. Acton, and C.W. Gilbreth (1975): Mapping X-Ray Heliometer for Orbiting Solar Observatory-8, Final Report. NASA CR-144710, 89 pp.

Wolfson, C.J., L.W. Acton, J.W. Leibacher, and D.T. Roethig (1977): Early Evolution of an X-ray Emitting Solar Active Region. Solar Physics, 55:181.

FREQUENCY OF CLASS M AND X FLARES BY SUNSPOT CLASS (1969-1976)

Karl J. N. Kildahl
U.S. Department of Commerce
National Oceanic and Atmospheric Administration
Environmental Research Laboratories
Boulder, Colorado 80303, U.S.A.

On 01 March 1969 the Space Environment Services Center adopted the revised classification of solar events based upon their peak x-ray emission in the 1 to 8 Angstrom wavelength range. This classification has continued and all flares are thus classified. Using the McIntosh Sunspot Classification all class M and X flares were catalogued for the time period 1969-1976. This paper shows that some classification of sunspot groups produce more M and X flares than others.

The C-M-X x-ray classification of Solar Flares was adopted by the Space Disturbance Forecast Center (SDFC) of ESSA, now known as the Space Environment Services Center (SESC) of NOAA on 01 January 1969. This new classification was prompted by the fact that the traditional optical importance of a solar flare (based on the area and brightness of the flare) is frequently not an adequate measure of the flare's geophysical importance. The C-M-X scheme was initiated in an attempt to classify flares according to their prompt (x-ray induced) geophysical effects (Baker, 1970). This classification was intended to supplement, but not replace, the optical classification of a flare. The original definitions were revised on 01 March 1969 so that the class C, M and X events are based upon the peak x-ray flux in the 1 to 8 Angstrom wavelength range. The 1-8 Å band was chosen because radiation at these wavelengths is largely responsible for the ionospheric disturbances which disrupt telecommunications. Early x-ray data were provided by two reliable satellite systems--the SOLRAD series of the Naval Research Laboratories and the VELA system operated by the Air Force. The SESC now receives data from the GOES-2 and GOES-3 satellites (Donnelly, et al., 1977) on a real time basis 24 hours a day. It is therefore easy to determine the x-ray class of any type of solar activity. This data is recorded in the forecast center of SESC, published in the Preliminary Report and Forecast of Solar Geophysical Data which is a weekly publication, and published in Solar-Geophysical Data-Prompt Reports (SGD). It is from SGD that the data for this study was taken (Solar Geophysical Data). The classes are defined as follows:

<u>Class</u>	<u>Peak 1-8 Å flux in watts per meter²</u>
C	greater than or equal to 10^{-6} but less than 10^{-5}
M	greater than or equal to 10^{-5} but less than 10^{-4}
X	greater than or equal to 10^{-4}

For descriptive purposes, a one-digit number from 1 to 9 may be appended to

these letter designations. The letter then acts as a multiplier. For example a C 3 burst would indicate an x-ray burst with peak flux in the neighborhood of 3×10^{-6} watts m^{-2} . This expanded classification is generally used only for description of events. Forecasts are issued in terms of the broad C, M, X categories.

Using data available from 1969-1976, a study was made in which the M and X flares were all catalogued using the sixty-three types of regions in the McIntosh Sunspot Classification (McIntosh, 1972; McIntosh, 1977) and the number of days each region type appeared on the disk. It was found that 12,411 classifications of sunspot groups were observed on the disk, and that 1,344 class M flares and 141 class X flares were observed. Table 1 gives a complete listing of all 63 types of regions and how many days that region class was observed on the sun during the period 1969-1976. Table 2 shows a complete listing of all 63 types of regions and the number of M-X flares (the first number is M flares and second number is X flares) which were observed in each type. Table 3 is a list of the eight highest producing sunspot types during the period, including the number of days that each class was observed and the number of class M-X flares associated with each type. Table 4 shows the flare occurrence by region type for this data set. The table shows the regions observed, the number of M-X flares and the number per day of flare occurrences from that region.

We see from Table 3 that the region Ekc was observed only 63 times but produced 149 class M flares and 21 class X flares. Region Fki appeared 47 times and produced 106 class M flares and 17 class X flares. The trained solar observer or solar forecaster could thus conclude that if either of these regions were observed on the visible disk that a class M flare is highly probable from that region during its appearance on the disk, and that a class X flare is also possible. We see from Table 1 that there are quite a few regions that are seldom seen on the solar disk. Table 2 would indicate that there are many regions that do not produce energetic flares. We find that the eight types listed in Table 3 produced 65% of all the class X flares and produced 50% of all the class M flares.

TABLE 1: NUMBER OF OCCURRENCES OF EACH SUNSPOT CLASSIFICATION

Regions 1969-1976

Year	Axx	Bxo	Bxi	Cro	Cri	Dro	Dri	Drc	Ero	Eri	Erc	Fro	Fri	Frc	Hrx
69	525	318	81	76	38	21	8	0	4	1	0	0	1	0	61
70	633	403	58	78	30	21	13	0	1	0	0	0	0	0	66
71	400	293	44	74	31	17	8	0	0	1	0	0	0	0	26
72	448	421	59	52	23	5	11	0	0	1	0	0	1	0	23
73	164	143	23	39	9	7	3	0	1	0	0	0	0	0	13
74	172	170	27	25	10	4	4	0	0	1	0	0	0	0	17
75	96	99	21	14	3	0	3	0	0	0	0	0	0	0	3
76	79	59	21	10	6	0	4	0	0	0	0	0	0	0	2
Totals	2517	1906	334	368	152	75	54	0	6	4	0	0	2	0	211

TABLE 1 (cont.)

Regions 1969-1976

Year	Cso	Csi	Dso	Dsi	Dsc	Eso	Esi	Esc	Fso	Fsi	Fsc	Hsx
69	55	56	110	56	2	8	25	9	3	3	0	340
70	303	65	227	90	5	32	21	0	8	1	0	490
71	168	15	101	37	6	12	11	0	0	2	0	393
72	185	29	56	33	3	22	11	0	2	1	0	306
73	44	13	15	8	0	1	1	0	0	0	0	100
74	69	13	28	10	0	6	9	0	0	1	0	172
75	49	7	12	6	0	1	0	0	0	0	0	73
76	16	13	4	6	4	0	0	0	0	0	0	89
Totals	1020	211	553	246	20	82	78	9	13	8	0	1963

Year	Cao	Cai	Dao	Dai	Dac	Eao	Eai	Eac	Fao	Fai	Fac	Hax
69	55	60	57	82	5	14	27	4	0	3	0	69
70	38	37	80	72	23	8	18	8	1	4	0	60
71	28	13	54	36	3	11	7	0	0	0	0	23
72	59	19	45	58	6	8	20	0	2	3	0	26
73	19	16	21	41	2	5	7	1	0	2	0	29
74	20	8	18	19	1	0	2	4	0	0	0	10
75	8	7	12	7	6	0	0	0	0	0	0	3
76	5	6	1	9	0	1	1	0	0	0	0	2
Totals	232	166	288	324	46	47	82	17	3	12	0	222

Year	Cho	Chi	Dho	Dhi	Dhc	Eho	Ehi	Ehc	Fho	Fhi	Fhc	Hhx
69	10	8	4	17	2	1	4	2	4	0	4	23
70	21	11	15	9	1	14	13	0	4	13	0	29
71	32	2	12	6	2	12	14	2	0	2	1	38
72	8	5	9	5	1	7	9	0	2	3	0	13
73	9	2	2	2	0	2	3	0	0	0	0	6
74	17	0	1	1	0	3	2	0	0	0	0	32
75	6	1	0	1	0	0	0	0	0	0	0	7
76	9	0	0	0	0	0	0	0	0	0	0	2
Totals	112	29	43	41	6	39	45	4	10	18	5	150

Year	Cko	Cki	Dko	Dki	Dkc	Eko	Eki	Ekc	Fko	Fki	Fkc	Hkx
69	13	10	11	23	31	18	5	19	3	1	7	7
70	10	6	13	17	14	13	23	17	11	9	5	12
71	5	1	9	12	7	7	24	4	1	18	3	13
72	11	4	3	9	12	11	16	19	3	11	5	1
73	10	2	5	12	12	3	7	1	1	1	0	3
74	3	4	2	9	9	0	2	3	0	1	7	0
75	0	1	0	5	3	0	4	0	0	6	0	1
76	0	0	0	1	12	0	0	0	0	0	0	1
Totals	52	28	43	88	100	52	81	63	19	47	27	38

12411 classifications of sunspot groups were observed.

TABLE 2: NUMBER OF FLARES ASSOCIATED WITH EACH SUNSPOT CLASS.

M-X Flares 1969-1976

Year	Axx	Bxo	Bxi	Cro	Cri	Dro	Dri	Drc	Ero	Eri	Erc	Fro	Fri	Frc	Hrx
69	8-1	8-1	12	5-1	0	5	2-1	0	0	0	0	0	1	0	4-1
70	13-1	9-1	2	2	5	0	2	0	0	0	0	0	0	0	2
71	1-1	10	1	2	2	1	1	0	0	0	0	0	0	0	0
72	5	5	4	2	0	0	1	0	0	0	0	0	0	0	0
73	1	4	1	0	0	0	1	0	0	0	0	0	0	0	1
74	2	3	0	0	0	0	0	0	0	0	0	0	0	0	0
75	1	0	0	9-1	0	0	0	0	0	0	0	0	0	0	0
76	0	2	0	0	0	0	0	0	0	0	0	0	0	0	0
Totals	31-3	41-2	20	20-2	7	6	7-1	0	0	0	0	0	1	0	7-1

Year	Cso	Csi	Dso	Dsi	Dsc	Eso	Esi	Esc	Fso	Fsi	Fsc	Hsx
69	7-1	4-2	23-2	6	1	1	2	0	0	6	0	8-1
70	20	5	22-3	18-1	0	8	13	0	6-1	2	0	53-4
71	6	2	3-1	3	3-1	2	4-1	0	0	4	0	11
72	4	2	1	1	0	2	2-1	0	0	0	0	10
73	3	3	0	0	0	0	0	0	0	0	0	5
74	0	0	1	3	0	1	1	0	0	3	0	5
75	0	0	0	0	0	0	0	0	0	0	0	0
76	0	0	1	0	1-1	0	0	0	0	0	0	1-1
Totals	40-1	16-2	51-6	31-1	5-2	14	22-2	0	6-1	15	0	99-6

Year	Cao	Cai	Dao	Dai	Dac	Eao	Eai	Eac	Fao	Fai	Fac	Hax
69	10	2	5	16-4	1	6-3	16	1	0	4	0	10
70	3	9	12-1	10	10-1	0	18	2-1	0	2	0	2
71	3	1	3-1	5	0	0	2	0	0	0	0	0
72	1	2	6	12-1	0	4-1	3	0	0	0	0	0
73	0-1	5	2	7-1	0	0	8-1	1-1	0	2	0	2
74	0	0	0	8-1	0	0	0	2-1	0	0	0	0
75	1	0	0	0	1	0	0	0	0	0	0	0
76	0	0	0	0	0	0	1	0	0	0	0	0
Totals	18-1	19	28-2	58-7	12-1	10-4	48-1	6-3	0	8	0	14

Year	Cho	Chi	Dho	Dhi	Dhc	Eho	Ehi	Ehc	Fho	Fhi	Fhc	Hhx
69	1	2	2	1	1	0	7-3	5	0	0	4	7-1
70	0-1	0	10	2	0	5	14	0	0	12	0	3
71	2	3	0	0	1	0	6-1	3	0	0	0	3
72	3	1	1	0	0	1	0	0	0	3	0	1-1
73	2	0	0	0	0	0	1	0	0	0	0	2
74	0	0	0	0	0	0	0	0	0	0	0	0
75	0	0	0	0	0	0	0	0	0	0	0	0
76	0	0	0	0	0	0	0	0	0	0	0	0
Totals	8-1	6	11	3	2	6	28-4	8	0	15	4	16-2

TABLE 2 (M-X Flares 1969-1976 cont.)

Year	Cko	Cki	Dko	Dki	Dkc	Eko	Eki	Ekc	Fko	Fki	Fkc	Hkx
69	3-1	2	5-1	20-3	35-4	3	26-5	30-5	0	0	11	4
70	4	2-1	3-1	5-1	11-1	7	45-4	73-9	6	79-13	14-6	2
71	0	0	2	5	2	0	8	0	0	14	0	1
72	5	1-1	3	3	3	6-1	6-1	31-6	0	9-2	1-1	0
73	1-1	1	1	0-1	10-2	4	8	4	0	0	0	0
74	0	0	0	7-1	4-2	0	9-1	11-1	0	4-2	13-6	0
75	0	0	0	2	3	0	1	0	0	0	0	0
76	0	0	0	0	4-1	0	0	0	0	0	0	0
Totals	13-2	6-2	14-2	42-6	72-10	20-1	103-11	149-21	6	106.17	39-13	7

Totals: 1344 M-Flares, 141 X-Flares, and 1485 Total M-X Flares.

TABLE 3. MOST PRODUCTIVE REGIONS 1969-1976

Region	Appearance	Class M Flares	Class X Flares
Hsx	1963	99	6
Dso	553	51	6
Dai	324	58	7
Ekc	63	149	21
Eki	81	103	11
Dkc	100	72	10
Fki	47	106	17
Fkc	27	39	13

TABLE 4

Class	Total # Days Observed	Total # Associated Class M Flares	Total # Associated Class X Flares	Ave. #* M Flares/ Day	Ave. #* X Flares/ Day
Axx	2517	31	3	.012	.001
Bxo	1906	41	2	.022	.001
Bxi	334	20	0	.059	.000
Cro	368	20	2	.054	.005
Cri	152	7	0	.046	.000
Dro	75	6	0	.080	.000
Dri	54	7	1	.129	.019
Drc	0	0	0	.000	.000
Ero	6	0	0	.000	.000
Eri	4	0	0	.000	.000
Erc	0	0	0	.000	.000
Fro	0	0	0	.000	.000
Fri	2	1	0	.500	.000
Frc	0	0	0	.000	.000
Hrx	211	7	1	.033	.005

TABLE 4 (cont.)

Class	Total # Days Observed	Total # Associated Class M Flares	Total # Associated Class X Flares	Ave. # [*] M Flares/ Day	Ave. # [*] X Flares/ Day
Cso	1020	40	1	.039	.001
Csi	211	16	2	.076	.009
Dso	553	51	6	.092	.011
Dsi	246	31	1	.126	.004
Dsc	20	5	2	.250	.100
Eso	82	14	0	.171	.000
Esi	78	22	2	.171	.026
Esc	9	0	0	.000	.000
Fso	13	6	1	.462	.077
Fsi	8	15	0	1.875	.000
Fsc	0	0	0	.000	.000
Hsx	1963	99	6	.050	.003
Cao	232	18	1	.078	.004
Cai	166	19	0	.114	.000
Dao	288	28	2	.097	.007
Dai	324	58	7	.179	.024
Dac	46	12	1	.261	.022
Eao	47	10	4	.213	.085
Eai	82	48	1	.585	.012
Eac	17	6	3	.353	.176
Fao	3	0	0	.000	.000
Fai	12	8	0	.667	.000
Fac	0	0	0	.000	.000
Hax	222	14	0	.063	.000
Cho	112	8	1	.071	.009
Chi	29	6	0	.207	.000
Dho	43	11	0	.256	.000
Dhi	41	3	0	.073	.000
Dhc	6	2	0	.333	.000
Eho	39	6	0	.154	.000
Ehi	45	28	4	.622	.089
Ehc	4	8	0	2.000	.000
Fho	10	0	0	.000	.000
Fhi	18	15	0	.833	.000
Fhc	5	4	0	.800	.000
Hrx	150	16	2	.107	.013
Cko	52	13	2	.250	.038
Cki	28	6	2	.214	.002
Dko	43	14	2	.326	.047
Dki	88	42	6	.477	.068

TABLE 4 (cont.)

Class	Total # Days Observed	Total # Associated Class M Flares	Total # Associated Class X Flares	Ave. # [*] M Flares/ Day	Ave. # [*] X Flares/ Day
Dkc	100	72	10	.720	.100
Eko	52	20	1	.385	.019
Eki	81	103	11	1.272	.136
Ekc	63	149	21	2.365	.333
Fro	19	6	0	.316	.000
Fki	47	106	17	2.255	.362
Fkc	27	39	13	1.444	.481
Hkx	38	7	0	.184	.000

$$^* \text{Ave. \# flares per day} = \frac{\text{Total \# Flares Associated with Class}}{\text{Total \# of Days Class was Observed}}$$

REFERENCES

- Baker, Donald M. (1970): Flare classification based upon x-ray intensity. AIAA Paper No. 70-1370.
- Donnelly, R. F., R. N. Grubb, and F. C. Cowley (1977): Solar x-ray measurements from SMS-1, SMS-2 and GOES-1. Information for Data Users.
- McIntosh Sunspot Classification. Solar-Geophysical Data: 1972, Descriptive Text, pp. 25-27 and in each annual descriptive text to the present.
- McIntosh, P. S. (1977): Solar flare predictions with a revised sunspot classification. Bull. Amer. Astron. Soc., 9:330, Abstract only.
- Solar Geophysical Data (Prompt Reports) Numbers 306-355, 1970-1974, U. S. Department of Commerce Monthly Publication, Boulder, Colorado, USA.

A PREDICTION METHOD FOR THE SOFT X-RAY FLUX OF SOLAR FLARES

D. L. Teuber, E. J. Reichmann, R. M. Wilson
NASA/Marshall Space Flight Center, Space Sciences Laboratory
Marshall Space Flight Center, AL 35812 USA

and

J. B. Smith, Jr.
NOAA/Space Environment Laboratory
Boulder, CO 80302 USA

An analytic method is described that allows prediction of peak X-ray flux and flux profile for solar flares. The method is based on full-disk proportional counter data from the X-ray event analyzer (X-REA) which was part of the Skylab ATM/S-056 experiment. The observed X-ray flux through all channels between 2.5 and 20 Å follows essentially a Chi-square distribution with five degrees of freedom. Higher order terms are successive derivatives of this distribution and can be obtained from a recursive property, but they are not required when about 90 percent of the cumulative power in the signal is sufficient for its representation.

At least four parameters are necessary for our empirical, general and orthogonal least-squares fits: the initial time and X-ray flux for the event and its maximum height and width (or relaxation time). The program which we describe starts with these four initial guesses and performs an iteration process. Several flares are described and classified in this manner.

Our method points to an impulse as the triggering mechanism for X-ray flares and demonstrates that the X-ray flare is purely a deterministic and predictable response to the impulse. Examples for the prediction method are shown from Skylab data, but it could equally be applied to present satellite solar observations.

1. INTRODUCTION

In recent years, solar physicists have investigated the nature of flares, their location and occurrence, and their peak-emission levels (e.g., Smith and Smith, 1963; Zirin, 1966; Tandberg-Hanssen, 1967; Noyes, 1976; Švestka, 1976a). While some success has precipitated, in particular, predicting the location and occurrence of flares (e.g., Martin and Ramsey, 1972; Smith, 1972; Švestka, 1976b; Martres *et al.*, 1977) and generating descriptive flare models (e.g., Priest, 1976; Švestka, 1976a), little has been revealed that allows the pre-

diction of flare peak-level emission. In this paper, we present a technique that allows an observer to know a priori flare-peak-level X-ray emission, based only on the early observations following flare initiation. The data used in this study come from the Skylab-borne X-ray event analyzer (X-REA), a system comprised of full-disk proportional counters (Underwood et al., 1977).

2. TECHNIQUE

2.1 Background

In a previous paper (Teuber et al., 1979), we presented a "principal component" analysis of solar flares in the soft X-ray flux between 2.5 and 20 Å. A disadvantage of the method is the requirement for a rather elaborate software system and large computer. Furthermore, it seems somewhat arbitrary to find common features of the X-ray flux through ten energy channels (i.e., looking for matched parameters over the entire spectral range).

In this report we make use of a more direct method for analyzing solar flares. We do this by either (i) applying an analytical expression to a channel of proportional counter data or (ii) solving a differential equation with a time-varying parameter. It can be shown that the analyzed flares in the 2.5-20-Å range are essentially deterministic responses with a predictable signature and that they can be classified with sufficient accuracy according to pulse height and width from an inferred origin.

The prediction of the time response is based upon "raw" data that are corrected only for extraneous points at aperture changes. We are limited in the number of data points used only by a sampling rate of one sample per 2.5 s and an observational window of generally up to 55 min (i.e., the duration of the daylight portion of an orbit).

While the technique described below has been used with the Skylab X-REA data, it could equally be applied to any proportional counter data (e.g., GOES). Also, while in the context of a prediction technique we emphasize strictly an empirical method, we note that more information on involved physical processes can be gleaned from it.

2.2 Analytic Expression

Mathematically, the density of the dependent variable x (X-ray flux) can be represented by a Chi-square distribution; i.e.,

$$F(x) = F(\chi^2) = K(f)T^{(f/2)-1}e^{-T/2}, \quad (1)$$

where f (degrees of freedom) equals 5, T (time) is the independent variable, and $K(f)$ is a constant whose value depends strictly on f . For practical purposes (see Teuber et al., 1979), we have selected the algebraic equation

$$Y = A(BT)^{3/2}e^{-BT}, \quad (2)$$

where Y (magnitude) corresponds to $F(x)$, T remains time, A is the pulse height, and B is the pulse width, to represent the distribution. (We note that the empirical function --equation 2-- has a close resemblance to the Chi-square distribution function --equation 1; however, its physical significance does not concern us here.) Figure 1 shows the similarity of the Chi-square distributions, represented by Y , for selected values of A and B , based on an arbitrary, normalized time scale; this time scale is the same for Figures 1 and 3. Curve 1 uses values of $A=2.44$ and $B=1.0$; curve 2 -- $A=1.9$ and $B=0.5$; and curve 3 -- $A=2.0$ and $B=2.0$. We note that, if these curves were properly scaled, they would then be representative of single-impulse, solar X-ray flares.

2.3 Differential Equation

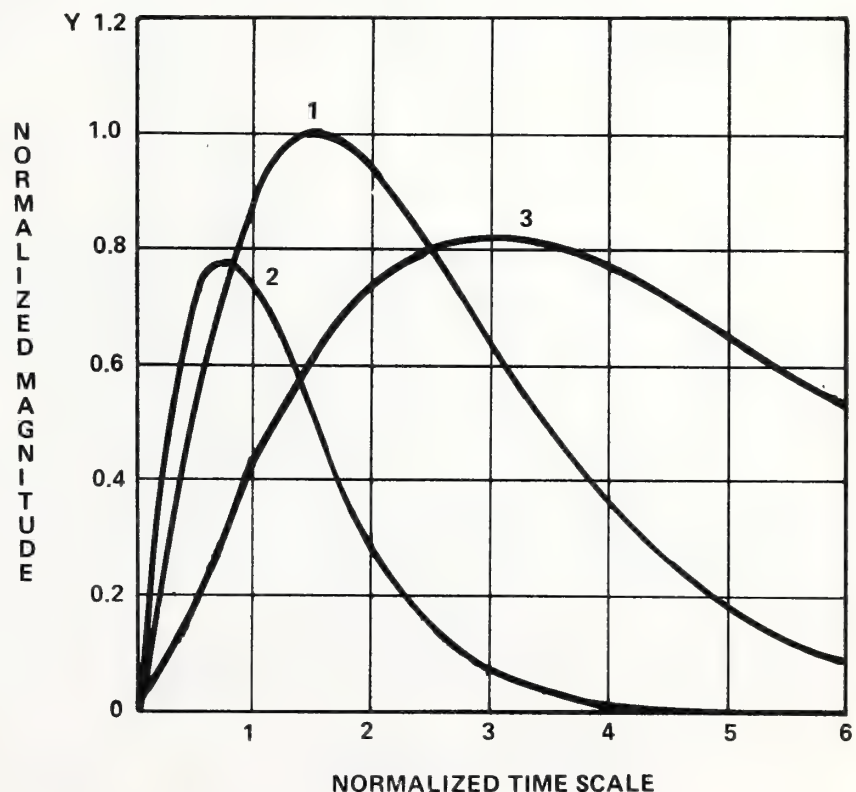
Identical curves to Figure 1 can be obtained as the solution of a differential equation with a time-varying parameter; namely,

$$\ddot{Y} + 2\dot{Y} + (1 - 3/4T^2)Y = 0, \quad (3)$$

where Y and T are defined as before, and \dot{Y} and \ddot{Y} are the first and second derivatives of Y . We note that the solution is unstable for $T \leq (3/4)^{1/2}$, and stable for $T > (3/4)^{1/2}$. For $T=0$, the time-varying parameter $(1 - 3/4T^2)$ becomes infinite and represents a singularity. We suggest that this may be supportive of Falciani *et al.* (1977) who have reported on the existence of a single triggering mechanism during the flash-phase of a solar flare.

Figure 2 depicts the solution of equation 3 by means of a flow chart. The

FIGURE 1. CHI-SQUARE DISTRIBUTIONS FOR SELECTED VALUES OF A AND B



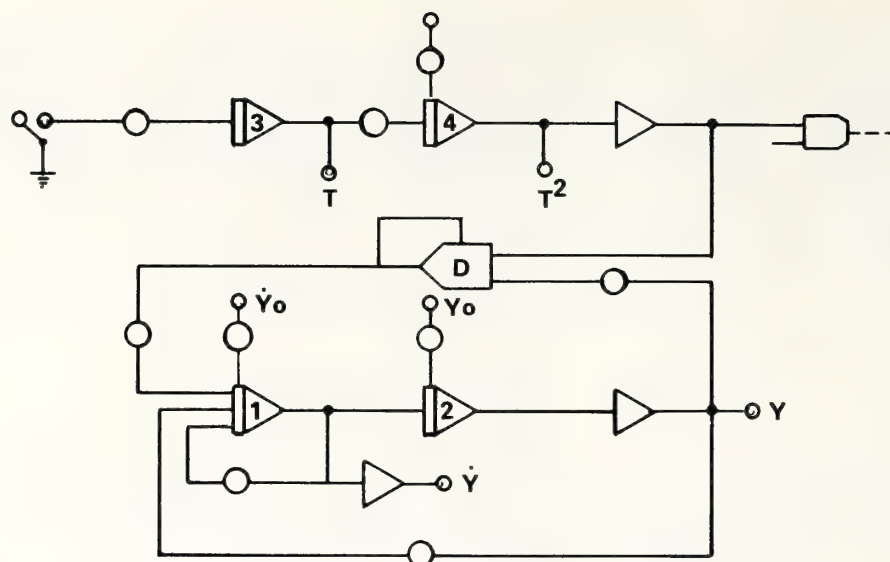


FIGURE 2. FLOW CHART FOR OBTAINING SOLUTION TO DIFFERENTIAL EQUATION

term Y_0 (following the Fortran convention) represents an equivalent impulse at the origin to the solution of equation 3. Y_0 is an initial condition. Three other parameters are required for a prediction using equation 3; namely, T_0 (the initial time or time when the impulse began), the identical time constants of integrators 1 and 2, and \dot{Y}_0 which corresponds to an equivalent impulse and serves as an additional input to integrator 1 at T_0 . To avoid overflow in the program at T_0 , a very large number (e.g., $1.0 + 38$, following the exponent convention discussed in section 3) has to represent the output of the divider (D) at T_0 . Integrators 3 and 4 are used to determine $1/T^2$ which goes through D to generate the solution for Y .

3. BASIS

In our paper on principal component analysis of solar flares in the soft X-ray flux (Teuber *et al.*, 1979), we showed that the first two largest eigenvectors are sufficient for an empirical curve-fit through proportional counter data. Making use of this fact, we can adapt the technique for flare prediction. To do this, we employ the templates depicted in Figure 3. Figure 3a illustrates the first eigenvector normalized in magnitude to 1.0 at normalized time scale $T=1.5$ and characterizes our standard Chi-square distribution with a fixed origin. Figure 3b shows the derivative of the first eigenvector (and is orthogonal to it) and is drawn to the same normalized time scale. In Figure 3a, the times when the eigenvector equals 36 percent ($1/e$) of the maximum amplitude occur at $T=0.34$ and $T=3.82$, and we note that the ratio of time durations T_2/T_1 is 2.0, where T_1 is the time duration from $T=0.34$ to $T=1.5$ and T_2 is the time duration from $T=1.5$ to $T=3.82$. The two extrema in Figure 3b occur at $T=0.28$ and $T=2.72$. We further note that the absolute magnitude of Figure 3b relative to Figure 3a, for practical curve-fits to the soft X-ray flux, is of only a few percent.

In Figure 4, we show logarithmically the 16-20-Å⁰, proportional-counter un-

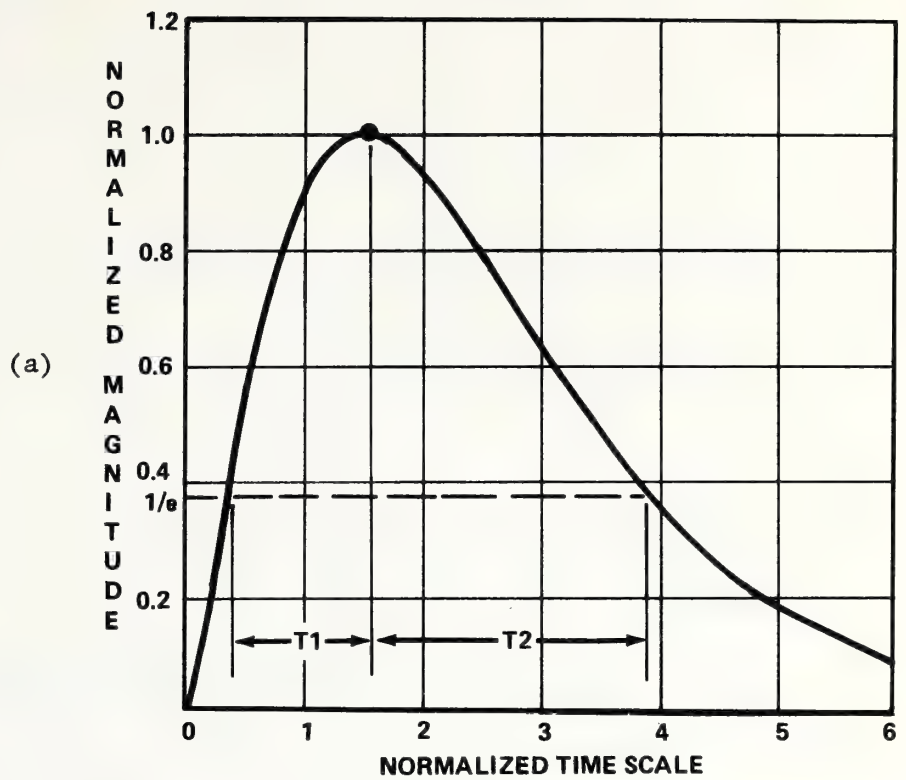
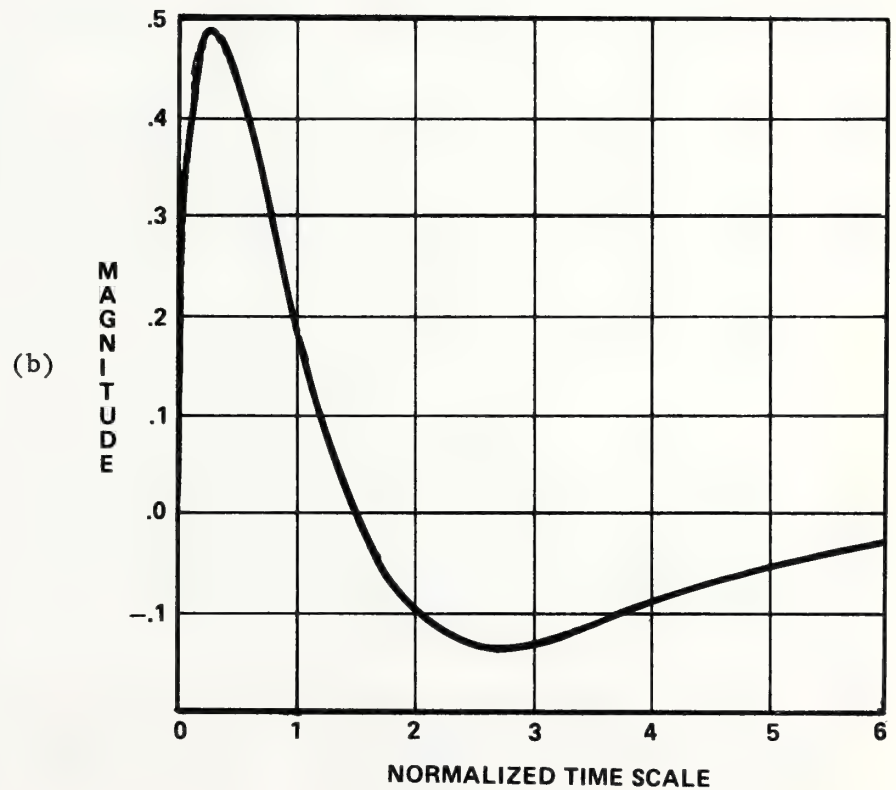


FIGURE 3. TEMPLATES OF
(a) FIRST EIGENVECTOR
AND (b) ITS DERIVATIVE



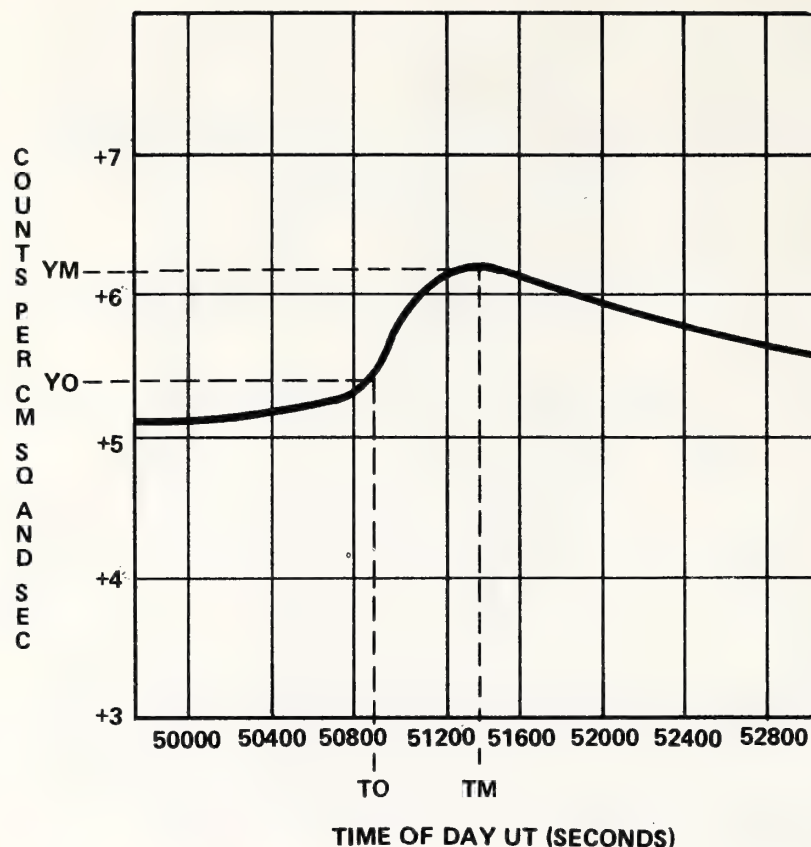


FIGURE 4. THE 15 JUNE 1973 1B/M3 FLARE FROM BOULDER AR131, AS RECORDED (RAW DATA) BY THE 16-20-Å CHANNEL OF THE X-REA

corrected record (raw data) for the X-ray flare of 15 June 1973, an optical class 1B and X-ray class M3 event, from Boulder region AR131 (McMath 12379) that peaked about 1415 UT. (This event has been extensively studied; e.g., see Wilson, 1976; Smith *et al.*, 1977; Krall *et al.*, 1978.) The terms YM and Y0 refer to maximum and origin values of X-ray flux, respectively. The time scale is shown in seconds of universal time (UT), where 1 day of UT equals 86400 s.

The data shown in Figure 4 can be normalized to the Figure 3a curve by the relation

$$Y = A [B(T - T_0)]^{3/2} e^{-B(T - T_0)} + Y_0 + R, \quad (4)$$

where $A = 2.44(YM - Y_0)$, $B = 3/[2(TM - T_0)]$, and R represents residual terms. The residuals include full-disk background X-ray flux variation ($Y_1(T - T_0) + Y_2(T - T_0)^2 + \dots$), which is normally quite small and, hence, negligible; the term A 1 times the values depicted in Figure 3b; and a term representing noise due to the instrument and to telemetry.

In their simplest mode, the generated fits are based only upon the initial guesses A, B, T_0 , and Y_0 . The computer program then minimizes by means of an orthogonal, generalized least-squares fit the deviation of a model function from the raw data. The performance index is derived from partial derivatives of Y

with respect to the parameters A, B, TO, YO. In all our guesses for different events, we find that the process converges to a final set of these four parameters within a few seconds (processor time) when less than 1000 data points are used. However, we must emphasize that the question of convergence is by no means an easy one since the boundaries for the guesses in A, B, TO, and YO are located on a hypersurface. When more than four parameters are tried (e.g., Y1, Y2, A1, and A2 in addition to the other four parameters with corresponding partial derivatives), it is best to repeat the iteration after A, B, TO, and YO have been determined. Then, and only then, do we find that it makes sense to release additional parameters which are quite insignificant anyhow. For too wide a margin of error in initial guesses (normally up to ± 50 percent in A and B), we observe that the iteration process does not converge but, instead, "blows up." Also, to avoid the same effect for negative values of T (i.e., times to the left of the origin in Figure 3a), we continue our template as an odd-function in the program.

As a supplement to Figure 4 and as an example for the quality of convergence, we present in Table 1 values of the parameters A, B, TO, and YO after a 10-cycle least-squares fit. Table 1 is presented below, where the positive and negative numbers following the first positive and negative numbers are the power of ten exponents. We note that the parameters converge rapidly and show small error (≤ 1 percent). We also include in Table 1 values of Y1 and Y2 (see equation 4 discussion) and note that they are effectively "zero" implying that for the 15 June 1973 event, the full-disk, background flux variation was completely negligible.

TABLE 1. ERROR VALUES OF PARAMETERS A, B, TO, AND YO FOLLOWING USE OF A 10-CYCLE LEAST-SQUARES FIT

PARAMETER	OLD VALUE	CHANGE	NEW VALUE	ERROR
A	0.268 +07	+0.167 -01	0.268 +07	0.122 +05
B	0.298 -02	-0.407 -10	0.298 -02	0.146 -04
TO	0.509 +05	-0.350 -03	0.509 +05	0.162 +01
YO	0.259 +06	-0.711 -02	0.259 +06	0.450 +04
Y1	0.000		0.000	
Y2	0.000		0.000	

4. EXAMPLE PREDICTION

The 15 June 1973 flare, discussed above, can now be used as an example for describing proportional counter data by a Chi-square distribution. We show in Figure 5a a superposition of raw data (wavy line), representing the X-REA 16-20-Å proportional counter channel, on the "best-fit" curve (smooth line). The best-fit curve was determined by the aforementioned 10-cycle least-squares fit analysis, using values of A, B, TO, and YO given in Table 1. The origin of the analytic curve is at T=50900, and this time can be regarded as the time of impulse initiation to be used solving the differential equation 3. (Another way to view the origin is to interpret it as that point where the residuals cross the zero line, becoming increasingly negative in value after a sharp initial positive increase.) We note that a loss in telemetry occurred at about T=52200,

and although our program does not interpolate for losses of reference signal, the effect on the quality of fit is negligible. (The quality of our fit can be expressed by a "figure of merit" that is derived from the residuals.) The total duration of the event included 854 data points or spanned 2135 s, and was limited to the orbital daylight portion, typically 1320 data points or 3300 s in length.

In Figure 5b, we show the residuals or differences between the computed and recorded data shown in Figure 5a. The most significant feature of Figure 5b is the rather large deviation in the residuals which occurs at about $T=51000$. (The maximum deviation depicted in Figure 5b can be enhanced by the use of an appropriate "matched filter" applied to the raw data; Teuber *et al.*, 1977 have discussed matched filtering applications.) We note that this deviation occurs shortly after flare onset, at a time which is about 20 percent of the time interval between flare onset and maximum emission. Thus, one could measure the deviation between recorded (raw) data and analytic (computed) data during this small increment of time, together with the count rate (slope), and determine an estimate of flare peak-level emission, approximate time of peak-level emission, and the event duration.

To ascertain the quality of such an estimate, we have selected a second event which we will analyze in "reverse order." That is, based on its residual deviations and count rate during the short interval of time following flare initiation, we will determine its (i) peak-level emission, (ii) time of peak-level emission, and (iii) time duration, and then we will compare the analytic curve with the actual recording to see the accuracy of the fit. The event used is the 27 November 1973 SB/M1 subflare from Boulder AR287 (McMath 12628) which peaked about 0313 UT. Figure 6a depicts the residuals for the best-fit over the total duration of the event, and Figure 6b shows the resultant best-fit (curve 1) which essentially is the raw-data curve. Also, shown in Figure 6b are the resultant curves (curves 2 and 3) which one would "estimate" if only selected parts of the residual curve (Figure 6a) from the origin to the arrows marked 3 and 2 were used for the estimate instead of the total event. Thus, curve 3 represents the estimate based only on the data points between the origin and the arrow marked 3 (Figure 6a), and similarly curve 2 is the estimate based only on the data points between the origin and the arrow marked 2. We see that, as the number of data points used in the analysis increases, a better estimate is apparent. (The confidence in the curve is a function simply of the array length.) Table 2 gives the A, B, TO, and YO values for curves 1, 2, and 3. TO and YO values for each of the curves are the same; i.e., $TO=0.115 +05$ (recall the exponent convention as stated in section 3) and $YO=0.119 +04$. The analysis is again based on the X-REA 16-20- \bar{A} proportional counter channel, as per the 15 June 1973 event. In addition to the improvement between estimate and real curves as larger array lengths (more data points) are employed, we see that, at least for this event, the value of A decreased while the value of B increased with the inclusion of more data points in the analysis. (We note that no convergence was possible in this event for fewer than 30 data points.)

In Table 3, we compare estimates of flare peak-level emission, time of peak-level emission, and duration, deduced from curves 2 and 3, with the actual event history shown in curve 1. Thus, we see that curve 1, based on 380 data points or the full array of 950 s, shows that the event peaked at ~ 11660 UT at a flux level of ~ 19555 and spanned ~ 370 s, based on the time duration at full-width-half-

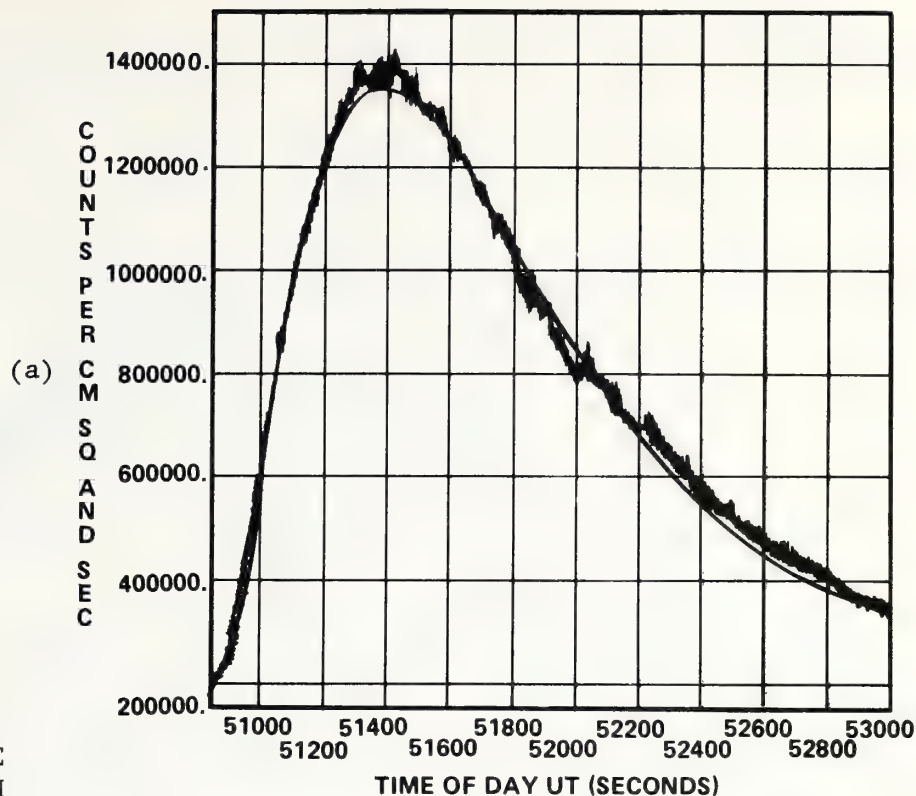
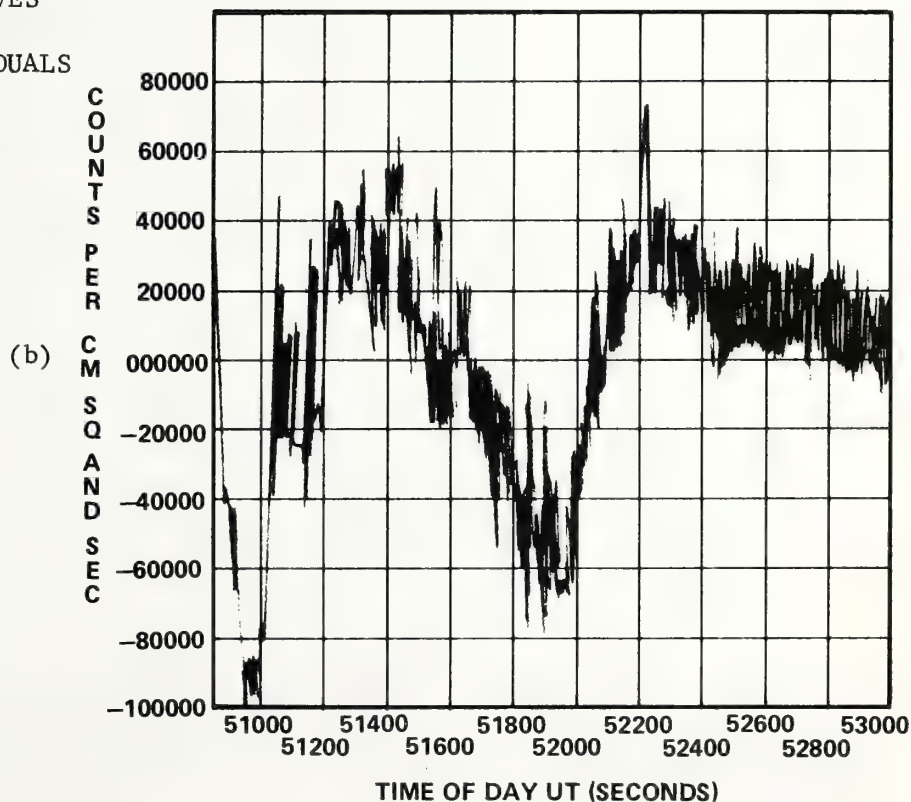


FIGURE 5. THE 15 JUNE
1973 1B/M3 FLARE FROM
BOULDER AR131 SHOWING
(a) SUPERPOSITION OF
RAW AND COMPUTED CURVES
OF THE X-REA 16-20-Å
CHANNEL AND (b) RESIDUALS



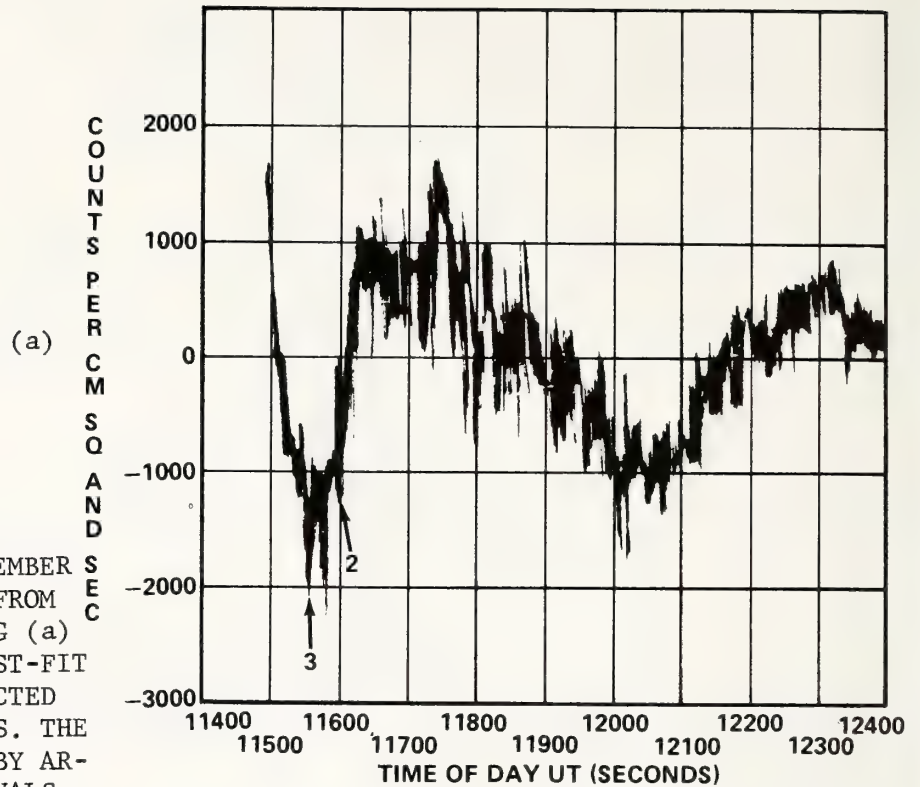


FIGURE 6. THE 27 NOVEMBER 1973 SB/M1 SUBFLARE FROM BOULDER AR287 SHOWING (a) RESIDUALS AND (b) BEST-FIT CURVES BASED ON SELECTED NUMBER OF DATA POINTS. THE NOS. 2 AND 3 MARKED BY ARROWS SHOW TIME INTERVALS OF RESIDUALS USED TO GENERATE PREDICTION CURVES 2 AND 3. CURVE 1 IS ESSENTIALLY THE RAW DATA CURVE.

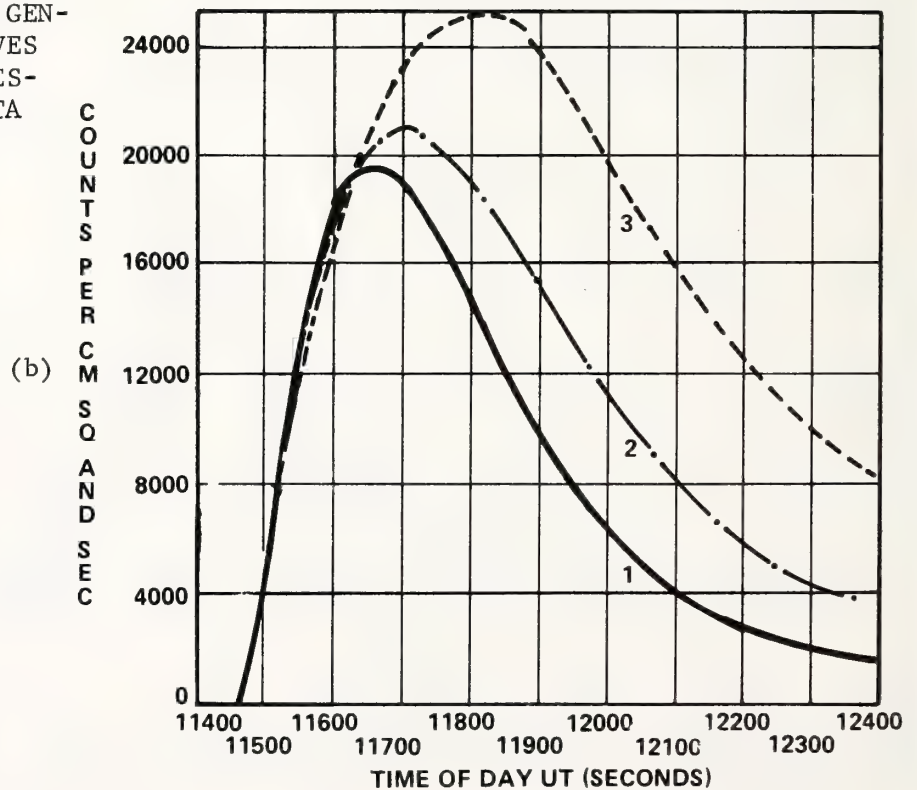


TABLE 2*. COMPARISON OF PREDICTED AND ACTUAL VALUES OF A, B, TO, AND YO FOR THE 27 NOVEMBER 1973 SB/M1 SUBFLARE FROM BOULDER AR287 FOR VARIOUS NUMBERS OF DATA POINTS ANALYZED

CURVE	A	B	TO	YO	DATA POINTS (No.)
1**	0.049 +05	0.829 -02	0.115 +05	0.119 +04	380
2	0.487 +05	0.625 -02	0.115 +05	0.119 +04	55
3	0.578 +05	0.423 -02	0.115 +05	0.119 +04	35

NOTES: * NO CONVERGENCE OBSERVED FOR FEWER THAN 30 DATA POINTS
 ** CURVE 1 IS ESSENTIALLY THE RAW-DATA CURVE

TABLE 3*. COMPARISON OF PREDICTED AND ACTUAL VALUES OF PEAK-LEVEL EMISSION, TIME OF PEAK-LEVEL EMISSION, AND FWHM DURATION FOR THE 27 NOVEMBER 1973 SB/M1 SUBFLARE

CURVE	TIME OF PEAK-LEVEL EMISSION	MAGNITUDE OF PEAK-LEVEL EMISSION	FWHM DURATION
1**	11660 UT	19555	370 s
2	11705 UT	20890	490 s
3	11815 UT	25100	640 s

NOTES: * BASED ON FIGURE 6b
 ** CURVE 1 IS ESSENTIALLY THE RAW-DATA CURVE

maximum (FWHM) emission (i.e., one-half of the peak-flux level occurs at ~ 11530 UT and ~ 11900 UT; the difference is ~ 370 s and represents the duration at FWHM emission). Curve 2, based on 55 data points or 137.5 s (~ 14 percent of the data), gives values slightly larger: time of peak-level emission, ~ 11705 UT (~ 45 s past actual peak occurrence); peak-level emission, ~ 20890 (~ 7 percent higher than the real case); and duration at FWHM emission, ~ 490 s (~ 32 percent longer than the curve 1 duration). Curve 3, based only on 35 data points or 87.5 s (~ 9 percent of the data), predicts a time of peak-level emission at ~ 11815 UT (~ 155 s past the actual peak-level emission time), a peak-level emission of ~ 25100 (~ 28 percent higher), and a FWHM-emission duration of ~ 640 s (~ 73 percent longer). Clearly, one can follow a curve-2 type approach as a prediction technique and deduce values for peak-level emission, time of peak-level emission, and FWHM-emission duration which are only slightly in error when compared to a detailed analysis of the full event.

5. REAL-TIME PREDICTION SCENARIO

In the preceding section we performed the prediction based on knowledge of the entire solar event. In this section we describe how one could apply the technique to a real-time event. This could be accomplished at a ground-

level receiver terminal (or from the Aft Flight Deck of a Spacelab mission) where a forecaster (or Payload Specialist) would be able to implement, from a variety of subroutines (perhaps, contained in a mini-processor of a Spacelab experiment), the optimum routine for the existing solar conditions. The exact details of the optimum subroutines being accomplished with the real-time data and the iterative procedures have been described in section 3.

Since the procedure for prediction is an iterative procedure and since the rise-time-to-peak intensity varies from less than a minute to tens of minutes for various events, a variety of subroutines should be examined to obtain accurate results. A subroutine for an iterative-prediction method would have the following characteristics. It will try to fit the measured flux data at the highest possible sample rate (e.g., 1.0 s^{-1} for GOES-type data or 2.5 s^{-1} for X-REA-type data) to equation 4 by a least-squares technique. As soon as a preset threshold in the background flux is exceeded, as well as a preselected rate as indicated by the differentiated data, an initial computation of parameter A and B is accomplished. The data are again sampled and new calculations made. After several iterations and before peak intensity has been reached, a satisfactory prediction of the total event characteristics will be available. The iterative least-squares method described in section 3 takes less than 10 s for 1000 data points on a modest size data acquisition computer. Consequently, periodic updates to the event are feasible while the event progresses. The monitor for convergence determines whether to continue the update or terminate the program.

Since several methods for accomplishing the prediction are possible, only additional test routines on real-time data will answer the remaining questions. The methods for display of the prediction results depend on the configuration of the data acquisition system. The output could be in the form of A and B printout (i.e., peak intensity and event duration) or in the form of a graphic display of the predicted curve superimposed on the real-time graphics display.

In general, real-time data, such as the existing GOES-spacecraft data, are required to determine the merit of this iterative predictive scheme. Many events should be sampled at the highest possible sample rate. The validity of equation 4 can be determined only by analysis of many and varied events. Equation 4 is simple enough for a predictive scheme and should be tried with existing real-time data. However, a more general equation may be appropriate for early predictive check (e.g., $x(t) = t^m e^{-t}$, where t is time, $x(t)$ is X-ray flux, and m is a constant between 0 and ∞). At this time our principle-component analysis scheme has shown equation 4 to be commensurate with the signal-to-noise ratio of existing data.

6. CONCLUSIONS

We have presented in this study a technique which, when applied real-time to full-disk, monitor-type proportional counter data (i.e., data that regard flares as point sources), will allow an investigator to predict the peak-level emission (flux), time of peak-level emission, and FWHM-emission

duration of a solar X-ray flare. The technique is based on principal-component analysis methods and the use of templates to describe solar X-ray flares. We have shown, based on an analysis of the 15 June 1973 1B/M3 flare from Boulder AR131, that a minimum of four parameters--A, B, T₀, and Y₀--is needed for the prediction. The analysis points to a single impulse occurring at the estimated origin (T₀, Y₀) with 90 percent of the cumulative power in the first (largest) eigenvector. The X-ray signature is then a deterministic response, which follows a Chi-square distribution.

We then applied the technique to the 27 November 1973 SB/M1 subflare from Boulder AR287 to ascertain quantitatively and qualitatively how the predicted and actual time-profile curves compare. A fairly good agreement between predicted and actual data, especially peak-level emission and time of peak-level emission, was observed. We also found that, as the array length (number of data points) used in the analysis increases, a better correlation is obtained.

Although not particularly stressed in the text of this report, we note that a convergent solution to the differential equation 3 appears to require: (i) processing of approximately 15 percent of the full-array data, with the present 2.5 s sampling rate, and (ii) knowledge of the parameters (initial guesses) to within a factor of about 2 or slightly more. We suggest that, through the use of higher sampling rates, a better understanding of the early portion of the flux profile may be deduced, thus lessening the conditions required for a convergent solution; i.e., a convergent solution will be obtained more precisely and, perhaps, even more quickly. Also, the use of higher sampling rates may resolve fine time-dependent structures that are not discernible with the 2.5-s sampling rate.

Additionally, we presented a scenario for applying the iterative predictive technique to a real-time data set. The scheme, whereby values for the parameters A and B are computed, was discussed and we note that this scenario may be applicable to GOES-type mission objectives and perhaps even to Spacelab-type mission objectives.

While the emphasis of the paper has been on the two aforementioned flares, we note that an additional ten events (class C0 to M1) have been analyzed over their full durations to ascertain common features, parameter values, etc. These events, together with the 15 June and 27 November 1973 events, are listed in Table A-1 in the Appendix. In each case the event array length was determined approximately as the difference between time of flare initiation and subsequent settling time to an equilibrium state in the X-ray flux. One feature common to all twelve events analyzed thus far is a similarity of residual curves; i.e., all events show residual curves which are strikingly similar to Figures 5b and 6a, namely a sharp positive pulse followed by a rather large negative dip occurring shortly after flare onset. We suggest that these events will show equally good agreement, as did the curve-2 prediction made in the previous section, regarding actual and predicted values of peak-level emission, time of peak-level emission, and FWHM-emission duration. (This will be the subject of a subsequent publication.)

Finally, while the present analysis has emphasized the prediction of certain single-pulse signature solar flare parameters based on the assumption that the X-ray flare is a deterministic response to a single impulse, it is by no means limited to application to single-pulse structured flares. We suggest that multiple-flux-peak events may also be explained as deterministic responses due to the superposition of several single impulses. (This too is presently being investigated and will be the subject of a subsequent publication.)

Acknowledgments. We wish to express appreciation to Dr. E. Tandberg-Hanssen (NASA/Marshall Space Flight Center) for reading the manuscript. A portion of this work was supported by Government Work Order H-12261-B (JBS).

REFERENCES

- Falciani, R., M. Giordano, M. Rigutti, and G. Roberti (1977): Comparison between some H α and X-ray flares. Solar Phys., 54:169.
- Krall, K. R., E. J. Reichmann, R. M. Wilson, W. Henze, and J. B. Smith, Jr. (1978): Analysis of X-ray observations of the 15 June 1973 flare in active region NOAA 131. Solar Phys., 56:383.
- Martin, S. F. and H. E. Ramsey (1972): Early recognition of major solar flares in H α . Solar Activity Observations and Predictions (eds., P. S. McIntosh and M. Dryer), Progress in Astroautics and Aeronautics (ser. ed., M. Summerfield), vol. 30, The MIT Press, Cambridge, MA, p. 371.
- Martres, M.-J., I. Soru-Escaut, and Y. Nakagawa (1977): H α off-band pre-flare activities. Astron. Astrophys., 59:255.
- Noyes, R. W. (1976): New developments in solar research. Frontiers of Astrophysics (ed., E. H. Avrett), Harvard University Press, Cambridge, MA, p. 41.
- Priest, E. R. (1976): The solar flare phenomenon. Physics of Solar Planetary Environments Proceedings of the International Symposium on Solar-Terrestrial Physics (June 7-18, 1976, Boulder, CO) (ed., D. J. Williams), vol.1, American Geophysics Union, Boulder, CO, p. 144.
- Smith, H. J. and E. v. P. Smith (1963): Solar Flares. The Macmillan Co., New York, NY.
- Smith, J. B. Jr. (1972): Predicting activity levels for specific locations within solar active regions. Solar Activity Observations and Predictions (eds., P. S. McIntosh and M. Dryer), Progress in Astronautics and Aeronautics (ser. ed., M. Summerfield), vol. 30, The MIT Press, Cambridge, MA, p. 429.
- Smith, J. B. Jr., R. M. Wilson, and W. Henze Jr. (1977): Morphology and physical parameters of a solar flare. Astrophys. J. (Letters), 216:L79.
- Švestka, Z. (ed.) (1976a): Flare build-up study (proceedings of the flare build-up study workshop, held at Falmouth, Cape Cod, MA, September 8-11, 1975). Solar Phys., 47:1

- Švestka, Z. (1976b): Solar Flares. Geophysics and Astrophysics Monographs, (ed., B. M. McCormac), vol. 8, D. Reidel Publ. Co., Dordrecht, Holland.
- Tandberg-Hanssen, E. (1967): Solar Activity. Blaisdell Publ. Co., Waltham, MA.
- Teuber, D., E. Tandberg-Hanssen, and M. J. Hagyard (1977): Computer solutions for studying correlations between solar magnetic fields and Skylab X-ray observations. Solar Phys., 53:97.
- Teuber, D. L., E. J. Reichmann, and R. M. Wilson (1979): Principal component analysis of solar flares in the soft X-ray flux. Astron. Astrophys., 80:218.
- Underwood, J. H., J. E. Milligan, A. C. deLoach, and R. B. Hoover (1977): S056 X-ray telescope experiment on the Skylab Apollo Telescope Mount. Appl. Opt., 16:858.
- Wilson, R. M. (1976): The 15 June 1973 1B/M3 flare: an overview of analysis results. NASA Technical Memorandum X-73357, Marshall Space Flight Center, AL.
- Zirin, H. (1966): The Solar Atmosphere. Blaisdell Publ. Co., Waltham, MA.

APPENDIX

Using the prediction method as just described (except that instead of employing the X-REA 16-20-Å proportional counter channel we use the 2.5-7.25-Å sum of channels), we have studied an additional ten events. We summarize the results of this analysis in Table A-1, showing the 10-cycle least-squares fit data for A and B based on a selected TO and YO input for each of the events. The flares are listed chronologically by date and the optical/X-ray class of each flare is shown below its corresponding date. The flare initiation time is expressed in hours and minutes UT and the array length employed in the analysis of each event is identified, where the array length represents the approximate number of data points from flare initiation to the time when the flux settles to an equilibrium value and occasionally to the end of the X-REA observing period. We emphasize that the parameters given in Table A-1 are based on the full array (total event) and not on the curve-2-type analysis performed in the text. All events display residual curves similar to each other and to those shown in Figures 5b and 6a.

TABLE A-1.* COMPUTED VALUES FOR PARAMETERS A, B, TO, AND YO FOR SELECTED FLARES

DATE	FLARE INITIATION (UT)	ARRAY LENGTH (APPROX. NO. OF DATA PTS.)	TO	YO	A	B
15 June 1973 (1B/M3)	1408	854	50900	17500	3.6 +05	4.2 -03
08 August 1973 (SF/CO)	1458	123	53880	2900	2.6 +03	8.3 -03

TABLE A-1. (Continued)

DATE	FLARE INITIATION (UT)	ARRAY LENGTH (APPROX. NO. OF DATA PTS.)	TO	YO	A	B
09 August 1973 (SN/M1)	1551	216	57050	3000	7.0 +05	1.2 -02
09 August 1973 (SF/C2)	2140	792	78000	2500	5.5 +04	7.5 -03
02 Sept. 1973 (SB/C4)	0042	475	02550	700	1.5 +04	1.5 -02
02 Sept. 1973 (SF/C4)	1600	400	47600	500	1.1 +04	1.0 -02
27 Nov. 1973 (SB/M1)	0311	380	11500	700	3.5 +04	1.5 -02
02 Dec. 1973 (1N/M1)	1513	1008	54800	2000	2.7 +04	7.5 -03
02 Dec. 1973 (SN/C5)	2005	240	72350	500	1.6 +04	1.5 -02
16 Dec. 1973 (SN/C0)	1316	983	47760	910	2.0 +03	2.5 -02
16 Dec. 1973 (SF/C2)	1954	504	71640	100	4.6 +03	1.0 -02
15 Jan. 1974 (SN/C6)	1420	1296	51600	180	1.0 +04	3.7 -03

NOTE: * PARAMETERS BASED ON FULL ARRAY ANALYSIS AND FOR THE 2.5-7.25- \AA SUM OF X-REA PROPORTIONAL COUNTER CHANNELS

THE STUDY OF EVOLUTION OF EXTREME ULTRAVIOLET SOURCES OVER SUNSPOTS AS GIVEN BY OSO- 4 DATA AND SOME IMPLICATIONS FOR PREDICTING SUNSPOT EVOLUTION AND FLARE ACTIVITY

E.V.Ivanov

Institute of Terrestrial Magnetism,
Ionosphere and Radio Wave Propagation
of the USSR Academy of Sciences

Moscow, USSR

The evolution of EUV sources over 24 sunspot groups with noticeable flare activity in 14 of them has been studied using spectroheliograms of the solar disk obtained both in O VI, Mg X, Si XII, Fe XVI lines and the Lyman continuum Ly C 800 on-board OSO-4 during its flight from October 25 to November 31, 1967. The change of source intensities is compared with the change of sunspot group areas and the flare activity index Q. Evolution changes of source intensities have been analyzed in each of above lines and shown the possibility of their use for predicting sunspot group evolution. A possibility is also explored for "quasi-steady current sheet" observations in the lines with excitation temperatures of $(3-8) \cdot 10^4 \text{K}$. Characteristic enhancements of emission intensity over 11 studied sunspot groups in C II, C III, O II, O III, and Si III lines are found to be 3-10, never exceeding 20, which is by 2-3 orders less than those estimated for quasi-steady current sheet.

In this work an attempt is made to study the evolution of emission sources over sunspot groups in the EUV spectrum lines with excitation temperatures $10^4 \text{K} - 3.5 \cdot 10^6 \text{K}$. We have used spectroheliograms of the solar disk in O VI, Mg X, Si III, Fe XVI lines and the Lyman continuum Ly C 800 obtained during the flight of OSO-4 from October 25 to November 31, 1967 [11]. The wavelengths and excitation temperatures of the analyzed emission lines are given in Table I. The spatial resolution of OSO-4 spectroheliograms is $1'$ and the spectral resolution is

Table I [11]

Ion	Wave-length \AA	Excitation temperature	
		T	K
Ly C	800	10^4	
O VI	1031	$3 \cdot 10^5$	
Mg X	625	$1.4 \cdot 10^6$	
Si XII	499	$2.2 \cdot 10^6$	
Fe XVI	335.4	$3.5 \cdot 10^6$	

about 3 \AA . A scan of the total disk (formation of a spectroheliogram) requires 5 min. A high quality of obtained spectroheliograms should be noted. Thus, for example, the dark current level of the photomultiplier was about 1 count per second, which for most chosen lines was by 2 orders of magnitude less than the

signal from an undisturbed solar region. The data obtained during the whole flight period are comparable within 20%. More details concerning the spectrograph specifications, experiment conditions and the quality of data see in [9, 11].

The period of OSO-4 observations was characterized by extremely high activity. From October 25 to November 31, 1967, more than 50 plages existed on the solar disk with sunspots or sunspot groups observed in 30 of them. We have studied evolution changes in 24 greatest sunspot groups, or rather intensity changes in the brightest cores of 24 plages with dimensions determined by spatial resolution, i.e. $\sim 1'$. A superposition of spectroheliograms, H_α filtrograms and Mount-Wilson magnetic charts [12] has shown that the brightest cores on spectroheliograms coincide with sunspot groups on H_α filtrograms and the greatest isogauss densities (i.e. greatest magnetic field gradients) on Mount-Wilson magnetic charts. It should be noted that the cores observed in Mg X, Si XII and Fe XVI lines were strictly connected with greatest magnetic field gradients and did not change their position throughout the observation period, whereas in Ly C and O VI they sometimes shifted during the field reconstruction in the group. It may be due to the fact that Mg X and Si III emission is produced in hot low arches in the region of strong magnetic field gradients (arch filament systems in X-rays), whereas O VI and Ly C emission is

mainly associated with the bases of colder high loops of comparatively weak fields which, therefore, undergo greater changes during the field reconstruction. There are numerous gaps in the data (sometimes as few as 1-2 spectroheliograms a day taken in one line) owing to a great number of lines involved (more than 50) and to the fact that only one line was registered during each satellite rotation. However the data are enough to study evolution changes of source intensities. On the other hand, there were periods of 1-3 days when spectroheliograms in Si XII and, particularly, in Mg X were obtained during each rotation (i.e. every 1.5 hours) allowing us to observe the source appearance from behind the limb and disappearance beyond the limb as well as to reveal quasiperiodic emission intensity variations over sunspots with a period of 5-7 hours, similar to those observed in soft X-rays by Melioransky et al. [2] and Wolfson et al. [15]. Figs. 1-8 show the evolution changes of spot areas (solid curve - the whole group, dashed curve - the leading spot), flare index $Q = \sum B \cdot \lg t$ (B being the flare importance, t - its duration in min, \sum - the sign of integration over a day [1]), and evolution changes of source intensity over sunspots in Ly C, O VI, Mg X, Si XII, Fe XVI for 18 greatest sunspot groups. (The daily means of evolution intensity changes are marked on the curves; the figure beside means the number of satellite rotations in which the given line was registered. J is expressed in relative units of count/second. The arrow indicates the moment of passage through the central meridian).

Except for the group McMath 9073, all spectroheliograms were obtained in intermediate intervals between noticeable flares, i.e. spectroheliograms and flares do not coincide in time. The flare data were taken from [12], the sunspot areas - from [3].

As seen from the figures, the evolution curves for EUV source intensities (particularly for well developed flare-active groups) are essentially similar to those for sunspot group areas (the intensities grow with the spot development and de-

crease with their decay), though some individual features may be seen associated with the group evolution (the change of Zürich class and compactness) and reconstruction of its magnetic field (from α to β configuration and the reverse).

In the "hottest" line Fe XVI ($T \sim 3.5 \cdot 10^6 K$), formed uppermost in the transition zone and in the lower corona, the source often occurs over the future group several days before its appearance. As the spots develop, the source intensity decreases. The most intensive emission in Fe XVI is observed over compact groups of Zürich class H, J, which are generally unipolar (α type according to Mt. Wilson classification). It is interesting to note an intensive emission in Fe XVI observed over a compact highly flare-active group of Zürich class H (McMath 9047) in which several proton flares were registered.

In Mg X and Si XII (with $T \sim 1.4 \cdot 10^6 K$ and $\sim 2.2 \cdot 10^6 K$ respectively) the source emission intensity grows with the development of sunspot group and the growth of its area. However at the end of the group lifetime, when the spots disappear, the behaviour of sources in Mg X and Si XII is often different: while the intensity in Mg X decreases, in Si XII it grows. Since the Mg X line is very sensitive to electron density in the source [14], such a behaviour suggests that the relative source height in the corona grows with disappearance of sunspots. It is accompanied with the temperature increase and electron density decrease in the source. An alternative explanation may be a decrease of electron density in the source due to its cooling after the spot disappearance or to the growing height of energy release by wave dissipation in the corona, i.e. to the growing "effective" height of the source.

The source in O VI ($T \sim 3 \cdot 10^5 K$) is more sensitive to the flare activity of sunspot groups than in other examined emission lines. Figs. 1-3 show a good correlation between the O VI source evolution and the flare index Q for the large sunspot groups with an area $S \gtrsim 300$ m.s.h. and high flare activity (dashed segments of the intensity curves correspond to gaps in the data and do not reflect real intensity variations within the gaps).

There is no such correlation for the small groups with low flare activity (figs. 4-8), where evolutionary effects seem to prevail (development or decay of the group, increase or decrease of the spot area etc.). The O VI spectroheliograms obtained just before and after the flare show strong fluctuations of the source before the flare and a slower (with respect to other lines) decrease of emission intensity after it. Similar source fluctuations in O VI before the flare were noted by Brückner [7].

The source behaviour in Ly C 800 ($T \sim 10^4 K$) formed in the upper chromosphere, resembles that in O VI, but the intensity change is less significant.

Summing up, it may be stated that though at present there exist no direct prediction methods based on EUV observations, these may be highly useful for predicting the development of sunspot groups, particularly at the initial stage of their development (brightening of Fe XVI sources preceding the spot occurrence), during their appearance from behind the limb (as given by UV and X-ray observations) and at the pre-flare stage (O VI source fluctuations before the flare). Comparing the evolution curves of Fe XVI, Si XII, Mg X, O VI and Ly C emission sources with those of isolated sunspot group (figs. 1-8), one can see that the appearance, development and structural changes of a sunspot group are differently manifested in the lines formed at different transition zone levels. It may be expected that the further investigations would reveal the intervals of EUV spectrum (lines) corresponding to a certain transition zone level (levels) which could be used for prediction of the spot group flare activity, development or decay, etc.).

OSO-4 spectroheliograms may be used to check another interesting possibility of solar flare prediction based on the

study of active regions in EUV spectral lines with excitation temperatures $(3-8) \cdot 10^4 \text{K}$. S.I.Syrovatsky and B.V.Somov [3, 12] have suggested the existence of one or more quasi-steady current sheets in an active region, in which the dissipating magnetic field may be a powerful source of EUV-emission. Such current sheet is stabilized when Joule heating and cooling by UV-emission are in equilibrium. Note that the effective temperature of emission must not exceed $\sim 8 \cdot 10^4 \text{K}$, otherwise the Joule heating is not balanced by emission leading to a quick destabilization and destruction of the current sheet [4, 5]. It is suggested that the energy accumulation in a quasi-steady current sheet may last for a long time (from tens of hours to several days), so that its emission may be used for flare prediction many hours before their occurrence. It is estimated [4, 13] that before large flares, the flux from a quasi-steady current sheet registered in C II, Si III, O II, O III, C III lines (corresponding to $T \sim (3-8) \cdot 10^4 \text{K}$) must be 2-5 times as much as the total flux from the solar disk (see Table 2).

Table 2 [4].

Ion	Wavelength $\lambda, \text{\AA}$	Ionization temperature T, K	Power of emission	
			$P_{i\lambda} \text{ erg} \cdot \text{s}^{-1}$	
			Current sheet	Whole Sun at moderate activity
C II	1335	$3 \cdot 10^4$	$4.8 \cdot 10^{26}$	$2.5 \cdot 10^{26}$
Si III	1206	$5 \cdot 10^4$	$2.8 \cdot 10^{26}$	$1.7 \cdot 10^{26}$
O II, III	833-845	$6 \cdot 10^4$	10^{27}	$6.2 \cdot 10^{26}$
C III	997	$8 \cdot 10^4$	$1.1 \cdot 10^{27}$	$2.5 \cdot 10^{26}$
	1176	$8 \cdot 10^4$	$5.7 \cdot 10^{26}$	$1.1 \cdot 10^{26}$

If the current sheet parameters are $a = 10 \text{ cm}$, $b = 7 \cdot 10^8 \text{ cm}$, $\ell = 10^{10} \text{ cm}$ (a , b and ℓ being respectively its half-depth, half-width and length), then for the flux values

given in Table 2 the enhancement (the ratio of current sheet intensity to that of an equal quiet Sun area) must be $\sim 10^3$. (Since 10^{10} cm on the Sun corresponds to $\sim 2'$, the geometric ratio of the current sheet area to that of the solar disk is ≈ 500). Besides that, since most emission from a quasi-steady current sheet should occur at temperatures less than $8 \cdot 10^4$ K, the source enhancement will sharply decrease as the temperature grows from $8 \cdot 10^4$ to 10^6 K. Real source enhancements over sunspots observed in different EUV lines show the reverse behaviour, i.e. the source enhancement grows as the temperature increases [10, 8] (Fig. 9). As shown by observations on OSO-4, 6 and others, 10^4 - 10^5 K is the range of effective temperatures where the total flux from the whole Sun is most stable (its fluctuations not exceeding 2% of the flux from the quiet Sun [11]), so, this spectrum region has been chosen for absolute calibration of on-board instruments. We have tried to find out how the source enhancements over sunspots in this spectrum range change under quiet conditions and during high flare activity, in particular, just before the flare.

Unfortunately, the C II, Si III, O II, O III, and C III spectroheliograms obtained on OSO-4 are very scarce and cover only the time interval from October 28 to November 12, 1967. Nevertheless, owing to high activity in this interval, 11 sunspot groups were registered, one of which (McMath 9047) was a complex compact group H with many powerful (including 3 proton) flares of great importance. Fig. 10 illustrates 2 most active and 2 less active of 11 groups. Unlike [10], where the average source and background intensities are used, we have estimated the enhancement values using the ratio of the most intensive core in a source (with dimensions of about $1'$) to the least intensive element of undisturbed equatorial region situated approximately at the same longitude. Though our enhancement values are, thus, something overestimated in comparison with [10], they never exceed 20. Characteristic enhancements were about 3-10, inclusive for spectroheliograms obtained 1-4

hours before proton flares of importance 1 and 2. No pronounced dependence has been found between the source enhancement several hours before flares and the flare activity of sunspot groups either in quiet or in active periods.

Summing up, the following may be stated:

1. Observations of EUV sources over sunspot groups in different lines give information about their energy power, magnetic configuration, future behaviour, and flare activity. It makes these data useful for predicting the sunspot group evolution.
2. Characteristic enhancements in EUV sources over sunspot groups observed at effective temperatures $3 \cdot 10^4 \text{K} - 8 \cdot 10^4 \text{K}$ are about 3-10, never exceeding 20 even immediately (1-4 hours) before proton flares of importance 1 and 2, which is by 2-3 orders less than the values for the cold quasi-steady current sheet estimated by Syrovatsky and Somov.

References

1. Borovik, V.N., E.V. Ivanov, and M.A. Livshits (1972): Correlation of local sources emission on λ 3.2 cm and sunspots flare activity. Solar-Terrestrial Physics, No. 3, Moscow, IZMIRAN, 269-295 (in Russian).
2. Melioransky, A.S., N.I. Nazarova, V.M. Pankov, and I.A. Savenko (1976): Quasi-periodic oscillations in the active region. In "Extra-atmospheric study of active regions on the Sun" (Proc. of the VIII Consultation of KAPG on solar physics), Nauka, Moskwa, 29-35 (in Russian).
3. Solnechniye Danniiye, Nauka, Leningrad.
4. Somov, B.V., and S.I. Syrovatsky (1976): Quasi-stationary dissipation of magnetic field in current sheets as a heating source for solar active regions. In "Extra-atmospheric study of active regions on the Sun" (Proc. of the VIII Consultation of KAPG on solar physics), Nauka, Moskwa, 126-131 (in Russian).

5. Syrovatsky, S.I. (1976): Current sheet characteristics and thermal trigger of solar flares. Pisma v A. Zh., Vol. 2, 35 (in Russian).
6. Syrovatsky, S.I. (1977): On the possibility to observe pre-flare current sheets on the Sun. Pisma v A. Zh., Vol. 3, 133 (in Russian).
7. Brueckner, G.E., N.P. Patterson, and V.E. Scherrer (1976): Spectroscopic far-ultraviolet observations of transition zone instabilities and their possible role in a pre-flare energy build-up. Solar Phys., Vol. 47, 127-146.
8. Foukal, P.V., M.C.E. Huber, R.W. Noyes, E.M. Reeves, E.J. Schmahl, J.G. Timothy, J.E. Vernazza, and G.L. Withbroe (1974): Extreme-ultraviolet observations of sunspots with the Harvard spectrometer on the Apollo Telescope Mount. Ap. J., Vol. 193, L 143-145.
9. Goldberg, L., R.W. Noyes, W.H. Parkinson, E.M. Reeves, and G.L. Withbroe (1968): Ultraviolet Solar Images from Space. Science, Vol. 162, 95.
10. Noyes, R.W., G.L. Withbroe, and R.T. Kirshner (1970): Extreme ultraviolet observations of active regions in the chromosphere and the corona. Solar Phys., Vol. 11, 388-398.
11. Reeves, E.M., W.H. Parkinson (1970): An atlas of extreme ultraviolet spectroheliograms from OSO-IV. Ap. J. Suppl., No. 181, Vol. 21.
12. Solar Geophys. Data, ESSA, Boulder, Colorado.
13. Somov, B.V. and S.I. Syrovatsky (1977): Current sheet as the source of heating for solar active regions. Solar Phys., Vol. 55, 391-399.
14. Withbroe, G.L. and J.B. Gurman (1973): Models of the chromospheric-coronal transition layer and lower corona derived from extreme-ultraviolet observations. Ap. J., Vol. 183, No. 1, 279-289.
15. Wolfson, C.J., L.W. Acton, J.W. Leibacher, and D.T. Roethig (1977): Early evolution of an X-ray emitting solar active region. Solar Phys., Vol. 55, 182-193.

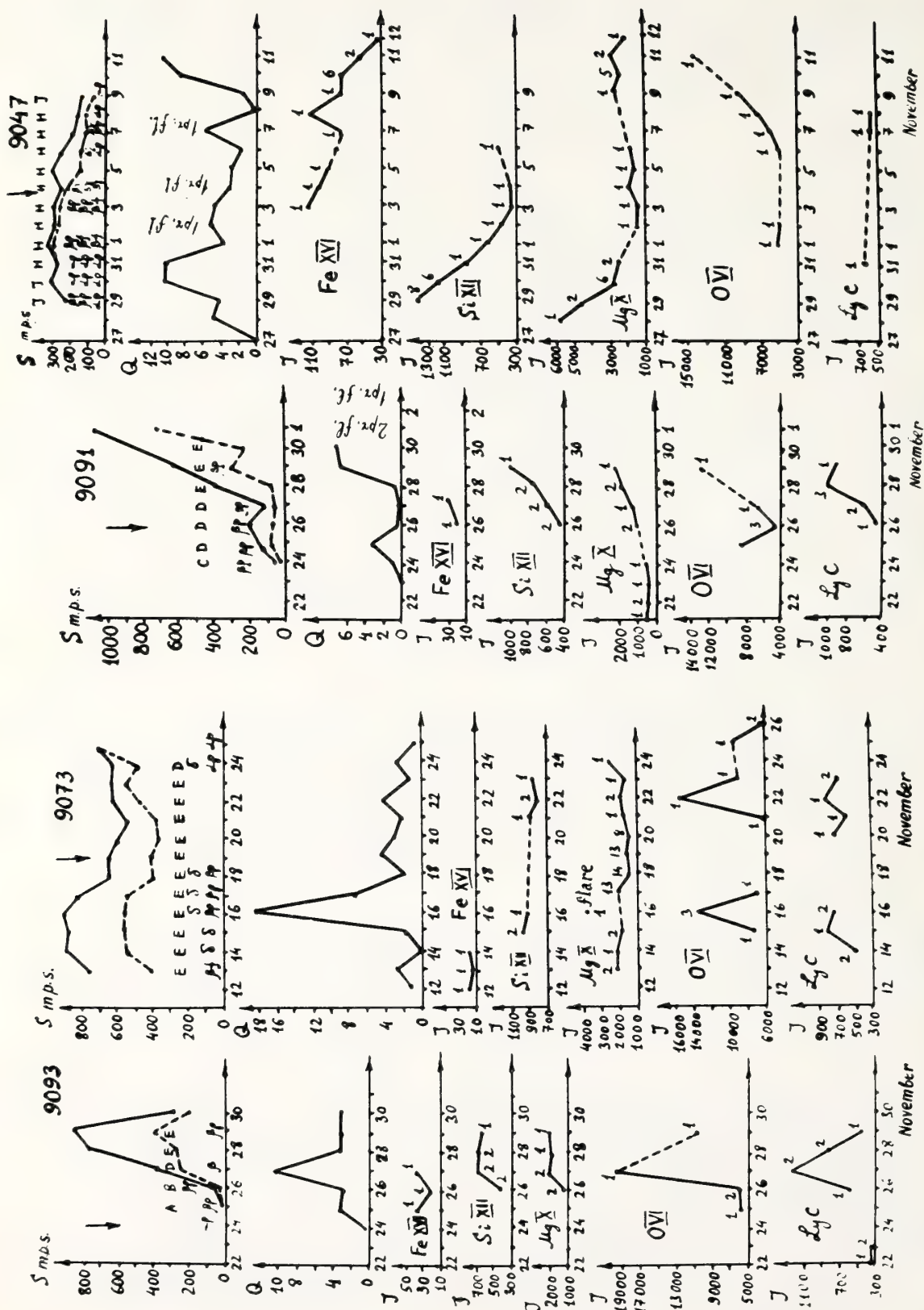


Fig. 1

Fig. 2

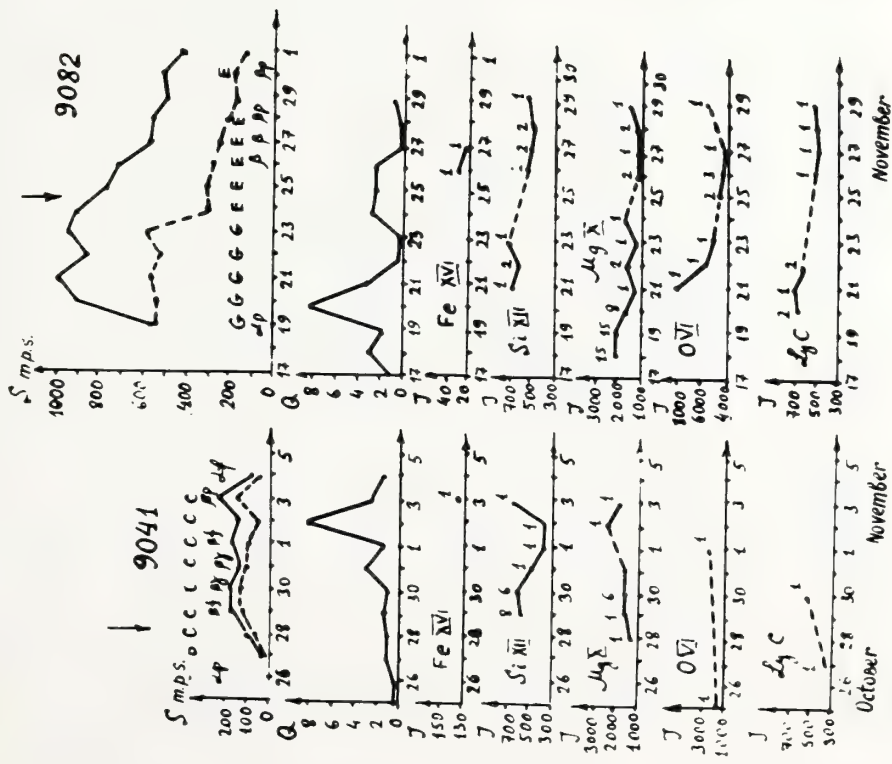


Fig. 3

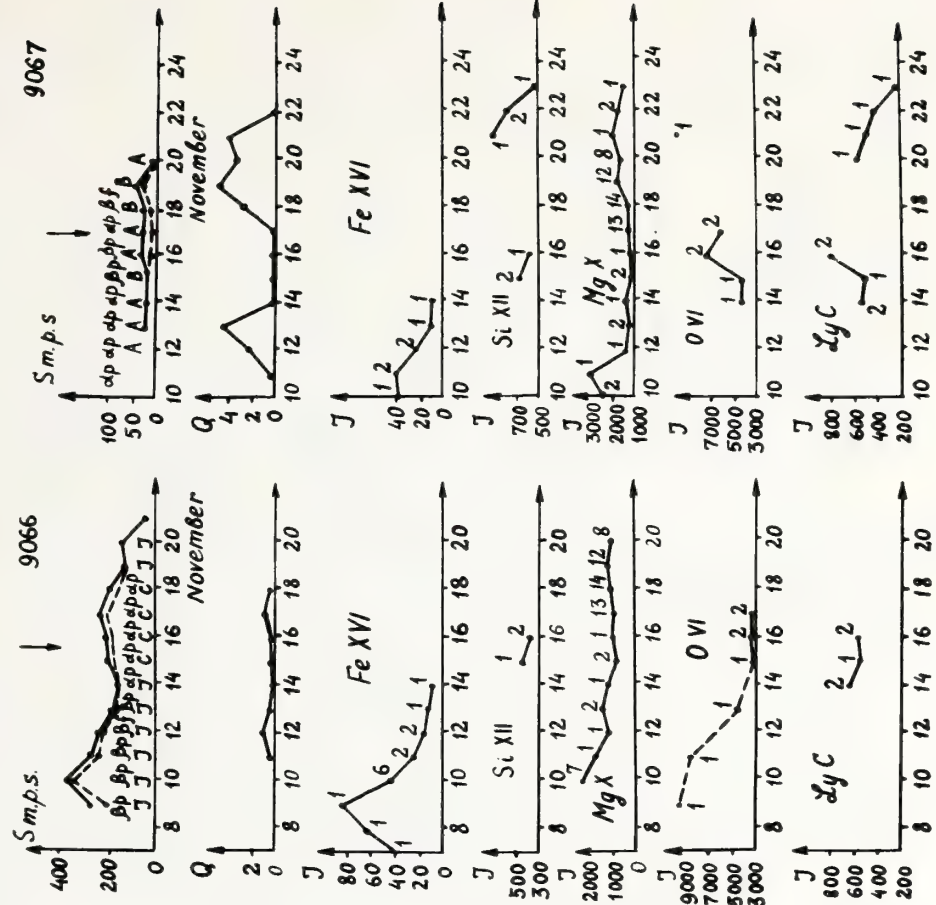
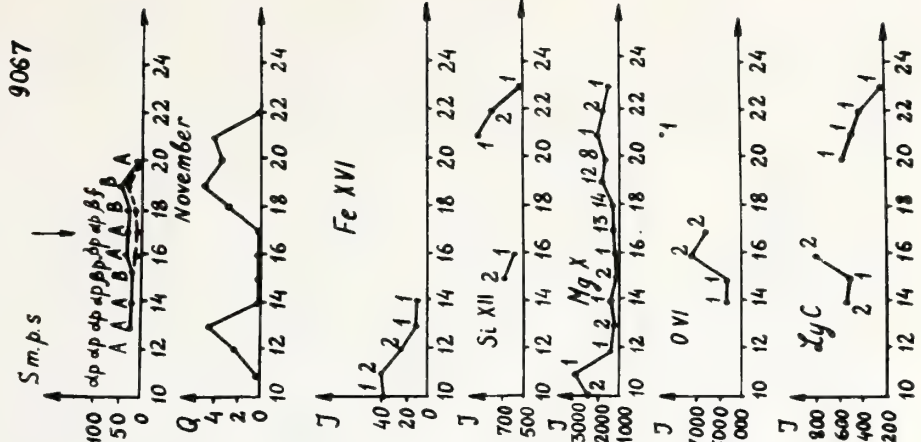


Fig. 4



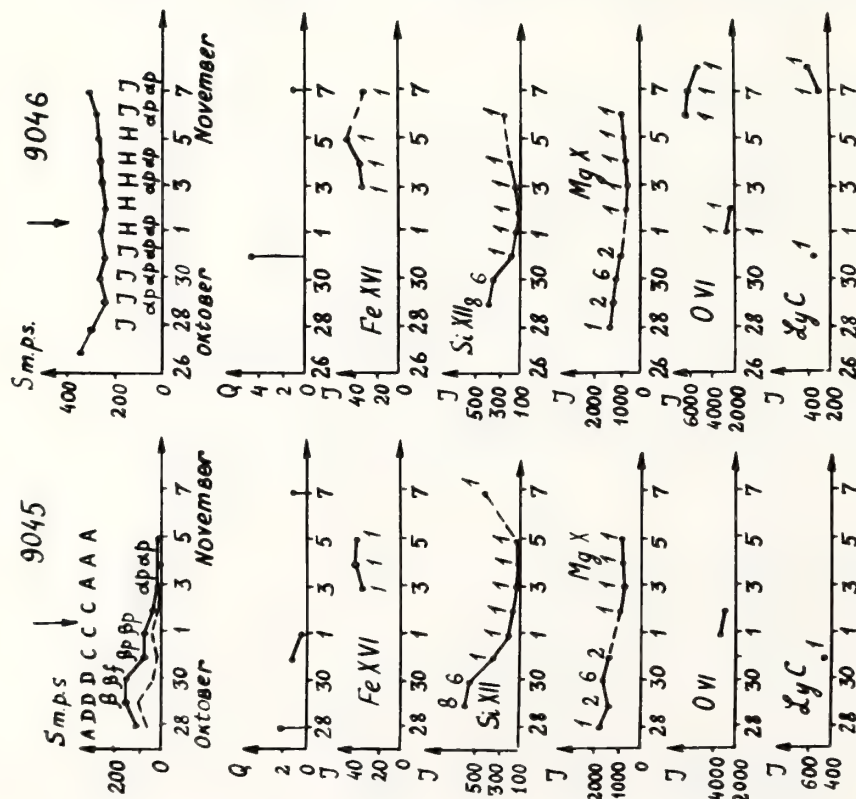


Fig. 5

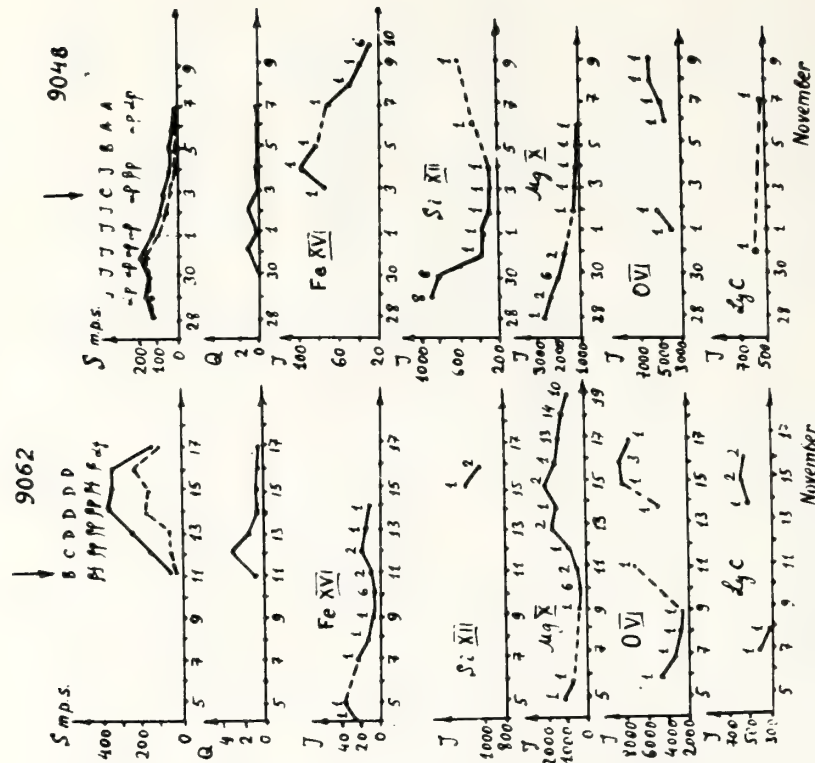


Fig. 6

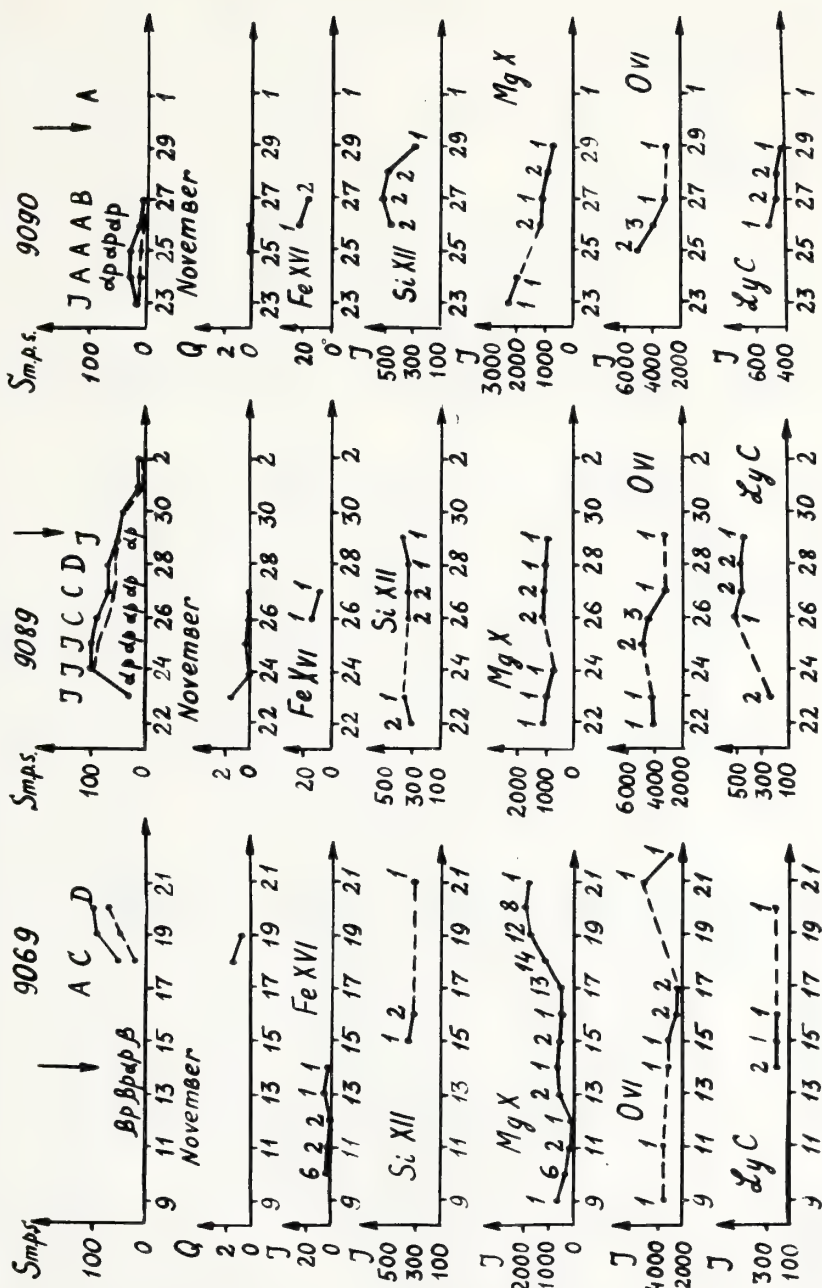


Fig. 7

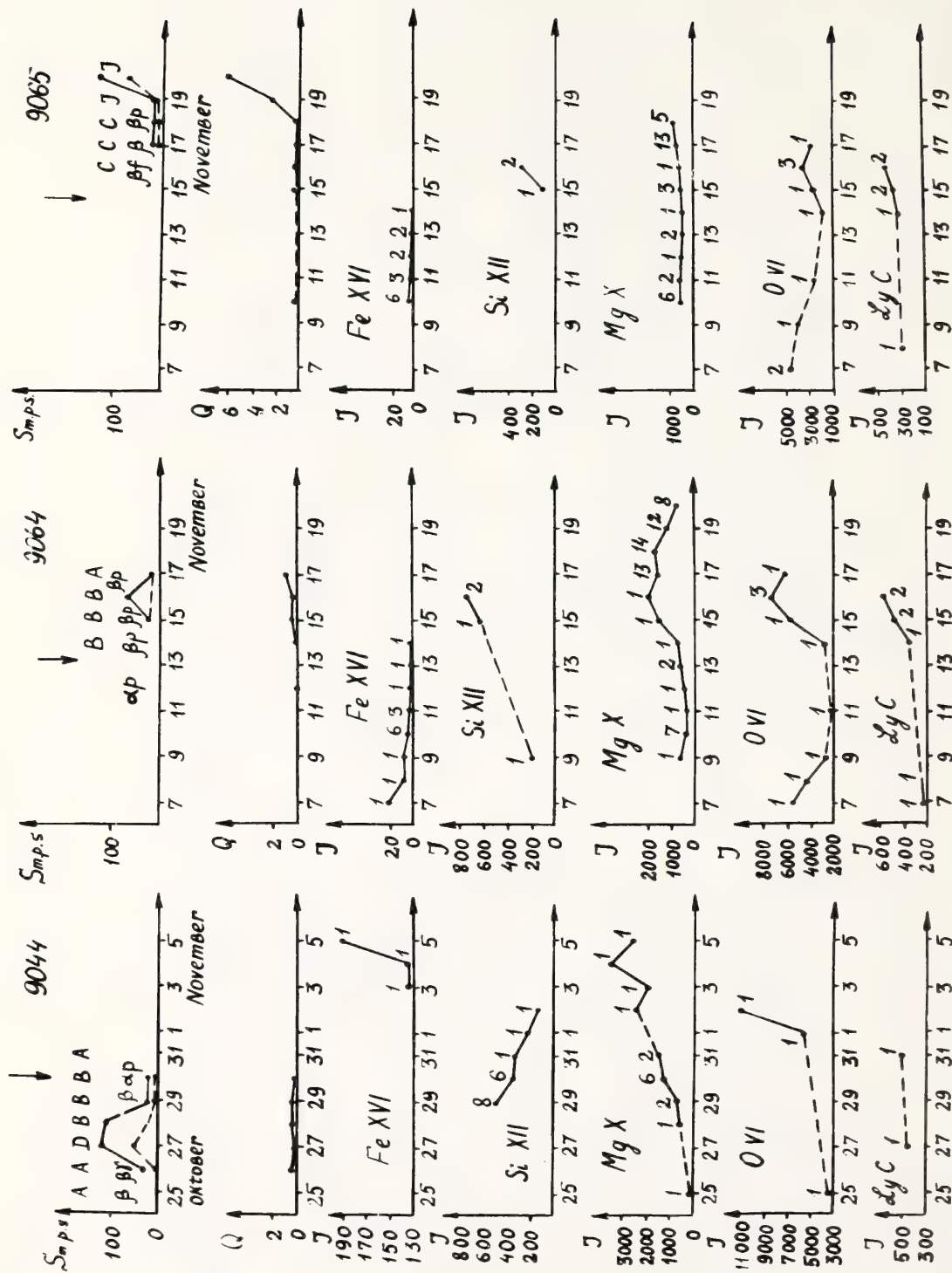
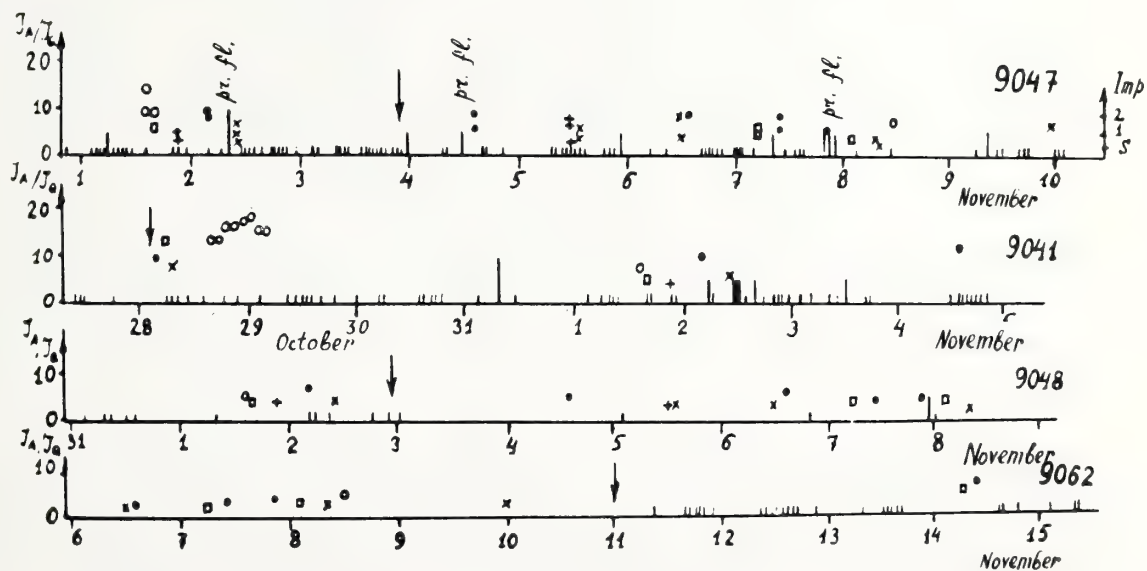
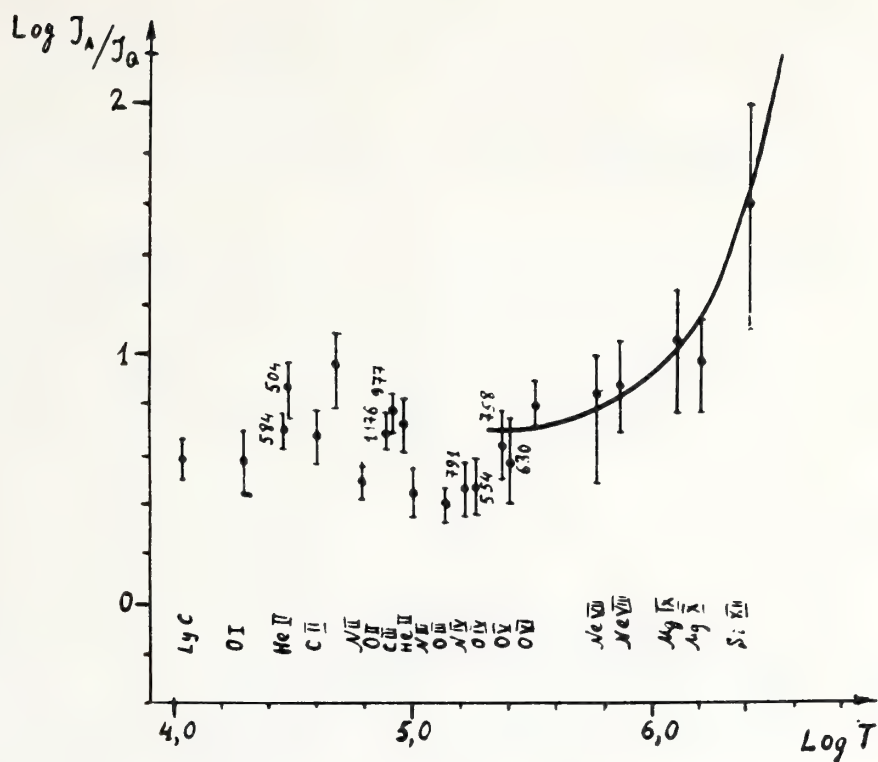


Fig. 8



A COMPUTATION SCHEME TOWARD
OBJECTIVE PREDICTION OF SOLAR FLARES

Tyan Yeh
Pure and Applied Science Division
Global Enterprises, Inc.
Louisville, Colorado 80027, U.S.A.

and

Yoshinara Nakagawa
Space Science Laboratory
NASA Marshall Space Flight Center
Huntsville, Alabama 35812, U.S.A.

A computation scheme is proposed for the calculation of the temporal evolution of the solar magnetic field. The region of computation is chosen with due consideration of the boundary conditions. The governing equations account for the plasma motion as driven by the magnetic force and the magnetic flux transport as convected by the plasma flow. The initial conditions are to be deduced from observed magnetogram data at the photospheric level. The temporal evolution simulated by the mathematical solution to the formulated initial-boundary value problem will provide a quantitative basis for objective prediction of the possible occurrence, locations, and magnitudes of solar flares.

There are observational evidences to indicate the existence of close relationships between occurrence of solar flares and evolving solar magnetic fields. For example, large active regions that are flare-poor are characterized by simple magnetic configurations with slow evolution, whereas small active regions that are flare-rich are characterized by rapid variations among their sunspots and other active-region structures (McIntosh, 1970). Therefore, the theoretical basis for flare forecasts lies in the analyses of

the temporal evolution of the solar magnetic field. In the past decade important improvements in flare forecasts have been made through intensive use of an observer's subjective evaluation of active-region structure and evolution (Smith, 1972). But, it is clearly desirable to eliminate the need for subjective experience and to move toward objective technique.

The eruption of a solar flare may be triggered by some kind of instability when the magnetic energy accumulated in a small region of the solar atmosphere exceeds a threshold limit. From the viewpoint of magnetohydrodynamics, accumulation of magnetic energy is nothing but the concentration of magnetic fluxes as caused by the motion of the solar plasma to which the magnetic field lines are frozen. Case studies of flare-rich active regions have suggested that shearing motions along the lines of polarity reversal are important to the build-up of flare energy and for creating the instability that releases the excessive energy (Tanaka and Nakagawa, 1973). Indeed, the nested distribution of such neutral lines determines the topological structure of the magnetic field in the corona (Yeh, 1978). Thus, the hydromagnetic interaction between the plasma motion and the magnetic field must be considered in a flare prediction model, if the locations of high concentration of magnetic energy are regarded as potential sites of flare occurrence.

We shall outline a computation scheme toward prediction of flares which is currently being pursued for implementation. To construct a mathematical model, we must specify the spatial extent of the region, the governing equations for the phenomenon of interest, the relevant conditions at the boundary of the region. These, together with the initial conditions, will determine a mathematical solution which describes the subsequent evolution of the plasma motion and the magnetic field in the region under consideration.

We choose a spherical layer containing the entire photosphere as the region of computation. The bottom level of the region lies below the photosphere and the top level lies above the photosphere. Inside the chosen region is the photosphere where occurrence of flares takes place. Since the emergence of magnetic fluxes to the photospheric level constitutes upward transport of magnetic energy from below the photosphere, to include this supply of energy in our consideration we should choose the bottom level of the region at some altitude where the upward motion of the plasma is negligible and hence the magnetic field lines are anchored. On the other hand, far above the photosphere the outward motion of the plasma forms the solar wind, to include this efflux of mass in our consideration we should choose the top level at some altitude where the plasma flow

become practically radial and hence the magnetic field lines are distended into the radial direction.

For the phenomenon of interest to our consideration, the relevant plasma motion is mainly driven by the magnetic force. The gradient force due to the thermal pressure and the gravitational force due to the solar mass are relatively small. Likewise, the field lines are essentially convected by the motion of the highly conducting solar plasma. The diffusion due to the electrical resistivity is ignorable. Therefore, we choose the following as the governing equations.

$$\frac{\partial}{\partial t} \rho + \nabla \cdot \rho \vec{u} = 0 \quad (1)$$

$$\frac{\partial}{\partial t} \vec{u} + (\vec{u} \cdot \nabla) \vec{u} = \frac{1}{\mu \rho} (\nabla \times \vec{B}) \times \vec{B} \quad (2)$$

$$\frac{\partial}{\partial t} \vec{B} + \nabla \times (\vec{B} \times \vec{u}) = 0 \quad (3)$$

Here ρ is the mass density, \vec{u} is the flow velocity, and \vec{B} is the magnetic field, μ being the magnetic permeability.

The boundary conditions are

$$\rho = \rho_1, \quad \vec{u} = 0, \quad \vec{B} = (\vec{B})_{t=0} \quad \text{at } r = r_1 \quad (4)$$

at the bottom level and

$$\rho = \rho_2, \quad \vec{u} \times \vec{r} = 0, \quad \vec{B} \times \vec{r} = 0 \quad \text{at } r = r_2 \quad (5)$$

at the top level. In other words, we assume that at the bottom level of the region the motion of the plasma diminishes to a standstill and consequently the frozen-in magnetic field remains at its initial value. And at the top level of the region the plasma flow becomes radial and the magnetic field also has no components perpendicular to the radial direction. The mass density is assumed to remain unchanged at the boundary.

To initiate the calculation for the temporal evolution, it is necessary to specify the initial values of the mass density, the flow velocity, and the magnetic field at every grid point of the entire region. At the present time, direct measurement of the flow velocity is not available at all, and observations of the magnetic field provide only the line-of-sight component at the photospheric level. Hence, the required initial conditions have to be deduced through theoretical modeling. For the magnetic field, we may assume that

at the initial time the magnetic field is not much affected by the electric currents inside the region. Accordingly, the current-free magnetic field

$$(\vec{B})_{t=0} = -\nabla\psi \quad (6)$$

can be determined from the gradient of a magnetic potential which satisfies Laplace equation

$$\nabla^2 \psi = 0 \quad (7)$$

subject to the conditions

$$\frac{\partial \psi}{\partial r} = -f(\theta, \phi) \quad \text{at } r = r_0 \quad (8)$$

at the photospheric level and

$$\frac{\partial \psi}{\partial \theta} = 0, \quad \frac{\partial \psi}{\partial \phi} = 0 \quad \text{at } r = r_2 \quad (9)$$

at the top level of the region. In other words, the top boundary is treated as a source-surface (Schatten et al., 1969). For the sake of simplicity, here we prescribe the radial component of the magnetic field, instead of the line-of-sight component, at the photospheric level. We remark that since the solenoidality of the magnetic field has been imposed on the magnetic potential, the subsequent magnetic field calculated from the induction equation will be divergence-free. Next, to calculate the initial velocity field, we may make use of two magnetic fields calculated in the manner just described at two suitably separated times. Their average can be taken as the initial magnetic field for our computation, whereas their difference quotient can be taken as the initial time-derivative of the magnetic field. The initial magnetic field and its time-derivative will enable us to calculate the initial velocity from the following induction equation

$$\nabla \times \left[(\vec{B})_{t=0} \times (\vec{u})_{t=0} \right] + \left(\frac{\partial \vec{B}}{\partial t} \right)_{t=0} = 0 \quad (10)$$

subject to the condition

$$(\vec{u})_{t=0} = 0 \quad \text{at } r = r_1 \quad (11)$$

at the bottom level. The resulting velocity field will not necessarily become radial at the top level. We have to tolerate this drawback. As to the initial mass density, we may assume a stratified distribution with a suitable exponential profile.

So far, we have outlined a computation scheme for the calculation of the evolving solar magnetic field in a global region containing the entire photosphere. If the computation is to be restricted to a local region

containing only a part of the photosphere, then additional boundary conditions at the lateral boundary must be imposed. We may assume that both the velocity and the magnetic field become vanishing there if the local region represents an active region and the lateral boundary of the local region is chosen sufficiently far away from the middle of the active region.

In summary, due to the complexity of the physical phenomenon which we try to simulate mathematically, we have to assume considerable simplifications for the governing equations as well as the boundary conditions. Furthermore, due to the scarcity of the observational data, we have to deduce the initial conditions through modeling. Inevitably, the proposed scheme contains some ad hoc elements to make the scheme deterministic. However, it will serve as a basis for future improvements. Hence, it seems worthwhile for testing and scrutiny. Hopefully, this will lead to the development of a practical method for objective predictions of the possible occurrence, locations, and magnitudes of solar flares.

Acknowledgments-- We thank Pat McIntosh for some discussion. The work performed by T. Yeh was supported by National Oceanic and Atmospheric Administration, Environmental Research Laboratories under contract 03-78-B01-103.

References

- McIntosh, P. S. (1970): in Ionospheric Forecasting, ed. by V. Agy, AGARD Conference Proceedings No. 49, 8-1.
- Smith, J. B. (1972): in Solar Activity Observations and Predictions, ed. by P. S. McIntosh and M. Dryer, MIT Press, Cambridge, Mass., 429-442.
- Schatten, K. H., J. M. Wilcox, and N. F. Ness (1969): Solar Phys. 6, 442.
- Tanaka, K., and Y. Nakagawa (1973): Solar Phys. 33, 187.
- Yeh, T. (1978): Solar Phys. 56, 439.

PROBABLE SHORT-TERM PREDICTION OF SOLAR ACTIVITY
I. PREDICTION OF THE EVOLUTION
OF ACTIVE REGIONS

E. I. Mogilevsky
Institute of Terrestrial Magnetism, Ionosphere and
Radiowave Propagation, Academy of Sciences
Moscow, 142092 U.S.S.R.

An analysis of the salient features of solar magnetic fields of solar activity phenomena permits one to substantiate the stochastic nature of the evolution of active regions and the necessity of applying a probabilistic method for predicting solar activity. The formalism of Markov processes and the Fourier spectra of magnetic field variations can be employed in constructing an algorithm for a short-term prediction of the evolution of the active solar regions.

1. INTRODUCTION

In solving the scientific and practically significant problem of short-term (1 to 10 days ahead) prediction of solar activity and, first, of the appearance of large solar flares, which determine a variety of geophysical phenomena of magnetic-ionospheric disturbance, radiation conditions in the vicinity of the Earth, etc., several quantitative methods have been suggested. They should in principle replace (or supplement) qualitative synoptical methods of forecasting solar activity that have been predominantly used so far. The practical tasks of astronautics (especially those prompted by prolonged space flights), wireless communication, etc., have led to the need not only to search for quantitative methods of prediction but also to solve a narrower problem of flare diagnostics from the available data (optical, radio, etc.) on a particular flare, it is necessary to determine the geoeffectiveness (the energy spectrum of solar cosmic rays in the vicinity of the earth, etc.) expected within the next few hours. The problems of flare diagnostics are solved by obtaining certain quantitative statistical relations from a given set of previously obtained teaching data and by determining the degree of correspondence between the observed parameters of the flare under study and the initial data using the previously obtained statistical "reference" relationships (Akinian et al., 1977). Although such a method of flare diagnosis has proved successful, it obviously cannot replace short-term prediction, both because it is highly limited by the relatively late acquisition of the data used and because in the frequently complex situations (say, in the presence of several intensively active regions simultaneously) diagnosis becomes extremely difficult.

In recent years, quantitative methods for predicting solar activity have been developed, which are based on the mathematical methods of "image recognition." The main idea of such methods is analogous to that underlying the method of flare diagnostics; i.e., a given set of characteristics for a number of active regions (ARs) (including flare-active regions) is used to find some algorithm for a precalculation, say, of flares from an optimum data base. A prediction is made according to that algorithm, using the set of initially observed data (Slutskaya and Stepanyan, 1974). Although use of such a method of prediction has not resulted in a substantial increase in reliability as compared with synoptical (qualitative) prediction, it is possible to make the following comments:

a) The "image recognition" prediction (a preflare situation) is, as a rule, independent of any heliophysical (or even working) model. This seeming advantage of a "purely empirical approach" in our opinion is its weakness. The choice of the characteristic parameters determining the evolution of ARs is almost arbitrary. This accounts for the fact that as many as several tens of activity indices which are at first sight different are often used. A statistical analysis has revealed that most of the solar indices used are not only closely correlated (i.e., yield no new information about the evolution of ARs) but represent a statistical assembly of intersecting sets. This precludes one from determining, within the framework of statistical methods, the most effective indices among them, which characterize physically significant parameters. Thus, the statistical method of recognition indicated above has no cognitive significance; it does not advance understanding of solar activity and flares.

b) By its very nature, "image recognition" assumes the existence of uniquely uniquely (often superficially) determined characteristics of the phenomenon to be investigated. The proof that such parameters (or only one parameter of this kind) exist is not then given but merely assumed. At the same time, all commonly used daily solar activity indices are insufficiently informative, especially for predicting such phenomena as flares. They describe arbitrarily chosen stationary states of ARs, but almost fail to characterize the most important features of AR evolution, the structural dynamics and energy content of magnetic fields, which determine both the development of flares and the evolution of practically all activity phenomena at every level of the solar atmosphere. Hence, despite the apparent perfection of mathematics (naturally, it was developed to solve entirely different problems), no appreciable success has been gained in predicting by this method because of the insufficient judiciousness (incompleteness and unsubstantiatedness) of the choice of the initial data indices. Moreover, in our opinion, no improvement along these lines is possible.

Without dwelling upon the discussion of limitations inherent in the formal statistical method of prediction, we note that a quantitative method for predicting solar activity and flares should rest on definite conceptions, deduced from observation, about the nature of solar phenomena. The mathematics of such a method should adequately describe the stochastic nature of the solar phenomena under consideration. In the two parts of the present paper, an attempt has been made to look for such a new approach toward the solution of the complicated problem of quantitative, short-term probabilistic prediction of both the evolution of active regions (part I) and the

development of flares (predominantly large) in flare-active regions (part II). It should be noted that at present merely the necessary substantiation of a possibility of such an approach is being attempted. The development of practical methods for utilizing the suggested approach must be solved in future investigations.

2. FORMALISM OF MARKOV PROCESS USED TO PREDICT EVOLUTION OF ACTIVE REGIONS

At the present time it is beyond doubt that practically all phenomena of solar activity (both evolutionary and fast) result from the dynamics of magnetic fields (in the solar atmosphere, where $\epsilon_{\text{mag}} > \epsilon_{\text{kin}}$) or manifest themselves in the magnetic field of ARs (in the photosphere and in the sub-photospheric regions, where $\epsilon_{\text{mag}} \lesssim \epsilon_{\text{kin}}$). The magnetic fields determine, directly or indirectly, the energy characteristics, rate of evolution, and features of development of ARs. Large-scale magnetic fields (the total magnetic field of the Sun, hierarchy of the "background fields", supergiant structures, and "giant granules") have a relatively low intensity (about several oersteds) at a significant altitudinal extension (up to the outer corona and the interplanetary medium). This indicates that the current systems that determine them occur rather deeply under the photosphere. These large-scale magnetic fields, within which there develop intense local magnetic fields of the various phenomena in ARs, do not decay into fine-structure elements. In contrast, the magnetic fields of solar-activity phenomena (sunspots, faculae, flocculi, and filaments such as protuberances, fibrillas, and coronal structures) consist, as indicated by the high spatial resolution observations made in recent years (Dunn and Zikker, 1973; Ramsey et al., 1977), of fine-structure filamentary magnetoplasma elements of small cross-section (to about 1 in) with high field intensity (to 2 or 3 kilo-oersteds in disturbed ARs and about 0.5 kilo-oersteds in "quiet" regions - in supergranule nodes). These thin magnetoplasma filaments (more frequently occurring in groups) "emerge" from the photosphere into the chromosphere and corona and, in the form of closed loops and arches, "sink" again into the photosphere at sites of the opposite polarity. The existence of such extended discrete magnetoplasma filaments is possible only when they contain extended or discrete-closed, as suggested previously (Mogilevsky, 1971), current systems, which are conventionally referred to as "subgranules". The indicated discrete filamentary structure of the solar magnetoplasma is its most important and basic property. It determines many characteristic features of solar activity phenomena: their high dynamicity which "contradicts" their apparently "complete frozenness" and, what is especially important for the following, their characteristic oscillatory (quasi-periodic) conditions. Attention has already been drawn (Mogilevsky, 1971) to the fundamental distinction between magnetoplasma within the solar atmosphere ("no walls") and laboratory plasma, where the distribution function for micro- (or structural macro-) particles and the conservation laws (for mass, energy, etc.) are determined by "impenetrable walls.". It is characteristic that for laboratory plasma having nonlinear properties (i.e., nonlinear effects in a plasma volume significantly exceed the influence of the confining walls), the property of forming discrete fine-structure filaments, which in principle alter many macroscopic properties of the magnetoplasma, is also

well pronounced (Samarsky et al., 1975). The "self maintenance" of the solar magnetoplasma, which is represented by the so-called integral structure relationship (Vlasov, 1966), does not answer the question of "how and where" the filamentary fine-structure elements of magnetoplasma are formed. (According to the integral structure relationship, if $f(q, p, t)$ is the distribution function for a statistical ensemble of elements, then the condition of "self-maintenance" of such an ensemble requires that there should be a definite relation between the magnetic field, currents, "density", macromotion and time, given by a certain function $\phi(T, \bar{B}, p, \bar{u}, t)$. This function determines the non-divergence of the integral of the distribution function

$$\int_{(\infty)} f(q, p, t) d\tau = \phi(T, \bar{B}, p, \bar{u}, t) \quad .$$

The integration here is over an infinite phase volume. This integral relationship, which has been substantiated by A. Vlasov for any interacting micro- and macro- (say, even stars) elements, leads necessarily to the existence of spatial structures.) This relationship does indicate the necessity of their existence, which has been confirmed recently by both direct and indirect observations (Dunn and Zikker, 1973; Ramsey et al., 1977).

In such a structured solar plasma, the effective electrical and heat conductivities in a volume exceeding the dimensions of the structural elements are the magnetic Reynolds number times lower than the classical values. Physically, this is due to the fact that in the medium between the "magnetic filaments," which suffer "bending oscillations," the conduction electrons are scattered by nonstationary magnetoplasma inhomogeneities (equivalent to "plasmons"), whose effective cross section is by far (to 5 or 6 orders of magnitude) greater than the classical Coulomb one. In the presence of closed current-whirl plasma condensations (Ermakov, 1969), which form filamentary strings, the solar plasma contained in a definite volume (for example, in structural filamentary elements of protuberances, chromospheric surges, etc.) may have a definite total magnetic moment. Hence, as has already been demonstrated (Mogilevsky, 1971), there inevitably appear macromagnetic oscillations of individual structures belonging to solar activity phenomena. Since they have definite characteristic parameters (mass, dimensions, magnetic fields), one would expect that the various solar activity phenomena must possess their natural (resonance) frequencies of oscillations. As indicated by the relevant studies (Mogilevsky et al., 1976; see, e.g., Figure 1, sunspots (of certain classes), flocculi, filaments, and fibrillas have various characteristic frequencies of oscillation, which are determined from the radial velocities and from the measured magnetic-field oscillations (Mogilevsky et al., 1973). The excitation of these natural oscillation spectra occurs because the structural magnetoplasma elements "sink" under the photosphere where (in the convective zone) they are subjected to an influence whose spectrum has the form of white noise or normal distribution. (The presence of a set of discrete frequencies or harmonics is due to the structural complexity of individual phenomena in ARs, which are made up by a number of magnetoplasma filaments.)

If ξ is the considered characteristic fluctuating parameter for a given phenomenon of solar activity (for example, the magnetic flux or the intensity of the S-component of the radio emission associated with the flux, etc.),

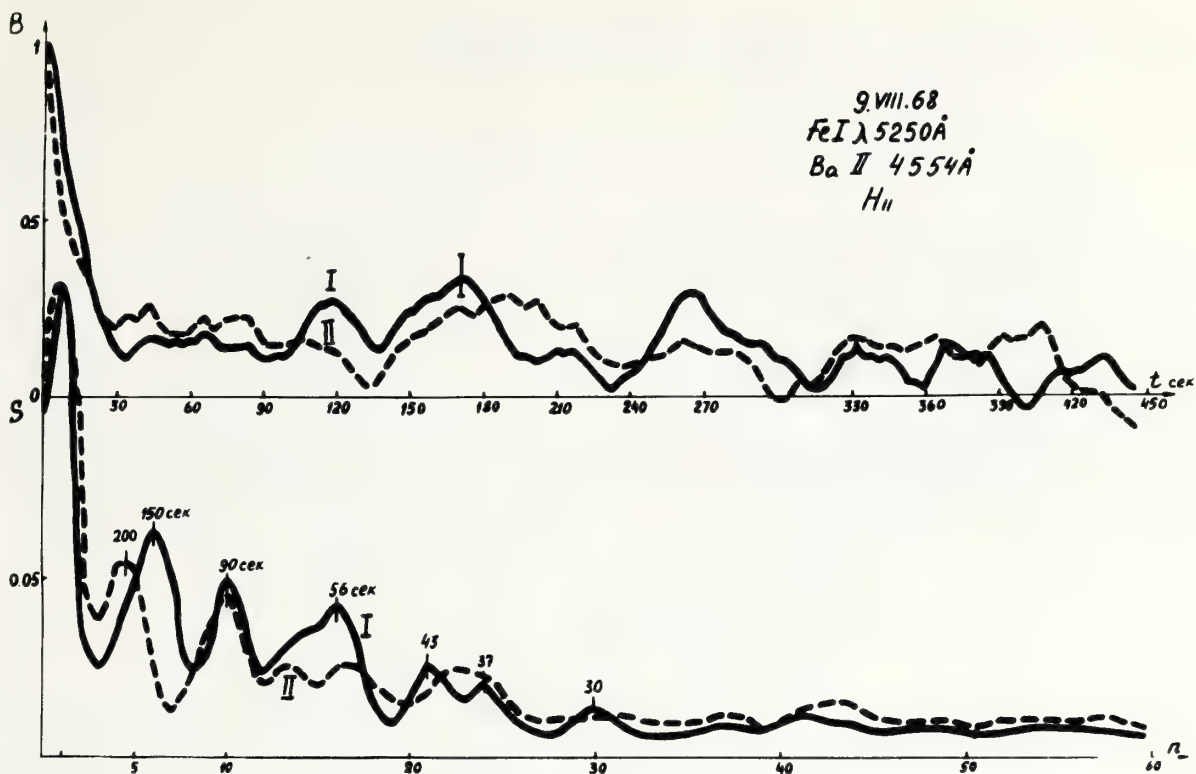


Figure 1a. An example of the autocorrelation functions and Fourier spectra of magnetic field variations in a sunspot umbra.

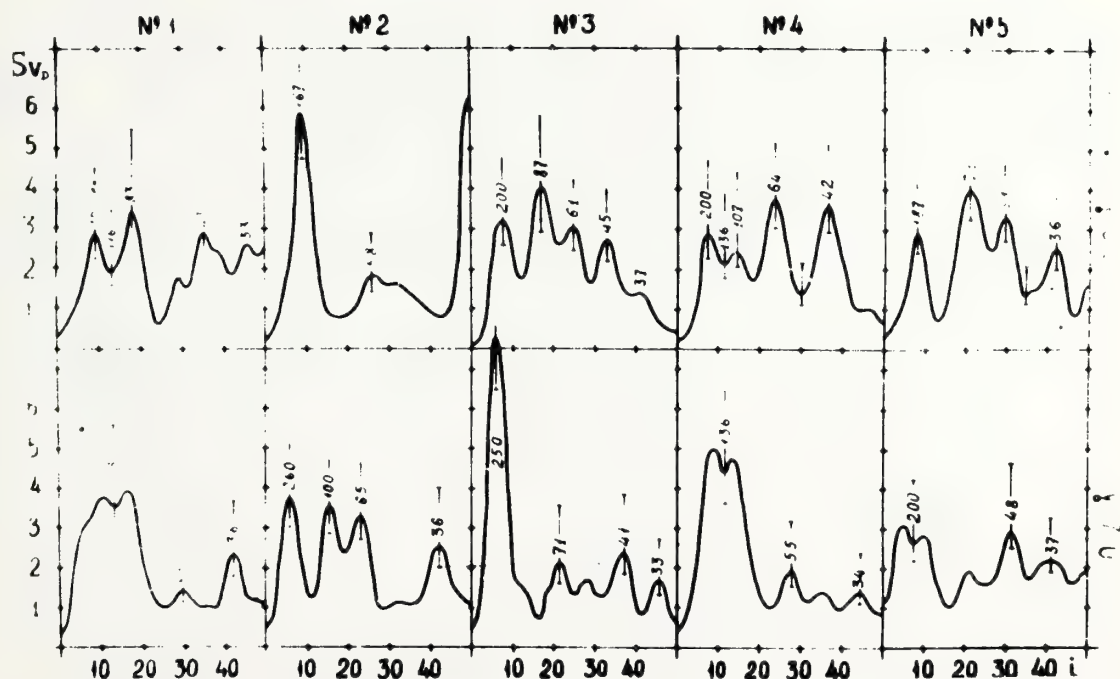


Figure 1b. Same examples of Fourier spectra for $(v_p)_{H\alpha}$ in AR - Mc Math 11976 accordingly: No. 1 - above a sunspot; No. 2 - in a fibril; No. 3 - in a flocculus; No. 4 - in a filament; No. 5 - in a flocculus behind an AR.

then in the presence of deterministic $F(\xi, t)$ and stochastic $\phi(\xi, t) Z(t)$ forces, the following stochastic equation should hold:

$$\frac{d\xi_i}{dt} + A_1 F(\xi_i, t) + A_2 \phi(\xi_i, t) Z(t) = 0 \quad (1)$$

Here, A_1 and A_2 are constants (related to the adopted normalization and initial conditions); $Z(t)$ has the above-mentioned spectrum of white noise or normal distribution, which determines the forced oscillations of the system under consideration. The deterministic forces (for example, the Coriolis forces, "lift forces", which determine the formation and emergence of magnetoplasma structures, etc.) also have (because of peculiarities of the convective subphotospheric zone) a fluctuating component which may be included in the third term of the expression (1). In this case, when we consider relatively fast fluctuations ($\lesssim 10^3$), the expression (1) is simplified as follows:

$$\frac{d\xi}{dt} + A' \phi_1(\xi_i, t) Z(t) = 0 \quad (1')$$

The validity of such a stochastic relation can be verified by making use of the successions of observations of the measured fluctuations of the S-component of radio emission from ARs, which, by virtue of the magnetic deceleration mechanism of emission, is directly associated with the magnetic field of an AR (Gontarev, 1975). Since the experimental data reasonably agree with the results of solving a stochastic equation of the type (1), this must imply that, according to Doobe's theorem, the adopted sequence of values of ξ_i corresponds to a Markov process (Tikhonov and Mironov, 1977). The applicability of the mathematics of Markov processes (i.e., processes without a consequence) for describing quasi-oscillatory conditions of magnetic fields or velocities in ARs makes it possible to construct a scheme of a quantitative prediction of AR evolution in terms of the probabilistic functions for AR states. It is important to emphasize once again that, in view of the heliophysical data on the fine structure of solar magnetoplasma, it is exactly this approach that is adequate to describe the nature of the development of the solar phenomena under investigation.

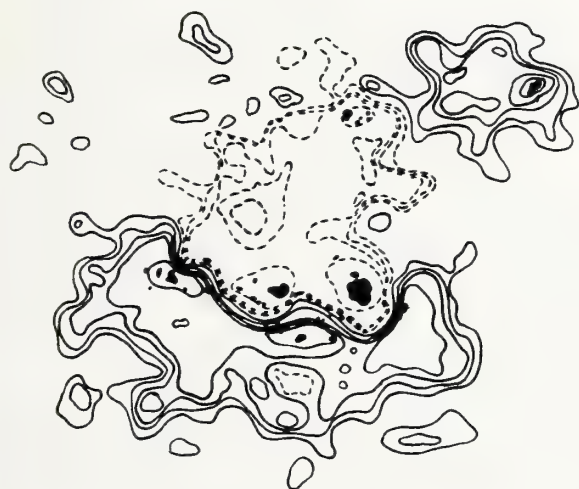
Over a decade ago, it was demonstrated (Leighton, 1964) that long-continued evolutionary changes in AR structure can be described by solving simultaneously the diffusion equation for the elementary AR components (in this context, the above-mentioned filamentary subgranular elements) and the differential rotation equation for the AR. Investigations of the development and decay of sunspots and their groups (Harvey and Harvey, 1973) have shown that concurrently with the diffusion process there occur flux (often of pulsed character) motions of elementary magnetic fields. These phenomena of the drift of the elementary components in the course of evolution of the magnetic field are readily traced on a successive series of maps of the magnetic field of ARs (see Figure 2). The penetration during the evolution of a field of one magnetic polarity within the field of the opposite sign (largely, into the region of prevailing magnetic flux) is a well-known fact. We note that, unfortunately, quantitative characteristics for such a phenomenon of field "drift" in the various phases of AR evolution have not



12.IX.1977



17.IX.1977



15.IX.1977



18.IX.1977

Figure 2a. An example of the evolution of magnetic field in AR Mc Math N 14942 - 43. in consequence of drift and diffusions.

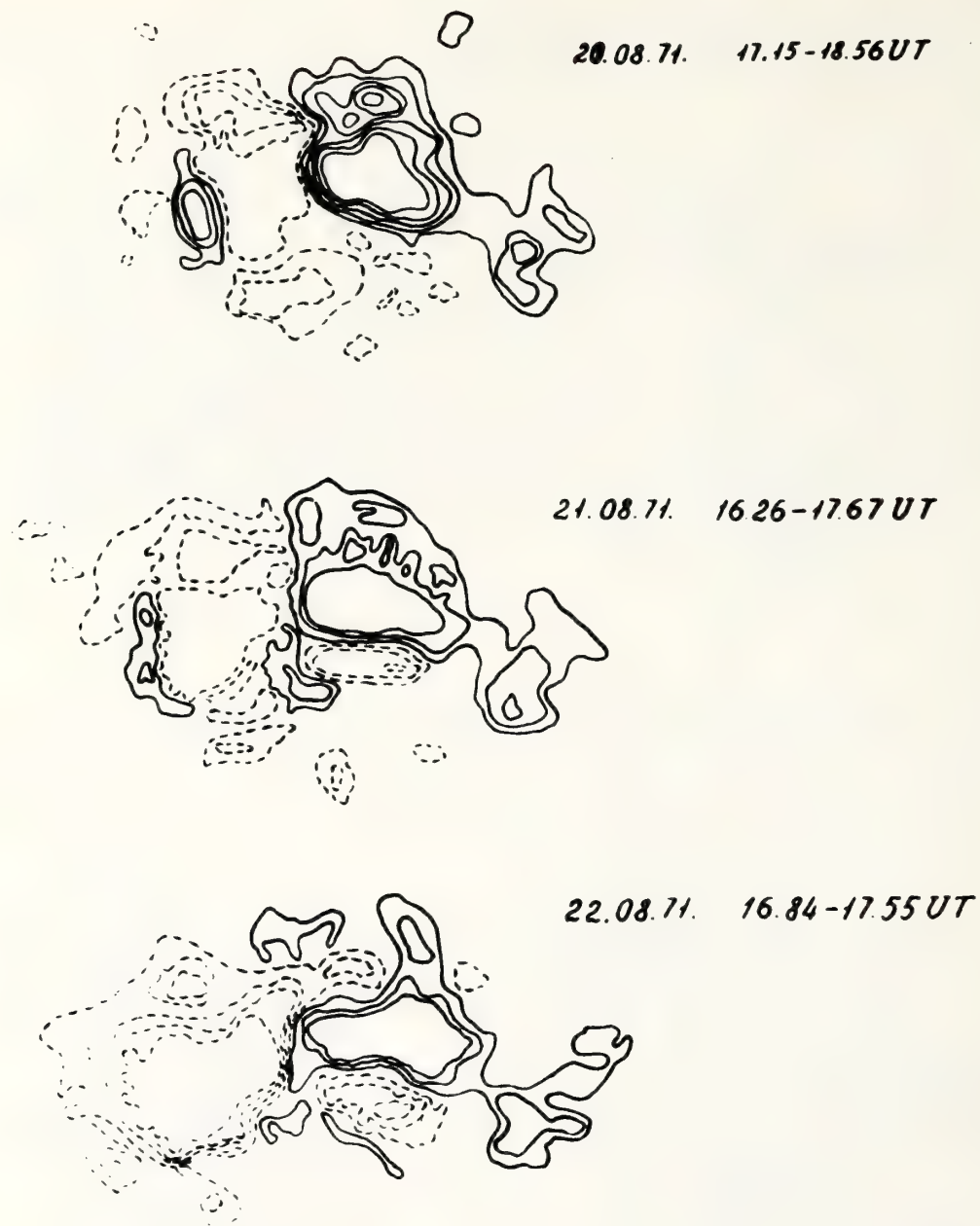


Figure 2b. The same for AR Mc Math N 11482.

yet been obtained. It will be noted that in general the phenomena of diffusion and drift can be used to describe all principal features of evolution, because the field emergence (or immersion) is generalized in these processes by a mathematically formal introduction of an "absorbing" or "semiabsorbing" screen (Tikhonov and Mironov, 1977). Thus, bearing the aforesaid in mind (the probabilistic description of evolution in the presence of field drift and diffusion), one may use as a prognostic equation for AR evolution the Fokker-Planck-Kolmogorov equation

$$\frac{\partial P(\xi_i, t)}{\partial t} = - \frac{\partial}{\partial \xi_i} \{a(\xi_i, t) P(\xi_i, t)\} + \frac{1}{2} \frac{\partial^2}{\partial \xi_i^2} \{d(\xi_i, t) P(\xi_i, t)\} \quad (2)$$

Here, $P(\xi_i, t)$ is the probability of an AR state, which is determined, in the general case, by the fluctuating parameters ξ_i ; $a(\xi_i, t)$ and $d(\xi_i, t)$ are the drift and diffusion coefficients, respectively.

In our case, for an assembly of discrete magnetoplasma structures constituting an AR, the state probability depends on a) the kinetic energy of "i" elements of the system, i.e., $\sum P_i^2/2m$, where $P_i = m\dot{r}_i$, m and r_i are the momentum, mass and coordinate of the center of the i-th element, respectively; b) the potential energy of the system, $U(r_i)$; c) the energy of interaction between the elements, $\psi_i = m\dot{r}_i + \mu\dot{r}_i + \gamma m/\gamma t$, where μ is the effective coefficient of "friction" between the elements. Then, as is known (Klyatskin, 1975), the probability for a state of the system is described by an equation of the Einstein-Fokker type. As will be shown below, there are reasons for believing that the description of the probability of the system under discussion may be given in the single-parameter form (say, in terms of magnetic flux), which, in the simplest case, may be one-dimensional (the distance from a conditional AR center); i.e., $\xi_i = x$. After integration over the elementary-component energy distribution (in the simplest case, their energy may be assumed to be equal and constant) we obtain a simplified Einstein-Fokker equation in the form

$$\frac{\partial P(\xi, t)}{\partial t} = - \frac{1}{\mu} \frac{\partial}{\partial x} \{P(\xi, t) \frac{\partial U}{\partial x}\} + \frac{D}{\mu^2} \frac{\partial^2 P(\xi, t)}{\partial x^2}, \quad (3)$$

where D is the effective diffusion coefficient for the macro-system under study.

Depending on the amount of available information, one may describe the evolution of ARs by simplifying equation (2) in the same manner as it has been done with the Einstein-Fokker equation or by using equation (3). Both these equations may be regarded as prognostic, i.e., as describing the time dependence of the AR state probability.

As an illustration of a practical calculation using an extremely simplified equation of the type (2) to give a quantitative description of the AR evolution probability with discrete possible states, one can cite an example from our work (Mogilevsky, 1972). From the general Kolmogorov equation for n_1 discrete states of AR it follows that

$$\frac{\partial P_{ik}(t)}{\partial t} = - \sum_i^{nk} \lambda_{ik} P_{ik}(t) + \sum_{jik}^{nk} \lambda_{kj} P_{ij}(t). \quad (4)$$

Here, $\lambda_{ik} = \lambda_{ki}$ are the discrete transition-"rate" coefficients of the type $i \rightleftharpoons k$; $\lambda_{ik} = n_{ik}/T$, where n_{ik} is the number of corresponding possible transitions over the interval T for which prediction is made. The set of

equations (4) for the possible discrete AR states may be solved (it reduces to a set of algebraic equations), in particular, using a teaching sequence of experimental data for a definite class of phenomena (or a phase in AR evolution). This example of a possible, extremely simplified, practical solution to a probabilistic prognostic equation, which has a purely illustrative value, indicates that even in our case, with many simplifying assumptions, we formally arrive at a scheme for a quantitative prediction after the pattern of the "image recognition method." Therefore, the image recognition prediction method may be considered the limiting case of the approach being discussed, in which the physical characteristics determining the evolution of ARs are extremely formalized. In the proposed approach, it is possible to simplify only to limits depending on the peculiarities of heliophysical data, which are determined by information about the observed properties of the parameters ξ , a , d (or μ and D). Their determination calls for the experimental search for global characteristics for AR evolution, which would reflect completely enough the energy content and structure of the magnetic field of ARs.

3. FOURIER SPECTRA USED IN TRACING EVOLUTION OF ACTIVE REGIONS

As the global characteristics just mentioned, one may use the space-time Fourier spectra of magnetic field fluctuations or corresponding Fourier spectra of the quasi-periodic component (QPC) of microwave radio emission from ARs. Here we present only several, most significant, results of the studies carried out so far.

a) The one-dimensional (or two-dimensional) Fourier spectra of the spatial distribution of the photospheric magnetic field, obtained with both low ($l > 15$ in) and high ($l \sim 3$ in) spatial resolution of magnetic maps, have made it possible to establish discrete spatial hierarchy structures of the photospheric magnetic field, which undergo change with the phase of AR evolution. In particular, the appearance of flare-active regions (for example, early in August 1972, July 1974) was preceded by a typical redistribution of the large-scale "background" field, namely, the emergence during 2 or 3 solar revolutions of a new discrete maximum with $l \approx 200$ in the Fourier spectrum of the field distribution across the disk. The high-resolution Fourier spectra had typical discrete maxima determined by the evolutionary phase of the AR (in the presence of one activity phenomenon or another). This indicates the possibility of tracing the evolution of the AR by using a succession of spatial Fourier spectra of the magnetic field.

b) The temporal Fourier spectra for the QPC of the magnetic field of ARs (specifically, within sunspots) varied, depending on the phase and character of evolution of the activity phenomenon being considered.

If it is possible in the future to accumulate an appropriately large amount of observational data (Fourier spectra of the QPC of magnetic fields in the various stages of the evolution of activity phenomena), such data will permit us to obtain a quantitative measure of change in the energy content and structure of magnetic fields in the course of AR evolution. In practice, however, it has turned out possible to use for this purpose the temporal

Fourier spectra of the QPC of microwave radio emission from ARs, whose variations correspond, as mentioned above, to those of the magnetic field of active regions. Moreover, microwave emission measurements (especially, very prolonged ones, for example, up to 10 h) are much simpler to make than the complicated measurements of magnetic field variations, which are carried out using the photoelectric magnetograph. Several results of radio emission QPC measurements, which are important for the prediction purposes, reduce to the following (Gontarev, 1975).

a) The spectrum of the quasi-periodic S component of radio emission from ARs contains a number of discrete periods (in the range from 10^2 to 10^3 s), namely, 900^s , 300^s , 180^s , and 100^s . The intensities (absolute and relative) of these maxima, however, vary significantly depending on the character of AR evolution. There is a typical quasi-period of about an hour, during which there occurs a successive "pumping" of energy from the shorter discrete periods to the longer ones. The character of this process of "re-pumping" changes depending on the evolution of ARs, thereby reflecting the energy balance and change of the magnetic structure of the AR.

b) When ARs are "quiet", one observes a comparatively stable and simple form of the Fourier spectrum for the radio emission QPC. Specifically, in the period range under consideration (10^2 to 10^3), there is only one reliable maximum ($T \approx 850 + 900$ s).

c) In the flare-active phase of AR evolution, the above-mentioned discrete maxima become nearly the same in magnitude, and rapid (about 10 or 15 m) changes in their intensities are observed. (The observations have thus far been made in the periods when flares \leq IMP. 1 occurred in solar ARs.)

d) Recent radio-emission E QPC measurements in the range from 10 to 150 s have revealed that during seven small-scale flares (five of them occurring in a single region at hour intervals) the shape of a Fourier spectrum changes drastically; that is, instead of a high peak around 100 s there appear one or two peaks with periods of 20 and 15 s. (The radio-emission data are still regarded as tentative, because further investigations are required to determine the possible contribution to these rapid fluctuations coming from atmospheric noises. The observations were made in alpine conditions (h about 3 km) for the "coronal" weather.) In the given case, it is essential that the entire Fourier spectrum of the QPC that existed during the whole optical flare (with floccule brightening and chromospheric eruption) has changed and, thus, deformed. Thus, the Fourier spectra of radio emission from ARs (both separately and, more so, in combination with the Fourier spectra for the magnetic-field QPC) may be regarded as the global characteristics of AR evolution which reflect the energy balance and structure of magnetic fields in the region under study. It should be stressed that radio emission from ARs takes a negligible portion of their energy. At the same time, being immediately associated with the evolution of the total energy balance of the magnetic field and with its variations, radio emission from ARs may be sufficiently representative in reflecting the main processes in the ARs and, therefore, may serve as a quantitative physical characteristic for predicting AR evolution. This, of course, does not imply that there exist no other characteristics suitable for predicting. It is important only that they should describe with sufficient completeness the oscillatory regime of the

magnetic field of ARs, which characterizes AR evolution. It is the task of the further search for global characteristics reflecting AR evolution to establish whether a single-parameter representation of AR evolution is possible. It may be, for example, a parameter characterizing the rate and amount of energy transfer from the lower to the higher QPC frequencies or the associated quantities characterizing the increase in the most significant discrete periods, whose existence determines one important stage in AR evolution or another.

The possibility of such a single-parameter representation follows, in principle, from the very character of the probabilistic prognostic equations. The same inference has been made in a quite recent theoretical work (Birn et al., 1978). In considering an analytical representation of AR evolution with a possible limiting transition to the flare state, these authors have demonstrated that in the case of a force-free magnetic field, which is given in the two-dimensional space, such a single-parameter (or, at worst, two-parameter) representation of the evolution of the energy and structure of the magnetic field is possible. The importance of representing the probability of an AR state using a minimal number (one or two) of determining characteristics consists not only in the fact that the prognostic equations are then solved in a rather straightforward manner. Such a single-parameter representation of AR evolution could be of a far-reaching significance in our understanding of the physical nature of solar activity phenomena, whereas the dependence of the AR state probability on many independent parameters inevitably results in a large spread of the probabilities calculated (in the limit, it leads to white noise). This practically rules out the possibility of a quantitative prediction of AR evolution.

4. REFERENCES

- Akinian, S. T., V. V. Fomichev, and I. M. Chertok (1977): Determination of solar proton parameters in the vicinity of the earth from radio outbursts. Geomagnetism and Aeronomy (Soviet), 17:10; 177; 596.
- Birn, J., H. Goldstein, and K. Schindler (1978): A theory of the onset of solar eruptive processes. Solar Physics, 57:81.
- Dunn, R. B., and J. B. Zihker (1973): The solar filigree. Solar Physics, 33:281.
- Ermakov, F. A. (1969): On the energetics of current-whirl condensations. Geomagnetism and Aeronomy (Soviet), 9:593.
- Gontarev, O. G. (1975): Candidate Dissertation, IZMIRAN, Moscow.
- Harvey, K., and J. Harvey (1973): Observations of moving magnetic features near sunspots. Solar Physics, 28:61.
- Klyatskin, V. I. (1975): The Statistical Description of Dynamical Systems with Fluctuating Parameters. Nauka Publishers, Moscow.

- Leighton, R. V. (1964): Transport of magnetic fields of the sun. Astrophys. J., 140:1547.
- Mogilevsky, E. I. (1971): Statistical model of small-scale discrete structure of magnetoplasma in active regions of the sun. In: Solar Magnetic Fields, Symp. JAU N 43, 480-486.
- Mogilevsky, E. I. (1972): Quantitative short-term prediction of proton and nonproton flares. Solar Activity Observations and Predictions, 30:411.
- Mogilevsky, E. I., V. N. Obdirko, and B. D. Shel'ting (1973): Spectrum of the low-frequency oscillations of the magnetic field of sunspots and low-frequency modulation of radio emission from active regions of the sun. Radiophysics (Soviet), 16:1357.
- Mogilevsky, E. I., V. G. Utrobin, and B. D. Shel'ting (1976): On quasi-periodic natural oscillations in active regions of the sun. In: Origination and Evolution of Active Regions of the Sun. Nauka Publishers, Moscow, 80-85.
- Ramsey, H. E., S. A. Scholman, and A. T. Title (1977): On the size, structure and strength of the small-scale solar magnetic field. Astrophysical J. Lett., 215:41.
- Samarsky, A. A., N. V. Zmitrienko, S. P. Kurdyumov, and A. P. Mikhailov (1975): Effect of metastable heat localization in a medium with non-linear heat conductivity. Doklady Akad. Nauk SSSR, 223:1344.
- Slutskaya, B. G., and N. N. Stepanyan (1974): Prediction of the evolution of active solar regions using the potential function method. Izv. Krymskoi Astrofizicheskoi Observatorii, 52:131.
- Stenflo, J. O. (1976): Influence of magnetic fields on solar hydrodynamics: experimental results. Proc. IAU, Vol. 36, Nice.
- Tikhonov, V. I., and M. A. Mironov (1977): Markov Processes. Soviet Radio Publishers, Moscow.
- Vlasov, A. A. (1966): Statistical Distribution Functions. Nauka Publishers, Moscow.

PROBABILISTIC SHORT-TERM PREDICTION
OF SOLAR ACTIVITY
II. PREDICTION OF FLARES IN FLARE-ACTIVE REGIONS

E. I. Mogilevsky
Institute of Terrestrial Magnetism, Ionosphere and Radio-
Wave Propagation Academy of Sciences
Moscow, 142092 USSR

A quantitative probabilistic prediction of the preflare state of active regions of the Sun can be made on the basis of a scheme for their evolutionary description (part I), the resultant flare being then treated as a threshold effect. This demands that the main currently-held ideas about the nature of solar flares should be revised. A model of large solar flares, in which the flare energy and matter are accumulated as MHD solitons in the magnetic field of the photosphere and are transferred to the corona of an active region by a system of shock waves, is discussed.

1. INTRODUCTION

Quantitative short-term prediction of solar activity and its geoeffectiveness falls naturally into three stages: a) the prediction of the evolution of solar active regions (ARs) (this has been discussed in part I); b) the prediction of a preflare situation and flares; c) the diagnosis of flares, i.e., determination of the degree and character of flare geoeffectiveness. The present paper discusses the second stage. To use optimally the observational data on preflare situations and flares to make quantitative probabilistic predictions, we shall briefly discuss some of the existing information on flares that we deem most important. (Rather complete recent reviews of the problem are available (Svestka, 1976; Rust, 1974), which seem to point out that a new approach toward the understanding of the nature of flares should be sought.) Subsequently, using a possible model for flares and assuming that we already can predict the evolution of ARs, we shall briefly consider a formal mathematical scheme for the quantitative probabilistic prediction. It will be noted that solution of the problem in hand is still just beginning. Appropriate conditions for a solution are not yet mature, in the realm of experiment (this is evidenced by the necessity of new efforts on the part of scientific community to organize and carry out the international program for the Solar Maximum Year) or especially in the

field of theory. And yet an attempt to look for a solution is justified because at least it would indicate promising routes for further investigations.

2. CHARACTERISTIC AR CONDITIONS FOR FLARE DEVELOPMENT

In our discussion of prediction of powerful flares, let us briefly consider some characteristic features of the origination evolution and of the preflare situation in ARs where large flares have occurred. (Only flares of importance 2B and above are, as a rule, geoeffective in the sense that they manifest the whole complexity of the geophysical phenomena determined by flares.) There is a vast amount of observational data on complex and powerful ARs (see, for example, Report UAG 24; 26; 28) where large flares have been observed. From these data, several authors have attempted to establish the morphological features of a preflare situation in ARs. The preflare characteristics of ARs refer largely to the following classes of phenomena.

a) Phenomena associated with the motion and, particularly, with the relative rotation of individual sunspots in a group. Motion of this kind (especially rotation) may be a source of the preflare energy accumulation in the magnetic field of an AR. The rotation of sunspots was repeatedly determined in flare-active groups, both in complex, predominantly bipolar groups (e.g., in the AR McMath 11482; group $\Psi_0 = -13^\circ$, $Z = 270^\circ$, August 1971; McMath 14942-43, groups $\Psi_0 = +8^\circ$ and $+16^\circ$, $Z = 200^\circ$ and 208° , September 1977) and in compact groups of the " δ " magnetic configuration, i.e., with nuclei of both polarities within a single half-shade (e.g., in the AR McMath 11976, group $\Psi_0 = +12$, $Z_0 = 15^\circ$, August 1972).

A detailed analysis of the rotation effect in these groups has been reported by several authors [Reports UAG 24, 28]. The measured values of daily rotation of the most active sunspots reach 10° to 15° . (In certain periods, rotations of about the same magnitude were recorded that occurred during several hours only.) The direction of rotation for the sunspots mentioned corresponds, as a rule, to that of the Coriolis force. The sunspot rotation directly manifests itself in the whorl-like structure of extended fibrillas and filaments. As a result, the line of magnetic polarity separation ($B_{11} = 0$) is S-shaped. This means not only that the field of the AR becomes more complicated (elongation of the zero line $B_{11} = 0^{**}$) but also that the field component $B_{\perp} \neq 0$ appears and the transition of the structure of the photospheric field of the AR to the force-free configuration takes place. (It will be noted that the elongation of the zero line $B_{11} = 0$ has served as one of the qualitative criteria for flare prediction.)

This highly important process of change in the AR magnetic-field structure is, however, evolutionary. No direct relation has been established so far between the rotation effect and the time of appearance of large flares. Estimates have been obtained for the magnitude of the increase (change) in the nonpotential (force-free) energy of the magnetic field in the group of August 1972 [Rust, 1973]. From table 1 contained

therein it follows that on all days (both "quiet" and those of large flares on 2, 4, and 7 of August) the calculated variations of the nonpotential field energy are on the order of 2 to 5×10^{31} ergs/day. The authors have also calculated the decrease of the nonpotential field energy, associating it with a large proton flare 7.08. It has turned out to be comparable with the total energy of flare emission. We have made a similar calculation for the most intense flare 4.08 in the same group, in which we used the magnetic-field maps of the Kitt Peak Observatory (obtained 6 h before and about 8 h after that flare) and the magnetic-field map in the group obtained at the IZMIRAN about 3 h after the onset of the flare. Within the estimation accuracy, we have obtained nearly the same values (about 1.5×10^{30} ergs/h) for the instances before and after the flare. These correspond to the average values of change in the energy of the nonpotential part of the field within the same group, both in "quiet" and "flare-active" periods. Hence it follows that the rotation effect and the related transition of the magnetic field to the force-free configuration is evolutionary. But no direct relation to the instant of appearance of large flares has been observed.

b) A typical phenomenon encountered in the evolution of the magnetic fields in the flare-active regions is a regular increase in the magnetic flux of one polarity and a decrease of that of the other polarity. This effect of approach of the magnetic-flux magnitudes on the eve of large proton flares has been investigated by a number of authors [e.g., Zvereva and Severnyi, 1970]. The effect has a character of evolutionary flux penetration of the enlarging field into the "pushed back" field of the other polarity. It is accompanied also by the diffusive expansion and division of structures (in the stage of decay of the AR). Such phenomena are observed, however, in the ARs with large changing sunspot groups, in which no flares have been practically observed (e.g., in the powerful group of October 1975). Thus the evolutionary character of change in magnetic flux cannot be immediately related to the appearance of flares.

c) It has been repeatedly mentioned [Svestka, 1976; Rust, 1974; Vorpahl, 1973] that the appearance of flares is associated with the "emergence" of magnetic fields of one polarity within the "older" field of the other polarity. But the "emergence" of the magnetic field in an AR occurs rather frequently (e.g., in the origination of sunspots and sunpores) without being accompanied by flares. Recently, attention has been called to the fact that the "emergence" of the magnetic field in an AR near the line $B_{11} = 0$ (close to filaments) is often accompanied by flares (true, of low intensity). This underlies the recently proposed flare model [Rust, 1974]. It should be noted that the conventional concept of "magnetic-field emergence" should be accepted only with caution. It is commonly accepted that certain magnetoplasma "tubes" under the photosphere are not in equilibrium, for the gas pressure in the surrounding medium is higher than in the "tubes." Since in the static case

$$P_{\text{ext.}} = P_{\text{int.}} + P_{\text{magn.}} \quad (1)$$

the "cold" plasma is caused to rise, under the influence of the Archimedes force, with the field. But then the concept of "magnetic tube" is not

substantiated. (Why should there be an isolated region possessing a high "natural" field?) And, most significantly, it is disregarded that within such a tube there exist, apart from the gas pressure, the dynamical forces associated with considerable velocities of the motion of matter observed at places of "emergence." In this case, one should use not the static relation of the type (1) but the generalized Bernoulli integral:

$$\varepsilon_{\text{kin.}} + \varepsilon_{\text{poten.}} + P_{\text{int.}} - \varepsilon_{\text{magn.}} = \text{const}, \quad (2)$$

where ε is energy density. Evidently, the equality (2) can be reached by using several possible relationships between the ε components in which $\Delta\varepsilon_{\text{poten.}} = \rho q (Z_1 - Z_2) = 0$ (no emergence) or a $\Delta\varepsilon = \varepsilon_{\text{poten.}} \geq 0$ (emergence or submergence). One can distinguish the effect of field "emergence" from that of local MHD disturbances in the already existing magnetic field, which, as will be shown below, may play the dominant role in the appearance of flares, by measuring simultaneously the time variations in the field (B) and the velocity of motion of the substance (\vec{v}). Such a relation exists only in certain cases (e.g., those associated with flares). Whereas MHD disturbances may occur as quasi-periodic field variations over wide periods, the field "emergence" may proceed only at "slower rates", because of viscosity, high electrical conductivity, and self-induction.

d) Of particular interest are the data on magnetic-field variations before and during flares. It is accepted that the flare energy is a realization of the magnetic-field energy in the corona of an AR (due to reconnections, current-layer breakdown, etc.), where the main flare phenomena take place. This should also affect the change in the structure of the photospheric magnetic field measured (abrupt changes in horizontal gradients, simplification of the overall structure, etc.). Attempts to elucidate the significant changes in the measured photospheric field of ARs during flares have failed to yield unambiguous results. This is due first to the incompleteness of factual information and to the difficulty in extracting it; usually, the photospheric B_{11} component alone is measured in ARs, whereas significant changes during flares may be expected also in the B_1 component, which is measured, if at all, with a sensitivity one-and-one-half order of magnitude lower than that for the B_{11} component. Direct measurements of the magnetic field in flare areas (in the corona) have been impossible so far. Nonetheless, from indirect determinations of the structure of chromospheric and coronal phenomena (arch and loop systems), it has proved possible to establish that during flares no significant field variations occur [Rust, 1973, 1974; Vorpahl et al., 1975]. The magnetoplasma loop structures of the corona (observed from X-ray patterns and in the emission lines of the corona and transition zone in the far UV) practically retain their geometry during flares. It is only their emission that increases (beginning from their tops) at that time. A similar result has been obtained for chromospheric arch systems (AFFS) [Korobova et al., 1976], from which it has also been possible to establish the conservation of the relative rotation of the arches with the increasing height of their summits. This corresponds to the "magnetic shears" constancy, which is possible when the whole current system in an AR is preserved. Finally, changes in the position of "quiet" hydrogen filaments, which are situated

along the line $B_{11} = 0$ and which reflect the structural variations of the magnetic field immediately before and after flares, also have the character of rather rapidly (7.5 m) attenuated pulses. (This pulsed regime of changes in $H\alpha$ -filaments before and during flares can be established only from a series of $H\alpha$ filter-diagrams obtained using an IPF with a narrow ($\Delta\lambda = 0.25 \text{ \AA}$) band moving along the $H\alpha$ contour.)

As in the photospheric magnetic field, the field variations in the flare regions differ little from the ordinary field variations due to AR evolution. To put it more exactly, during flares one observes relatively fast ($t \approx 5$ to 10 m), pulsating (rapidly restored), variations in the magnetic field that occur against the background of the "ordinary" evolutionary (slow) variations in the AR field structure.

Until now it has been impossible to establish with certainty what changes in the structure and magnitude of the magnetic field precede flares or accompany them. At this writing it is clear only that the above-listed evolutionary changes in fields are somehow associated with the origination of a preflare situation. To determine under what real, qualitative and quantitative field changes in AR conditions large flares occur, one should advance a working flare model. The subsequent directed experiments will enable the most promising model to be chosen. A method for quantitative flare prediction should, of course, be based upon a realistic model for flares and preflare situations in ARs.

3. RELEASE OF FLARE ENERGY

It is commonly believed that a flare is a "point" explosion and that the entire (or almost entire) energy of flares (even large ones) is liberated during a very short time (≈ 10 to 10^2 s). The variety of flare phenomena is the consequence of the original (occurring in the initial "flash-phase") "instantaneous" energy release. However, some ground-based and satellite-borne observation data are at variance with such a conception [Vorpahl et al., 1975; Withbroe, 1978; Rust, 1974]. An especially convincing proof that in powerful solar flares energy is released during a long time is the observation of γ -lines in two proton flares of August 1972 [Chupp et al., 1973]. According to the observational conditions onboard spacecraft OS07, during flares γ -lines were recorded 4.08 from the onset to the maximum (when the satellite was in the shade of Earth) and 7.08 after the maximum practically during the entire $H\alpha$ flare. (Here γ -lines with energies of 0.5, 2.2, and 4.2 MeV are meant, which arise, respectively, in the positron and electron annihilation and in the excitation of the O and C nuclei under the bombardment by powerful fluxes of particles continuously accelerated during flares.)

A more detailed examination of optical and radio observations of a number of flares [Ishkov et al., 1978] has shown that large flares are composed of a succession of discrete (often overlapping) components of "elementary flares." The authors have been able to establish some of the characteristics of these discrete components. Optically, this is a local

short-duration, abrupt brightening of parts of flocculi with subsequent chromospheric eruptions (surges or AFFS) in the adjacent regions. In the radio band, to these elementary flares, there correspond discrete outbursts (radio outburst components of the types IV and IV_{dm}). The elementary, short-duration (from several seconds to tens of seconds) outbursts in X-rays are grouped in time around the "elementary flares." Thus a flare model should explain the prolonged (during the entire flare, i.e., 1 or 2 h for very large flares) process of discrete energy release. This energy is not only spent on emission; it also determines the long-continued dynamical flare phenomena (arch and loop systems, surges, oscillations, and deformations of the "quiet" filaments in ARs) in the chromosphere and corona (including the coronal flare "transients"). The total energy spent on these long-continued dynamical flare phenomena in the chromosphere and corona (including the energy spent to the ejection into the interplanetary medium of geoeffective corpuscular fluxes) is more than an order of magnitude higher, as estimates have shown [Svestka, 1976], than the combined energy of all kinds of flare emissions. For the largest flares, the upper limit on the total flare energy is estimated to be between 5×10^{32} and 5×10^{33} ergs. When considering the possibility of the preflare accumulation of that energy in the magnetic field of the corona of an AR, one should remember that in large flares about 10^{16} to 10^{17} g of solar matter escape from the AR into the interplanetary medium and to the coronal transients only. But the amount of the solar substance participating in large flares is apparently still greater, because the above estimates have ignored the flux of substance, which descends to the AR photosphere and which exists for a long time during the flare.

Can such amounts of energy and matter be stored and released during large flares in the AR corona? Even the over-estimated values for the whole amount of substance in the AR corona (taking into account the increased density in coronal condensations) do not reach 10^{16} g. During large flares the substance of the AR corona is far from being ejected completely; on the contrary, (judging from the intensity of emission) it is substantially augmented during and after an optical flare. If before the onset of a flare there had been a process of substantial accumulation of substance in the AR corona, the amount of which exceeded the "norm" by at least an order of magnitude, it would have led inevitably to the yet unobserved hundredfold preflare increase in emission intensity. Therefore, the "flare" substance should be supplied continuously or discretely to the AR corona during the whole flare.

The possibility of the preflare accumulation of the above amount of energy in the nonpotential part of the magnetic field of the AR corona has been discussed by several authors [Sturrock et al., 1976]. Irrespective of the particular mechanism of accumulation and subsequent utilization of the energy released during a flare, there are obvious difficulties associated with the fact that the "plasma factor" $\beta = 8\pi P/B^2$ is much less than unity in the corona. An increase in energy in the magnetic field of a helicon structure of the plasma filament that passes from the photosphere to the corona (e.g., in twisting the photospheric "foundations") has been discussed recently [Parker, 1976]. The penetration of such a filament into the corona leads to its expansion, enhancement of currents, and appearance of high

instability to small-scale disturbances. In the case of the force-free magnetic-field structure in the corona (which is quite probable) the restrictions on the energy accumulation are still more severe. As calculations have shown [Jockers, 1976], for a local force-free magnetic field there is a well-defined upper limit on the toroidal component energy (and therefore, the total field energy) in solar and stellar atmospheres, which is considerably lower than the flare energy indicated above. Moreover, because of the integral character of current systems of the force-free magnetic field, it is possible to obtain not more than 10% of the total field energy during the flare time ($< 10^3$ s). This means that the preflare energy stored in the field should exceed by another order of magnitude that spent during the flare, which is hardly possible. It will be noted that here we discuss the magnetic field energy in a large volume of the entire coronal condensation. The difficulties associated with the expenditure of energy in a thin (≈ 1 cm) current layer, to which a significant amount of adjacent plasma should be transported with the field, have been discussed in a recent monograph [Kaplan et al., 1977]. When to these theoretical difficulties one adds the above-mentioned observational facts (changes in the coronal field structure, which have not yet been established even for large flares and which should accompany the coronal field annihilation, etc.) it becomes clear that to overcome these difficulties one should assume that the flare energy stored locally in the photosphere is supplied to the AR corona during the occurrence of all flare phenomena. Such an assumption, which has already been discussed in the literature, is also suggested when considering the large material of flare observations in the $H\alpha$ emission and X-rays and in the range λ 3835 Å [Zirin, 1978] from the character of excitation during the flare of the narrow lines of rarely-occurring elements and from the numerous $H\alpha$ observations of flare evolution upon the limb. The consideration of nonlinear effects (the development of abnormal thermal and electrical conductivities in the downward propagation of a flux of "heating" electrons towards the chromosphere) also leads to the necessity of looking for a mechanism of transport of the flare energy and substance from the photosphere to the corona of the AR.

4. TRANSPORT OF FLARE ENERGY

Consider the following scheme for energy accumulation in a local magnetic field of the photosphere with a subsequent transfer of this energy to the AR chromosphere and corona. In complex flare-active regions containing sunspot groups of the magnetic classes " δ ", " γ ", or " $\beta\gamma$ ", where, as a rule, there occur large flares and where, as has been mentioned above, the evolutionary transition of the magnetic field to the force-free configuration takes place, i.e., everywhere (or at least within the zonal region) $\text{rot } \mathbf{B} = \alpha(r, t) \mathbf{B}$. However, at the photospheric level (and still more so, within the subphotospheric layers of ARs), where the plasma factor $\beta = 8\pi P/B^2 \geq 1$ at a finite conductivity σ , the existence of a stable force-free field is possible if a special type of hydrodynamical motion takes place: $\text{rot } \mathbf{v} = \alpha(r, t) \mathbf{v}$ (i.e., the so-called Gromeko-Beltrami type motion). According to Sreenivasan and Thompson (1974), in this case, the

condition for the preservation of the force-free structure is the simultaneous fulfillment of two relationships:

$$\text{rot } (\bar{\mathbf{B}} \cdot \nabla) \mathbf{v} = \alpha (\bar{\mathbf{B}} \cdot \nabla) \bar{\mathbf{v}} \quad (3)$$

and

$$\text{rot } (\bar{\mathbf{v}} \cdot \nabla) \bar{\mathbf{B}} = \alpha (\bar{\mathbf{v}} \cdot \nabla) \bar{\mathbf{B}} .$$

Together with the induction equation (at $\alpha(r, t) = \text{const}$), one can obtain from (3) the following expression:

$$\frac{\partial}{\partial t} \left(\frac{B^2}{2} \right) + B^2 (\nabla \mathbf{v}) = \bar{\mathbf{B}} \{ (\bar{\mathbf{B}} \cdot \nabla) \mathbf{v} \} - \frac{\alpha^2}{\mu \sigma} B^2 = Q , \quad (4)$$

where μ is the magnetic permeability. At $Q = 0$, equation (4) expresses the law of conservation of the magnetic-field energy. When $Q > 0$, the magnetic energy increases at the expense of the kinetic energy, whereas at $Q < 0$ it decreases (with the increasing kinetic energy); we have

$$\alpha^2 \gtrless \mu \sigma \frac{\bar{\mathbf{B}} \{ (\bar{\mathbf{B}} \cdot \nabla) \bar{\mathbf{v}} \}}{B^2} \quad \left\{ \begin{array}{l} > \text{field increases} \\ < \text{field decreases} \end{array} \right. . \quad (5)$$

The case of periodic changes in Q is also possible. This leads to an oscillatory regime for the field and velocities in the force-free magnetic field region and for the Gromeko-Beltrami motions. The relative preflare stationarity of the force-free structure imposes, according to Kruger [1976], a restriction upon the upper limit for the values of the parameter $\alpha < 0.45$. The lower limit (apart from the trivial $\alpha = 0$ implying that the nonpotential part of the field is absent, which is out of the question) can be estimated by substituting in (5) the possible values for the quantities in the right-hand side. Then $\alpha \gtrsim 0.01$. Thus, for the stationary force-free magnetic field, the modulus limit will be $0.01 < \alpha < 0.45$.

We shall consider our problem of determining the oscillatory regime in ARs under the following conditions:

a) The magnetic field in the AR area under study is horizontal; there arise only transverse disturbances. This corresponds to the above condition of appearance of the flare foci near the zero line ($B_{11} = 0$), i.e., close to AR filaments, where $B \neq 0$.

b) Taking into account the increase in temperature and ionization degree with depth h , we find that at a certain value h_0 , for which $kT \gtrsim \chi$ (χ being the ionization potential for hydrogen and helium), there results a "complete frozenness." In the standard model for the Sun, we have $h \ll 1$, where 1 is the dimension of the region characterized by $B_{11} = 0$ and $B_1 \neq 0$. (When $h \lesssim 5 \times 10^8$ cm, $1 \gtrsim 5 \times 10^9$ cm, which is in accord with the observations of the field in the vicinity of the "zero" line). We consider the region of the regime under investigation to be flat.

The peculiarity of the motions in the force-free magnetic field of the photosphere that we are considering is that all macromotions of matter are exercised about the force lines of the field. The poloidal velocity component is directed along the toroidal field component, and the toroidal

velocity component is directed along the poloidal field component. In such a case (with the condition that the field is force-free), the averaged energy values for each respective component are equal to one another. Such a peculiar "rigid" coupling of the field with the motions exercised in a layer of thickness h , where

$$\beta \frac{8 \pi P}{B^2} \geq 1,$$

makes it possible to reduce our problem to that of plasma oscillations in a high magnetic field. We consider the long-wave ($\lambda \geq h_2$) transverse field disturbances. Within the subphotospheric layer there occur variations in the field, density, and temperature. This means that at the wavelength λ the phase velocity of disturbance propagation varies; i.e., we can, while considering small disturbances, reduce the determination of non-linear plasma oscillations in the magnetic field with dispersion to the familiar problem of gravitational waves in shallow water [Karpman, 1973]. For small disturbances, i.e., for

$$\delta \bar{B} = \frac{\bar{b}}{\bar{B}} \ll 1, \quad \delta \bar{v} = \frac{\bar{v}}{\bar{v}} \ll 1,$$

if at the base of the layer

$$r = h_0, \quad b_0 = v_0 = 0$$

and within the layer $\bar{K}(r)$ is the wave vector (a function of distance) $r \lesssim \lambda$, equation (4) is transformed according to a previously considered scheme [Karpman, 1973] (after eliminating terms quadratic in \bar{b} and \bar{v}) to the following set of equations:

$$\left. \begin{aligned} \frac{\partial \bar{v}}{\partial t} + (\bar{v} \nabla) \bar{v} &= - \frac{\bar{B}}{4\pi\rho} \nabla b \\ \frac{\partial \bar{b}}{\partial t} + \nabla(\bar{B} \cdot \bar{v}) + 2\varepsilon \nabla \Delta \bar{v} &= 0 \end{aligned} \right\} \quad (6)$$

Here ε is the dispersion length for the transverse MHD disturbances, which is given by

$$\varepsilon = C_A(r) / \sqrt{2} w_{0,1}(r) \quad (7)$$

where $C_A(r)$ is the Alfvén velocity as a function of depth r ; $w_{0,1}(r)$ is the Langmuir frequency in the subphotospheric plasma.

The set (6) is a formal analog of nonlinear equations for gravitational waves in shallow water in the Boussinesque approximation. Since the layer thickness h_0 is finite, for one-dimensional transverse field disturbances in coordinate r , we obtain the discrete oscillation spectrum desired:

$$\begin{aligned}\bar{b} &= \sum_j b_j \exp i [(k_j Z) - w_j(k)t] \\ v &= \sum_j v_j \exp i [k_j (r - \lambda/2) - w_j(k)t] \quad j = 0, 1, 2, \dots\end{aligned}\tag{8}$$

and the dispersion equation of the type

$$w_j(k) = C_A(r)k_j - \varepsilon k_j^3 \tag{9}$$

In the adopted approximation for the oscillatory regime of the subphotospheric layer under study, the steady-state solution of (8) goes over to a system of isolated waves (solitons). To emphasize the MHD nature of these waves, we shall refer to them as "macromagnetic solitons." They represent local regions with interconnected (with respect to oscillations of the components B_{\perp} of the field and \bar{v}_{11} of the velocity) increase and subsequent decrease of variable intensity amplitudes. Within the h layer there should exist inhomogeneities in field and velocity. These are the discrete supergranular cells of the AR, which are observed on the "surface" (in the photosphere). These discrete structures have their own periods of oscillation. (In the photosphere, they reach about 300 s) Because of the nonlinear properties of the medium, there should take place the fragmentation of the initial energy proceeding in a period of about 3,000 s (oscillations of the entire AR taken as a whole) with the predominant increase in the amplitudes corresponding to oscillations of one or several discrete magnetoplasma structures. This should result in the appearance of a train of damped nonlinear waves, macromagnetic solitons. An analogous process has already been treated theoretically [Benzhemen, 1970], and the train character of nonlinear gravitational waves in shallow water has been established. It can be readily seen that the energy flux proceeding at the Alfvén velocity v_A of about 10^6 cm/sec, is, for the amplitude $b_{\perp} \sim 3 \times 10^{23}$ G, wavelength $\lambda \approx 3 \times 10^9$ cm and period $t \approx 10^3$ s, equal to about 4×10^{31} ergs. If, in a macromagnetic soliton, we have $\langle \varepsilon_{\text{magn.}} \rangle = \langle \varepsilon_{\text{kin.}} \rangle$, then, for the same wave parameters, the estimated upward flux of substance from the photosphere reaches 10^{18} g. During large flares of this kind, solitary train disturbances (with amplitudes decreasing relative to that of the soliton with which the onset of the flare may be associated) may occur in sequences (up to ten, depending on the disturbance energy accumulated at the "base" of the layer, which determines the entire preflare situation in the AR). Evidently, this is quite sufficient to ensure the energy release and "substance" in large flares.

Up to now, we have not discussed the dissipative processes and the questions concerning the transfer of soliton energy to the region of the coronal flare. These problems have already been examined [Sokolov et al., 1977; Kosovichev and Popov, 1978] and the results obtained may be regarded as quite consistent with the model under review. In the region of the macromagnetic soliton (local increases and decreases of field and velocity), two essentially dissipative processes may be operative. Ascending above the photosphere, the soliton magnetoplasma forms a skinning layer with filamentary currents. The dissipation of the latter leads to heating and subsequent emission, which is seen on the limb as a "swelling" of the

flare region "with brightening". The same increase in the velocity (field) in the soliton acts as a "piston", exciting in the chromosphere and corona a system of ascending shock waves. The gas dynamical flow thus produced consists of a succession of shock waves separated by the descending "cold plasma". Calculations have shown that, in this way, about 4×10^{30} ergs of energy are removed from a single soliton to the corona (at $\lambda = 3 \times 10^9$ cm) and about 10^{16} g of the substance. During a flare, the whole system ($n \geq 10$) of discretely traveling solitons may supply to the corona the amounts of energy and substance that will be sufficient for all flare phenomena to develop. As a consequence of these powerful dissipative processes, the macromagnetic solitons will not appear directly in the solar atmosphere of an AR.

5. QUANTITATIVE PROBABILISTIC FLARE PREDICTION

The scheme just considered, despite its understandable incompleteness, corresponds qualitatively to the main observational data listed above. On the other hand, it contains the idea of the single-parameter representation of evolution; only when a certain threshold value of the soliton amplitude is reached will a flare process occur. Thus, for $b \leq 1$ to 10 G., the energy flux is considerably lower than the flare energy. In this case, one should observe only the preflare heating of the AR by weak damped sinusoidal oscillations of field and matter rather than a curtailed wave front (with transition to "overturning", which corresponds to the onset of the flare). Using these concepts and taking into account that the preflare evolution of the magnetic field of ARs corresponds to a Markov process (see part I), we formulate the quantitative probabilistic flare prediction as the determination of the threshold effect of the AR evolution over the prediction interval (c, d) . If $a(\xi_0)$ and $d(\xi_0)$ are, respectively, the coefficients of drift and diffusion of the parameter ξ at the moment of the preflare state, t_0 , the predicted flare probability P_{cd} is given by the Pontryagin equation [Tikhonov and Mironov, 1977]:

$$\frac{\partial P_{cd}}{\partial t} = a(\xi_0) \frac{\partial P_{cd}}{\partial \xi} + d(\xi_0) \frac{\partial^2 P_{cd}}{\partial \xi^2} \quad (10)$$

It is then assumed that the probability for the $P(\xi_{t_1})$ state where t_1 is the initial moment of the prediction interval (c, d) , has already been determined in the first stage of the prediction (see part I). The solution of equation (10) has the form [Tikhonov and Mironov, 1977]

$$P_{cd} = 1 - \sum_k C_k A_k(\xi_0, \gamma_k) \exp(-\gamma_k^2 t) \quad , \quad (11)$$

where γ_k and C_k are constants determined by the initial (at $t = t_1$) conditions and normalization; $A_k(\xi_0, \gamma_k)$ are the eigenvalues of the solution of the characteristic equation. To use the prognostic equation (10), one should determine from a series of observations the most probable values for the coefficients of drift $a(\xi_0)$ and diffusion $d(\xi_0)$ in the periods immediately preceding large flares, i.e., at

$$\xi_t = t_1 = \xi_0.$$

The proposed model and scheme for the quantitative probabilistic flare prediction have been constructed to assure correspondence with the principal phenomenological properties of the preflare AR evolution and the main flare energy characteristics. The questions of how flares develop at different levels in the AR atmosphere, the problem of the acceleration and escape from an AR of the solar cosmic rays, etc., have been deliberately omitted. From the standpoint of solving the flare prediction problem it appears to us that it is more important to understand the class of problems discussed herein, almost traditionally disregarded in the literature on solar flares. Finally, it should be noted that the proposed scheme may be verified experimentally (establishment of characteristics of local field and velocity disturbances in the AR photosphere (near the line $B_{11} = 0$) and their relation with the sites of flare development at all levels of the AR atmosphere, etc.). The degree of reality of the proposed models (for AR and flare evolution) will also determine the practical value of the probabilistic scheme for solar activity prediction.

6. REFERENCES

- Benzhemen, T.B. (1970): Instability of periodic wave trains in nonlinear systems with dispersion. In: A Nonlinear Theory of Wave Propagation, 83-104.
- Chupp, E.L., E.J. Forrest, P.P. Higbie, A.N. Suri, C. Tsai, and P.P. Dunphy (1973): Solar gamma ray lines observed during the solar activity of August 2 to August 11, 1972. Nature, 241:333.
- Ishkov, V.N., E.I. Mogilevsky, and V.P. Nefed'ev (1978): On the correspondence between the optical and radio phenomena in the eruptive phase of the proton flare of August 4, 1972. Solar Data, 1:72.
- Jockers, K. (1976): Upper limits in the toroidal component of force-free magnetic fields in stellar atmospheres in the context of solar and stellar flares. Solar Physics, 50:405.
- Kaplan, S.A., S.B. Pikel'ner, and V.N. Tsitovich (1977): Plasma Physics of the Solar Atmosphere. Nauka Publishers, Moscow.
- Karpman, V.I. (1973): Nonlinear Waves in Dispersive Media. Nauka Publishers, Moscow.
- Korobova, Z.B., V.N. Ishkov, and E.I. Mogilevsky (1976): Eruptive chromospheric phenomena observed during the flare of August 2, 1972. In: Physics of Solar Activity.
- Kosovichev, A.G., and Uy.P. Popov (1978): Some features of shock wave propagation in the solar atmosphere. Preprint N 73 IPM, Acad. Sci. USSR, Moscow.

- Kruger, J. (1976): General stability analysis of force-free magnetic fields. J. Plasma Physics, 15:15.
- Parker, E.N. (1976): Basic properties of magnetic flux tubes and restrictions on theories of solar activity. Astro-phys. and Space Sci., 44:107.
- Report UAG, 24; 26; 28, etc. WDC-A Solar-Terr. Physics.
- Rust, D.M. (1973): Analysis of the August 7, 1972 white light flare: changes in the magnetic and velocity fields. Solar Physics, 33:205.
- Rust, D.M. (1974): Observations of flare-associated magnetic field changes. In Flare-related magnetic field dynamics, 243:267.
- Sokolov, V.S., S.S. Katsnelson, A.G. Kosovichev, and V.S. Slanin (1977): Skinning process stability of the magnetic field in the solar active regions. Solar Physics, 51:293.
- Sreenivasan, S.R., and D.L. Thompson (1974): Velocity fields which preserve cylindrically symmetric force-free magnetic fields. Physica, 78:321.
- Sturrock, P.A., P.J. Baum, J.M. Beckers, C.E. Newman, E.R. Priest, E.R. Rosenberg, D.F. Smith, and D.G. Wentzel (1976): Report on the solar physics-plasma physics workshop. Solar Physics, 46:411.
- Svestka, Z. (1976): Solar Flares. D. Reidel
- Tanaka, K., and Y. Nakagawa (1973): Force-free magnetic fields and flares of August 1972. Solar physics, 33:187.
- Tikhonov, V.I., and M.A. Mironov (1977): Markov Processes. "Soviet Radio" Publishers, Moscow.
- Vorpahl, J.A. (1973): Flares associated with emerging flux regions. Solar Physics, 28:115.
- Vorpahl, J.A., E.G. Gibson, P.V. Landecker, M.L. Mackenzie, and J.H. Underwood (1975): Observations of the structure and evolution of solar flares with a soft X-ray telescope. Solar Physics, 45:199.
- Withbroe, G.L. (1978): The thermal phase of large solar flares. Astro-physical J., 225:614.
- Zirin, H. (1978): Studies of solar flare using optical, X-ray and radio data. Solar Physics, 58:95.
- Zvereva, A.M. and A.B. Severnyi (1970): The magnetic fields and proton flares of July 7 and September 2, 1966. Izvestiya Krymskoi Astrofizicheskoi Observatorii, 97:56-57.

FORECASTING FLARE ACTIVITY BY PATTERN RECOGNITION TECHNIQUE

V. A. Burov
Institute of Applied Geophysics
Goscomhydromet, Moscow, U.S.S.R.

J. W. Hirman and W. E. Flowers
Environmental Research Laboratories, NOAA
Boulder, Colorado 80303, U.S.A.

Results of the pattern recognition technique applied to problems of forecasting flare activity of solar active regions on the next day are considered. Verification score of the obtained solution rule is more than 90%.

1. INTRODUCTION

The forecasting of flare activity is one of the most important and most complicated problems of solar activity forecasting. The synoptic method is virtually the only method presently used for forecasting. The existence of some internal relationships between various phenomena is the basis of this method. Since quantitative characteristics of these relationships are unknown or known only approximately, subjectivity (experience and forecaster's skill) is a great factor in forecasting, and results in inadequate predictions by different forecasters from the same original data.

The absence of objective criteria and formal procedures of forecasting is an inherent drawback of this method. The need for an objective technique for flare forecasting has long been recognized. A pattern recognition technique for flare activity forecasting, i.e., a technique constituting an objective approach to forecasting, is presented here.

2. DATA FOR THE TECHNIQUE

The original information (20 parameters in all) is a table of daily observation data, characterizing the active regions from Jan. 1, 1977,

until Aug. 1, 1977. The proper data are the observations of the active regions in white light, H-alpha, radio, and X-ray wavelength in a coded form. The list of the parameters and the key-code are given in Table 1. Four parameters (interaction with another region, radio bursts and/or sweep, proton events, and large flares have been excluded on the basis of a preliminary visual check of the data. It is possible that these parameters may be informative, but their significance hardly changes from region to region in the given period of time and in terms of the chosen codification. The original codes of the remaining 16 parameters were changed. Changes (data compression) were based on the following:

- Physical idea about the evolution of the active regions and solar flare.
- Formal conceptions of the expediency of data compression, if this parameter value (grade) occurs infrequently, it unites with the neighboring grade into a larger one.

The new code is that shown in Table 1. In the period of time studied there were too few events of M-class for the results to be statistically significant. So the problem is formulated as follows: to predict whether, within the coming 24 hours, flares of C-class and larger will occur in a given active region.

3. FIRST STAGE OF THE SOLUTION

The problem was solved in several stages by the pattern recognition algorithm, "TOPOL" (Burov, 1976). In accordance with the recommendations of the algorithm in teaching, 10 vectors (cases) of the first class and 32 vectors of the second class were used at the initial stage. The first class comprised the active regions, where within the coming 24 hours flares of C-class and larger were observed, and the second class comprised active regions without flares within the next 24 hours.

The selection that was examined contained 16 vectors of the first class and 94 of the second class. Although there were about 40 events of the first class, complete information (about all 16 parameters) exists for only 26 events. That is why at this stage of the problem solution only 26 vectors of the first class were used.

Accuracy of the determining rule evaluated according to the size of risk function (Berlyand et al., 1978) and obtained by the independent examining consequence (i.e., forecasting) was $R(d) = 0.11$, which corresponds to a verification score of 89% and is 38% for the first class and attains a level of 96% for the second.

Table 1.--Parameters and key codes.*

No.	Parameter	Old code	New code
1	Spot class (C)	0 ----- 0 1,2 ----- 1 3 ----- 2 4,5 ----- 3	
2	Magnetic class (M)	0 ----- 0 1 ----- 1 2 ----- 2 3,4,5 ----- 3	
3	Magnetic field strength (H)	0,1 ----- 0 2 ----- 1 3,4 ----- 2	
4	Magnetic gradients (G)	0,1 ----- 0 2,3,4 ----- 1	
5	Sunspot dynamics (D)	0 ----- 0 1,2,3 ----- 1	
6	Stage of development (S)	0 ----- 0 1 ----- 1 2 ----- 2 3,4,5 ----- 3	
7	Leader emerged (L)	0 ----- 0 2 ----- 1 3,4,5 ----- 3	
8	Relationships with nearest sector boundary (B)	0 ----- 0 1 ----- 1 2,3,4 ----- 2 5,6,7 ----- 3	
9	Plage compactness (K)	0 ----- 00 1,2 ----- 01 3 ----- 10 4,5 ----- 11	
10	Main NL orientation (O)	0 ----- 00 1 ----- 01 2,3,4 ----- 11	
11	Neutral line complexity (N)	0 ----- 0 1 ----- 1 2,3,4 ----- 2	
12	Neutral line temporal changes (N)	0 ----- 0 1,2 ----- 1	
13	Associated filament (F)	0 ----- 0 1,2,3,4 ----- 1	
14	Bright points (P)	0 ----- 0 1 ----- 1 2,3 ----- 2	
15	Emerging flux (E)	0 ----- 0 1,2,3,4 ----- 1	
16	Largest flare (I)	0 ----- 0 1,2,3 ----- 1	

* From Hirman and Flowers (1977).

4. SECOND STAGE OF THE SOLUTION

At the second stage of the solution a hierarchy of parameter importance was established to exclude the least informative parameters from the input data.

Reducing the number of parameters is extremely desirable because some are absent at the moment of the operative forecast for technical reasons. We emphasize (Burov, 1976; Berlyand et al., 1978) that the evaluation of the relative importance of the information and, correspondingly, the hierarchy obtained, may change, depending on the algorithm used and the method of evaluation, insofar as their change causes the change of space metric.

In the problem being solved here, the parameter importance is evaluated according to the change in quality of the determining rule with the exclusion of the considered parameter from teaching and examination.

It should be noted that the verification score of the second class is significantly high (96%), and we are, to a greater extent, interested in improving the quality of the first class.

If we take into account only part of the correctly classified first class vectors, all parameters may be divided into four groups in order of decreasing importance:

1. P, B;
 2. N, O, E;
 3. D, M, C;
 -
 4. H, G, S, L, K, V, F, I.
- (A)

Symbols are given in Table 1, and group 4 parameters do not improve recognition quality.

If we take into account summary (for the first and the second classes) recognition quality, then the hierarchy looks like this:

1. B, V, F;
 2. P, N, D, K;
 3. S, O, L, H;
 -
 4. G, C, M, E, I.
- (B)

The evaluations obtained may be used to exclude some of the parameters from the mass of original data. Since we are to a greater extent interested in the first class, it is natural to take the set (1+2+3) from (A) variant. It should be noted that variant (1+2+3) (A) comprises half of the parameters. The determining rule accuracy obtained by using only these 8 parameters of the original 16 was as follows:

In the forecast (variant d)-83% (60% on the first class and 88% on the second), and in the epignosis (i.e., when examining consequence is chronologically before the teaching material) it is 84% (variant β) (70% on the first class and 88% on the second).

The addition to these parameters of information about F and V (i.e., those missing from group I variant (B) did not improve the recognition quality. Reduction of the original parameter number made it possible to increase the number of vectors in the first class to 34, and in the second class to 183. Then the most frequently occurring signs from variants were combined. The recognition quality, obtained by using these signs on 217 vectors, is characterized by the following figures: general-89%; in the first class-82%; in the second-90%.

5. FINAL STAGE OF SOLUTION

The essential meaning of the determining rule in such a procedure is cumbersome, since voting (i.e., relating a vector to i class) may be done in many ways. It should be emphasized that at the present stage the main problem is not to reveal the essential meaning of the determining rule, but rather to find the maximum level of class division, which is more essential for practical forecasting. However, we may try to reveal the essential meaning by a slight algorithmic change and by simplifying the rule formation procedure; having taken the signs chosen at the last stage, and having analysed the examination results, we may be convinced that there are second-class signs in almost all the vectors of the second class, and that there are practically none in the first class.

First-class signs also occur in the second-class vectors. In other words, second-class signs correspond to the definition "sufficient," and first-class signs correspond to the definition "necessary." Then by considering any second-class sign to be "sufficient," and any first class sign "necessary," active regions may be classified according to the following rule: Within the coming 24 hours no flares of C-class or larger will occur in a given active region, if any of the following four conditions is satisfied:

- No spots in the active region.
- No kinks of the neutral line, bright points, and no isolated pole in region, no AFS present or new EFR emerges within existing spot group or within 5 degrees of it.
- Region is located within 30 degrees of the Hale boundary; no isolated pole in region; no AFS present or no new EFR emerges within existing spot group or within 5 degrees of it.
- No bright points, no isolated pole in region, no AFS present or new EFR emerges within existing spot group or within 5 degrees of it, no dynamics in the group.

If none of these conditions is satisfied, a flare will occur, if any of the following conditions is satisfied:

- Magnetic classification of β , $\beta\gamma$, or δ , and there are more than three kinks on the neutral line.
- The neutral line is oriented to E-W, east-west, hairpin, circular or reverse polarity region, and there are bright points along the neutral line or fluctuation.
- There are bright points along the neutral line or brightness fluctuation, and more than three kinks in the neutral line.

If in the active region there are no "sufficient" or "necessary" signs we may expect a flare only in the case where within 24 hours at least one flare has occurred in the region and the class of the group in Zurich classification modification exceeds 2 according to Table 1.

Examination of 685 vectors on the material collected Aug. 1, 1977-Dec. 30, 1977, by such a scheme gave the following results: general verification score is 92%; in the first class it is 52%, in the second, 96%.

Verification of such a rule on the whole material of 1977 (except those cases when a flare occurred on the day of a group appearance, or when information was lacking on most parameters) gave the following results for 1,358 events: general verification score is 94%; in the first class it is 56%, in the second, 96%.

It should be noted that verification score of climatological forecast is 92%.

6. ACKNOWLEDGMENTS

The authors express their gratitude to Dr. G. S. Ivanov-Holodniy, whose participation made possible the implementation of the present work, as well as to N. I. Kantserskaya for her assistance in computer calculations.

7. REFERENCES

Berlyand, B. O., V. A. Burov, and N. N. Stepanyan (1978): Izvestiya Krymskoy astrofizicheskoy observatorii, t. 60.

Burov, V. A. (1976): Prognozirovanie nekotorykh evolyutsionnykh karakteristik aktivnykh oblastey, v sb. Evolutsiya aktivnykh oblastey. Trudy VIII Mezhdunarodnogo konsultativnogo soveshchaniya po fizike Solntsa. Irkutsk.

Hirman, J. W., and W. E. Flowers (1977): An objective approach to region analysis for flare forecasting. Space Environment Laboratory, Boulder, Colorado.

Vapnik, V. N., and A. N. Chervonenkis (1974): Teoriya raspoznavaniya obrazov. M., Nayka.

D. DIAGNOSIS OF SOLAR FLARE ELECTROMAGNETIC RADIATION
AND SHORT-TERM PREDICTIONS OF PARTICLE RADIATION

APPLICATION OF INTEGRATED RADIO BURST FLUXES TO THE
PREDICTION OF SOLAR ENERGETIC PROTON FLUX INCREASES.

William R. Barron
Space Physics Division
Air Force Geophysics Laboratory
Hanscom AFB, MA 01731

Pradip Bakshi
Physics Department
Boston College
Chestnut Hill, MA 02167

Solar radio burst integrated fluxes and related energetic solar protons were studied. It was found that the time-frequency integrated radio fluxes were best related to the peak > 10 MeV proton fluxes when they were appropriately adjusted for the solar longitudinal position of the related flare. In particular, the longitudinal correction e^{nA} , where A is the angular distance in radians between the flare location and a standard reference longitude A_0 , gave the best correlations ($r \approx 0.82$) with $n=2$ and $A_0=57^\circ\text{W}$.

The study of solar flares and their related radio burst and particle emissions has long occupied the attention of solar-terrestrial physicists. With the advent of earth satellites a bit more than two decades ago, the proliferation of information about the earth, its environment and the interaction of solar activity upon both has been quite astounding. We will look here at two quantities of solar emission and a relationship between them.

In 1967 it was reported by Castelli et al (1) that when a solar radio burst occurred, which had a U-shaped peak flux spectrum, there was generally an increase in the flux of energetic protons from the sun into the ionosphere of the earth. The larger increases of solar energetic protons were usually associated with the occurrence of polar cap absorption events (PCA's) and increases in auroral activity. The U-shaped radio spectrum was found in the 1 m to 1 cm interval of the radio spectrum, with the minimum of the U found in the vicinity of $\lambda = 10\text{-}30$ cm. The magnitude of the peak radio fluxes at the high side of each rising

arm of the U is of the order of 1000 solar flux units ($1 \text{ sfu} = 10^{-22} \text{ W M}^{-2} \text{ Hz}^{-1}$) and larger.

The solar radio burst data for sunspot cycle 20 has been studied to see whether or not it was able to give some information as to the nature of the particle emissions associated with the burst (2, 3). It was found that the width of the U-shaped radio spectrum was related to the hardness of the peak flux vs energy spectrum of the emitted protons in the > 10 to > 100 MeV energy interval. The finding was that, if the radio-U was wide, the particles showed a hard energy spectrum; i. e., there were relatively more of the higher energy particles emitted. Likewise, if the radio-U was narrow, there were relatively fewer of the higher energy particles.

The prediction of the peak proton flux by means of the radio flux from the associated flare has generally been attempted with the peak radio flux or the time integrated flux of the radio burst at only one frequency of observation (4, 5, 6, 7). Straka (4) attempted an analysis at five of the frequencies observed at the AFGL Sagamore Hill Radio Observatory, taking them one at a time. Recently (8) the integrated radio fluxes at these same five frequencies, 8800, 4995, 2695, 1415, and 606 MHz, were integrated together and the combined frequency-time integrated flux values were tested as a prediction of > 10 MeV proton fluxes. The correlation of the particle peak flux with the integrated radio flux was about 0.75. When the particle peak fluxes were multiplied by a correction factor of e^{3A} (5) the correlation improved to 0.80. The quantity A is the angular distance, in radians, from the longitude of the flare involved to the foot point of the magnetic field lines connecting the sun to the earth, taken to be 57° West longitude in this consideration. As shown in Figure 1a, the factor of e^{NA} was tested to find what value of N would provide the best correlation. It was found that the best correlation, 0.82, was obtained for $N=2.0$. Figure 1b shows the result of testing the 57°W foot point value. As can be seen the correlations at 50°W and 57°W are essentially the same, and higher than those outside the interval between them. The best-fit parabola to the points shown has a maximum at 56.85°W . Figure 2 is a plot of the peak > 10 MeV proton fluxes, each multiplied by the longitudinal correction factor e^{2A} , vs the integrated radio flux in the frequency interval from 606 to 8800 MHz. The best-fit straight line to the data is also indicated. The expression for the best-fit straight line is $Y=1.69X-1.08$, where $X=\text{Log (time-frequency integrated radio flux)}$ and $Y=\text{Log (}> 10 \text{ MeV peak proton flux times } e^{2A})$.

The data illustrated in Figure 2 is representative of particle and radio burst activity in the years 1966 to 1973, or sunspot cycle No. 20. Three additional points, indicated by \square and their dates, are included

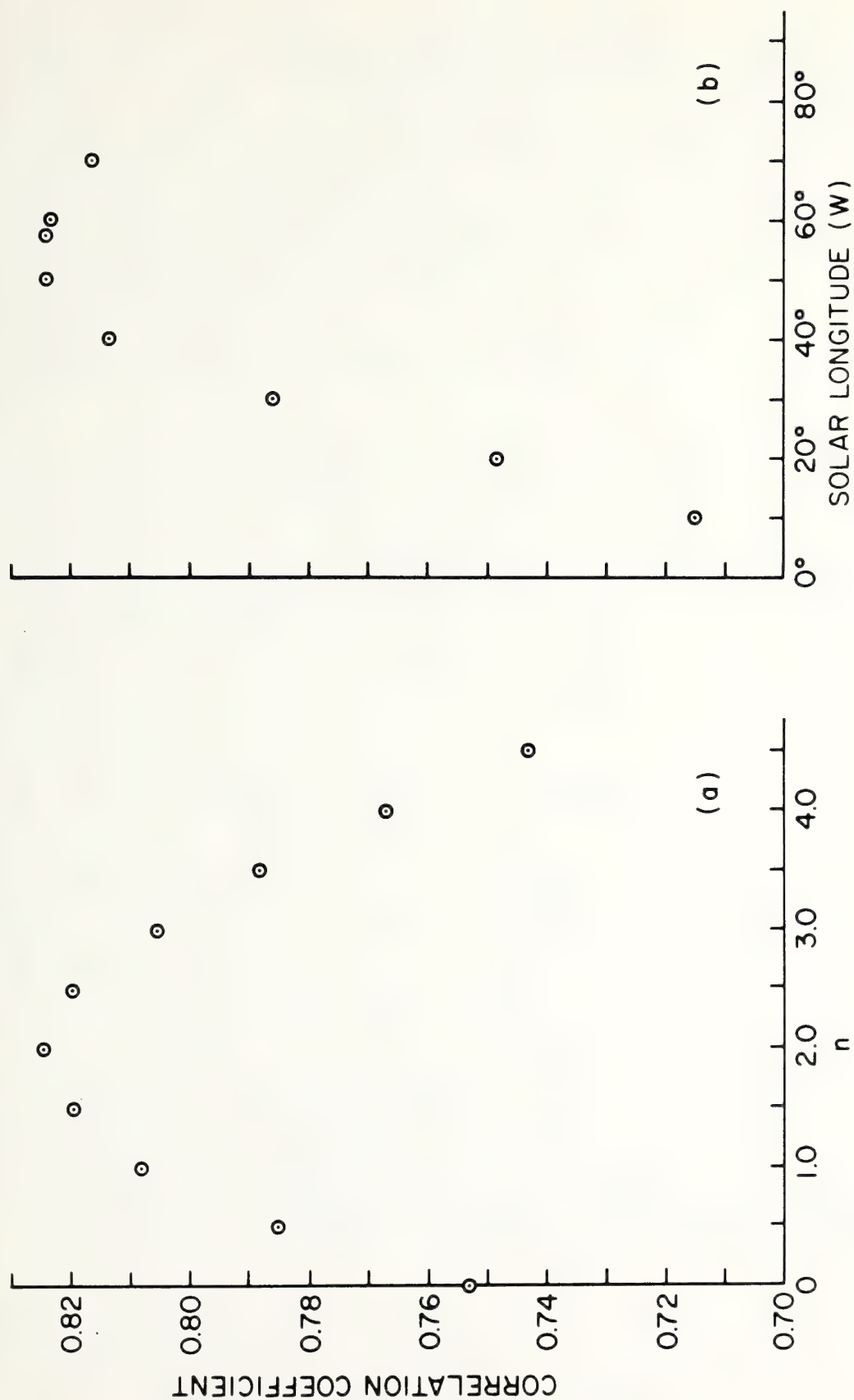


FIGURE 1. THE EFFECTS OF TWO VARIABLE PARAMETERS UPON THE CORRELATION OF INTEGRATED RADIO FLUXES WITH PEAK >10 MeV PROTON FLUXES.

(a) VARIABLE n FOR e^{nA} WITH $57^\circ W$ AS THE REFERENCE LONGITUDE.

(b) VARIABLE REFERENCE LONGITUDES FOR DETERMINING A IN e^{2A} .

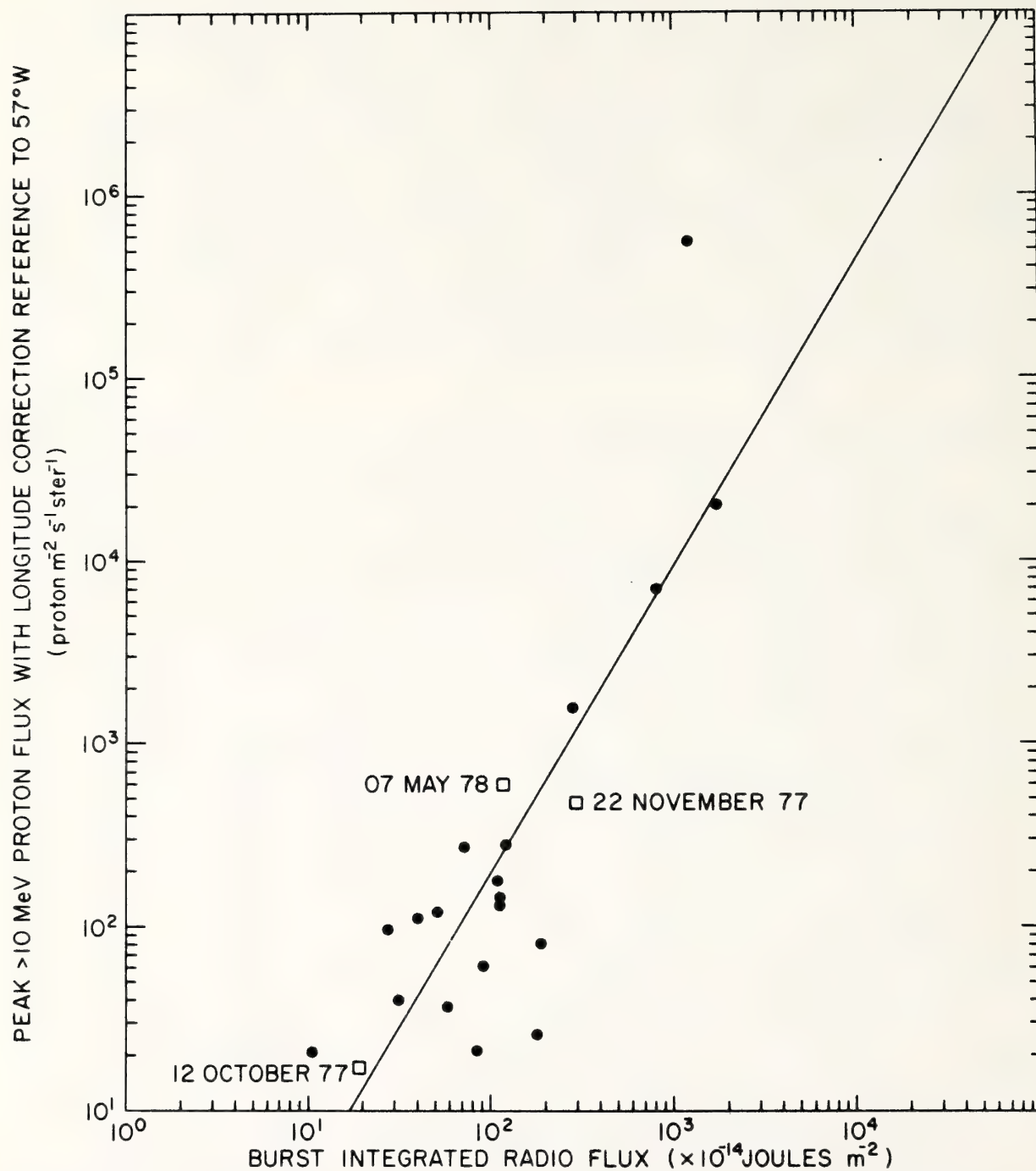


FIGURE 2. CORRELATION OF PEAK >10 MeV PROTON FLUX (WITH LONGITUDE CORRECTION) WITH BURST INTEGRATED RADIO FLUX.

in the plot. Two of them, 22 November 1977 at 1004 UT and 07 May 1978, at 0330 UT had high latitudes of occurrence, 24°N , which should make them Cycle No. 21 phenomena. The third, 12 October 1977 at 0152 UT, occurred at a latitude of 07°N which may make it a remnant occurrence of cycle No. 20. The radio bursts, observed at the AFGL Sagamore Hill Radio Observatory, the Manila Observatory, in the Philippines, or the Athens Observatory, Athens, Greece, all had U-shaped peak flux spectra with sufficiently high fluxes to indicate that there had been an emission of energetic protons. The time-frequency integrated radio fluxes were obtained and associated with the satellite observed peak proton flux, corrected for the solar longitude of the flare involved. The plotted points indicate the results of the associations. As may be seen the points all fit the population trend quite well.

A recent paper by Helms (9) has discussed the association of changes in the height of the polar D-region with the incident proton flux. These height changes, due to electron density changes, influence the characteristics of trans-polar radio wave propagation. It may well be that the results of the research by Helms can be combined with the results reported here to provide a prediction of height change for the polar D-region before it actually takes place.

REFERENCES

1. Castelli, J. P., J. Aarons, and G. A. Michael, Flux Density Measurements of Radio Bursts of Proton-Producing Flares and Non Proton Flares, J. Geophys. Res., 72, 5491, 1967.
2. Bakshi, P., and W. R. Barron, Spectral Correlations Between Solar Flare Radio Bursts and Associated Proton Fluxes, II, Rep. AFCRL-TR-75-0579, Air Force Cambridge Research Laboratories, Hanscom Air Force Base, Massachusetts, 1975.
3. Bakshi, P., and W. R. Barron, Prediction of Solar Flare Proton Spectral Slope From Radio Burst Data, J. Geophys. Res., 84, 131, 1979.
4. Straka, R. M., The Use of Solar Bursts as Predictors of Proton Event Magnitudes, AFCRL Space Forecasting Research Note No. 2, 1970.
5. Cliver, E. W., Parent Flare Emission at 2.8 GHz As A Predictor of the Peak Absorption of Polar-Cap Events, Naval Electronics Laboratory Center Report NELC/TR 2015, 1976.
6. Newell, D. T., Forecasting Peak Proton Flux and PCA Event Magnitudes Using Flash-Phase Integrated Radio-Burst Flux Density, AFCRL-72-0543, Environmental Research Papers, No. 415, Air Force Cambridge Research Laboratories, L. G. Hanscom Field, Bedford, MA, 1972.
7. Akinyan, S. T., V. V. Fomichev, and I. M. Chertok, Determination of the Parameters of Solar Protons in the Neighborhood of the Earth from Radio Bursts. 1. Intensity Function, Geomagnetism and Aeronomy, 17, 5, 1977.
8. Bakshi, P., and W. R. Barron, Prediction of the Proton Flux Magnitudes from Radio Burst Data, AFGL-TR-78-0100, Scientific Report No. 2, Air Force Geophysics Laboratory, Air Force Systems Command, United States Air Force, Hanscom Air Force Base, MA, 1978.
9. Helms, W. J., Polar D-Region Electron Density Profiles During A Solar Proton Event, Radio Science, 13, 853, 1978.

PREDICTION OF SOLAR FLARE PROTON SPECTRUM FROM RADIO BURST CHARACTERISTICS

Pradip Bakshi
Physics Department
Boston College
Chestnut Hill, MA 02167
and

William R. Barron
Air Force Geophysics Laboratory
Hanscom AFB, MA 01731

A real time prediction scheme for the solar flare proton spectrum based on various features of the antecedent U-shaped peak flux density radio burst spectrum is described. The proton spectral slope is predicted from a ratio of two frequencies characterizing the U-shaped radio spectrum. The proton event magnitude is predicted from the radio spectral energy integrated over a given frequency range and the flare location. Illustrative examples involving recent flare events demonstrate its capabilities for prediction.

1. INTRODUCTION

Solar flare radio spectra have served as predictors of significant proton events for quite some time (Castelli, Aarons and Michael, 1967, Castelli, 1968, Castelli and Aarons, 1970, Straka and Barron, 1970, Straka, 1970, O'Brien, 1970, Castelli and Giudice, 1972, Newell, 1972). The earliest studies (Castelli, Aarons and Michael, 1967, Castelli, 1968) provided a yes-no criterion in terms of the existence or otherwise of a U-shaped radio spectrum signature. Subsequent studies (Straka and Barron, 1970, Straka, 1970, Newell, 1972) correlated various integrated radio flux density measures to the magnitude of the proton events as measured by the peak proton flux with $E > 10$ MeV. In a series of studies, we have tackled the problem of predicting the slope of the proton spectral profile (Bakshi and Barron, 1974, Bakshi and Barron, 1975, Bakshi and Barron, 1979), and we have also taken a closer look at the problem of predicting the proton event magnitudes (Bakshi and Barron, 1978); combined, these studies provide a complete scheme for the real time prediction of the complete proton flux spectral profile. We summarize here the main selection criteria, the radio parameters used in prediction

and the results for the twentieth solar cycle, which lead to correlation formulas to be employed for future predictions. Some examples of predictions based on this approach are also discussed.

2. SELECTION CRITERIA AND RADIO PARAMETERS

The radio peak flux density versus frequency profile for a given event is examined to determine whether it has a U-signature, defined by a rising spectrum on the high frequency side, a dip in the middle, and again a rising spectrum on the low frequency side. The range of frequencies covered is from a few hundred to several thousand MHz. The peak flux densities on the high as well as the low-frequency side should generally be at least 1000 solar flux units and the minimum at the dip of the U should generally exceed 100 units, ($1 \text{ sfu} = 10^{-22} \text{ W M}^{-2} \text{ Hz}^{-1}$).

If this condition is met, it indicates a high probability of occurrence of a proton event. To determine the spectral characteristics of the proton peak flux profile we employ the following features of the radio flux data.

(i) To determine the proton peak flux spectral slope, we need (Bakshi and Barron, 1979) the radio frequency ratio (ω_3/ω_2), which essentially defines the width of the U, where ω_3 is the frequency at which the high-frequency branch of the U spectrum attains its maximum flux density and ω_2 is the frequency at which the U spectrum attains its minimum flux density.

(ii) To determine the proton peak flux magnitude for $E > 10 \text{ MeV}$, we need (Bakshi and Barron, 1978) several features concerning the flare data. The primary parameter is the energy ϵ received in the radio frequency band 606 to 8800 MHz during the time interval of the U-event. This is calculated by a time integration of the incident radio flux density at each of the discrete frequencies 606, 1415, 2695, 4995, and 8800 MHz, followed by a frequency integration over the stated range. On general physical grounds, one can expect this energy to be well correlated to the energy carried away by the protons at the source. We can thus expect a better correlation by introducing a proton energy factor ρ , which depends on the proton spectral slope and which can be estimated from the radio frequency ratio (ω_3/ω_2). Correlations would also improve if allowance is made for the proton propagation effects which depend on the longitudinal location of the flare.

3. PREDICTION OF PROTON SPECTRAL SLOPE

Our extensive study (Bakshi and Barron, 1979) of the events of the twentieth solar cycle led to the relation

$$\beta = \frac{1.185}{\{\log_{10}(\omega_3/\omega_2)\}^{1.01}} \pm 0.45 \quad (1)$$

where β is the proton spectral slope for the integral spectrum $I(>E \text{ MeV}) = AE^{-\beta}$, and (ω_3, ω_2) are the radio frequencies defined in section 2. Equation (1) essentially indicates that wider U's (large (ω_3/ω_2)) are associated with harder proton spectra (small β) and narrower U's (small (ω_3/ω_2)) are associated with softer proton spectra (large β), as was originally proposed (Bakshi and Barron, 1974, Bakshi and Barron, 1975). The power law form represented by equation (1) gave a significantly better correlation ($r \approx 0.77$) as compared to a straight line or an exponential form. The statistical distribution of individual events has been given in Figure 3 of Bakshi and Barron, 1979. Since the slope was determined over the integral spectral range $> 10 \text{ MeV}$ to $> 60 \text{ MeV}$, the prediction applies strictly over only that range, or perhaps a bit beyond, from 5-100 MeV.

4. PREDICTION OF PROTON SPECTRAL MAGNITUDE

We have shown (Bakshi and Barron, 1978) that restricting the time integration for the radio flux density to the duration of the interval characterizing the U leads to a significant improvement in the correlations between I_{10} , the peak flux of protons with energies $> 10 \text{ MeV}$ and the time-integrated radio flux at any frequency. Further improvement is obtained by carrying out a frequency integration over the range 606 to 8800 MHz and using ϵ the radio-energy in this range as the correlation variable.

As regards the proton variable, significant improvement is obtained upon using $I_{10}e^{3A}$, where A is the magnitude in radians of the angular distance of the flare location from the standard reference longitude 57°W . The factor e^{3A} compensates for the propagational attenuation, and provides a better correlation. The choice of e^{3A} is somewhat arbitrary, and based on past usage (Cliver 1976); we show elsewhere in these proceedings that further improvement is obtained upon using a slightly different attenuation factor.

In principle, one would expect the proton energy content $10\rho I_{10}$ [with $\rho = \beta/(\beta-1)$], rather than the proton flux I_{10} to correlate well with the radio energy ϵ . However, we found no significant difference in the correlations of ϵ with $I_{10}e^{3A}$ and $I_{10}\rho e^{3A}$, both giving a coefficient $r \approx 0.80$.

The best fit straight lines for correlations between $\log \epsilon$ and $\log (I_{10}e^{3A})$ or $\log (I_{10}\rho e^{3A})$ lead to relations (Bakshi and Barron, 1978)

$$I_{10} e^{3A} = (0.115) \epsilon^{1.77} (5.14)^{\pm 1}, \quad (2)$$

$$I_{10} \rho e^{3A} = (0.76) \epsilon^{1.655} (4.82)^{\pm 1}, \quad (3)$$

where the last factor represents one standard deviation in each case. To predict I_{10} , in units of protons $\text{cm}^{-2} \text{sec}^{-1} \text{ster}^{-1}$, first calculate the radio parameter ϵ for that event in units of 10^{-14} Joules m^{-2} , then either use (2) to predict $I_{10} e^{3A}$ and divide that by e^{3A} using the observed value of A or use (3) to predict $I_{10} e^{3A_p}$ and divide that by e^{3A_p} , where $\rho = \beta/(\beta-1)$ is obtained from the radio data by employing (1). The second method, equation (3), cannot be used if ω_3/ω_2 is so large that β is close to or less than unity.

5. ILLUSTRATIVE PREDICTIONS

We now apply the results described in the preceding two sections to "predict" the proton flux characteristics for some recent flare events, using the radio data as the input. Three events are considered, with radio data observed at the AFGL Sagamore Hill, Manila, or Athens Observatory:

TABLE I

Index	Date	Location	ω_3 MHz	ω_2 MHz	ω_3/ω_2	$J^\epsilon \text{ M}^{-2}$	A
1	10.12.77	07 ^{ON} 07 ^{OW}	9400	2000	4.70	19×10^{-14}	0.872
2	11.22.77	24 ^{ON} 40 ^{OW}	8800	1415	6.22	298×10^{-14}	0.297
3	05.07.78	24 ^{ON} 68 ^{OW}	8800	1415	6.22	123×10^{-14}	0.192

Applying equation (1), we can predict the spectral slope of the associated proton peak fluxes. In the following table, the predictions are compared with the actual slopes obtained from the observed particle data as reported in the Solar Geophysical Data Bulletins:

TABLE II

Index	β predicted	β observed
1	1.77 ± 0.45	1.59
2	1.50 ± 0.45	1.45
3	1.50 ± 0.45	0.80

There is excellent agreement for event nos. 1 and 2, while the third event falls outside one standard deviation. As a group, these blend well with the study population of Figure 3 in Bakshi and Barron, 1979.

Applying equation (2), we can predict $I_{10}e^{3A}$ for the proton event, and a division by e^{3A} provides the proton-magnitude I_{10} :

TABLE III

Index	$I_{10}e^{3A}$ predicted	e^{3A}	I_{10} predicted	I_{10} observed
1	21	13.7	1.5	2.8
2	2755	2.44	1129	259
3	575	1.78	323	415

There is good agreement for event nos. 1 and 3, while event no. 2 falls just inside the one standard deviation factor $(5.14)^{\pm 1}$.

Applying equation (3), we can predict $I_{10} \rho e^{3A}$ for the proton event. Then a division by e^{3A} and by $\rho = \beta/(\beta-1)$, where $\beta = \beta_{\text{predicted}}$ is taken from Table II, provides the proton magnitude I_{10} :

TABLE IV

Index	$I_{10} \rho e^{3A}$ predicted	e^{3A}	ρ	I_{10} predicted	I_{10} observed
1	99	13.7	2.30	3.1	2.8
2	9455	2.44	3.00	1291	259
3	2186	1.78	3.00	409	415

There is excellent agreement for event nos. 1 and 3, while event no. 2 falls just outside the one standard deviation factor $(4.82)^{\pm 1}$.

6. CONCLUDING REMARKS

We have developed a complete scheme for the prediction of the proton peak flux profile in the range > 10 to > 100 MeV, using the real time radio data as the input. Equation (2) or (3) provides the magnitude I_{10} , which along with the slope β provided by Equation (1) is sufficient for obtaining the proton integral flux over the entire energy range. The illustrative examples, taken from a later period, seem to bear out the validity of this approach. Besides providing a practical prediction scheme, our empirical results suggest that there is a simple relationship between the proton slope and the width of the radio U. Explaining this, then, is an interesting question posed for current and future theories.

QUANTITATIVE FORECASTS OF SOLAR PROTONS BASED ON SOLAR FLARE RADIO DATA

S. T. Akinyan, I. M. Chertok, V. V. Fomichev
IZMIRAN, 142092 Moscow, USSR

A method of quantitatively estimating the energetic proton flux from solar flares is developed on the basis of the analysis of radio burst characteristics and proton parameters ($E > 10, 30$ and 60 MeV) for the reference period 1965-1969. The expected maximum intensity and temporal parameters of the proton event near the Earth are calculated from the radio data. Verification of the method was carried out using independent data from the period 1970-1977. Control calculations show that there is good agreement between the proton parameters calculated from radio data and ones observed near Earth.

1. INTRODUCTION

Quantitative diagnosis of proton flares is becoming more and more important as well as the prediction of solar activity. The objective of our diagnosis is to determine promptly the kind of particles, their quantity and arrival time near the Earth, by observing the current solar flare. Quantitative diagnosis provides this information in advancing intervals from tens of minutes to tens of hours and is the basis of the corresponding short-term warning system.

Among the different electromagnetic radiations accompanying a flare, the radio emissions prove to be most suitable for the diagnostics due to the simplicity and feasibility of observations. Besides that, it is of key importance that the emission of various radio frequencies is generated at essentially different altitudes in the solar atmosphere. The microwave bursts produced in the chromosphere or lower corona make it possible to estimate the particle acceleration in the flare, whereas the bursts in the meter and decameter ranges generated in the solar corona yield information on particle access into interplanetary space as well.

The radio bursts data relevant to the proton-flare diagnostics were discussed in numerous works (Castelli and Guidice, 1976; Straka, 1970; Croom, 1971; Böhme, 1972; Sakurai, 1972; see also Smart and Shea, 1978). However, it should be noted that the main advantages of the radio emission were insufficiently used, and some important features of solar cosmic ray propagation were disregarded.

In recent papers (Akinyan et al., 1977; 1978 a, b; 1979) we made an attempt to develop the available techniques of the proton flares diagnostics. The following aspects of the proposed method may be considered as an innovation: (a) The dependence of the proton flux parameters and of the mode of their relationships to radio bursts in the centimeter and meter ranges on flare heliolongitude has been consistently included. (b) Information about the conditions of proton access into interplanetary space, which may be derived from the meter component of radio emission, has been taken into account. (c) The relationship between the frequency spectrum of microwave bursts and the energy spectrum of protons was used (see Bakshi and Barron, 1975). (d) Unified technique has been applied for determination of the proton parameters in various energy ranges ($E > 10, 30$ and 60 MeV). (e) Besides the maximum intensity, provisions have been made for estimating the time parameters (the moments of commencement and maximum intensity of protons relative to microwave burst maximum, the decreasing rate of the particle flux), which make it possible to calculate the time-intensity profiles of protons. The well-known parameters of microwave bursts at frequencies 3 and 9 GHz, such as the maximum intensity $S_{3,9}$, integrated flux during the increasing phase $R_{3,9}$ and total integrated flux of the burst $P_{3,9}$, were used as initial parameters for estimating the proton flux.

The most realistic approach to solving the problem of the quantitative diagnostics of proton flares is reduced to direct comparison of the characteristics of radio bursts of a certain flare with the parameters of solar cosmic rays registered after this flare near the Earth. The regularities inferred from such comparison for events that occurred during some reference interval are expressed through definite supporting functions, which then may be used in real time for prompt diagnostics of observed flares.

As a reference interval, the period 1965-1969 has been taken. Also, data for some large proton events in 1971 and 1972 were used. The proton events with maximum intensity $J(E > 10 \text{ MeV}) \gtrsim 1 \text{ cm}^{-2}\text{s}^{-1}\text{sr}^{-1}$ identified unambiguously with the flares on the solar disc are treated. The results of the analysis of the reference interval and the method of estimating the proton flux parameters by radio data developed on this basis are given (Akinyan et al., 1977, 1978a, b). Section 3 is devoted to a verification of the method by the independent data for control period 1970-1977. Here the proton flare criterion is also formulated, and the examples of diagnostics for some events are presented (Akinyan et al., 1979). The analysis of the reference period and the control calculations were largely based on the information on radio bursts and proton fluxes presented in NOAA Solar-Geophysical Data and Catalog (Svestka and Simon, 1975). Use was also made of unpublished time-intensity profiles of microwave radio bursts registered in observatories of Canada, England, GDR, Japan and USSR.

2. ANALYSIS OF THE REFERENCE PERIOD

2.1 Intensity Function

In comparing the information on radio bursts and proton fluxes, we assumed that the azimuthal propagation of particles takes place mainly in the

solar corona (see e.g. Reinhard and Wibberenz, 1974). Therefore, the analysis of the reference period begins with the consideration of the proton flares within a so-called optimal longitude interval (OLI, heliolongitudes 20-80 West). Proton flux parameters and the character of their relationship with radio bursts do not depend on heliolongitude θ in this interval. The dependences of intensity J of the > 10 , > 30 and > 60 MeV protons observed near the Earth, and each of six initial parameters of microwave bursts at 3 and 9 GHz ($S_{3,9}$, $R_{3,9}$, $P_{3,9}$) are analyzed.

The typical relationship, which is revealed in this case, is illustrated by Figure 1. Here the dependence between J of > 10 MeV protons and the initial parameter S_3 is shown. It can be seen that there is a definite spread. Apart from peculiarities of individual events, the spread is caused by a number of factors that influence the proton flux intensity, e.g. the escape condition for the particles from the flare region (see subsection 2.2) are not taken into account. However, the relationship between J and S_3 is sufficiently pronounced and may be described by the intensity function $J(S_3)$ - the curve shown in Figure 1 and corresponding empirical expression (Akinyan et al., 1977). The analogous intensity functions were also determined for other initial parameters (Akinyan et al., 1978a, b).

2.2 Longitude Attenuation Function

After determining the intensity function $J(x)$ by the events within the OLI (x -one of initial parameters $S_{3,9}$, $R_{3,9}$, $P_{3,9}$), a so-called attenuation value may be calculated for each event under consideration. The attenuation value ϕ is defined as the ratio of the proton intensity observed near the Earth J_0 to the intensity J_c calculated on the basis of the initial parameter x using the intensity function $J(x)$. The value $\phi = J_0/J_c$ makes it possible to transfer from the OLI to an arbitrary flare longitude θ and takes into account the conditions of particle access into the interplanetary space and the energy spectrum of protons.

There are reasons to suppose that a definite quantitative correspondence exists between the conditions of particle access into the interplanetary space and the intensity of the starting component of the meter radio emission containing type II and IV bursts, which are generated at large altitudes in

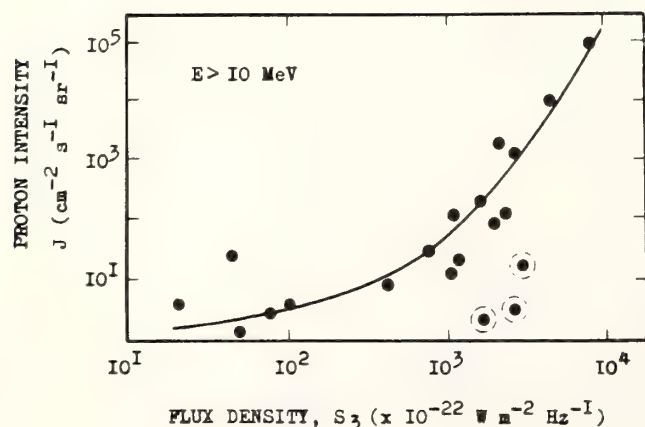


Figure 1. Maximum intensity of > 10 MeV protons J versus parameter S_3 for flares localized in the OLI.

the corona (Akinyan et al., 1977). Let us subdivide all events under consideration into two groups depending on the intensity of meter component. Radio bursts with a flux density $F > 5000$ s.u. ($1 \text{ s.u.} = 10^{-22} \text{ W m}^{-2} \text{ Hz}^{-1}$) at the frequencies $f \approx 245 \text{ MHz}$ (with the dynamic spectra containing type II-IV bursts of importance ≥ 3) form a category of events with an intensive meter component. Radio bursts with $F < 5000$ s.u. (type II-IV bursts of importance 1 and 2) are attributed to a category of events with a weak meter component.

Then, the distribution of events with different characteristics of the diagrams of "attenuation value ϕ versus heliolongitude θ " were analyzed. The diagrams obtained by this analysis are analogous to that shown in Figure 2. Here the dependence of ϕ on θ for parameter R_3 and > 10 , $> 30 \text{ MeV}$ protons is illustrated (a), as well as for parameter P_9 and $> 10 \text{ MeV}$ protons (b). Dark and light signs correspond to the events with intensive and weak meter component, respectively.

These diagrams indicate the following effects:

(a) In each of the energy ranges within the OLI, the attenuation (hence the proton flux intensity) fails to exhibit any systematic heliolongitude dependence. For such events, the value ϕ is characterized by a certain spread around $\phi = 1$.

(b) Outside the OLI, the proton fluxes detected near the Earth are markedly attenuated, the attenuation effect enhancing tens and hundreds of times (ϕ decreases accordingly) as the east longitude of flares increases.

(c) The difference between the events with intensive and weak meter component can be clearly seen. The character of the difference confirms the

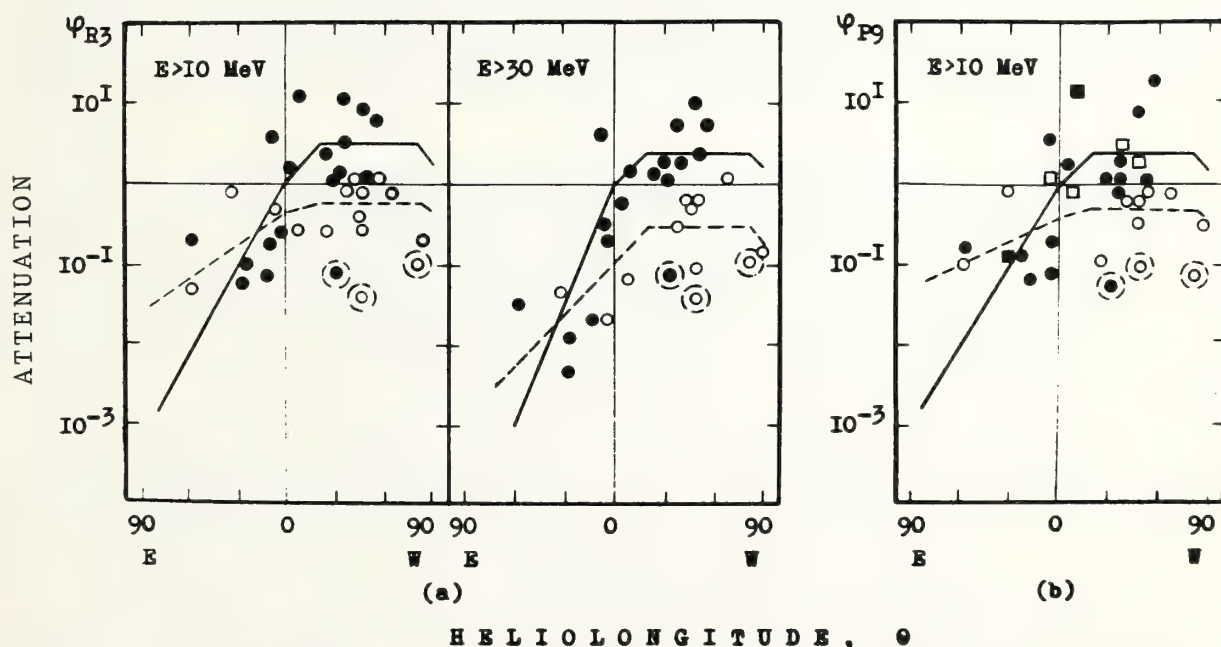


Figure 2. "Attenuation value ϕ as a function of flare longitude θ ". Diagrams for initial parameters R_3 (a) and P_9 (b).

assumption made above that the meter radio emission intensity reflects the conditions of the particles that escape from the flare region. Within the OLI, the events with intensive meter component (i.e. with favorable conditions of particles access) are mainly localized in the region $\phi > 1$. This fact means that the events are characterized by more intensive proton fluxes. The events with weak meter component, for which the particle-escape conditions are unfavorable, are localized in the region $\phi < 1$. At the same value of the initial parameter, such events are associated with less intensive proton fluxes.

Outside the OLI, on the eastern part of the solar disc, the inverse relationship between the events with intensive and weak meter component is observed. In this case, the events with weak meter radio emission are located higher on the diagrams (i.e. in the region of larger values ϕ) as compared with events involving intensive meter bursts. In other words, the proton fluxes from the flares located outside the OLI and accompanied with intensive radio emission are attenuated much more strongly than the proton fluxes from the flares with weak radio emission. This effect reflects the fact that under favorable escape conditions (intensive meter radio emission) the bulk of particles leave the Sun directly from the flare region and propagate aside from the Earth. On the other hand, when the conditions of particles access into the interplanetary space directly from the flare region are unfavorable (weak meter component), the particles have to propagate mainly along the solar surface. In this case, the relative number of protons detected near the Earth increases.

The said differences between the groups of events with intensive and weak meter component may be conveniently included by inserting separate longitude attenuation Functions $\phi_{1,2}(\theta)$ for each group. Such functions are shown in Figure 2 by solid and dashed lines for events with intensive and weak meter components, respectively. More detailed information on the longitude attenuation functions for all the initial parameters are given by Akinyan et al. (1977; 1978a, b).

(d) For the events associated with eastern flares, the effect of longitude attenuation of proton fluxes is enhanced with increasing particle energy. This regularity is observed for both groups of the events, i.e. with either intensive or weak meter components. The attenuation effect is also enhanced with increasing east longitude of the flare, which results in a steepening of the proton energy spectrum. This effect is in agreement with the results obtained by Van Hollebeke et al. (1975), which revealed the steepening of the proton energy spectrum with increasing eastern longitude of flares by a statistical analysis of the data on the spectrum of individual events.

(e) In using the parameters of the microwave bursts at 9 GHz, for flare diagnostics, besides the effects mentioned above, it is necessary to take into account also the frequency spectrum of the radio bursts. Akinyan et al. (1978a, b) have revealed that the events, in which the high frequency maximum of U-shaped spectrum of the microwave bursts is located at $f_{\max} < 8.8$ GHz (in Figure 2b these events are marked by squares), are characterized by larger intensities of > 10 MeV protons, i.e. by a softer energy spectrum. The effect is weaker for the > 30 MeV protons and it is not quite seen for the > 60 MeV ones. To take into account this effect, the additional corrective

coefficient k is introduced. The concrete values of this coefficient for different initial parameters were obtained by Akinyan et al. (1978a, b).

2.3 Time Dependence Functions

To carry out a total quantitative diagnostics of proton flares, besides the estimations of the maximum intensity, it is also necessary to determine in good time the main time parameters of the proton fluxes: the time delays between the arrival at the Earth of the first protons from a given flare Δt_1 and the time of maximum proton intensity Δt_2 with respect to the time of maximum of the microwave radio burst, as well as an exponential decay time-constant τ .

Akinyan et al. (1977) determined the corresponding supporting functions $\Delta t_1(\theta)$, $\Delta t_2(\theta)$ and $\tau(\theta)$ by a statistical analysis of the reference sample of events for 1965-1969. It was revealed that all time parameters Δt_1 , Δt_2 and τ do not depend on heliolongitude of solar flares θ on the western hemisphere and increase gradually with eastern distance from the central meridian. Besides that, the events with intensive microwave burst ($S_3 > 1000$ s.u.) and weak meter component have a tendency to larger delays Δt_1 and Δt_2 within the OLI. This effect is connected with the circumstance that such combination of microwave and meter radio bursts corresponds to the most unfavorable conditions for particles to escape from the flare region.

2.4 Calculation Procedure for Proton Flux Parameters

The supporting functions described above permit the rapid calculation of the time-intensity profiles of > 10 , > 30 and > 60 MeV proton fluxes near the Earth, taking into account a flare heliolongitude, conditions of particle access into the interplanetary space and its energy spectrum. The calculation procedure for the proton flux parameters is reduced to the following:

After the radio emission accompanying a given flare has been recorded, one first must determine whether the flare is a proton flare. For this purpose, there is a so-called "yes-no" criterion (see subsection 3.1). If the flare satisfies the proton criterion, then the necessary initial data (heliolongitude, parameters of microwave and meter radio emission) are substituted in the corresponding supporting functions, and the maximum intensity and time parameters of proton fluxes are calculated.

With a glance to the regularities described in subsection 2.2, the general expression for calculating the maximum proton intensity near the Earth for every energy range by the given initial parameter x has the form

$$J = k \phi_{1,2}(\theta) J(x) \quad (1)$$

where $J(x)$ and $\phi_{1,2}(\theta)$ are the supporting intensity function and longitude attenuation function. $\phi_{1,2}(\theta)$ is selected in accordance with the intensity of the meter component. Coefficient k depends on the frequency spectrum of microwave bursts when the parameters at 9 GHz are used as initial ones.

In calculating the time parameters Δt_1 , Δt_2 and τ , the corresponding time supporting functions are used (see subsection 2.3). On the whole, the maximum intensity and time parameters allow one to have practically at the moment of flare maximum the information on the expected time profiles of > 10 , > 30 , > 60 MeV protons on some days in advance.

3. VERIFICATION OF THE METHOD BY INDEPENDENT DATA

To verify the main regularities and the method of the quantitative diagnostics of solar flares, the control calculations of proton parameters have been carried out by independent data on the radio bursts and proton fluxes for 1970-1977 (Akinyan et al., 1979).

3.1 Selection of Proton Events

The first step of the control calculation was a systematic examination and analysis of data on all radio bursts registered by the world network of solar radio observatories during the control interval, and the selection therefrom of the events satisfying the proton flare criterion.

In the control calculations, the proton events were selected by a criterion that is a modification of the well-known criterion of the U-shaped frequency spectrum suggested by Castelli and his collaborators (see Castelli et al., 1976). It was believed that a flare may be followed by a proton flux with maximum intensity $J(E > 10 \text{ MeV}) \gtrsim 5 \text{ cm}^{-2}\text{s}^{-1}\text{sr}^{-1}$ at the orbit of the Earth, providing the characteristics of the accompanying radio bursts satisfy the conditions:

(a) The maximum intensity S of a microwave radio burst at any frequency in the range 5-9 GHz must have $S \gtrsim 500 \text{ s.u.}$

(b) The frequency spectrum of a microwave burst is characterized by an increasing maximum flux density with frequency in any part of the range from 3 up to 9 GHz.

(c) The duration of a microwave burst at a level of 0.5 of the maximum intensity at the boundaries of frequency range 3-9 GHz exceeds 3.5 and 2 minutes, respectively.

(d) Over the meter range, in the initial phase of the event during the microwave burst lifetime, type II and/or type IV bursts are observed with flux density $F > 300 \text{ s.u.}$ at $f \lesssim 245 \text{ MHz.}$

As a result of the analysis of radio data for 1970-1977, the control sample of the events was selected which consists of 30 radio bursts completely satisfying the proton criterion and 4 sufficiently intensive bursts being exceptions (Akinyan et al., 1979). The events of 24 January 1971 and 2-7 August 1972 are excluded from the control consideration since they have been already used in the reference sample of events.

3.2 Comparison of the Calculated and Observed Proton Parameters

Calculations of the expected parameters of > 10 , > 30 and > 60 MeV protons for each of the events selected by the proton flare criterion were carried out in accordance with the scheme described in subsection 2.4 by substituting the particular values of the initial parameters, data on flare heliolongitude and character of the meter radio emission into the corresponding supporting functions, which have been defined on the basis of the reference sample of events. A maximum intensity of proton fluxes was calculated by formula (1) for every initial parameter separately S_3 , R_3 , P_3 , S_9 , R_9 and P_9 . As a result, one has six values of calculated intensities J_C for every event in each energy range. In addition, the intensity values calculated from the initial parameters at 3 GHz were averaged (\bar{J}_3). Similarly, those at 9 GHz were averaged (\bar{J}_9). Finally, all six intensity values calculated from the initial parameters at 3 and 9 GHz were averaged ($\bar{J}_{3,9}$).

Table 1 gives the values of the correlation coefficient between the observed proton flux intensity J_O and the values J_C calculated by separate initial parameters as well as by results of averaging. The typical relation between J_O and J_C is illustrated in Figure 3, where the solid and open circles represent the events on the western and eastern hemispheres, respectively. It is evident that the calculated and observed intensities are in fairly good accordance. For most initial parameters the correlation coefficient between J_O and J_C $r \sim 0.75-0.80$; in averaging it amounts $r \sim 0.80-0.85$. Over all the energy ranges the observed intensities, on one hand, and the calculated values \bar{J}_3 , \bar{J}_9 and $\bar{J}_{3,9}$, on the other hand, in 75-80% of the events do not differ by more than a factor of 2 and in 80-90% of the events - under factor of 2.5.

Table 1. Correlation coefficients between the observed and calculated proton intensities

Energy of protons MeV	f = 3 GHz				f = 9 GHz				
	S_3	R_3	P_3	\bar{J}_3	S_9	R_9	P_9	\bar{J}_9	$\bar{J}_{3,9}$
E > 10	0.84	0.74	0.71	0.86	0.81	0.80	0.77	0.79	0.85
E > 30	0.69	0.82	0.82	0.85	0.81	0.73	0.89	0.80	0.85
E > 60	0.72	0.85	0.84	0.87	0.83	0.75	0.85	0.81	0.87

In the control calculations, the time parameters of proton fluxes (time delays Δt_1 , Δt_2 and damping constant τ) also showed positive results. These values for the events of the control sample are calculated by the same scheme as the maximum intensity, i.e. by substituting the necessary initial data into the corresponding time supporting functions established by the reference sample of events (see subsection 2.3). The analysis has revealed that at all heliolongitudes there is a fairly good agreement between calculated and observed values of the time parameters. In particular, on the western

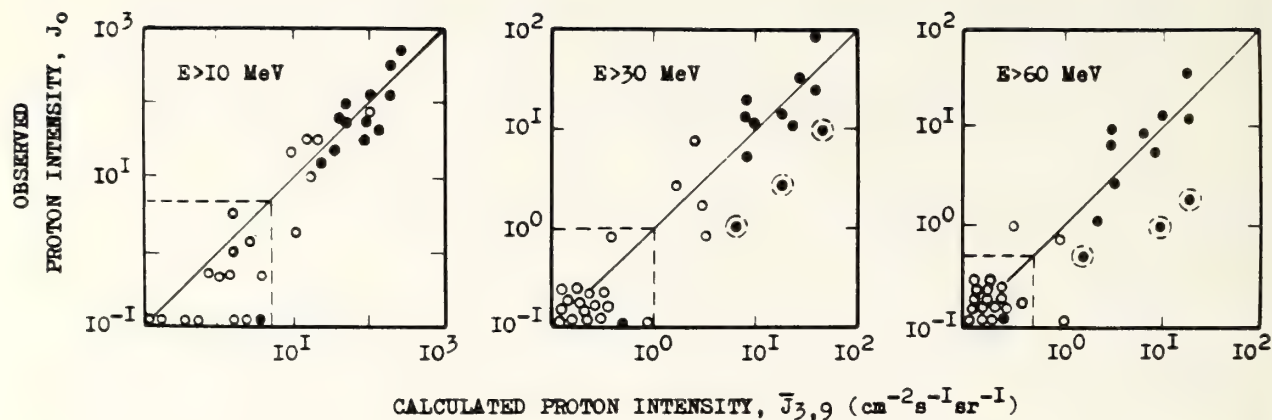


Figure 3. Correlation between the observed proton intensity \bar{J}_0 and calculated ones $\bar{J}_{3,9}$ for the > 10 , > 30 and > 60 MeV protons near the Earth.

hemisphere for most events, the calculated values Δt_2 for the > 10 MeV protons differ from the observed ones by less than 2 hours, the average delay being about 4 and 8 hours for events with favorable and unfavorable conditions of particles access, respectively. On the eastern hemisphere a spread is greater, but the time delay Δt_2 increases, also, and it amounts to 70-80 hours near the eastern limb. Similar results were derived for the time parameters Δt_1 , Δt_2 and τ in other energy ranges. As concerns the damping constant τ , for western flares the difference between the calculated and observed values is under one hour, with the average value $\tau \sim 9$ hours. On the whole, the calculated time-intensity profiles of the proton fluxes are sufficiently like the observed ones. It may be judged, in particular, by the examples presented in Figure 4. Shown here are time-intensity profiles of protons and energy spectra for most large proton events during last years in April and May, 1976, and in September and November, 1977. In each of the panels, the dashed and solid lines represent the insitu observations (Avdyushin et al., 1977, 1978) and results of the calculations which are carried out by radio data in accordance with the method outlined above.

3.3 Analysis of Unidentified Events

In the control calculations, along with estimations of the proton flux parameters expected from the flares selected by the proton criterion, one should bear in mind the reverse problem: using the information on all known proton flux increases near the Earth over the control period 1970-1977, to analyze those that were omitted in the radio emission considerations. Such an analysis has been made by Akinyan et al. (1979). As was expected, a greater part of these events were reliably identified with beyond the limb flares, and for this reason its diagnostics could not be carried out. The analysis of the rest of the omitted events is indicative of sufficiently good justification for the proton criterion formulated above. It permitted, in particular, to select almost all the proton flares that took place on the disk over the control interval. The number of evident omissions is relatively low: 2-5 flares of weak and moderate proton intensity ($J(E > 10 \text{ MeV}) \lesssim 25 \text{ cm}^{-2}\text{s}^{-1}\text{sr}^{-1}$). The number of possible omissions does not exceed 5-7, most

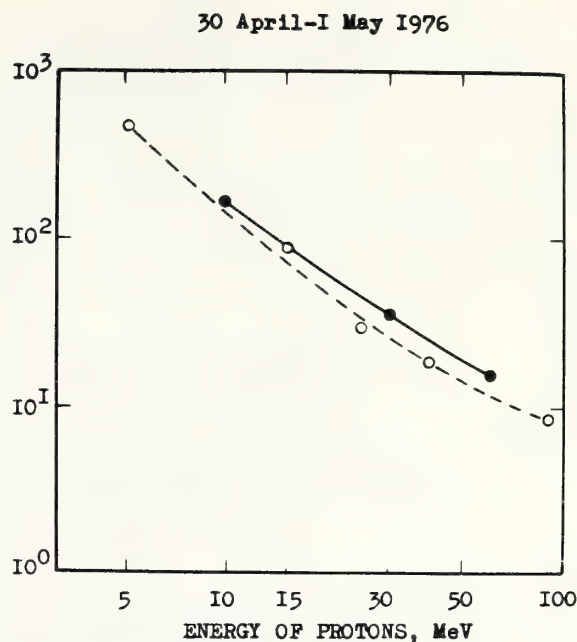
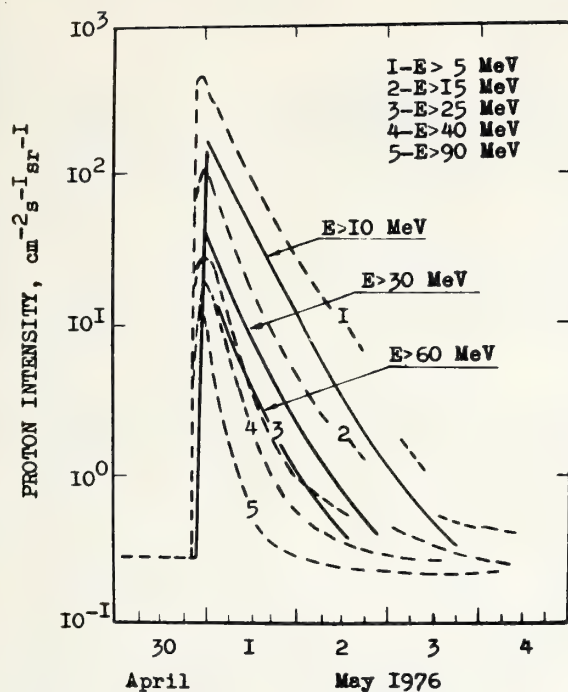


Figure 4(a). Time-intensity profiles and energy spectra of protons near the Earth. The solid and dashed lines represent the calculations and in situ observations, respectively.

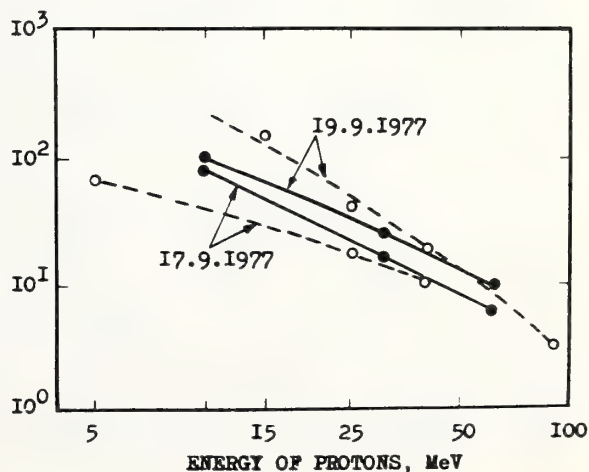
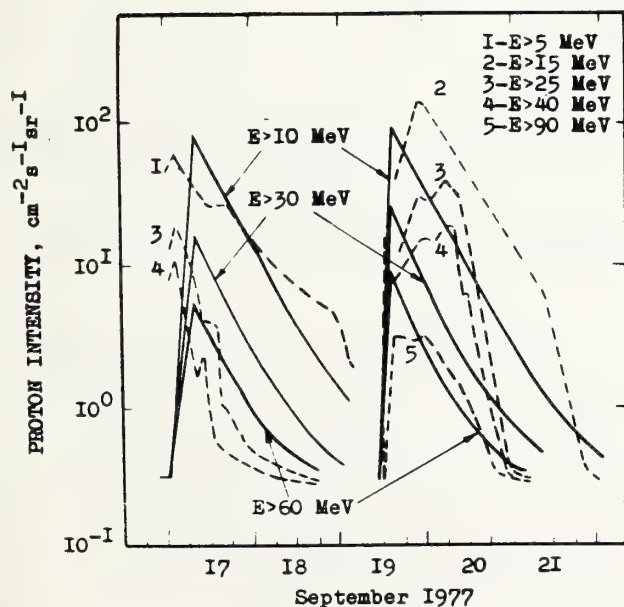


Figure 4(b)

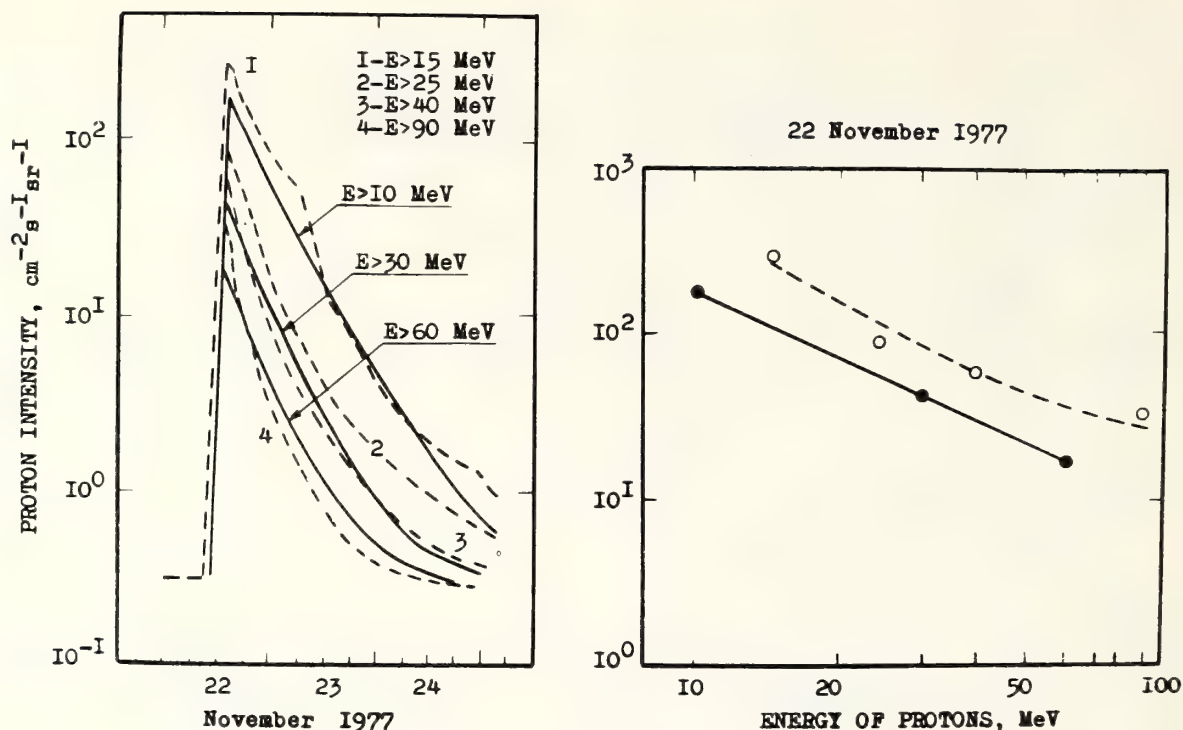


Figure 4(c)

of them being low intensity events as well. As far as "false alarms" are concerned, two events can be attributed thereto with certain reservations.

4. CONCLUSIONS

Our consideration of the reference sample of proton events (1965-1969) and the positive results of the control calculations for 1970-1977 shows that radio data may be successfully used for a quantitative diagnosis of proton flares. In this case, the possibility exists to take into account the flare heliolongitude, the conditions of particles escape from the flare region and the energy spectrum of protons.

Based on radio bursts information and using certain criteria, one can certainly select from numerous flares only those that should be considered to be proton flares. Then by the known supporting functions, one can calculate promptly the expected parameters of the > 10 , > 30 and > 60 MeV protons near the Earth. The positive results of the control calculation indicate the stability of the main regularities that form the basis of the suggested method, and show the possibility of its practical application for the quantitative diagnosis of proton flares under real conditions.

The authors would like to express their gratitudes to Prof. A. E. Covington (Canada), Drs. D. L. Croom and L. D. J. Harris (England), Drs. A. Krüger and A. Böhme (GDR) and S. Enome (Japan), who have presented at our disposal unpublished time-intensity profiles of some radio bursts.

REFERENCES

- Akinyan, S. T., V. V. Fomichev, and I. M. Chertok (1977): Determination of solar protons parameters near the Earth by radio bursts. I. Intensity function. II. Longitude attenuation function. III. Time parameters. Geomagn. i Aeronomiya, 17:10, 17:177; 17:596.
- Akinyan, S. T., M. M. Alibegov, V. D. Kozlovskii, and I. M. Chertok (1978a): On the quantitative diagnostics of proton flares by characteristics of microwave radio bursts at frequency \sim GHz. Geomagn. i Aeronomiya, 18:410.
- Akinyan, S. T., V. V. Fomichev, and I. M. Chertok (1978b): Estimations of solar proton intensity by integrated parameters of microwave radio bursts. Geomagn. i Aeronomiya, 18:577.
- Akinyan, S. T., V. V. Fomichev, and I. M. Chertok (1979): Results of quantitative diagnostics of proton flares by radio bursts for control interval 1970-1977. Geomagn. i Aeronomiya, (in press).
- Avdyushin, S. I., N. K. Pereyaslova, Yu. M. Kulagin, M. N. Nazarova, and I. E. Petrenko (1977): Observations of solar cosmic rays by "Meteor" satellite in March-May 1976. World Data Center A for Solar-Terrestrial Physics, Report UAG-61, pp. 157-164.
- Avdyushin, S. I., N. K. Pereyaslova, Yu. M. Kulagin, M. N. Nazarova, I. E. Petrenko, S. T. Akinyan, V. V. Fomichev, and I. M. Chertok (1978): Solar cosmic rays and radio bursts in September and November 1977. World Data Center A for Solar-Terrestrial Physics, Report UAG, (in press).
- Bakshi, P., and W. R. Barron (1975): Spectral correlations between solar flare radio bursts and associated proton fluxes. II. AFCRL Rpt. TR-75-0579.
- Böhme, A. (1972): Spectral behavior and proton effects of type IV broad-band continua. Solar Phys., 25:478.
- Castelli, J. P., and D. A. Guidice (1976): Impact of current solar radio patrol observations. Vistas Astron., 19:355.
- Croom, D. L. (1971): Forecasting the intensity of solar proton events from the time characteristics of solar microwave bursts. Solar Phys., 19:171.
- Reinhard, R., and G. Wibberenz (1974): Propagation of flare protons in the solar atmosphere. Solar Phys., 36:473.
- Sakurai, K. (1972): Some characteristics of microwave type IV radio bursts and acceleration of solar cosmic rays. Publ. Astron. Soc. Pacif., 84:531.
- Smart, D. F., and M. A. Shea (1978): Prediction of the solar proton time-intensity profiles for the 30 April 1976 event. Space Research, XVIII, pp. 373-376.

Solar-Geophysical Data, NOAA, U. S. Department of Commerce, Boulder, Colo. 80302.

Straka, R. M. (1970): The use of solar radio bursts as predictors of proton event magnitudes. AFCRL Rpt. 70-0002.

Svestka, Z., and P. Simon (eds.) (1975): "Catalog of Solar Particle Events, 1955-1969", D. Reidel Publ. Co., Dordrecht.

Van Hollebeke, M. A. I., L. S. Ma Sung, and F. B. McDonald (1975): The variation of solar proton energy spectra and size distribution with heliolongitude. Solar Phys., 41:189.

DETERMINATION OF PCA VALUE FROM THE CHARACTERISTICS OF SOLAR RADIO BURSTS

S. T. Akinyan, I. M. Chertok, and E. M. Zhulina
IZMIRAN, 142092 Moscow, USSR

The dependence between the maximum PCA value and parameters of solar radio bursts at 3 and 9 GHz is analyzed for the period 1965-1969. The effect of the longitude of the flare is taken into account. To estimate the conditions for proton access into interplanetary space, the intensity of the meter component is used. The energy spectrum of protons is determined from the frequency spectrum of microwave bursts. A method for estimating PCAs from radio data is formulated. The results of a verification with independent data for the periods 1955-1964 and 1970-1977 are given.

1. INTRODUCTION

The definite regularities characterizing the relationship between the parameters of the proton fluxes and radio bursts accompanying a flare were established by Akinyan et al. (1977; see also Akinyan et al., Quantitative diagnostics of solar proton flares by radio data, presented at this workshop). From these regularities, a method has been formulated, which makes it possible to calculate promptly the expected parameters of the >10, >30, and >60 MeV protons near the Earth from meter and microwave radio burst data. The heliolongitude of the flare and the conditions for proton access into interplanetary space are taken into account.

Moreover, a quantitative diagnostic of proton flares has a second objective, namely, estimating the polar cap absorption (PCA) accompanying the flare. Generally speaking, the PCA value can be estimated from the preliminarily calculated intensity of the >10 MeV protons, J , using the well-known empirical relation $J = 20 A^{1.7}$ (Driatsky, 1974), where A is the daytime absorption in dB from a 30 MHz riometer. However, it seems reasonable to use the method proposed by Akinyan et al. (1977) for PCAs directly. This approach automatically allows for the contribution of particles with various energies to the absorption, including protons with $E < 10$ MeV.

It should be emphasized that we are speaking about the estimation of the absorption caused by protons, which relatively rapidly leave the flare region in the form of an independent flux. The effects of low energy protons that arrive at the Earth with the flare-generated shock waves are not taken into consideration.

Attempts to establish a relationship between the PCA value and the parameters of corresponding microwave radio bursts have already been made (Straka, 1970; Croom, 1973). However, a number of important factors, i.e., the influence of the flare heliolongitude, the conditions for protons escaping from the solar corona (meter radio component) and the energy spectrum of the particles (frequency spectrum of microwave radio bursts), were disregarded.

In Section 2 of this paper, the main effects, determined from the analysis of PCA and radio burst data for the reference interval 1965-1969, are described, and a method for estimating the PCA value from these effects is formulated (Akinyan et al., 1978; Akinyan and Chertok, 1979). The results of a verification of the method from independent data for the periods of 1955-1964 and 1970-1977 are given in Section 3 (Akinyan et al., 1979).

The information on flares, radio bursts, and PCA events, published in NOAA Solar Geophysical Data, IAU Quarterly Bulletin on Solar Activity and Catalogs (Švestka and Simon, 1975; Driatsky et al., 1979), are used.

2. ANALYSIS OF THE EVENTS FOR A REFERENCE SAMPLE

The reference sample consists of the PCA events with maximum value $A \geq 0.4$ dB for the period 1965-1969 as well as a number of large events for 1971 and 1972 that have been unambiguously identified with flares on the solar disk. According to Akinyan et al. (1978) and Akinyan and Chertok (1979), the regularities characterizing the relationship between PCA and solar radio emission are essentially analogous for all considered initial parameters of the microwave bursts at 3 and 9 GHz: maximum intensity, S , integrated flux of the increasing phase, R , and total integrated flux, P . Therefore, in order to illustrate these regularities here it is sufficient to consider one parameter only, for example, maximum flux density for a burst at 3GHz, S_3 .

In analyzing the PCA events, we assumed that the azimuthal propagation of protons takes place in the corona (see Reinhard and Wibberenz, 1974).

Following Akinyan et al. (1977), let us first of all consider the PCA events associated with the flares which are localized in a so-called optimal longitude interval (OLI; the heliolongitudes 20-80° West). Within this interval, the influence of the flare longitude on the parameters of proton fluxes is insignificant. Figure 1 shows the relationship between the peak intensity of microwave radio bursts at 3 GHz, S_3 , and the maximum PCA value, A , for the events localized in the OLI. One can see that there is a definite spread. This is partly due to the fact that the important factors that influence the PCA value, such as the conditions for particles escaping from the corona and the energy spectrum of protons, are omitted. However, on the whole, a certain dependence exists between the values of A and S_3 . It will be characterized by the intensity function $A(S_3)$, i.e., by the curve shown in Figure 1 and the corresponding empirical expression (Akinyan et al., 1978).

We can calculate for each event a so-called attenuation value, ψ , determined as the ratio of the observed absorption, A_0 , to the absorption, A_c , calculated from the parameter S_3 in accordance with the intensity function $A(S_3)$. The value $\psi = A_0/A(S_3)$ allows for a transfer from the OLI to an arbitrary flare longitude and therefore permits the analysis of proton access into interplanetary space and the influence of the proton energy spectrum on the estimation of the PCA value.

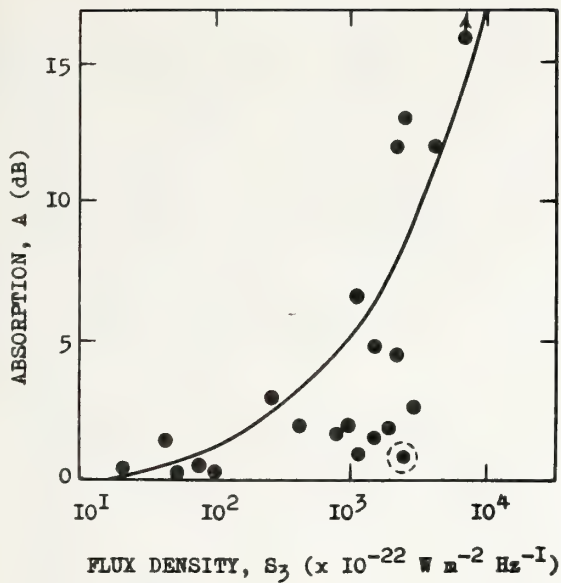


Figure 1. Maximum absorption values A versus parameter S_3 for flares localized in OLI.

Let us analyze the mode of distribution of the events with different characteristics in the "attenuation value ψ - flare heliolongitude θ " diagram (Figure 2). In order to take into account the conditions for particles escaping from the flare region, the events are divided into two categories. The first category consists of the events with an intensive meter component which is supposed to correspond to favorable escape conditions. The events of this category have the following observational characteristics: maximum flux density at frequencies $f \leq 245$ MHz, $F \geq 5000$ f.u. (1 f.u. = $10^{-22} \text{ W m}^{-2} \text{ Hz}^{-1}$) or a dynamic spectrum containing type II or IV bursts of importance ≥ 3 . The second category is formed from the rest of the events with a weak meter component, i.e., with unfavorable escape conditions.

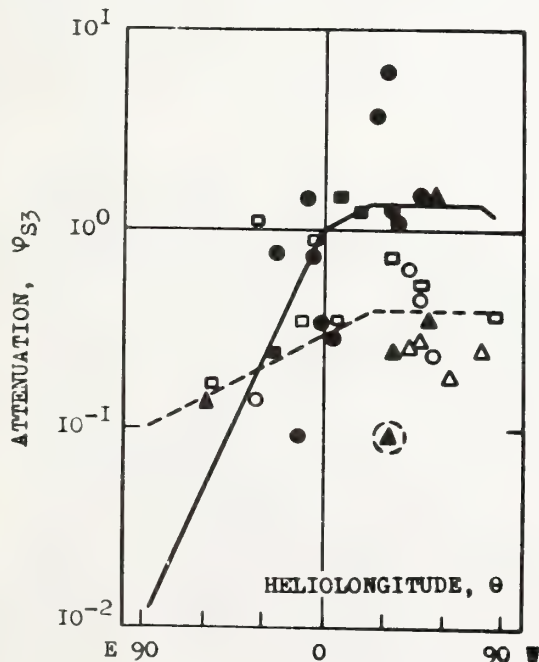


Figure 2. "Attenuation value ψ - flare longitude θ " diagram. Black signs represent events with a favorable escape condition (intensive meter component). White signs represent those with an unfavorable escape condition (weak meter component).

Information on the proton energy spectrum may be obtained from the analysis of the frequency spectrum of the microwave radio bursts. Let us separate into a group the events with a "soft" radio spectrum, in which at the high frequency part of the U-shaped spectrum of the burst, the flux density peaks at $f_{\max} < 8.8$ GHz. The events of this group are marked by squares in Figure 2. When the event satisfies one of the following conditions: $f_{\max} > 15$ GHz, $\alpha < 0.5$ and $f_{\max}/f_{\min} > 10$, it is attributed to a group with a "hard" radio spectrum (triangles). Here α is the index of the power frequency spectrum in the region $f > f_{\max}$, and f_{\min} is the frequency at which the intensity in the decimeter region attains its minimum (see Bakshi and Barron, 1975). The rest of the events are classified as the intermediate radio spectrum (circles).

The analysis of Figure 2 shows that for the PCA events, the same effects take place which have been revealed by Akinyan et al. (1977) for the relationship between the proton flux parameters and radio bursts. These effects may be briefly described as follows:

1. Within the OLI, the attenuation value ψ , and consequently, the absorption value do not show any systematic dependence on the flare longitude θ .
2. Outside the OLI a visible attenuation of the absorption is observed: the value ψ decreases when the eastern flare longitude increases.
3. There is a clear difference between the events with intensive and weak meter components. Within the OLI, the former are mainly concentrated in the region $\psi > 1$ (higher absorption) whereas the latter are localized in the region $\psi < 1$ (relatively small absorption). Outside the OLI, at the eastern half of the solar disk the relation is inverse: the PCA events from the flares with intensive meter component experience stronger attenuation than those with the weak meter component. This effect may be taken into account by two longitude attenuation functions $\psi_{1,2}(\theta)$. In Figure 2, these functions are shown by the solid and dashed lines for the events with intensive and weak meter components, respectively.

The qualitative interpretation of the effects described above was proposed by Akinyan et al. (1977, 1978) in the context of azimuthal propagation of coronal protons. In particular, these effects confirm the assumption that the intensity of the meter radio bursts and the conditions for particles escaping from the flare region are correlated, and also testify to the importance of consistently including the flare longitude.

Indeed, when the meter component is intensive (the open magnetic field configuration), the particles escape more or less freely into interplanetary space directly from the flare region in a form of a relatively narrow (in longitude) beam. On the other hand, when the meter radio emission is weak (the closed magnetic field), the immediate escape of particles is difficult, and they are forced to leave the flare region, propagating mainly in the azimuthal direction along the solar surface. Then, the intensity of proton fluxes arriving at the Earth, and consequently, the absorption from the proton flares with an intensive meter component and localized in the OLI, is higher due to a free quasiradial escape of the particles. However, when such flares occur outside the OLI, on the eastern hemisphere, the bulk of protons propagate far from the Earth, and the corresponding events are considerably weakened. But, if a proton flare with a weak meter component takes place on the eastern hemisphere, then as a result of the preferential azimuthal propagation of the particles, the relative quantity of protons reaching the western hemisphere and arriving at the Earth increases, and the attenuation value, ψ , happens to be relatively small for such events.

4. In analyzing the PCA events, an additional effect, connected with peculiarities of the frequency spectrum of the microwave radio bursts, is revealed. The proton flares with the "soft" frequency spectrum (the squares in Figure 2) are followed by relatively strong absorption. It is believed to be due to the fact that for these events the corresponding proton fluxes are characterized by a very soft energy spectrum as well. The analysis shows that within the OLI, the index of the differential energy proton spectrum in the range of 10-30 MeV is satisfied when $\gamma \geq 3.2$. On the other hand, the proton flares with "hard" radio spectra, which corresponds to the most hard energy proton spectra ($\gamma < 2.25$) are accompanied by relatively small absorption (the triangles in Figure 2). To take this effect into account, an additional corrective coefficient, k , is introduced, which must be multiplied by the appropriate longitude attenuation function, $\psi_{1,2}(\theta)$ (Akinyan et al., 1978; Akinyan and Chertok, 1979).

Bearing in mind the regularities described above, the general expression for estimating the maximum PCA value from a flare with heliolongitude θ and a radio burst intensity at 3 GHz, S_3 , has the following form

$$A = k \cdot \psi_{1,2}(\theta) \cdot A(S_3) \quad (1)$$

where $A(S_3)$ and $\psi_{1,2}(\theta)$ are functions of intensity and longitude attenuation. The latter is chosen with respect to the meter component intensity of the radio bursts; k is a corrective coefficient which takes into account the character of the frequency spectrum of the microwave radio bursts.

Concrete expressions of the functions of intensity and longitude attenuation as well as the meaning of the coefficient k for various initial parameters $S_{3,9}$, $R_{3,9}$, and $P_{3,9}$ are given by Akinyan et al. (1978) and Akinyan and Chertok (1979).

In order to estimate the time parameters characterizing the delay of the onset and the maximum of the absorption with respect to the microwave burst maximum, one can use the corresponding time functions for the proton fluxes obtained by Akinyan et al. (1977).

3. RESULTS OF THE CONTROL CALCULATION

It is necessary to verify with independent data the established regularities and the method for the quantitative diagnostic of the proton flares. We carried out the preliminary verification with data for 1955-1964 and made a detailed control calculation of the PCA value with data for 1970-1977.

The verification for the period 1955-1964 (Akinyan et al., 1978) is insufficient because for many events the information on the radio bursts was incomplete. For the same reason, in estimating the PCA value, we have restricted ourselves to two initial parameters, namely, the maximum burst intensity at 3 and 9 GHz, i.e., S_3 and S_9 . The results of the comparison of the observed absorption values A_0 with the values A_c , calculated from the initial radio parameter S_3 for the PCA events during the magnetoquiet conditions, are illustrated in Figure 3a. One can see that on the whole the agreement between the values A_0 and A_c is rather good: the correlation coefficient is sufficiently high, $r \approx 0.91$. When the parameter S_9 is used for calculation of the absorption, the correlation coefficient is $r \approx 0.88$.

In analyzing the period 1970-1977, the events were selected on the base of a definite proton flare criterion (Akinyan et al., 1979). For every event, the absorption value was calculated from formulas analogous to equation (1), by substituting the initial parameters $S_{3,9}$, $R_{3,9}$ and $P_{3,9}$ into the corresponding supporting functions which have been established by the reference sample of the PCA (see Section 2). As a result, there are six calculated absorption values. In addition, we averaged the absorption values calculated from the initial parameters at 3 and 9 GHz, as well as over all of the initial parameters at both frequencies, i.e., one has three more calculated values, \bar{A}_3 , \bar{A}_9 , and $\bar{A}_{3,9}$.

The typical relationship between the observed absorption values A_0 and the calculated ones A_C is illustrated in Figure 3b, where the values $\bar{A}_{3,9}$ are given as A_C ; black and white circles correspond to the events on the western and eastern solar hemispheres, respectively. One can see that the calculated absorption values are quite close to the observed ones. In particular, in 80 percent of the events, the relative difference, δA , between the calculated values $\bar{A}_{3,9}$ and the observed absorption does not exceed $\delta A \approx 0.5$, and in 55 percent of the events $\delta A \leq 0.3$. Moreover, the correlation coefficient between the values A_0 and A_C is equal to $r \approx 0.81, 0.76, 0.73, 0.81, 0.81$, and 0.82 for the parameters S_3, R_3, P_3, S_9, R_9 , and P_9 , respectively, and $r \approx 0.80, 0.83$, and 0.83 for the averaged values \bar{A}_3, \bar{A}_9 , and $\bar{A}_{3,9}$.

This the analysis of the events for the reference sample and the positive results of the control calculations show that radio data (in particular, data on the intensity, integrated parameters, and frequency spectrum of the microwave radio bursts, as well as on the intensity and dynamic spectrum of the meter component) indicate it is possible to make timely estimates of the expected value of the PCA by taking into account the flare heliolongitude, the escape conditions of protons into the interplanetary space, and its energy spectrum.

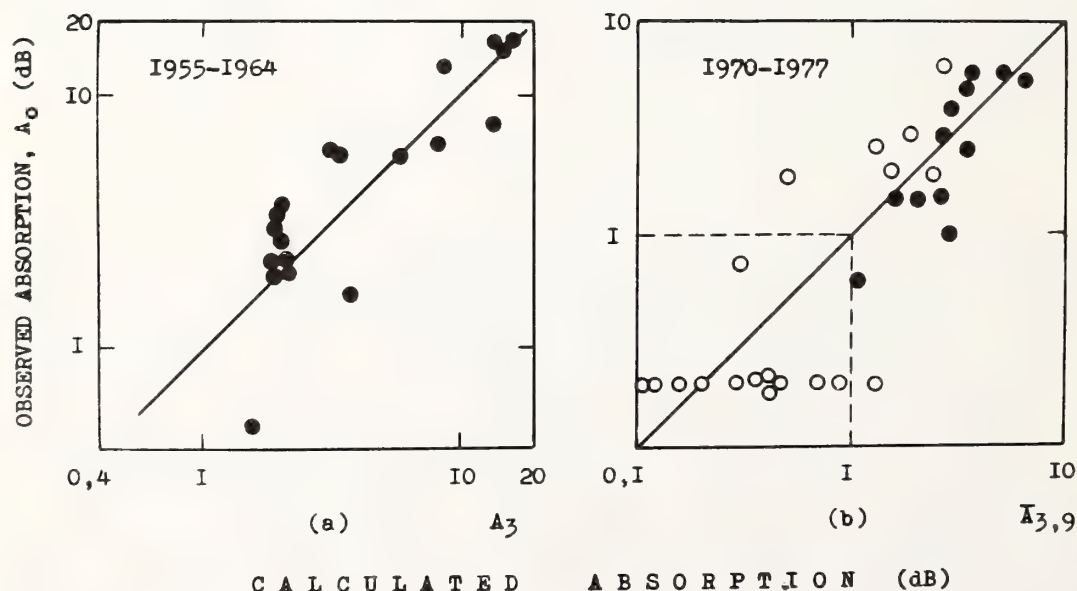


Figure 3. Correlation between observed absorption values A_0 and calculated values A_C (a) and $\bar{A}_{3,9}$ (b) for periods 1955-1964 and 1970-1977, respectively.

REFERENCES

- Akinyan, S. T., V. V. Fomichev, and I. M. Chertok (1977): Determination of solar proton parameters near the Earth by radio bursts. I. Intensity function. II. Longitude attenuation function. III. Time parameters. Geomagn. i Aeronomiya, 17:10, 177, 596.
- Akinyan, S. T., E. M. Zhulina, and I. M. Chertok (1978): Estimations of PCA value by characteristics of solar radio bursts. Geomagn. i Aeronomiya (in press).
- Akinyan, S. T., and I. M. Chertok (1979): Relationship between PCA value and integrated parameters of microwave radio bursts. Geomagn. i Aeronomiya (in press).
- Akinyan, S. T., E. M. Zhulina, V. A. Ulyev, I. M. Chertok, and A. V. Shirochkov (1979): Control calculation of PCA value by data on solar radio bursts from the period 1970-1977. Geomagn. i Aeronomiya (in press).
- Bakshi, P., and W. R. Barron (1975): Spectral correlations between solar flare radio bursts and associated proton fluxes. II. AFCRL Rpt. TR-75-0579.
- Croom, D. L. (1973): Solar microwave bursts and polar cap absorption. Planet. and Space Sci., 21:707.
- Driatsky, V. M. (1974): Nature of anomalous absorption of cosmic radio emission in the lower ionosphere of high latitudes. Gidrometeoizdat, Leningrad.
- Driatsky, V. M., V. A. Ulyev, and A. V. Shirochkov (1979): Catalog of the PCA events for 1970-1977. Preprint AANII, Leningrad (in press).
- Quarterly Bulletin on Solar Activity, I.A.U., Eidgenössische Sternwarte, Zürich.
- Reinhard, R., and G. Wibberenz (1974): Propagation of flare protons in the solar atmosphere. Solar Phys., 36:473.
- Solar Geophysical Data, NOAA, U.S. Department of Commerce, Boulder, Colo.
- Straka, R. M. (1970): The use of solar radio bursts as predictors of proton event magnitudes. AFCRL Rpt. 70-0002.
- Švestka, Z., and P. Simon (Eds.) (1975): Catalog of Solar Particle Events, 1955-1969. D. Reidel Publ. Co., Dordrecht.

PREDICTION OF SOLAR PROTON EVENTS USING HARD X-RAY EMISSION

S. R. Kane and R. P. Lin
Space Sciences Laboratory, University of California
Berkeley, California 94720

Impulsive solar flares are known to produce energetic (10 - 100 keV) electrons in what is generally called the "first stage" of acceleration (cf. Kane, 1974; Lin, 1974). The electrons in the vicinity of the flare region on the Sun produce hard X-rays (~ 20 keV) by bremsstrahlung and microwave radio emission by the synchrotron process. Some of the large impulsive flares have a "second stage" of acceleration in which higher energy (~ 100 KeV) electrons and energetic (~ 10 MeV) protons are produced. Some of these energetic protons propagate away from the Sun through the interplanetary space and produce pronounced effects on the earth's environment. It is therefore important to predict whether a flare is likely to produce energetic protons.

The characteristics of the impulsive electron spectrum produced in a flare are expected to be an important parameter in determining the probability of proton acceleration in that flare. A "remote sensing" of this electron spectrum at the Sun is possible through either the observations of the hard X-ray or microwave emission of the flare. Previous studies of the prediction of solar proton flares primarily used the spectral characteristics of the radio emission (cf. Castelli and Barron, 1977; Bakshi and Barron, 1979). An alternative approach, which could lead to a more reliable short-term prediction of solar proton events, is to examine the hard X-ray emission associated with solar flares. Compared to the radio emission, which depends critically on the details of the magnetic field and density structure in the source region, the hard X-ray emission depends primarily on the average ion density in the X-ray source. Thus, the hard X-rays are expected to provide more accurate and reliable information about the energetic electrons in the flare and hence about the possibility of a solar proton event.

A study using the 10 - 50 keV X-ray measurements made with ionization chambers aboard the OGO-1 and OGO-3 satellites (Arnoldy et al, 1968; Kane and Winckler, 1969) indicated that solar proton events are usually produced by those flares which produce a hard X-ray (~ 20 keV) energy flux $\sim 5 \times 10^{-5}$ ergs cm⁻² sec⁻¹ as seen at 1 A. U. (Lin and Hudson, 1976). Thus by monitoring the emission of solar X-rays ~ 20 keV with an experiment aboard a spacecraft such as ISEE-3 (Anderson et al, 1978; Kane and Anderson 1978), which is in a heliocentric orbit and hence continuously monitors the Sun, it is possible to know if a flare is likely to produce a solar proton event. Since the protons with energy ~ 10 MeV arrive near the earth much later than the hard X-rays, an advance warning of ~ 20 minutes could be obtained in real time.

ACKNOWLEDGEMENTS: This research was supported by NASA under contract NAS5-22307.

REFERENCES

- Anderson, K. A., S. R. Kane, J. H. Primbsch, R. H. Weitzman, W. D. Evans, R. W. Klebesadel, and W. P. Aiello (1978): 1978 IEEE Trans, Geosc. Electronics, GE-16, 157.
- Arnoldy, R. L., S. R. Kane, and J. R. Winckler (1968): Ap. J., 151, 711.
- Bakshi, P., and W. Barron (1979): J. Geophysic. Res., 84, 131.
- Castelli, J. P., and W. Barron (1977): J. Geophys. Res., 82, 1275.
- Kane, S. R. (1974): in Gordon Newkirk, Jr. (ed.) Coronal Disturbances, IAU Symp. 57, p. 105.
- Kane, S. R., and K. A. Anderson (1978): Paper No. SS 18, presented at the Fall Meeting of the American Geophysical Union, San Francisco, 4-8 December.
- Kane, S. R., and J. R. Winckler (1969): Univ. of Minnesota Cosmic Ray Tech Rep. CR-135.
- Lin, R. P., 1974, Space Sc. Rev., 16, 189.
- Lin, R. P., and H. S. Hudson (1976): Solar Phys., 50, 153.

DIAGNOSTICS OF SOLAR FLARES AND FORECAST OF THEIR GEOEFFECTIVENESS

Frolov S.G.

Institute of Applied Geophysics, Goscomhydromet.

Information content of parameters characterizing electromagnetic radiation of solar flares is studied. Diagnostic solving rules are obtained which allow to make a distinction between solar flares resulted in generation of cosmic radiation protons with high energies creating irradiation doses of a certain threshold level in the near Earth cosmic space as well as geoeffective interplanetary shock waves and flares which do not result in such geoeffective processes. Regression equations are derived which are used for the forecast of irradiation characteristics of solar protons (integral flux, spectrum rigidity index, irradiation dose) for the forecast of the time of shock wave arrival and the extent of the geomagnetic field disturbance.

The investigation of problems concerned with early diagnostics of solar flares and forecast of their geoeffectiveness is an urgent problem of solar-terrestrial physics. This is explained by the dominant effect of electromagnetic radiation fluxes, highly energetic corpuscles and solar plasma generated by solar flares which cause in the near Earth space the disturbance of radio wave propagation on the lighted side of the Earth, deteriorate radiological situation in the near Earth space (NES), initiate severe geomagnetic disturbance and so on.

As a rule flux generation of flare electromagnetic radiation lasts from several minutes to several tens of minutes, the time of propagation to the Earth takes about 8 minutes, their geoeffective impact time is not more than tens of minutes. Protons of solar cosmic rays (SCR), a component of flare highly energetic corpuscular radiation present the greatest radiation hazard and have the following temporal characteristics: generation - several tens of minutes, propagation from the Sun to the Earth - several hours, geoeffective impact - several days. The injection of highly turbulent plasma into interplanetary space leads as a rule (in powerful flares) to the origination of geoeffective interplanetary shock waves (GISW); their propagation time lasts from several tens of hours to 2-3 days, geomagnetic disturbance caused by them lasts several days.

Highly energetic flux intensities of SCR protons and geomagnetic disturbances correlate with flare strength - this is explained by the fact that the main fraction of flare energy is released as magnetohydrodynamic motions transferred to the solar wind and through it they affect the Earth's magnetosphere and as highly energetic SCR protons /1/. Considering this and comparing the characteristic time of generation, propagation and geoeffective impact of solar flare radiation component it should be supposed that the components of electromagnetic radiation in X-ray and optical ranges being closely connected with the process occurring during a flare may be important indications of GISW generation and SCR fluxes and hence they can be used as predictors when diagnosing solar flares and forecasting their geoeffectiveness in spite of a relatively small fraction of internal energy released. The same is true for flare radio emission. For example bursts of types II and IV are predictors of shock wave motion in the solar corona and of SCR generation /2/.

Forecast of SCR protons or flare geomagnetic disturbances with the use of predictors of soft X-ray, radio emission and

optical radiation can be divided into two steps: a) at the first step the fact of generation by a solar flare of SCR highly energetic protons or GISW is established or expected level of irradiation in NES from SCR higher than a given threshold - source flare diagnostics; b) at the second step the following is forecasted: quantitative characteristics of SCR protons (integral flux of protons, spectrum rigidity index, irradiation dose for the selected protection of space vehicles); GISW arrival time to the Earth, and disturbance degree of geomagnetic field. Taking into account the necessity of obtaining both qualitative and quantitative forecasting characteristics as well as the presence of discrete and continuous predictors, the problem in such a formulation was solved by multidimensional regression analysis.. To distinguish more informative predictors an algorithm developed on the basis of method synthesis was used sieving and decrease of square error sum neglecting i - variable at each elimination of step of n -predictors of the original multitude /3/. At the step of diagnostics a solving rule was given as

$$f(x) = b_0 + \sum_{i=1}^n b_i x_i ; \quad (1)$$

where $x = \{x_i\}$, $i = 1 \dots n$ - predictor multitude. Quality criterion of the solving rule was determined by expectation of a penalty function $c(f)$

$$\phi = M[c(f)] ; \quad (2)$$

as $c(f)$ a square of recognition error was chosen $c(f) = [y - f(x)]^2$. The procedure of solving rule derivation was reduced to the determination of vector \vec{B} which realizes $\min_{\vec{B}} M[c\{y - f(x, \vec{B})\}]$. At the second step the oriented detection of multidimensional regressions connecting the forecasting quantitative characteristics of flare geoeffectiveness with the optimum predictor composition was carried out.

The analysis of heliogeophysical situation for the period of 1967 to 1974 /4-7/ determined the initial flare ensemble which was used in solving of diagnostics problems and forecasting of

geoeffective characteristics, there were 100 flares all in all. a relatively small volume of sampling was explained by the necessity to meet the requirements of purity and homogeneity of data including high reliability of identification of GISW and SCR which was realized allowing for the real time of delay of these processes and the completeness of predictor set where we used: x_1, x_2 - area and flare brightness in H_α ; x_3, x_4, x_5 - maximum intensity, time of decrease and relation of increase time to decrease time of X-ray burst in the range of 2-12Å; x_6 to x_{10} - spectral types of radio burst from I to V respectively (for type IV a broadband component in the metre range of wavelength was used. x_6 to x_{10} are quantified as 1 or 0 if radio burst of corresponding type is observed or it doesn't). For the sake of convenience the mentioned predictors were normalized approximately in the range of 0+1. The estimation of event division level into classes - P (P - the sum of events correctly distributed with classes) was carried out by education and examination method, statistical significance of the obtained regression equations and their coefficients were derived by classical methods /8/.

SOLAR FLARE DIAGNOSTICS AND FORECASTING OF SCR PROTON RADIATION CHARACTERISTICS

Radiation characteristics of SCR protons in NES essentially depend of flare strength, its heliocoordinates, interplanetary parameters determining particle transfer and occurrence of GISW during the effective phase of SCR event. Depending of power and dynamical characteristics of flare integral SCR proton fluxes vary within the range of $10^3 + 10^9 \text{ cm}^{-2} \text{ ster}^{-1}$, spectrum rigidity index - γ varied from 0.3 to 5, irradiation dose - from tens of millirad to hundreds of rad. As it follows from theoretical models /9,10/ and experimental results /4/, the process of SCR proton propagation in the interplanetary space is symmetric to the force line of interplanetary magnetic field (IMF) originat-

ing from the region of $\lambda_0 = 40-60^\circ\text{W}$ of the solar disk and passing through the Earth. When heliolongitude of flares is moved apart by $130-160^\circ$ to the West (W) or to the East (E) from the corotation point of a given force line SCR proton flux is decreased almost as much as two orders of magnitude. On the other hand GISW propagating in the interplanetary environment with velocities notably exceeding the velocity of the quiet solar wind considerably straiten out force lines that leads to the approach of the force line to the Earth along which protons were injected if the flare occurred to the east of λ_0 or recession from the Earth if the flare occurred to the west of λ_0 . This effect which we observed in 60% of all the considered events leads to the appearance in time profiles of SCR events of positive or negative intensity variations accordingly. The magnitude of such variations as a rule amounts to $0.5-2$ orders of magnitude depending on the degree and direction of effective angular distance variation between heliolongitudinal flare λ and corotation point of IMF force line passing through the Earth - λ_0 . Taking into account these peculiarities of SCR proton propagation from the initial event ensemble 40 flares were selected where SCR proton generation with the energy more than 60 Mev (class A) occurred, and 50 flares where there was no such a generation (class K). At the step of diagnostics of solar flares that generate or do not generate SCR protons by means of statistical analysis using the above mentioned algorithm we obtained several solving rules in which P division level is within the limits of 0.85-0.95. Parameters of X-ray were the most informative for example $P(x_3, x_4, x_5, x_9) = 0.95$, $P(x_3, x_4, x_9) = 0.91$, $P(x_3, x_4) = 0.85$ /13/. Similar results are obtained for the division of flares into classes for which irradiation level in NES is higher or lower than the assumed threshold D_0 for the fixed protection of space vehicle T_i . Proceeding from the practical requirements real-time diagnostics four thresholds were chosen $D_0(T_i)$: $D_0 = 10$ and 200 mrad for

$T_1 = 0.3 \text{ g/cm}^2 \text{ Al}$, $D_0 = 10$ and 50 mrad for $T_2 = 1 \text{ g/cm}^2 \text{ Al}$ and $D_0 = 1 \text{ mrad}$ for $T_3 = 3 \text{ g/cm}^2$. Thus for example for $D_0 = 10 \text{ mrad}$ and T_2 solving rules are obtained with $P(x_1, x_3, x_4, x_6, x_7, x_{10}) = 0.94$;

$P(x_1, x_3, x_4, x_7) = 0.90$; $P(x_3, x_4) = 0.83 / 14/$. Confidence intervals for \bar{P} and coefficients of multiple correlation - which is in the interval of $0.74-0.85$ are equal to ± 0.06 and 0.08 respectively and are provided with 0.95 probability.

The comparison of calculation results for sampling for the increasing branch (1967-1969) and decreasing branch (1970-74) of solar activity allows us to hope that the quality of event division into classes must no considerably depend 11 year cycle phase /14/.

For the forecast of proton quantitative characteristics of SCR, i.e. of integral proton flux - I ($E > 60 \text{ Mev}$), irradiation dose $D(T_i)$, and proton spectrum rigidity index (in the flux maximum - γ_M and on the whole for an event - γ_i), regression correlations were obtained using SCR events (class A) data:

$$Y = b_0 + \sum_{i=1}^n b_i x_i ; \quad (3a)$$

or

$$Y = b_0 + \sum_{i=1}^n b_i x_i + \sum_{i=1}^n b_{ii} x_i^2 ; \quad (3b)$$

where $Y = \lg I$ ($E > 60 \text{ Mev}$); $Y = \lg D(T_i)$; $Y = \gamma_M$; $Y = \gamma_i$.

Table 1 gives the main statistical characteristics of equations: a) residual dispersion - S^2 at optimum predictor composition $\{x_1, \dots, x_k\}$; b) mean estimation of general statistical significance of regression equation - A ; c) relative mean deviation of the forecasting magnitude - $S/\bar{Y} / 13, 14/$.

Let us note that the regression equation for integral flux is obtained allowing for flare heliolongitude effect (according to model /9/) and equations for the dose (regression form -(3b)) are obtained for flares in heliolongitudinal interval $30^\circ \text{E} - 90^\circ \text{W}$ thereby in both cases we tried to diminish the effect of flare heliocoordinates, propagation process and GISW on forecasted characteristics. This naturally has lead to some

narrowing of the class of SCR events for which it is possible to use these regression data in practical work. Obtained results, however, meet the main requirements of practical forecasting of SCR proton radiative characteristics. Thus for example, before SCR arrival or accumulation of permissible dose it is possible to estimate both the magnitude of the expected dose with the accuracy of 2 to 6 times depending on the protection thickness and spectrum rigidity index with accuracy not more than 34%.

MAIN STATISTICAL CHARACTERISTICS OF FORECASTING REGRESSIONS

Table 1

y	S^2	$\{x_1, \dots, x_k\}$	A	$s/\bar{y}, \%$
$\lg I(E > 60_{\text{MeV}})$	0.14	1,4,5	3.2	10
$\lg D(T_2)$	0.54	1,2,3	2.1	36
$\lg D(T_3)$	0.38	1,2,3,5	2.4	22
r_m	0.30	1,3,5	2.0	30
r_i	0.43	1,3,5	2.0	34
t	100	2,5,7,8,9	2.4	25
$A_p(\text{max})$	210	1,5	2.0	50

DIAGNOSTICS AND FORECAST OF EFFECTIVE INTERPLANETARY SHOCK WAVES FROM SOLAR FLARES

The initial ensemble of solar flares which was used for diagnostics and forecasting of flare geomagnetic disturbances comprised 36 events where GISW were generated and 48 events without any. GISW delay time was determined by SC record on the Earth /11/. As a result of statistical analysis two solving rules were obtained where the level of class division P was 0.92 ± 0.06 and 0.88 ± 0.06 for predictor composition

$\{x_2, x_3, x_4, x_7\}$, $\{x_3, x_4, x_7\}$ respectively /15/. These results confirm physical assumptions for identification of a geoeffective shock wave sources according to selected predictors with relatively high degree of reliability.

For the delay time of shock wave arrival to the Earth - t which was used in sampling changed in the interval of 17-70 hours after elimination of non-informative indicators, regression equation of (3a) type was obtained - see Table 1, with residual dispersion $S^2=100$ and predictor composition $\{x_2, x_5, x_7, x_8, x_9\}$ which is characterized by coefficients of multiple correlation within confidence limits $0.72 \leq R \leq 0.88$ and mean relative error of arrival time - 25% /15/.

Index A_p was taken as a feature of extent of geomagnetic field disturbance often used both in practical work on diagnostics and geomagnetic disturbance forecast and in research. Namely - maximum value for the period of a given disturbance. Values $A_p(\max)$ varied from 10 to 120 in the considered sampling. After elimination of non-informative features equation of type (3a) was obtained - see Table 1- its correlation coefficient is within confidence limits $0.70 \leq R \leq 0.82$ and mean relative error $A_p(\max)$ is not more than 50%. This result allows to use the equation for forecasting estimations of geomagnetic disturbance intensity.

As it is shown in a number of investigations /2,7,12/ there are factors influencing the character, intensity and duration of flare geomagnetic disturbances: the direction of large-scale solar magnetic field, asymmetry of shock wave front, source heliocoordinates, parameters of solar wind energy transfer process to the magnetosphere. In a given problem of geomagnetic disturbance forecast they were not taken into account and part of statistical spread of data used may be connected with this.

All the obtained regression equations are significant according to F - criterion at the level of $\alpha = 0.05$, regression

coefficient errors are within the limits of 20-60%. An additional test of solving rules and regression equations was carried out with events of August 2-7, 1972 and it provided satisfactory results /14-15/

The results of this paper testify to a statistically significant relationship between selected predictors of solar flare electromagnetic radiation and parameters characterizing their geoeffectiveness. The obtained solving rules and regression equations are a formalized method of quantitative forecast of solar flare geoeffectiveness consisting of the following aspects:

1) practically after acquisition of data on X-rays, optics, and radio emission it is possible to make the diagnostics of solar flare with high reliability for:

- SCR proton geoeffective flux generation;
- creation of irradiation levels in NES higher or lower than a certain threshold;
- GISW generation;

2) solar flare being attributed to a geoeffective class it is possible to forecast quantitative characteristics of geoeffectiveness:

- SCR proton integral flux with energy more than 60 Mev, then recalculating it for NES considering the effect of heliolongitude according to model /9/;
- irradiation doses for protections 1 and 3 g/cm²Al;
- spectrum rigidity index in the event maximum for SCR event as a whole;
- time delay of GISW arrival to the Earth;
- geomagnetic field disturbance degree.

The present method can be used for varying information volume and part of the obtained here results is used in practical work.

REFERENCES

1. Somov, B. V., S. I. Syrovatsky (1976): Uspekhi fiz. nauk, 120, 217
2. Akasofu, S.-I., S. Chapman Solnechno-zemnaya fizika, M., "Mir", t.2, 1975.
3. Tomin, Yu. A. (1974): Trudy VNIIGMI-MTsD, vyp.1, 70.
4. Solar Geophysical Data, 1967-1974.
5. Sarris, E. T., S. D. Sawhan (1973): Solar Physics, 28, 519.
6. Geomagnetic Data, IAGA Bulletin, 1967-1974.
7. Pudivkin, M. I., A. D. Chertkov (1976): Solar Physics, 50, 213.
8. Rokhvarger, A. E., A. Yu. Shevyakov (1975): Matematicheskoe planirovanie nauchno-tekhnicheskikh issledovaniy, M., "Nauka".
9. Burlaga, L. F. (1967): J. Geophys. Res., 71, 4449.
10. Lupton, J. R., E. G. Stone (1973): J. Geophys. Res., 78, 1007.
11. Burlaga, L. F., K. W. Ogilvi (1969): J. Geophys. Res., 74, 2815.
12. Ivanov, K. G., N. V. Mikerina, L. V. Evdokimova (1974): Geomagnetism i aeronomiya, t.14, No.5, 777.
13. Bezruchenkova T. M., N. A. Mikryukova, N. K. Pereyaslova, and S. G. Frolov: Geomagnetism and Aeronomy, 17, 880-885.
14. Bezruchenkova T. M., N. K. Pereyaslova, and G. S. Frolov (1978): Geomagnetism and Aeronomy, 18, 992-997.
15. Frolov S. G. (1978): Dokl. AN SSSR, 243, No.3, 615-617.

ON SOME PECULIARITIES OF THE GENERATION OF SOLAR FLARE ELECTROMAGNETIC AND CORPUSCULAR RADIATION

M. N. Belovsky and Yu P. Ochelkov
Institute of Applied Geophysics
Moscow, U.S.S.R.

1. INTRODUCTION

During chromosphere flares electrons, protons, α -particles, etc. are accelerated to high energies. According to the estimates of Pinter (1972) accelerated electrons account for 10^{29} ergs and protons for 10^{31} ergs. Protons accelerated in the flare go to interplanetary space and, propagating in it, approach the Earth's orbit. Linear theory describes well enough the process of solar proton transport in interplanetary space. Therefore the measure of a number of flare accelerated protons N_p can be a proton flux at the maximum of proton event I recorded with the help^p of satellites. (Belovsky et al., 1978).

The acceleration of electrons in a flare is evidenced by radio emission and X-ray as well as by registration of them in space by satellites. At present there are numerous data on microwave radio bursts of type IV which are generated by flare-accelerated electrons. Though the mechanism of microwave burst emission has not been determined yet (gyro-synchrotron emission is preferable), nevertheless it is generally assumed that the radiation process can be described by linear equations. (Jokipiy, 1976). Therefore radio emission flux at maximum T can be a measure of the number N_e of electrons accelerated in the flare

$$T \sim N_e.$$

The investigation of proton event distribution function with intensity I at the maximum and microwave burst with intensity T at the maximum gives the opportunity, as will be shown, to find the relation between the numbers of flare-accelerated electrons and protons, as well as to answer the question whether protons with energy 10 MeV are always generated in chromosphere flares accompanied by microwave radio bursts. It is impossible to answer the question by simply counting the proton event numbers since the satellite can fail to record a proton event because of threshold counter sensitivity and background proton flux value (Shvestka, 1976).

In view of further presentation it is very important to preserve the power form of distribution functions in case of the linearity processes transforming the distribution functions. Let $L_{p,e}(N_{p,e})$ be the function of

distribution with the number of flare-accelerated electrons N_e and protons N_p . Let us find the relation with the function $L_r(T)$ of radio burst distribution^p with intensity at the maximum and the function $f(I)$ of proton event distribution with intensity at the maximum. Since there^p is no unique relation between N_e and T or between N_p and I because of the variety of conditions in the radiation region, proton release, and propagation, it is necessary to apply the probability approach. Through $\sigma_{p,e}(N_{p,e}, T_{p,r})$, we denote the probability of registration of a proton event with $T_{p,r}$ intensity at the maximum within single intensity interval at the generation^p of protons in the flare or the corresponding probability of registration of microwave burst with $T_{p,r}$ intensity at the maximum within single intensity interval at the generation of N_e electrons. Since the processes are linear

$$\sigma_{p,e}(N_{p,e}, T_{p,r}) = \sigma\left(\frac{N_{p,e}}{T_{p,r}}\right) \frac{1}{N_{p,e}}.$$

Then

$$L_{p,r}(T_{p,r}) = \int_0^{\infty} dN_{p,e} \sigma_{p,e}\left(\frac{N_{p,e}}{T_{p,r}}\right) \frac{1}{N_{p,e}} L_{p,e}(N_{p,e}). \quad (1)$$

Denoting $\frac{N_{p,e}}{T_{p,r}} = x$, rewrite (1) as

$$L_{p,r}(T_{p,r}) = \int_0^{\infty} dx \sigma_{p,e}(x) \frac{1}{x} L_{p,e}(xT_{p,r}) \quad (2)$$

If $L_{p,e}(xT_{p,r})$ is a power function then from (2) it follows that

$L_{p,r}(T_{p,r})$ is also a power function of the same power.

Further we need the following distribution functions: $L_r(t)$, $\phi_r(T)$ and $f(I)$, $F(I)$ -respectively differential and integral functions^r of radio burst and proton event distributions with intensity at the maximum; $L_r(T, I)$, $\phi_r(T, I)$ -differential and integral distribution functions which were accompanied by proton events at the maximum $>I$ (proton ratio bursts); $f(I, T)$, $F(I, T)$ -differential and integral functions of proton event (preceded with^p radio bursts with maximum intensity $>T$) distributions with intensity at the maximum. Differential and integral functions are related as

$$F(T) = \int_T^{\infty} dT' f(T').$$

Since radio bursts with the assumed value of intensity T at maximum are accompanied by proton flares of various intensities, it is necessary to consider the probability of observation of proton events with intensity I at the maximum within the single intensity range after the radio burst with T intensity: $w(T; I)$.

Accordingly

$$w(T, I) = - \frac{\frac{\partial}{\partial T} f_p(I, T)}{L_r(T)} . \quad (3)$$

When proton event intensities are not connected with the corresponding radio burst intensity, the following relationship is valid:

$$f_p(I, T) = f_p(I) \phi_r(T) .$$

For (3) we obtain $w(T, I) = f_p(I)$. It is a trivial case, which means that the probability of recording^p the proton event does not depend on radio burst intensity and it is determined only by the function of proton event distributions.

Let us consider the problem of normalization of $w(T, I)$. Having integrated (3) over I we obtain

$$\int_0^{\infty} dI w(T, I) = \frac{- \frac{\partial}{\partial T} \int_0^{\infty} dI f_p(I, T)}{L_r(T)} .$$

Two cases are possible:

$$\int_0^{\infty} dI f_p(I, T) \phi_r(T)$$

and

$$\int_0^{\infty} dI f_p(I, T) = \phi_r(T, 0) < \phi_r(T) .$$

In the first case we obtain

$$\int_0^{\infty} dI w(T, I) = 1 .$$

In the second one

$$\int_0^{\infty} dI w(T, I) = \frac{L_r(T, 0)}{L_r(T)} < 1$$

where $L(T, 0) = - \frac{\partial}{\partial T} \phi_r(T, 0)$.

The first case is realized if all the microwave bursts are followed by proton events; the second case corresponds to the presence of two families of radio bursts: proton bursts followed by proton events with the assumed proton energies (in our case > 10 MeV) and by non-proton bursts which are not followed by the generation of assumed energies.

In the second case we perform renormalization by the introduction of a new function,

$$w_o(T, I) = w(T, I) \frac{L_r(T)}{L_r(T, 0)}$$

Then we obtain again $\int_0^{\infty} dI w_o(T, I) = 1$.

As shown below the second case is realized; therefore it is necessary to introduce additional differential and integral function of proton radio burst distribution:

$$L_r(T, 0), \phi_r(T, 0).$$

According to the definition,

$$\lim_{I \rightarrow 0} L_r(T, I) = L_r(T, 0) .$$

It is easy to demonstrate that the following relationships of the considered distribution functions are valid:

$$f_p(I) = \int_0^{\infty} dT w_o(T, I) L_r(T, 0) . \quad (4)$$

$$\phi_r(T, I) = F_p(I, T) = \int_0^{\infty} \int_0^{\infty} dT' dI' w_o(T', I') \phi(T', 0) \quad (5)$$

$$\phi_r(0, I) = F_p(I) \quad (6)$$

Equation (6) means that the total number of proton events (with intensity $I > 0$) coincides with the total number of proton radio bursts.

2. DISTRIBUTION FUNCTION

To determine distribution functions in this paper, observation data of radio bursts at frequencies 8800 and 2695 MHz carried out at Sagamore Hill and Manila Observatories are used as well as data of patrol observations of protons with E 10 MeV by Explorer 34 and 41 published in Solar Geophysical Data (1967-1974)^P. The period of radio observations is selected to be coincident with that of satellite observations of protons. The period from May 23, 1967, to December 31, 1972, was considered except for intervals from May 3 to June 22, 1969 and from Nov. 15, 1971 to Feb. 1, 1972 when satellite data of patrol observations were absent.

Altogether during the period mentioned 323 and 209 radio bursts with maximum intensity $T > 100$ units ($10^{-22} \text{ W m}^{-2} \text{ Hz}^{-1}$) at frequencies 8800 and 2695 MHz, and 87 proton events with maximum intensity of the proton flux $I > 0.1$ part $\text{cm}^{-2} \text{ s}^{-1} \text{ ster}^{-1}$ were observed according to Solar Geophysical Data (1967-1974) and Van Hollebeke et al. (1975).

On the basis of observation data at the mentioned frequencies, distribution functions $\phi_r(T)$ and $\phi_r(T;0,1)$, $\phi_r(T;1)$, $\phi_r(T;10)$ i.e., the distribution function of radio burst numbers with intensity accompanied by proton events with $I > 0.1; 1; 10$ part. $\text{cm}^{-2} \text{ s}^{-1} \text{ ster}^{-1}$ respectively, were obtained. As it turned out, integral function $\phi_r(T)$ is easily approximated by expression $\phi_r(T) = CT^{-\alpha}$ that is in agreement with Kakinuma and Yamashita (1969), Scalize (1970), and Belovsky and Ochelkov (1977). Kakinuma and Yamashita (1969) and Scalize (1970) obtained $\phi_r(T)$ for intensities of radio bursts beginning with $T > 10$ units. The value of α is close to the value obtained by Belovsky and Ochelkov (1977). Expressions for $\phi_r(T)$ have the following forms:

$$\phi_r(T) = 10^{3.99} T^{-0.75}; \quad V = 8800 \text{ MHz} \quad (7)$$

$$\phi_r(T) = 10^{4.33} T^{-0.97}; \quad V = 2695 \text{ MHz} \quad (8)$$

The best approximation for experimental functions of proton radio burst distribution is obtained as

$$\phi_r(T, I) = M(T+T_0)^{-\alpha}:$$

$$\phi_r(T;0,1) = 10^{3.88} (T+970)^{-0.75}, \quad (9)$$

$$\phi_r(T;1) = 10^{3.88} (T+1700)^{-0.75}, \quad (10)$$

$$\text{and} \quad \phi_r(T;10) = 10^{3.86} (T+4500)^{-0.75} \quad (11)$$

for observations at the frequency of 8800 MHz;

$$\phi_r(T;0,1) = 10^{4.26} (T+308)^{-0.96} \quad (12)$$

$$\phi_r(T,1) = 10^{4.30} (T+644)^{-0.96} \quad (13)$$

$$\text{and} \quad \phi_r(T,10) = 10^{4.20} (T+1026)^{-0.96} \quad (14)$$

for observations at frequency 2695 MHz. It follows from (9)-(14) that parameter T_0 , characterizing the location of "break" at the integral distribution function, increases with the increase of threshold intensity of proton events. Fig. 1 shows experimental and smoothing functions of distribution for observations at 8800 MHz. ($\phi_r(T)$, $\phi_r(T;0,1)$, $\phi_r(T;1)$, and $\phi_r(T;10)$ are shown in curves 1-4, respectively.

According to (5) the integral distribution function of number of proton events of intensity $F(I, T)$ is equal to the integral distribution function of proton radio burst number $\phi_r(T, I)$ at the same arguments T and I . Having determined the value of $F(I, T)$ from $\phi_r(T, I)$ for three values of I ($I=0.1; 1; 10$) at fixed $T = 0, 100$, and 1000 units, and under the assumption that $F(I, T) = m(I+I_0)^{-\beta}$ we obtain values of parameters m , I_0 , and β .

Values of parameters of distribution functions $F(I, T)$ at three fixed values of T ($0, 10^2$, and 10^3 units) for observations at frequency 8800 and 2695 MHz are summarized in Table 1.

Table 1

v T	8800 MHz			2695 MHz		
	0	10^2	10^3	0	10^2	10^3
m	$10^{1.52}$	$10^{1.50}$	$10^{1.39}$	$10^{1.59}$	$10^{1.53}$	$10^{1.28}$
I_o	0.322	0.365	0.650	0.022	0.086	1.130
β	0.38	0.37	0.31	0.30	0.28	0.26

Directly from data of proton event observations it is possible to obtain the corresponding integral functions $F(I, T)$ at $T=0$, 10^2 and 10^3 units and to compare them with calculations. The degree of agreement between smoothing and experimental functions was obtained according to Ramanovsky's rule for the $P(x^2)$ criterion (Metropolsky, 1971). It appeared that function $\phi_r(T, I)$ --equations (9)-(14) as well as function $F(I, T)$ -Table 1--is a good approximation for an experimental series of distribution. According to Table 1, I_o is an increasing function of T and parameter $\beta \approx \alpha/e$.

By setting I in $F(I, T)$ equal to zero, it is possible to determine the total number of proton events with energy more than 10 MeV which were preceded by radio bursts with $T > 10^2$ and 10^3 units. During the whole period of time considered here protons were accelerated to 10 MeV only in 15% of the flares accompanied by radio bursts at 8800 MHz with $T > 10^2$ units and 53% of the flares accompanied by radio bursts with $T > 10^3$. The total number $\phi_r(T, 0)$ of proton radio bursts at any T is determined by the expression

$$\phi_r(T, 0) = n[T + T_o(0)]^{-\alpha} \quad (15)$$

where $n = 1^{3.86}$; $T_o(0) = 780$ units; $\alpha = 0.75$ for 8800 MHz
 $n = 10^{4.21}$; $T_o(0) = 170$ units; $\alpha = 0.96$ for 2695 MHz.

The form of asymptotic function $\phi_r(T, 0)$ is chosen to be similar to the form of function $\phi_r(J, I)$, and parameters n , $T_o(0)$ and α were selected according to expressions (9)-(14) and Table 1. From expressions (7), (8), and (15) it follows that the total number of radio bursts $\phi_r(T)$ does not coincide with the total number of proton flares $\phi_r(T, 0)$, and the fraction of proton radio bursts increases with the increase of T intensity.

3. DISCUSSION OF THE RESULTS

According to the results of the paper the function of microwave burst distributions $\phi_r(T)$ has a power form, eqs. (7) and (8). The power form of distribution function is preserved for a sufficiently large range of burst intensity variations: from $T = 10$ units to $T = 5 \times 10^4$ units. As shown above,

the power form of function $\phi_r(T)$ results in the power distribution of the number of flare-accelerated electrons that should be considered in any theory of particle accelerations in flare regions. However, the power character of distribution function cannot be preserved to $T = 0$. At present the behavior of differential distribution function $L(T)$ at low $T < 10$ units is not clear. At sufficiently low T the distribution function can become constant or have a maximum.

Proton radio bursts also have power distribution at sufficiently high intensity, and power α coincides with power for the distribution function $\phi_r(T)$ (see equations (7)-(8), and (9) through (14). At low intensities one can see the deviation from power law. The integral distribution function as it was shown is well described by the expression

$$\phi_r(T, I) = K[T + T_0(I)]^{-\alpha}.$$

Function $\phi_r(T, I)$ at high T is transferred to the power one, and at low T it is constant. The characteristic intensity $T_0(I)$ at which the distribution function has a break depends on proton event intensity I . As I increases T_0 is also increased. Since $\phi_r(T, I) \neq \phi_r(T, I_0)$ evidently there is a relation between microwave radio burst intensities and proton event intensities. It follows from this that the acceleration of electrons and the acceleration of protons in a flare are related processes.

It is rather important that power β in $F(I, T)$ is different from α in $\phi_r(T, I)$: $\alpha \approx (2 \text{ to } 2.5)\beta$. The only explanation for the fact (in case of linearity of the radio burst emission process and of proton transfer) can be a non-linear relation between the numbers of flare-accelerated electrons and protons.

At low intensity of proton events $F(I)$ is different from the power one. As we have shown, it is well described by the expression of the form $F(I) = m(I + I_0)^{-\beta}$ and at $I \ll I_0$ is approaching the constant. Function $F_p(I, T)$ is also well described by the same expression where β is close to the power for $F_p(I)$ and I_0 is an increasing function T .

According to the above results $\phi_r(T) > \phi_r(T, 0)$. It means that in some flares accompanied by microwave radio bursts the acceleration of protons to 10 MeV does not occur. The probability of proton acceleration to 10 MeV is related to the number of accelerated electrons and growth with N_e increase.

Evidently the difference of $\phi_r(T, 0)$ from $\phi_r(T)$ is in a great value of $T_0(0)$ at which "the break" of distribution function takes place.

All the regularities found can be explained in the following way. As mentioned before it is necessary to draw a conclusion concerned with non-linearity of relation T and I : $I \sim T^\gamma$. As the analysis of observation data shows, $\gamma = 2 \text{ to } 2.5$. It means that the probability $w_0(T, I)$ is

$$w_0(T, I) = w_0\left(\frac{T^2}{I}\right) \frac{1}{T^2}.$$

Although at present it is difficult to draw a certain conclusion on the explicit form of function $w(T^2/I)$, nevertheless certain limitations for its form can be derived. Since T and I are poorly correlated, $w(T^2/I)$ has no sharp maximum. (As the analysis shows, the correlation coefficient for $\log T$ and $\log I$ is equal to 0.5 to 0.6.) Another important thing is a sharp precipice of $w(x^2)$ function at low x ($x^2 = T^2/I$) which will be approximated by the presence of a factor as θ function:

$$w_0(x^2) = \tilde{w}_0(x^2)\theta(x^2 - x_0^2) .$$

The presence of such a precipice results from the impossibility of generating any amount of protons at a fixed number of electrons. Besides, $w(x^2)$ should satisfy the condition

$$\int dx w\left(\frac{1}{x}\right) = 1 .$$

Let us take the differential function of proton radio burst distribution as

$$L_r(T, 0) = \frac{A}{[T + T_0(0)]^{\alpha+1}} .$$

Then from (4) it follows that

$$f_p(I) = \frac{1}{I^{\frac{\alpha+2}{2}}} \int_0^\infty dx \frac{w_0(x^2)}{x^2} \frac{A}{\left[x + \frac{T_0(0)}{\sqrt{I}}\right]^{\alpha+1}} .$$

Having integrated over I from I to ∞ we obtain

$$F_p(I) = \frac{2A}{\alpha} \int_{x_0}^\infty dx \frac{\tilde{w}_0(x^2)}{x^3 [x\sqrt{I} + T_0(0)]^\alpha} . \quad (16)$$

From (16) it follows that

$$F_p(I) = \frac{2A}{\alpha} \frac{1}{I^{\alpha/2}} \int_{x_0}^\infty dx \frac{\tilde{w}_0(x^2)}{x^{\alpha+3}} ; I \gg \frac{T_0^2}{x_0^2} = I_0(T)$$

$$\frac{1}{T_0^\alpha(0)} \int_{x_0}^\infty dx \frac{\tilde{w}_0(x^2)}{x^3} \sim \text{const}; I \ll I_0(T)$$

Such a form of $F_p(I)$ is in a good agreement with the experimental distribution function. Then let us consider functions $F_p(I, T)$ and $\phi_r(T, I)$. From (5) it follows that

$$\phi_r(T, I) = F_p(I, T) = 2A \int_T^{\infty} \frac{dT'}{[T' + T_0(0)]^{\alpha+1}} \int_{x_0}^{T'^2/I} dx \frac{\tilde{w}_0(x^2)}{x^3} . \quad (17)$$

At $T \gg \sqrt{I} x_0$ we obtain

$$\phi_r(T, I) = F_p(I, T) = \int_T^{\infty} \frac{dT'}{[T' + T_0(0)]^{\alpha+1}} \int_{x_0}^{\infty} dx \frac{\tilde{w}_0(x^2)}{x^3} \sim \text{const.} \cdot \phi_r(T)$$

which is consistent with experimental data.

At $T \ll \sqrt{I} x_0$ we obtain

$$\phi_r(T, I) = F_p(I, T) = \int_{\sqrt{I} x_0}^{\infty} \frac{dT'}{[T' + T_0(0)]^{\alpha+1}} \int_{x_0}^{T'^2/I} dx \frac{\tilde{w}_0(x^2)}{x^3} \sim \text{const.} \cdot \frac{1}{I^{\alpha/2}} .$$

This is also in a good agreement with the experimental dependence.

The burst intensities to which the break of distribution function corresponds, as it follows from (17), are determined by the relationship $T_0(I) = \sqrt{I} x_0$, $T_0(I) \gg T_0(0)$. The increase of proton event intensities as much as 10^3 times results in 3 times increase of $T_0(I)$. According to (9) to (14) $T_0(I)$ varies as much as 2 to 3 times. This small discrepancy is related to the fact that this expression is applicable at $T_0(I) \gg T_0(0)$. In our case $T_0(I)$ is close to $T_0(0)$.

4. CONCLUSIONS

From the analysis of distribution functions it is possible to arrive at the following conclusions:

The proton and electron accelerations result from different mechanisms, genetically related to each other.

The number of accelerated protons is related to the number of accelerated electrons through the relationship $N_p \sim N_e^\gamma$ where $\gamma \sim 2$ to 2.5.

The distribution functions of the number of flare-accelerated electrons have a power form within the large range of argument variation.

In flares accompanied by radio bursts at frequencies 8800 and 2695 MHz the proton acceleration to 10 MeV occurs only in a part of the flare. The fraction of proton flares (flares with $E_p > 10$ MeV) increases with the increase of radio event intensities.

The results obtained are not contradictory with modern ideas on particle acceleration in flares. So it is possible that the electrons are accelerated in electric fields at the break of current sheet and protons, whereas their interacting with plasma turbulence resulted from instability development in the flare region.

5. ACKNOWLEDGMENTS

The authors express their gratitude to P.V. Sasorov for useful consultations and discussions of the paper.

6. REFERENCES

- Belovsky, M.N., Yu.P. Ochelkov (1977): Doklady Akad. Nauk USSR, 236:1331.
- Belovsky, M.N., Yu.P. Ochelkov, T.S. Podstrigach, M.A. Fasakhova (1978): V sb. Radioisluichenie Solntsa, vyp.4, 44, "Leningradsky universitet", Leningrad.
- Jokipiy, I.R. (1976): V sb. Nablyudeniye i prognoz solnechnoy aktivnosti, 213, "Mir", Moscow.
- Kakinuma, T., Enoma S. Yamashita (1969): Proc. Res. Inst. Atmos. Nagoya Univ., 16:127.
- Mitropolsky, A.K. (1971): Tekhnika statisticheskikh vychesleniy, "Nauka", Moscow.
- Pinter, S. (1972): IV Leningradsky mehzdunarodny seminar, 63, Leningrad.
- Scalize, E., Jr. (1970); Publ. Astr. Society Japan, 22:483.
- Shvestka, Z. (1976): V sb. Nablyudeniye i prognoz solnechnoy aktivnosti, 126, "Mir", Moscow.
- Solar Geophysical Data, 1967-1974.
- Van Hollebeke, M.A.Y. et al. (1975): Solar Phys., 41:189.

PREDICTION OF SOLAR FLARE CORPUSCULAR INTENSITY ON THE BASIS OF RADIO BURST OBSERVATIONS

A. P. Molchanov and I. E. Pogodin
Research Institute of Physics,
Leningrad State Zdanov University
USSR 198904, Leningrad, Petrodvoretz prospekt Perwogo Maja 100

A method allowing the improvement of the quality of flare proton flux prediction on the basis of flare radio emission is suggested.

The maximum intensities of proton fluxes with energy greater than 10 MeV reaching the Earth (J_E) after major solar flares were statistically considered, together with various parameters (X_E) of radio bursts connected with these flares in the band 200-20,000 MHz. These data support the conclusion that the principal particle acceleration processes take place at heights where radio bursts with frequencies of the order of one or a few gigahertz are generated (Pogodin, 1978a). Emission at lower frequencies is connected with the region in which particles are accelerated away from their main acceleration region. From this (Figure 1), it is possible to indicate cases of effective particle acceleration with an impulse component on the basis of the relationship τ_R/T at some gigahertz, where τ_R and T are the increasing phase and the whole duration, respectively. Moreover, the large values of τ_R/T at lower frequencies may indicate the existence of the so-called open magnetic field structure in the flare region, which allows the outflow of accelerated particles into space. Considering the magnetic field structure orientation in the flare region, it is possible to estimate the character of the "solar" spreading of particle fluxes accelerated during the flare (Molchanov and Pogodin, 1976).

By taking into account the complex condition (\vec{z}) acting on the particle fluxes (J_S) moving from the solar flare to the Earth, and by also taking into account complex flare radio emission parameters, we can consider the following relations (Molchanov and Pogodin, 1978):

$$J_S = f|_Y(X_S); \quad J_E = \prod_i \eta_i(z_i) \cdot J_S; \quad X_E = \prod_j \xi_j(z_j) \cdot X_S \quad (1)$$

$$J_E = \prod_i \eta_i(z_i) \cdot f|_Y(\prod_j^{-1} \xi_j(z_j) \cdot X_E) \quad (2)$$

If $f(x)$ is a uniform function of order n , then $f(k \cdot x) = k^n \cdot f(x)$,

$$J_E = [\prod_i \eta_i(z_i) \cdot (\prod_j \xi_j(z_j))^{-n}] f|_Y(X_E) \quad (3)$$

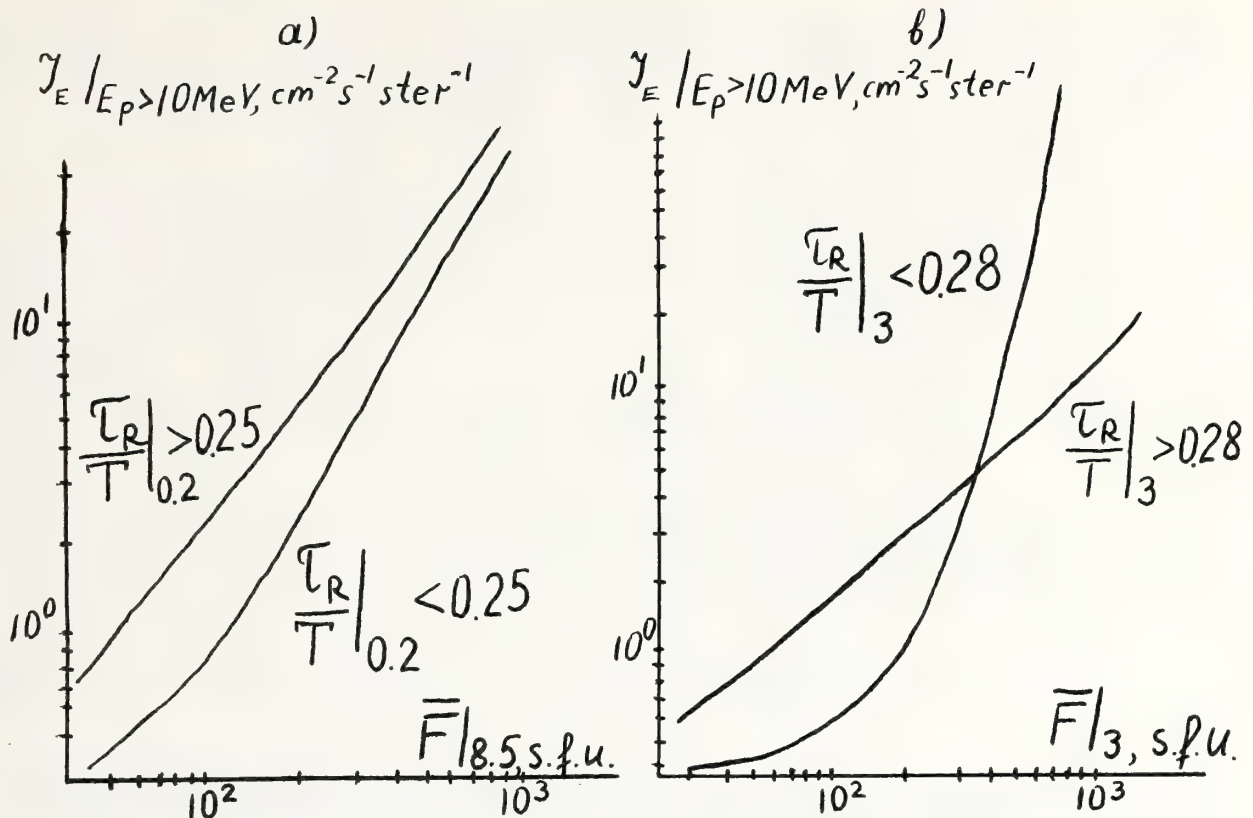


Figure 1. Effective particle acceleration on the basis of the relationship, τ_R/T .

These functions, taking into account the independent action of some concrete factors in linear approximation, may be found by the method suggested in Molchanov and Pogodin (1978), in which the following factors were investigated and described (Figure 2):

- the main spiral structure of the interplanetary magnetic field η_λ (Molchanov and Pogodin, 1978)
- local deformations of this structure resulting from the spreading of particle fluxes of previous flares $\eta_{\lambda, \Delta t k, k-1}$ (Molchanov and Pogodin, 1977)
- the above mentioned magnetic field orientation in the flare region on the sun $\eta_{B\phi}$ (Molchanov and Pogodin, 1976)
- the equatorial zone of particles escaping in space $\eta_{\phi_s | \phi_*}$ (Pogodin and Tertishnikov, 1977)
- the angular directivity of particles out of the flare region in the sun η_{ϕ_*} (Pogodin, 1978b)
- the Carrington longitude of flares on the sun η_L (Pogodin, 1978b)
- the closeness of the flare location to the sector structure boundaries η_{ss} (Pogodin, 1978b).

Statistical estimations of radio burst directivity ξ_θ (Pogodin, 1978b) resulted in the fact that its variations are much less while variations of many of the functions η_i , for example η_λ , approach the same order of magnitude.

The above results, derived from "proton" flares in 1964-1969 (Svestka and Simon, 1975) and corresponding radio bursts (Solar geophysical data) show that the usage of radio burst parameters indicates some condition of

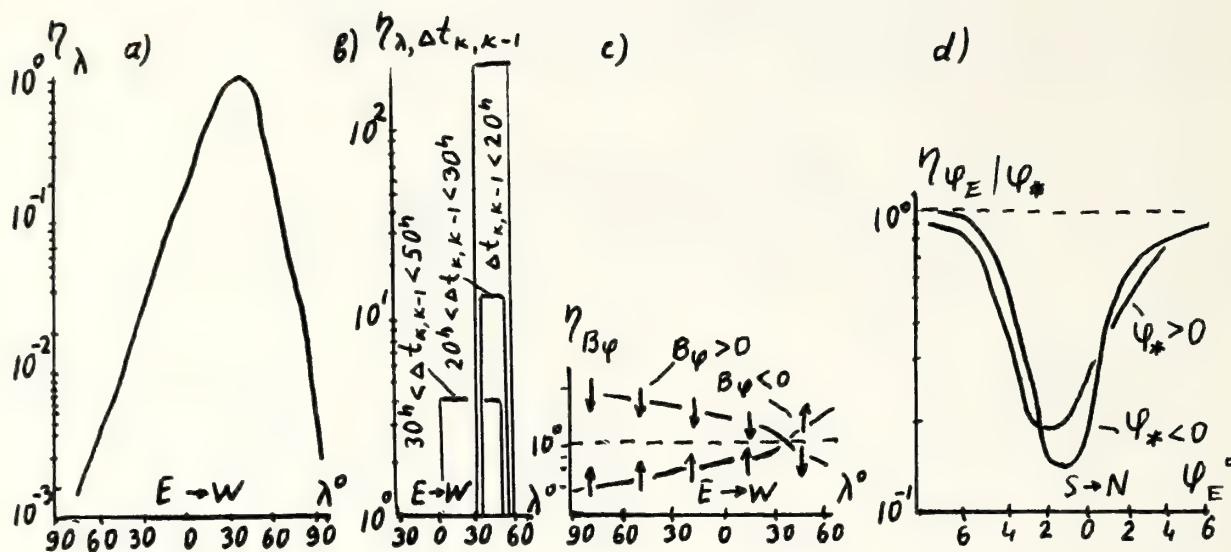


Figure 2. Diagrams showing factors referred to in Molchanov and Pogodin (1978).

accelerated particle generation and that these particles in space y increase the correlation of proton flux with basic parameters by 0.1. Additionally using only the first four functions η_i succeeds in increasing the correlation by 0.1-0.15 (Pogodin, 1978b). Without using the noted parameters, the considered correlation, even for the optimal basic radio burst parameters (they are energetic characteristics at some 1-7 GHz such as maximum and mean radio fluxes, increasing phase and the whole burst energy) usually does not exceed 0.6-0.7.

These parameters and conditions, the usage of which led us to improve the quality of prediction of expected near-Earth proton fluxes after solar flares, may be of some use in predicting the polydimensional volume by analogy.

The special algorithm of such prediction has been generated (Pogodin, 1978c). It allows one (using basic information) to obtain the probability distribution of observation of various particle flux values. The algorithm also works well for an incomplete array of basic parameters, but it gives less prediction reliability.

REFERENCES

- Molchanov, A. P., and I. E. Pogodin (1976): On the magnetic field structure in the solar proton region. Vozniknovenije i razvitije aktivnykh oblastej na Solnze. Nauka, Moscow, pp. 199-202.
- Molchanov, A. P., and I. E. Pogodin (1978): Solar flare consequences prediction. Radioizluchenie Solnza, Leningrad State University, 4:3-29.
- Molchanov, A. P., I. E. Pogodin, and E. P. Tertishnikov (1977): On the registration of high energetic proton fluxes from the consequential flares on the sun near the Earth. Solnechnye dannye, 3:74-81.

- Pogodin, I. E., and E. P. Tertishnikov (1977): The determination of some characteristics of the space zone near the solar equatorial plane. Solnechnye dannye, 4:95-100.
- Pogodin, I. E. (1978a): Flare localization in solar atmosphere on the basis of radio observations. Doklady Akademii Nauk of the USSR, 243:596-599.
- Pogodin, I. E. (1978b): Microwave radio emission of solar flares connected with high energetic particle fluxes. Kandidatskaja dissertacija, Leningrad.
- Pogodin, I. E. (1978c): About one method of the prediction of some kinds of solar-terrestrial connections. Radioizluchenie Solnza, Leningrad State University, 4:29-43.
- Svestka, Z., P. Simon, et al. (1975): Catalog of solar particle events 1955-1969. Reidel, Holland.
- Solar geophysical data (1964-1970): ESSA, U.S. Department of Commerce, Boulder, Colorado, USA.

E. ERRATA

VOLUME I:

- page 164 In the table heading, R_m and $R_m^{(4)}$ should read R_M and $R_M^{(4)}$.
(maximum) (maximum)
- page 167 Value for R_m in the table should read "3.6 to 5.2."
- page 378 The prediction technique presented in this paper has been revised since the publication of Volume I. For further details, contact W. W. Vaughan, Space Sciences Laboratory, Marshall Space Flight Center, Alabama 35812, U.S.A.

VOLUME 11:

- page 72 The equation and following sentence should read:
- $$\rho = \rho_0 \frac{F_{20}}{100} \{1 + 0.19 [\exp (0.0055 z) - 1.9] \cos^6 \frac{\psi}{2}\}$$
- where $\log \rho_0 = -16.021 - 0.001985 z + 6.363 \exp (-0.0026 z)$. In this expression, ρ is the density in gm/cm³ at altitude z in km ($200 \leq z \leq 700$); F_{20} is . . ."
- page 117 Line 3 of the Conclusion should read: ". . . ATS-6) in eclipse at geosynchronous orbit and geomagnetic activity: by observation, by a simple . . ."
- page 149 Throughout this paper, the variable for frequency should be changed from w to ω .
- page 150 Equation (2) should read:
$$\delta_1 = \frac{1}{\sqrt{2\pi\sigma_1\omega}} = \frac{1}{2\pi} \sqrt{\frac{T}{\sigma_1}}$$
- page 202 Item 4 should read: "Space power systems have the potential to significantly modify the ionosphere locally; and globally when used for long periods and in large numbers."
- page 450 Figure 6 caption should read: "Proton motion across a discontinuity. Multiple discontinuity traversals produce . . ."
- page 467 In caption of Figure 3, change "deconvolved" to "decoded." In Table 1, fourth column, change "Deconvolve" to "Decode."
- page 469 Last paragraph, "GEOS satellites" should be "GOES satellites."
- page 471 Line 4, change "deconvolution" to "decoding."
- page 535 Section 2.3, second paragraph, change time reference to GLT.
- page 540 Figure 9 caption should read: "The positions of the plasmopause (small circles) and the equatorial boundary of the DR current (crosses) as a function of geomagnetic activity. . . ."



F. INTERNATIONAL SOLAR-TERRESTRIAL PREDICTIONS WORKSHOP PARTICIPANTS

S.I. Akasofu
Geophysical Institute
University of Alaska
Fairbanks, AK 99701

E.C. Aken
City Service Pipeline Co.
P.O. Box 300
Tulsa, OK 74102

Vern Albertson
Electrical Engineering Dept.
University of Minnesota
Minneapolis, MN 55455

Joe H. Allen
NOAA-NGSDC, D64
Boulder, CO 80302

Richard S. Allen
A.F. Geophysics Lab.
Hanscom AFB
Bedford, MA 01731

Richard C. Altrock
Air Force Geophysics Lab
Sacramento Peak Observatory
Sunspot, NM 88349

David N. Anderson
Ionosphere Physics Group
Space Environment Lab
NOAA-ERL
Boulder, CO 80303

Paul Argo
Electromagnetic Propagation Div.
NOSC
San Diego, CA 92152

William Atwell
Rockwell International
1840 NASA Road One
Houston, TX 77058

Rich Babcock
HQ AWS/DNPP
Scott AFB, IL 62225

Robert Backstrom
Kirtland AFB
Albuquerque, NM 87116

Daniel N. Baker
Los Alamos Scientific Lab
Group P-4/MS 436
Los Alamos, NM 87545

Pradip Bakshi
Boston College
Chestnut Hill, MA 02167

Les Barclay
Home Office
Waterloo Bridge House
Waterloo Road
London SE1 8VA ENGLAND

W.R. Barron
AFCL/PHP
Hanscom AFB
Bedford, MA 01731

Santimay Basu
Emmanuel College
Boston, MA 02115

Sunanda Basu
Emmanuel College
Boston, MA 02115

A.D. Belmont
Research Division
Control Data Corp.
2800 E. Old Shakopee Rd.
Box 1249
Minneapolis, MN 55440

Paul Bernhardt
Radioscience Lab
Stanford University
Stanford, CA 94305

Wolfgang Boerner
University of Illinois
Chicago, IL 60680

D.H. Boteler
University of British Columbia
Vancouver, B.C. CANADA

G.M. Brown
Dept. of Physics
University College of Wales
Aberystwyth, Wales, U.K.

J. Bryson
SESC
NOAA ERL SEL
Boulder, CO 80303

Ronald Buhmann
NOAA EDIS
Boulder, CO 80303

Joseph Cain
USGS
MS 964
Box 25046
Denver, CO 80225

G.A. Caldwell
Natl. Bureau of Standards
Boulder, CO 80303

Wallace H. Campbell
USGS Box 25046
Denver Federal Center MS 964
Denver, CO 80225

D.P. Cauffman
ST-5
NASA Headquarters
Washington, DC 20546

Yam T. Chiu
Space Sciences Laboratory
The Aerospace Corp.
P.O. Box 92957
Los Angeles, CA 90009

Hugh Chivers
University of California S.D.
P.O. Box 109
La Tolla, CA 92705

T. Clark
SESC
NOAA ERL SEL
Boulder, CO 80303

Helen E. Coffey
NOAA EDIS
Boulder, CO 80303

Ray Conkright
NOAA EDIS
Boulder, CO 80303

F.E. Cook
Warning Section and IUWDS/RWC
Ionospheric Prediction Service
162-166 Goulburn Street
P.O. Box 702
Darlinghurst N.S.W. 2010
AUSTRALIA

S. Cruickshank
SESC
NOAA ERL SEL
Boulder, CO 80303

Elmer Curry
P.O. Box 35822
Tulsa, OK 74135

T. Damboldt
Forschungsinst. der DPB
P.O. Box 800
611 Darmstadt WEST GERMANY

George Davenport
Patterson AFB, OH

Ken Davies
Ionospheric Physics Group
Space Environment Lab
NOAA/ERL
Boulder, CO 80303

Peter Davies
EDIS, NOAA
Boulder, CO 80303

S.D. Deshpande
Dept. of Applied Physics
College of Engineering
Amravati 666 603, INDIA

Robert Doherty
DRPLI
1898 So. Flatiron Ct.
Boulder, CO 80303

V. Domingo
Space Science Department
ESTEC
Noordwijk, NETHERLANDS

Delia E. Donatelli
Regis College Research Center
235 Wellesley St.
Weston, MA 02193

Richard F. Donnelly
1-2119, SEL
NOAA/ERL
Boulder, CO 80303

Murray Dryer
NOAA ERL SEL
Boulder, CO 80303

David S. Evans
NOAA Research Lab
Space Disturbance Lab
Boulder, CO 80303

Joan Feyman
Boston College
Chestnut Hill, MA

W. Flowers
SESC
NOAA ERL SEL
Boulder, CO 80303

P.F. Fougere
Air Force Geophysics Lab
Hanscom AFB, MA 01731

Edward Fremouw
Physical Dynamics, Inc.
P.O. Box 3027
Bellevue, WA 98009

Henry Garrett
Air Force Geophysics Lab/PH
Hanscom AFB, MA 01731

Alberto Giraldez
Liara
Libertador 327
1638 Vincente Lopez
Buenos Aires, ARGENTINA

William Goddard
University of Manitoba
Winnipeg, Manitoba CANADA

R.A. Goldberg
Code 961
NASA Goddard Space Flight Center
Greenbelt, MD 20771

John M. Goodman
Code 7950
Naval Research Lab
Washington, DC 20375

E.R. Greenstadt
TRW Space Systems Group
R. 1280
1 Space Park, Bldg. R-5
Redondo Beach, CA 90278

J.B. Gregory
Inst. for Space & Atmospheric
Studies
University of Saskatchewan
Saskatoon, CANADA S7N 0W0

J.K. Hargreaves
Dept. of Environmental Science
University of Lancaster
Lancaster, LA1 4YQ ENGLAND

G.K. Hartmann
Max-Planck Inst. for Aeronomie
Postfach 20
D-3411 Katlenburg-Lindau 3
WEST GERMANY

Karen L. Harvey
Solar Physics Research Corp.
4720 Calle Desecada
Tucson, AZ 85718

Elaine Hatfield
SRI International
333 Ravenswood Ave.
Building 44
Menlo Park, CA 94025

Richard M. Head
Solar-Environmental Sciences, Inc.
P.O. Box 4338
Scottsdale, AZ 85258

Gary R. Heckman
1-2010, SESC-SEL
NOAA/ERL
Boulder, CO 80303

Ruth Hedeman
McMath-Hulbert Observatory
Pontiac, MI 48055

David Hickman
Aerospace Corp.
P.O. Box 92957
Los Angeles, CA 90009

Paul R. Higbie
Los Alamos Scientific Lab
Group P-4/MS 436
Los Alamos, NM 87545

J. Hirman
SESC
NOAA ERL SEL
Boulder, CO 80303

R.E. Holzer
Inst. of Geophysics & Planetary
Physics
University of California
Los Angeles, CA 90024

Donald Horan
Naval Research Laboratory
Washington D.C. 20375

Jaroslave Hruska
Division of Geomagnetism
Energy, Mines and Resources
1 Observatory Crescent
Ontario, CANADA KYA 0Y3

Robert D. Hunsucker
Geophysics Institute
University of Alaska
College, AK 99701

Herbert Hunter
Box 58
Reading, MA 01867

W.L. Imhof
Dept. 52-12, Bldg. 205
Lockheed Palo Alto Research Labs
3251 Hanover St.
Palo Alto, CA 94304

Samuel L. Irwin
Explorer Pipeline Co.
P.O. Box 2650
Tulsa, OK 74101

R.G. Johnson
Lockheed Research Lab
3251 Hanover St.
Palo Alto, CA 94303

R.H. Jones
Dept. of Biometrics
Univ. of Colo. Medical Center
Denver, CO 80262

Joann C. Joselyn
1-3034 SEL
NOAA/ERL
Boulder, CO 80303

K. Kawasaki
Geological Survey
Federal Center MS 964
Denver, CO 80225

John A. Klobuchar
AFGL-PHP
Hanscom AFB
Bedford, MA 01731

Z. Klos
Space Research Center
Polish Academy of Sciences
Ordonia 21, Warsaw, POLAND

Patrick Lassudrie-Duchesne
CNET MIR, rue de Tregastel
22301 Lannion, FRANCE

Susan McKenna Lawlor
St. Patrick's College
Mayrooth
Co. Reldare, IRELAND

Reinhard Leitinger
Inst. for Meteorologic and Geophysics
Universitat Graz Halbarthgasse 1
Graz, AUSTRIA A-8010

Mae Lethridge
Dept. of Meteorology
Pennsylvania State Univ.
University Park, PA 16802

J. Virginia Lincoln
EDIS-D63
RB3-131
NOAA
Boulder, CO 80303

D.S. Lund
Mail Code 0560
Denver Division
Martin Marietta Aerospace Corp.
P.O. Box 179
Denver, CO 80201

L.R. Lyons
NOAA/ERL
Space Environment Lab
Boulder, CO 80303

Robert H. Manka
Atmospheric Sci. Sect
National Science Foundation
Washington, DC 20550

Sara F. Martin
5212 Maryland Ave.
La Crescenta, CA 91214

Katsuhide Marubashi
Upper Atmosphere Research Sect.
Hiraiso Branch
Radio Research Lab
Nakaminato, IBARAKI 311-12 JAPAN

S. Matsushita
High Altitude Observatory
NCAR
Boulder, CO 80307

P. McIntosh
SESC/NOAA/SEL/R43
325 S. Broadway
Boulder, CO 80303

Robert L. McPherron
University of California
Inst. of Geophysics
6846 Slichter Hall
Los Angeles, CA 90024

Michael Mendillo
Astronomy Dept.
Boston University
Boston, MA 02215

George Millman
General Electric Co.
Electronics Systems Division
Bldg. 4, Room 47
Court Street Plant
Syracuse, NY 13221

J. Murray Mitchell, Jr.
NOAA
Silver Spring, MD

A.P. Mitra
Radio Science Division
Natl. Physics Lab
Hillside Rd.
New Delhi 110012 INDIA

P.B. Morris
c/o Commanding Officer
R. 4309 Transpoint Bldg.
2100 2nd St.
Washington, DC 20590

Paul Mutschlecner
Los Alamos Scientific Lab
P.O. Box 1163, MS 436
Los Alamos, NM 87545

Donald F. Neidig
Air Force Geophysics Lab
Sacramento Peak Observatory
Sunspot, NM 88349

V.N. Obridko
IZMIRAN
c/o Akademgorodok
Troitsk
Moscow Region, 142092 USSR

Tadahiko Ogawa
Aeronomy Lab
NOAA ERL, Bldg. 24
24-1102
Boulder, CO 80303

Takashi Okuzawa
NOAA/ERL/SEL/R43
Boulder, CO 80303

Bill Olsen
McDonnell Douglas Astronautics Co.
5301 Bolsa Ave.
Huntington Beach, CA 92647

Roger Olson
Aspen Institute
1919 14th St., No. 811
Boulder, CO 80302

Vernon G. Patterson
A.F. Global Weather Center 7515
Offutt AFB, NE 68113

George A. Paulikas
Bldg., A6, Mail Station 2403
Space Sciences Lab
The Aerospace Corp.
P.O. Box 92957
Los Angeles, CA 90009

N.K. Pereyaslova
Inst. of Applied Geophysics
107258, Glebovskaya Str.,
Moscow, USSR

W.R. Piggott
British Antarctic Survey
Madingley Rd.
Cambridge CB3 0ET ENGLAND

Margo Leftkin Pokempner
1-3413
NTIA, ITS 3
Boulder, CO 80303

Helen Dodson Prince
McMath-Hulbert Observatory
895 Lake Angelus Rd.
Pontiac, MI 48055

E. Prior
NASA Langle Research Center
Hampton, VA 23665

Guo Quanshi
Purple Mountain Observatory
Nanking, Kinagsu CHINA

Boyde E. Quate
Boyde E. Quate & Assoc.
P.O. Box 7065, Holland
Station
Suffolk, VA 23437

Ram Rastogi
c/o J.A. Klobuchar
AFGL-PHP
Hanscom AFB, MA 01731

J.B. Reagan
Lockheed Palo Alto Research
Lab
3251 Hanover St.
Palo Alto, CA 94304

B.M. Reddy
Radio Science Division
Natl. Physical Lab
Hillside Rd.
New Delhi 110012 INDIA

C.L. Rino
Stanford Research Inst.
Menlo Park, CA 94035

Donald E. Robbins
Mail Code SC4
NASA/Johnson Space Center
Houston, TX 77058

E.C. Roelof
John Hopkins Univ./Applied
Physics Lab
Johns Hopkins Rd.
Laurel, MD 20810

Charles M. Rush
NTIA/ITS
Boulder, CO 80303

C.T. Russell
Space Science Center
Inst. of Geophysics & Planetary
Physics
Univ. of California
Los Angeles, CA 90024

David Rust
Solar Physics Group
American Science & Engineering Co.
955 Massachusetts Ave.
Cambridge, MA 02139

Mangal Sain
All India Radio
Research Dept.
Indraprastha Estate
New Delhi 110012 INDIA

H.H. Sargent III
SESC/NOAA/ERL/SEL R43
325 S. Broadway
Boulder, CO 80303

J. Schafer
Radioastronomisches Institut
der Universität Bonn
5300 Bonn-Endenich
Auf dem Hugel 71 WEST GERMANY

K.H. Schatten
Code 961
NASA Goddard Space Flight Center
Greenbelt, Maryland 20771

Warren A. Schlueter
Mission Research Corp.
735 State St.
P.O. Drawer 719
Santa Barbara, CA 93105

Manfred Scholer
Max-Planck Inst. for Physik &
Astrophysik
Institut für Extraterrestrisch
Physik
8046 Garching, Muneen GERMANY

Jim Secan
AFGWC/TSIS
Offut AFB, NE 68113

Peggy Ann Shea
PHE, Space Physics Lab
Air Force Geophysics Labs
L.G. Hanscom Field
Bedford, MD 01731

A.V. Shirochkov
Arctic & Antarctic Research Inst.
nab. Fontanki 34
Leningrad D-104 USSR

S. Silverman
Space Physics Lab
Air Force Cambridge Research
Hanscom Field, MA 01730

P. Simon
Ursigrammes, DASOP
Observatoire
92190 Meudon FRANCE

Donald G. Singleton
Navigation Group
Weapons Res. Est
GPO Box 2111
Adelaide S.A. 5001 AUSTRALIA

J.A. Slavin
Inst. Geophysics
Univ. of California
Los Angeles, CA 90024

Jack Slowey
Smithsonian Inst.
Astrophysics Observatory
Cambridge, MA 02138

Don F. Smart
Space Physics Division
AFGL/PHG
Hanscom Field AFB
Bedford, MA 01731

Georgellen Smith
SRI International, 333 Ravenswood RD.
Menlo Park, CA

Jesse B. Smith, Jr.
Space Sciences Lab, ES-52
Marshall Space Flight Center
Huntsville, AL 35812

H. Soicher
DRDCO-COM-RF
U.S. Army CORADCOM
Ft. Monmouth, NJ 07703

D. Speich
SESC
NOAA ERL SEL
Boulder, CO 80303

W.N. Spjeldvik
NOAA/ERL
Space Environment Lab
Boulder, CO 80303

James Sroga
P.O. Box 92960
Worldway Postal Center
SAMS0/WE
Los Angeles, CA 90009

Arnold Starr
Sept. 7, 12WS
Holloman AFB, NM 88330

K. Stasiewicz
Space Research Center
Polish Academy of Sciences
Ordona 21, Warsaw POLAND

E. Stassinopoulous
Code 601
NASA Goddard Space Flight Center
Greenbelt, MD 20771

N.N. Stepanyan
Crimean K Astrophysical
Observatory
334413, p/o Nauchny
Simferopol USSR

J. Sutori K
SESC
NOAA ERL SEL
Boulder, CO 80303

E.R. Swanson
Naval Electronics Lab Center
271 Catalina Blvd.
San Diego, CA 92152

W. Swider
Air Force Geophysics Lab
Hanscom AFB, MA 01731

Thomas F. Tascione
Air Force Global Weather Control
TSIS
Offutt AFB, NE 68113

M. Teague
Code 601
NASA/Goddard Space Flight Center
Greenbelt, MD 20771

R. Thompson
OFGWD/WPE
Offutt AFB, NE 68113

Eivind Thrane
Norwegian Defense Research
Establishment
Div. for Electronics
P.O. Box 25
Kjeller, NORWAY

John Gethyn Timothy
LASP
University of Colorado
Boulder, CO

Kurt Toman
RADCC-EEP
Hanscom AFB, MA

P.V. Tyron
Nat'l. Bureau of Standards
Boulder, CO 80303

Bruce T. Tsurutani
Jet Propulsion Lab/183-401
4800 Oak Grove Drive
Pasadena, CA 91103

A.L. Vampola
The Aerospace Corp.
P.O. Box 92957
Los Angeles, CA 90009

William W. Vaughan
Atmospheric Science Division
NASA Marshall Space Flight Center
AL 35802

D.F. Vecchia
Nat'l. Bureau of Standards
Boulder, CO 80303

James I. Vette
Code 601
Goddard Space Flight Center
Goddard, MD 20904

Richard R. Vondrak
Radio Physics Lab
SRI International
Menlo Park, CA 94025

John M. Wilcox
Inst. for Plasma Research
Vis Crespi
Stanford Univ.
Stanford, CA 94305

Hurd C. Willett
Mass. Inst. of Technology
Cambridge, MA

Donald J. Williams
1-3050, SEL
NOAA/ERL
Boulder, CO 80303

Jim Williams
NOAA ERL SEL
Boulder, CO 80303

R. Gareth Williams
Southampton University
c/o Physics Dept.
Southampton, ENGLAND

G. Wortham
AFGW/SESC
NOAA ERL SEL
Boulder, CO 80303

Bill Wright
Ionospheric Physics Group
Space Environment Lab
NOAA/ERL
Boulder, CO 80303

Tyan Yeh
Eastern Research Service
Louisville, CO 80207

Lin Yuan-zhang
Peking Observatory
Peking, CHINA

Ding You-ji
Yunnan Observatory
Kunming, Yunnan CHINA

R.A. Zevakina
IZMIRAN
p/o Akademgorodok
Troitsk
Moscow Region 142092 USSR

PENN STATE UNIVERSITY LIBRARIES



A000070945478